TIME DEPENDENT DEFORMATIONS OF HARDENED CEMENT PASTE FROM 20°C TO 725°C

Wiranjith Priyan Solomon Dias

A thesis submitted for the Degree of
Doctor of Philosophy of the University of London
and the
Diploma of Imperial College

1986

Civil Engineering Department
Imperial College of Science and Technology
University of London

parentibvs meis

ABSTRACT

This thesis is primarily concerned with an experimental investigation into time dependent deformations of unsealed hardened cement paste at temperatures from 20°C to 725°C. This is supplemented by the testing of mechanical properties, microstructural investigations and computer modelling of the aggregate-paste interaction of an idealized concrete subjected to a temperature rise.

The main focus of the research is on basic creep, which is defined as the load induced time dependent deformation of a specimen when loaded after achieving thermal, hygral and dimensional equilibrium at a given temperature. The time required to achieve such stability varied from one temperature to another, depending on the extent and rate of the physical and chemical transformations taking place. Loading prior to dimensional equilibrium resulted in an enhanced creep response. Pre-heating to higher temperatures before loading diminished the creep response, and pointed to the existence of a temperature induced microstructural stabilization effect, which counteracted strength reduction caused by temperature.

The time function of basic creep obeyed a power law relationship. The temperature function showed a marked increase above 600°C. Activation energy studies were undertaken to obtain a temperature dependence for basic creep, and also to suggest underlying mechanisms for elevated temperature creep. The stress function was investigated only in a very limited manner.

Shrinkage strains occurring during first heating were also measured. Their time dependence was modelled mathematically by a logarithmic master curve for the variable temperature phase and an exponential type formula for the isothermal phase.

The strength and elastic properties, both at temperature and on post-cooling, indicated a densifying effect of temperature and load, within certain limits. They also showed that the over-riding effect of temperature on these properties was structural rather than thermal.

The polysilicate content measurements revealed that load and temperature applications increased the degree of polymerization at temperatures up to 120°C, but that higher temperatures caused depolymerization. Percentage weight loss was found to be a better index of temperature induced stabilization, i.e. reduction of creep potential, than was the degree of polymerization, at temperatures above 300°C.

The computer modelling predicted the formation of matrix cracks in a specimen of the idealized concrete, i.e. spherical glass inclusions in a paste matrix, heated to and maintained for 7 days at 120°C, despite stress relaxation due to transient creep.

ACKNOWLEDGEMENTS

This work was carried out during the headship of Professor John Dougill, to whom I am grateful for the opportunity to undertake research in the Concrete Section, and for his interest in my subsequent progress.

Dr. Patrick Sullivan has been a source of encouragement from virtually my first day at Imperial College. My interest in Concrete Materials led me to work under his supervision, and I would like to thank him for his guidance and advice.

It was indeed my good fortune to have Dr. Gabriel Khoury working in the section as a Research Fellow. His comprehensive experience gave me quick access to the state of the art in high temperature concrete research. I am especially grateful to him for his ready availability for many valuable discussions and his critical evaluation of my manuscript.

I would like to thank Mr. Brian Grainger at the Central Electricity Research Laboratories in Leatherhead for going out of his way to help me in many ways, especially in the casting of specimens and in the loan of the furnace for the hot strength tests. My thanks are also due to Mr. Dennis Hitchings of the Department of Aeronautics at Imperial College, who spent much of his valuable time helping me to use the finite element package FINEL. Karen Scrivener and Alison Crumbie in the Department of Metallurgy and Materials Science helped me to obtain the electron microscope images.

The experimental work could not have been performed without the help of Messrs. Roy Loveday, Peter Jellis, Roy Baxter and the rest of the technical staff in the Concrete Laboratories, and Mr. Gupta Singh in the Public Health Section. Messrs. Richard Packer and Andrew Chipling produced photographs of the highest quality. A special word of thanks is due to Miss Patricia O'Connell, who typed this thesis to perfection.

The opportunity for studying and living in London for over 3

years was made possible because of a scholarship received from the Commonwealth Scholarships Commission in the U.K. I would like to record my thanks to them and also to the British Council, who administered the scholarship. Towards the end of my stay, financial assistance was also received from the Mountbatten Fund and the Leche Trust. I am also indebted to the Department of Civil Engineering at the University of Moratuwa, Sri Lanka, for their willingness to release me to pursue research overseas.

Finally, it gives me much pleasure to make mention of the many supportive communities in London that enabled me to enjoy my stay here and contributed either directly or indirectly to the completion of this thesis - my friends in Lillian Penson Hall and at All Souls Langham Place, my flatmates at 100, Lexham Gardens and my colleagues at Imperial College, in whose number it was my privilege to have Samantha and Premini Hettiarachchi. I should also add that my overall experience was enhanced by Britain's liberal press, London's cultural life and the Haldane Library's collection of classical music cassettes.

TABLE OF CONTENTS

LIST OF TABLES

LIST OF FIGURES

FOREWORD

> "We must not say, let us begin by inventing principles whereby we may be able to explain everything; rather we must say, let us make an exact analysis of the matter and then we shall try to see, with much diffidence, if it fits in with any principle".

The above quotation from Voltaire was used in the introduction to a paper on high temperature creep by Professor J.E. Dorn in 1954 (47). It emphasises the need for the experimental researcher to be grounded in empiricism, to be true to the observed data. If the above was the case for Dorn, whose experiments were on metals, much more should it be the case for those who venture to research the far more complex materials of cement paste and concrete.

However, the purpose of all scientific research is to find underlying unity, to undergird the particularity of individual observations with the generality of a theoretical framework. It is hoped that this thesis reflects, in some way, a balance between the empirical and theoretical approaches. While being essentially in Voltaire's camp, it seeks also to identify with Newton, as quoted by Krausz and Eyring in their book on Deformation Kinetics (90) :

> "I wish we could derive the rest of the phenomena of nature by the same kind of reasoning from mechanical principles, for I am induced by many reasons to suspect that they may all depend upon certain forces by which the particles of bodies by some causes hitherto unknown, are either mutually impelled towards each other, and cohere in regular figures, or are repelled and recede from each other; which forces being unknown, philosophers have hitherto attempted the search of nature in vain; but I hope the principles here laid down afford some light either to that or some truer method of philosophy".
>
> The Principia, Isaac Newton

CHAPTER 1 - INTRODUCTION

1.1. BACKGROUND FOR RESEARCH PROGRAMME

The properties of concrete at elevated temperatures have attracted considerable research interest over the last half century or more. The major application of this research has been in fire resistance studies and more recently, in the design of pre-stressed concrete pressure vessels. High temperature data would be important for ultimate limit state studies in both the above cases. In the latter case, a proper design for the working state would also require a knowledge of the high temperature properties of concrete, albeit at comparatively lower temperatures.

Figures 1.1 and 1.2 indicate the kind of temperatures that could be envisaged in fires and advanced gas cooled reactors (AGRs) respectively. In Figure 1.2, the upper temperature limit of interest, representing a disaster situation, is 650°C while the lower limit, representing a service condition, is 55°C. It might be possible however, to increase this operating temperature, thus reducing cooling costs, provided experimental data is available as design inputs. The temperatures involved in fire can be much higher than the above, as shown in Figure 1.1. The BS 476 furnace curve is used for fire tests on structural elements and assemblies.

At temperatures of the above magnitudes, the time-dependent behaviour of concrete becomes comparatively more significant than at ambient temperatures. Attention should be paid both to its detrimental effects, such as increased deflection and loss of pre-stress due to creep and shrinkage, as well as its beneficial effects, such as stress relaxation.

1.2. LAYOUT OF THESIS

This investigation is primarily concerned with the basic creep of hardened cement paste at temperatures from 20°C to 725°C. Although

experimentation on hardened cement paste, as opposed to concrete, is perhaps a step removed from the real world of concrete construction, it was considered to be a more fundamental approach, both because hardened cement paste is in fact the creeping medium in concrete and also because interference from aggregate effects would be eliminated. Furthermore, very little experimentation has been performed to date on hardened cement paste at these high temperatures, especially at temperatures above 100°C. The reasons for concentrating on cement paste are further elaborated in Chapter 3.

In practice, concrete elements and structures could experience creep loading under various combinations of moisture, temperature and shrinkage conditions. It is neither possible nor even desirable to simulate all these conditions experimentally. A better approach is to investigate the limiting cases thoroughly, and seek to interpolate the properties for intermediate conditions, which in turn should be experimentally verified. In the present investigation, most of the specimens were loaded at a combination of conditions that corresponded to maximum temperature, hygral equilibrium and cessation of shrinkage. These conditions of loading are further discussed in Chapter 3.

The heterogeneous nature of concrete has led to its characterization at different structural levels (180). Hence, concrete materials research can be conducted at the micro-level (which is related to the structure of the hardened cement paste), the meso-level (where the influence of pores, cracks and aggregate inclusions are accounted for) and the macro-level (which consists of obtaining material laws for structural design inputs). All three of these levels have been researched in the present project. Most of the experimentation was conducted at the macro-level; data was obtained on basic creep, shrinkage, transitional thermal creep, thermal strains, static and dynamic moduli of elasticity and hot strength. The micro-level investigations consisted of polysilicate content determination and scanning electron microscopy. The computer modelling of the aggregate-paste interaction constituted a meso-level investigation.

A review of the literature on high temperature properties of

concrete is given in Chapter 2. This chapter is divided into four sections: (a) creep, (b) shrinkage and thermal strain, (c) strength and elastic properties and (d) microstructure. The purpose of the literature review is both to provide the general background within which this work was undertaken, and to identify areas of research potential. The latter is realized explicitly in Chapter 3, which also describes test procedures and materials. The creep rigs, which were the main experimental apparatus used, are described in Chapter 4.

The experimental results are presented, analysed and discussed under the headings given in the literature review, in Chapters 7, 6, 5 and 9 respectively.

Chapter 8 seeks to establish a theoretical basis for the temperature dependence of basic creep via an activation energy approach. Values of activation energy are also used to make tentative conclusions regarding creep mechanisms at elevated temperatures.

Chapter 10 describes the formulation and solution of the computer model for simulating the aggregate-paste interaction under thermal loading. It also contains additional experimental results which were obtained as input data for the model.

Chapters 5, 6, 7 and 9 are essentially empirical in approach, while Chapters 8 and 10 are more theoretical. The final chapter identifies some themes common to the different results obtained, and draws some general conclusions. It also recommends areas for future research.

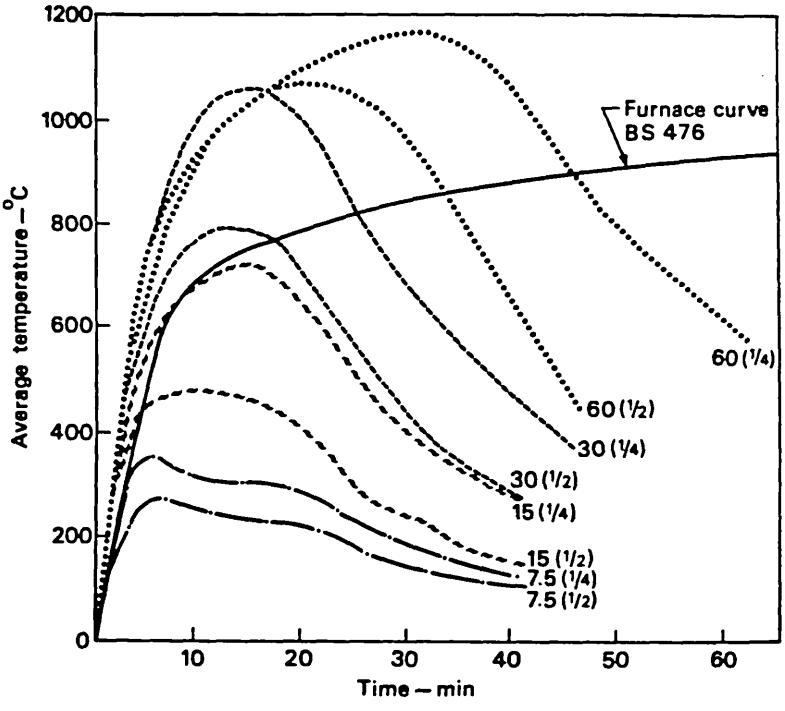

(60 (½) means fire load 60 kg/m² floor area and ventilation 50% of one wall)

Figure 1.1 - TEMPERATURES EXPERIENCED DURING FIRE (FROM MALHOTRA (98))

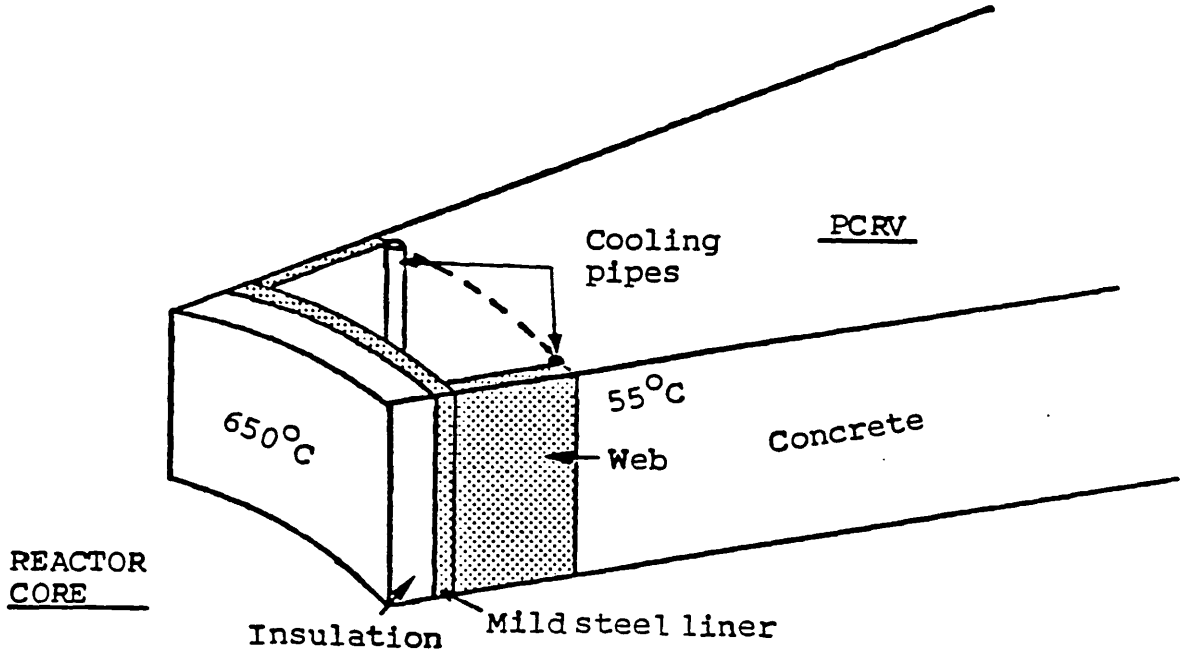

Figure 1.2 - TYPICAL TEMPERATURES REACHED IN AN ADVANCED GAS-COOLED REACTOR (FROM KHOURY (84))

CHAPTER 2 - LITERATURE REVIEW

This literature review sets out the general background within which the present investigation was undertaken, and helps to identify potential areas for research. It is divided into four sections, namely Creep, Shrinkage and Thermal Strain, Strength and Elastic Properties and Microstructure.

2.1. CREEP

Geymayer (58) has made a detailed review of creep tests, most of which have been performed in the temperature range below 100°C. Anderberg and Thelandersson (3), Neville et al (119) and Khoury (84) have made reviews on creep tests performed up to higher temperatures. The following review of literature, however, is made with a particular emphasis on its relation to the present investigation.

2.1.1. Creep of Concrete at Elevated Temperatures

Although many investigators have studied the creep of concrete at high temperatures, analysis and comparison of their results is a difficult task. This is due, not only to the inherent variability of concrete itself, but also to the fact that time dependent strain behaviour is sensitive to temperature and load history. Hence, the different kinds of pre-conditioning and test procedures employed by different investigators have given rise to significantly different results.

While there are no direct tensile tests at elevated temperature reported in the literature, a few flexural creep investigations have been carried out (66, 164). Illston and Sanders (79) performed torsional creep tests on thin walled hollow cylindrical mortar specimens, in order to minimize undesirable stress gradients as well as to isolate volumetric movements caused by thermal expansion.

However, most high temperature creep tests have been performed

in compression, and here too, most of the investigators have confined themselves to uniaxial compression tests on cylindrical specimens. Some exceptions to this are Marechal (100), who tested square prismatic specimens under uniaxial compression, Arthanari and Yu (6), who tested square slabs under biaxial compression and Bazant et al. (14), who tested cylindrical specimens under triaxial compression.

Table 2.1 gives an indication of the different parameters involved in the performance of concrete creep tests at elevated temperatures. It should be appreciated that the first three parameters (i.e. initial moisture condition, sealing condition and the time of load application) contribute, in smaller or greater measure, to determine the history of the specimen.

The importance of the initial moisture condition indicates the dominant role of evaporable moisture on the creep of concrete, especially in the temperature range below 100°C. For example, as apparent in Figure 2.1, Marechal's quartzite concrete shows a distinct creep maximum at 50°C when initially moist. However, this maximum disappears in specimens which were pre-dried at 105°C for 30 days.

The sealing condition of the specimen during the heating and loading periods has been considered to be a very important parameter. A sealed specimen would not permit the diffusion of moisture to the surroundings and hence exhibit a reduced amount of shrinkage during the heating phase. Furthermore, it is likely that hydrothermal reactions within the concrete would be promoted by the presence of this moisture within the specimen (91). An unsealed specimen, on the other hand, would lose moisture to its surroundings and experience considerable shrinkage (which would, of course, be superimposed on the thermal expansion of the specimen) during the heating phase. The testing of concrete in the sealed condition could be considered as an attempt to understand behaviour in thick walled, massive concrete structures, while the testing of unsealed concrete could be considered as an attempt to simulate conditions in thinner concrete sections or in surface regions.

The sealing of concrete specimens has been achieved in

different ways. Nasser and Neville (116) maintained their specimens in a water bath set to the desired temperature throughout the heating and loading phases. It must be appreciated, however, that this technique can be employed only at temperatures below 100°C. The other technique commonly employed has been to encase the specimen in a watertight foil or jacket (65, 113). A drawback in this technique is the possibility of moisture diffusion taking place to the surface of the specimen and collecting in the space between the specimen and the jacket (113). Bazant et al. (14) achieved sealed conditions by the use of a triaxial testing rig and a flexible membrane around the specimen. They contend, in fact, that the only way to achieve a sealed, "zero moisture loss", condition at elevated temperature is by triaxial testing, since pressure must be applied on the concrete surface to prevent moisture loss.

The time of load application is also a very critical parameter in discussing creep at elevated temperatures. It is, in fact, the parameter by which the type of ensuing creep is defined. For example, if the load is applied in the absence of shrinkage under isothermal conditions, the resulting creep is called basic creep. The absence of shrinkage at elevated temperatures can be achieved by waiting till the end of the shrinkage phase (99).

If, however, the load is applied while drying shrinkage is taking place, not only is this shrinkage superimposed on the basic creep, but an additional component of creep called drying creep is introduced.

Furthermore, if the load is applied before the heating phase, cement paste (130), mortar (79) and concrete (87) specimens have been found to undergo a significantly large amount of creep during heating. This has been called transitional thermal creep and has been observed only during the first time of heating to a given temperature; it is absent during cooling. In the case of moist, unsealed specimens loaded prior to heating, transitional thermal creep would be superimposed on basic creep, drying creep, shrinkage and thermal expansion.

2.1.2. Uniaxial Basic Creep of Unsealed Concrete

The uniaxial basic creep of unsealed concrete is now considered in more detail, since the present investigation concentrates on this area. Table 2.2 gives the parameters employed by different investigators, while Figures 2.1 and 2.2 give a comparison of their results.

(a) Comparison of Results

Two difficulties were encountered when making this comparison. The first is the fact that durations of creep tests vary from one investigator to another, ranging from 3 hours (4) to 11 months (115). For this reason, it has not been easy to find a time at which to make a suitable comparison between all the investigators. The 3 hr (Figure 2.2) and 60 day (Figure 2.1) creep strains have been chosen so as to obtain as much information as possible from the comparisons.

The second difficulty is the task of normalizing the creep strains to a common parameter. Although the practice in the past has been to normalize such data on the basis of specific creep (i.e. creep strain per unit stress) (3, 58), the approach here is different. In this study, the creep data has been normalized on the basis of the creep corresponding to an equal stress/strength ratio. This approach has been chosen on the basis of Neville's work (119), which indicates that creep is proportional to the stress/strength ratio, especially at smaller stresses. Although the exact nature of this proportionality is not very clear at elevated temperatures, creep strains in this comparative study have been normalized with respect to an equal stress/cold strength ratio. If it is assumed that most concretes lose strength with temperature in an approximately similar fashion, normalizing creep strains on the basis of an equal stress/cold strength ratio would be a reasonable method of making comparisons between the results of different investigators. The value of stress/cold strength chosen is 0.1, because most of the present investigation was carried out at a value close to this. If an investigator has used more than one stress level in his study, the data corresponding to the lowest stress level has been normalized and used in this study.

(b) Pre-heat duration

Perhaps the most important consideration when investigating the basic creep of concrete at high temperatures is the time of load application (i.e. the pre-heat duration). Unsealed concrete loses moisture and hence undergoes shrinkage during heating. If the measured creep strains are to be free from the effects of shrinkage and drying creep, not only must the specimen achieve thermal and hygral stability, but it must also achieve dimensional stability as well (i.e. it must be loaded after shrinkage has ceased). This is borne out by Bazant et al. (14) who reported that shrinkage increased significantly even after the cessation of drying (calculated on the basis of pore pressure equalization). They also reported that the creep associated with drying was considerable, long after drying terminated. Reutz (146) (reported in ref. (3)) too found a significant difference between sealed hardened cement paste specimens that had been subjected to a 3-day pre-heat duration at a temperature of 80°C, compared to those that had not been thus pre-heated. (See Figure 2.3). In this case, however, since these specimens were sealed, and not heated to excessive temperatures, it is likely that the reduction in creep for the pre-heated specimens was due to the cement paste achieving an increased maturity, and hence a reduced creep potential.

Various investigators have made different attempts to overcome the problem of pre-heat duration in unsealed concrete specimens. Hannant (65) for example, loaded his unsealed specimens just one day after reaching thermal stability, but subsequently did not report the results because he realized that specimens at different temperatures would have different rates of drying, thus making comparison impossible (Figure 2.4). Anderberg and Thelandersson (4), who loaded their specimens shortly after thermal stability, have claimed that companion control specimens did not undergo any shrinkage over the 3 hour creep test period, and hence concluded that the measured creep strains were in fact basic creep strains. The above claim, however, is at variance with the experience of most other investigators.

England and Ross (50) also loaded their specimens shortly after thermal stability, but measured shrinkage on control specimens

and corrected the measured creep strains for this shrinkage. However, it is now widely accepted (180) that this kind of shrinkage compensation is not sufficient to obtain the required basic creep, because of the additional drying creep component which cannot be isolated. Many other investigators, however, have completely ignored the possible effects of shrinkage, and made no shrinkage compensation.

Perhaps the investigator with the best approach to the problem to date has been Marechal (99). Not only did he employ a pre-heat duration of 14 days prior to loading, in order to eliminate most of the shrinkage, but even after that, he monitored any additional shrinkage on control specimens and compensated for this in the measured creep strains. The significantly lower strains obtained by Marechal (Figure 2.1) in comparison with other investigators indicate the justification for his rigorous approach, which would have probably eliminated all the shrinkage and most of the drying creep effects from the measured creep strains.

Figure 2.1 also shows Hickey's (71) results, where the concrete was loaded prior to heating. Hence the measured strains include not only basic creep, drying creep and shrinkage strains, but also transitional thermal creep strains. This, no doubt, is why Hickey's results form an "upper bound" for the creep strains shown in Figure 2.1.

Geymayer, in his review of the literature on high temperature creep tests (58), draws attention to another possible effect of the duration of pre-heating. In all the tests he surveyed, he found a maximum for the creep rate (defined as the average slope of the creep vs. log time plot over an arbitrary duration of time, not including the first day) at temperatures between 50°C and 100°C (Figure 2.5). In some cases, a similar maximum was obtained for the total creep (measured over periods of 60-107 days) as well (Figure 2.6). Geymayer found that the maxima for both the creep rate as well as the total creep were more pronounced for specimens that had been pre-heated for durations of 2 weeks or more. This total creep maximum below 100°C is visible in most of the results plotted in Figures 2.1 and 2.2.

Another consideration with regard to the heating phase is the rate of heating. Excessive rates of heating not only give rise to undesirable temperature (and hence stress) gradients in the specimen (3, 86), but may also cause explosive spalling (168, 169).

(c) Age at Testing and Pre-conditioning

Increased hydration that takes place with age would increase strength and reduce the creep potential of concrete. In addition, pioneering work by Lentz (93) has shown that polymerization of silicate chains takes place long after cement hydration has ceased. This then can be considered to be a major phenomenon associated with the long-term ageing process in concrete, causing a densification of the structure of hardened cement paste and reducing its creep potential. Furthermore, Parrott (128) has shown that a correlation exists between the degree of polymerization and the amounts of the irreversible components of shrinkage and creep in hardened cement paste specimens. It can, therefore be expected that ageing and drying (whether temperature induced or otherwise) of concrete would increase the degree of polymerization and affect the creep response.

Evidence regarding the effect of age and pre-conditioning at temperature is scanty. Gillen (60) has reported that concretes at ages of 35 and 187 days tested at temperatures up to 650°C showed no significant difference in their creep responses. Arthanari and Yu (6), who investigated creep behaviour at temperatures up to 80°C, found that the effect of age on the creep response reduced with increasing temperature. Therefore, when considering the creep behaviour of concrete maintained at elevated temperatures, the foregoing evidence seems to indicate that the effect of temperature tends to eliminate, or over-ride the effect of age.

However, it is interesting to note that concrete which has been pre-heated to a higher temperature and creep tested at a lower temperature, experiences less creep than when tested at the lower temperature. This phenomenon was observed by Theuer (170) (reported in ref. (119)), who found that unsealed concrete pre-dried at 110°C exhibited very little creep when tested in the temperature range -3 to

51°C; he also found that the amount of creep was independent of the test temperature within this range. Marechal (100) who pre-heated his concrete to the much higher temperatures of up to 400°C also found that pre-heating reduced the creep rates obtained at lower temperatures (Figure 2.7). Marechal explains this phenomenon by stating that "it is possible that the number of bonds liable to be activated has decreased".

Parrott (129) and Day and Gamble (43) have also pre-heated 28 day old hardened cement paste specimens to temperatures up to 95°C and have observed lower basic creep at ambient temperature. This may perhaps have been due to accelerated curing induced by temperature, since the specimens, in both cases, were in a sealed, saturated state. Nevertheless, the above-mentioned authors have correlated the decrease in irrecoverable basic creep with an increase in the degree of polymerization. Day and Gamble have, however, also reported an opposite effect of pre-heating (i.e. an increase in creep) when the hardened cement paste specimens were mature - i.e. 2.5 years old (43).

(d) Strength

The strength at testing, which reflects the water/cement ratio of the concrete, has been considered to affect the creep response only in as much as it changes the stress/strength ratio. This has been generally verified in practice, although some reports claim that higher strength concrete exhibits more creep, especially at very high temperatures (c. 650°C), despite being loaded to the same stress/strength ratio (60, 176).

(e) Aggregate volume percentage and type

Neville (117) has shown that the aggregate volume percentage is a significant factor in determining the creep response of concrete, because the aggregate serves as a restraint to the creep of the hardened cement paste. Where our comparative study is concerned, the aggregate volume percentages vary only slightly from each other (Table 2.2).

The type of aggregate employed would affect the creep response in three ways. Firstly, aggregates having different stiffnesses would give varying degrees of restraint to the creep of the cement paste and hence result in different concrete creep values.

Secondly, the coefficient of thermal expansion of the aggregate would determine the degree of incompatibility, during heating, between the expanding aggregate and the shrinking cement paste (48). This would tend to induce stresses at the interface, which however would be relieved to an extent by transitional thermal creep of the cement paste. The degree of bond weakening (or even cracking) during this heating phase may be reflected in subsequent strain response to creep loading. The effect of thermal cycling on the aggregate-paste bond for different aggregates has been studied in detail by Campbell-Allen and Desai (30).

Finally, creep at elevated temperatures will be affected by the aggregate itself if it is unstable, or breaks up at a particular temperature. The creep behaviour reported by Gross for gravel concrete (63) as shown in Figure 2.2 shows a sharp increase in creep at 400-450°C, which could be attributed to the fact that gravel tends to disintegrate at these temperatures. However, the fact that both Khoury's lightweight aggregate concrete (85) as well as Gillen's calcareous aggregate concrete (60) show increased creep at the same temperature of around 650°C may indicate that a more fundamental cause (such as the behaviour of the hardened cement paste itself) is responsible for this increase.

2.1.3. Mathematical Formulations

The mathematical formulations for basic creep are conveniently classified into time, temperature and stress functions. Although they are discussed separately, they cannot, strictly speaking, be assumed to be uncoupled.

(a) Time Function

Most of the mathematical formulations for the time function

of high temperature creep of concrete, whether sealed or unsealed, have been of the logarithmic form,

$$\epsilon_c = a + b \log t, \qquad (2.1)$$

or of the more general power law form,

$$\epsilon_c = At^n, \qquad (2.2)$$

where ϵ_c represents the creep strain and t the time under load, while a, b, A and n are constants.

Marechal (99, 100) plotted his creep strains against the logarithm of time and obtained a linear relationship. The slopes of the straight lines varied with temperature, and were a measure of the creep rate. Other authors (65, 113, 116) found a bilinear relationship, with a point of inflection at either 21 or 50 days.

Day and Gamble (41) fitted the flow component of their creep strain results with a formula of the form.

$$\epsilon_c = C_1 (1 + \log_e C_2 t) \qquad (2.3)$$

where C_1 and C_2 are constants. This formula was derived theoretically, considering creep as a thermally activated exhaustion process.

Browne and Blundell (27) however, discovered that their results from sealed limestone concrete specimens were best fitted by a log-log plot of creep vs. time. They found that this relationship, which in fact is a power law formulation of the time function, tallied with experimental results for periods as long as 6 years. (It is known that the logarithmic formulation tends to underestimate long term creep). Furthermore, replotting the results of Marechal (99), Hannant (65) and Neville (116) on a log-log basis, they demonstrated the suitability of the power law formulation for these results as well. Although an attempt was made to determine the dependence of the exponent n on temperature, the results were largely inconclusive. If

at all, there seemed to be a reduction of the value of n with an increase in temperature.

Khoury (84) found that the results of his tests carried out over 7 days on unsealed lightweight aggregate concrete were best fitted by a power law relationship in the period from 1 to 7 days. Gillen (60), who tested 3 kinds of concrete in an unsealed condition for only 5 hours, found the best fit for his results to be a power law time function as well. Anderberg and Thelandersson (4) also chose a power law function to model their experimental results. All three investigators above, although experiencing some variation in the values for the exponent n at different temperatures, have considered n not to be a function of temperature, thus uncoupling the time and temperature functions, albeit within certain temperature limits.

The power law function has also been recommended by Wittmann and Setzer (184), on the basis of a comparative study of four creep functions. Table 2.2 gives an indication of the values for the exponent n, obtained when fitting a power law time function to creep results from unsealed concrete specimens at elevated temperatures. It should be noted that the values of n for Anderberg and Thelandersson (4), Gillen (60) and Khoury (84) are those that they have reported themselves; the values of n for Marechal's (100) results are those obtained by Browne and Blundell (27), while those for England and Ross (50) and Gross (62) have been calculated in this present study.

Bazant and Osman (15) have proposed a slightly different form of the power law time function, which, if age effects are ignored, reduces to

$$J = \frac{1}{E_o} + \frac{\phi}{E_o} t^m \qquad (2.4)$$

where J = total strain including the initial elastic strain,

t = time

and E_o, ϕ and m are constants, to be obtained by non-linear optimization. It is claimed that this function gives a better fit than equation (2.2) for experimental results at very short durations. The original form of the power law function (equation 2.2) requires a

separation of the initial elastic strains (which would always contain some creep strain in the finite time duration elapsed) from the total strain, in order to obtain the creep strains, whereas this form of the function does not require such a separation.

Gross, in the mathematical treatment of his creep results (63), did not directly relate the creep strain to time, but rather linearized a log-log plot of the creep rate with time.

(b) Temperature Function

Many researchers have adopted a rate-theoretical approach to study the creep deformation of concrete and employed the Arrhenius relation to model the temperature dependence of basic creep. The Arrhenius relation is given by

$$\dot{\epsilon}_c = A \exp(-Q/RT) \qquad (2.5)$$

where $\dot{\epsilon}_c$ is the creep rate and T the absolute temperature. Q is the activation energy while R is the gas constant; A is a material constant, which can be considered to be stress dependent, as will be discussed later. Provided, therefore, that the change in basic creep of concrete with temperature is due purely to a thermal effect, a linear relationship should be obtained between $\ln \dot{\epsilon}_c$ and $1/T$.

Marechal (100) obtained such a linear relationship for pre-dried concrete over a temperature range of 20-400°C, under 3 different stress levels (Figure 2.8a). He obtained values for activation energy of 13.4-16.3 kJ/mole for 5 different concretes, irrespective of the stress level. Wittmann and Setzer (184), on analysing Hannant's (65) results for sealed concrete in the temperature range 27°C-82°C obtained a value for activation energy of 28.0 kJ/mole. This value was independent of time, the same value being obtained at 100 and 300 days after loading (Figure 2.8b).

Reutz (146) (reported in ref. (84)), who investigated hardened cement paste in the temperature range 20°-80°C also obtained a linear relationship between $\ln \dot{\epsilon}_c$ and $1/T$ (and a value for activation energy of 15.5 kJ/mole) when his specimens were pre-dried. However, no such linear relationship was obtained when the specimens were initially

moist (Figure 2.8c). Khoury's results from testing unsealed lightweight aggregate concrete in the temperature range 165°-724°C (84) indicated reasonable linearity in the temperature range 165°-500°C, yielding a value for activation energy of 7.3 kJ/mole. Above this temperature, however, he found the negative slope of the curve increasing considerably, giving an activation energy value of 167.8 kJ/mole (Figure 2.8d). This change was explained as being the possible result of a change of state. The evidence from Reutz's results for initially moist specimens also seems to confirm that the Arrhenius relation approach is not applicable over temperature ranges where significant changes in structure take place.

Some investigators have sought to fit empirical curves to experimental data, in order to obtain a temperature function for creep. Gillen (60) expressed the temperature function as an exponential curve of the form

$$\epsilon_c = k \exp(cT) \qquad (2.6)$$

where ϵ_c is the creep strain and T, the temperature in °C; c and k are material constants. This curve, however, does not fit the experimental results too well (Figure 2.9a).

Anderberg and Thelandersson (4) normalized their creep strains with respect to the stress/hot strength ratio, ν_T and expressed the temperature function, also as an exponential curve of the form

$$\epsilon_c/\nu_T = k_1 \exp(k_2(T-20)) \qquad (2.7)$$

where ϵ_c is the creep strain, ν_T is the stress/hot strength ratio and T is the temperature in °C; k_1 and k_2 are material constants. Here again, there is a fairly large scatter above 400°C, which reflects, also, a difficulty in normalizing creep strains with respect to the stress/hot strength ratio (Figure 2.9b).

Khoury (84) used a quadratic expression of the form

$$\epsilon_c = a + bT + cT^2, \qquad (2.8)$$

(where ϵ_c is the creep strain and T, the temperature in °C, while a, b and c are constants), to fit a curve to his results in the temperature range 165°-500°C (Figure 2.9c). The sharp increase in the creep response with temperature above 500°C (Figure 2.2) made it difficult to fit an empirical expression in that range.

In some cases, the temperature function has been approached as a technique for predicting basic creep at elevated temperatures from a known creep response at a reference temperature. Illston and Sanders (80) approached the problem by first dividing basic creep into delayed elastic strain and flow components. A linear relationship was fitted between delayed elastic strain and temperature. However, the variation of flow with temperature was obtained by deriving a "master curve", where flow was plotted against a weighted maturity, m' defined as

$$m' = \int \theta'(\theta' dt), \qquad (2.9)$$

where θ' was measured from a base temperature of -10°C. Hence, the effects of thermal agitation were incorporated in the delayed elastic strain component, while effects of increased maturity (which is a function of both temperature and age) were incorporated in the flow component. This prediction technique was tested in the temperature range 20°-76°C for sealed mortar.

Other researchers (53, 109) have suggested the use of the time shift principle for predicting the creep of concrete at high temperatures. According to this principle, if the creep responses of a material at different temperatures have similar shapes when plotted on a logarithmic time scale, a change of temperature can be considered to be equivalent to a shift of the logarithmic time scale. Such materials are called "thermorheologically simple", and a shift function can be defined, such that the creep response with time, at a higher temperature is obtained by the operation of this shift function on the known creep response at a reference temperature. Tests performed in the temperature range 20°-93°C seemed to indicate that sealed concrete is "thermorheologically simple" in this range. The effect of age on creep has also been modelled on the basis of a time-shift principle

(109). Sullivan (165) used a different time-temperature equivalence technique to extrapolate creep results from one temperature to another.

Bazant and Panula (18) used a double power law to account for the effects of age and time under load. The age effect also reflected the increased maturity due to temperature exposure. The effect of thermal agitation in increasing the creep potential was incorporated in the creep coefficient, ϕ_T, in their expression for total strain (i.e. creep + elastic strain),

$$J(t, t') = (1/E_o) + (\phi_T/E_o)\,(t'^{-m}_e + \alpha)(t - t')^{n_T} \qquad (2.10)$$

where t' is the age at loading, while (t - t') is the time under load, t'_e is the effective age (reflecting an equivalent maturity), which is given by

$$t'_e = \int_o^{t'} \beta_T\,(t'')\,dt'' \qquad (2.10a)$$

ϕ_T is the creep coefficient at temperature T, which is related to the coefficient, ϕ_1, at the reference temperature by

$$\phi_T = \phi_1\,(1 + C_T) \qquad (2.10b)$$

E_o is a material constant while C_T, n_T and β_T are functions of temperature.

None of the prediction models above account for the dehydrating effect (in the case of unsealed specimens) or the weakening effect (in the case of sealed specimens) of exposure to high temperatures. This is because the models have been developed largely for sealed concrete at temperatures below 100°C.

(c) Stress Function

The rate-theoretical approach can be extended to include the dependence of the creep rate on stress (100). Hence, the constant A in equation (2.5) can be written

$$A \propto \sigma^{\alpha/kT}, \tag{2.11}$$

and, for a given temperature we have

$$\dot{\epsilon}_c = B\sigma^{\alpha/kT}, \tag{2.12}$$

where $\dot{\epsilon}_c$ is the creep rate, σ is the stress and T is the absolute temperature. k is the Boltzmann's constant, while α and B are material constants.

Marechal (100) obtained a linear relationship between ln $\dot{\epsilon}$ and ln σ for pre-dried concretes at temperatures up to 400°C. It was found that the slopes of the lines were independent of temperature, giving a constant value for the exponent, $^{\alpha}/_{kT}$, equal to 0.82. This implies, of course, that α varied as T (Figure 2.10).

Other authors (56) have suggested the use of the relation, based also on rate-theoretical considerations,

$$\dot{\epsilon}_c \propto \sinh(c\sigma) \tag{2.13}$$

where $\dot{\epsilon}_c$ is the creep rate and σ the stress, c being a constant.

A more empirical approach to a stress function has been to relate the total creep strain to the stress/strength ratio.

Investigators have reported different findings regarding the proportionality between creep and the stress/strength ratio. Nasser and Neville (116) reported that creep was linearly related to the stress/cold strength ratio for sealed concrete at stress/cold strength ratios up to 0.7 and temperatures up to 96°C, but found that the straight lines did not always pass through the origin, giving positive abscissae. Wang (176) also showed that a linearity exists between creep and the stress/cold strength ratio for unsealed concrete at stress/cold strength ratios of 0.4 and 0.6 and temperatures up to 427°C; his lines passed through the origin as well.

Other investigators (113, 115, 152) have demonstrated a

linearity between creep and stress/hot strength ratio for sealed and unsealed concrete at stress/hot strength ratios up to 0.45 and temperatures up to 232°C. It must be borne in mind, however, that changes in strength at temperatures up to 232°C may not be very significant, especially for unsealed concrete (91, 115).

Anderberg and Thelandersson (4) tested unsealed concrete at stress levels up to 80-100% of the hot strength. An attempt to normalize creep strains with respect to the stress/hot strength ratio indicated that there was approximate linearity between creep and the stress/hot strength ratio for stress/hot strength values up to 0.6-0.8 at temperatures up to about 400°C, but poor linearity above this temperature.

2.2. SHRINKAGE AND THERMAL STRAIN

Shrinkage and thermal strains are experienced simultaneously by concrete when heated in a moist, unsealed state. In order to best unravel the complexity of this phenomenon, the behaviour of the hardened cement paste is considered first, after which the influence of the aggregate is introduced.

2.2.1. Behaviour of Hardened Cement Paste

The heating of hardened cement paste causes both the time dependent response of shrinkage (due to the influence of temperature on moisture migration), as well as a thermal expansion, which can be considered to be time-independent, and a function of temperature.

The presence of a time dependent response implies that strains exhibited by the paste will depend on the rate of heating and duration of exposure to temperature. Wittmann and Lukas (181), when measuring thermal expansion of a water stored specimen in the range 20°-70°C, found that the initial expansion was considerably reduced by time-dependent shrinkage, with an actual net decrease in length at the upper end of the temperature range (Figure 2.11a). Lea and Stradling (92) measured the strains in unsealed hardened cement paste specimens

at temperatures up to 800°C, the measurements at each temperature being taken after the achievement of length stability (Figure 2.11b). While Wittmann and Lukas reported that this stability was achieved after a few hours in the range 20°-70°C, Lea and Stradling reported great difficulty in achieving stability in the range 100°C-491°C, in some cases having to keep the specimen at a particular temperature for a week or more at a time. This delay in achieving length stability is also reported by Bazant et al, in their tests on sealed cement paste (14) and Marechal, in his tests on unsealed concrete specimens (99).

When considering Figures 2.11a and b it seems that hardened cement paste, when heated until length stability, experiences an expansion in a temperature range from ambient temperature to some temperature below 100°C. At higher temperatures, it undergoes a net contraction due to the increasingly over-riding shrinkage phenomenon, caused by the effect of the higher temperatures on moisture migration. However, Lea and Stradling (92) found an interesting reversal in the trend of strain at 491°C. (See Figure 2.11b). This expansive effect has been explained as that arising from the thermal expansion of unhydrated cement grains, which are interspersed within the matrix of hydrated cement paste. Harada's work also indicated a similar strain reversal, albeit at the higher temperature of around 700°C (67).

The time-independent thermal expansion component is itself very difficult to measure, because of its dependence on the moisture state of the cement paste. Zoldners (189) distinguished between the true thermal expansion based on kinetic molecular movements and the superimposed apparent thermal expansion caused by a hygrothermal volume change associated with moisture migration. He gives a value for the average coefficient of true thermal expansion of around 10 x 10^{-6}/°C, which is close to the measured expansion of hardened cement paste in either a desiccated or saturated state. Cement pastes with intermediate moisture conditions yield higher values for the measured coefficient of expansion, due to hygrothermal effects. (Figure 2.12).

2.2.2. Influence of Aggregate

The behaviour of concrete can be considered to be the behaviour of hardened cement paste as modified by aggregate inclusions, the most important parameter being the aggregate volume content. The size and grading of aggregate have been shown as being not very important when considering its effect of modifying cement paste strains (103).

The shrinkage of hardened cement paste is modified by aggregate in proportion to its stiffness, with greater stiffness giving greater restraint and hence less shrinkage in the concrete (145). It has been shown, however, that even small differences in the volume content of aggregate can significantly affect the shrinkage of concrete (139). Most of the commonly used aggregates can be considered to undergo only elastic and not time-dependent deformation, although some aggregates do experience shrinkage themselves (118).

The thermal expansion of concrete is determined by the coefficients of expansion of aggregate and paste (and, of course, their relative volume proportions). Harada et al (67) showed that the thermal expansion of concrete would be increased both when using aggregates with a higher coefficient of expansion (for a given volume content of aggregate) as well as when using higher volume contents of a given aggregate. (See Figure 2.13). This latter result was also obtained by Walker et al. (174) who showed that the coefficient of expansion of concrete is approximately the weighted average of the coefficients of its aggregate and matrix constituents; they also showed that the coefficient of expansion of the aggregate could be determined by extrapolation from tests on concrete with differing proportions of coarse aggregate in the mortar matrix.

The coefficients of expansion of aggregates vary widely. Zoldners (189) suggested that the main factor which determined thermal expansion was the proportion of quartz. He classified them broadly as rocks with a high quartz content (e.g. quartzite and sandstone) having coefficients around 12 x 10^{-6}/°C, those with little or no quartz (e.g. limestone) having coefficients around 5 x 10^{-6}/°C and those with a

medium amount of quartz (e.g. granite, basalt) having coefficients in between the above values. These coefficients of thermal expansion are not themselves constant with temperature. Furthermore, some aggregates have certain "critical" temperatures. For example, when quartz is heated to 573°C, it is transformed from α-quartz to β-quartz, with a sudden volume expansion of about 2.4%, causing shattering of the rock structure; basalt, which shows fairly low expansion up to 600°C, expands rapidly above 900°C, due to developing gases.

Most practical concretes undergo a net expansion at elevated temperatures, (despite the fact that cement paste experiences shrinkage when heated), since they have a significant volume proportion of aggregate (50-75%). The actual values of the expansion coefficients of concretes are quite close to those of the aggregate itself, but some investigators have reported transition temperatures of 150°C (30) and 260-427°C (136), above which there is an increase in the measured coefficient of expansion. These increases have been associated with the end of the drying phase (136).

The above-mentioned difference between the strains in the aggregate and cement paste can give rise to thermal incompatibility. Dougill (48) suggested that the difference between strains (see Figure 2.14) indicated a measure of the degree of damage sustained by the concrete in being heated. Lea and Stradling (92) considered the cement paste surrounding a sand grain as a thick-walled sphere and studied the effect of temperature on the circumferential tensile stress in the cement; this study, which was confined to an elastic analysis, concluded that concrete or mortar could not withstand a sustained temperature of even 100°C without breaking up of the cement paste. Khoury (84) has suggested however, that these "parasitic stresses" would be relieved to a large extent by transitional thermal creep in the cement paste, during first heating of the concrete. Campbell-Allen and Desai (30) showed that aggregate-paste bond as well as other mechanical properties depend not only on the degree of thermal compatability between aggregate and cement paste, but also on the chemical interaction between them.

On exposure to temperature, the integrity of concrete as a composite material can be disrupted either by the breakdown of bond between aggregate and cement paste, or by the degradation of the aggregate itself. One indication of the degree of this disruption is the residual strain on cooling back to ambient temperature. Although concrete at temperature will show a net expansion, provided there has been no bond or aggregate breakdown, it should show a residual contraction when cooled back to ambient conditions, because of the shrinkage that would have been experienced during the heating phase. The cooling process may itself give rise to bond breakdown.

Table 2.3 gives a comparison between results obtained by some investigators, with regard to the test temperature after which the concrete showed a residual expansion. It must be emphasised that the temperature at which disruption starts would be lower than the 'critical' temperature, as defined in the table, since a reversal in the trend of residual strain would have occurred at a lower temperature than the temperature at which residual contraction became residual expansion. This phenomenon can be considered to parallel the behaviour of hardened cement paste as reported and explained by Lea and Stradling (92), where the unhydrated cement grains were considered to behave as aggregate inclusions in a matrix of hydrated paste. Figure 2.15a shows Zoldners' (188) results; it is interesting to note that concrete made with expanded slag (an artificial lightweight aggregate) shows an increasing amount of residual contraction up to a temperature as high as 900°C. Figure 2.15b indicates Marechal's results (102) for porphyry concrete; the interesting features here are firstly, the initial path reversibility up to a given temperature (with respect to first heating, first cooling and second heating), and secondly, the residual contraction being increased with a rise in temperature up to 400°C (indicating that the concrete has preserved its integrity up to this temperature); however, there seems to be a sudden expansion beyond 500°C, with path irreversibility and residual expansion (indicating that the concrete has now lost its 'integrity').

Khoury (84) also made a comparison between the residual strains from concretes made with different aggregates heated at 0.2°C/min or 1°C/min under different levels of stress/cold strength.

His results for 3 concretes made with gravel, lytag (sintered pulverized fuel-ash) and basalt are shown in Figure 2.16. Here we find that when heated and cooled in an unloaded condition, only the lytag concrete exhibits residual con traction. The basalt concrete registers approximately zero strain, while the gravel concrete shows a considerable residual expansion.

From the above discussion it is clear, therefore that the type of aggregate would significantly affect the thermal strain behaviour of concrete. Not only does the coefficient of expansion of the aggregate largely govern the coefficient of expansion of concrete, but the thermal integrity of the concrete also depends on the coefficient of expansion of the aggregate, the bond between the aggregate and the paste matrix, and the thermal stability of the aggregate itself.

2.2.3. Influence of Rate of Heating and Loading

Apart from the thermal incompatibility between aggregate and cement paste, the concrete specimen would be subjected, during the heating (and cooling) phase to a thermal gradient across its section. This gradient would, in turn, give rise to a stress gradient, the magnitude of which would depend on the rate of heating. Excessive rates of heating could cause disruption because of tensile stresses set up in the interior of the specimen. On the other hand, a slow rate of heating would minimize the stress gradients within the specimen. It would also allow both these 'gradient' stresses as well as the 'incompatibility' or 'parasitic' stresses affecting the aggregate-paste bond to be relieved by creep. Experimental and theoretical studies regarding the effects of the rate of heating can be found in the literature (4, 84, 174).

If concrete is heated for the first time under load, it undergoes, in addition to simultaneous shrinkage and thermal expansion, a creep component as well, which, depending on the load level, could result in a net contraction of the specimen. This creep component, known as transitional thermal creep, is exhibited only on first time heating under load (3, 87). It has been reported that the coefficient of thermal expansion is insensitive to load level during subsequent

heating cycles (152).

2.2.4. Mathematical Treatment of Shrinkage

In the attempt to model the shrinkage of concrete mathematically, two approaches have been adopted.

The empirical approach consists in fitting a convenient mathematical relationship to observed data. Generally speaking, this approach has resulted in the time function of shrinkage being represented by variants of a hyperbolic function (17, 24, 162), whose 'basic' form can be considered to be

$$\epsilon_{st} = \frac{t}{A + t}\,\epsilon_{s\infty} \qquad (2.14)$$

where ϵ_{st} is the shrinkage at time t (from the commencement of drying), $\epsilon_{s\infty}$ is the ultimate shrinkage and A is a constant. The effects of ambient humidity, size and age have generally been incorporated by using empirically obtained factors (32).

Other approaches have sought to correlate the shrinkage phenomenon with linear diffusion or evaporation, which can be treated theoretically. These approaches have generally led to the time function of shrinkage being expressed as variants of an exponential function (19, 94, 182) whose 'basic' form can be considered to be

$$\epsilon_{st} = \epsilon_{s\infty}\,(1 - e^{-\alpha t}) \qquad (2.15)$$

where ϵ_{st} is the shrinkage at time t (from the commencement of drying), $\epsilon_{s\infty}$ is the ultimate shrinkage and α is a constant. The effects of humidity, size, age and temperature on shrinkage have been given a semi-theoretical treatment by Bazant and Panula (17), with size dependence being based on diffusion theory and temperature dependence on activation energy concepts.

2.3. STRENGTH AND ELASTIC PROPERTIES

The compressive strength and elastic properties of concrete, as affected by elevated temperature, have been studied even more extensively than its strain behaviour. As such, the following review is very general in nature, and confined to the uniaxial compressive behaviour of unsealed concrete only.

2.3.1. Compressive Strength of Concrete - Testing Conditions Employed

Although some investigators have reported a monotonic loss in strength with increase of temperature, the general trend of strength variation with temperature for unsealed concrete is best represented by Figure 2.17, taken from a review by Blundell et al. (23). The initial drop in strength to a minimum at a temperature below 100°C can be ascribed to swelling in the cement gel, with consequent weakening of Van der Waal forces, caused by thermal agitation of water molecules. This minimum point varies in the literature from 50°C to 100°C (67, 82, 83, 84, 188). The increase in strength at temperatures above 100°C is probably due to the densification of the cement paste caused by desiccation. The point of the strength maximum varies in the literature from 150°C to around 300°C (67, 69, 82, 91, 92, 151, 188). The drop in strength beyond this would be due to a variety of chemical and physical causes, affecting the paste, the aggregate-paste bond, and in some cases, the aggregate itself. A detailed analysis of these effects has been made by Khoury (84).

Table 2.4 indicates the various testing conditions employed by different investigators to study the way concrete strength is affected by elevated temperature. It must be appreciated that the results obtained reflect not only the effect of temperature, but also the effects of the conditions employed during testing.

Where hot strength is concerned (i.e. the strength of concrete at a given elevated temperature), Malhotra (97) has reported that specimens stressed during heating showed a smaller percentage reduction in strength than those unstressed during heating, the difference in percentage reduction being 4% at 200°C and increasing to 21% at 500°C.

However, Abrams (1) found that stress levels from 0.25 to 0.55 of the cold cylinder strength applied during heating had little effect on the strength of concrete at temperature. Anderberg and Thelandersson (4) also claimed that there was no difference between the strength of loaded concrete which was heated to failure and that of heated concrete which was loaded to failure.

Many investigators have studied the effect of temperature on concrete by determining the residual strength on cooling back to room temperature. Most of them have both heated and cooled their specimens in an unstressed state at slow rates of heating and cooling. Malhotra (97) has reported residual strengths to be around 20% lower than the corresponding hot strengths iin the temperature range 200-450°C.

The stressing of concrete during heating can have two effects. Firstly, it may have the beneficial effect of "densifying" the cement paste, both physically (by strengthening the Van der Waal forces in the solid skeleton and also reducing porosity) and chemically (by the polymerization of silicate chains). Secondly, it can prevent the detrimental effect of cracking that may arise due to differential movements between the aggregate and cement paste on heating. However, Khoury (84) has suggested that concrete could accommodate such differential movement between its constituents because of stress relief obtained from the large transient thermal creep strains in the cement paste. He has further stated that cooling may cause greater disruption in concrete because cement paste does not exhibit such creep strains during cooling. The above considerations would perhaps contribute towards an understanding of the results quoted in the two preceding paragraphs.

Where the effect of duration at temperature is concerned, most investigators agree that the strength of unsealed concrete is not dependent on the duration of exposure at temperatures above 250°C (82, 157). At temperatures below 200°C too, the variation in strength with duration at temperature is not very significant, in some cases the strength actually increasing with time (82, 89). (See Figure 2.18a).

Harada et al. (67) have investigated the effect of extended storage in air on post-cooled concrete specimens. Specimens heated to temperatures below 500°C showed autogenous recovery after an initial loss of strength (see Figure 2.18b), but those heated above 500°C exhibited cracks which did not close. Weigler and Fischer (177) found that the maximum decrease in strength occurred 3 days after post-cooling, and that the decrease in strength was greater for specimens exposed to higher temperatures. They also found that the improvement in strength when stored in water was greater for higher pre-exposure temperatures. An interesting phenomenon with respect to post-cooling exposure has been reported by Lea and Stradling (92). They found that concrete specimens exposed to a temperature above 400°C exhibited severe cracking after a few days of storage in air. The effect of post-cooling exposure on strength is no doubt a result of rehydration, the hydration of cement giving rise to strength enhancement, and the rehydration of dissociated Calcium hydroxide (whose dissociation temperature is around 400°C or more) being disruptive in nature, since it is accompanied by a considerable volume expansion.

Some investigators have reported that concrete strength is a function of the maximum temperature reached and not affected by temperature cycling, up to a temperature of 200°C (89, 157). However, Campbell-Allen found that all mechanical properties deteriorated with an increasing number of cylces for maximum temperatures of 200°C and 300°C. He also found that this deterioration took place at both slow and fast rates of cycling and concluded that it was due to thermal incompatibility between the aggregate and paste (30, 31).

2.3.2. Other Factors Affecting Strength

Some of the other factors that may affect the strength of concrete at elevated temperatures are now considered.

Abrams (1) has reported that the original strength had little effect on the percentage reduction in strength, whether tested in the hot or residual condition. Similarly, Malhotra (97) also reported

that neither age (beyond an age of 3 months) nor water/cement ratio (in the range 0.375-0.65) had any effect on the proportion of strength reduction due to temperature. He has mentioned however, that leaner mixes, while having a lower intrinsic strength than richer mixes, showed a smaller porportional reduction in strength when heated to any given temperature.

Fast rates of heating and cooling could affect strength, if they cause thermal gradients in the specimen, capable of setting up disruptive tensile stresses. Campbell-Allen and Desai (30) have shown, however, that heating and cooling rates of 60°C/hour and 100°C/hr respectively did not produce macroscopic stress gradients that affected their results on cylinders 8 in x 4 in dia. On the other hand, Khoury (84) has reported consistently lower strengths in specimens heated at a slower rate (0.2°C/min as opposed to 1°C/min.). He has attributed this to hydrothermal reactions which produce weaker hydrates and which would be more pronounced at the slower rate of heating (since more water would be available for the reactions for a longer time).

The type of aggregate could affect the strength of concrete either by the onset of parasitic stresses due to thermal incompatibility between the aggregate and cement paste, or by the break-up of the aggregate itself, if it is thermally unstable. This influnce of aggregate has already been discussed in Section 2.2. Comparative studies between strengths of concretes made with different aggregates have been undertaken by many researchers (1, 30, 31, 67, 188).

The strength of concrete exposed to temperature is influenced by chemical effects as well. For example, if concrete is heated to a temperature above the dissociation temperature of Calcium hydroxide and cooled back to room temperature, continued exposure in air would cause rehydration of Calcium hydroxide, which is a disruptive process because it is accompanied by volume expansion (92). Then again, chemical interaction between the aggregate and cement paste can either strengthen or weaken the bond between them (30). Furthermore, the heating of concrete produces chemical changes in the cement paste

which can either enhance or reduce the strength of concrete.

2.3.3. Elastic Properties

The static modulus of elasticity of concrete falls more sharply with an increase in temperature than strength does. Some researchers have sought to demonstrate a linear variation of elastic modulus with either temperature (10, 83) or weight loss (152). The work of Sullivan and Poucher (167) has indicated that the drop in elastic modulus with temperature is fairly sharp for temperatures below 100°C and above 300°C, but less marked in the range 100°C-300°C. (It should be noted that these investigators performed their tests in flexure). Weigler and Fischer (177) have actually reported a slight increase in elastic modulus in the temperature range 150°C-300°C. Gross (63) found a minimum and maximum for this modulus at 60°C and 110°C respectively. However, in general, it seems that the drop in elastic modulus is related to moisture loss and is more pronounced than strength loss with temperature for unsealed concrete.

Stress-strain curves obtained for concrete and hardened cement paste at elevated temperatures indicate an increasing strain at failure with increasing temperature (10, 69). Harmathy and Berndt have reported, however, that prolonged exposure at temperatures above 260°C reduces the plasticity of hardened cement paste. They have also reported that the changes in elastic modulus and strain at failure are more pronounced for cement paste than for lightweight concrete (69).

Marechal's tests (101) indicated a maximum for the modulus of elasticity at around 50°C, and a consistent drop with increasing temperature thereafter. He also found that the change in modulus was negligible when cooling back from a given temperature (see Figure 2.19) and stated that variations in modulus were due, not to thermal effects, but to irreversible changes in state caused by temperature. This seems to be confirmed in the experiments performed by Sullivan and Poucher (167), who found no difference between the 'hot' and 'residual' elastic moduli.

Walther and Pareth (175), who investigated the post-cooled

mechanical properties of specimens previously tested for either creep or shrinkage at a temperature of 200°C, found that the modulus of elasticity of the creep specimens was about 13-14% higher than that of the shrinkage specimens, perhaps indicating a degree of consolidation under load.

Khoury (88) found that a variety of concretes heated under load for temperatures up to 600°C showed little change in the modulus of elasticity at temperature, whereas those heated under load but cooled without load exhibited a considerable reduction. (See Figure 2.20).

The dynamic modulus of elasticity, as measured by pulse velocity techniques, is considered to be a sensitive measure of the degree of cracking in a material, despite the increase of experimental scatter with increasing exposure temperature, according to Logothetis and Economou (95). Their results indicate that the pulse velocity of post-cooled concrete decreases monotonically with exposure temperature, with a proportionately steeper drop in the temperature range 300°C-500°C (see Figure 2.21a). Khoury has reported a sharp drop in the post-cooled dynamic modulus of elasticity above 600°C, which was also the temperature above which his lightweight concrete specimens showed a large increase in basic creep (84). (See Figure 2.21b).

The Poisson's Ratio was reported by Marechal to behave similarly to the modulus of elasticity, with respect to temperature change (101). Parrott (125) found the Poisson's Ratio of sealed hardened cement paste to be around 0.275 at ambient temperature. He also found that this value decreased with increasing moisture loss. Some investigators have found similar Poisson's Ratios for both elastic and creep strains (65), though others have found the opposite (125).

2.4. MICROSTRUCTURE

2.4.1. Chemistry and Microstructure of Hardened Cement Paste

There is considerable difficulty in describing hardened cement paste at the microstructural or chemical level. The hydration of

Portland Cement gives rise to a hardened paste consisting of solid as well as water phases. However, there is much controversy regarding both the physical structure of the solid phase as well as the nature of the water phases. There is also uncertainty regarding the chemical composition of the solid phase.

(a) Chemistry

Hardened cement paste consists of crystalline, semi-amorphous and amorphous phases. This semi-amorphous nature has made it difficult to assess both the quantitative composition of the paste as well as the stoichiometry of its components. Diamond (46) has made an estimate that fully hydrated cement paste consists of 70% CSH gel, 20% $Ca(OH)_2$, 7% aluminates and sulpho-aluminates and 3% minor constituents (including unhydrated clinker). It must be appreciated that most pastes are not fully hydrated and would contain a greater proportion of unhydrated cement.

The main component of the hydrated products is the CSH gel. Although its stoichiometry is sometimes quoted as $C_{1.5}SH_{1.5}$ (143), the CSH is present in a semi-amorphous form and its molar ratio is variable; the C/S ratio is generally about 2-3 (45), while the H/S ratio (based on the d-dried state) in a hydrated C_3S paste has been found to be less by around 0.5 than the C/S ratio (35). The Calcium hydroxide produced is mainly crystalline in nature.

As the hardened paste ages, it has been shown (93) that the monomeric silicate anions (SiO_4^-) initially present in the CSH gel are polymerized by the bonding of silicate chains. This process is known to continue even after hydration has ceased.

(b) Physical Structure of Gel

The morphology of the CSH gel varies as hydration proceeds, with an initially fibrous morphology giving way to a more flattened one. At early stages the $Ca(OH)_2$ can be seen as hexagonal crystals; subsequently however, as deposits of $Ca(OH)_2$ grow larger, they tend to encapsulate other phases, losing their hexagonal outline in the

process. Aluminate and sulphoaluminate crystals are cubic or hexagonal (46).

Researchers have differed considerably in their description of the physical structure of the CSH gel. The most important characteristics of the gel are its colloidal and probably layered structure, large internal surface area and high sensitivity to the water phase. There are three main models in use today for describing the properties and explaining the behaviour of hardened cement paste.

(i) The Powers model - this was the first of the models to be proposed and was based on studies of water sorption isotherms. According to this model, hardened cement paste has a minimum porosity of 28% (i.e. "gel pores" which are accessible only to water molecules) and a high specific surface of around 200 m^2/gm. Any volume not filled with gel is called capillary space. The structure is held together by Van der Waals forces on the large surface area, while length changes such as swelling, shrinkage and creep are caused by "disjoining" pressures in the gel water.

(ii) The Feldman-Sereda model - this model is based on measurements of length change, stiffness, helium inflow characteristics etc. during sorption and desorption at controlled relative humidities. It ascribes a layered structure to the CSH gel and considers the "interlayer" water as part of the CSH gel, contributing to its rigidity. This model, therefore, does not involve the concept of gel pores and suggests a smaller specific surface, which should be measured by a fluid that does not cause interlayer penetration (e.g. methanol, nitrogen, helium etc.). According to this model, the cement paste derives its strength from a combination of Van der Waals forces, siloxane (-Si-O-Si), hydrogen and calcium-silica (-Si-O-Ca-O-Si-) bonds. Length changes are caused by a combination of factors which include reduction of the solid surface energy due to the physical interaction of the surfaces with H_2O molecules, penetration of H_2O molecules between layers of CSH gel, menisci effects due to capillary

condensation and ageing effects, considered to be a further agglomoration of sheets, which increases the interlayer area and reduces the specific surface.

(iii) The Munich Model - this model is not so much a physical description of the CSH gel, but rather a mathematical description of the paste characteristics, based on thermodynamic considerations and sorption studies at controlled relative humidities. The strength of the paste is considered to be affected by adsorption, which causes a reduction in surface free energy, which in turn reduces the Griffith's critical stress. Between relative humidities of 2% and 42%, length changes are ascribed to changes in surface free energy; at higher humidities these changes are considered to be due to the disjoining pressure of water which separates surfaces held together by Van der Waals forces.

(c) Porosity

The pore structure of hardened cement paste significantly influences its mechanical behaviour. Total porosity, pore size distribution and the average pore size and shape can be considered to be the relevant parameters of the pore structure.

The determination of total porosity and pore size distribution has proved to be difficult, not only because of structural alterations caused to the paste in the process of measurements (e.g. the collapse of the pore structure on drying) but also because of discrepancies between different methods of measurement. Sorption measurements, using fluids such as nitrogen and water vapour are capable of measuring only a small range of pore sizes, between a few tens and several hundreds of Angstroms. Water consistently gives higher porosities due to its smaller molecular size enabling it to penetrate "interlayer" or "gel pore" spaces, which are not accessible to other fluids. Mercury intrusion porosimetry (MIP) is capable of measuring pore sizes from 30Å to as high as 1000 μm.

The total porosity increases with increasing w/c ratio and

decreases with increasing age, although the variation with age beyond 3 days has been reported to be small (2).

The pore size distribution as obtained from sorption data gives a pore size maximum at pore diameters of around 30-50Å (44). This maximum, however, is not obtained when using mercury porosimetry. Diamond (44) has made a critical comparison between the capillary condensation and mercury porosimetry methods for obtaining pore size distributions. He found that the volume mean pore diameters from capillary condensation studies ranged from 42-105Å, while those from mercury porosimetry studies ranged from 230-1900Å. Diamond has also suggested that the "missing" pore volume in MIP studies (i.e. the difference between the total pore volume measured by immersion in a suitable liquid, and the pore volume intruded by mercury) is not in ultra fine pores but rather in pockets of gel encapsulated aby $Ca(OH)_2$ strata growing through the cement paste (44). Meanwhile, optical microscopy studies have revealed that 30-50% of the pore volume is greater than 15 μm and cannot be picked up by MIP, either because they are virtually "closed" without any interconnection, or because the path to these pores lies through much finer pores which cannot be intruded at low pressures. Nevertheless, it was considered that Mercury Intrusion Porosimetry was an adequate technique for reflecting microstructural changes in the cement paste (2).

2.4.2. Effect of Elevated Temperature

Table 2.5 indicates the different changes that take place in hardened cement paste when heated to temperatures up to 900°C. This table incorporates the most significant changes in the paste that are reported in the literature. Some of the tests are dynamic in nature, in the sense that there is a continuous increase in temperature (at a predetermined rate) while the various phenomena are being observed. Tests such as these (e.g. Differential Thermal Analysis-DTA and Differential Thermogravimetry-DTG) would tend to indicate temperatures that are higher than the "true" temperature for a given change. There are also differences in results from one investigator to another. Fairly typical DTA results are given in Figure 2.22. Another possible drawback in some of these tests (e.g. porosity measurements) is that

they are difficult if not impossible to perform at temperature, but have to be carried out after cooling back to room temperature. Hence the results may reflect the effects of cooling in addition to the effects of temperature.

Heating the unsealed cement paste to 100°C has the effect of removing most of the evaporable water. It also causes an increase in the degree of polymerization (43, 129) and a minimum in the porosity at 80°C (83), which suggest that heating to 100°C is generally beneficial to the hardened cement paste. Furthermore, increased hydration (which is beneficial) and hydrothermal reactions (which are largely detrimental) could take place at temperatures up to 200°C, although these phenomena would not occur in unsealed specimens as much as in sealed specimens (84).

Piasta et al. (138) have reported that the proportion of unhydrated grains decreases up to a temperature of 300°C. (See Figure 2.23a). They have also found, however, that depolymerization takes place beyond 100°C, as indicated by the shift in the infra-red absorption band at 980 cm^{-1} towards lower wave numbers (Figure 2.23b).

By the time the paste is heated to 400°C, the CSH gel has lost most of its bound water, with DTA and DTG peaks occurring between 150–400°C (49). However, the increase in porosity due to this moisture loss is not as great as expected (148).

Temperatures ranging from 400–600°C have been quoted as the dissociation temperature of Calcium hydroxide (49, 61, 68, 135, 155). The reason for this discrepancy is the nature of the test involved (i.e. whether 'static', 'semi-static' or 'dynamic').

The increase in pore volume from 300–600°C is also greater than one would expect from the corresponding weight loss in that temperature range (148). Furthermore, the pore structure begins to get coarsened at around 550–600°C (154), as indicated in Figure 2.24.

Beyond 600°C, the most significant changes are the chemical transformations that take place in the cement paste, with the formation

of β-C_2S and β-CS and the conversion of any original β-C_2S to α'-C_2S (68, 121, 153). Decarbonation also takes place beyond 700°C (49, 155).

An interesting phenomenon reported by Lea and Stradling (92) and Harada et al (67) is the reversal of shrinkage. However, they have reported widely differing temperatures and strain values for this phenomenon. (See Figure 2.25). This may be attributable either to the differing nature of the tests (i.e. 'static' vs. 'dynamic') or to the different w/c ratios used, or to both the above reasons.

2.4.3. Degree of Silicate Polymerization

(a) Factors Affecting Polymerization

The pioneering work in silicate polymerization for cement paste was done by Lentz (93), who recovered the silicate structures of hydrating Portland Cement paste as trimethylsilyl derivatives and studied the variation in silicate fractions from 1 day to 14.7 years. He found that the orthosilicate fraction decreased continuously while the derivative referred to as a polysilicate (having a degree of condensation of 4 anions or more) increased continuously throughout the period of investigation. The above evidence, coupled with the behaviour of the dimer fraction, which showed an initial rise but a subsequent fall (see Figure 2.26), led him to conclude that the hydration reaction was similar to a condensation type polymerization, the high proportion of orthosilicate in the original Portland Cement being converted to polysilicate fractions via the dimer. Parrott (124) however, using the same results from Figure 2.26 together with his own results on degree of hydration pointed out that the rate of development of the polysilicate phase was considerably greater than the rate of hydration. This suggested an ageing process distinct from hydration and characterized by silicate polymerization, a concept now held widely.

Thermal treatment of cement paste has have been found to change the degree of polymerization significantly. Day and Gamble (43) found an increase in their polysilicate descriptor after heat

treatments up to 92°C on saturated specimens of both young and mature hardened cement pastes. (See Figure 2.27). Parrott (127, 128, 129) has reported a similar phenomenon for heat treatments up to 95°C and has also suggested that this increase is due to an acceleration by heat curing of the silicate polymerization that normally takes place at room temperature (127). It is interesting to note however, that Piasta et al. (138) have reported depolymerization of the silicate anion at temperatures above 100°C, based on infrared spectroscopy performed on unsealed cement paste specimens heated from 20°C to 800°C (Figure 2.23b).

The effect of drying upon silicate polymerization can be gleaned from the results reported by Bentur et al. (22) for pastes of both low and high degrees of hydration. The general trend of their findings suggests that the degree of condensation of the anion is increased by drying, whether in the shrinkage tests performed at 53% RH or in the 11% RH conditioning done prior to derivatization. This increase is markedly less significant for the well hydrated pastes.

Apart from temperature, the other major factor affecting polymerization is load. Day and Gamble (43) found that loading (to a stress/strength ratio of 0.25) of sealed, saturated specimens under both isothermal as well as variable temperature conditions (at temperatures up to 92°C) caused an increase of polymerization in young (i.e. 28 day) specimens but depolymerization in mature (i.e. 2.5 year) specimens. A similar tendency is evident in the results of Bentur et al (22) for silicate paste specimens at ambient temperature, having degrees of hydration ranging from 29% to 93%, the well hydrated pastes being depolymerized by load (i.e. stress/strength = 0.1) while the low hydration pastes were increased in degree of condensation. Parrott's tests on loading sealed, saturated cement paste specimens under variable temperature regimes up to 60°C (132) indicated very significant increases in the degree of polymerization.

(b) Correlation with Time Dependent Strains

Perhaps the greatest significance of a polysilicate descriptor or index is the possibility of correlating it with time dependent

strains. Since the degree of polymerization would reflect the degree of stabilization of the microstructure, it would be expected, all other factors being equal, that the potential for shrinkage and creep could be related in some fashion to the degree of polymerization at the start of drying and loading respectively. Parrott (127, 128, 129) treated saturated cement paste specimens to various temperatures up to 95°C and after cooling them back to room temperature, measured their shrinkage at a controlled relative humidity and subsequently, their creep upon loading. He found a very definite reciprocal correlation between creep and the degree of polymerization after thermal pre-treatment as indicated in Figure 2.28. He also found an equally definite correlation between the initial shrinkage and subsequent creep, which therefore implied a correlation between the polysilicate content and shrinkage as well. Furthermore he discovered (128) that it was the irrecoverable components of shrinkage and creep that were affected by the heat curing and that they could be correlated particularly well with polysilicate content after heat curing; these irrecoverable strains did not correlate very well with measured changes in either porosity or combined water content. Conversely, elastic strains, creep recovery strains and cube strengths did not show any dependence on changes in polymerization. Day and Gamble (43) also found a similar correlation between creep and polysilicate content at the time of loading for 28 day specimens of hardened cement paste. However, no such relationship could be found for specimens of 2.5 years' age.

Thus far we have discussed the correlation of creep with the degree of polymerization at the time of loading. The next consideration has to do with changes in the degree of polymerization during loading. There are two conflicting views in this regard. According to one school of thought, load contributes to the stabilization process and hence, would presumably increase the degree of polymerization. The other opinion held is that load does not actually increase stabilization, but merely gives it "directionality", resulting in an observable creep behaviour. Hence the application of load during changes of phase in the material would result in a creep response; examples of this are the large creep strains observed during early hydration (171), carbonation (126) and temperature rise (which could be considered as an increase in the rate of polymerization) (132).

Parrott observed a remarkable similarity between the development of transitional thermal creep and the degree of polymerization as shown in Figure 2.29. However, this does not really help us to choose between the two views expressed above. Day (40), on the other hand found a fairly definite contribution of load towards the degree of polymerization. He also showed that the change of magnitude in the polysilicate index during loading, irrespective of sign, was related to flow, with young and mature specimens giving separate linear relationships.

2.4.4. Mechanisms of Creep

A large volume of review literature has been written on the mechanisms of creep (78, 84, 119, 180). This ensuing summary seeks only to identify the most widely held theories and also to investigate briefly how well they explain creep at high temperature.

The seepage theory and the viscous theory of creep are the two most commonly held theories regarding the mechanism of creep. The seepage theory ascribes to the water phase a predominant role in the creep process, unifying the phenomena of shrinkage and creep as those that are caused by an imbalance in hygral equilibrium, leading to diffusion of water. It is capable of explaining creep and shrinkage recovery as a reversal of the diffusion process. The increased creep at high temperatures is explained by the lower viscosity and higher diffusivity of the water phase at these temperatures. It cannot explain creep at very high temperatures when most if not all the gel water has been lost.

The viscous theory ascribes to the water phase only a modifying role in a process that is largely governed by gel particle movement. The viscous theory cannot explain creep recovery. The increase in creep at high temperatures is explained by the increased viscosity of the gel, and hence this theory can accommodate the high creep strains obtained at temperatures where dehydration is virtually complete.

Basic creep manifested in concrete has been considered by

Illston (77) to be divided into two components - viz. delayed elasticity and flow. Delayed elasticity is considered to be the delayed response of the composite material to the creeping medium, after "attenuation" by inert material. Flow, on the other hand, is the unattenuated response. After some time (i.e. when internal stress redistribution has taken place), concrete exhibits only flow. Delayed elasticity has been linked to the recoverable component of creep and flow to the irrecoverable component.

Other mechanisms that are associated with creep are micro-cracking and molecular bond formation. Microcracking can take place due to excessive load or due to thermal strains (caused by temperature gradients or parasitic stresses, or both). Bond formation - i.e. the polymerization of the hardened cement paste - takes place both under load as well as upon thermal treatments up to a temperature of 95°C, and reduces the further creep potential of the paste (43, 129). The degree of polymerization has been correlated with the potential for irrecoverable creep and shrinkage (129).

Wittmann (180) has approached mechanisms of creep and shrinkage by classifying them into 'real' and 'apparent' mechanisms. 'Real' mechanisms are those of a fundamental nature, generally seated in the cement paste, while 'apparent' mechanisms are due to internal stress redistributions. Delayed elasticity and drying creep are considered to be apparent mechanisms.

Treating creep as a rate process has been a useful way of giving it a theoretical basis. The temperature dependence of creep is expressed by the Arrhenius relation

$$\dot{\epsilon}_c = A \exp\left(-Q/RT\right) \qquad (2.16)$$

where $\dot{\epsilon}_c$ is the creep rate

Q is the activation energy

R is the gas constant and

A is a constant, incorporating the stress dependence.

Using an activation energy approach again, the stress dependence of the creep rate can be expressed as

$$A = A_1 \sinh((V/RT)\sigma) \qquad (2.17)$$

where V is the activation volume

σ is the stress and

A_1 is a constant, incorporating the time dependence.

This rate theoretical approach is presented with greater detail in Section 8.1.

Investigator (1)	Initial Moisture Condition	Sealing Condition	Time of Load Application	Applied Stress State	Temp. Range	Types of strain(2)
England, G.L. and Ross, A.D. (50) (1962)	Moist	unsealed	After thermal stability on heating	Uniaxial Compression	20-140°C	bc, dc, sh
Nasser, K.W. and Neville, A.M. (116) (1965)	Saturated	sealed (water stored)	13 days after heating	Uniaxial Compression	21-96°C	bc
Hickey, K.B. (71) (1967)	moist	unsealed	1 day before heating	Uniaxial Compression	23-143°C	ttc,bc,dc,sh,te
Arthanari, S. and Yu, C.W. (6) (1967)	moist	sealed (epoxy resin)	After thermal stability on heating	Biaxial Compression	20-80°C	bc
Nasser, K.W. and Lohtia, R.P. (113) (1971)	saturated	sealed (water-tight jacket)	13 days after heating	Uniaxial Compression	2-232°C	bc
Marechal, J.C. (100) (1972)	moist, predried	unsealed	14 days after heating	Uniaxial Compression	20-400°C	bc
Illston, J.M. and Sanders, P.D. (79) (1973)	saturated	sealed (water stored)	Before heating	Torsion	20-76°C	ttc, bc
Bazant,Z.P.,KIM,S.S.and Meiri,S. (14) (1979)	saturated	sealed (triaxial pressure)	After thermal stability on heating	Triaxial compression	100-300°C	bc
Khoury, G.A. (84) (1983)	moist	unsealed	Before heating	Uniaxial Compression	20-600°C	ttc,bc,dc,sh,te

Notes - (1) - In some cases, these researchers may have investigated more than one pre-treatment, condition, time of load application or stress state. However, only one parameter is given, for purposes of exemplifying the ensuing types of strain.

(2) - Notation is as follows:- ttc - transitional thermal creep; bc - basic creep; dc - drying creep; sh - shrinkage; te - thermal expansion.

TABLE 2.1. PARAMETERS EMPLOYED IN INVESTIGATING CREEP OF CONCRETE AT ELEVATED TEMPERATURES.

Investigator	w/c ratio	Agg. Vol. %[1]	Agg. Type	Strength[2] at test (N/mm^2)	Age at Test	Conditioning	Preheat duration	Shrinkage Compensation	Temperature Range (°C)	Stress[3] Range	n value in $\varepsilon = At^n$
England, G.L. and Ross, A.D. (50) (1962)	0.45	71%		28 N/mm^2	10 days	1 day - in mould 3 days - under water 6 days - 90% RH and 17°C	Thermal Stability	Yes	20°-140°C	0.24 f'_c	0.09-0.41
Marechal, J.C. (4) (100) (1972)			Quartzite	35 N/mm^2	1 year	98% RH	14 days	Yes	20°-400°C	$0.14f'_c$- $0.42f'_c$	0.214-0.345
Anderberg, Y and Thelandersson, S. (4) (1976)	0.60	69%	Quartzite	41 N/mm^2	19-24wks	5 days - water cured then - 65% RH and 20°C	Thermal Stability	No	20°-840°C	$0.11f'_c$- $0.90f'_c$	0.50
Gross, H. (63) (1975)	0.60	68%	Gravel	42 N/mm^2	6-12 mths	1 day - under hessian in mould 6 days - water stored 4 weeks -under damp hessian then - air at 50% RH and 20°C	1 day	No	20°-450°C	$0.2f'_c$- $0.66f'_c$	0.21-0.41
Nasser, K.W. and Marzouk, H.M. (115) (1981)	0.60	75%	Dolomite and Horn-blende	46 N/mm^2	35 days	7 days - moist curing at 21°C 28 days - sealed	13 days	No	71°-232°C	$0.18f'_c$- $0.37f'_c$	
Gillen, M. (4) (60) (1981)	0.71	72%	Calcareous	23.2 N/mm^2	90 days	7 days - 100% RH 83 " - 50% RH	Thermal Stability	No	22°-649°C	$0.3f'_c$- $0.6f'_c$	0.40 ± 0.05
Khoury, G.A. (84) (1983)	0.795	65.3%	Lytag	50 N/mm^2	37-51 days	100% RH and 20°C	1-3 days	No	165°-724°C	$0.125f'_c$- $0.244f'_c$	0.36

Notes (1) - In some cases, this has been calculated, on the basis of a concrete specific gravity of 2.4 and an aggregate specific gravity of 2.6.
(2) - This gives the cold strength of the creep test specimen; in some cases, average values are given, while in others, cylinder strengths have been obtained by multiplying cube strengths by a factor of 0.75.
(3) - f'_c refers to the cold strength of the creep test specimen.
(4) - These investigators have tested other types of concrete as well; however, only one type is displayed in the table.

TABLE 2.2. PARAMETERS EMPLOYED IN TESTING UNIAXIAL BASIC CREEP OF UNSEALED CONCRETE.

Investigator	Type of Aggregate	AGG. Vol. %	Effective w/c ratio	Rate of heating	Critical(*) Temperature
Sullivan, P.J.E. and Poucher, M.P. (167) (1971)	Gravel Silica Sand	47.2% 27.4%	0.56	1-2 °C/min.	350°C
Zoldners, N.G. (188) (1971)	Gravel	72%	0.56	Shock	300°C
	Limestone	71%	0.58	Shock	380°C
	Sandstone	69%	0.61	Shock	380°C
	Expanded Slag	59%	0.25	Shock	-
Marechal, J.C. (102) (1972)	Porphyry			0.2 °C/min.	500°C
Kaplan, M.F. and Roux, F.J. (82) (1972)	Quartzite Sileceous Sand	43-44% 27-28%	0.50-0.58	0.58 °C/min.	250-400°C
Khoury, G.A. (84) (1983)	Basalt	67.3%	0.45	1°C/min.	400-600°C

Note (*) - The critical temperature is defined, for the purpose of this table, as that temperature at which residual contraction becomes residual expansion.

TABLE 2.3. RESIDUAL STRAIN REVERSAL TEMPERATURES FOR CONCRETES WITH DIFFERENT AGGREGATES.

Investigator	Hot Strength		Residual Strength		Effect of Duration		Effect of Cycling	Temp. Range (°C)
	Unstressed During Heating	Stressed During Heating	Unstressed During Cooling	Stressed During Cooling	At Temperature	On Post-Cooling		
Lea, F.C. and Stradling, R.E. (92) (1922)	✓							200-1030
Malhotra, H.L. (97) (1956)	✓	✓	✓					200- 600
Zoldners, N.G. (188) (1960)			✓					20- 800
Campbell-Allen, D. and Desai, P.M. (30) (1967)			✓				✓	20- 300
Harmathy, T.Z. and Berndt, J.E. (69) (1966)	✓				✓			20- 760
Saemann, J.C. and Washa, G.W. (151) (1957)	✓							-57- 232
Lankard, D.R. et al. (91) (1971)	✓		✓					20- 260
Abrams, M. (1) (1971)	✓	✓	✓					21- 871
Harada, T. et al. (67) (1972)	✓		✓		✓	✓		20- 700
Weigler, H. and Fischer, R. (177) (1972)			✓			✓		20- 750
Gross, H. (63) (1975)				✓				20- 450
Kasami, H. et al. (83) (1975)			✓		✓			20- 300
Anderberg, Y. and Thelandersson, S. (4) (1976)	✓	✓						20- 800
Kottas, R. et al. (89) (1979)	✓				✓		✓	20- 200
Seeberger, J. et al. (157) (1981)			✓		✓		✓	20- 250
Kaplan, M.F. and Roux, F.J. (82) (1972)	✓		✓		✓			21- 400
Khoury, G.A. (84) (1983)			✓	✓				20- 724

TABLE 2.4. VARIOUS TESTING CONDITIONS EMPLOYED TO STUDY THE EFFECT OF ELEVATED TEMPERATURE ON COMPRESSIVE STRENGTH OF UNSEALED CONCRETE.

TEMP. (°C)	0	100	200	300	400	500
WATER	20°C→100°C: Loss of evaporable water.	150-200°C: Max. value for rate of desorption. (D) (68) 100-200°C: Endothermic peak in DTA curve. (D) (135) 176°C: Peak in DTG curve. (S-S) (49)			301°C & 398°C: Peaks in DTG curve. (S-S) (49)	
POLYMERI - ZATION	20°C→95°C: Increase in degree of polymerization with increasing temperature. (43,129)	100°C→800°C: Depolymerization of SiO_4^{-4} anion. (138)				
CSH GEL		110°C: No change in chemical composition from XRD test. (83)				
POROSITY	80°C: Min. in pore volume between 75-75000 Å w.r.t. temp. range 20-110°C. (83)	100°C: Permeability increased by 2 orders of magnitude despite little change in porosity; widening of pore necks. (13)	20°C→300°C: Increase of total pore volume small compared with weight loss. (148)			
$Ca(OH)_2$					400°C: Weight change; dissociation. (S) (61) 430°C: Peak in DTG curve; dissociation. (S-S) (49)	
MICRO - CRACKING				300°C: Beginning of significant microcracking. (137)	491°C: Reversal of increasing shrinkage in hcp (w/c= 0.18). (S) (92)	

(cont...)

Note 1:- Symbols S,S-S and D stand for Static, Semi-Static and Dynamic respectively, indicating the nature of the test. Figures in parantheses are references.

Note 2:- An arrow (→) between two temperatures indicates that the change described takes place over the range between the temperatures. A dash (-) between temperatures indicates that the temperature of interest lies between the two temperatures quoted.

TABLE 2.5. CHANGES IN CEMENT PASTE UPON HEATING.

TEMP.(°C)	500	600	700	800	900
WATER					
POLYMERI - ZATION					
CSH GEL		600°C→700°C: Decomposition of CSH to β-C_2S.(D) (153)	700°C→800°C: Formation of ultimate dissociation products C_2S & CS.(D) (68) 705°C: Original β-C_2S converted to β-C_2S.(D) (121) 785°C: Endothermic peak linked with wt. loss.(D) (153)	800-900°C: Exothermic peak in DTA curve; formation of β-CS.(D) (135)	
POROSITY	300°C→600°C: Increase in pore volume large compared with weight loss. (148) 550-600°C: Increase in "main pore radius". (154)			600°C→900°C: Further increase in pore volume; decrease in pore volume under 200 Å. (148) 20°C→850°C: Increase in porosity by c.40%. (68)	
$Ca(OH)_2$	500-600°C: Peak in DTA curve; dissociation.(D)(68) 500-600°C: Min.in $Ca(OH)_2$ by TG method.(D) (138) 500°C: Max. $CaCO_3$ content by TG method.(D) (138)		729°C: Peak in DTG curve; decarbonation.(S-S) (49)	850°C: Peak in DTA curve; decarbonation.(D) (155)	
MICRO - CRACKING			700-800°C: Reversal of increasing shrinkage in hcp (w/c=0.30).(D) (67)		

Note 1:- Symbols S,S-S and D stand for Static,Semi-Static and Dynamic respectively, indicating the nature of the test. Figures in parantheses are references.

Note 2:- An arrow (→) between two temperatures indicates that the change described takes place over the range between the temperatures. A dash (-) between temperatures indicates that the temperature of interest lies between the two temperatures quoted.

TABLE 2.5 CHANGES IN CEMENT PASTE UPON HEATING (CONT.).

Fig.2.1– 60–DAY CREEP STRAINS NORMALIZED TO STRS./COLD STRENGTH=0.1

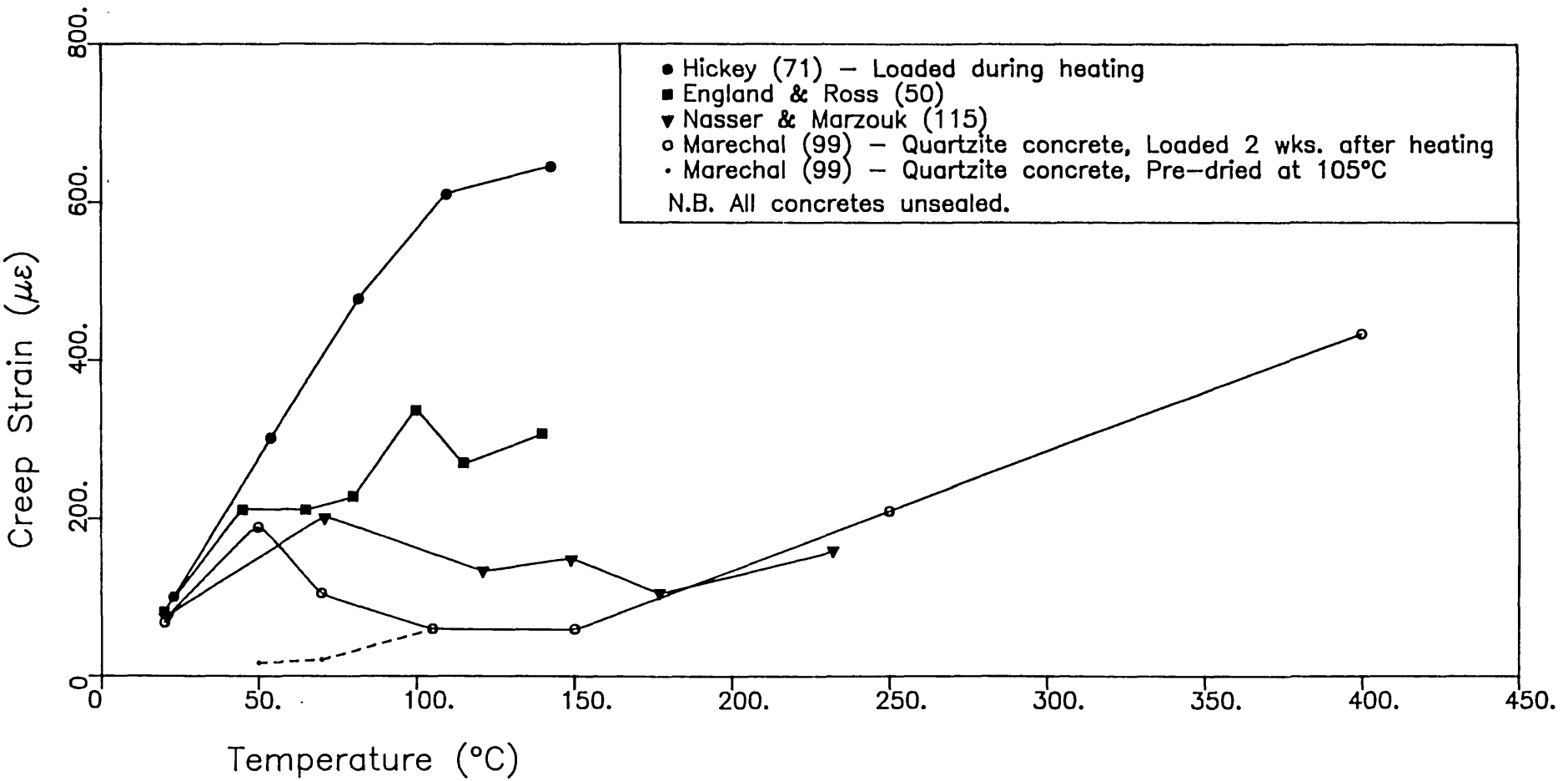

Fig.2.2– 3–HR. CREEP STRAINS NORMALIZED TO STRS./COLD STRENGTH=0.1

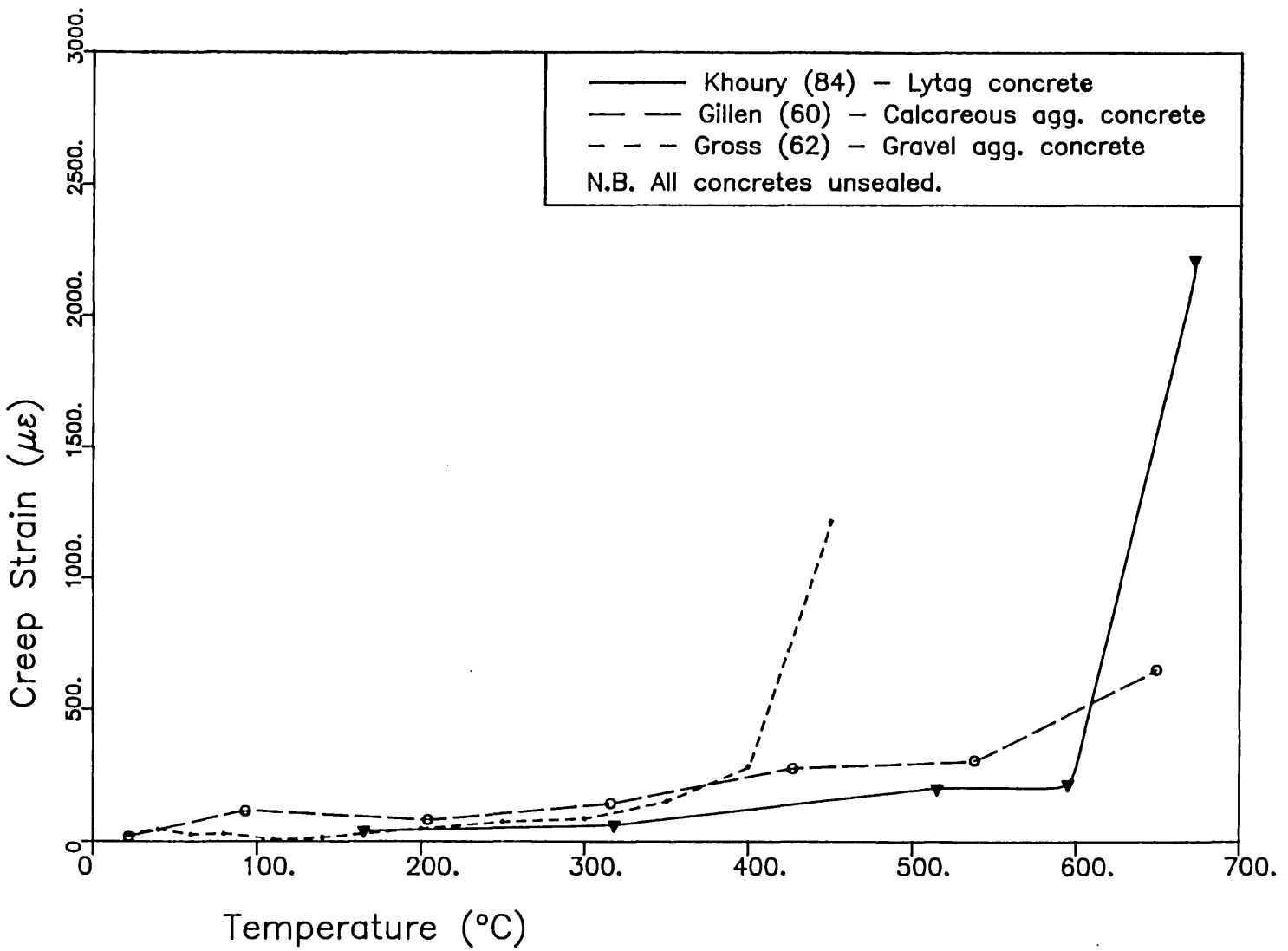

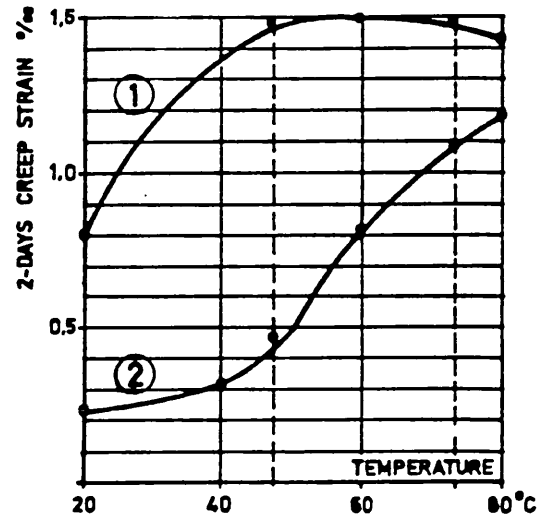

Figure 2.3 - CREEP STRAINS FOR SATURATED,SEALED CEMENT PASTE SPECIMENS. 1-LOADED AFTER HEATING TO TEST TEMPERATURE. 2-LOADED AT TEMPERATURE AFTER 3 DAYS' THERMAL TREATMENT AT 80 C.(FROM ANDERBERG & THELANDERSSON (3),AFTER REUTZ (146))

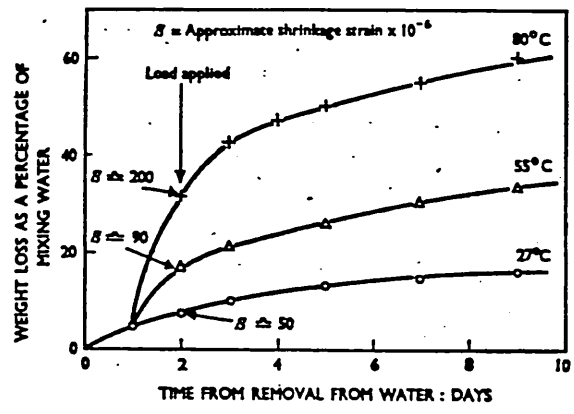

Figure 2.4 - MOISTURE LOSS FROM UNSEALED CONCRETE CYLINDERS PRIOR TO CREEP LOADING.(FROM HANNANT (65))

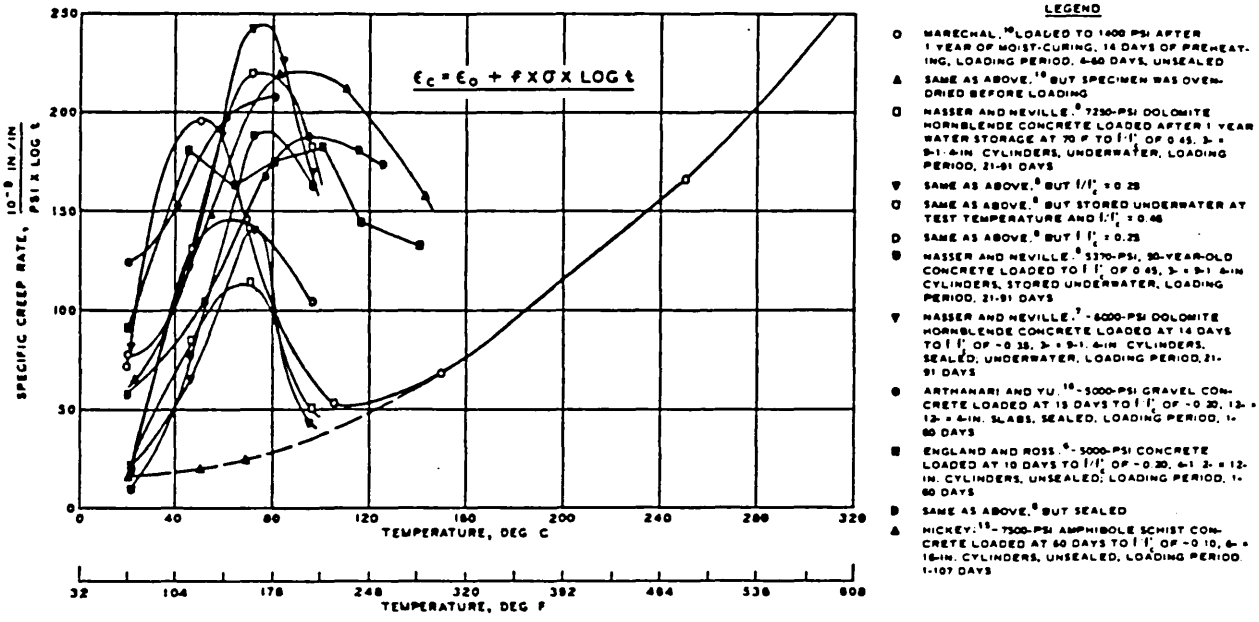

Figure 2.5 - INFLUENCE OF TEMPERATURE ON CREEP RATE. (FROM GEYMAYER (58))

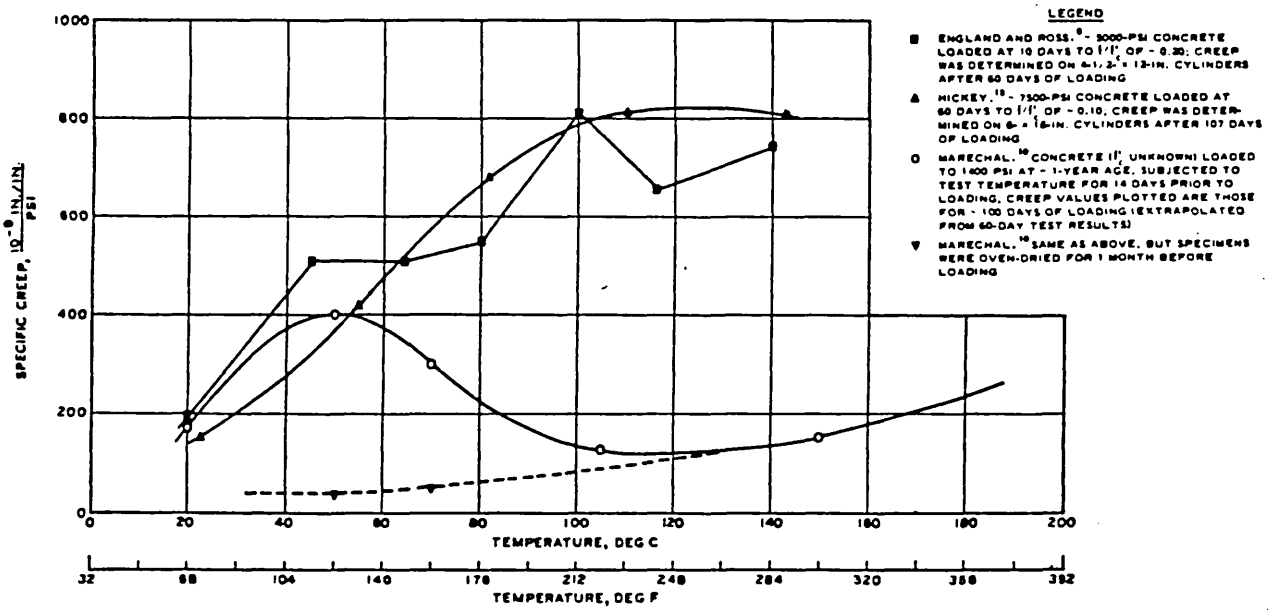

Figure 2.6 - INFLUENCE OF TEMPERATURE ON CREEP OF UNSEALED SPECIMENS AFTER 60,100 OR 107 DAYS' LOADING. (FROM GEYMAYER (58))

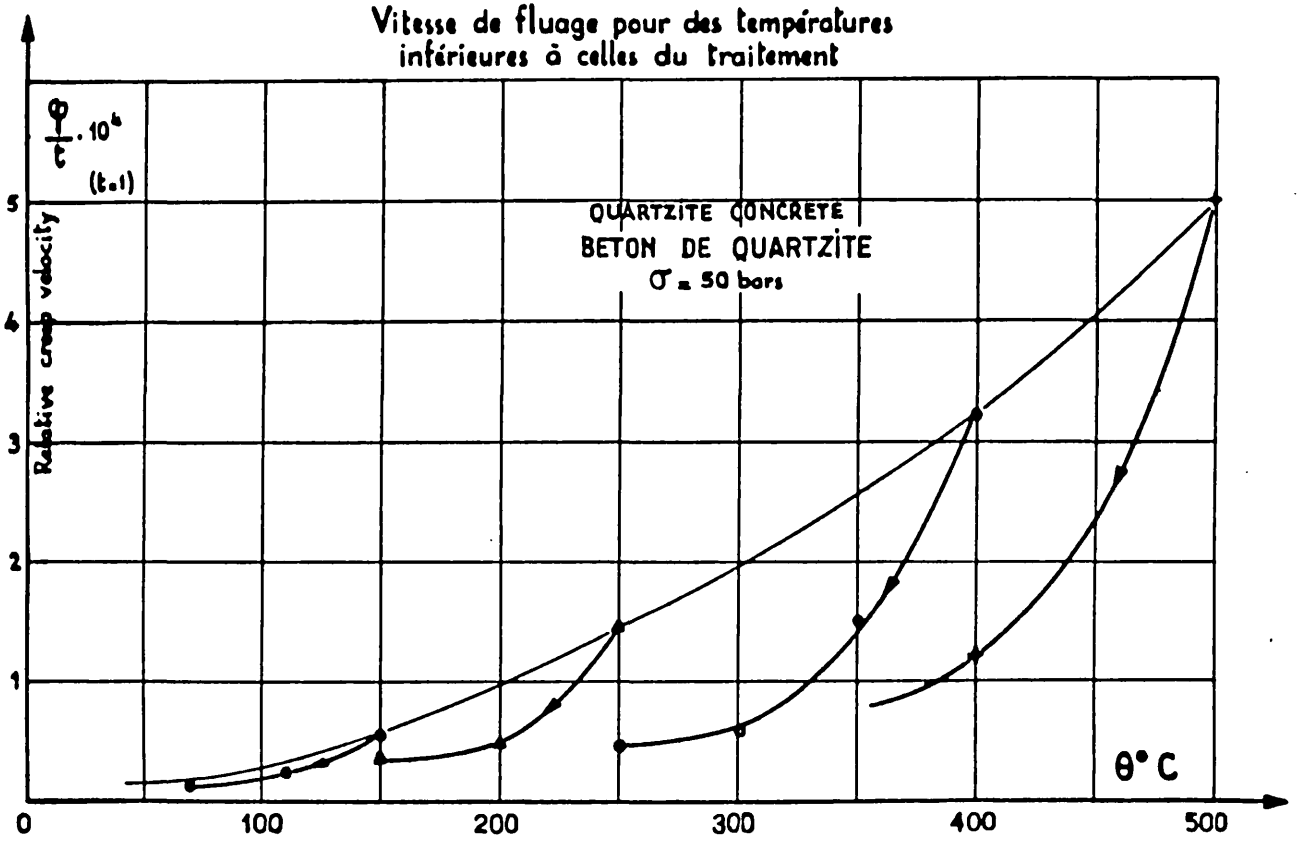

Figure 2.7 - CREEP RATE OF QUARTZITE CONCRETE, 1DAY AFTER LOADING, AT TEMPERATURES LOWER THAN PREHEAT TEMPERATURE. (FROM MARECHAL (100))

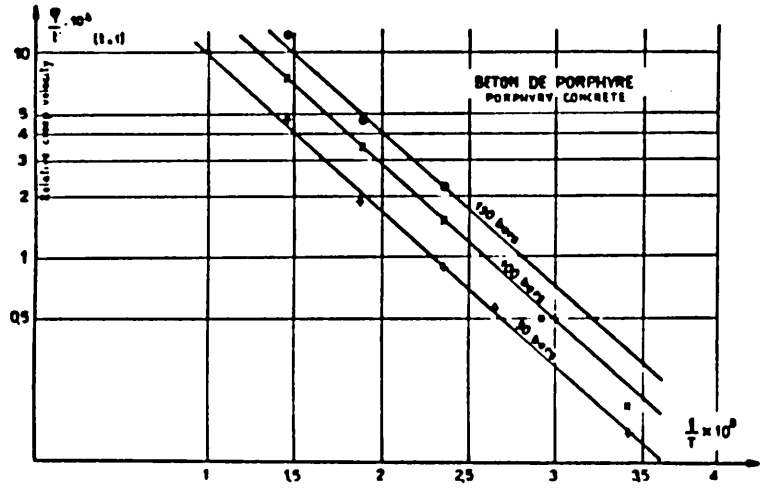

(a) PORPHYRY CONCRETE AT DIFFERENT STRESS LEVELS. (FROM MARECHAL (100)

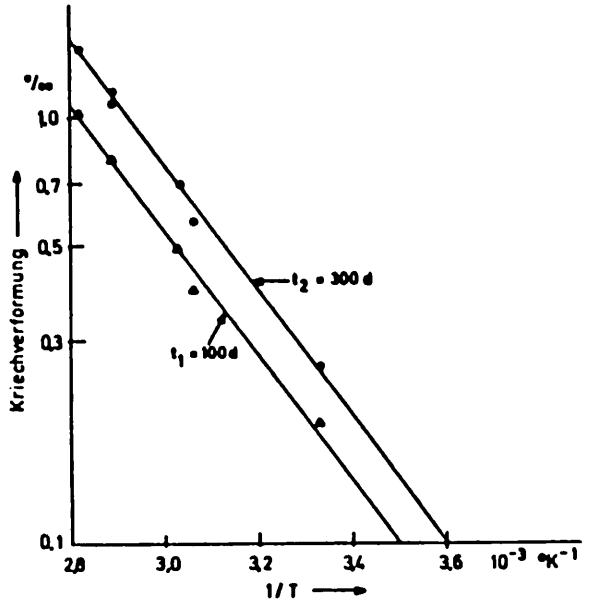

(b) SEALED CONCRETE AT DIFFERENT TIMES AFTER LOADING. (FROM WITTMANN & SETZER (184))

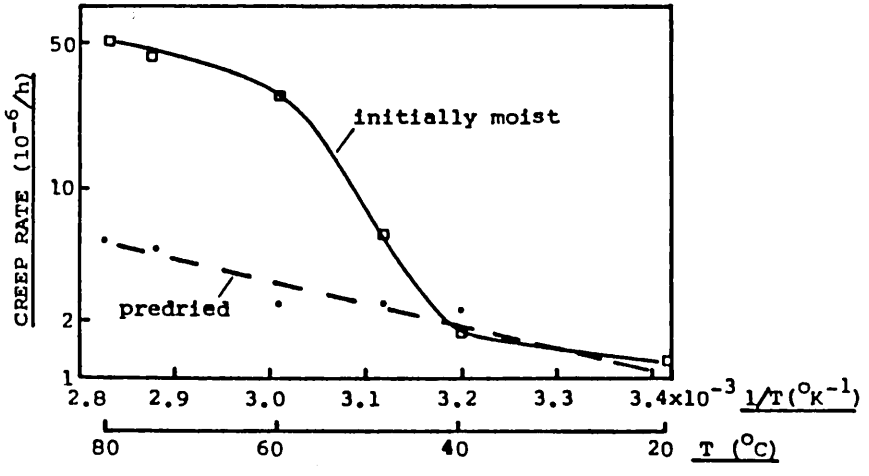

(c) MOIST AND PREDRIED CEMENT PASTE. (FROM KHOURY (84), AFTER REUTZ (146))

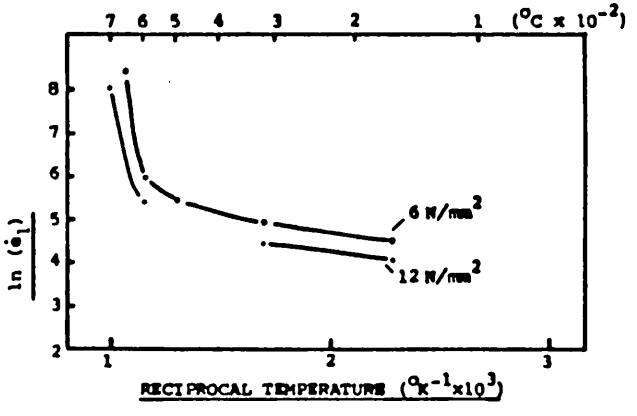

(d) LYTAG CONCRETE AT 2 STRESS LEVELS. (FROM KHOURY (84))

Figure 2.8 - ARRHENIUS PLOTS OF CREEP RATE vs. RECIPROCAL TEMPERATURE.

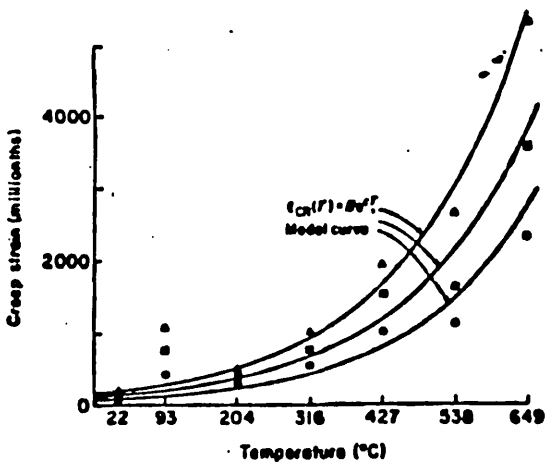

(a) EXPONENTIAL MODEL, 3 STRESS LEVELS.(FROM GILLEN(60))

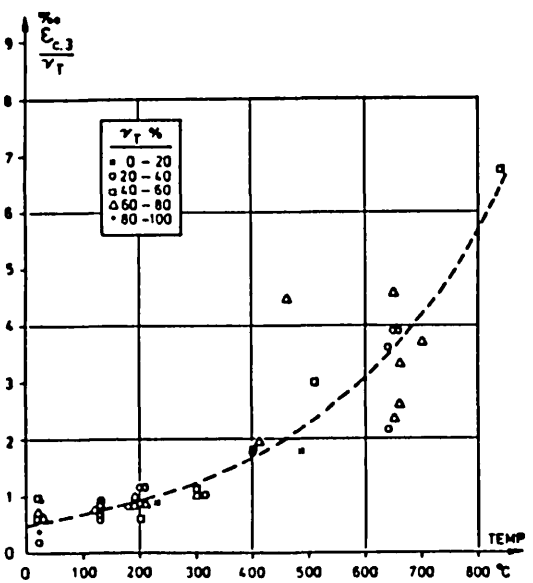

(b) NORMALIZATION W.R.T. STRESS/HOT STRENGTH.(FROM ANDERBERG & THELANDERSSON (4))

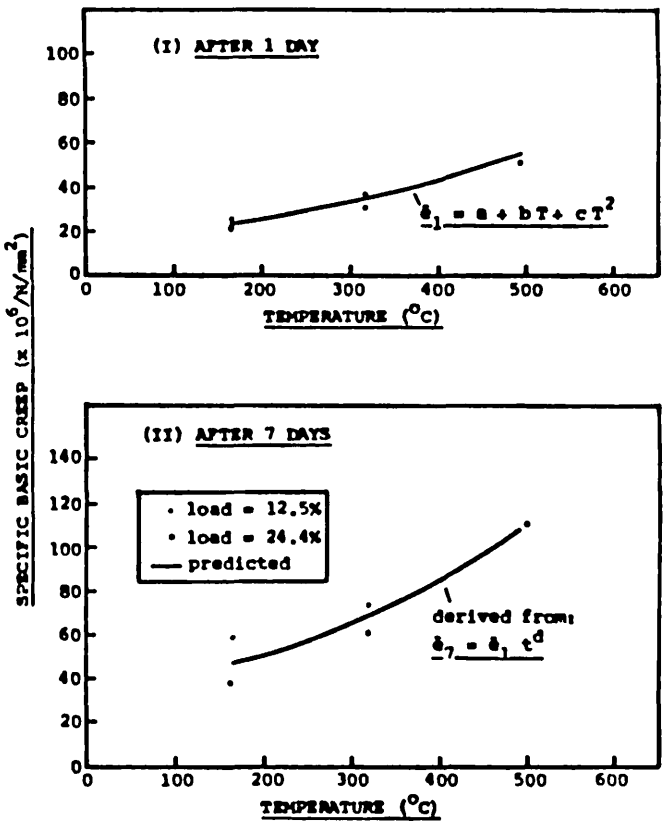

FIGURE 8.16: SPECIFIC BASIC CREEP-TEMPERATURE RELATION OF LIGHTWEIGHT AGGREGATE CONCRETE AT ONE AND SEVEN DAYS AFTER LOADING AT TWO LEVELS. EXPERIMENTAL RESULTS (POINTS) ARE COMPARED WITH MATHEMATICALLY DERIVED RELATION (CURVES).

a = 20.252
b = -0.003537
c = 0.0001473
d = 0.36
t = 1 - 7 days
T = 165 - 500°C

(c) QUADRATIC EXPRESSION.(FROM KHOURY (84))

Figure 2.9 - EMPIRICAL RELATIONSHIPS FOR TEMPERATURE FUNCTION OF CREEP.

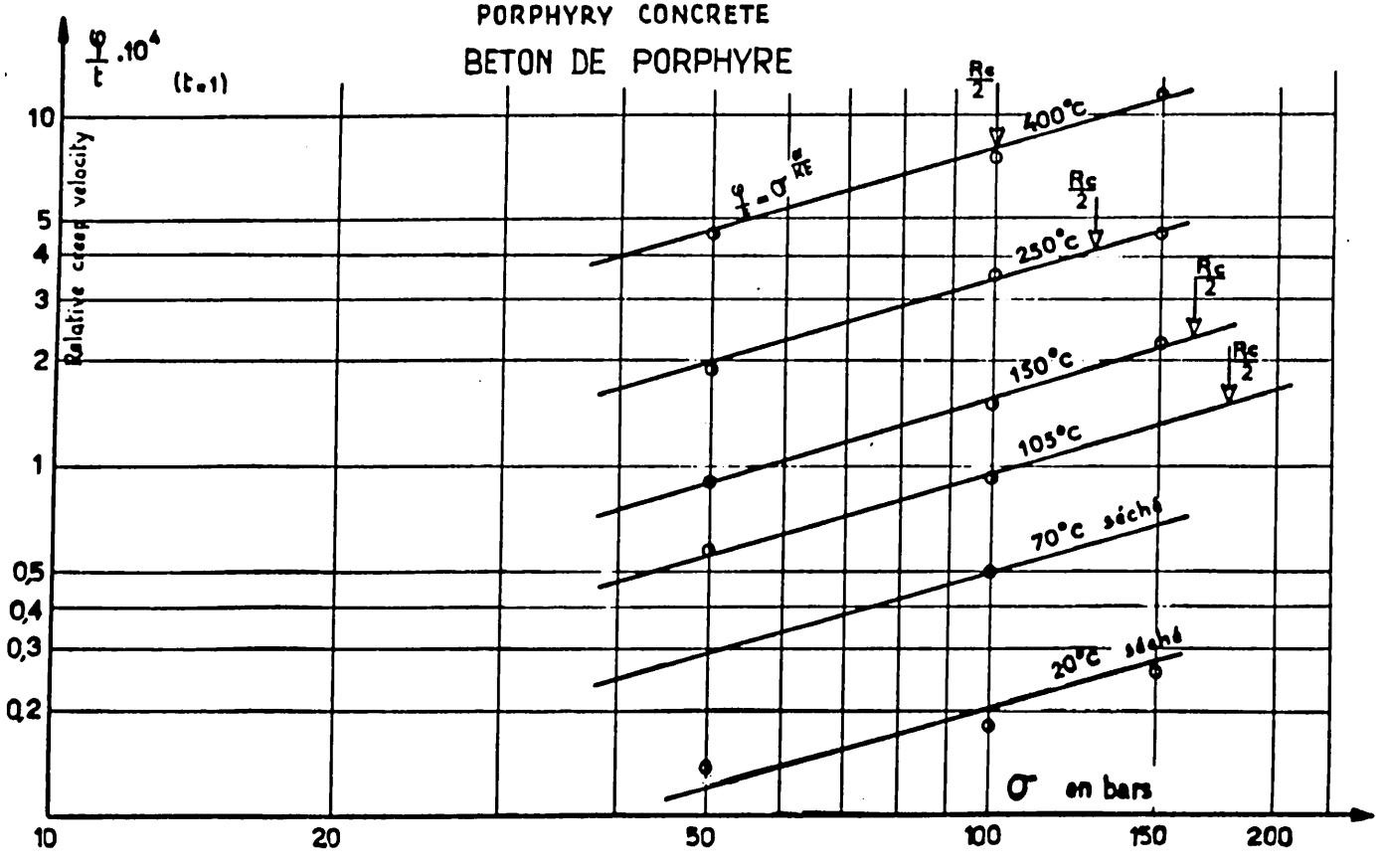

Figure 2.10 - RELATIONSHIP BETWEEN CREEP RATE AND STRESS LEVEL.(FROM MARECHAL (100)

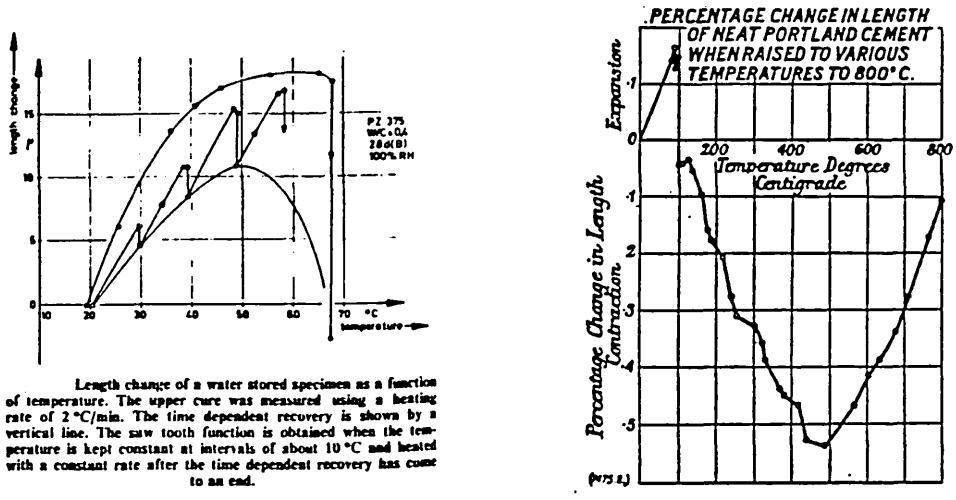

Length change of a water stored specimen as a function of temperature. The upper cure was measured using a heating rate of 2 °C/min. The time dependent recovery is shown by a vertical line. The saw tooth function is obtained when the temperature is kept constant at intervals of about 10 °C and heated with a constant rate after the time dependent recovery has come to an end.

(a) (b)

Figure 2.11 - THERMAL STRAINS OF HARDENED CEMENT PASTE AT SUSTAINED ELEVATED TEMPERATURES. (a-WITTMANN & LUKAS (181), b-LEA & STRADLING (92))

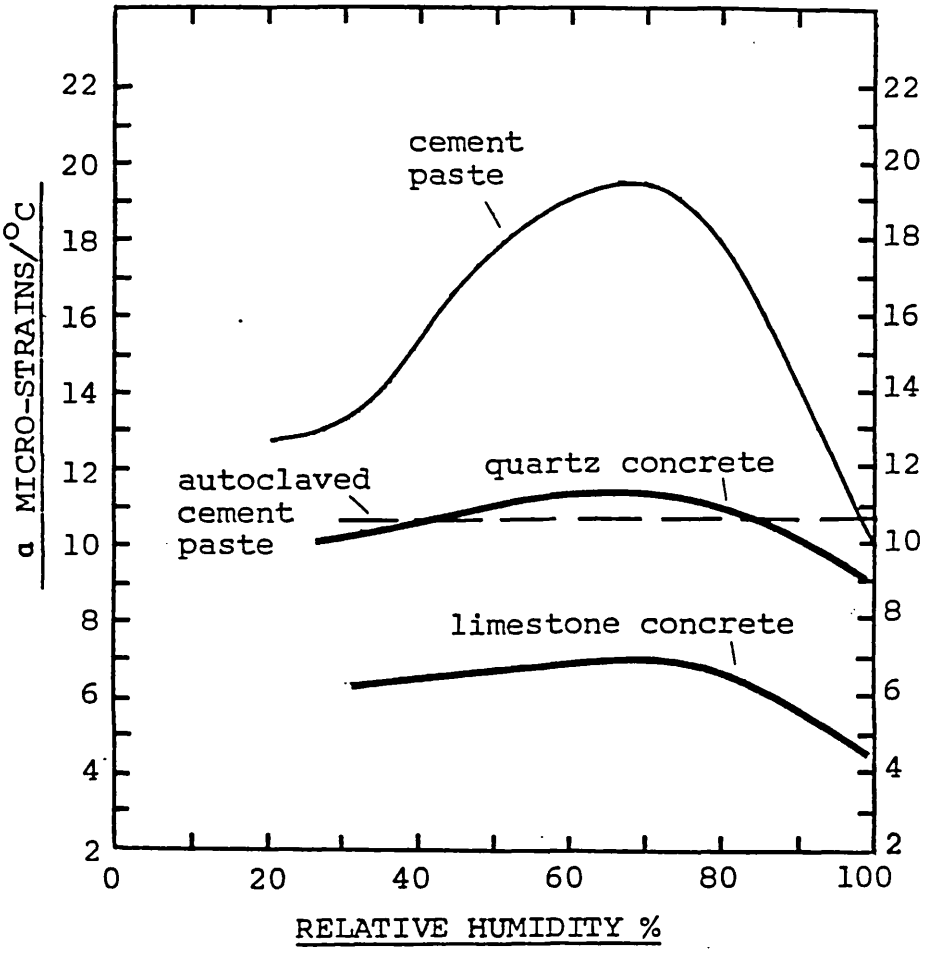

Figure 2.12 - EFFECT OF MOISTURE STATE ON THE COEFFICIENT OF THERMAL EXPANSION OF CEMENT PASTE AND CONCRETE. (FROM KHOURY (84))

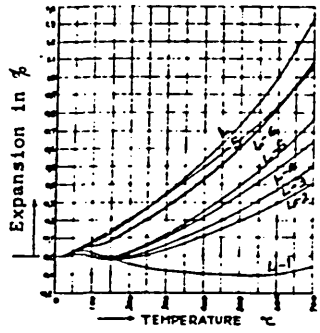

(a) LIMESTONE AGGREGATE
L: expansion of limestone
L-1 to L-5: mortars (1:1 to 1:5)
L-6: concrete (1:1.9:2:2.85)

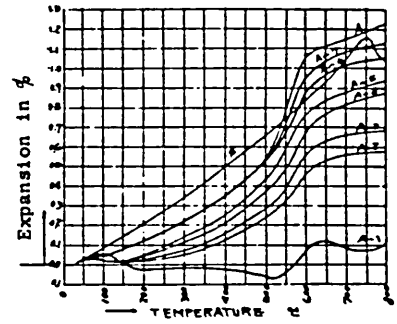

(b) SANDSTONE AGGREGATE
A: expansion of sandstone
A-1 to A-5: mortars (1:1 to 1:5)
A-6 & A-7: concrete
(1:2.0:2.5 & 1:2.3:2.9)

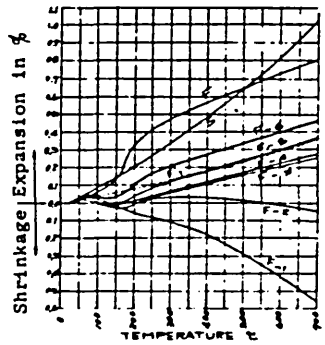

(c) ANDESITE AGGREGATE
F: expansion of andesite
F-1 to F-5: mortars (1:1 to 1:5)
F-6: concrete (1:2.0:3.0)

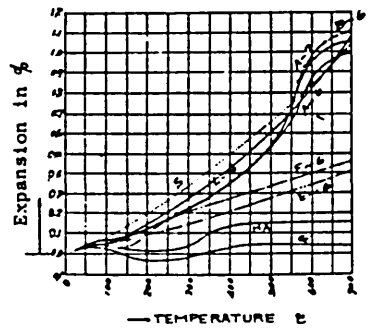

(d) CONCRETES WITH DIFFERENT TYPES OF AGGREGATES
A-6 & A-7: sandstone, as in (b)
B-6: another sandstone (1:1.8:3.6)
L-6: limestone concrete (1:1.9:2.85)
F-6: andesite concrete (1:2.0:3.0)
E-6: another andesite (1:1.7:3.4)
G: expans. of pumice concrete
HA: expans. of cinder concrete
S: expans. of reinf. steel

Figure 2.13 - EFFECT OF AGGREGATE VOLUME CONTENT AND TYPE ON THE THERMAL STRAINS OF CONCRETE.(FROM ZOLDNERS (189),AFTER HARADA ET AL.(67)

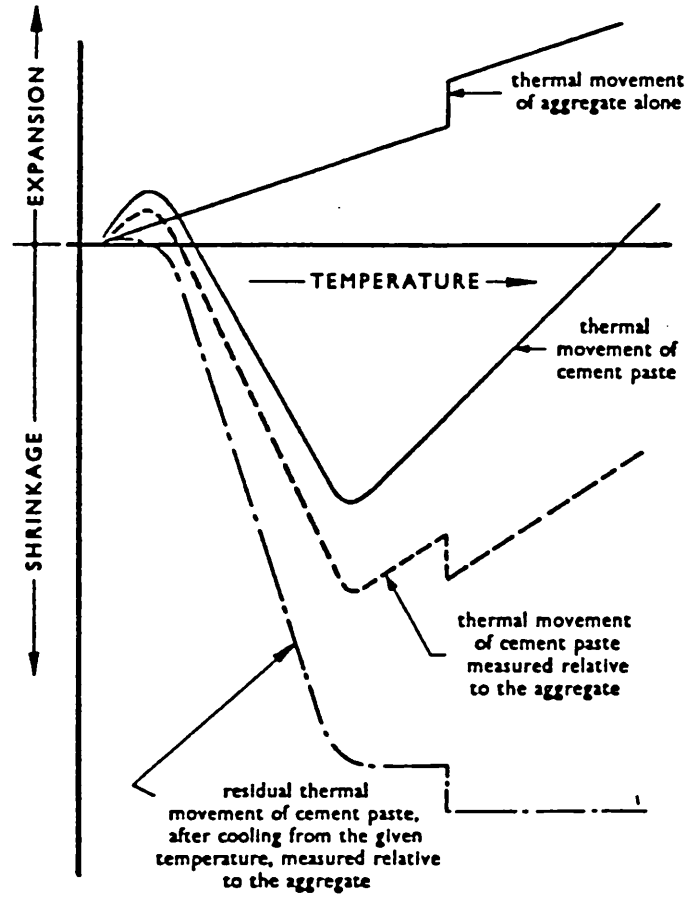

Figure 2.14 - THERMAL MOVEMENT OF CEMENT PASTE RELATIVE TO A TYPICAL SILECEOUS AGGREGATE.(FROM DOUGILL (48))

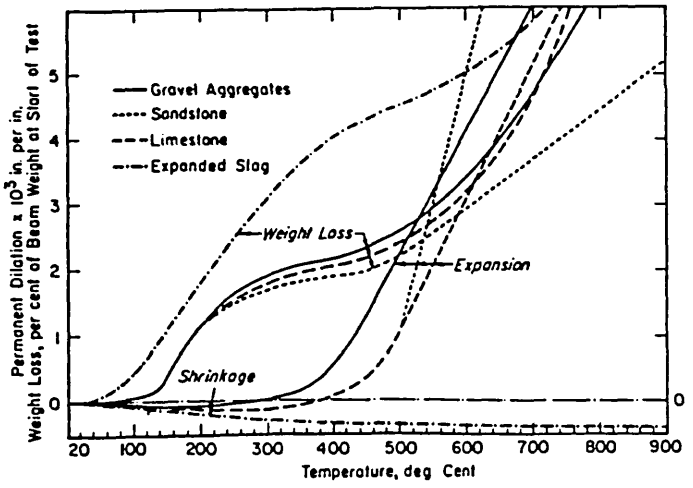

Figure 2.15(a) - THERMAL STRAINS AND WEIGHT LOSSES OF CONCRETES MADE WITH DIFFERENT AGGREGATES.(FROM ZOLDNERS (188))

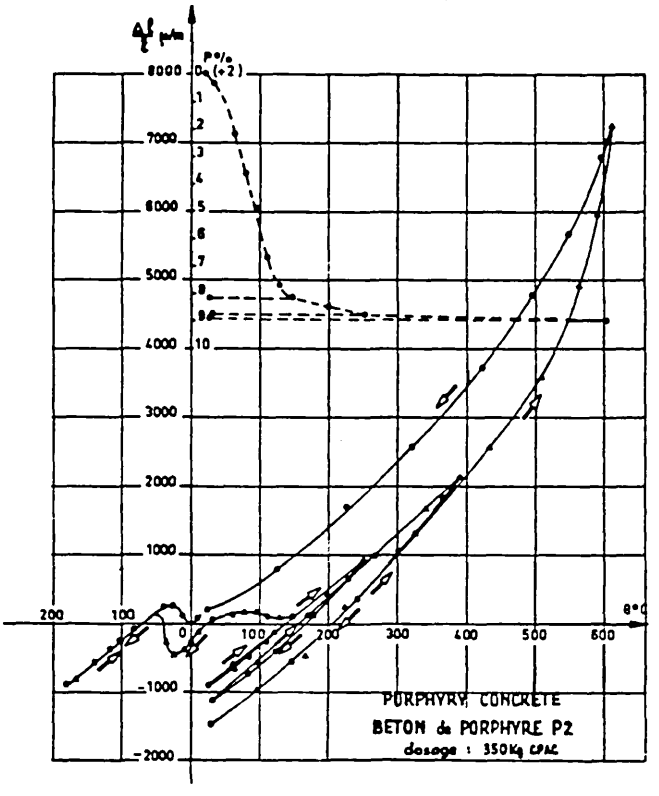

Figure 2.15(b) - THERMAL STRAIN BEHAVIOUR OF PORPHYRY CONCRETE. (FROM MARECHAL (102))

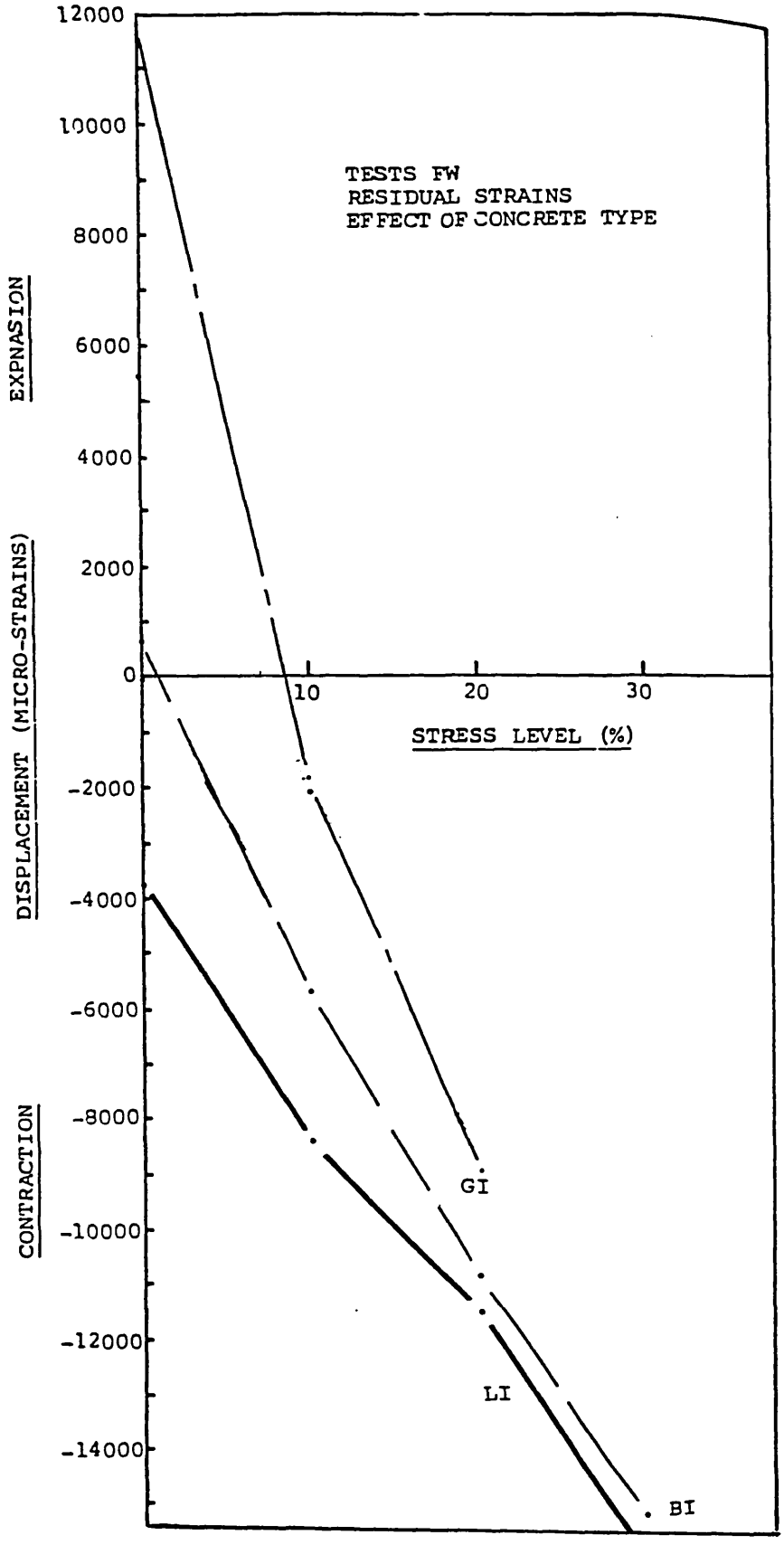

Figure 2.16 - RESIDUAL STRAINS OF CONCRETE MADE WITH DIFFERENT AGGREGATES AFTER HEATING TO 600 C UNDER VARIOUS STRESS LEVELS.NOTE:-GI=GRAVEL,BI=BASALT,LI=LYTAG. (FROM KHOURY (84))

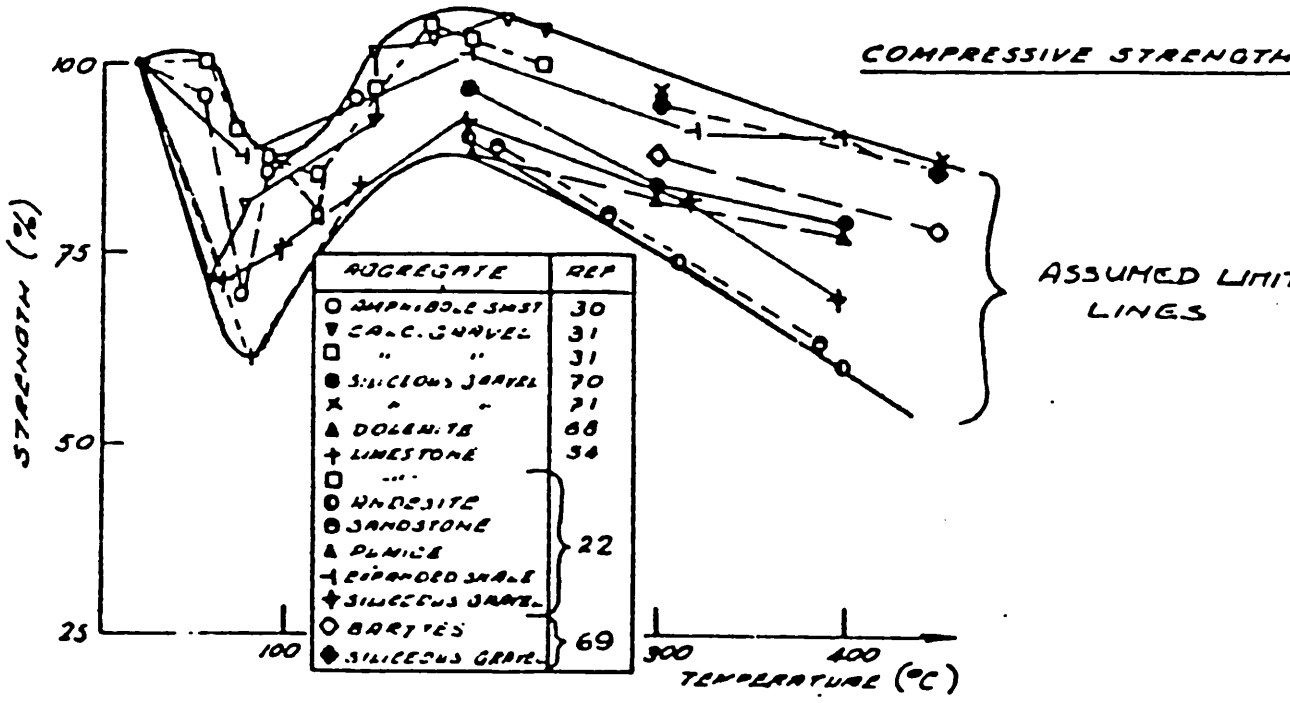

Figure 2.17 - VARIATION OF COMPRESSIVE STRENGTH WITH TEMPERATURE. (FROM BLUNDELL ET AL.(23))

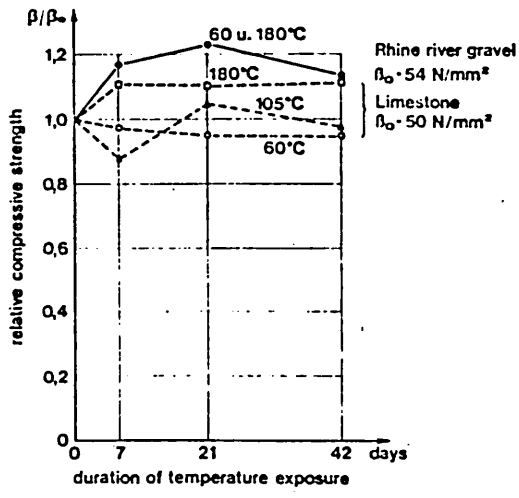

Figure 2.18(a) - EFFECT OF DURATION AT TEMPERATURE ON HOT STRENGTH OF UNSEALED CONCRETE.(FROM KOTTAS ET AL.(89))

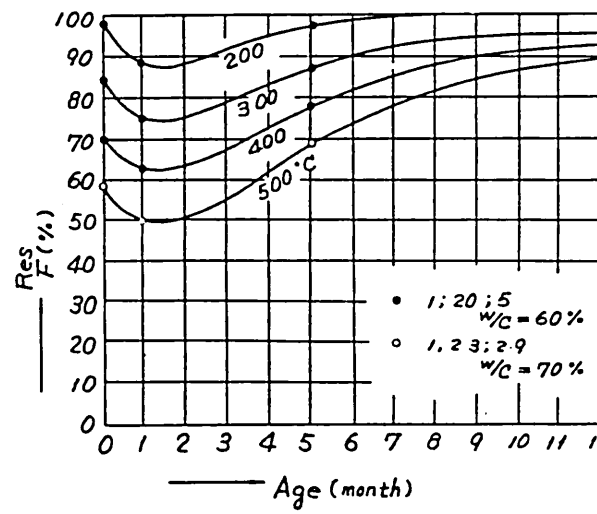

Figure 2.18(b) EFFECT OF POST-COOLED EXPOSURE DURATION ON CONCRETE STRENGTH. (FROM HARADA ET AL.(67))

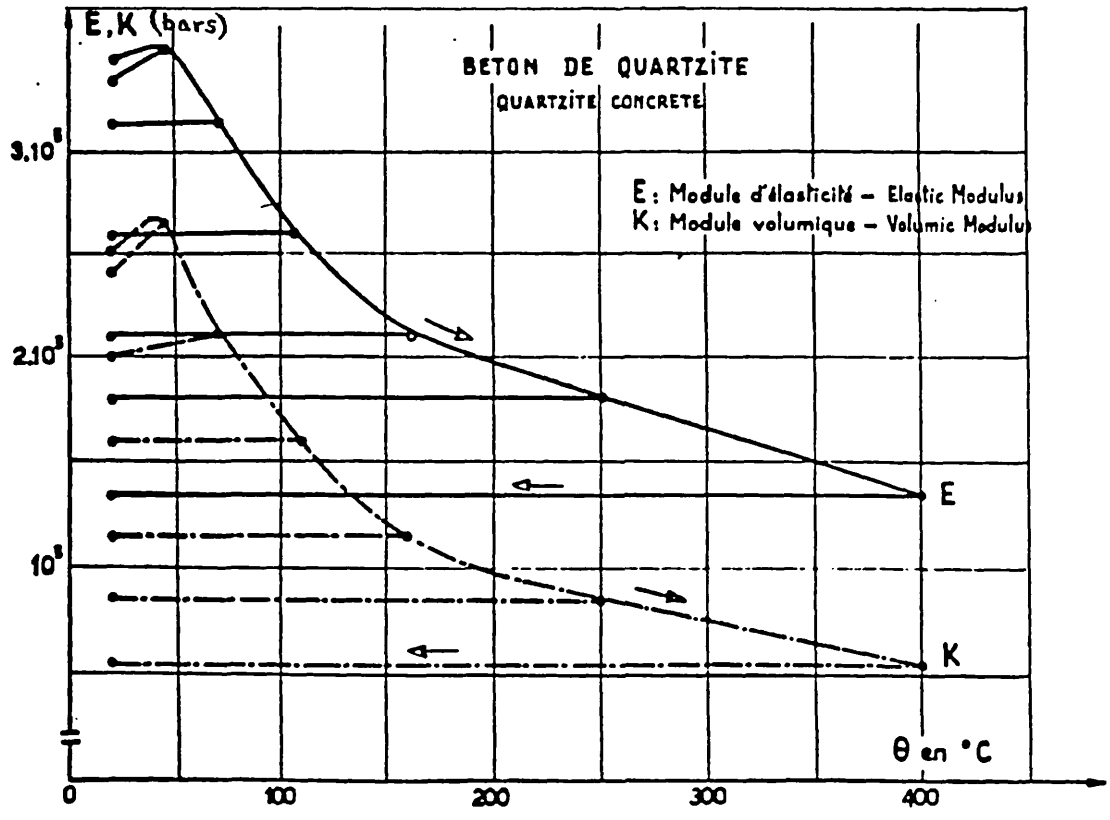

Figure 2.19 - VARIATION OF ELASTIC MODULI WITH TEMPERATURE ON HEATING AND COOLING.(FROM MARECHAL (101))

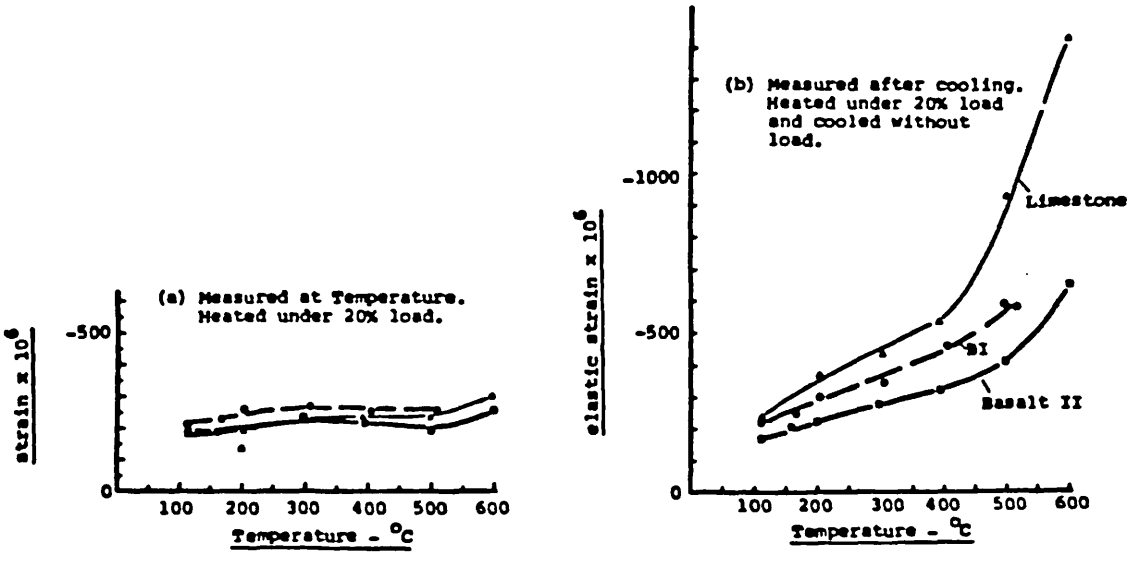

Figure 2.20 - EFFECT OF TEMPERATURE LEVEL ON ELASTIC STRAINS OF CONCRETES SUBJECTED TO VARIOUS THERMAL AND LOAD CONDITIONS.(FROM KHOURY ET AL.(88))

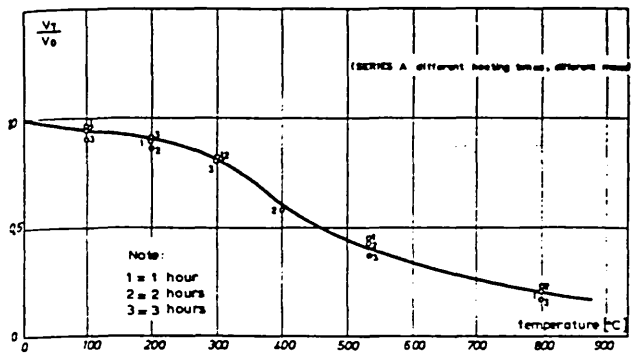

Figure 2.21(a) - VARIATION OF ULTRASONIC PULSE VELOCITY WITH EXPOSURE TEMPERATURE.(FROM LOGOTHETIS & ECONOMOU (95))

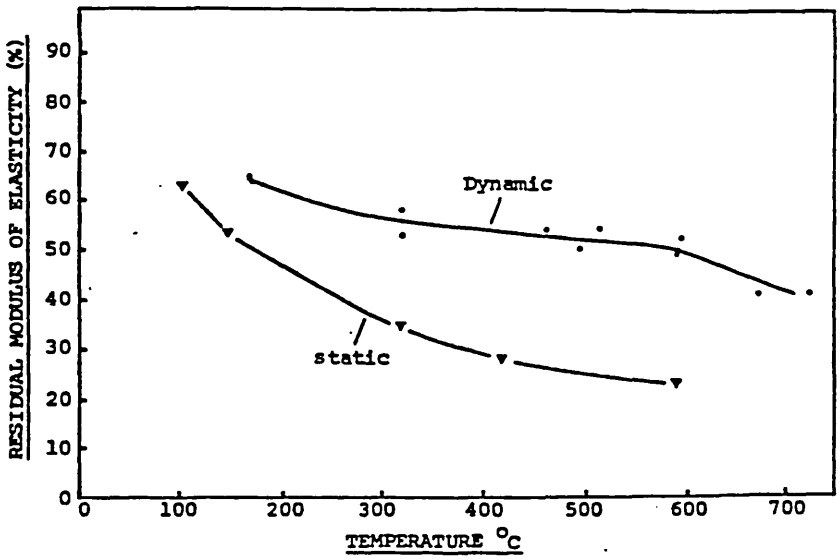

Figure 2.21(b) - VARIATION OF DYNAMIC AND STATIC ELASTIC MODULI WITH EXPOSURE TEMPERATURE.(FROM KHOURY (84))

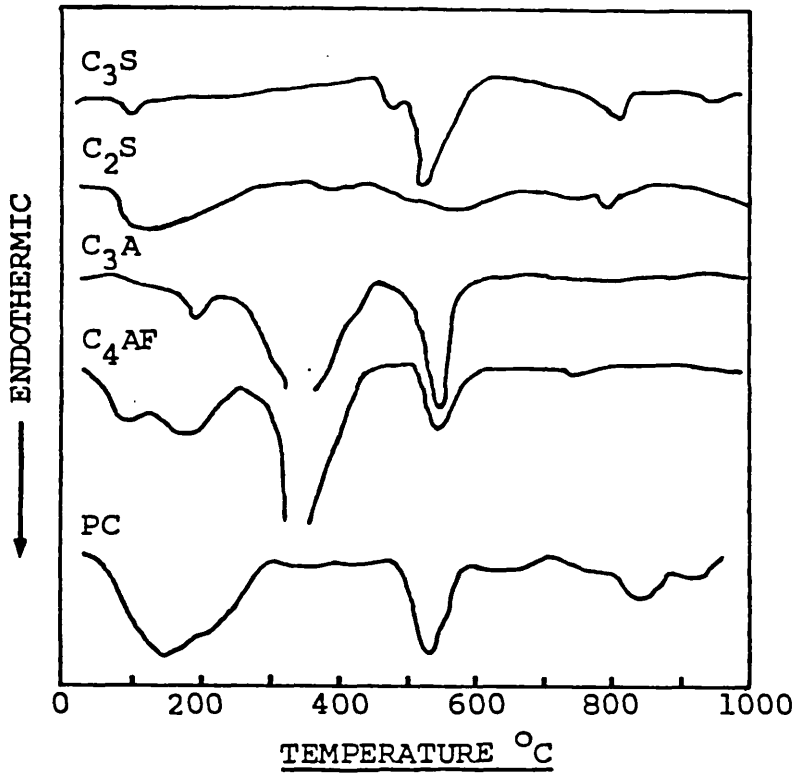

DTA MEASUREMENTS OF PORTLAND CEMENT PATSE AND ITS MAIN HYDRATED CONSTITUENT COMPOUNDS

a) Endothermic peaks at 500-600°C caused by dehydration of $Ca(OH)_2$ which is notably absent in hydrated C_2S.
b) Exothermic peak between 800°C and 900°C caused by formation of wollastonite.
c) Hydrated C_3A and C_4AF behave similarly. Endothermic peak between 300°C and 400°C caused by dehydration of C_3AH_6
d) Endothermic peak between 100°C and 200°C caused by loss of evaporable and CSH water.

Figure 2.22 - TYPICAL DTA CURVES FOR PORTLAND CEMENT PASTE AND ITS MAIN HYDRATED CONSTITUENT COMPOUNDS.(FROM KHOURY (84))

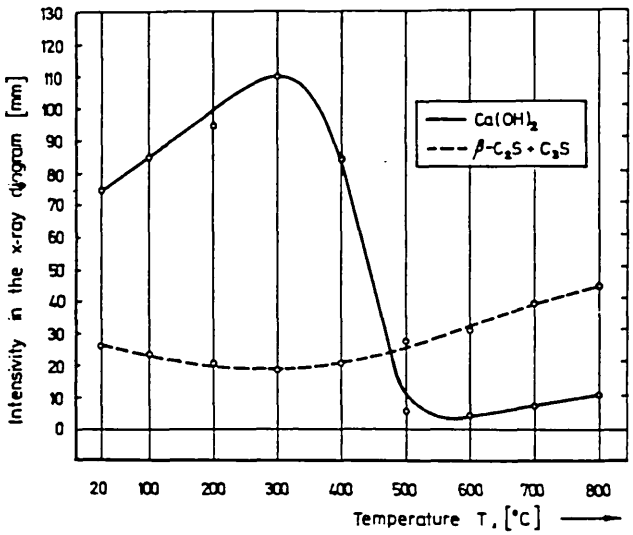

Figure 2.23(a) - THE AMOUNTS OF $Ca(OH)_2$ AND β-C_2S+C_3S IN OPC PASTES (AGE=28 DAYS,W/C=0.4) AFTER EXPOSURE TO 3 HOURS' HEAT.(FROM PIASTA ET AL.(138))

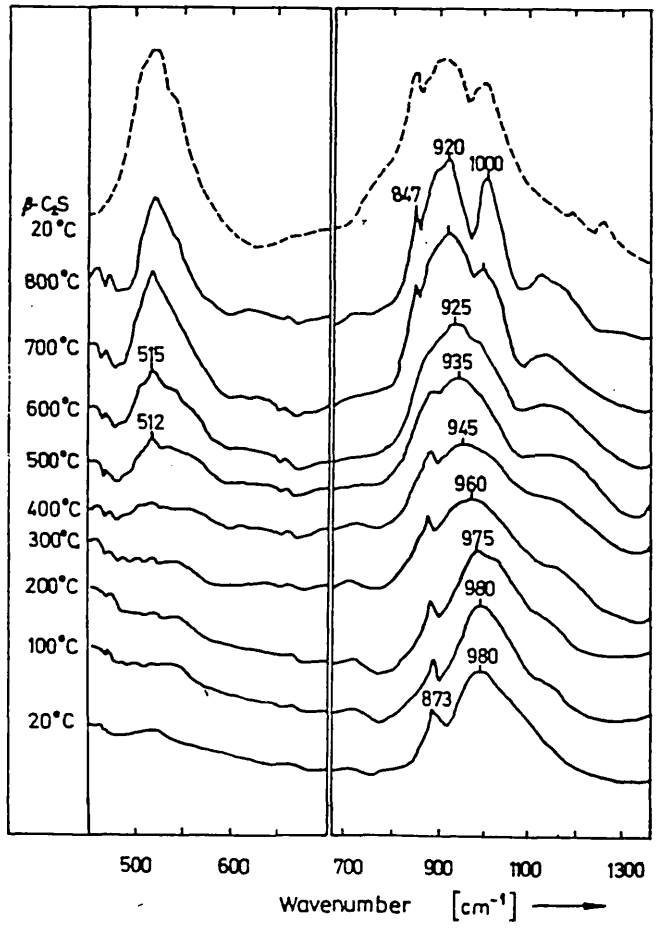

Figure 2.23(b) - INFRARED ABSORPTION SPECTRA OF OPC PASTE AFTER EXPOSURE TO 3 HOURS' HEAT.(FROM PIASTA ET AL.(138))

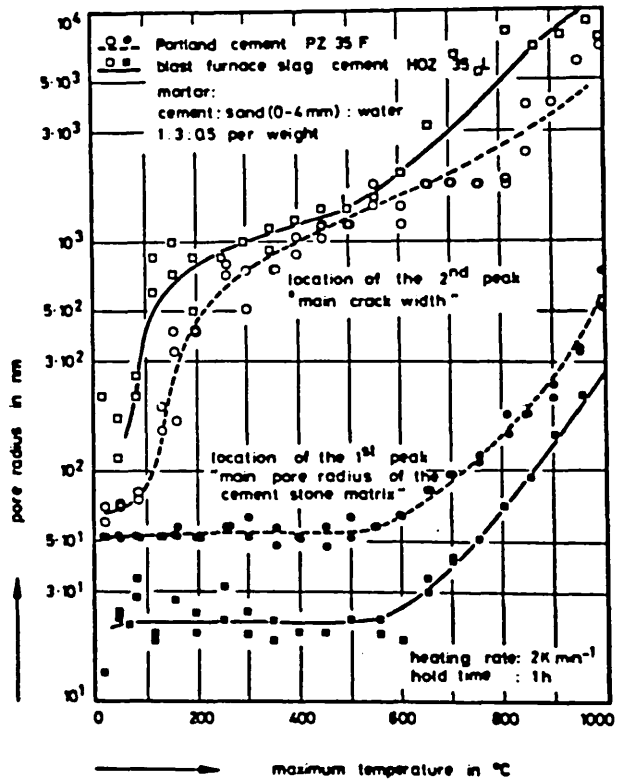

Figure 2.24 - LOCATION OF THE MAXIMA OF THE DIFFERENTIAL PORE SIZE DISTRIBUTION OF THERMALLY EXPOSED MORTAR SPECIMENS. (FROM SCHNEIDER & DIEDERICHS (154))

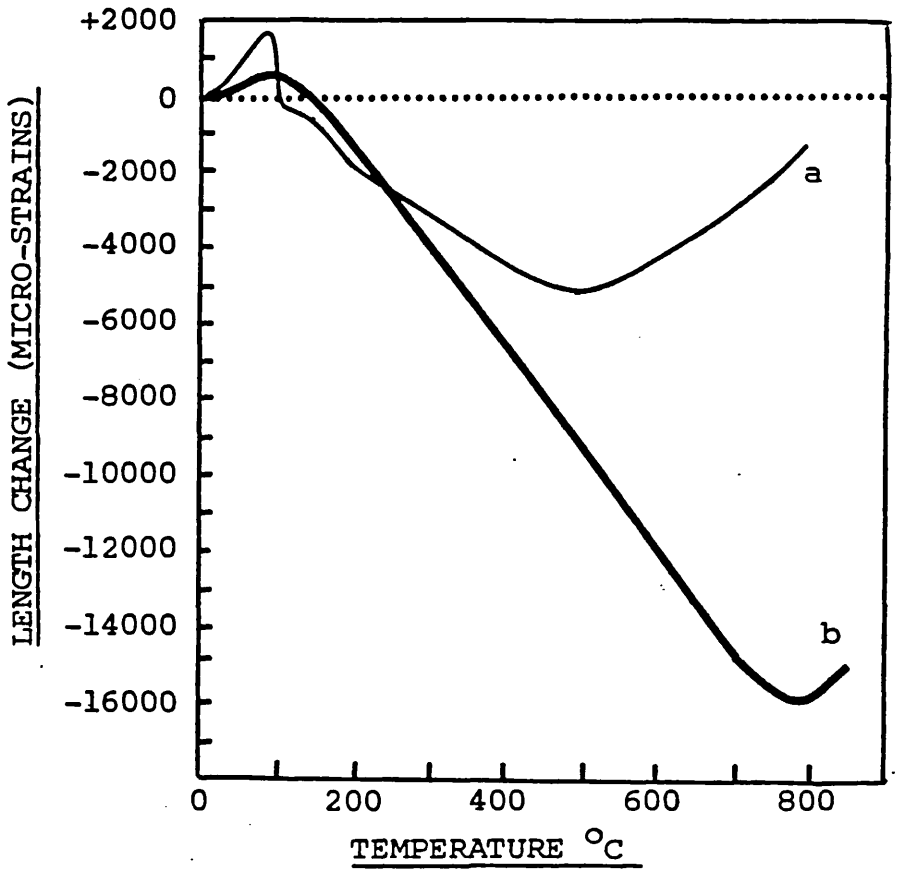

Figure 2.25 - LENGTH CHANGE OF CEMENT PASTE UPON HEATING.a-LEA & STRADLING (92),b-HARADA ET AL.(67).(FROM KHOURY(84))

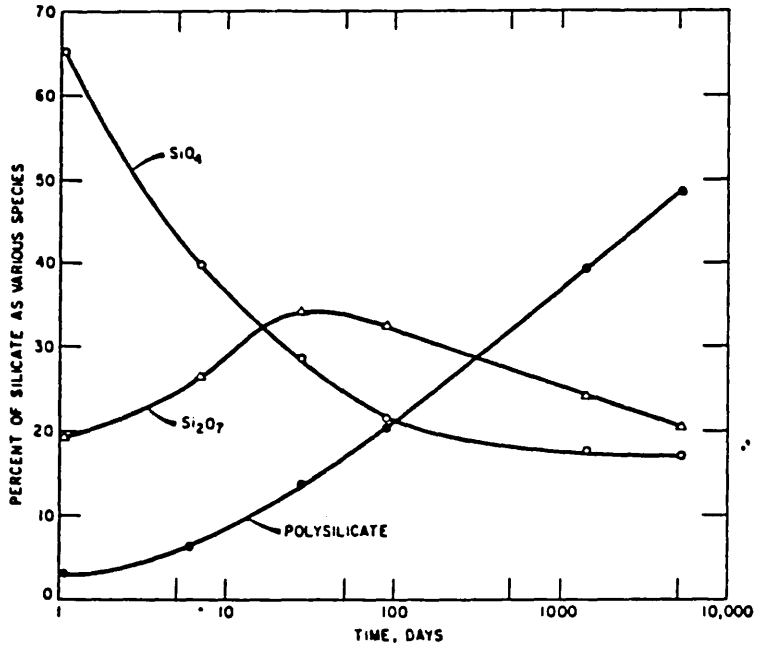

Figure 2.26 - CHANGES IN SILICATE STRUCTURE OF PORTLAND CEMENT PASTE WITH AGE.(FROM LENTZ (93))

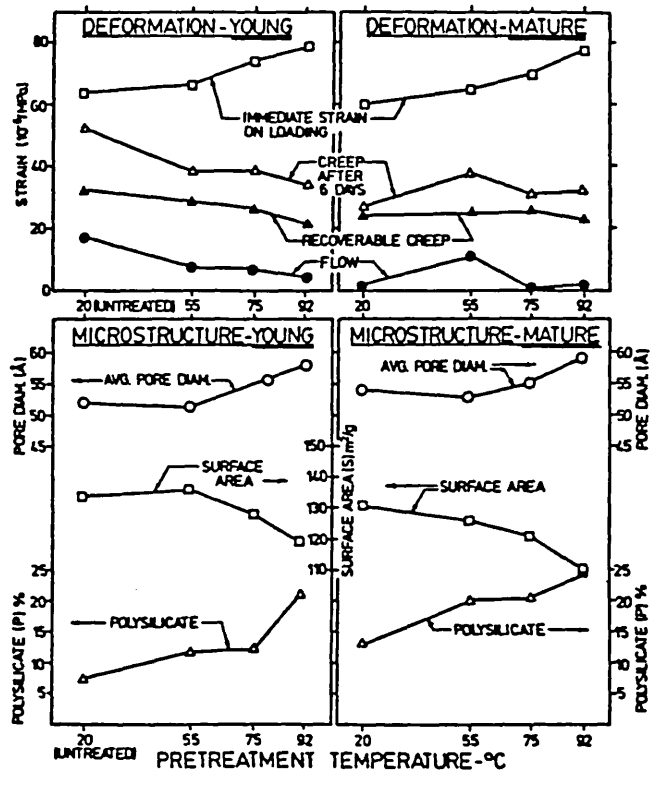

Figure 2.27 - EFFECTS OF THERMAL PRETREATMENTS ON MICROSTRUCTURE AND DEFORMATION UPON SUBSEQUENT LOADING.(FROM DAY & GAMBLE (43))

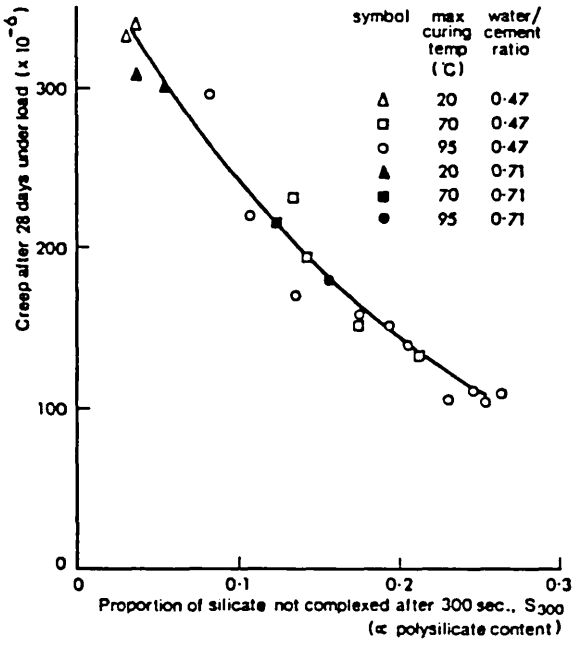

Figure 2.28 - RELATIONSHIP BETWEEN CREEP AND POLYSILICATE CONTENT AFTER THERMAL PRE-TREATMENT.(FROM PARROTT (127))

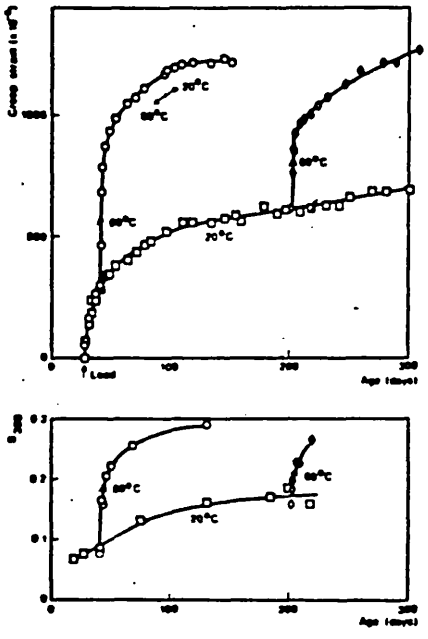

Figure 2.29 - DEVELOPMENT OF CREEP STRAIN AND POLYSILICATE INDEX WITH AGE AND TEMPERATURE,UNDER LOAD.(FROM PARROTT (132))

CHAPTER 3 - APPROACH TO THE PROJECT

3.1. AREAS OF INVESTIGATION

The review of literature indicates that high temperature research on concrete properties in general and creep in particular has suffered from a considerable lack of uniformity, due to the large number of parameters involved. Some of the major differences include methods of curing, durations of pre-heating prior to loading and types of aggregate used in the concrete (4,60,63,84,100,113). Therefore, it was proposed to design this project to be more fundamental in approach, in order that the results would be more general.

It has been well established that creep of concrete is seated in the cement paste, with the aggregate acting as a restraint to movement (117). The paste exercises a dominant role in other properties such as strength and shrinkage as well. Furthermore, when considering the behaviour of concrete at high temperatures, it is clear that its properties would be affected by any thermal instability of the aggregate or weakening of the aggregate-paste bond. Hence, results of tests done on various concretes would be affected by the specific nature of the type of aggregate used. (See Figures 2.2, 2.13, 2.16, 2.17). Therefore, this present programme sought to concentrate largely on establishing the behaviour of hardened cement paste at elevated temperatures. Subsequently, a few tests were carried out on fly-ash replaced pastes and concrete (i.e. OPC paste modified by coarse aggregate) specimens. The aggregate employed was single sized spherical glass marbles. This "idealized" aggregate was used to facilitate numerical modelling carried out at the micromechanical level.

The decision to test unsealed samples was based on a variety of reasons, not the least of which was the availability of experimental facilities. As pointed out in the literature review, a truly sealed test (especially at temperatures in excess of 100°C) would have required triaxial testing facilities at high temperature (14), which were not immediately available, whereas the laboratories already

possessed facilities for testing uniaxial compressive creep at temperatures up to 750°C.

Furthermore, it was felt that much information had yet to be learnt about unsealed uniaxial behaviour, especially since no such programme had been previously undertaken for hardened cement paste over a comprehensive range of temperatures. Another reason for testing unsealed samples was to complement the extensive work done on transient thermal creep for unsealed specimens (84) with basic creep results for unsealed specimens at high temperatures.

3.1.1. Creep

Given that tests were to be carried out on unsealed hardened cement paste, it was clear that a decision had to be made regarding the moisture condition of the specimens at the time of test. Whereas the easiest way to control the moisture condition in a sealed specimen is to maintain it in a saturated condition, the most convenient way to control the moisture condition in an unsealed specimen is to dry it out completely. Hence, where the creep tests were concerned, it was decided to load the specimens after hygral equilibrium at the temperature of interest.

At the same time, given the fact that creep strains are known to be highly sensitive to the nature of the pre-treatment prior to loading (Figure 2.1), it was decided to load the specimens not merely after thermal and hygral equilibrium, but after dimensional equilibrium as well (i.e. after all expansion or shrinkage had ceased). In any case, the only way of ensuring hygral equilibrium (both with respect to moisture loss as well as internal moisture movement) was to assume that such moisture movements were reflected in dimensional changes and to ensure that dimensional equilibrium was achieved. Furthermore, it was felt that dimensional equilibrium would reflect microstructural stabilization, not only of hygral changes but of other chemical reactions as well. This appreciation of the need to wait until dimensional equilibrium prior to loading (in order to measure basic creep) seems to have been ignored by most researchers except one (99), despite the wide recognition that creep results are affected in the

presence of shrinkage (180). Hence, for the purpose of this research programme, the basic creep of unsealed specimens was considered to be the load induced time dependent deformation of a specimen which is loaded while being in thermal, hygral and dimensional equilibrium at a given temperature.

The options for the point of loading are schematically presented in Figure 3.1. Loading at point A, the start of the temperature rise, would result in the measured strains comprising of transient thermal creep (which would include drying creep), shrinkage and expansion. If loading is performed at the end of the temperature rise, i.e. at point B, the measured creep strains would still contain drying creep and shrinkage components. In order for the creep strains to be free of these components, the load must be applied at point D, i.e. at the end of the shrinkage phase, or thereafter. Figure 10.6 shows the difference between the creep responses arising from loading at points A, B and D for a 120°C maximum temperature level. Figure 7.1. shows the differences in the 1-day creep strains for loading at some point C compared to loading at the point D. It also shows that the creep response is the same whether the load is applied at point D, which is the end of the shrinkage phase, or any point E after this time. Hence, loading at point D or thereafter would result in the "lower bound" creep response which has been defined as basic creep; loading at point A would result in the "upper bound" creep response called transient thermal creep. Most of the present study was concerned with the lower bound responses at various temperatures, although a few specimens were loaded at point A to obtain the upper bound responses. The intermediate responses can be interpolated as explained in Section 10.2.

It is convenient to study basic creep by considering its dependence on time, temperature and stress. Since the time function of creep has been fairly well investigated, it was decided to use existing formulae from the literature and check their correlation with the results obtained in this study. The temperature function was considered to have the greatest potential for investigation, a mathematical basis being sought via an activation energy approach. The stress function was not rigorously investigated, due to time

constraints on the experimental programme.

3.1.2. Shrinkage and Thermal Expansion

Since dimensional stability was sought prior to creep loading the specimens, it was possible to measure shrinkage and thermal expansion, and the time dependence thereof. It was also possible to measure the "ultimate" values of the above, as opposed to time-dependent values (c f. Figure 2.11a). Furthermore, since hardened cement paste was used, the strain measurements, both at temperature as well as when cooled back to ambient temperature, were expected to be free from effects of aggregate type and content (c f. Table 2.3).

3.1.3. Strength and Elastic Properties

Modulus of elasticity (both static and dynamic) and residual strength tests were planned as additional tests to be performed on the creep test specimens. Here again, it was felt that the use of hardened cement paste specimens as opposed to concrete would give a clearer indication of the effect of temperature on the properties of the paste itself, especially in pulse velocity measurements.

A separate programme was, however, planned to measure hot strength. It was hoped that these results could be used, not only to get an indication of the way that temperature caused strength variation, but also to interpret the creep results in the light of these strength variations.

3.1.4. Microstructure

It was seen in the literature review that the degree of polymerization both before as well as during time dependent strains could be correlated with these strains. Furthermore, temperature was seen to have a marked effect on the polysilicate content. Since temperature and time-dependent strain are the main foci of the "macro-level" investigations, it was considered that silicate polymerization tests would lead to the most suitable characterization

or description of the microstructure. Hence, it was decided to conduct a series of tests, concurrent with the creep tests, in order to establish the effects of temperature and load on the degree of polymerization of the cement paste. Although a significant correlation has been demonstrated between polysilicate formation and load and temperature application for sealed, saturated specimens of hardened cement paste (43, 128), no such work has been carried out to date on unsealed specimens.

Another aspect of the "micro-level" investigations was the limited amount of Scanning Electron Microscopy which was performed to explain certain phenomena described in Chapters 5 and 6.

An attempt was also made to model numerically the internal stresses and overall strains set up during the heating of an idealized two-phase material, the results being compared with experiments performed on the "idealized" concrete.

3.2. EXPERIMENTAL PROGRAMME

The experimental programme consisted of Test Series I-VIII as indicated in Table 3.1. Most of the testing was performed on the creep rigs, since time dependent strains in general and basic creep in particular were the main phenomena investigated.

3.2.1. Basic Creep Tests

The detailed programme of testing is described in Table 3.2. Since it was felt that the temperature function should be investigated as thoroughly as possible, the approach adopted was to reduce the temperature intervals as far as possible, with fewer replicates at each temperature, rather than spacing out the temperature intervals for the sake of increasing the number of replicates. This approach ensured that temperatures of interest were not "missed out"; it was also considered a better approach for the purpose of establishing a trend. Furthermore, the performance of the apparatus, as measured by the proving tests described in Section 4.4 and the analysis of differences

between replicates (Section 7.1) justified the validity of this approach. The need to "economize" on the number of specimens per condition, and indeed the necessity to omit testing the stress function, arose due to the unexpected delay for specimens to reach dimensional stability, especially at the lower temperatures. (See Section 6.1).

The parameters involved in the basic creep tests are described below. While some of these were kept unchanged throughout the investigation, others were changed, to a greater or lesser degree.

The following parameters were kept unchanged throughout the investigation.

(a) Curing

Although eleven batches of specimens were cast, the method of curing was kept identical throughout the test programme. After casting, specimens were kept in a humidity room at 100% RH and 20°C. They were demoulded after one day and continued to be stored in the humidity room for a total of 14 weeks, after which their ends were ground and then allowed to air dry (i.e. at around 60% RH and 20°C). See (f).

(b) Specimen Size

It has been suggested that the creep response of concrete at temperature is a function of specimen size (60). This was not investigated however, all the specimens being cast to a standard size of nominal dimensions 62.5 mm ϕ x 187.5 mm. The diameter was kept as small as possible to avoid the build up of large thermal gradients during heating or cooling (84), but was not allowed to be smaller than around 5 times the maximum size of aggregate used (141). The length was chosen to give a height to diameter ratio sufficient to ensure uniaxial compressive loading in the middle of the specimen.

(c) Rates of Heating and Cooling

The rates of heating and cooling would also govern thermal

and moisture gradients, and hence stress gradients set up within the specimen. Previous research performed at Imperial College had established that reducing this rate below 1°C/min. was unnecessary (84). Hence, during this test programme, all specimens were heated and cooled at approximately 1°C/min.; when cooling was done to bring a specimen from a pre-heat to a test temperature, this was carried out at $^1/_2$°C/min.

The following parameters were kept constant for most of the test programme, changes being made to investigate specific points of interest.

(d) Water/Cement Ratio

A water/cement ratio of 0.3 by weight was used for the hardened cement paste specimens. An increase of this ratio would have caused bleeding and segregation, leading to non-uniform specimens (141); a decrease of this ratio would have caused difficulty in mixing. However, a few specimens employing water/cement ratios of 0.225 and 0.375 were tested. These served to check whether critical temperatures for paste behaviour were influenced by the water/cement ratio of the mix. Where the fly-ash mixes and the concrete were concerned, the ratio of water to binding material (i.e. cement and fly-ash) was maintained at 0.3.

(e) Strength

A few references in the literature claim that creep response at temperature cannot be normalized with respect to a stress/cold strength ratio alone, but is a function of cold strength as well (60, 176). No attempt was made to make a detailed investigation regarding this in the present programme. However, the variation of water/cement ratio for hardened cement paste specimens provided the opportunity to investigate this parameter in a limited way.

(f) Age

For most of the test programme, the age at loading was

between 14 and 28 weeks, during which period the specimens were drying in air. It was expected that additional hydration and strength gain would be minimal during this drying period, especially after the specimens had been cured at 100% RH and 20°C for the first 14 weeks. (This was confirmed as indicated in Section 3.3). The change in the degree of silicate polymerization during this period of 14–28 weeks was not expected to be very large either. (This was confirmed as described in Section 9.3). The ages of specimens used for different series of tests are given in Table 3.1.

(g) Stress/Strength Ratio

The creep response was studied on the basis of normalizing creep with respect to the stress/cold strength ratio. This technique had been used previously and had proved to be both useful and informative (62, 84). Most of the tests were performed at a stress/cold strength ratio of 0.11.

(h) Duration of Loading

In most of the creep tests, the duration of loading was 7 days. This period is short when compared to creep tests performed at ambient temperatures, but long when compared to some high temperature creep tests reported in the literature (4, 60). The period of 7 days was chosen as a compromise. On the one hand, it was a period that would have accounted for a significant proportion of the total creep (63), and one within which the trend of the creep behaviour was expected to be recognizable; on the other hand, it was a period short enough to have enabled a satisfactory number of tests to be performed. However, a few tests were performed for a longer period of around 6 weeks, in order to confirm the time function for creep.

The following parameters were the main variables in the test programme.

(i) Duration of Heating

As explained in Section 3.1, the specimens were maintained at

a given temperature until dimensional stability was achieved. This resulted in different specimens (at different temperatures) being heated for unequal periods of time, since dimensional stability was achieved in different durations of time at different temperatures. This was unavoidable, in order to perform as many tests as possible. However, the programme of testing established that the creep response of a specimen was not affected by any additional heating beyond the point of achieving dimensional stability. (See Section 7.1).

(j) Pre-heat Temperature

The range of temperatures investigated was 20°C-725°C, the lower limit being the average room temperature, and the upper limit being the temperature at which hydraulically bound cement paste would have lost most of its binding capacity. Temperatures around 400°C, at which Calcium hydroxide begins to dissociate (61), and 600°C, at which it was suspected that there would be a sudden change in creep behaviour (85), were more carefully investigated. The various temperatures used in the investigation are given in Table 3.2.

(k) Test Temperature

In most cases, specimens were loaded at temperatures to which they were heated. However, some tests were carried out after cooling to lower temperatures. The schedule for this series of tests is given in Table 3.2. Each pair of pre-heat and test temperatures were chosen to span ranges of temperatures of interest. This procedure of heating to a given pre-heat temperature and then cooling to different test temperatures was employed, among other things, to satisfy the conditions under which activation energy analyses could be performed - i.e. it enabled test specimens at different temperatures to have the same initial structure, on account of being pre-heated to the same upper temperature. These considerations are further elaborated in Section 8.2.

3.2.2. Silicate Polymerization Tests

Although the main part of this project was concerned with

investigations at the phenomenological or macro level, some experimentation was undertaken at the microstructural level, both to supplement as well as to perhaps explain certain observations at the macro level. It must be mentioned that these investigations were not as well planned as the macro-level experiments, since they were envisaged only mid-way in the project. However, some valuable information regarding high temperature behaviour of cement paste was obtained even with the limited amount of experimentation performed.

Most of the investigators quoted in the literature review in Section 2.4.3 performed their thermal treatments under saturated specimen conditions, the temperatures not exceeding 95°C. In many of the cases, the loading was applied under saturated conditions as well. Furthermore, the same saturated conditions were maintained, in most cases, for the polymerization tests.

The situation in the present investigation was somewhat different. In the first instance, the macro-level investigations concerned unsealed specimens which were either dried to dimensional stability prior to creep loading at given temperatures or heated under load to desired temperature levels. Since the polysilicate tests were performed either on these specimens or others subjected to similar heat treatments, saturated conditions were not maintained. The implications of this moisture loss will be discussed later in Section 9.2. Furthermore, most of the temperature range of interest lay above 100°C, for which range quantitative polysilicate testing has not previously been done, although Piasta et al (138) noted some qualitative trends using infra red absorption.

The programme of testing is shown in Table 3.3. An attempt has been made to concentrate on temperature treatments below 100°C (i.e. 50°C and 90°C) and one just above (i.e. 120°C), in order to make comparisons with the results of other researchers. However, as stated previously, the limited planning of these experiments led to the following drawbacks.

(a) The number of temperature points at which pre-treatment was done was limited.

(b) Only a few Series I and II specimens were tested for degree of polymerization.

(c) The ages of specimens varied from 15 to 40 weeks, being at 100% RH for 14 weeks after casting and air dried at around 60% RH thereafter. However, the effect of age upon polysilicate content was determined and found not to be significant. (See Section 9.3).

3.2.3. Other Tests

The detailed programme of testing for Series III and VI specimens is given in Table 3.4. The Series III specimens were all loaded to a stress/cold strength ratio of 0.11 prior to heating to the specified temperature. The tests on the Series IV specimens, i.e. the "idealized" concrete specimens, are described in Chapter 10.

The Series VI specimens were tested in a jacket furnace on an Amsler compression testing machine. Most of the specimens were crushed at the maximum temperature. Two specimens, however, which were heated to 460°C, were crushed after slow cooling to 410°C and 310°C respectively.

The scanning electron microscopy was performed on a few selected specimens using a JEOL JSM 35-CF Scanning Electron Microscope at an accelerating voltage of 20 kV. The various conditions to which these specimens were exposed to are described in Chapter 9. Back scattered electron images of polished surfaces and secondary electron images of fracture surfaces were obtained.

3.3. MATERIALS

3.3.1. Mix Details and Specimen Size

Although a total of 7 different mixes were used in this investigation (see Table 3.5), most of the testing was performed on a single mix - i.e. OPC paste with w/c = 0.3 (Mix Code A). Mixes B and C were used to investigate the effects of changing the w/c ratio;

mixes X, Y and Z were used to study the effects of cement replacement with pulverized fuel ash. Only one "concrete" mix was used - an "idealized" two phase concrete consisting of roughened single sized glass spheres (of nominal dia. 12 mm) in an OPC paste matrix.

The specimens used in the creep rigs were cylindrical in shape with nominal dimensions 62.5 mm ϕ x 187.5 mm. The diameter was kept small enough to reduce to tolerable limits, the thermal and stress gradients during heating and cooling at 1°C/min. (84); on the other hand, it was large enough to accommodate a maximum aggregate size of 12 mm without causing too much inhomogeneity (141). The nominal length to diameter ratio of 3 was considered sufficient to ensure uniaxial compressive loading in the middle of the specimen.

3.3.2. Casting and Curing

Nine batches (consisting of 18 cylinders and 12 no. 2 inch cubes) of Mix A were cast during the project, the casting being spread out over the duration of the project so that the age of specimens at any given time of testing could be kept at 14-28 weeks. The casting was done at the Concrete Laboratories of the Central Electricity Generating Board (C.E.G.B.) at Leatherhead. A Benton Creteangle pan mixer (of capacity 14 litres) was used for mixing, and the cylinders cast in 3 layers while being compacted on a vibrating table. Vibration was carried out until most of the entrapped air was removed, care being taken, however, to prevent bleeding. Steel moulds were used to cast the cubes while split plastic moulds tightened with jubilee clips were used to cast the cylinders. A few cylinders in some batches had thermocouples embedded in them at intervals along their axes, while others had studs cast in at both ends, in order to monitor subsequent shrinkage in air.

The specimens were then stored in a humidity room at 100% RH and 20°C. Temperature readings from the embedded thermocouples indicated that the average cylinder temperature rose to a maximum of 47°C around $6^{1}/_{2}$ hrs after casting. This is the order of temperature rise that a large pour of concrete would be subjected to in practice. Twenty four hours after casting, the specimens were demoulded, weighed,

marked up and returned to the humidity room. The cubes were removed from the humidity room and crushed at 7, 28 and 98 days after casting.

The cylinders were kept in the humidity room for a period close to 14 weeks and then transported to the Imperial College laboratories in a humidity box. They were kept moist while their ends were ground plane and perpendicular to their axes. After this, at an age of 14 weeks, they were placed in laboratory conditions, which averaged around 60% RH and 20°C through a year. The shrinkage of specimens having studs cast into them was monitored periodically. The cylinder strength was also checked at ages of 14 and 28 weeks. The rest of the cylinders were used for the experimental programme, between the ages of 14 and 28 weeks.

The mixes B, C, X, Y and Z had only a few specimens each and hence were cast at the Imperial College laboratories using a small table mixer and a vibrating table. Subsequent curing however, was carried out in identical fashion to Mix A, at the C.E.G.B. laboratories.

Where the idealized concrete mix, λ_{1}^{CN} was concerned, commercially available glass marbles (i.e. soda-glass spheres) of diameter 12.5 mm were used as the single sized aggregate. These were roughened in a ball mill using Carborundum powder of grade 100. The roughened spheres were assumed to have a nominal diameter of 12 mm and the concrete mix designed to give an aggregate volume content of 50%. The water absorption of the spheres was found to be zero and the specific gravity 2.5. The mixing was done on the Creteangle pan mixer at the C.E.G.B. laboratories. Since the w/c ratio of the paste was kept at 0.3, in order to avoid problems with low workability, the water was first mixed with the cement, and the marbles gradually added into the paste. Vibrating, curing, grinding and air drying procedures were identical to those of Mix A.

3.3.3. Strength Development

The development of cube strength for Mix A is indicated in Figure 3.2. The 28-day strength was 86% of the strength at 14 weeks,

by which time it was expected that strength development would be negligibly small. This was borne out by the strength tests performed on cylinders, which did not show any significant change in strength during the 14 to 28 week period of air drying (Figure 3.3). A single cylinder tested at 46 weeks also indicated that strength gain in air after 14 weeks of curing was negligible, if non-existent. Hence, any specimen from any batch tested while being air dried beyond 14 weeks (and especially between the ages of 14 and 28 weeks) could be considered to have a strength of 99 N/mm^2.

It may be noted that the brittleness of the hardened cement paste has caused a fair (although not unreasonable) degree of scatter in strength results; furthermore, it has resulted in the fairly high ratio of cylinder to cube strength of 0.95 (at an age of 14 weeks).

The strength development of mixes B, C, X, Y, Z and CN are indicated in Figure 3.4.

3.3.4. Shrinkage in Air

The shrinkage of hardened cement paste specimens in air was monitored on selected specimens having studs cast into their ends. Three specimens per batch were used for 2 batches. Weight changes were noted simultaneously. The fitted linear relationship ($r^2 = 0.97$) between shrinkage and weight loss indicated in Figure 3.5 was taken as representative for all hardened cement paste specimens. It must be remembered, however, that the length change between the ends of the studs is a combination of shrinkage and induced strain, set up as a result of radial moisture gradients (73). The actual shrinkage can be measured only if and when dimensional stability is reached.

3.4. EXPERIMENTAL PROCEDURES

3.4.1. Creep Rig Tests

Although these tests, which formed the bulk of the project, are described here, the apparatus referred to is not described until the following chapter.

All specimens were weighed and measured prior to testing. These weights were used to determine the amount of shrinkage undergone since air drying, by using the regression line in Figure 3.5, and also to calculate the weight loss percentages. A PUNDIT Ultrasonic pulse velocity tester was used to determine the pulse velocity and hence dynamic modulus of elasticity of the specimens before they were transferred to the creep rigs.

The specimens were placed between the end platens after ensuring that the faces of both the specimen as well as the platens were clean and free from grit. Three thermocouples were attached to the top, middle and bottom, longitudinally along the specimen surface, using a ceramic binder. After the sliding furnace was lifted into place, any spaces between the covers and the furnace wall were plugged with ceramic wool to reduce heat losses and hence thermal gradients within the furnace.

The specimens were "bedded down" by cycled loading and then tested for static modulus of elasticity. After this, the load was removed and the specimens heated at 1°C/min. until the desired temperature. In the Series III tests, the specimens were heated under load and maintained at temperature for the desired period of creep measurement. Where the other test series were concerned, the specimens were kept at maximum temperature until dimensional stability was achieved. Where it was not possible to achieve complete stability, a deformation of 30 $\mu\epsilon$/day was considered small enough to assume stability. In this phase, strains were recorded at 10 minute intervals during the first day, which included the temperature rise period, and at 4 hourly intervals thereafter. After achieving dimensional stability at the pre-heat temperature, the Series II specimens were cooled at $^1/_2$°C/min to the desired test temperature and again allowed to stabilize dimensionally.

The specimens were then loaded to the required load level in steps of 57.5 kg weights acting via the 1:15 lever arm of the creep rig and strains recorded at every 10 second step for the determination of the static elastic modulus. Subsequently, strains were recorded at 10 second intervals for the first 5 minutes, 5 minute intervals for the

first day and 4 hourly intervals thereafter. In most cases, basic creep tests were conducted for 7 days' duration. However, three specimens were tested for 40 days and a few specimens for just 1 day.

After the period of creep testing, the specimens were cooled back to room temperature while under load at a rate of approximately 1°C/min. They were tested for static modulus of elasticity while in the rig and after removal from the rig, for dynamic modulus of elasticity. The weights and dimensions were recorded as well. Some of the specimens were crushed in a Contest compression testing machine to determine residual strength while others were exposed to the atmosphere to observe post-cooled behaviour.

The temperature and load applications for Test Series I, II and III are schematically depicted in Figure 3.6.

3.4.2. Hot Strength Tests

An Amsler compression testing machine of capacity 30 tons was used to crush the cylinders for the hot strength tests. The loading rate employed was 49 $N/mm^2/min$, which was identical to that used in determining cylinder cold strength. An insulated furnace was used to house the specimen between the platens of the testing machine. (See Figure 3.7). In order to protect the machine platens from the high temperatures within the furnace, the specimen was crushed between 2 square steel platens, located within the furnace and separated from the machine platens by Sindanyo spacers. A perforated metal cage surrounding the specimen within the furnace served to protect the furnace lining during the specimen failures, which were often brittle and explosive. A single hinged door (itself provided with insulated heating elements) provided access into the furnace cavity. The furnace could, however, be separated along a vertical plane into 'front' and 'rear' portions.

The power to the furnace was supplied via a Eurotherm temperature controller which had a Pt/Pt-Rh control thermocouple and a Chromel-Alumel cut-off thermocouple. It was able to generate a uniform ramp signal with respect to control thermocouple voltage up to

a desired maximum temperature; a cut-off temperature could also be pre-set, as a safety measure. The thermoucouples were placed in cavities extending into the walls of the furnace. Since the control thermocouple voltage output was not strictly linear with temperature, it was not easy to maintain a uniform temperature rise (as opposed to voltage rise). Hence, it was sought to err on the slower side and maintain the rate of heating below 1°C/min. at all times. Where the test temperature was lower than a pre-heat temperature, it was not possible to control the rate of cooling. However, this did not exceed $^{1}/_{2}$°C/min.

Three Chromel-Alumel thermocouples attached to the top, middle and bottom of the specimen surface and passing through an aperture in the side wall of the furnace were connected to a Solatron data logger and used to monitor the temperature of the specimen. The logitudinal thermal gradients along the specimen were somewhat greater than those experienced in the creep rigs, the maximum being around 3°C/cm.

The specimens used for the hot strength tests were somewhat greater in age than those used in the creep rigs, being tested at ages between 41 and 52 weeks. This was not however, expected to make any significant difference, the strength development being virtually stable by 14 weeks. (See Figure 3.3).

Time constraints did not permit the heating of these specimens, prior to testing, for the kind of durations employed in the basic creep tests. However, here again the evidence from the literature is that the effect of duration at temperature on strength is minimal, especially at temperatures above 250°C. Hence it was decided to crush the specimens after periods of 3 days' heating in the temperature range 300-700°C and 4 days' heating in the temperature range 50°C-215°C. The specimens pre-heated to 460°C were cooled to 410°C and 310°C respectively on the 3rd day after heating and crushed on the following day. Another consequece of time constraints was that only one specimen per condition was tested. However, since fairly close temperature intervals were employed, it was expected that the results would be able to indicate significant trends.

The furnace and temperature controller used in this series of tests were kindly supplied by the Central Electricity Research Laboratories in Leatherhead.

3.4.3. Silicate Polymerization Tests

(a) Determination of Polysilicate Content

The methods used by investigators for the quantitative determination of polysilicate fall into two main categories. The first method, which was used by Lentz (93), and later in a modified form by Bentur et al (22) consists in first converting the silicates in the sample into silicic acid, using hydrochloric acid according to

$$SiO^{4-}_4 + 4HCl \rightarrow H_4SiO_4 + 4Cl^-$$

The silicic acid produced is unstable and will condense into higher degrees of polymerization unless it is "end blocked" with a trimethylsilyl compound to form a stable product according to

$$H_4SiO_4 + 4Me_3SiCl \rightarrow (Me_3Si)_4SiO_4 + 4HCl$$

The resulting compounds should contain silicates having the same degree of condensation as the original material. These compounds are recovered and analysed, usually by gas chromatography, to determine the different degrees of condensation and their relative amounts in the original sample.

The second method, outlined in detail by Funk and Frydrich (55), also first converts the silicates into silicic acids. A paramolybdate solution is then added, which reacts with the silicic acid present according to

$$H_4SiO_4 + {}^{12}/_7\ Mo_7O_{24}^{-6} + {}^{72}/_7\ H^+ \rightarrow H_4SiMo_{12}O_{40} + {}^{36}/_7\ H_2O$$

The method is based on the fact that the rate of reaction with the paramolybdate is dependent on the degree of condensation of the silicic acids, a lower degree of condensation giving a faster rate of reaction and vice versa. Monitoring the rate of reaction allows an estimate of

the relative proportion of low to high molecular weight silicate species to be made. Funk and Frydrich used a titration method to follow the reaction. Other researchers such as Parrott (134) and Day (40) have simplified the procedure by using a spectrophotometer to monitor the colour change involved in the paramolybdate-silicic acid reaction.

The first method has the advantage of being able to distinguish between the different silicate species and their relative amounts, whereas the second method can only give an indication of the degree of polymerization, lumping the amount of polysilicate as well as the length of silicate chain into a single index. However, since such an index seems to be all that is required for correlation with time-dependent strain behaviour and since the method is much simpler to carry out, especially if the reaction is monitored by a spectrophotometer, it was decided to use this second method in the current investigation.

(b) Experimental Details

Where the pre-treatments involved loading, a small portion from the middle of the Series I, II or III specimens was taken for the polysilicate tests, after they had been compression tested to determine residual strength. Where the pre-treatments involved only heating, miniature cylindrical specimens of 10 mm dia. x 40 mm, cast in a specially manufactured mould were used. These were cured and air dried under the same conditions as the creep specimens, and were heated in the same creep rig furnaces at the same rates of heating.

The samples were ground and the portion passing a 150 μ sieve taken for the subsequent testing. After being cooled in the furnace, the samples were stored in a desiccator until the polysilicate testing. This meant that any rehydration due to atmospheric moisture would have been largely eliminated, although the same could not be said regarding carbonation from atmospheric carbon-dioxide. However, tests done on samples at different time intervals showed excellent replication and it was concluded that any effect of carbonation on the polysilicate measurements was negligible.

The reagents and procedures for the testing was virtually identical to those used by Parrott and Taylor (134). Samples were dissolved in methanolic HCl, which was prepared by mixing 16 ml of conc. HCl (S.G. 1.16) in methanol and making up the solution to a litre. It has been shown that silicic acid is much more soluble in methanolic HCl than in aqueous HCl and also that undesirable condensation is much slower in methanol than in water (55); furthermore, the use of the methanolic reagent also eliminated the possibility of any rehydration in these pre-dried samples. The complexing agent was a 10% solution of Ammonium paramolybdate.

A portion of around 100 mg of the ground sample was dissolved in a beaker containing 100 ml of the methanolic HCl, being stirred vigorously for exactly one minute, while being maintained in a water bath at a temperature of 25°C. This one minute period was pointed out by Funk and Fridrich (55) as being the maximum time within which the silicate should be dissolved, in order to obtain defined and uniform silicic acids in solution. The contents of the beaker were quickly filtered through a fast action filter paper until around 25 ml of filtrate was obtained. The filtration took around 15 seconds to perform.

Meanwhile, a beaker serving as the reaction vessel had been prepared and kept in the same 25°C water bath. The medium for the reaction was essentially 170 ml of distilled water acidified by a few drops of conc. HCl to a pH of 1.6. The complexing reaction would result in the formation of α-molybdosilicic acid, β-molybdosilicic acid or a mixture of the two, depending on the pH value of the reactants. In order to obtain a linear response of spectrophotometer absorbance with time for a single silicate species, it is necessary to ensure that only one type of acid is produced. Truesdale and Smith (172) found that α- and β- forms of the acid are produced in isolation only in the pH ranges 3.8 to 4.8 and 1.0 to 1.8 respectively. They also found that the time required to attain maximum absorbance varied with pH but was constant in the pH ranges 1.6 to 3.0 and 3.8 to 4.2. Hence the two feasible pH ranges that could be used were 1.6 to 1.8 for obtaining β-molybdosilicic acid and 3.8 to 4.2 for obtaining α-molybdosilicic acid. The former range was chosen because β-molybdosilicic acid has a

higher absorbance of incident light/mole than α-molybdosilicic acid, thus making the spectrophotometer results more sensitive to the extent of complexing.

10 ml of the 10% paramolybdate solution was added to the above-mentioned reaction medium. Into this solution was added 20 ml of the filtrate containing the dissolved silicates, and a stop clock activated to follow the rate of reaction. It has been found (134) that condensation beyond formation of dimer would be insignificant during the approximately 2 minute period between the start of dissolution of silicate and the start of the complexing reaction.

The complexing reaction was followed using a 10 mm cell in a Cecil Instruments CE 393 Digital Spectrophotometer set at 410 nm. A view of the experimental set up is given in Figure 3.8. Readings were taken at 5 minute intervals from the start of the complexing reaction for a duration of 35 minutes. At each stage, the reading given by the solution drawn from the reaction vessel was compared against a reading given by distilled water in an identical 10 mm cell. At various times in the test programme, absorbence readings were taken of the reaction vessel solution without dissolved silica - i.e. a solution of 170 ml distilled water acidified to pH 1.6, 10 ml of 10% ammonium paramolybdate solution and 20 ml methanolic HCl. The average reading for the absorbence of this solution was 0.008 units on the spectrophotometer. This value was subtracted from all measurements taken.

Before commencing these experiments, anhydrous Portland Cement samples of differing weights, which would contain only the monosilicate phase, were dissolved in methanolic HCl and the above procedure carried out in order to check the linearity of spectrophotometer absorbence values with weight of sample. The absorbence readings, taken at 300 seconds after the start of complexing, are shown in Figure 3.9. The response can be considered linear up to around 0.45 units, fairly linear up to around 0.6 units, but non-linear around 0.9 units. Hence the weights of subsequent samples were adjusted such that the silicate in solution produced maximum absorbence readings which were around 0.45 units or slightly above, in order both to preserve linearity as well as to maximize sensitivity.

Test Series	Apparatus	Material	Description
I	Creep Rig	hcp, w/c = 0.3	Shrinkage and Basic Creep etc. in temp. range 20-670°C at stress/cold str. = 0.11 Age 14-28 wks
II	Creep Rig	hcp, w/c = 0.3	Shrinkage and Basic Creep etc. in temp. range 20-635°C of pre-heated specimens at stress/cold strength = 0.11 Age 14-28 wks
III	Creep Rig	hcp, w/c = 0.3	Transitional thermal creep in temp. range 50-300°C at stress/cold strength = 0.11. Age 14-40 wks. (See Ch. 10)
IV	Creep Rig	Idealized Concrete w/c = 0.3 Agg vol = 50%	Shrinkage and thermal strain in temp. range 50-300°C. Age 14-28 wks. (See Ch. 10)
V - A V - B	Creep Rig	hcp, w/c =0.225 and 0.375 hcp + pfa(w/s=0.3)	Shrinkage and Basic Creep etc. in temperature range 525-725°C. Age 14-28 wks.
VI	Jacket Furnace and Amsler	hcp, w/c = 0.3	Hot strength tests, corresponding to Series I and II (See Ch. 5). Age 40-52 wks.
VII	Spectrophotometer	hcp, w/c = 0.3	Degree of polymerization, corresponding to Series I, II and III (See Ch. 9).
VIII	Scanning Electron Microscope	hcp hcp + pfa	Polished and fracture surface studies to possibly explain some shrinkage and strength phenomena. (See Ch. 9).

TABLE 3.1. OVERALL EXPERIMENTAL PROGRAMME.

Test Series	Varying Parameter		Preheat Temperature (°C)																			
			20	35	50	70	90	120	150	200	300	375	400	425	460	500	525	560	600	635	670	725
I	Stress/cold strength	0.11	2		1	1	1	1	1	2	2(*)	1	2	2	2(*)	2	1	2(*)	2	1	1	
II	Test Temperature (°C)	600																		1		
		560																		1		
		525																		1		
		~~500~~																1				
		460																1		2		
		~~325~~													1			1				
		300													1	1		1		2		
		200									1				1							
		120									1									1		
		90						1														
		70						1														
		50				1		1			1									1		
		35				1																
V-A	w/c	0.225															1		1			
		0.375																		1		1
V-B	% PFA (w/w)	10																	1			
		25																	1			
		40																	1			

Note (*) - Includes a long-term test.

TABLE 3.2. EXPERIMENTAL PROGRAMME FOR TEST SERIES I, II AND V.

Maximum Temp. (°C)	20	50	90	120	120	120	300	300	460	460	560	635	635
Test Temp. (°C)	20	50	90	50	90	120	120	300	300	460	560	600	635
Unloaded	8[1]	3	3			3		3		3	3		3
Loaded after heating (Series I and II)				2	1		1	2	2	1		1	
Loaded during heating (Series III)		3	3			3		3					

Note:- (1) 2 specimens each tested at ages of 15, 21, 29 and 37 weeks.

(2) Unloaded specimens are of size 10 mm ϕ x 40 mm; loaded specimens are of size 62.5 mm ϕ x 187.5 mm.

(3) Load level applied corresponds to a stress/cold strength of 0.11.

TABLE 3.3. EXPERIMENTAL PROGRAMME FOR TEST SERIES VII.

Test Series	Varying Parameter		Maximum Temperature (°C)												
			50	90	120	150	200	300	350	400	460	500	560	600	700
III			1	1	1		1	1							
VI	Test Temperature (°C)	700													1
		600												1	
		560											1		
		500										1			
		460									1				
		400								1	1				
		350							1						
		300						1			1				
		200					1								
		150				1									
		120			1										
		90		1											
		50	1												

TABLE 3.4. EXPERIMENTAL PROGRAMME FOR TEST SERIES III and VI.

Mix Code	A	B	C	X	Y	Z	CN
Cement	1.0	1.0	1.0	0.90	0.75	0.60	1.0
P.F.A.	-	-	-	0.10	0.25	0.40	-
Aggregate	-	-	-	-	-	-	1.435
Water	0.3	0.225	0.375	0.3	0.3	0.3	0.3
P.F.A. Content ($^{W}/_{w}$) %	-	-	-	10	25	40	-
Water/blend ratio	0.3	0.225	0.375	0.3	0.3	0.3	0.3
Agg./cement ratio	-	-	-	-	-	-	1.435
Agg. S.G. (SSD)	-	-	-	-	-	-	2.5
Agg. Content ($^{V}/_{v}$) %	-	-	-	-	-	-	50
Slump (mm)	-	-	-	-	-	-	100
Cube Str (N/mm^2) 7 day	74.5						
28 day	89.9			89.9	75.8	60.1	78.1
98 day	105.1	113.2	66.8	102.2	95.9	89.6	86.8
Cylinder Str. (N/mm^2) 98 day	99.4	118.9 (*)	68.1 (*)	101.1 (*)	101.0 (*)	86.8 (*)	27.7 (*)

Note (*) - Not very reliable, since only one specimen used.

TABLE 3.5. MIX DETAILS.

Fig.3.1 – LOADING CONDITIONS FOR CREEP TESTS

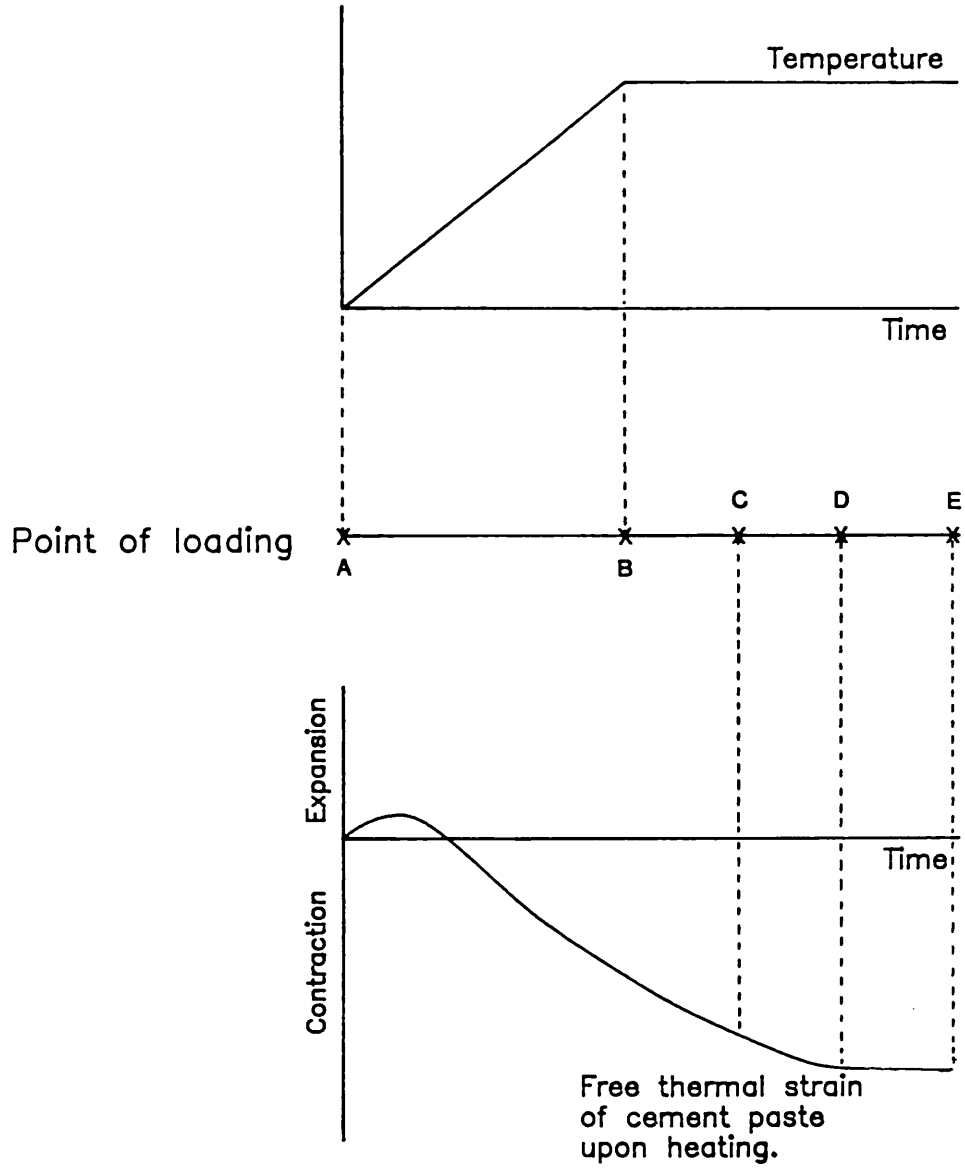

Fig.3.2 – DEVELOPMENT OF CUBE STRENGTH – MIX A (OPC w/c=0.3)

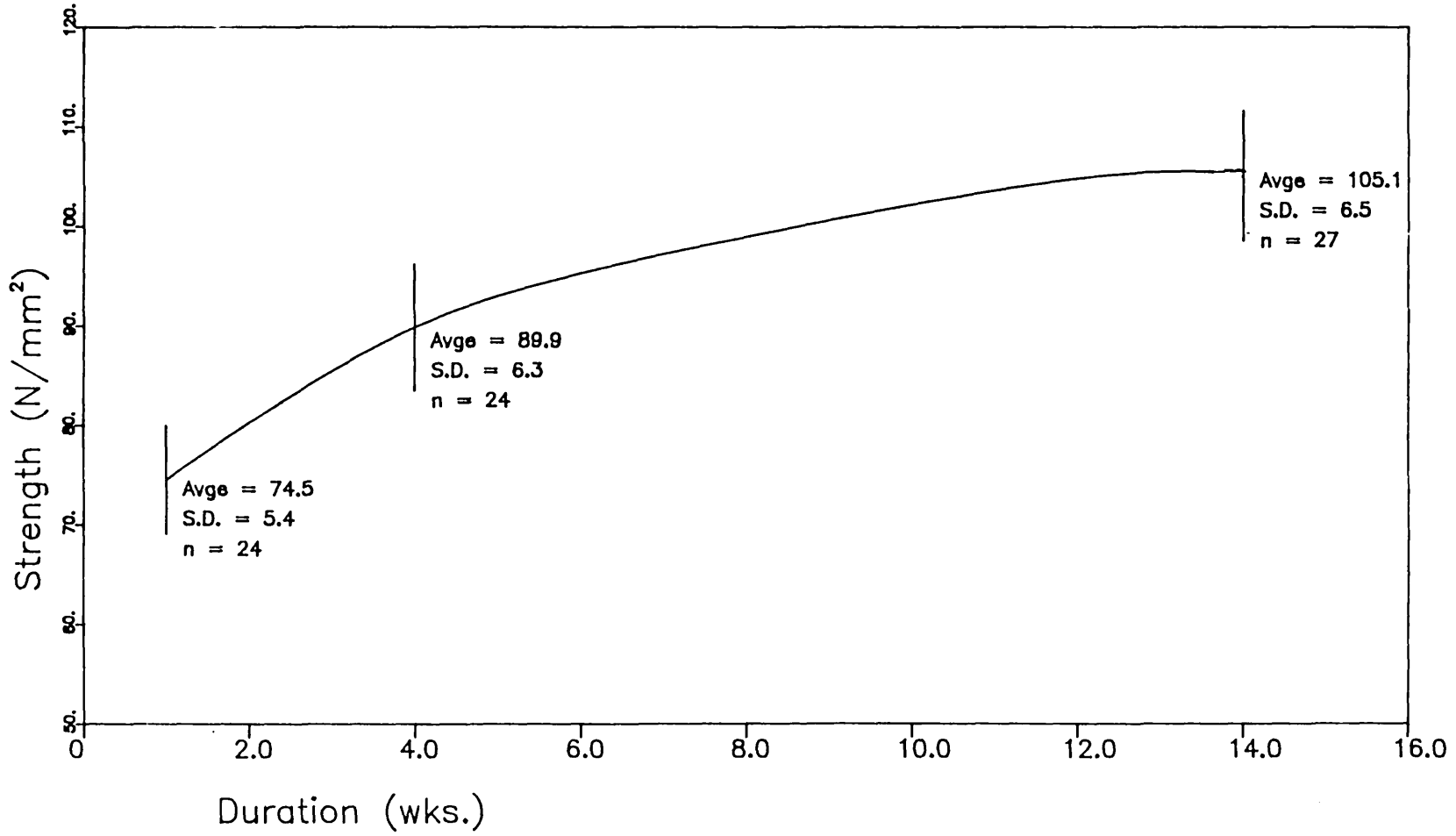

Fig.3.3 – CYLINDER STRENGTHS – MIX A (OPC w/c=0.3)

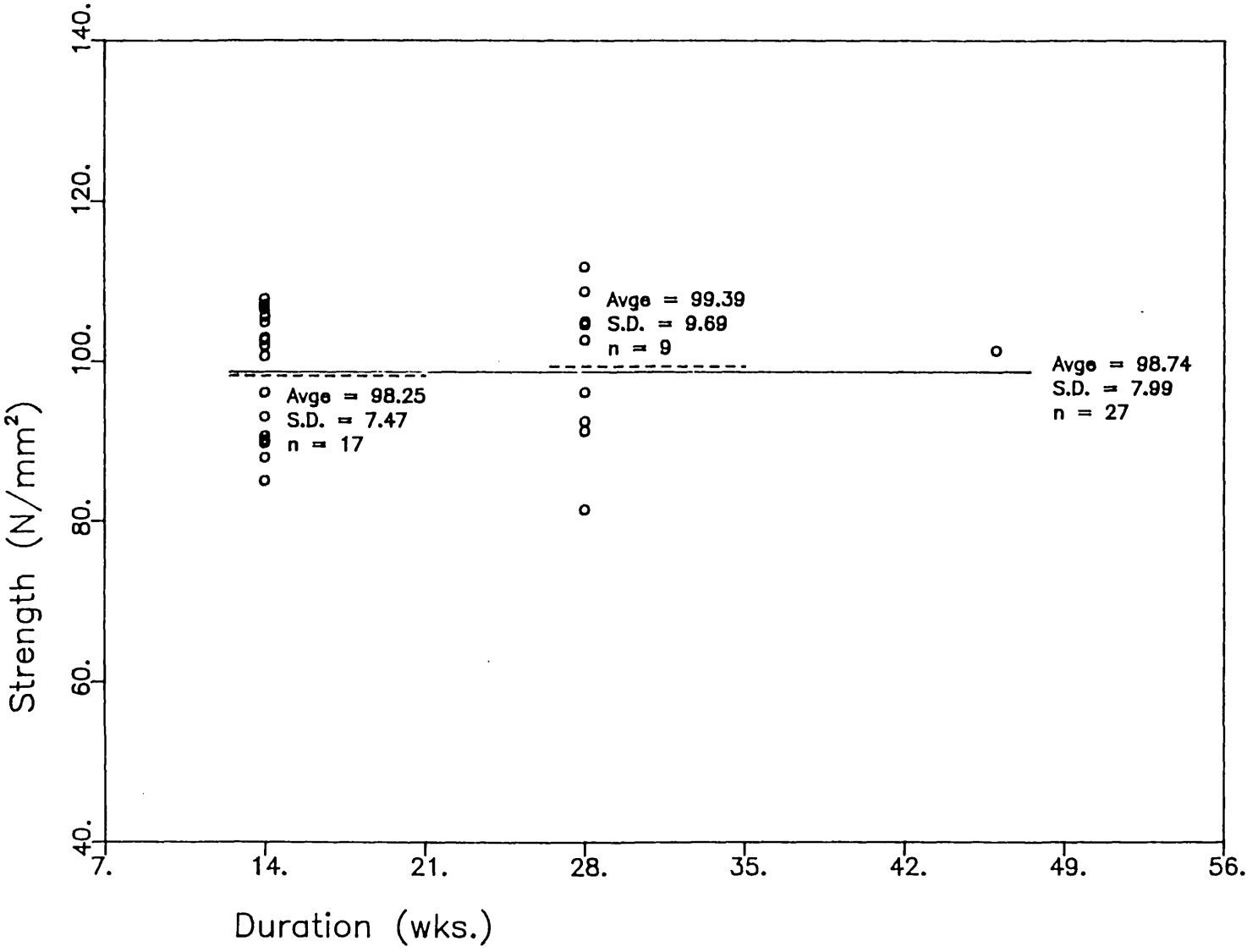

Fig.3.4 – CUBE STRENGTHS – VARIOUS MIXES

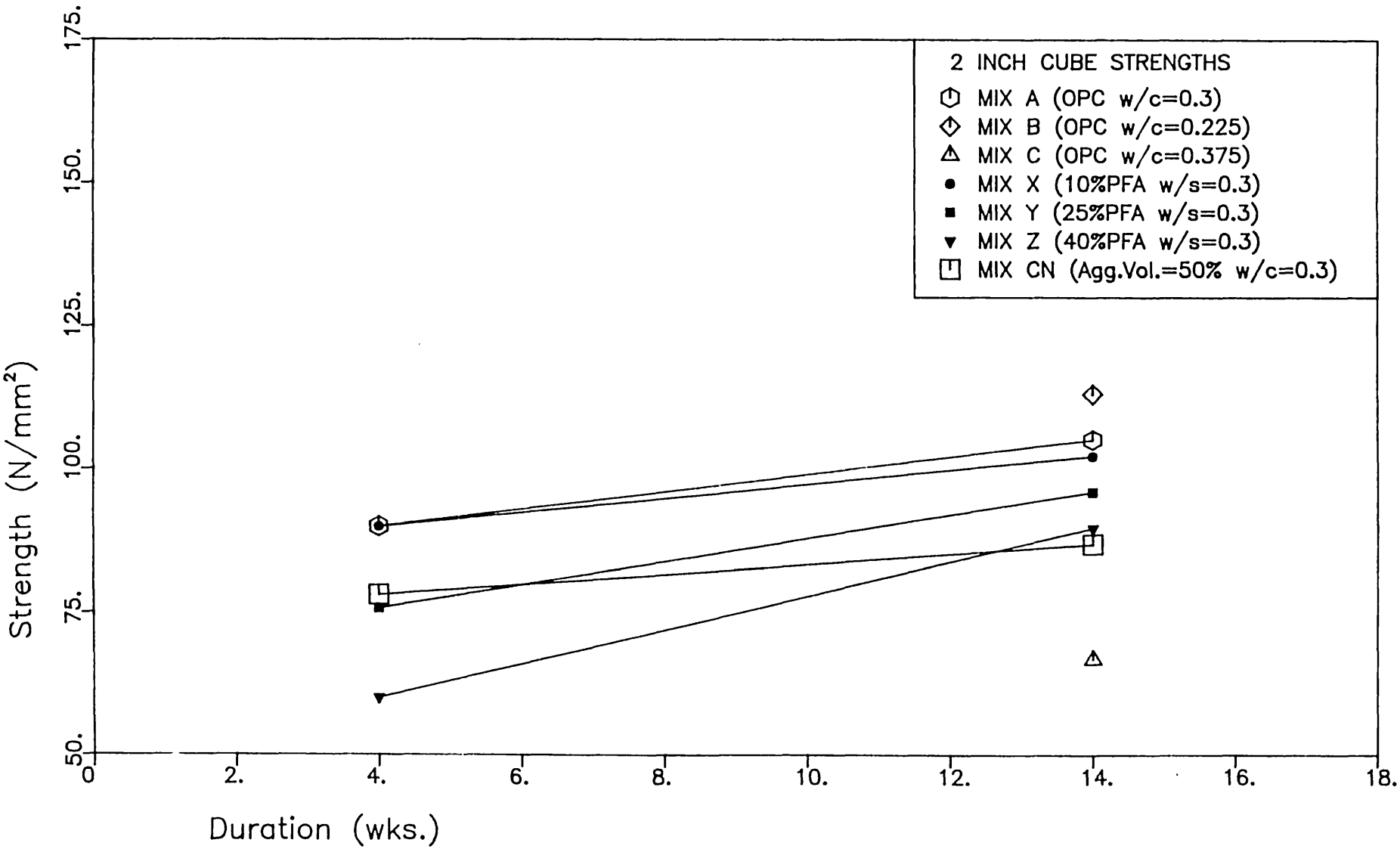

Fig.3.5 – SHRINKAGE IN AIR vs. WEIGHT LOSS

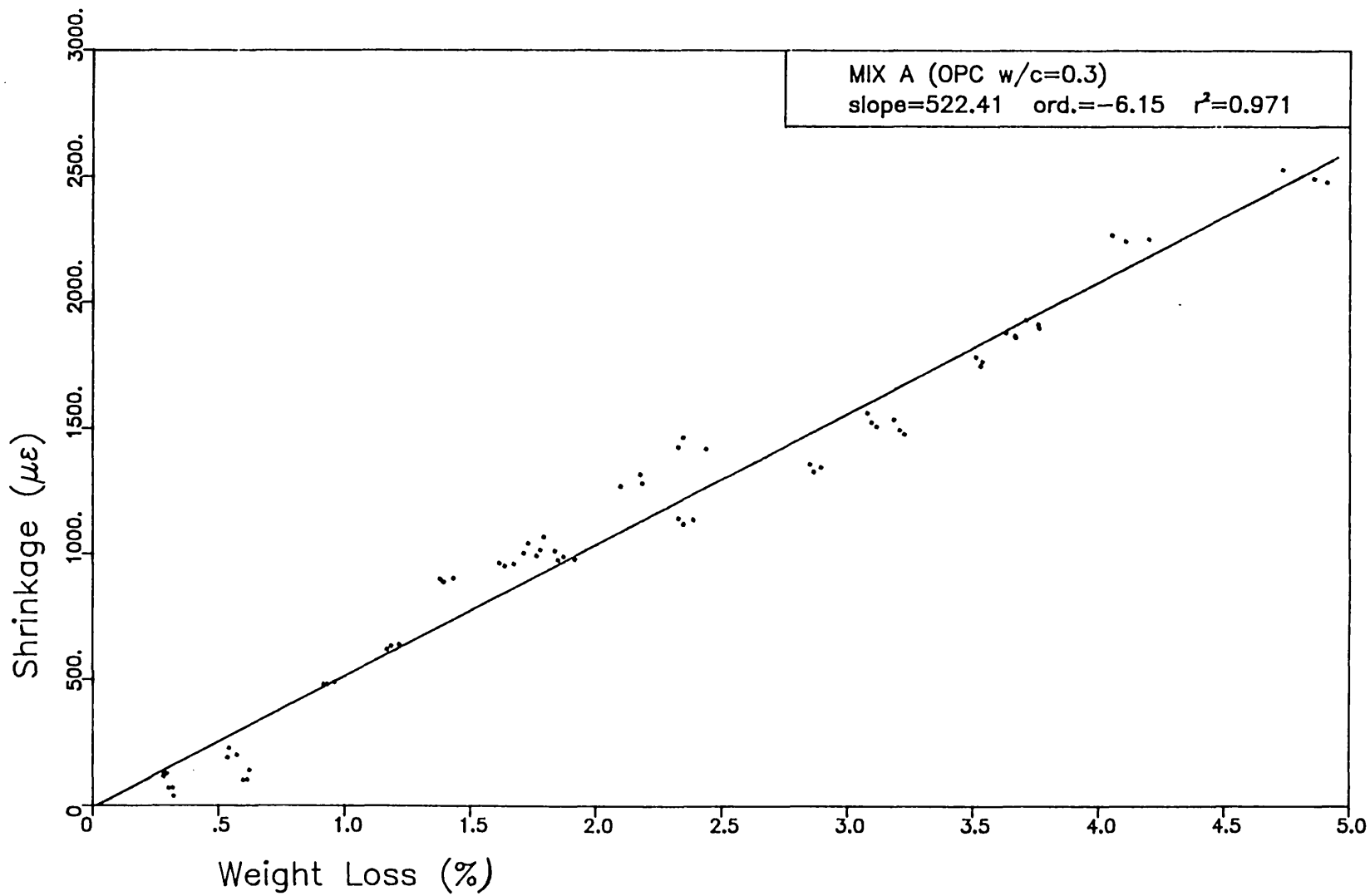

Fig.3.6 – HEATING & LOADING SEQUENCES FOR CREEP RIG TESTS

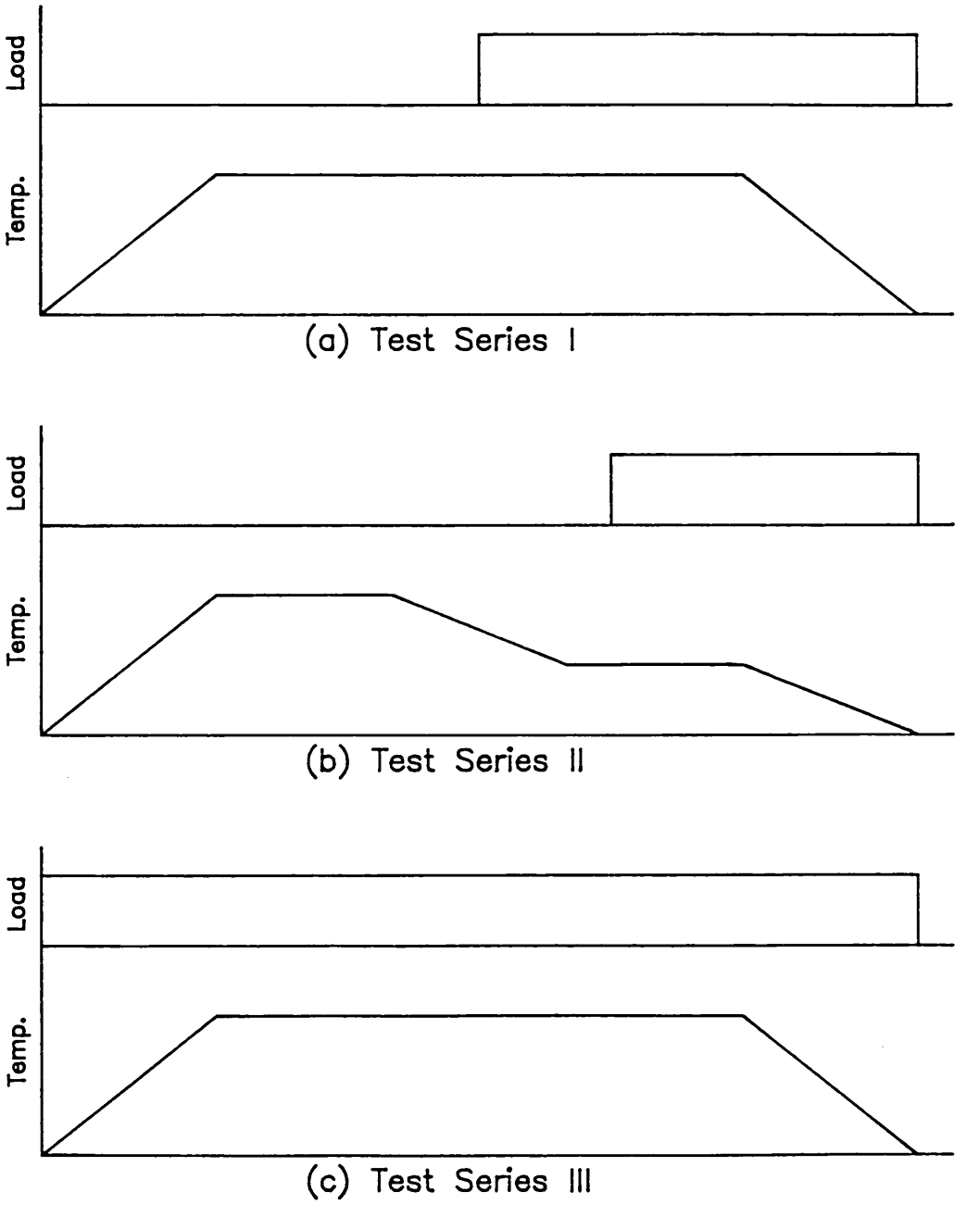

N.B. Not to scale. Horizontal axis is Time.

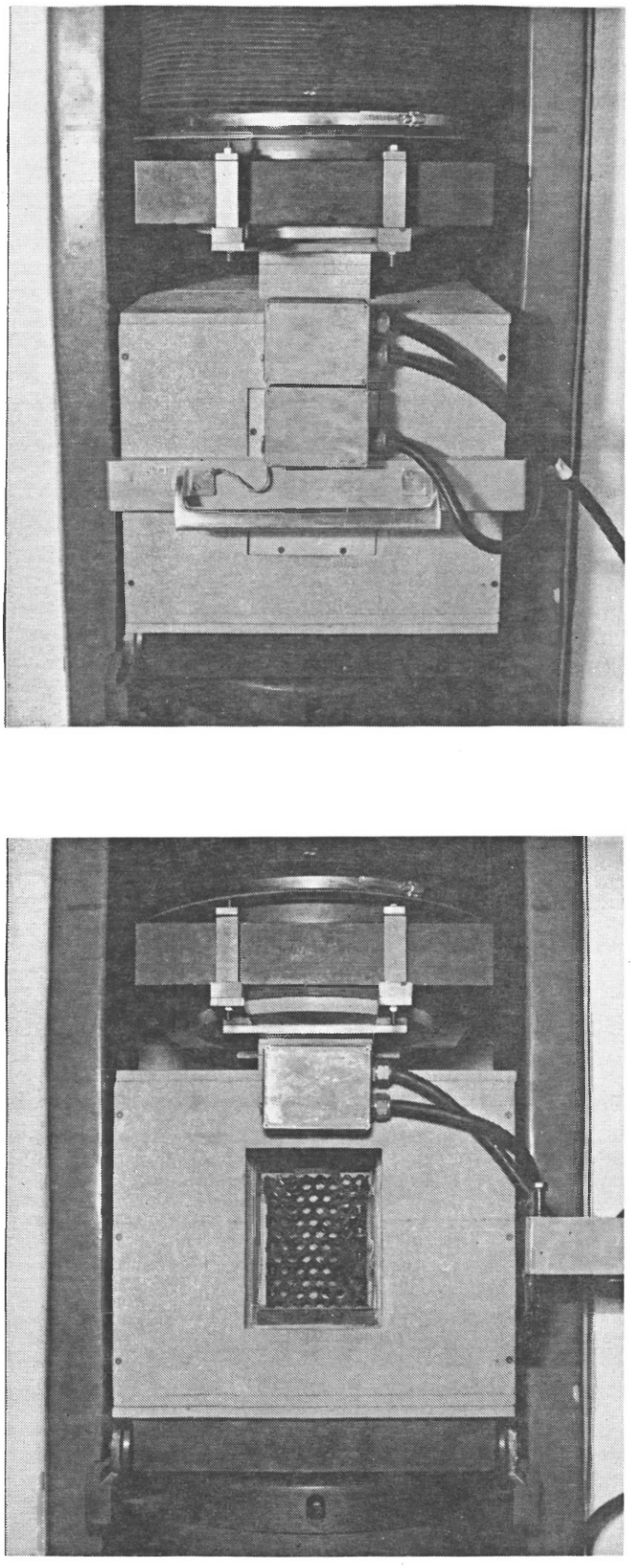

Figure 3.7 - APPARATUS FOR HOT STRENGTH TESTS.
SINDANYO SPACERS SEPARATING SPECIMEN FROM AMSLER PLATENS CAN BE SEEN IN TOP FIGURE, WHILE BOTTOM FIGURE SHOWS METAL CAGE SURROUNDING SPECIMEN IN FURNACE CAVITY.

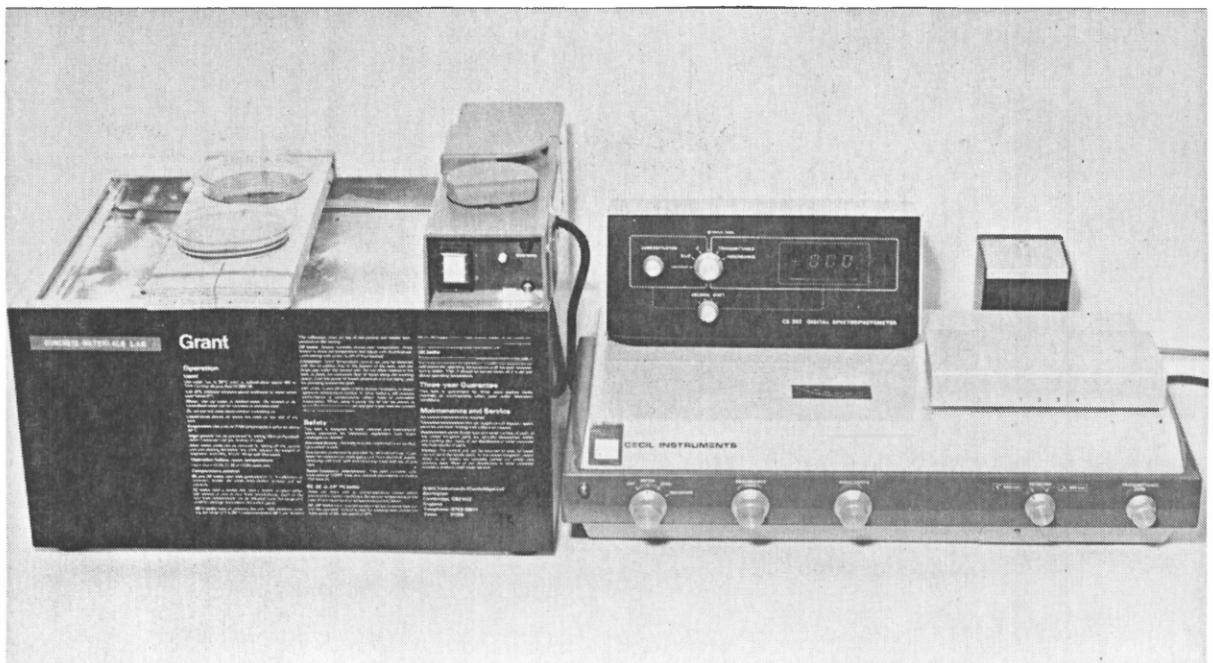

Figure 3.8 - APPARATUS FOR POLYSILICATE CONTENT DETERMINATION, SHOWING WATER BATH MAINTAINED AT 25 C AND DIGITAL SPECTROPHOTOMETER.

Fig.3.9 – SPECTROPHOTOMETER ABSORBENCE vs. SAMPLE WEIGHT

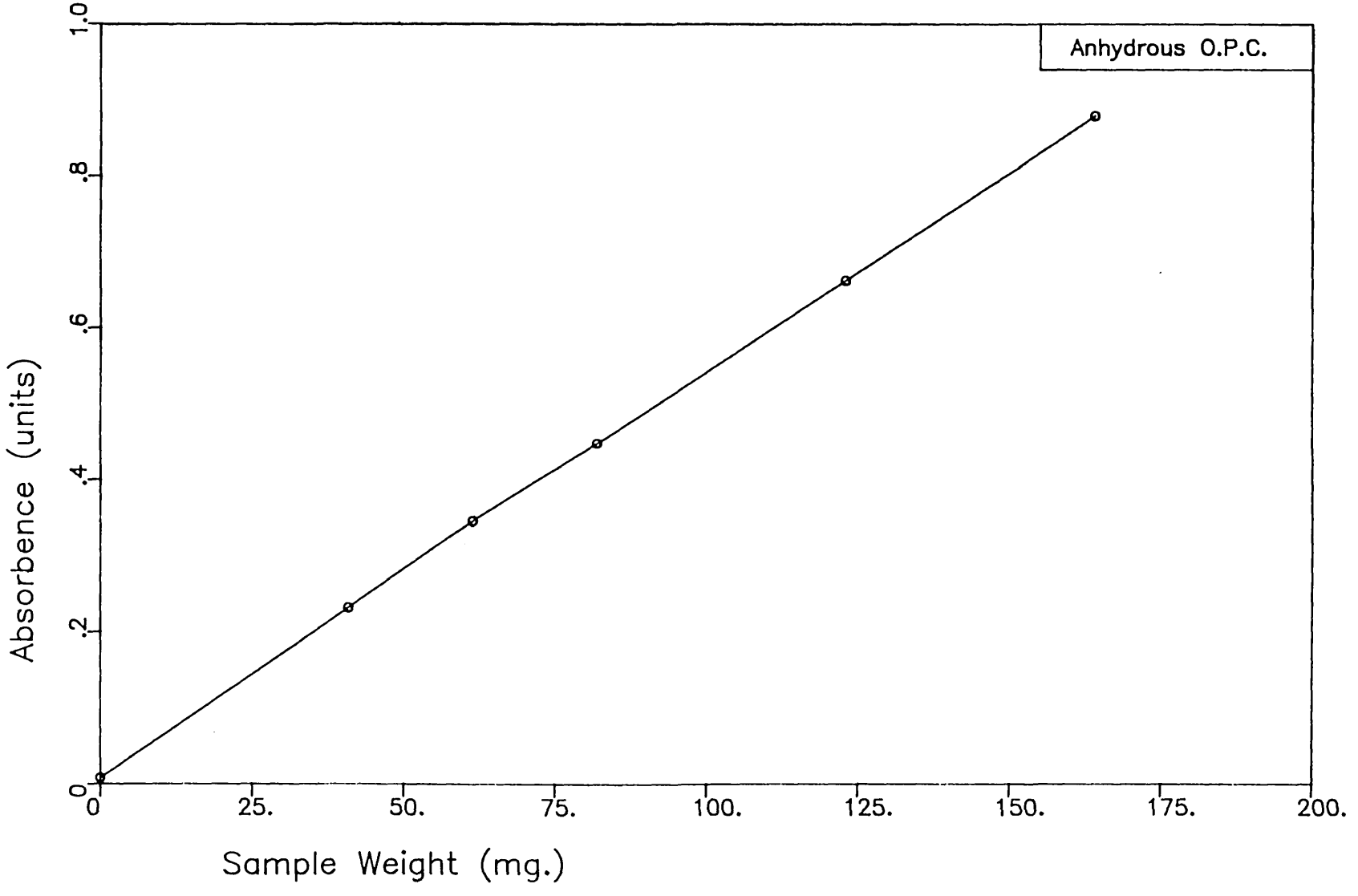

CHAPTER 4 - APPARATUS

4.1. INTRODUCTION

The main apparatus consisted of three identical creep test rigs fitted with adjustable furnaces. These rigs were designed by Gross (62) and subsequently modified by Khoury (84). A few additional modifications carried out during the course of the present experimental investigation are described in the next section.

Schematic representations of the apparatus are given in Figures 4.1 and 4.2. Its essential features are heating, loading and measuring systems which are independent of each other. The heating system has a feedback loop in order to establish control. The measuring system is connected to a computerized data logging facility.

The main component of the heating system for each rig is the furnace. This is in the form of a thick walled hollow cylinder of internal diameter 178 mm, and houses the cylindrical specimens of dimensions 62.5 mm ϕ x 187.5 mm. Each furnace consists of three zones which are wired and controlled independently. A temperature control unit regulates the power supply to each zone on the basis of the difference between the actual temperature and the pre-set temperature signal. This signal is specified simultaneously to the controllers of all three zones by a ramp generator, according to a pre-programmed time-temperature path. The actual temperatures of each of the three zones are measured by three separate thermocouples (one for each zone) and provide the feedback loop to the control system.

The loading of the specimens is performed by a yoke system through a lever arrangement, which magnifies an applied gravity load by a ratio of 15:1.

The measuring system for each test rig consists of five thermocouples and a displacement transducer. The total axial deformation in the specimen is transmitted to a d.c. displacement transducer, via invar rods connected to the end platens. The

transducer assembly is placed beneath the furnace and away from the heated region. Chromel-Alumel type K thermocouples are used to measure the surface temperature at the top, middle and bottom of the specimens. Two other thermocouples are attached to the invar connecting rods, in order to make allowance for the expansion of invar when obtaining the axial deformation of the specimen under transient temperature conditions.

The thermocouples and transducers from all three test rigs are connected to a datalogger, which is controlled by and sends information to a dedicated microcomputer. The data is processed by the computer and directed to a display unit. Permanent storage of data is made on a print-out as well as on a magnetic disc.

A more detailed description of the apparatus is given in a subsequent section of this Chapter.

4.2. MODIFICATIONS TO EXISTING APPARATUS

4.2.1. Programmable Temperature Control Unit

The manual device for pre-setting the heating rate and desired temperature was replaced by a programmable control unit, enabling an entire time-temperature path to be pre-set. This path can have up to a maximum of five linear sections, including controlled cooling phases (provided the required cooling rate is slower than the natural cooling rate), as well as heating and constant temperature ones. This capability of controlling the rate of cooling was required when performing the series of tests where specimens were cooled from pre-heat temperatures to lower temperatures prior to creep loading.

4.2.2. Computerized Data Logging Unit

An ORION datalogger, incorporating a clock mechanism and capable of measuring up to 200 channels was used to measure the signals from the transducers and thermocouples. A dedicated APPLE IIE microcomputer was used to control as well as to receive data from the datalogger. The data thus received was then processed by the computer

and displayed on a visual display unit. It was also stored permanently on a print-out of an on-line printer and on a magnetic disc.

A significant advantage in the use of this datalogger is its ability to convert signals from the thermocouples directly into temperatures by means of an inbuilt calibration, thus eliminating the need for a separate calibration of thermocouples. The signals from the transducers however, are fed to the computer as voltages, which have to be converted to linear displacements by means of an independent calibration, stored in the computer program.

4.2.3. Transducer Mounts

The grub screw holding the transducer in place on the lower link plate was replaced by a collette (a threaded split sleeve and nut arrangement), mounted on the link plate. The outer casing of the transducer is held tight when the nut is tightened on the split sleeve. Not only is this method of holding the transducer more secure, but it also prevents any indentation of the transducer casing by grub screws.

4.2.4. Wheels on Lower Link to Intermediate Plate

The vertical positioning of the yoke system was facilitated by the introduction of a hand wheel mounted on ball bearings, to replace the nut which had previously to be turned by a spanner.

4.3. DESCRIPTION OF APPARATUS

The apparatus can be conceptually divided into heating, loading, measuring and data processing systems, as depicted in Figure 4.1. However, a physical description is made easier by considering it as consisting of the creep test rigs (which incorporate loading, heating and measuring systems), the temperature control units (which are part of the heating system) and the data acquisition and processing system.

A description of these three sections of the apparatus is

given below. A detailed description of the design criteria used for the fabrication of the creep test rigs is given by Gross (62), while Khoury (84) has given an extensive discussion regarding the design of the temperature control units.

Labelled diagrams of the apparatus are given in Figures 4.7 to 4.16 and the individual components listed in Appendix 1. Views of various parts of the apparatus are shown in Figures 4.17 to 4.20.

4.3.1. Creep Test Rigs

(a) The main frame

The main frame consists of four upright posts of hollow cross section, welded to horizontal plates at the top, bottom and an intermediate level of the rig. The two front posts are always maintained in compression, while the rear posts are in tension. Since the front posts are always in compression, they have a larger cross-section than the rear ones.

(b) Loading system

The loading system is schematically depicted in Figure 4.3. It consists, essentially, of the following:-

1. A suspension rod to carry the 'dead' weights.
2. A lever arm to magnify the load in the ratio 15:1.
3. An assembly transmitting the force from the 'load' arm of the lever to the specimen.

The dead weights used for loading the specimen are slotted cylindrical discs, weighing between 57 and 58 kg. The design load of 10 tons thus corresponds to 12 weights piled up onto the weight pan. The length of suspension required to accommodate the design load is 1200 mm.

The use of gravity loading was preferred to methods such as hydraulic or spring loading, which would have involved loading against

a reaction frame. Not only is gravity loading the most simple form of loading for this apparatus, but loading against a reaction frame would have involved the complications of continuous load compensation as the specimen deformed with time. Gravity loading does not entail these complications, and is perhaps the most effective way of maintaining a constant load on specimens experiencing time dependent deformations.

The load from the suspension rod is transmitted to the 'effort' arm of the lever through the rear hanger. The lever arm is supported at its fulcrum by a mounting fixed to the front edge of the top plate, thus ensuring that the front posts are always in compression under load. The distance between the fulcrum and the rear hanger is 900 mm, while the distance between the fulcrum and the front hanger (which transmits the magnified load to the specimen) is 60 mm, thus achieving a load ratio of 15:1. The front hanger, fulcrum and rear hanger are all mounted on knife edges. A threaded arm with a movable counterweight, forming an extension to the front end of the lever arm, enables the lever system to be brought into static equilibrium at zero load conditions.

The assembly transmitting the force from the 'load' arm of the lever to the specimen is made up of the front hanger, the upper universal joint, the upper pulling rod, the yoke system, the lower pulling rod, the lower universal joint and the lower link to the intermediate plate. The hanger is pivoted on the front knife edge of the lever arm, while the lower link is threaded through a wheel which bears on the intermediate plate, enabling adjustments to the assembly to be carried out. In order that the load is applied to the specimen in a truly axial direction, it is transmitted through the upper and lower universal joints (which are seated on ball bearings) and the spherical bearing in the yoke system.

The yoke system which houses the specimen converts the tension in the pulling rods to a compression on the specimen. This yoke system is the part of the assembly exposed to the furnace heat, and is hence made of temperature resistant titanium alloy, except for the parts experiencing working loads in excess of 5 tons, which are made of incoloy alloy.

(c) Furnaces

The furnaces used to heat the specimens are thick walled hollow cylinders of 178 mm bore, which house both the specimen as well as the yoke system. The power required for heating is minimized by making the clearance between the furnace wall and the yoke system as small as possible, and also by providing Sindanyo end caps to the furnace. The furnace is axisymmetric, has no 'windows', and is lined with a temperature resistant ceramic liner. It contains three heating zones which are independently controlled by means of a temperature sensing feedback mechanism. It is therefore possible to minimize temperature gradients along the length of the specimen. Each zone has a resistance of around 50 Ω and the recommended upper voltage is 170 volts. The safe operating temperature is 750°C. The end caps are made of four layers of Sindanyo of thickness 10 mm. The top end cap has apertures to admit the upper pulling rod and thermocouples, while the lower end cap has apertures to admit the lower pulling rod and the invar rods of the strain measuring device. These apertures were plugged with ceramic wool, in order to reduce convection heat losses.

The furnaces are connected to a sliding assembly in order that they may be lowered to expose the yoke system for positioning or removal of specimens. It consists of two circular pipes, on which two brackets fitted with linear bearings slide. The furnace holding ring is welded to the brackets. A strong high tensile steel cable connects the sliding bracket via a pulley to a counterweight, which hangs inside the left front post, and which facilitates the vertical movement of the furnace.

The furnaces were built by Donaldson Furnaces Ltd.

(d) Thermocouples

All thermocouples are of the Chromel-Alumel type K with insuquartz sheathing capable of withstanding temperatures up to 800°C. They were supplied by Saxonia Electrical Wire Ltd. All thermocouples (which sense temperatures within the furnace) are connected to junction boxes located on the creep rig, from which point compensating wire is

used for connections, either to the temperature controllers or to the datalogger.

There are eight thermocouples used in each furnace. Three of these are placed adjacent to each of the three zones of the furnace wall, and are continuously monitored by the temperature controllers. The other five thermocouples are connected to the datalogger. Three of these are fixed to the top, middle and bottom of the specimen; the other two are fixed to each of the two invar rods connected to the top end platen of the specimen.

The thermocouples were fixed to the surface of the specimen by means of a high temperature resistant cement by the trade name Autostic, supplied by Carlton Brown & Partners Ltd. The fixing of the thermocouples to the specimen surface enables the measurement of actual surface temperature (which is slightly different from the furnace wall temperature or the temperature of the air surrounding the specimen). A disadvantage in fixing the thermocouples by means of the cement is the depression of the temperature reading caused by moisture evaporation from the cement during heating. This effect is reduced by using only a small quantity of cement, and is eliminated if the cement is dried prior to heating.

(e) Transducers

The displacements produced by the strain measuring device are measured by a d.c. displacement transducer, supplied by Sangamo Weston Controls Ltd. It is energised by a 10 volt d.c. power supply and the output voltage scanned by the datalogger. The supply voltage is also scanned by the datalogger. Any drift in the supply is compensated for by "normalizing" the output voltage from the transducer to correspond to a supply voltage of 10 volts. This is performed at the data processing stage and the procedure is written into the computer program.

The transducer has a linearity of 0.1% and an accuracy of ±1 micron (which is about 5.5 microstrains for a specimen approximately 187.5 mm long). It has a travel of 5 mm on each side of its

electrical zero position, and hence a total travel of 10 mm (which corresponds to about 55,000 microstrains, and more than sufficient for all measurements envisaged). The transducer is placed away from the heat affected region, by means of the strain measuring device.

(f) Strain Measuring Device

The strain measuring device enables the relative displacement between the specimen's end platens to be measured by the transducer which is placed outside the furnace. The device consists of two pairs of invar rods, attached, within the furnace to each end platen and outside the furnace to two link plates, remote from the furnace heat. The link plates are firmly attached to the invar rods by means of grub screws which can be tightened by alan keys. Where a rod has to pass through a plate, a ptfe sleeve is fitted to the aperture in the plate, so that frictional resistance to movement is minimized.

The transducer, which is mounted on the lower link plate, measures the relative movement between link plates. In order to obtain the strains in the specimen during transient temperature conditions, allowance has to be made for the thermal expansion or contraction of the invar rods. The link plates are connected to the invar rods in such a way that a compression in the specimen results in an increase of the distance between the link plates. Hence, any unforeseen compression failure of a specimen within the furnace would not cause damage to the transducer.

The measurement of the strain in the specimen through its end platens introduces the possibility of some errors, which are dealt with in the section on calibration tests.

4.3.2. Temperature Control System

The temperature control system consists of the programmable ramp generator (which specifies the pre-set temperature signal), the automatic digital controllers (which supply the required electrical power to the furnace elements) and the control thermocouple feedback system.

(a) Programmable Ramp Generator

This unit supplies the pre-set temperature signal (which can be of constant value or a linear function of time) to the automatic temperature controllers. A pre-determined time-temperature path consisting of a maximum of five linear segments (including cooling as well as heating and constant temperature phases) can be programmed. A cut-off maximum temperature can also be specified.

Three channels of output are available, each channel being connected to all three controllers of each furnace. Therefore, the three controllers of a given furnace receive the same signal from the ramp generator, but operate separately, depending on the feedback received from the control thermocouples.

The programmable ramp generator was custom built by Mr. Andrew Raby, formerly of Imperial College, and has the following specifications:-

Programmable temperature range (including cut-off temp.) = 0-999°C
Programmable time range = 0 - 65535 minutes (≙ 45 days)
Programmable heating rate = 0 - 999 °C/min.
(Note:- the maximum cooling rate cannot exceed the rate of natural cooling).

When the program is being run (i.e. when the ramp generator is in the 'RUN' mode), a digital display indicates the channel (Nos. 1-3), the current phase (Nos. 1-5), the current pre-set temperature, and the rate of change (in degrees C/min) of this pre-set temperature.

(b) Automatic Digital Controllers

When configured in a control system, the controller is a high gain, negative feedback amplifier. Nine automatic digital controllers (3 per furnace) were supplied by Solid State Controls Ltd.

The set point voltage from the ramp generator and the control thermocouple output are compared in the controller, which then turns

on or off, for varying proportions of time over a one second cycle, a solid state relay (triac) which in turn switches the heating element on or off.

There is an inherent time lag in the response of the element, as well as between the element and the control thermocouple, which causes, in effect, a damping of the thermocouple output. This effect, together with some slight damping in the controller itself, prevents instability in the control loop.

The following are the salient features of the controllers:-

Output drive:- Output triac switches 15 amp at 240 VAC (3.6 kW) for resistive load only.

Output switching differential:- Comparison between setpoint and actual temperature signals to within 25 μV, which is equivalent to $^1/_2$°C for standard thermocouples.

Indicating accuracy of display:- 3°C.

Cold junction compensation:- provided.

Fail safe facility:- heater turned off if control thermocouple goes open circuit. (This facility is in addition to the cut-off at the maximum temperature specified).

(c) Control Thermocouples

The control thermocouples form the feedback loop to the temperature controllers. Since each of the three zones in each furnace is independently controlled, there are three control thermocouples per furnace. They are also of the Chromel-Alumel type K with insuquartz sheathing.

The thermocouples are positioned as close as possible to the heating elements. This arrangement is more desirable than the alternative one of positioning the control thermocouples on the specimen itself (see Fig. 4.4). The feedback loop consists of a heat link and an electrical link (i.e. the thermocouple current). In

order for effective control to be maintained, the time lag for the feedback must be as short as possible. Since the electrical link can be considered to be virtually instantaneous, this time lag is governed by the heat link. In arrangement 1, the heat link b-c is mainly conductive and the physical distance b-c relatively short. However, in arrangement 2, not only is the physical distance b-c greater, but the heat link itself is of a convective nature, and hence much slower than in arrangement 1. The slow response time in arrangement 2 would result in a fluctuation of specimen temperature about the pre-set signal, while arrangement 1 would tend to produce a specimen temperature curve that gradually approaches the pre-set signal. The latter has been considered more desirable and hence arrangement 1 adopted.

The drawback in this arrangement however, is that the temperature being controlled is that of the furnace lining and not of the specimen itself. There would be a time lag before the specimen itself reached this temperature. Furthermore, the maximum temperature attained by the specimen may be a little lower than the pre-set maximum temperature. The latter however was remedied by suitably increasing the pre-set maximum temperature slightly beyond the desired maximum temperature of the specimen.

4.3.3. Computerized Data Logging and Storing System

(a) Hardware

All the measured data (i.e. transducer and thermocouple readings) from the three furnaces are logged by a Solartron 3530A ORION Data Logging System which is controlled by an APPLE IIE Microcomputer, acting as a dedicated microprocessor. The logged data is fed into the computer in its raw state, to be processed and printed on an EPSON MX-100 Dot Matrix Line Printer. In addition, the processed data is stored on a floppy disc while part of the data is displayed on the APPLE IIE Monitor.

The Data Logging System has facilities to take measurements through 200 channels which can be allocated to 8 tasks. Both

analogue and digital type inputs can be accommodated. The type of measurement to be taken through each channel has to be specified and the logger is activated when a task is defined and triggered. The output can either be displayed on the logger monitor or obtained as a print-out; alternatively, it can be sent to an external device such as a computer.

In the experiments described herein, nineteen channels were utilised. Channels 1-15 were used to measure temperatures from the K-type (i.e. Chromel-Alumel) thermocouples and channels 17-19 used to measure voltages from the three d.c. transducers; channel 20 was used to monitor the voltage output from the d.c. power supply.

The logger was programmed to take readings by scanning the channels at a rate of 100 channels per second. The interval between readings or scans varied in durations ranging from 10 seconds to 4 hours, depending on the stage of the experiment. It was also possible to take a single reading at a given time.

The data logger was connected to the microcomputer by a standard IEEE-488 interface bus. The interface bus was used both to send commands from the microcomputer to the data logger as well as to transmit data from the logger to the computer. Hence, the data logger functioned both as a "listener" as well as a "talker".

The microcomputer has an internal Random Access Memory of 64 k. It has seven ports for peripheral connections. Two of these ports were used for an IEEE-488 interface for the data logger connection and a Centronics interface for the line printer connection. A third port was used for an interface connecting two disc drives. One of these disc drives contained the disc with the computer programs while the other contained the disc on which data was stored.

The line printer has a 9 x 9 dot matrix print head with bidirectional printing at 100 CPS. In normal character size (10 characters per inch), it can print a maximum of 136 characters per line. It also has a buffer of 1 k.

A schematic diagram of the computerized data logging and storing system is shown in Figure 4.5.

(b) Software

The computer program used for the logging and storing operation is based on the flowchart shown in Figure 4.6.

The program has the following features:-

1. Data input is fully interactive.

2. The printing of titles and creation of a storage file can be bypassed if necessary.

3. The "central core" of the program is the routine of checking whether the datalogger is requesting service in order to transmit data. The program returns control to this routine after each step, except when an entry has been made on the keyboard.

4. When the specified time interval between scans is small (low values of k), since the computer does not have time to process the data before the next service request, it merely stores the raw data in a numeric array. All the data from a single scan forms a line or row of the array.

5. As the interval between scans is increased (this is done via the keyboard), the computer goes on to process the array of raw data, a line at a time, and sends the output to the monitor and the printer. Subsequently, as shown in the flowchart, it stores the processed data on the storage disc as well.

6. Three kinds of entries can be made via the keyboard, as indicated in the flowchart. The datalogger can be halted, recommenced, or set to scan the channels at a different time interval by using the Command Codes. After the logger has

been halted, the transducer 'zero' and the initial time and temperature values can be altered by an interactive data entry routine; this routine is initiated by entering 'R' on the keyboard. The program can be halted by entering 'X' on the keyboard.

7. The calibrations for the invar rod expansion and transducer voltages are stored as data in the program.

4.4. CALIBRATION TESTS

Calibration tests were performed on the apparatus, primarily to ensure the proper functioning of the strain measuring devices. The efficiency of the heating arrangement in minimizing axial temperature differentials and producing uniform rates of heating and cooling was also investigated.

4.4.1. Strain Measurement via End Platens

The specimen strains are obtained by measuring the relative displacement between its end platens. This could introduce two sources of error. Firstly, since the entire length of the specimen is used as a gauge length, the measured strains may not be indicative of uniaxial behaviour alone (which would occur towards the mid-height of the specimen), but be affected by triaxial confinement effects (set up due to friction between the platens and specimen ends) in the regions close to the platens. Secondly, there may exist imperfect contact between the platens and the specimen ends, the "closing up" of which during loading would reflect larger apparent strains than the specimen actually undergoes.

Care was taken to minimize errors from the latter source by ensuring that both the specimen ends as well as the platen faces were clean and free from dust. Furthermore, specimens were always bedded down prior to any test, by repeated loading (and unloading) to the load level subsequently employed in the test.

However, in order to investigate both the above "platen effects", the transducer readings were calibrated against readings from strain gauges placed at the mid-height of the specimens (3 gauges per specimen arranged at 120° intervals around its circumference). The averaged results for all 3 rigs are indicated in Figure 4.21. This shows that although there is a discrepancy between the transducer and strain gauge results at lower load levels, the slope of the transducer readings becomes parallel to that of the strain gauge readings beyond a load of around 1.7 tons (i.e. the load induced by 2 of the 57.5 kg weights). Hence, it may be concluded that the strain measurements via end platens taken at load levels in excess of 1.7 tons can be considered to be reliable. All strains measured in this investigation have been obtained at load levels in excess of the above.

4.4.2. Strain Measurement in Transient Temperature Regimes

Since the displacement between end platens has to be transferred to the link plates (carrying the transducer) via invar rods, any measurements made in non-isothermal conditions must account for the thermal expansion or contraction of the invar rods. The invar rod expansion figures, obtained from the National Physical Laboratory (N.P.L.), Teddington, are stored in the computer program.

The calibration of the system was performed by measuring the thermal expansion of a copper cylinder using the strain measuring system in the apparatus, and comparing this with expansion figures for a sample of copper (from the same cylinder), again provided by the N.P.L.

The results of the 4 tests performed are given in Table 4.1 and Figure 4.22. They show that the strain measuring system performed well, both with respect to repeatability (as indicated by the low standard deviations for the 4 tests as percentages of the averages) as well as with respect to accuracy (as indicated by the experimental expansion values being within 4% difference of the reference sample over the entire temperature range of 25°C-600°C). Furthermore, since the calibration test results are sensitive to the accuracy of temperature measurements as well, it may be concluded that the entire

system (consisting of thermocouples and the strain measuring device) could be relied upon to measure strains accurately and repeatedly, under all temperature regimes.

It should be mentioned that previous calibration tests performed on the strain measuring system (84, 166) serve as confirmatory evidence of its proper functioning.

4.4.3. Efficiency of Heating and Cooling Systems

The heating and cooling system were expected to provide a uniform rate of change of average specimen temperature and also ensure that longitudinal temperature differentials in the specimen were kept to a minimum. Figures 4.23-4.25 indicate its performance in typical tests carried out on cement paste and copper specimens. The heating and cooling curves for the cement paste, although not obtained from the same specimen, are results of tests performed on the same furnace.

Figure 4.23 shows the change of specimen temperatures with time for both heating and cooling regimes. The deviation from the specified rates of both heating and cooling for the cement paste specimens is noticeable in the lower temperature range; it is more clearly seen when the rate of change of temperature is plotted (Figures 4.24, 4.25).

When considering the response of the copper specimen (Figure 4.24) the initial rate of heating builds up only gradually to the desired 1°C/min., because of the thermal inertia of the system. The subsequent increase in the heating rate above 1°C/min. is probably due to compensation for the previously slow rate of heating. The cement paste specimen shows an even greater period of heating below 1°C/min. In addition to the thermal inertia of the system, this would be due to the heat absorbed in the loss of evaporable water. The subsequent compensation is therefore greater than that for the copper specimen. The minimum in heating rate at around 540°C may be due to the endothermic dissociation of $Ca(OH)_2$. As would be expected, a compensating rise is exhibited thereafter. The sharp drop in heating rate at the end of the trace signals the reaching of the pre-set

maximum temperature.

The longitudinal temperature differentials (measured on the surface of the specimen) indicated on the same figure show maxima corresponding to periods of higher heating rate, which is to be expected. The maximum at around 100°C would correspond to the loss of evaporable moisture, which could set up thermal gradients due to latent heat effects. The maximum longitudinal temperature difference is 17°C which would correspond to an average longitudinal thermal gradient of approximately 1°C/cm. This was considered small in comparison to the radial thermal gradient of 3°C/cm expected to be developed at the heating rate of 1°C/min. (84).

Figure 4.25 shows the rate of cooling to be remarkably constant at the desired rate of 0.5°C/min in the upper temperature range. Below 315°C however, it is apparently not possible to maintain this rate because natural cooling is slower. The longitudinal temperature differentials are in general smaller than those during the heating regime. The increase in these differences below the temperature of 315°C may be due to the fact that the rate of cooling is continuously changing in this range. The differences seem to drop when the cooling rate approaches zero, near the pre-set temperature desired.

Temperature (°C)	100	200	300	400	500	600
Invar Rod expansion (με)	133	591	1765	3334	5034	6788
Copper Reference expansion (με)	1274	3051	4882	6775	8728	19734
Test 1 (με)	1227	2982	4820	6785	8861	10986
Test 2 (με)	1236	2940	4783	6784	8901	11128
Test 3 (με)	1253	2999	4832	6699	8631	10650
Test 4 (με)	1200	2950	4819	6756	8773	10847
Average of 4 Tests (με)	1229	2968	4814	6756	8792	10903
Std. Deviation (με)	22	27	21	40	120	204
Std. Dev. as % of Av. (%)	1.8	0.9	0.4	0.6	1.4	1.9
Av. as % of Ref. (%)	96.47	97.27	98.60	99.72	100.73	101.57
Average - Reference (με)	-45	-83	-68	-19	+64	+169

Note:- All strains are measured from 25°C.

TABLE 4.1. CALIBRATION OF STRAIN MEASURING DEVICE FOR TRANSIENT TEMPERATURE REGIMES

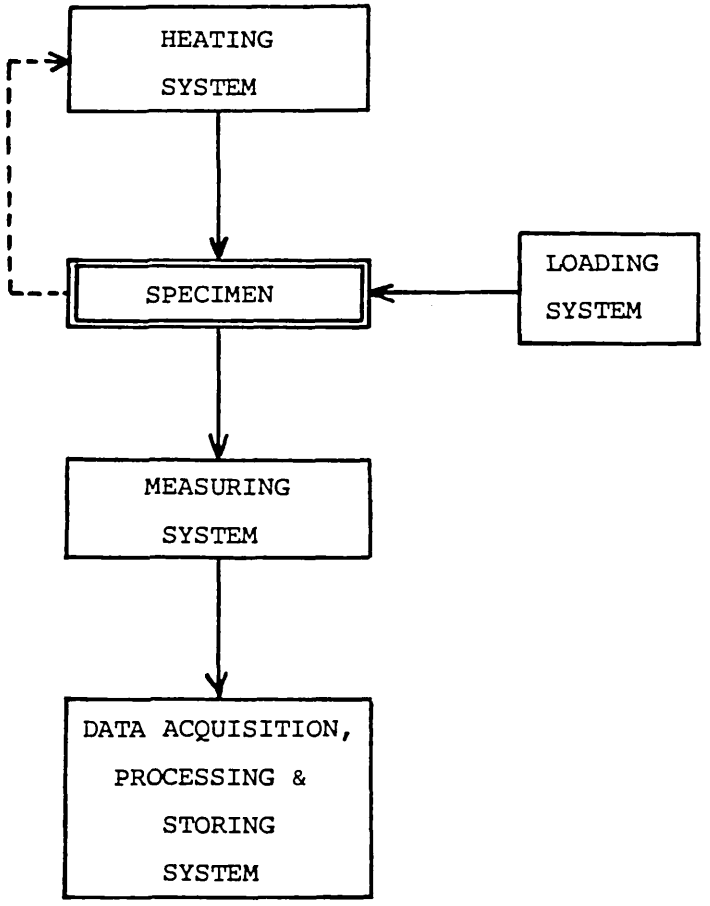

Figure 4.1 - CONCEPTUAL REPRESENTATION OF APPARATUS.

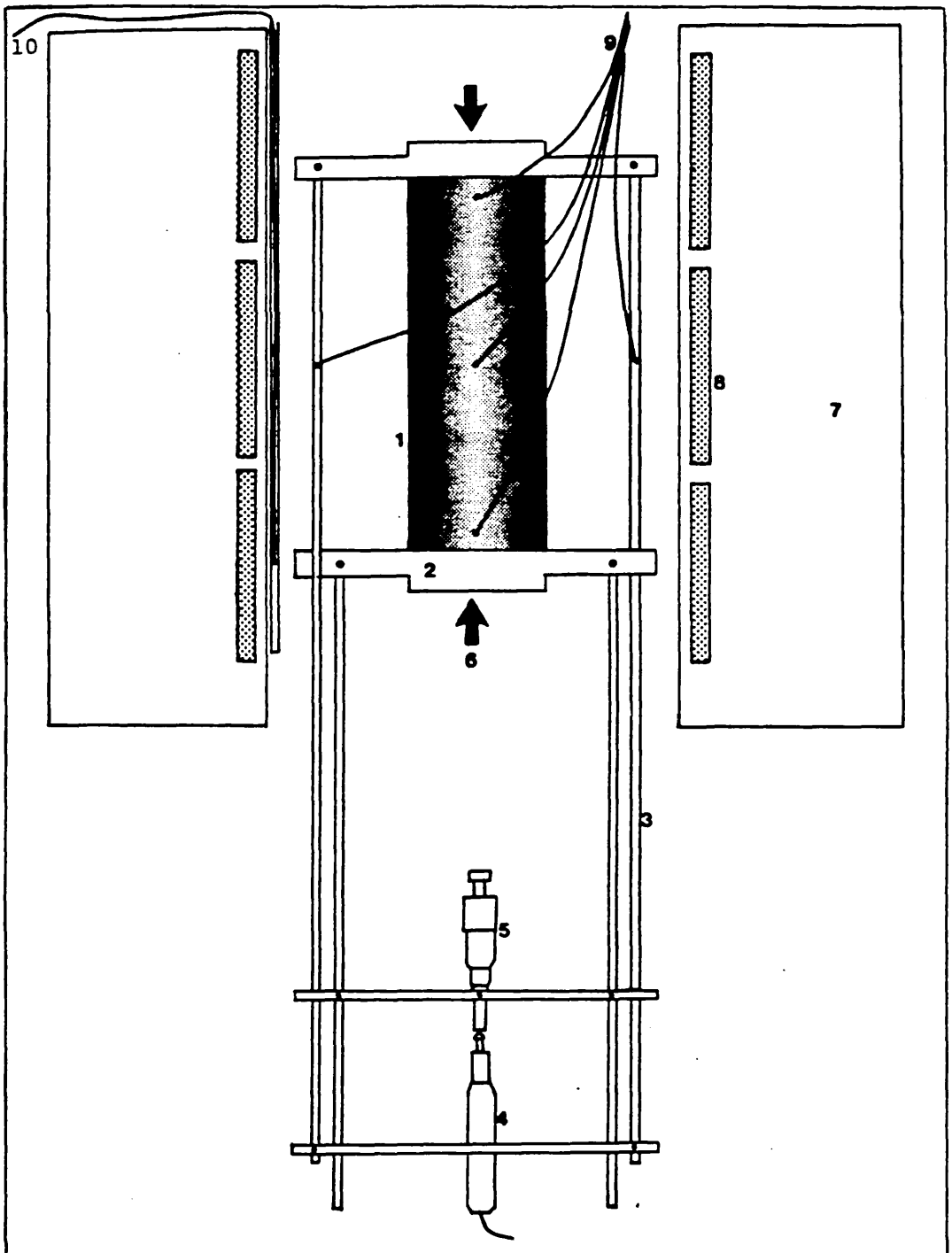

DIAGRAM SHOWING A SCHEMATIC REPRESENTATION (NOT TO SCALE) OF:

1) CONCRETE SPECIMEN 2) END PLATENS 3) INVAR RODS
4) TRANSDUCER 5) MICROMETER 6) APPLIED LOAD 7) FURNACE
8) INDEPENDENT HEATING ZONES 9) MEASURING THERMOCOUPLES
10) CONTROL THERMOCOUPLES

Figure 4.2 - SCHEMATIC REPRESENTATION OF APPARATUS.(FROM KHOURY (84))

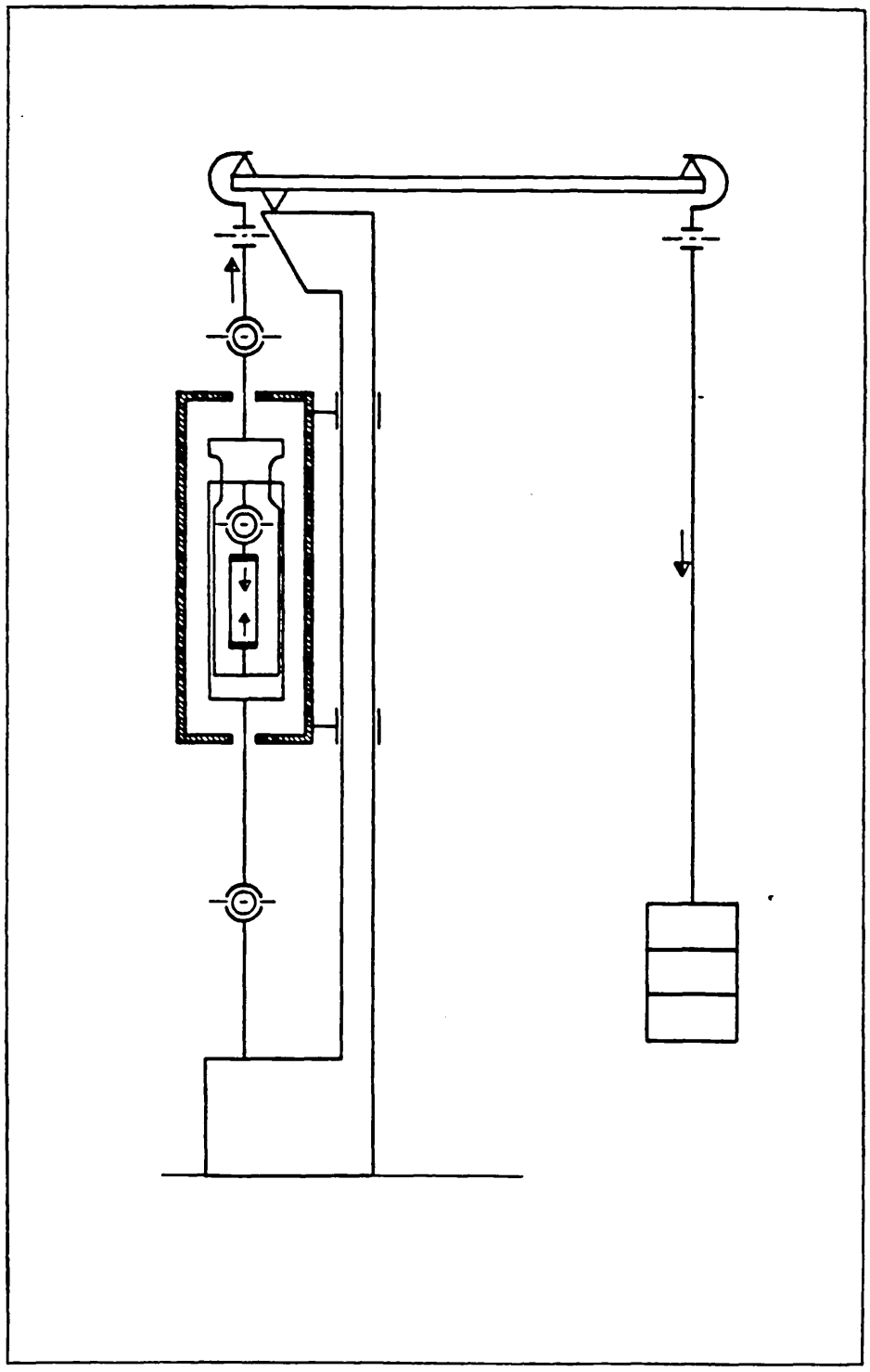

Figure 4.3 - MECHANICAL LOADING SYSTEM OF CREEP TESTING MACHINE.
(FROM GROSS (62))

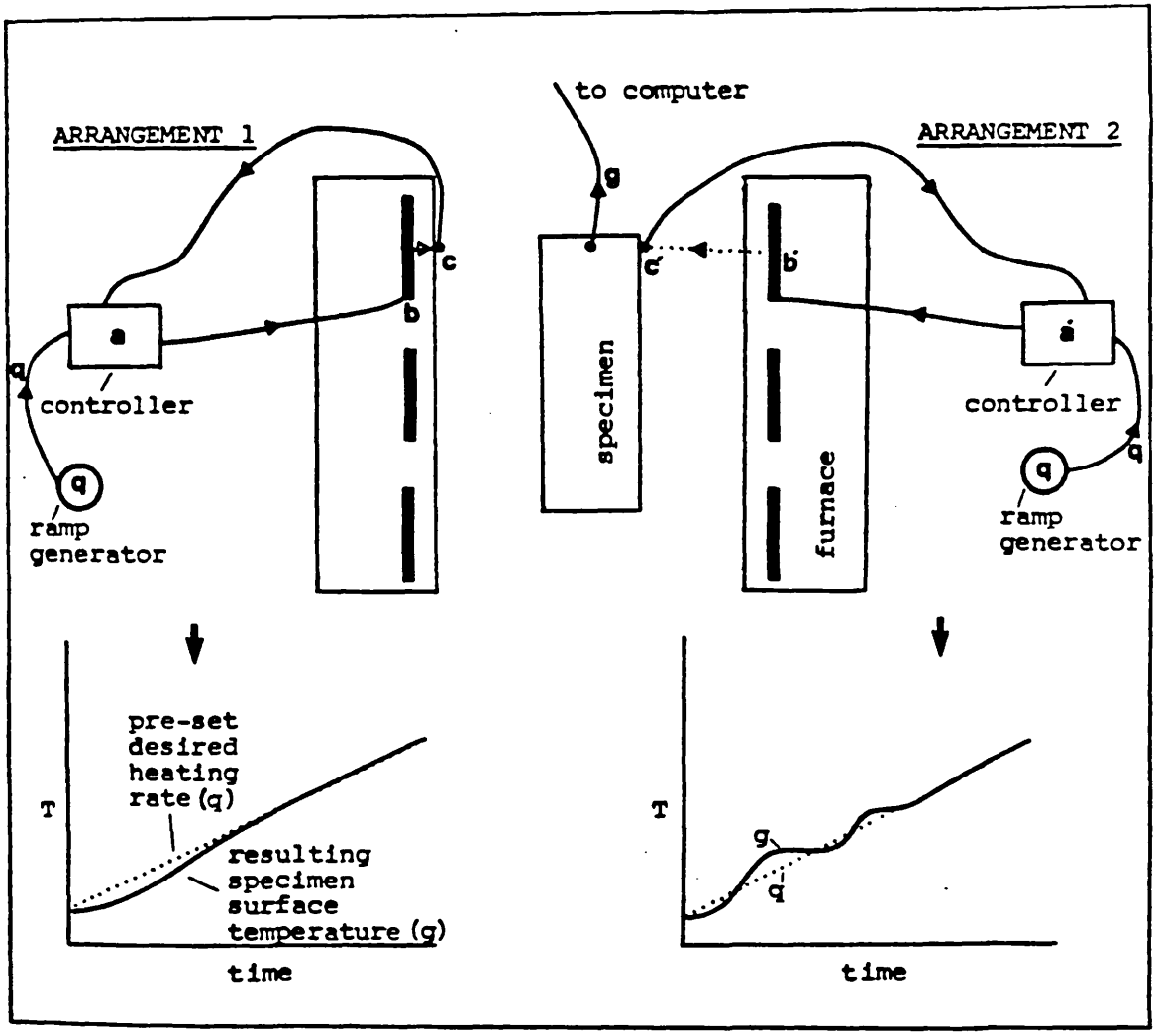

TRANSIENT TEMPERATURE RESPONSE AT THE SPECIMEN'S SURFACE WHEN CONTROL THERMOCOUPLES ARE PLACED (1) AT THE FURNACE'S INNER FACE AND (2) ON THE SPECIMEN. THE SET SIGNAL OF CONSTANT TEMPERATURE INCREASE FROM THE RAMP GENERATOR BEING THE SAME.

Figure 4.4 - FEEDBACK FROM CONTROL THERMOCOUPLES.(FROM KHOURY (84))

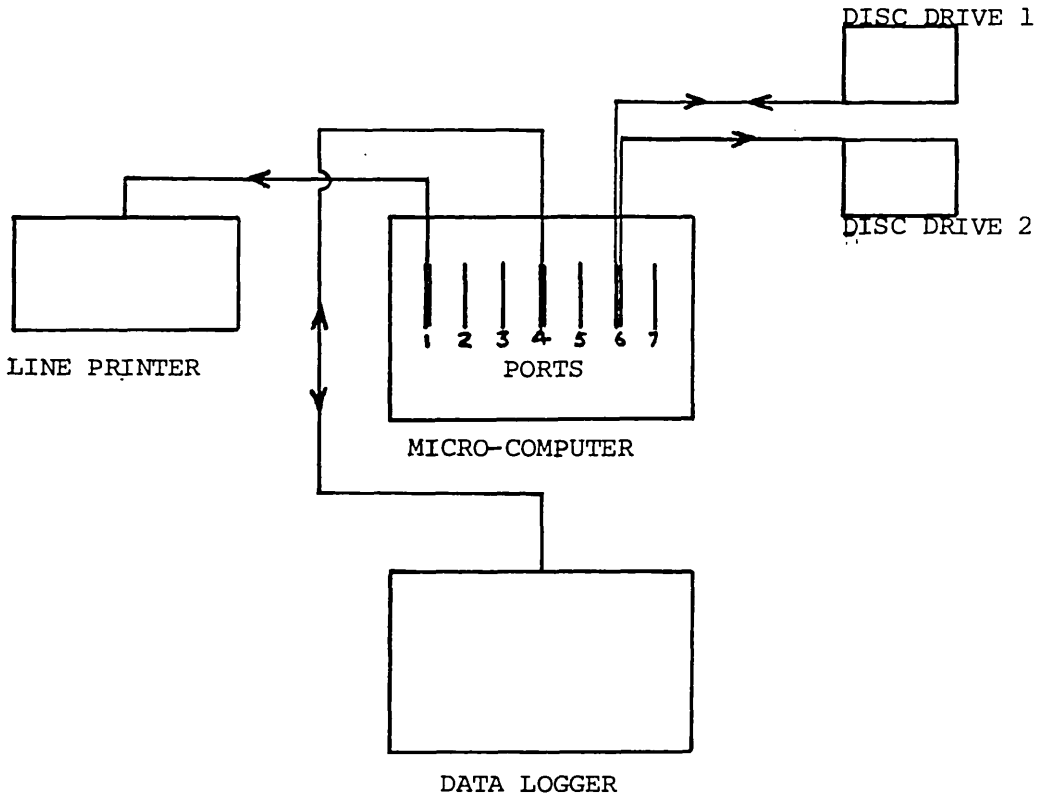

Port No. 1 - Centronics Interface Card
Port No. 2 - IEEE-488 Interface Card
Port No. 3 - Disc Drive Interface Card

Note:- Arrows indicate direction of information flow.

Figure 4.5 - DATA ACQUISITION, PROCESSING & STORING SYSTEM.

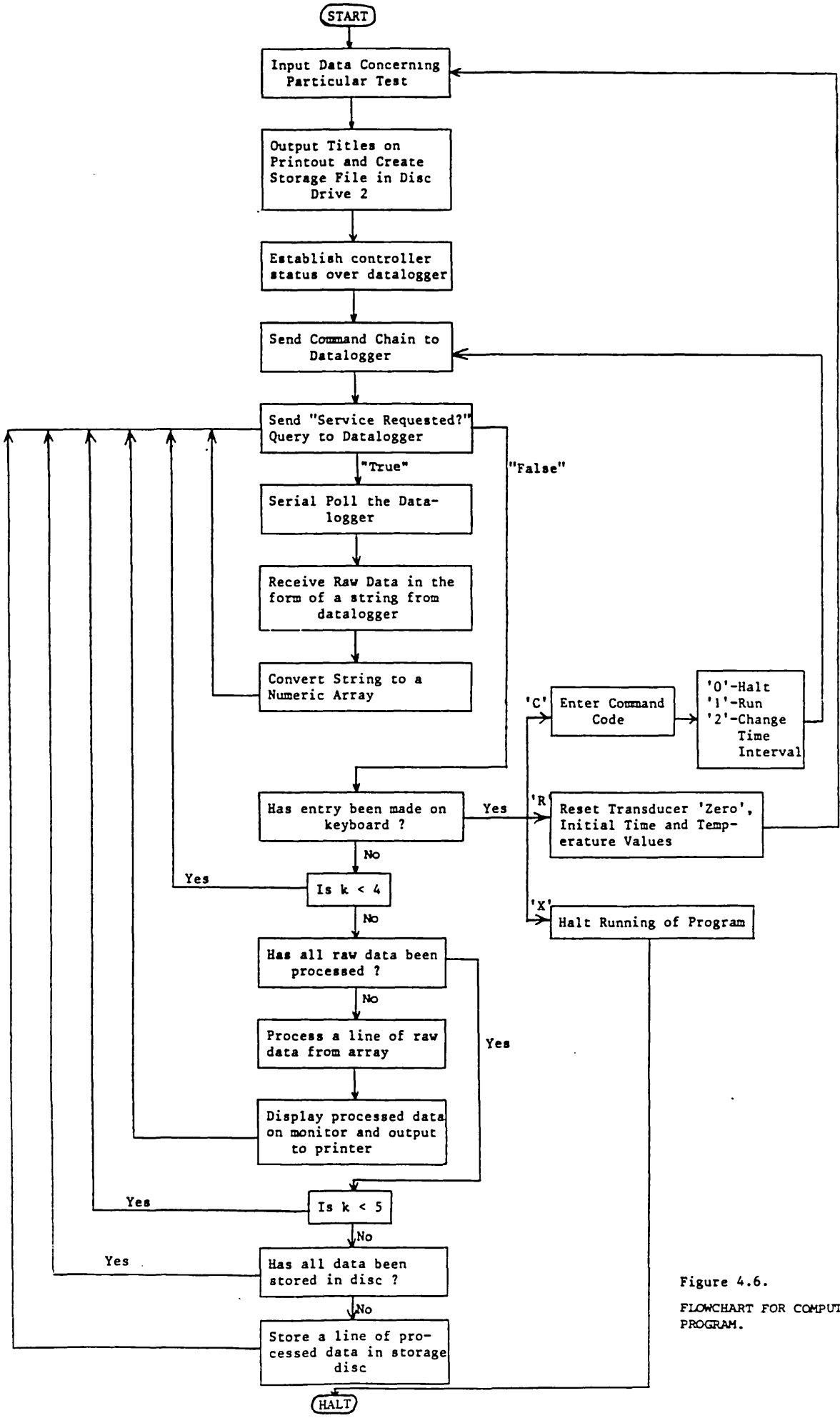

Figure 4.6.

FLOWCHART FOR COMPUTER PROGRAM.

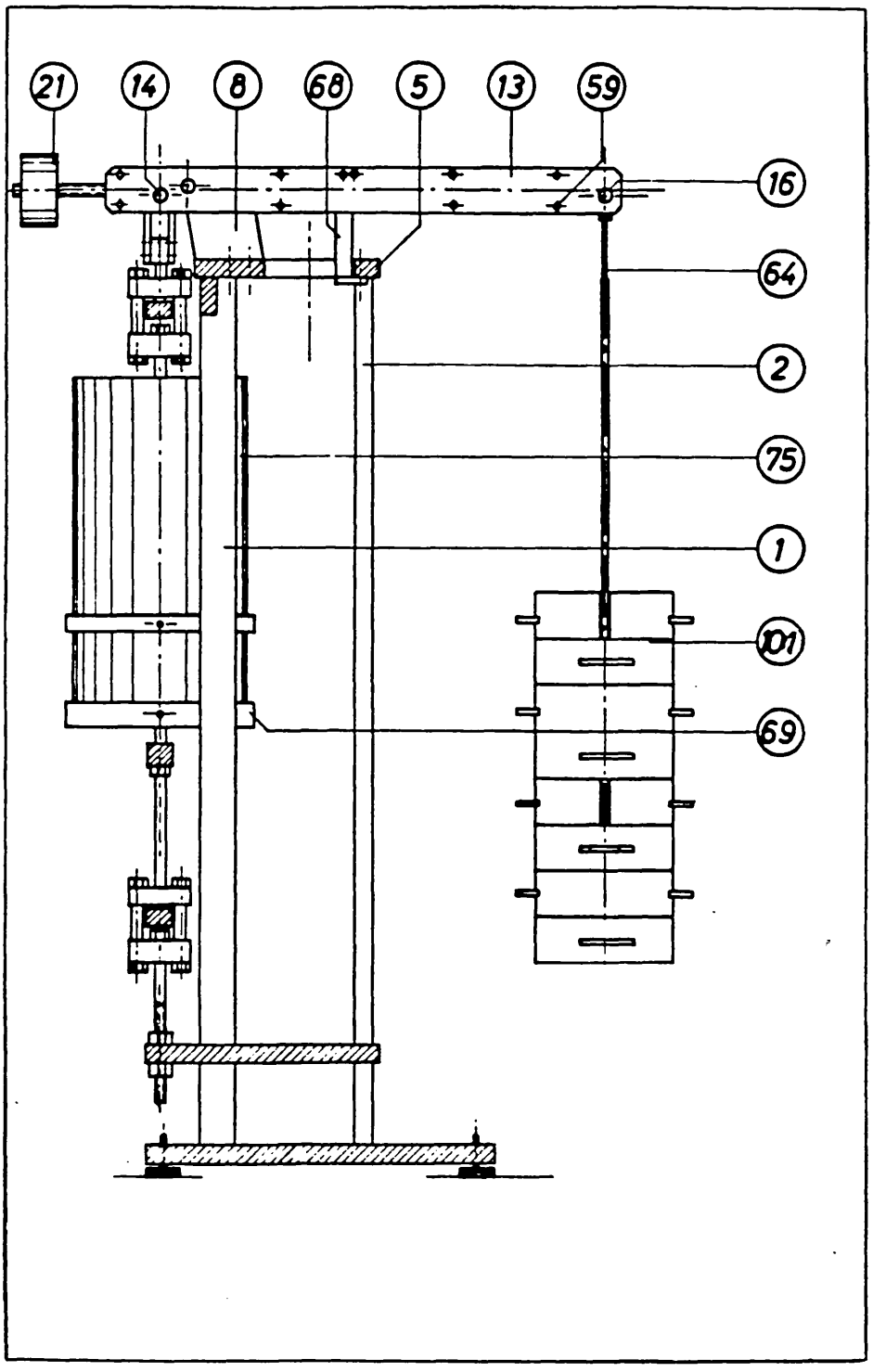

Figure 4.7 - END ELEVATION OF CREEP TESTING MACHINE.(FROM GROSS (62))

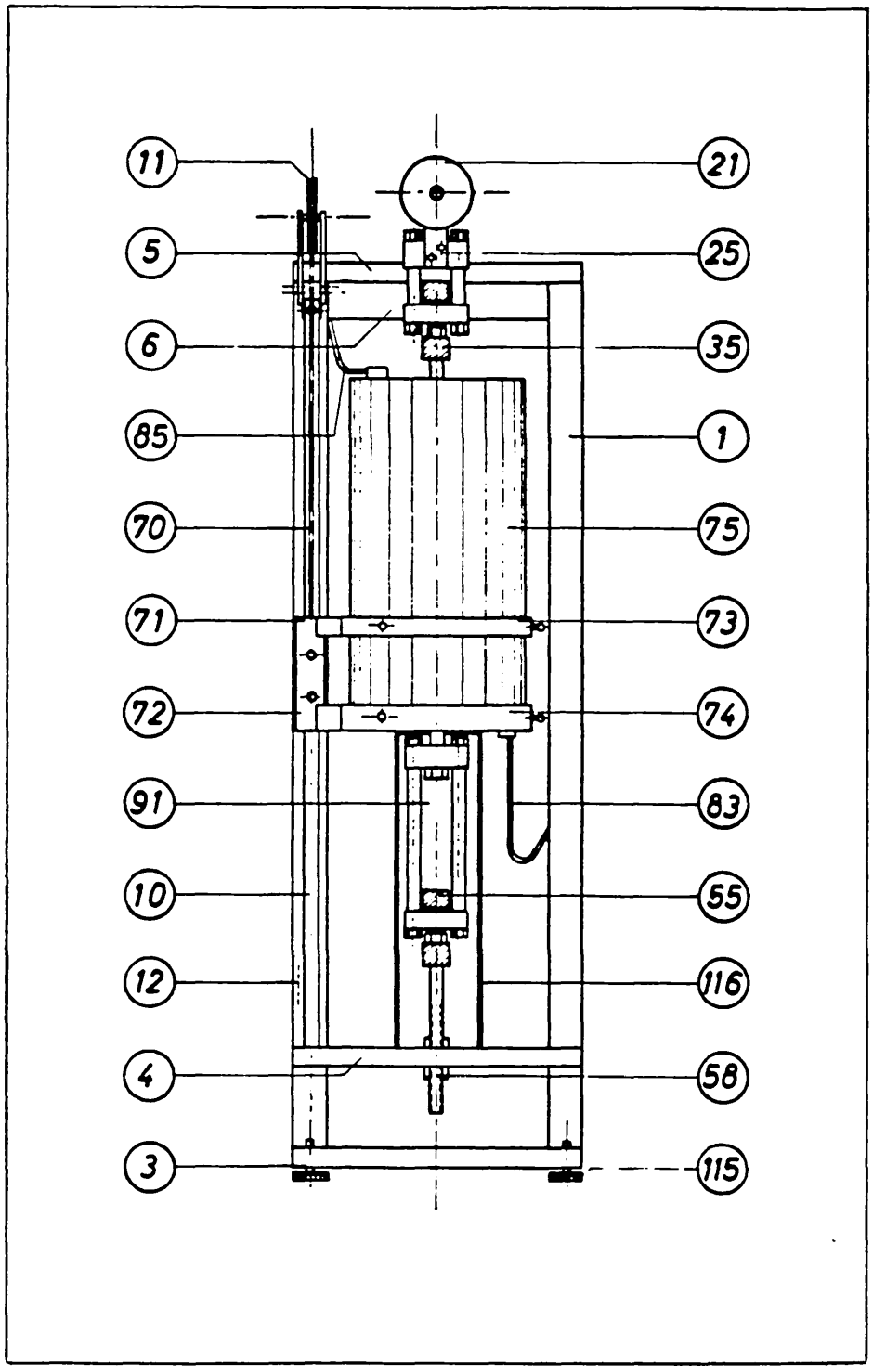

Figure 4.8 - FRONT ELEVATION OF CREEP TESTING MACHINE.(FROM GROSS (62))

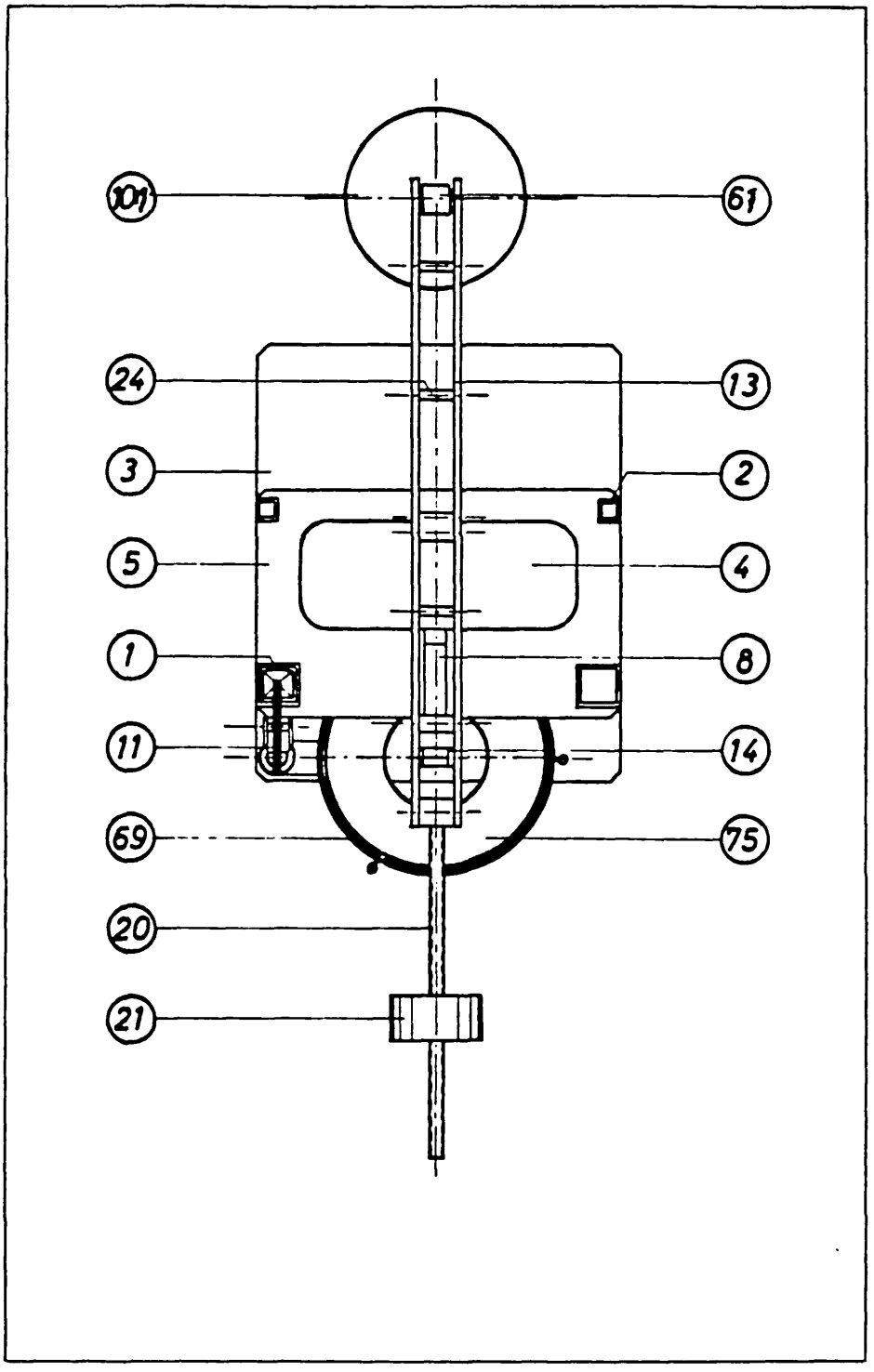

Figure 4.9 - PLAN OF CREEP TESTING MACHINE.(FROM GROSS (62))

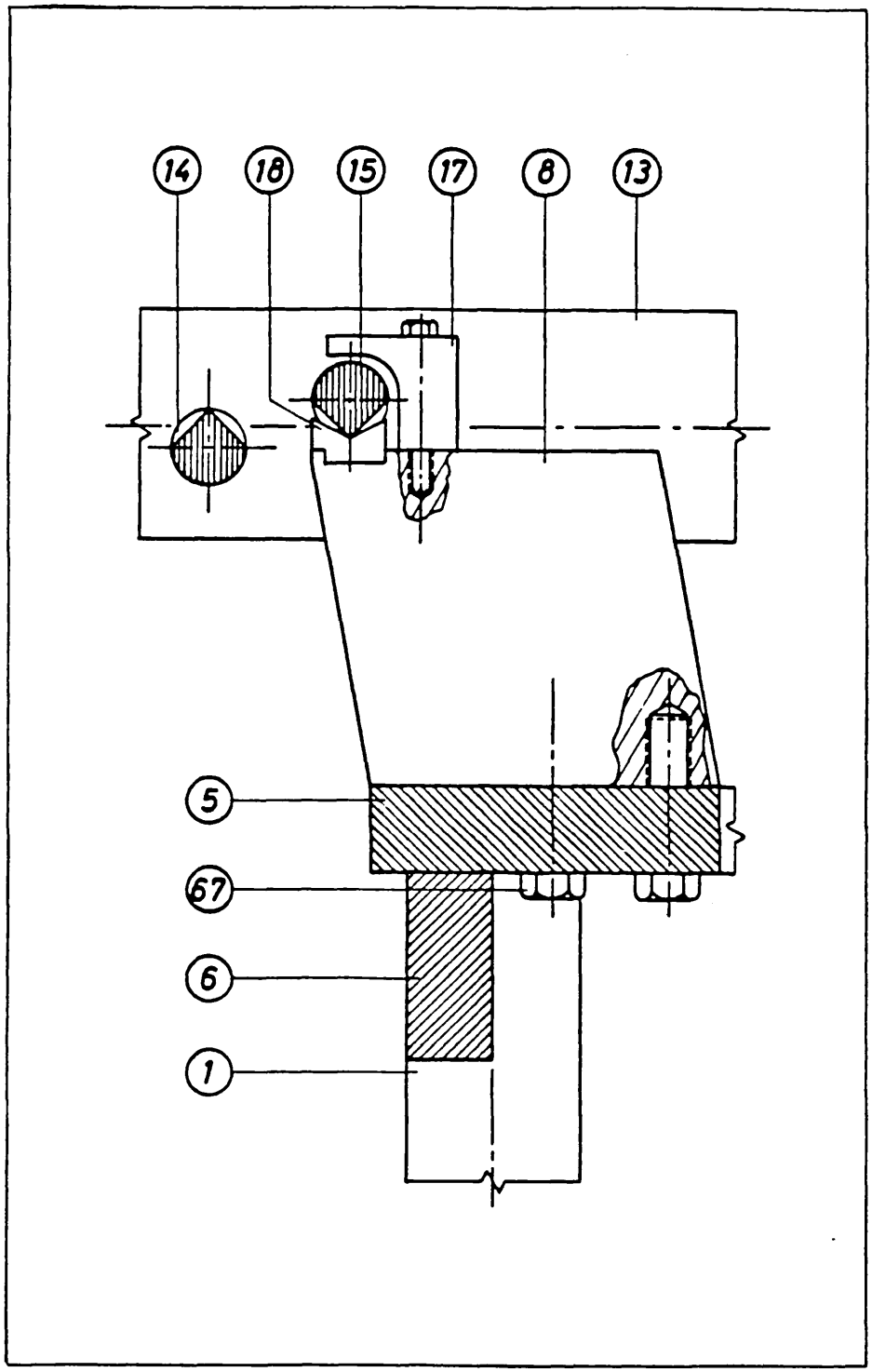

Figure 4.10 - FULCRUM OF LEVERARM SYSTEM.(FROM GROSS (62))

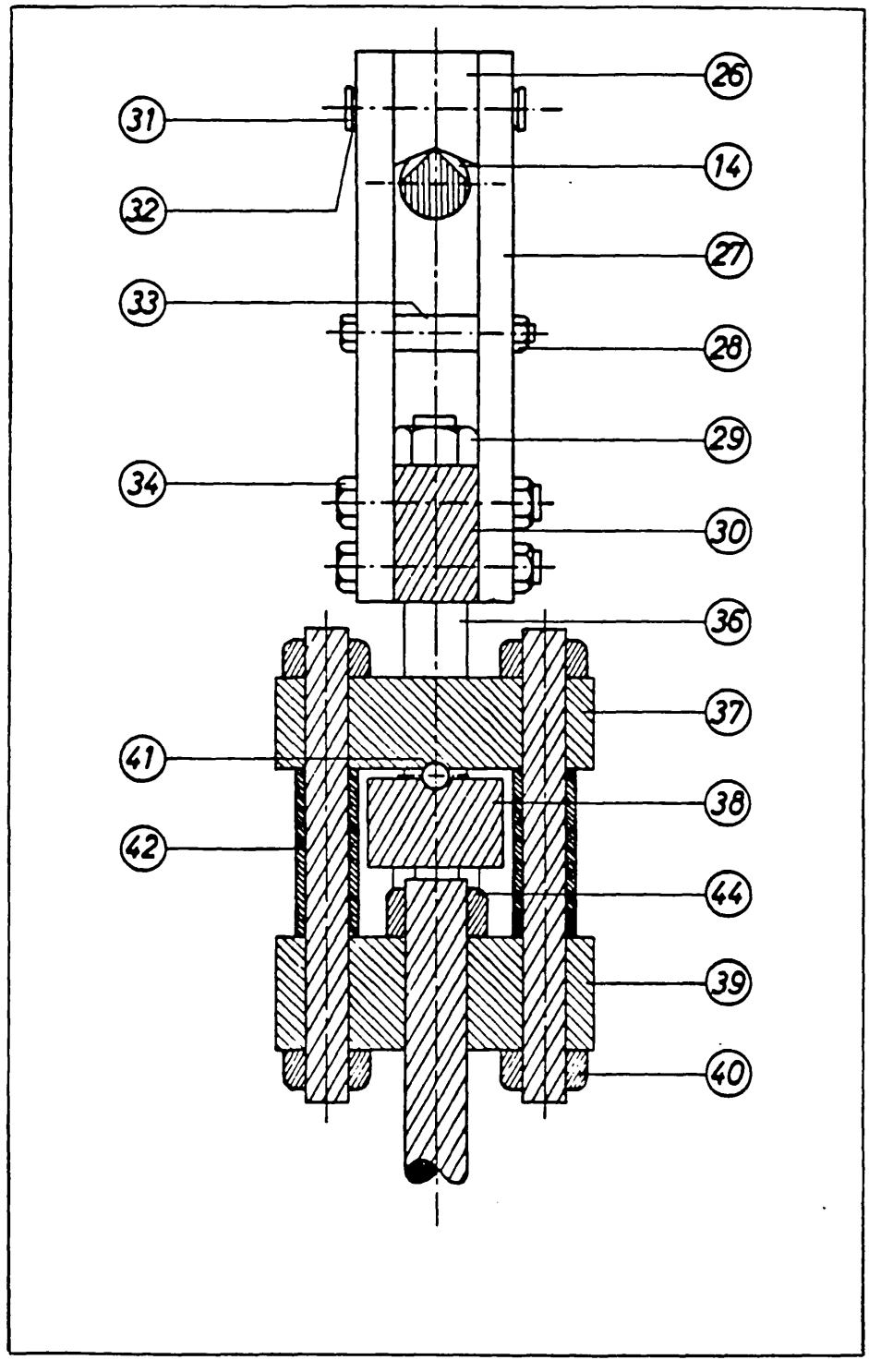

Figure 4.11 - FRONT HANGER AND UPPER UNIVERSAL JOINT.(FROM GROSS (62))

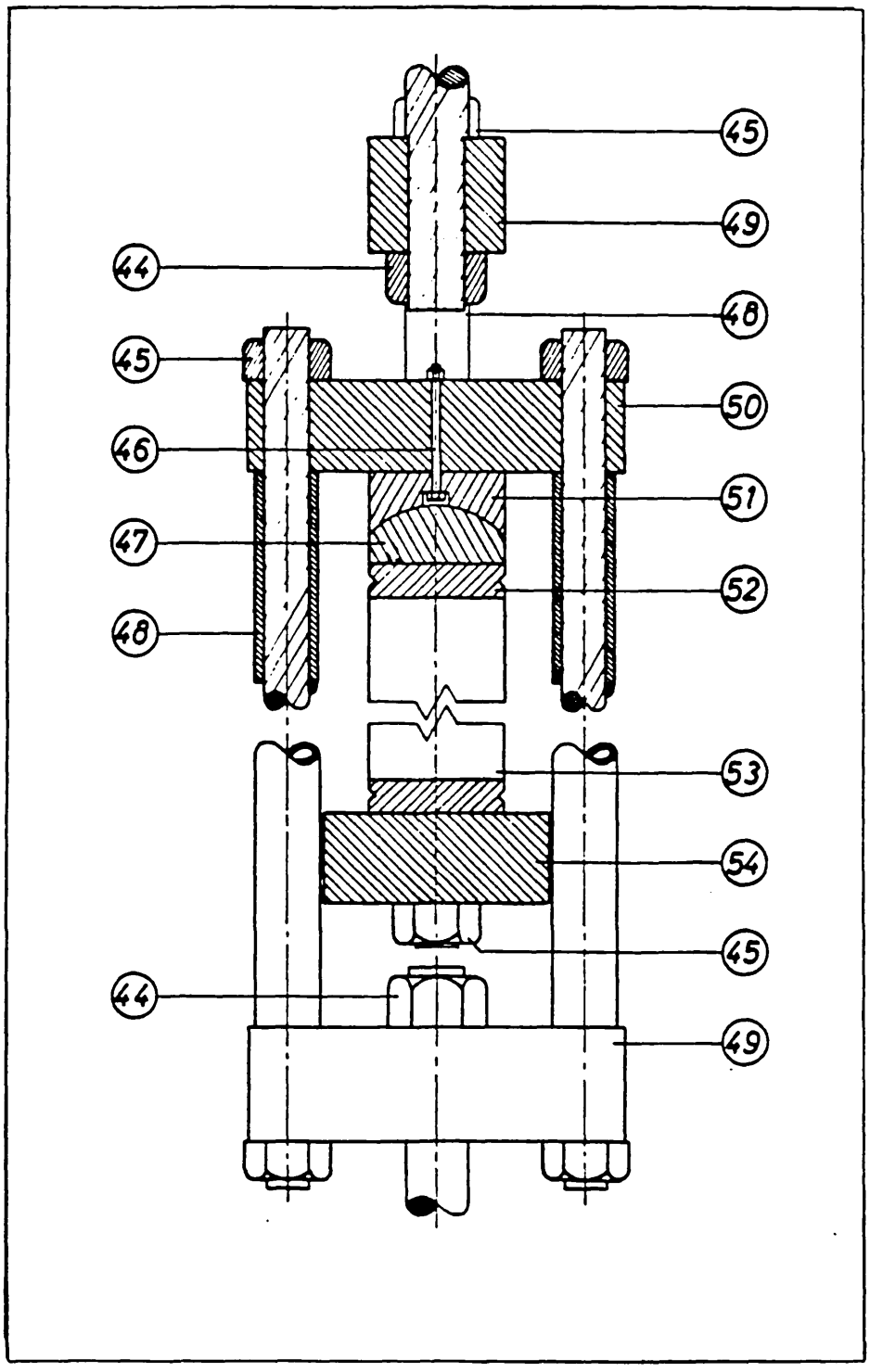

Figure 4.12 - HIGH TEMPERATURE RESISTANT YOKE SYSTEM.(FROM GROSS (62))

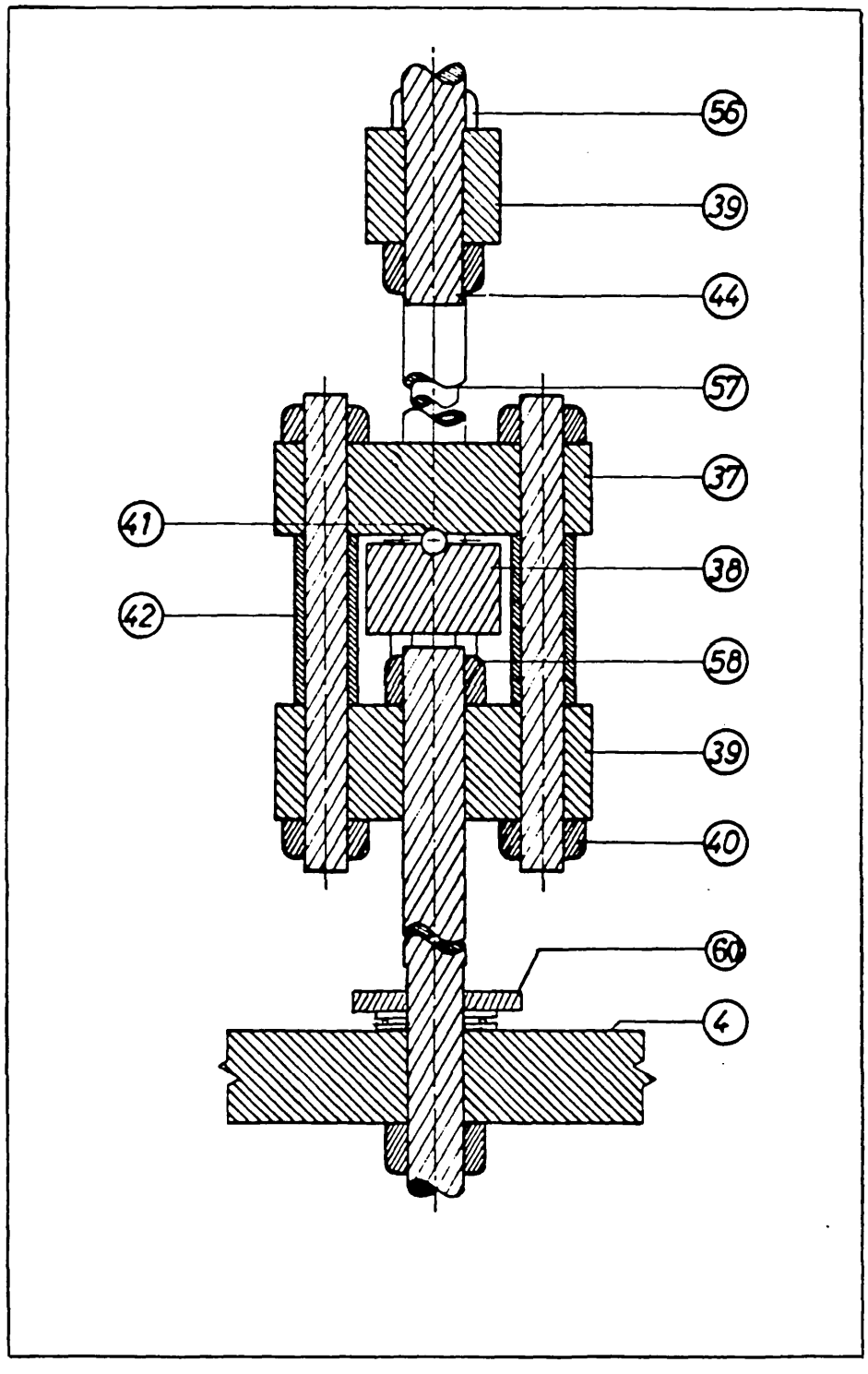

Figure 4.13 - LOWER UNIVERSAL JOINT AND LINK.(FROM GROSS (62))

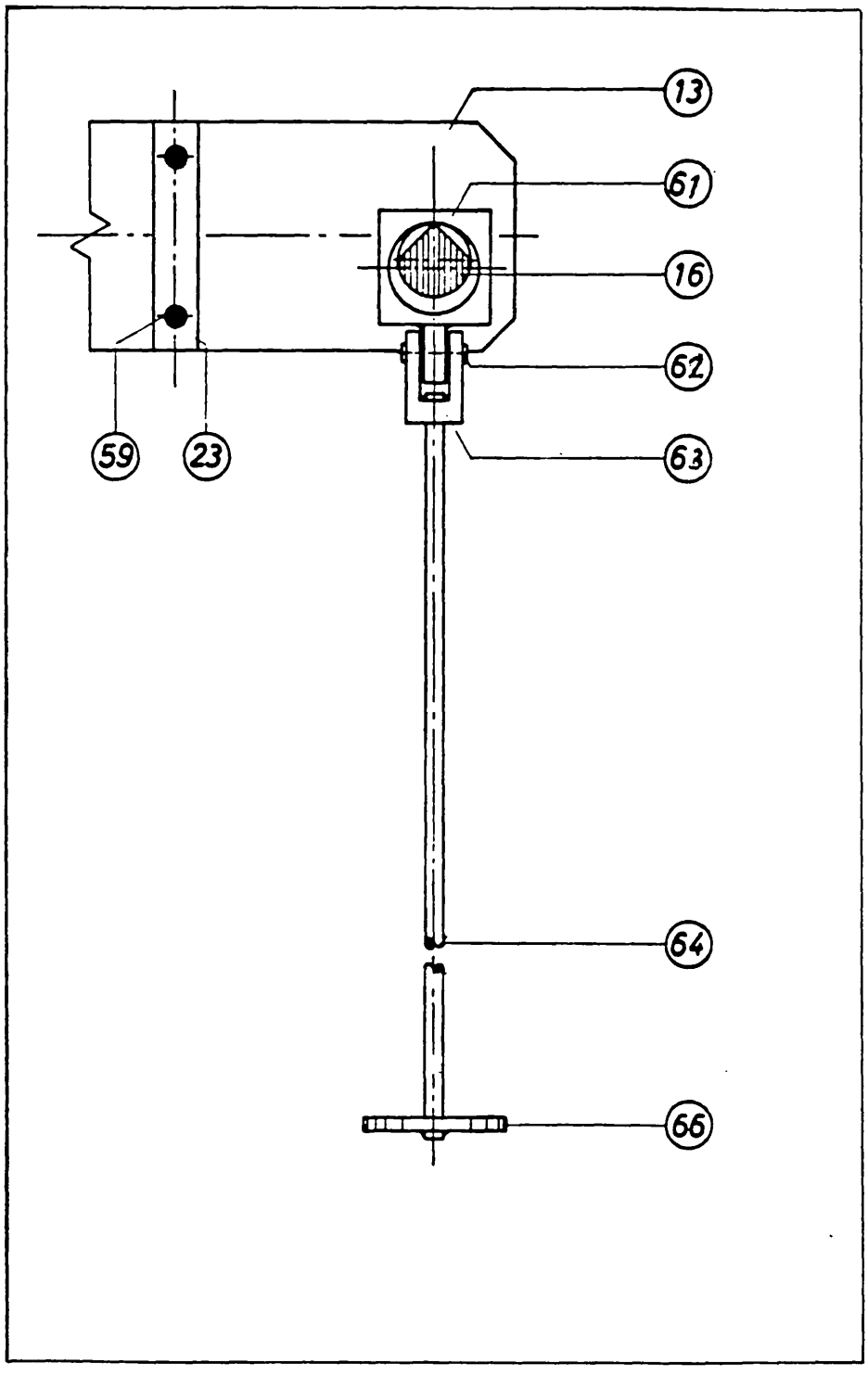

Figure 4.14 - REAR HANGER AND SUSPENSION.(FROM GROSS (62))

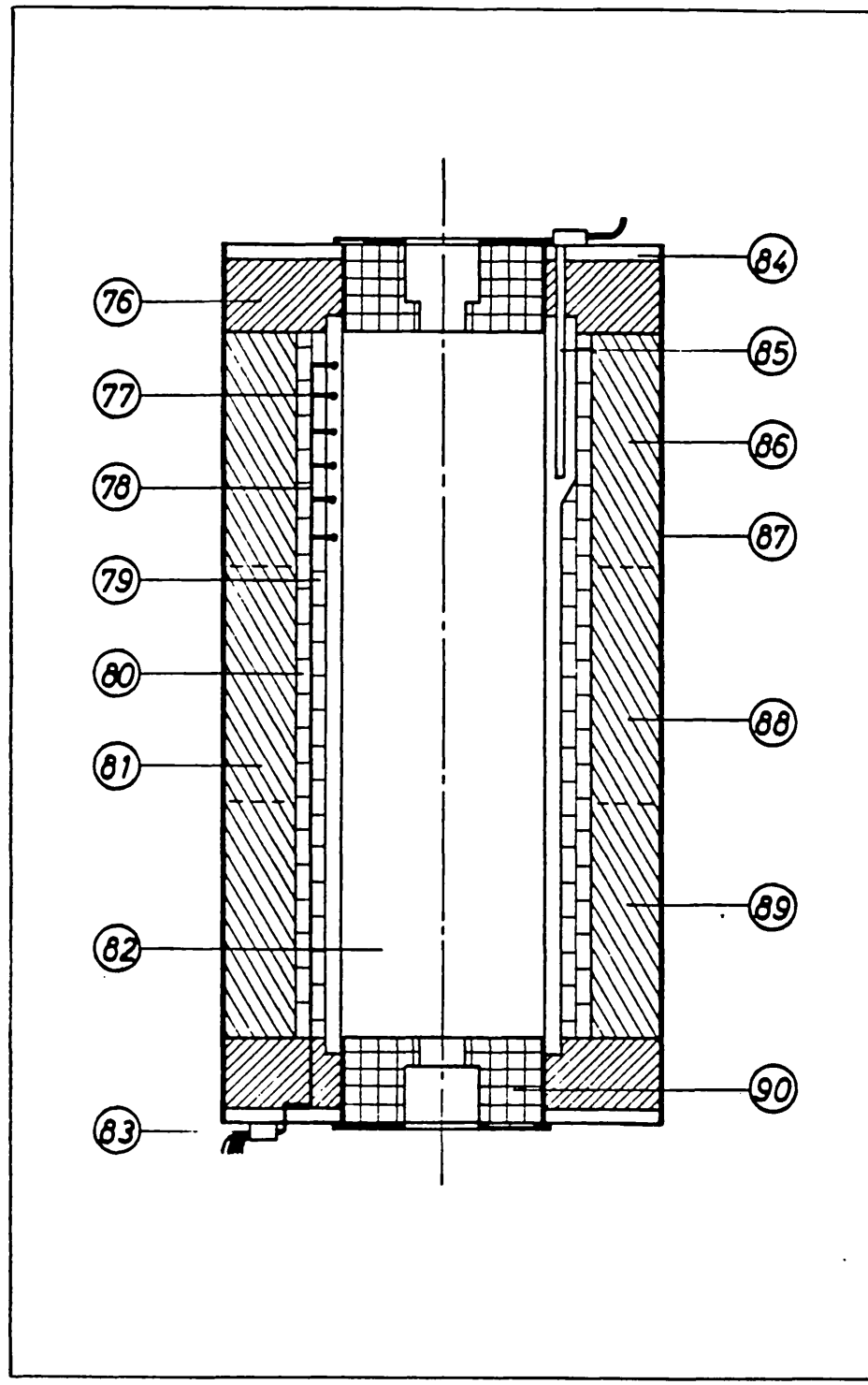

Figure 4.15 - 7" BORE THREE ZONE FURNACE.(FROM GROSS (62))

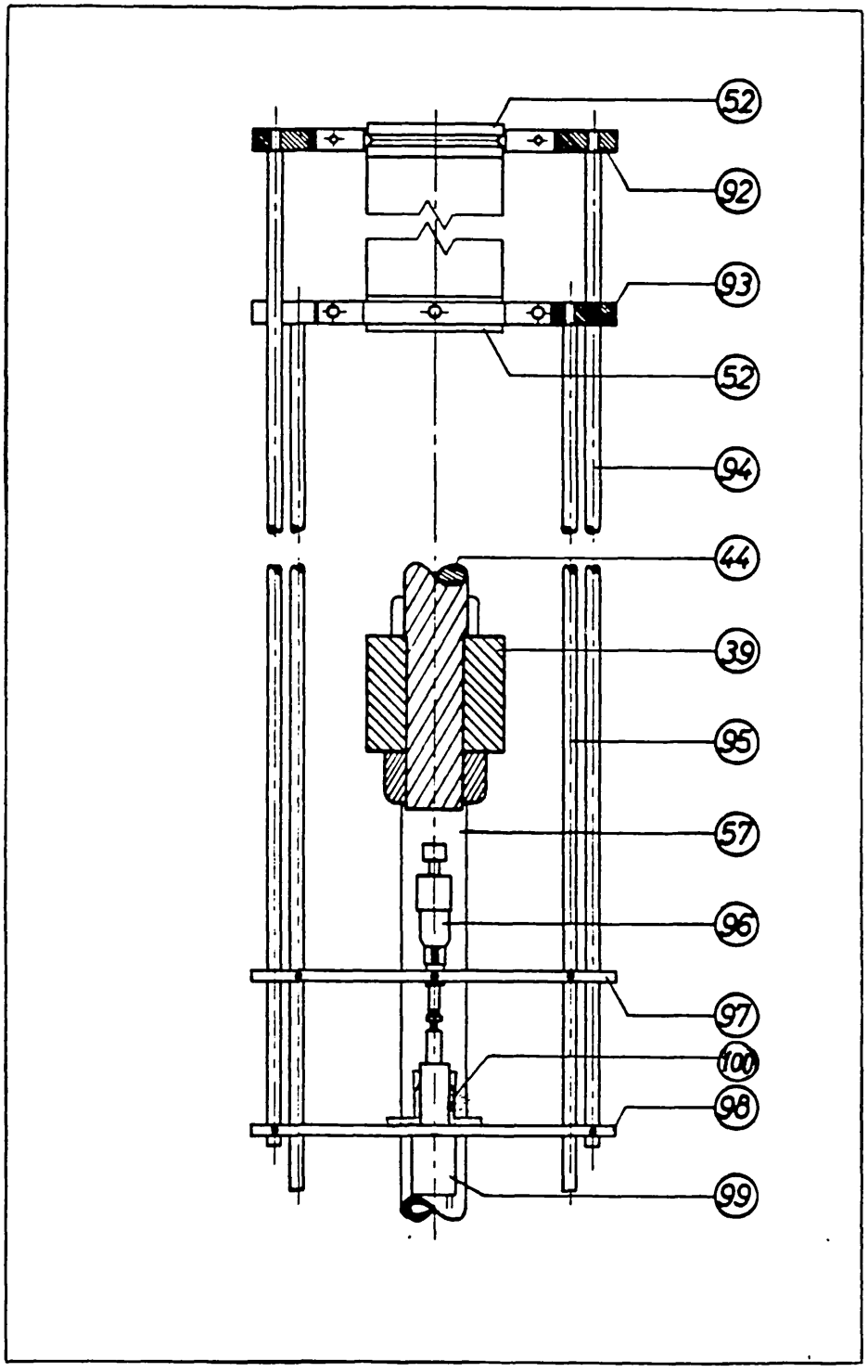

Figure 4.16 - STRAIN MEASURING DEVICE AND TRANSDUCER.(FROM GROSS (62))

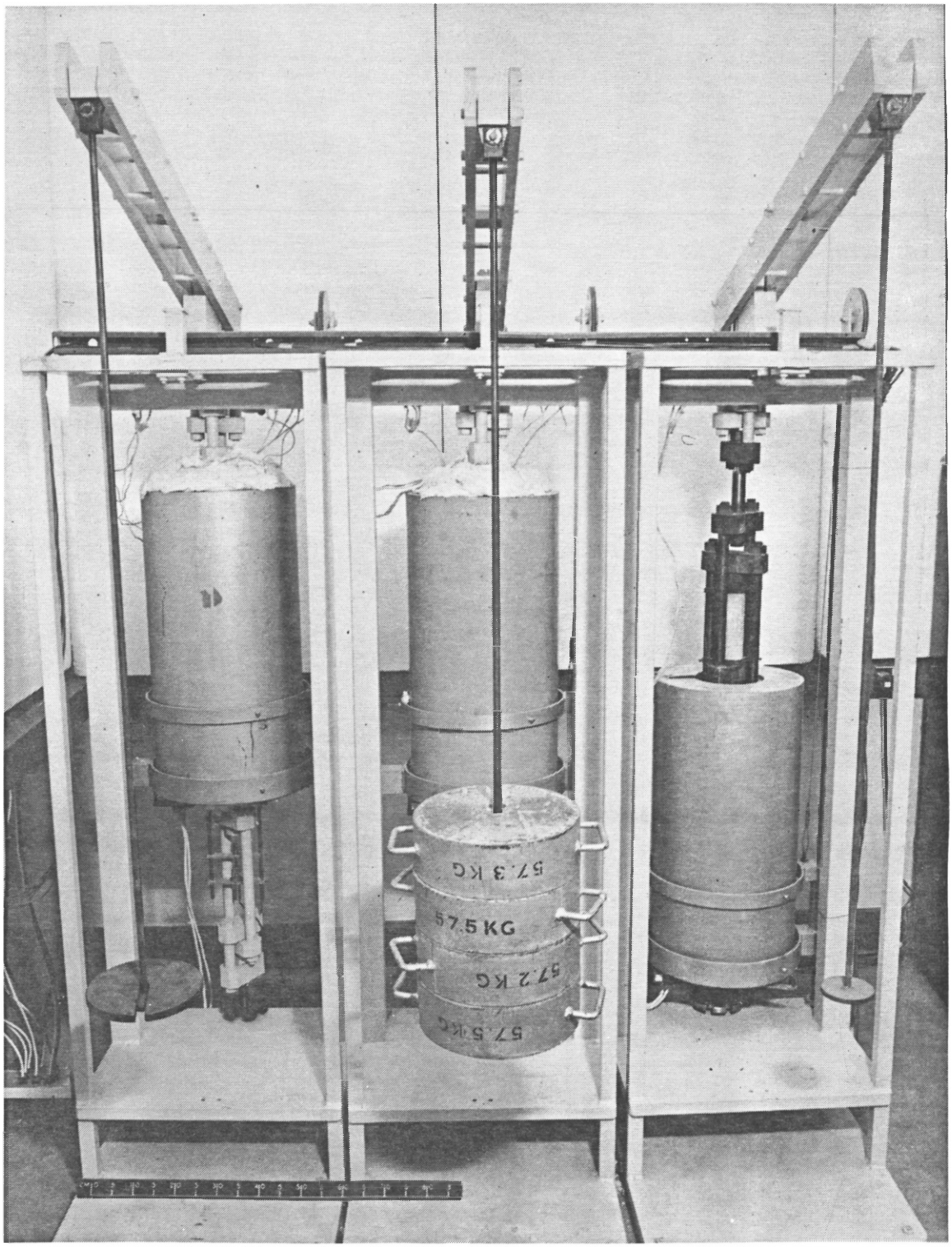

Figure 4.17 - GENERAL VIEW OF CREEP TEST RIGS.

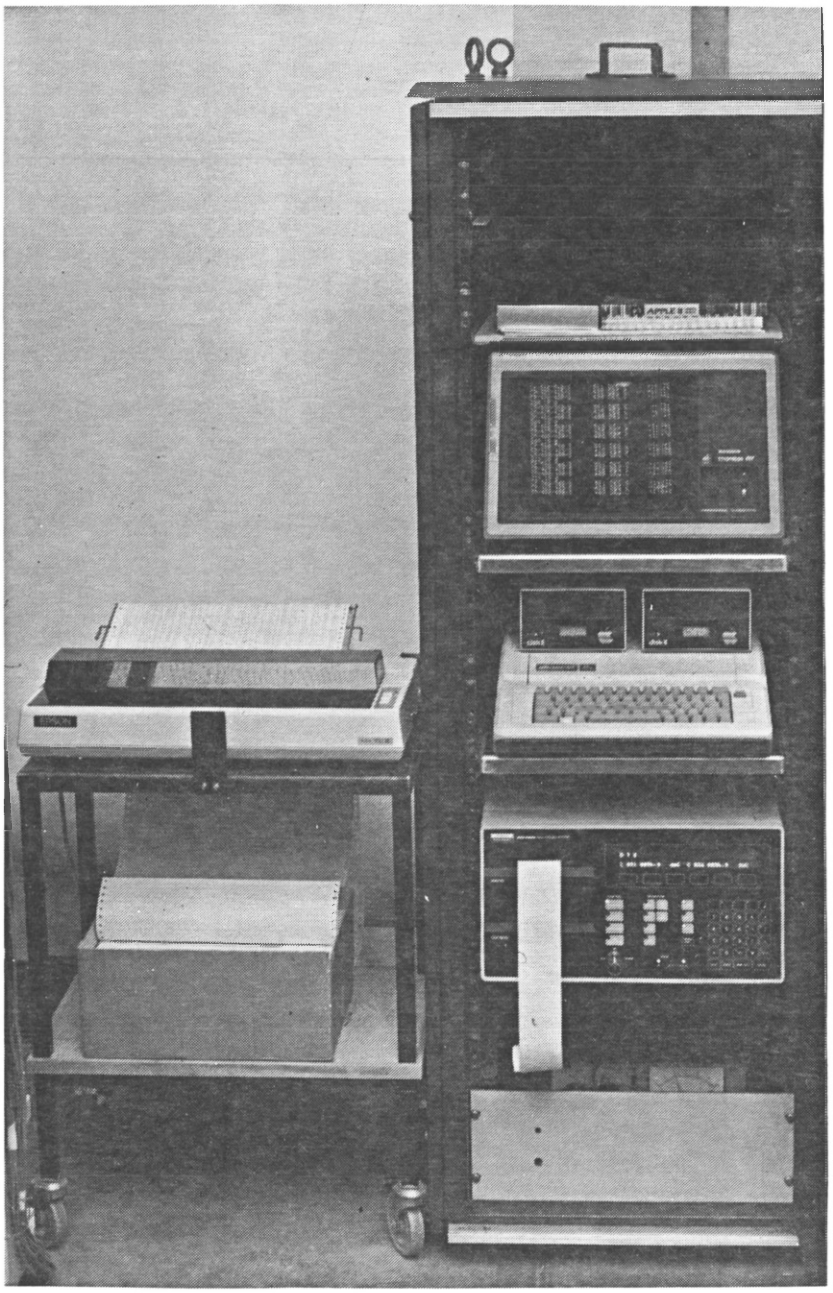

Figure 4.18 - VIEW OF DATA ACQUISITION,PROCESSING AND STORING SYSTEM.

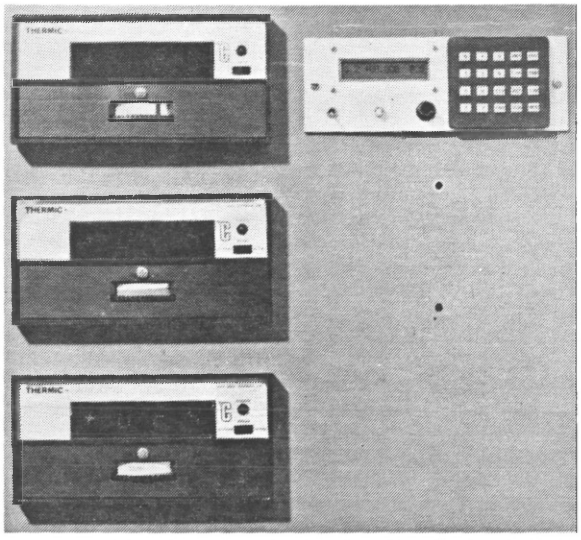

Figure 4.19 - PROGRAMMEABLE TEMPERATURE CONTROL UNIT AND DISPLAY.

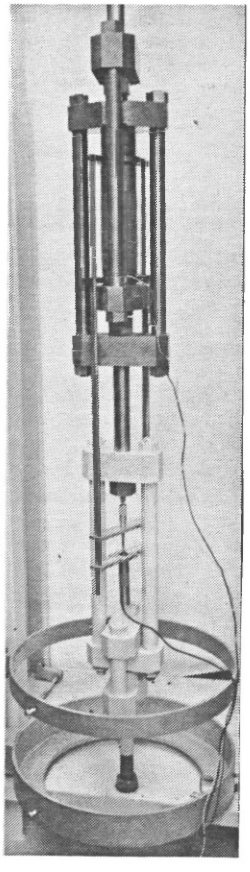

Figure 4.20 - VIEW OF STRAIN MEASURING SYSTEM.(DETAIL FROM GROSS (62))

Fig.4.21– CALIBRATION TEST FOR PLATEN EFFECTS

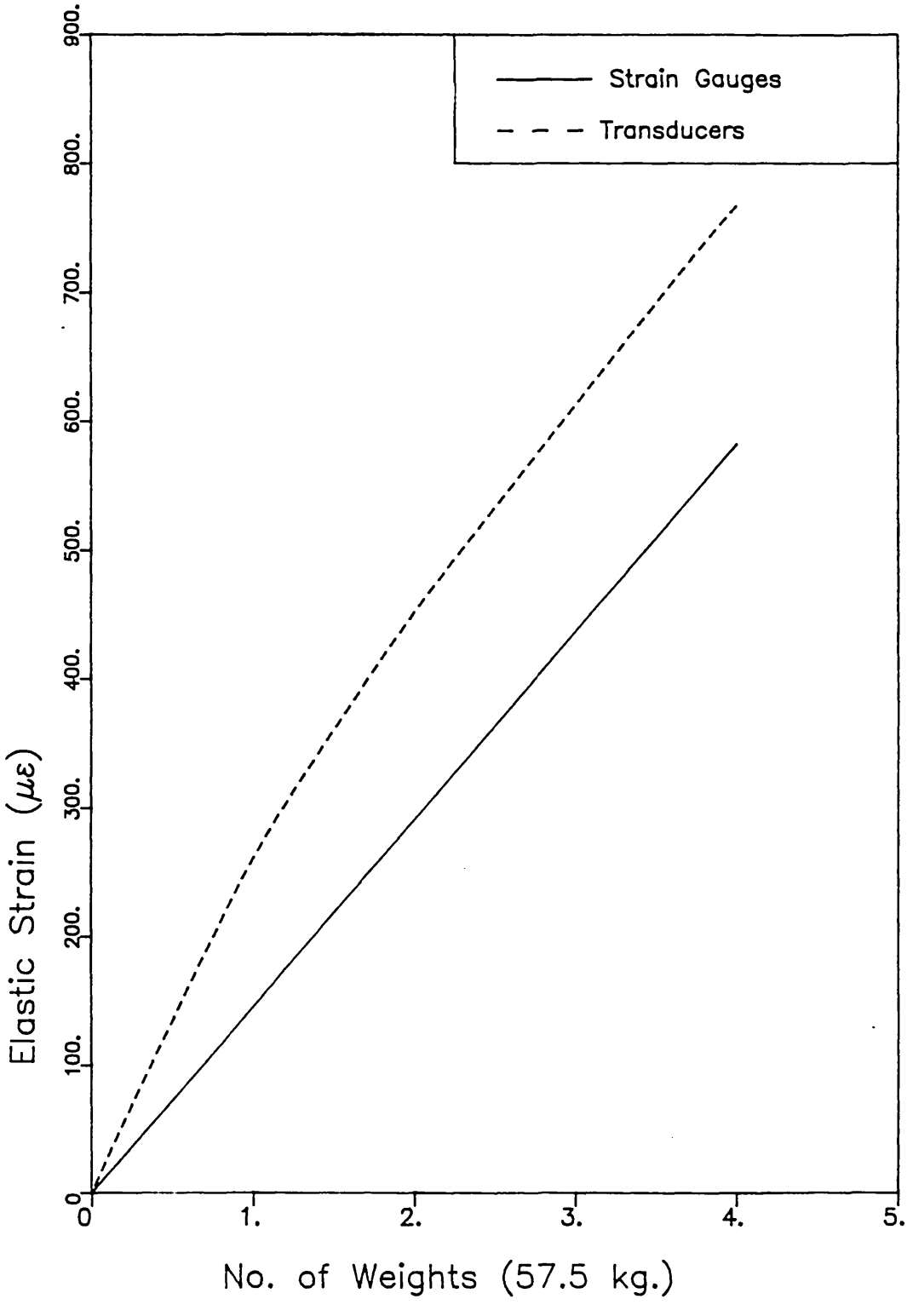

Fig.4.22 – SYSTEM CALIBRATION TEST

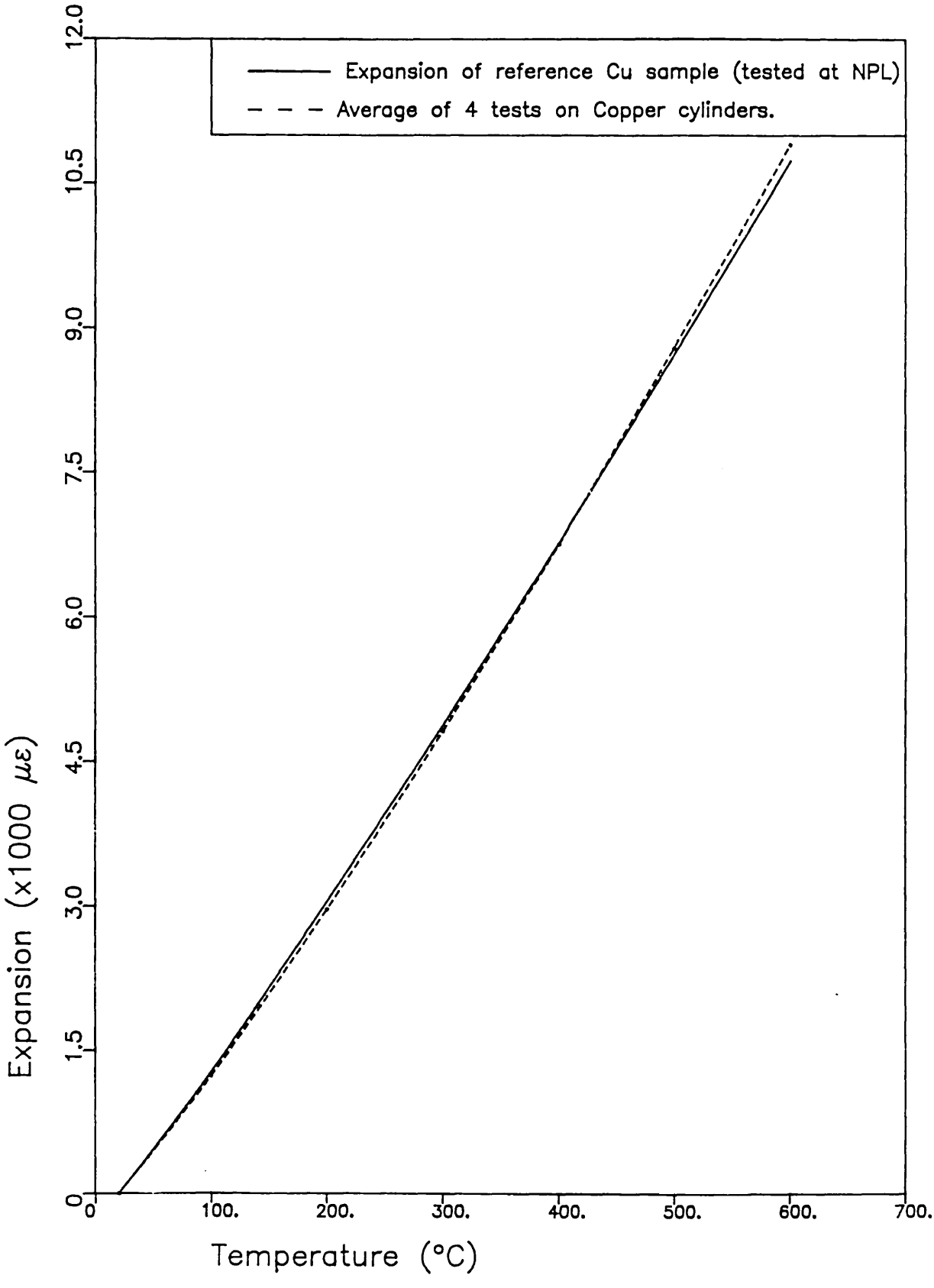

Fig.4.23 – TEMPERATURE vs. TIME CURVES

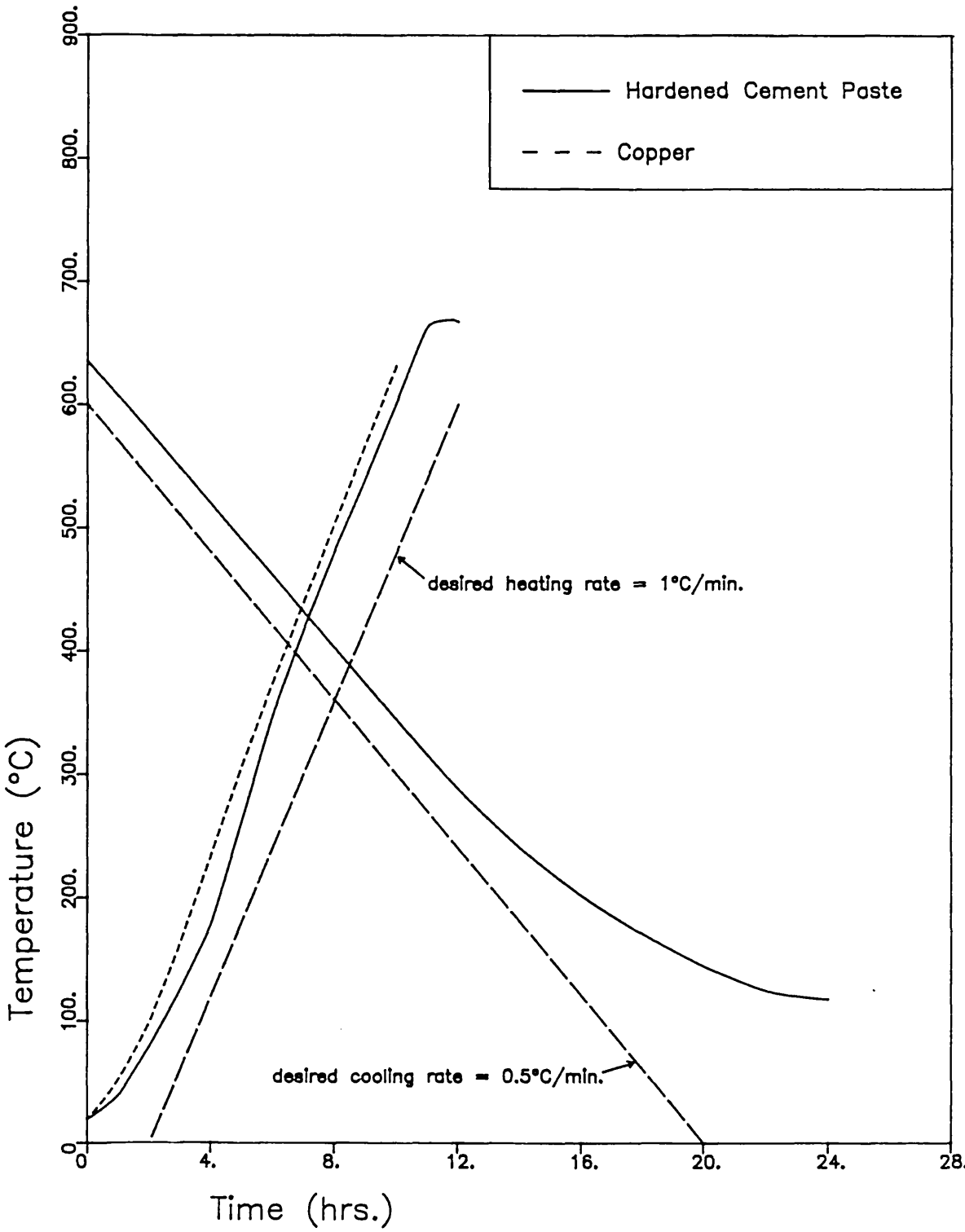

Fig.4.24 – HEATING RATE VARIATIONS & LONG^{L} TEMPERATURE DIFFERENTIALS

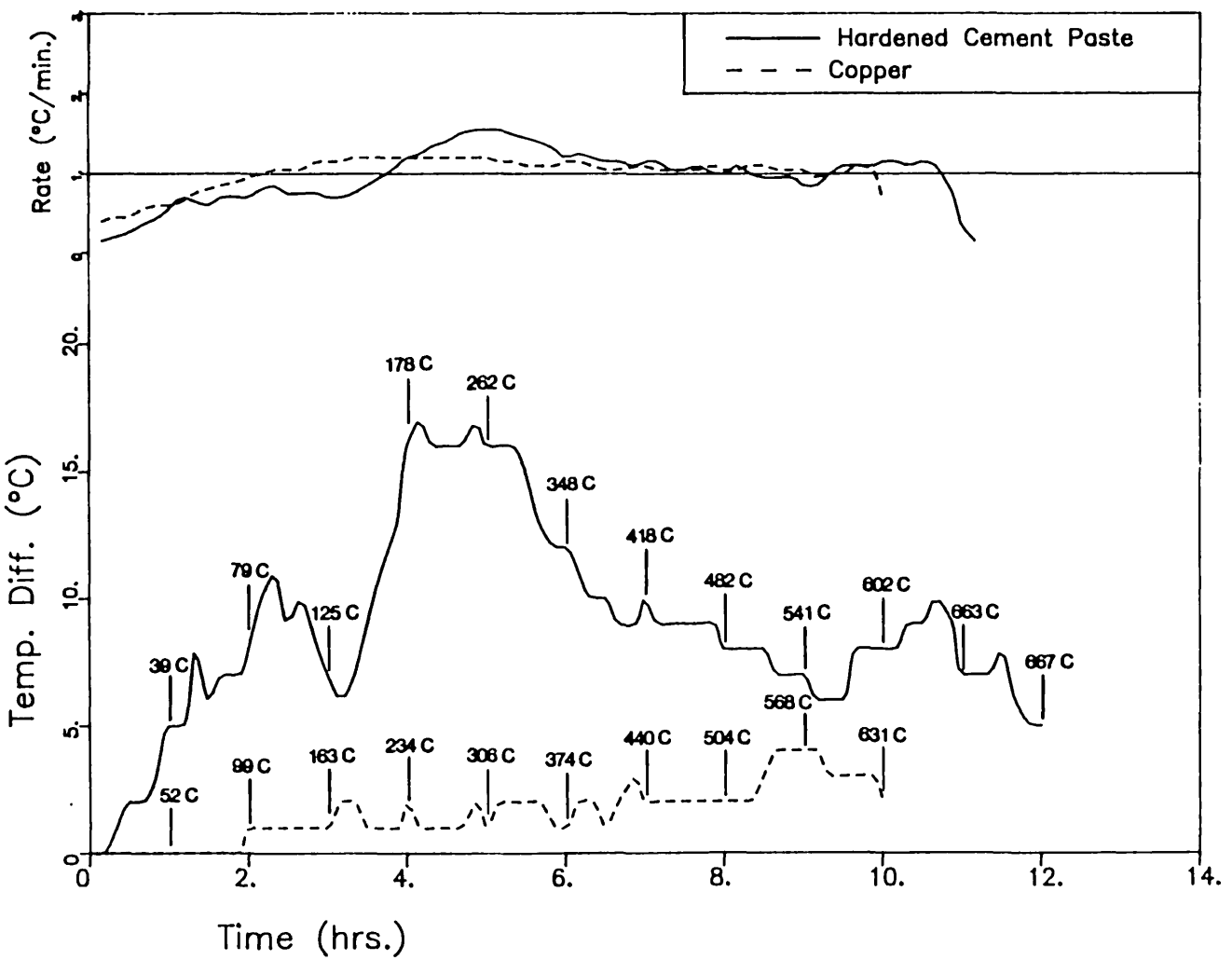

Fig.4.25 – COOLING RATE VARIATIONS & LONG^{L} TEMPERATURE DIFFERENTIALS

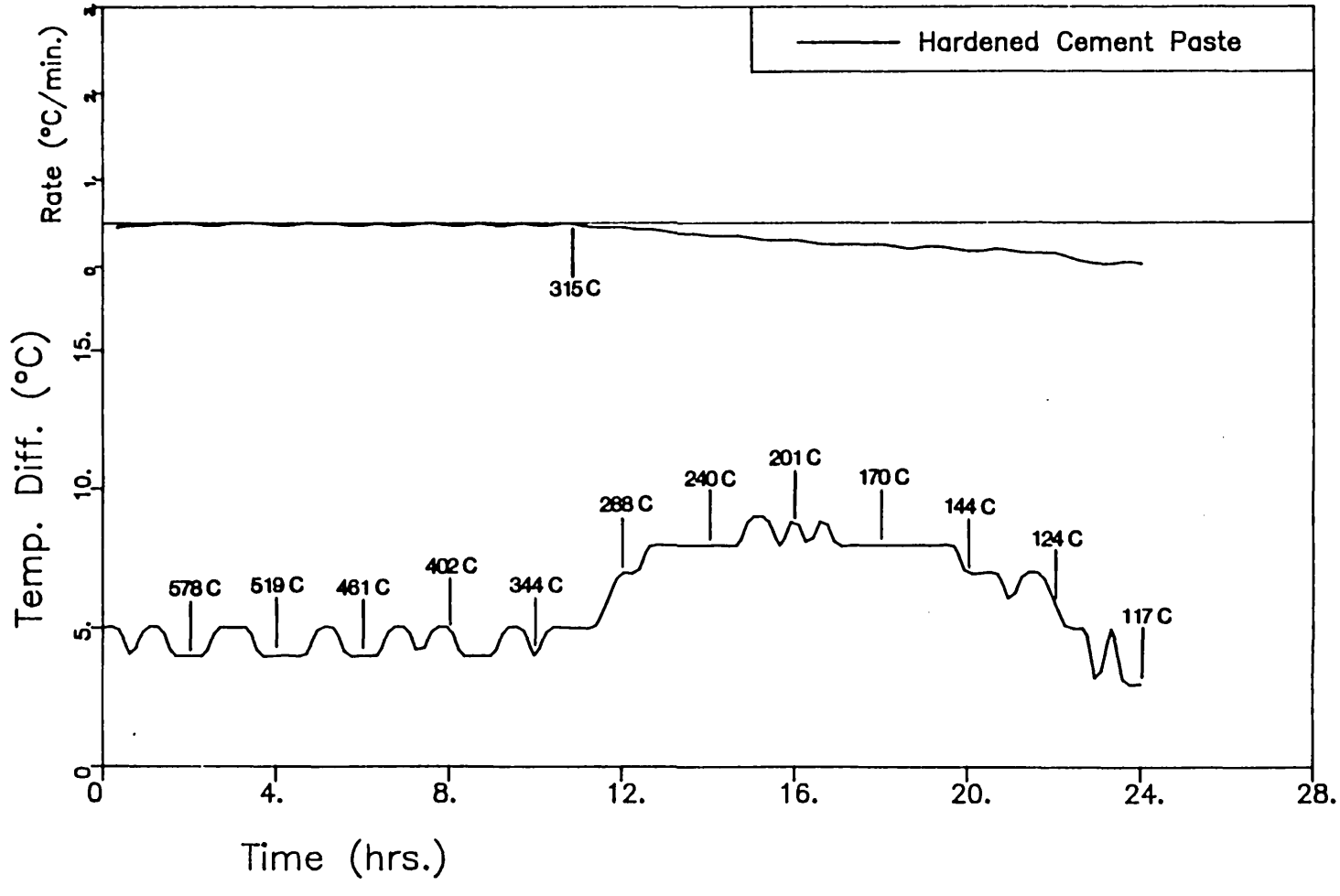

CHAPTER 5 - STRENGTH AND ELASTIC PROPERTIES

Although the main body of the present investigation is concerned with time dependent deformations in cement paste, strength and modulus of elasticity measurements that were carried out will be reported and discussed first. In addition to giving a more complete picture of the behaviour of cement paste in the temperature range studied, some of these results will be used in the analysis of time dependent strain measurements.

5.1. MODULI OF ELASTICITY

The modulus of elasticity measurements were carried out in conjunction with Test Series I-III, performed on the creep rigs and described in Section 3.4.

5.1.1. Static Modulus

The static modulus of elasticity results, both at temperature and upon post-cooling are indicated in Figures 5.1 and 5.2 respectively. They are represented as percentages of the initial static modulus of elasticity, prior to testing, of each specimen. Normalization in this fashion was expected to reduce if not eliminate errors due to test rig and specimen variability. The mean initial static modulus of elasticity for 56 specimens tested was 20.11 kN/mm^2 and the standard deviation 3.23 kN/mm^2.

Let us consider first the results of Test Series I, indicated by solid lines in Figures 5.1 and 5.2 for tests at temperature and upon post-cooling respectively. Although Figure 5.1 shows a fairly sharp drop in modulus from ambient to around 200°C, a significant drop becomes apparent in Figure 5.2 only after 120°C, up to which temperature there is an actual increase in value over the initial modulus. Where both figures are concerned, the modulus does not seem to change much between 200°C-300°C, which is similar to findings by other investigators (167, 177). Above 300°C, there is another sharp

drop till around 460°C after which there seems to be a level plateau again until 600°C; beyond this, there is a final drop.

An attempt to explain these results is made by examining the relationship between weight loss and modulus (solid line in Figure 5.3). The residual or post-cooled modulus has been selected because it would not contain any thermal component that may be present at temperature; furthermore, since the specimens were cooled under load, distortion of the results due to cracking arising from thermal gradients is expected to be minimal if not non-existent. The figure shows a reasonable correlation between weight loss and modulus except for the points beyond 600°C (which have not been used to obtain the correlation). The variation of weight loss with maximum temperature is given in Figure 5.4.

Both Figures 5.1 and 5.2 show a reasonably constant modulus from 50°C to 90°C and 50°C to 120°C respectively, although their values differ considerably. This range would correspond to the loss of physically held water. The increase in modulus at 120°C in Figure 5.1 may be due to a physical densification effect. A similar effect was reported by Gross (63) who found a minimum for the static modulus of elasticity at 80°C. The increase in modulus above the initial value up to a temperature of 120°C in Figure 5.2 would again be due to a densification effect, caused both by drying as well as loading during the creep test and the cooling phase. This would seem to be confirmed by the Series III results showing an even greater increase above the initial value; these specimens were loaded during the heating phase as well as the constant temperature and cooling phases.

The constant modulus shown between 200°C-300°C (despite the loss of weight in that range - and this too probably due to the loss of chemically combined water) is an interesting phenomenon. Here too it may be that the detrimental effect of losing chemically combined water is offset by a physical densification due to drying out. In this context it is pertinent to note Rostasy's (148) findings that the increase in porosity up to 300°C was much smaller than expected, given the amount of moisture lost at that temperature.

Despite an increase in weight loss above 635°C (due perhaps to decarbonation), the corresponding drop in modulus is much greater, as indicated by Figure 5.3. This could perhaps be explained as being due to the increase in the main pore radius of cement paste which takes place at that temperature, as reported by Schneider and Diederichs (154). (See Figure 2.24).

The trends of the Series II results in Figures 5.1 and 5.2 are not too definite, but seem to indicate that the moduli at test temperatures are approximately equal to, if not greater than the moduli at the pre-heat temperatures. (The specimens pre-heated to 300°C in Figure 5.2 are exceptions to this trend). This is in agreement with Marechal's (101) results (shown in Figure 2.19) and confirms his hypothesis that the change in modulus is due primarily to a change in the structure of the material which is temperature induced, and not due to temperature itself. However, the slight increase in modulus shown at some lower test temperatures (despite the fact that cooling to these temperatures took place without load, creating potential for microcracking) may indicate that a small part of the change in modulus is due to a purely thermal effect.

Figure 5.5 shows (in the broken line) the ratio between the percentages of the moduli at temperature and upon post-cooling. The ratio is always less than unity, because of densification caused by loading in the creep and cooling phases, prior to post-cooled testing. Walther and Pareth (175) have also reported that post-cooled creep specimens showed a 13-14% increase in residual modulus of elasticity over corresponding shrinkage specimens, the test temperature in their case being 200°C. The fact that the overall trend in Figure 5.5 is downward with increasing temperature also serves to confirm the previously stated suggestion that there is a thermal effect which contributes to the decrease in modulus with temperature.

5.1.2. Dynamic Modulus

The pulse velocity and dynamic modulus of elasticity, derived from pulse velocity tests performed upon post-cooling, are normalized in the same fashion as the static modulus results and shown in Figures

5.6 and 5.7 respectively. (The mean initial dynamic modulus of elasticity for 56 specimens tested was 27.75 kN/mm^2 and the standard deviation 1.01 kN/mm^2). The trends seem to be clearer and the scatter reduced, in comparison with the static modulus results.

The Series I results (in solid lines) can be described as having an essentially monotonic drop in value from ambient to around 500°C (with a sharp drop from 375°C to 425°C), a level plateau thereafter and another sharp drop beyond 600°C. They compare well with the results of Logothetis and Economou (95) which also indicate a steeper decline in modulus between 300°C and 500°C, the wider temperature range perhaps being a result of fewer experimental points. (See Figure 2.21a). The sharper drop beyond 600°C was also found by Khoury for lightweight concrete (84).

When comparing these results with the static modulus results, it can be seen that the increase above the initial modulus (Figure 5.2) and the 'level plateau' beween 200°C and 300°C (Figures 5.1 and 5.2) are absent from Figures 5.6 and 5.7. The pulse velocity measurements seem therefore, to be more sensitive to moisture loss than to densification. The broken line in Figure 5.3 seems to indicate a better correlation for dynamic modulus with weight loss than for static modulus. In this context it is interesting to note that the Series III specimens, despite reflecting a pronounced densification effect in Figure 5.2, do not give pulse velocity or dynamic modulus results that are very different to the Series I specimens, especially at lower temperatures.

The Series II results show similar trends as in Figures 5.1 and 5.2, but the reduced 'scatter' makes for more apparent 'horizontality'. One conclusion that could be drawn from this is that, since pulse velocity techniques are expected to be sensitive to cracking, very little if any cracking is caused by cooling from pre-heat to test temperatures. Hence the structure of the material at the pre-heat temperature could be considered as being maintained at test temperatures. This is a very important consideration for one of the assumptions made in Section 8.2.

The ratios of percentage values of dynamic to static modulus on post-cooling are shown in Figure 5.5 in solid line. Although there is a fair degree of fluctuation, there does not seem to be any visible overall trend with temperature; this is to be expected since both measurements were performed on post-cooling and would not incorporate any 'thermal' effects. The values of this ratio are consistently less than unity, which indicates that the change in the dynamic modulus of elasticity with temperature is greater than that in the static modulus of elasticity.

5.2. STRENGTH

Figure 5.8 shows the variation of hot strength with temperature. Although there is a significant drop in strength giving a minimum at 120°C, the original strength is regained with a further increase in temperature, and maintained until 300°C. Beyond this point however, there is a rapid drop in strength with temperature. The minimum in strength around 100°C is consistent with many investigators' findings (see Figure 2.17) and has been attributed to the thermally energised swelling of physically bound water layers.

The regaining of strength is probably caused by a densification effect due to drying, as described previously in the section on elastic moduli.

The rapid drop in strength after 300°C should be seen in the light of Fischer's results (54), which also indicated such a drop in strength for unsealed cement mortar after this same temperature. It is also interesting to note that Abrams' (1) unstressed concretes did not start losing strength until 300°C irrespective of the type of aggregate. (See Figure 5.11). It would seem therefore, that 300°C is a critical temperature with respect to loss of strength for unsealed Portland Cement concretes, due to a phenomenon in the cement paste matrix itself. Recent electron microscopy studies by Piasta (137) indicated that microcracking increased significantly beyond 300°C, first around $Ca(OH)_2$ crystals and then around grains of unhydrated cement.

The strength of specimens tested after being cooled down from the pre-heat temperature of 460°C seems to be essentially constant, adding weight to the observations made earlier regarding the 'structural' as opposed to the 'thermal' effect of temperature.

Figure 5.9 shows the results of the post-cooled residual strength tests done in conjunction with the creep test Series I-III. The Series I results (in solid line) show a minimum at 50°C followed by a regain in strength and a drop beyond 120°C, with sharp drops in the range 425°C-500°C and 560°C-600°C. (The result at 200°C is ignored). It is interesting to note that the minimum at 50°C is less pronounced and occurs at a lower temperature than in the hot strength results. This again would be due to some densification, both by prolonged exposure to temperature, as well as by loading.

The Series III results show this minimum at 120°C, as in the hot strength results. However, it is not clear why the Series III results are in general lower than the Series I results, given that the Series III specimens were under load during heating as well as during constant temperature and cooling, and given that they showed higher residual static moduli than the Series I specimens.

The Series II results are similar to the elastic modulus and hot strength results, the broken lines being essentially 'horizontal' in nature. Two of the specimens pre-heated to 635°C and cooled to 50°C and 120°C showed large expansive strains (see Section 6.4) and failed upon loading. This phenomenon is probably due to moisture absorption, leading to the disruptive rehydration of dissociated Calcium hydroxide (see Section 5.3).

Figure 5.10 indicates the ratio of hot strength to the Series I residual strengths. The peaks at 50°C and 300°C and the trough at 120°C could be explained by the shapes of the graphs in Figures 5.8 and 5.9. The monotonic drop of this ratio with temperature beyond 300°C would seem, again, to point to a thermal effect that also contributes to the reduction in hot strength.

5.3. POST-COOLED EXPOSURE TO ATMOSPHERE

Selected specimens from the Series I test programme were not tested for residual strength but wrapped in cling film for subsequent testing. It was discovered, however, that the cling film was not impermeable to atmospheric moisture, with the specimens gaining in weight. Although no significant signs of distress were visible on the specimens on their removal from the furnace, all specimens heated to 400°C or above exhibited severe cracking to the point of disintegration after a few days. (See Figure 5.12).

A similar phenomenon to the above was noted by Lea and Stradling (92); although they did not obtain the critical temperature accurately, they estimated a lower limit of 400°C. Harada et al (67) have also reported an initial loss in strength prior to subsequent strength gain for specimens of silica concrete exposed to atmosphere after being heated to varying temperatures for a short period. (See Figure 2.18b). They stated that concrete heated to 500°C exhibited large cracks which did not close. The small temperature intervals employed in the present investigation, however, enable us to estimate the temperature of concern fairly accurately. It is interesting to note that a specimen heated to 375°C shows no signs of distress whatever, but one heated to 400°C is cracked severely (Figure 5.12a).

This would lead us to conclude that 400°C is the critical temperature, above which Portland Cement concrete cannot be sustained for any significant period, without disintegration on subsequent post-cooled exposure to atmospheric moisture. The reason for this disintegration is the expansive and hence disruptive rehydration of dissociated $Ca(OH)_2$, which is accompanied by a 44% volume increase (135). The temperature of dissociation of $Ca(OH)_2$ is quoted in the literature as ranging from 400°C-600°C. (See Table 2.5). However, if 'static' temperature conditions are maintained, Calcium hydroxide will dissociate at 400°C (61), which temperature coincides with the critical temperature for concrete deduced from the results of this present investigation. The higher critical temperature of 500°C obtained by Harada et al (67) is probably due to the fact that their specimens were maintained at temperature for only a short period,

which may not have given sufficient time for a significant dissociation of $Ca(OH)_2$ to take place.

The figures also indicate that the specimen surface assumes a whitish hue when exposed to temperatures of 560°C and above (Figures 5.12b and c) and that cracking becomes very severe when the temperature of exposure is above 600°C. The whitish hue may be due to the formation of Calcium carbonate, which has been reported to be considerable around 500-600°C (138).

Since the above-mentioned disintegration on post-cooled exposure to air is attributed to the dehydration of dissociated $Ca(OH)_2$, some tests were performed on mixes where the OPC paste was partially replaced (i.e. 10%, 25% and 40% by weight) with PFA. DTA and other analyses have shown that PFA would reduce the amount of $Ca(OH)_2$ due to 'pozzolanic' reactions (64, 86). It was found in fact that even a 10% PFA replacement completely eliminated all visible surface cracking due to post-cooled exposure to air for specimens heated up to 600°C. (See Figure 5.12e).

Although it was not possible to make a visual distinction between the 3 PFA mix specimens on post-cooling, their strengths before heating and after post-cooled exposure showed some interesting distinctions, as seen in Table 5.1. Where the strength after 98 days' hydration is concerned, mix Z (40% PFA) seems to differ from the other two, due probably to the high proportion of PFA. It is interesting to note that mixes X and Y show strengths similar to that of mix A (0% PFA; w/c = 0.3). However, the percentage strength retained on post-cooled exposure to air for 4 months after heating to 600°C shows an increasing trend from mixes with low to high PFA replacement. It is possible that this increasing trend reflects the decreasing amounts of $Ca(OH)_2$ present in the hydrated pastes prior to heating, and hence the decreasing amount of disruption of the paste structure upon exposure to atmospheric moisture after heating to 600°C. In order to make more definite conclusions, specimens of mixes X, Y and Z should be tested for strength after heating to 600°C, but before any significant post-cooled exposure to air takes place; this would make it possible to isolate the strength variation due to post-cooled exposure alone.

It should be noted that the percentage strength retained for a mix A specimen, soon after cooling to room temperature from 600°C, is 36.9%. Since mixes Y and Z retain percentage strengths of this order or more even after post-cooled exposure to air, it may be concluded that sufficient replacement of OPC with PFA could eliminate the previously mentioned critical temperature of 400°C for Portland Cement concretes.

5.4. CONCLUSION

In concluding this chapter, an attempt will be made to highlight temperatures of significance for the mechanical properties of unsealed cement paste and draw together some of the threads brought out in the discussion so far.

The temperature range 50-120°C is characterized by a minimum in strength which can be attributed to the swelling of water layers in the paste causing weakening of bonds. The static elastic modulus decreases, in general, with temperature until around 200°C, where it levels off up to around 300°C. This latter temperature seems to be especially important, with both strength and elastic modulus dropping markedly beyond 300°C. This corresponds, at the microstructural level, to the point at which microcracking begins to increase rapidly (137). Chemically speaking, the next temperatures of significance are 400°C, at which the dissociation of Calcium hydroxide takes place, and 425°C, at which most of the moisture loss is complete. These phenomena would seem to be reflected at the macro-level by a sharp drop in dynamic modulus of elasticity around 400°C and a levelling off of the values of elastic moduli beyond 460°C. The final temperature of interest is 600°C, beyond which the elastic moduli again drop sharply. At the microstructural level, the start of a sharp increase in the main pore radius of the cement paste has been detected at this temperature (154).

A fairly dominant thread in this chapter has been the concept of densification, reflected in the enhancement of mechanical properties. Perhaps the first reference to this phenomenon is

Gilkey's contribution in 1937, where he reported that concrete specimens air dried prior to testing had higher compressive strengths than those moist at testing (59). Since then, the beneficial effects, within limits, both of thermally induced drying as well as simultaneous loading have been observed and reported (1, 83, 97, 175). The enhancement of properties on drying would be due to increased physical or chemical bonds between solid surfaces in the cement gel. Loading would have a confining effect on the specimen and inhibit crack development and propagation; in addition, it could promote solid to solid bonds and possibly reduce porosity.

This present investigation has shown that thermal drying contributes to the improvement of strength and perhaps even static modulus of elasticity. This effect was seen to commence at temperatures as low as 50°C, but under some conditions was reflected only at temperatures in excess of 120°C. Thermal drying ceased to be beneficial above 300°C, when microcracking and dehydration of the gel caused a deterioration of mechanical properties. The effect of load also tended to improve the mechanical properties; loading during the heating phase in addition to that at constant temperature and cooling phases was in general more beneficial than loading during the latter two phases alone. It seemed however, that the effects of densification, either by drying or loading, were not reflected in the pulse velocity measurements.

Another feature with regard to these strength and elasticity results was their possible correlation with porosity and moisture loss. The elastic moduli showed good correlation with moisture loss, the dynamic modulus in particular being seen to be more sensitive to the moisture condition than to densification effects.

The strongest link with porosity changes reflected in this investigation is probably the sharp drop in elastic moduli above 600°C, at which temperature the main pore radius of cement paste has been found to increase rapidly (154). Another correlation with porosity is the fact that the porosity of cement mortar has been found to show little change up to 300°C but to increase quickly thereafter (148); the strength and static modulus of elasticity results here were also

found to decrease fairly rapidly after this temperature of 300°C. One piece of evidence regarding porosity seems to be contradictory to findings here as well as those of other investigators. Kasami et al found a minimum for porosity in the pore size range 75Å -75000Å at 80°C (83). This however, seems to coincide with a minimum for strength, whereas a maximum would have been expected.

The final thread to be discussed will be the structural versus the thermal effect of temperature. All mechanical properties showed that the over-riding effect of temperature on cement paste was structural as opposed to thermal - i.e. once the material was heated to a given temperature, its behaviour was characteristic of that temperature and not, in general, dependent on any lower temperature it was cooled to prior to testing. However, the evidence seemed to indicate that a slight contribution from a thermal effect was also present.

Mix	A	X	Y	Z
% PFA	0	10	25	40
w/s Ratio	0.3	0.3	0.3	0.3
98-day strength (N/mm^2)	98.74	101.1	101.0	86.8
Strength after heating to 600°C and cooling back to R.T. (N/mm^2)	36.4	-	-	-
Strength after post-cooled exposure to air (N/mm^2)	0	27.6	36.8	34.7
Percentage strength Retained(*) (%)	36.9	27.3	36.4	40.0

(*) For mix A, this refers to the strength retained immediately after cooling back to room temperature; for the other mixes this refers to the strength retained after a 4 month post-cooled exposure to air.

TABLE 5.1. STRENGTH REDUCTION DUE TO HEATING AND POST-COOLED EXPOSURE TO AIR.

Fig.5.1 – STATIC MODULUS OF ELASTICITY AT TEMPERATURE

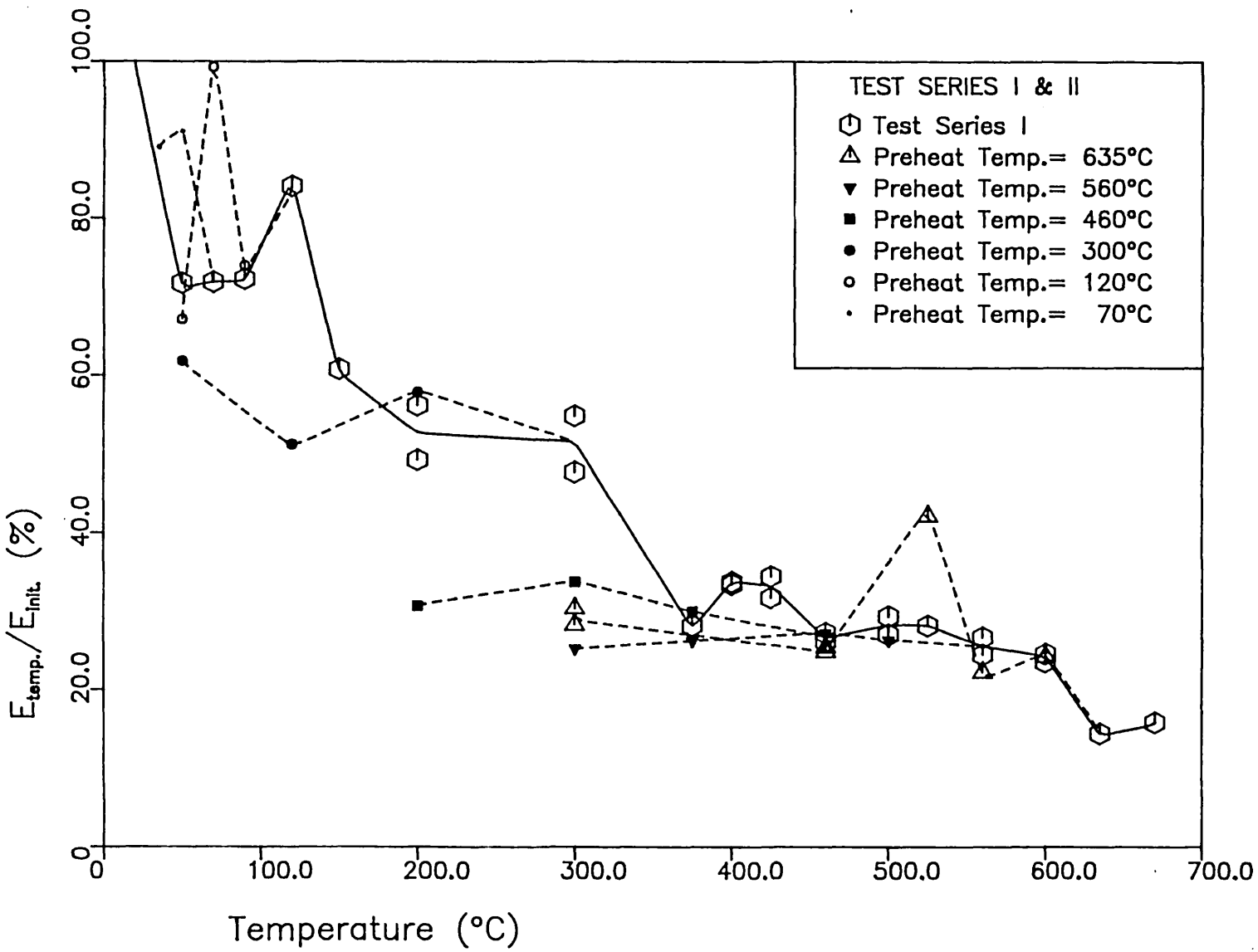

Fig.5.2 – RESIDUAL STATIC MODULUS OF ELASTICITY

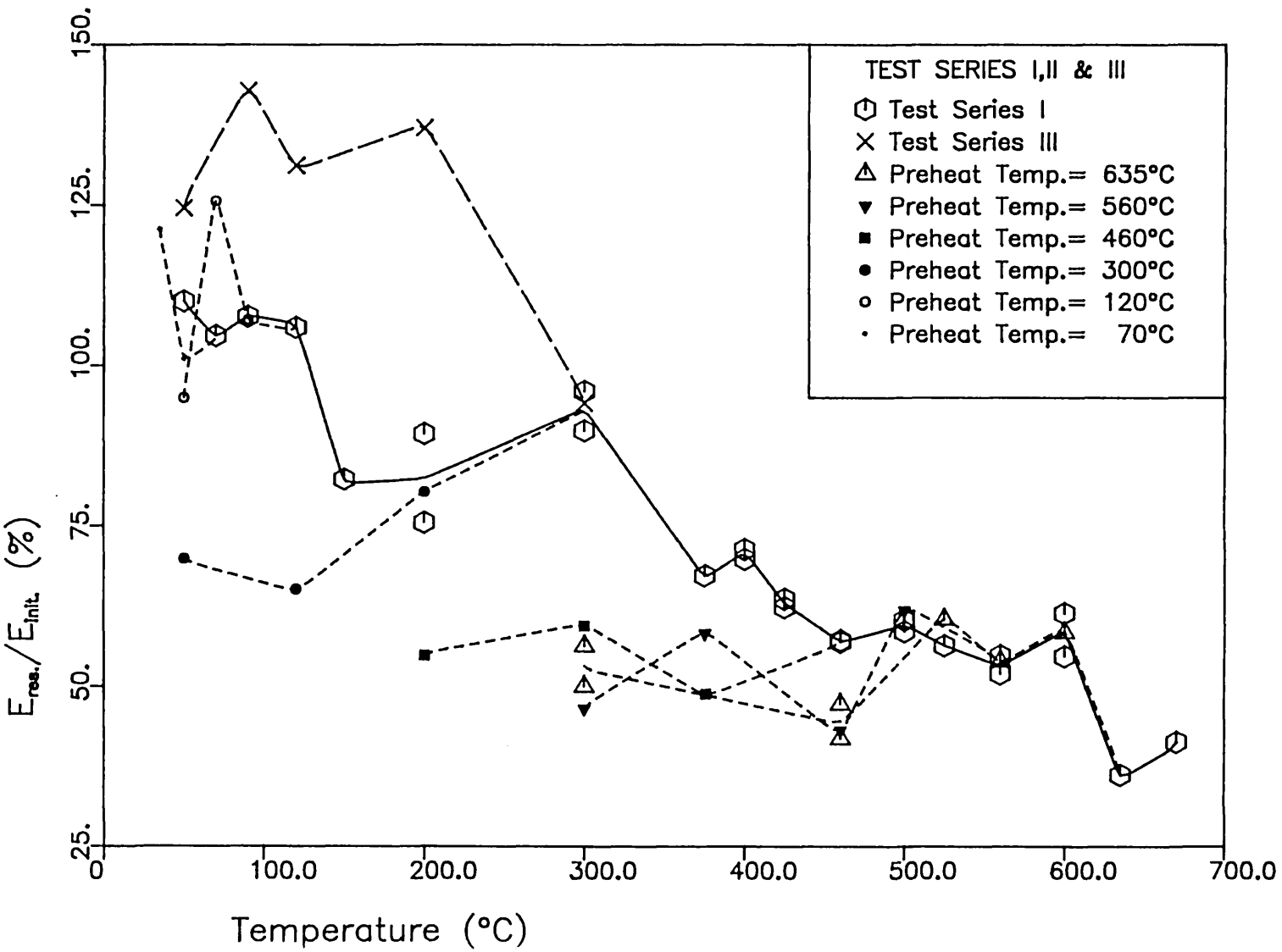

Fig.5.3 – RESIDUAL MODULUS OF ELASTICITY vs. WEIGHT LOSS

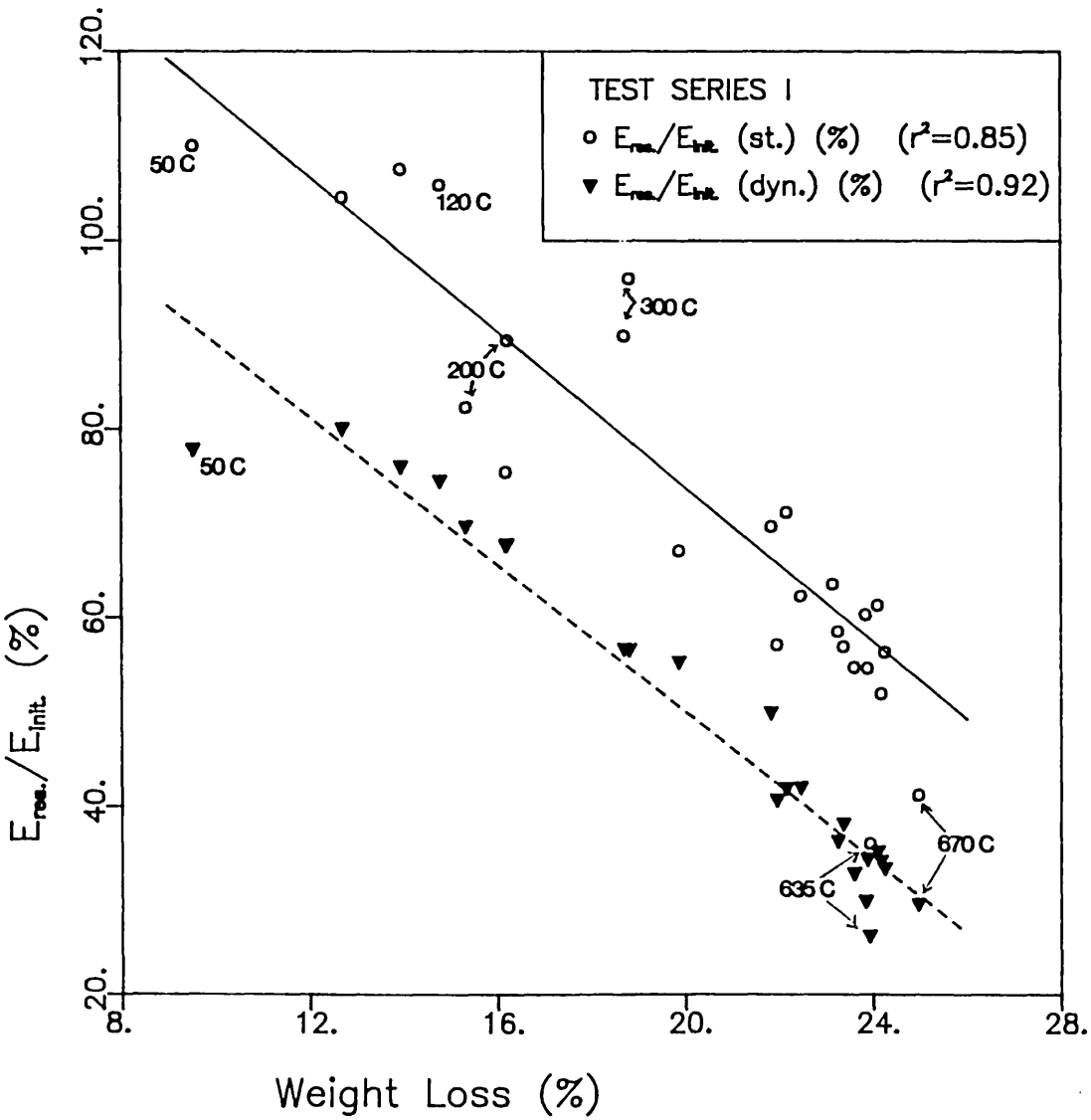

Fig.5.4 – TOTAL WEIGHT LOSS

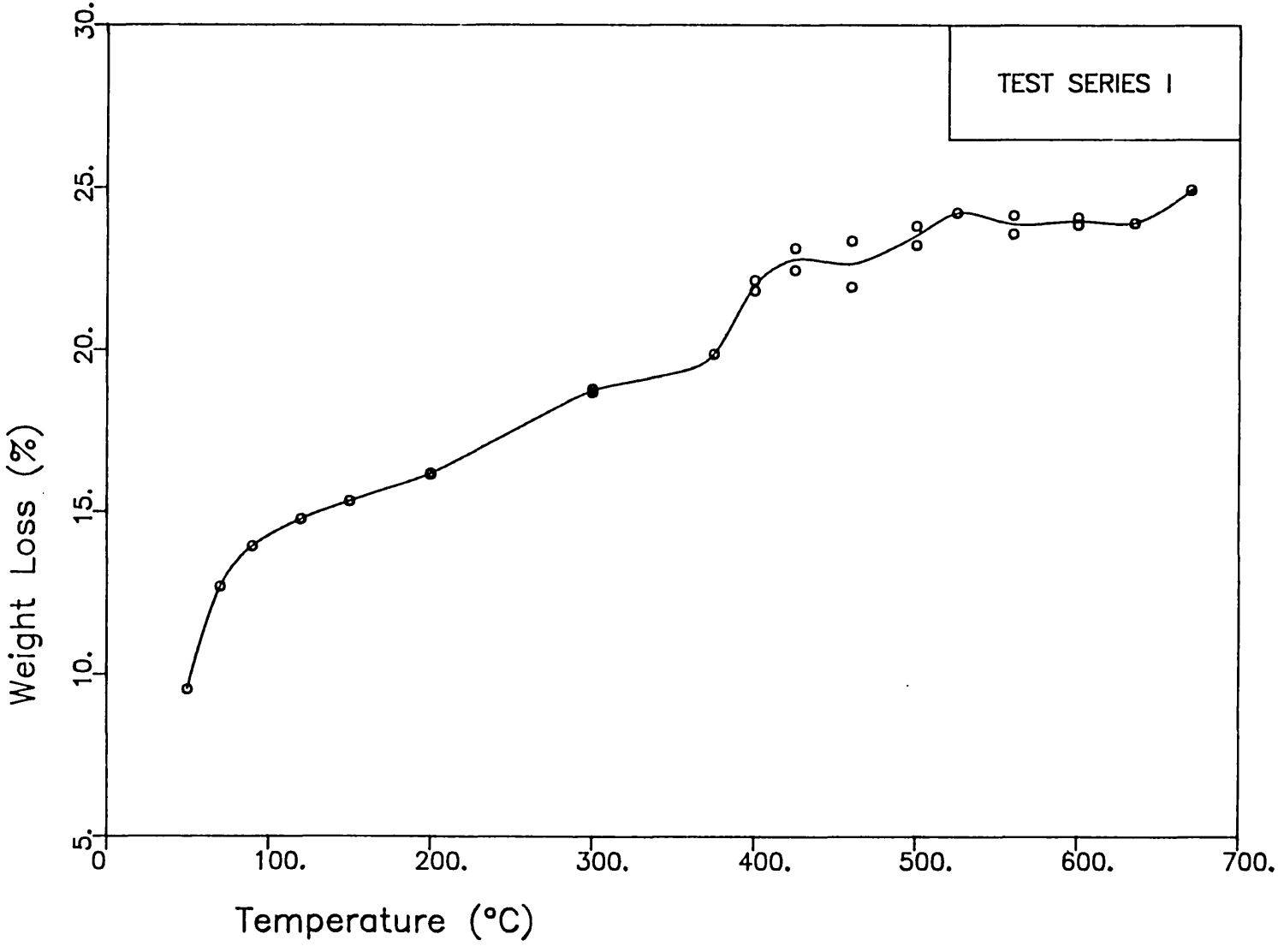

Fig.5.5 – RATIOS OF ELASTIC MODULI

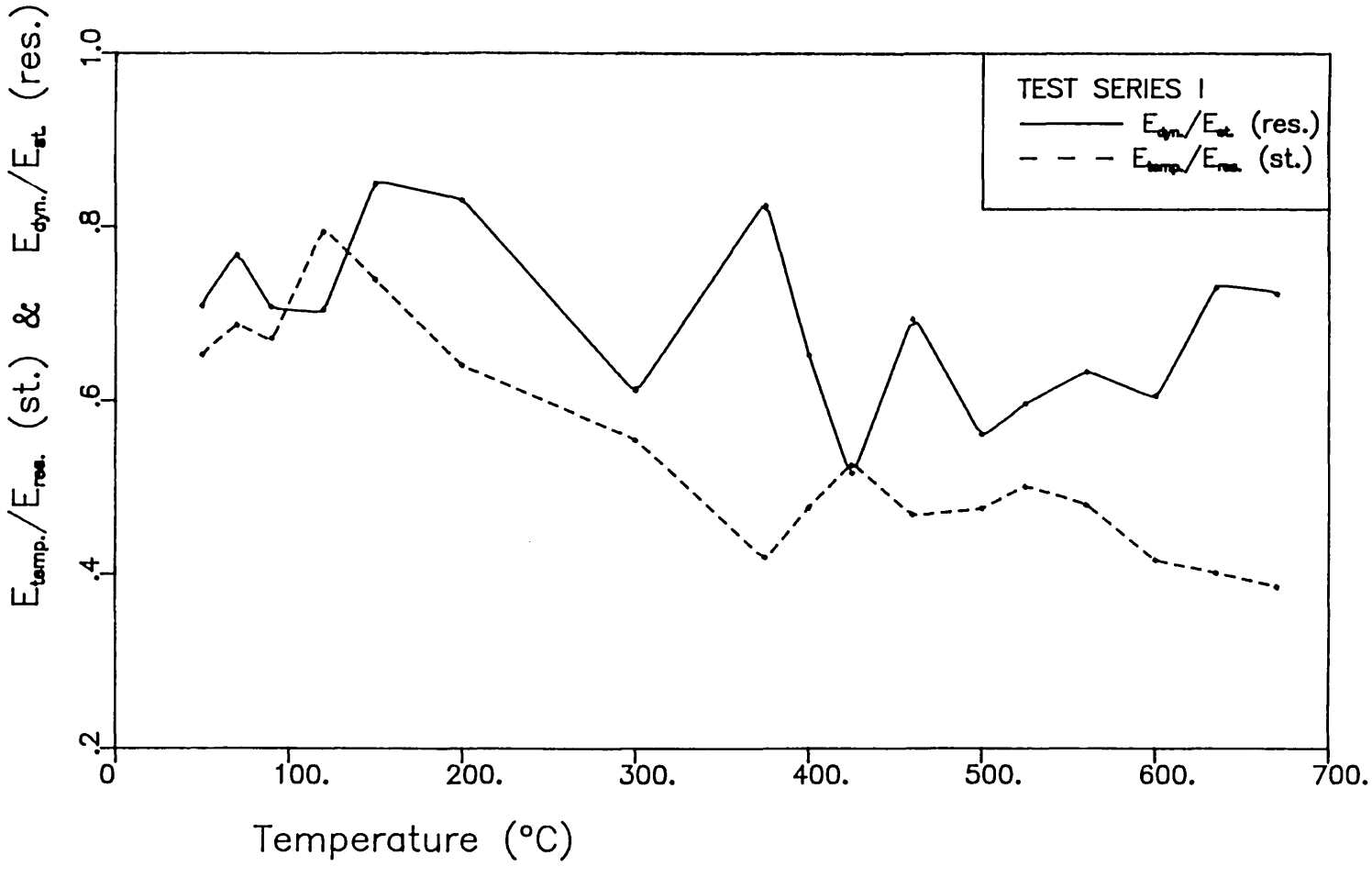

Fig.5.6 – RESIDUAL PULSE VELOCITY

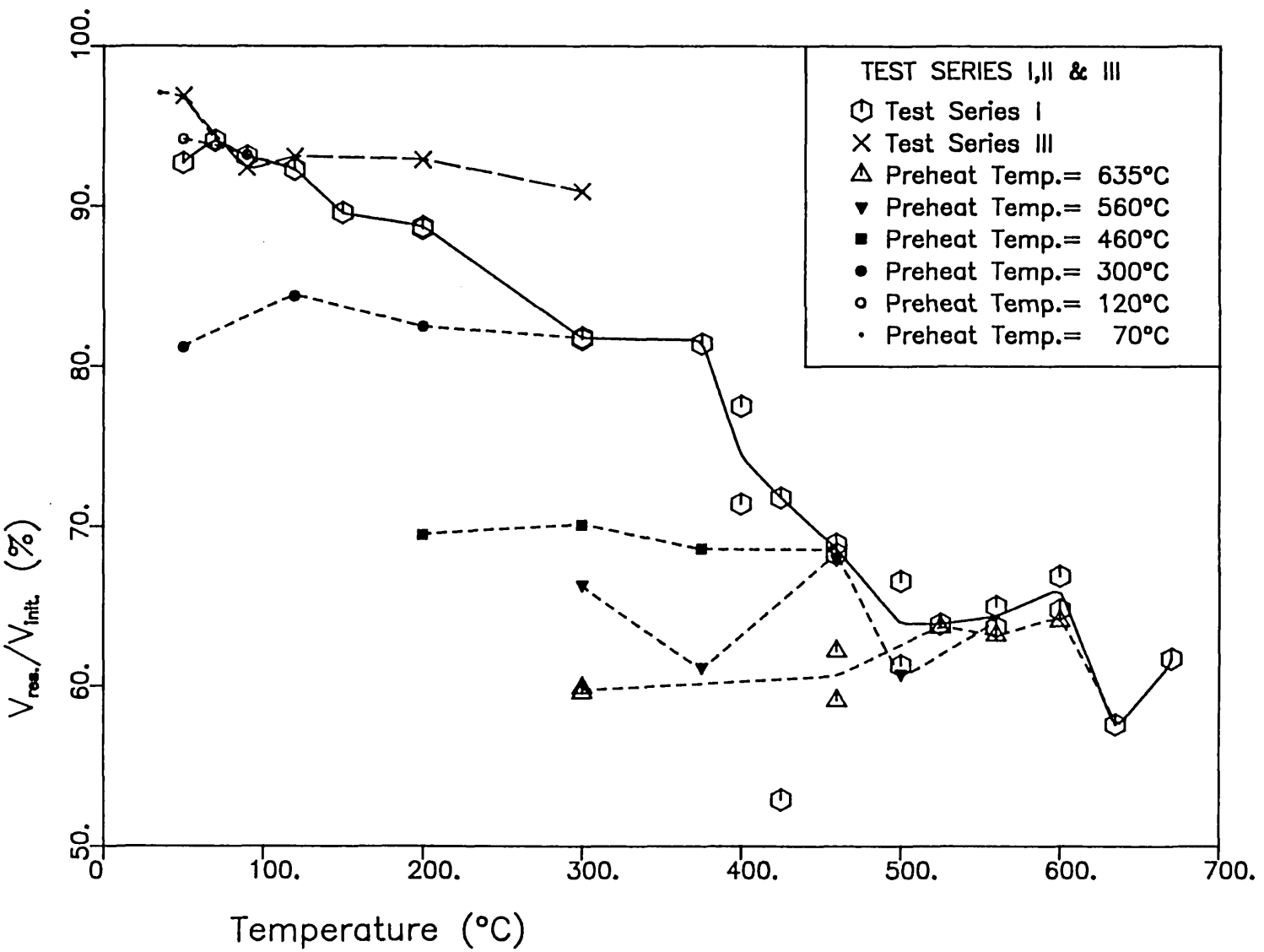

Fig.5.7 – RESIDUAL DYNAMIC MODULUS OF ELASTICITY

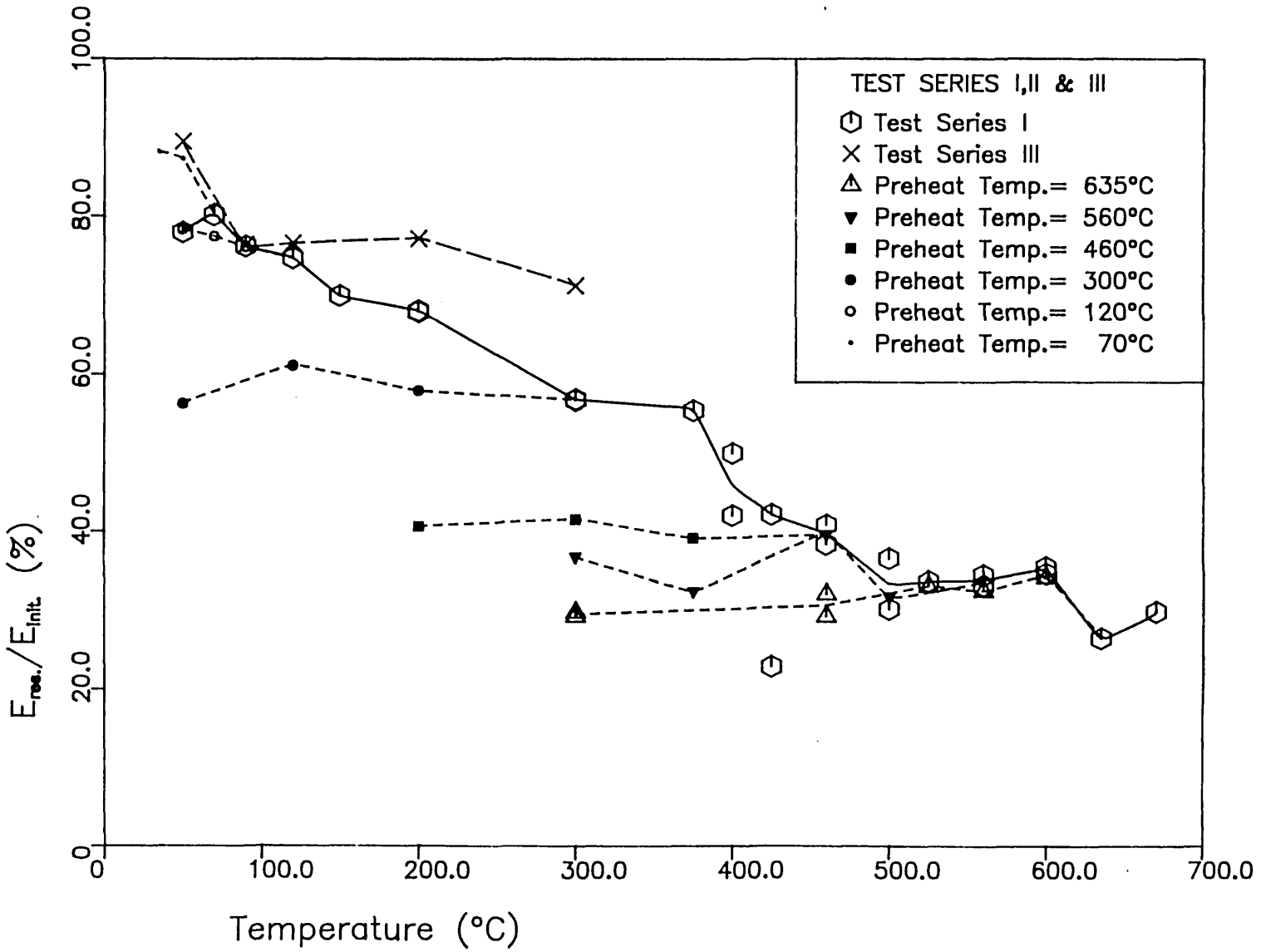

Fig.5.8 – HOT STRENGTH

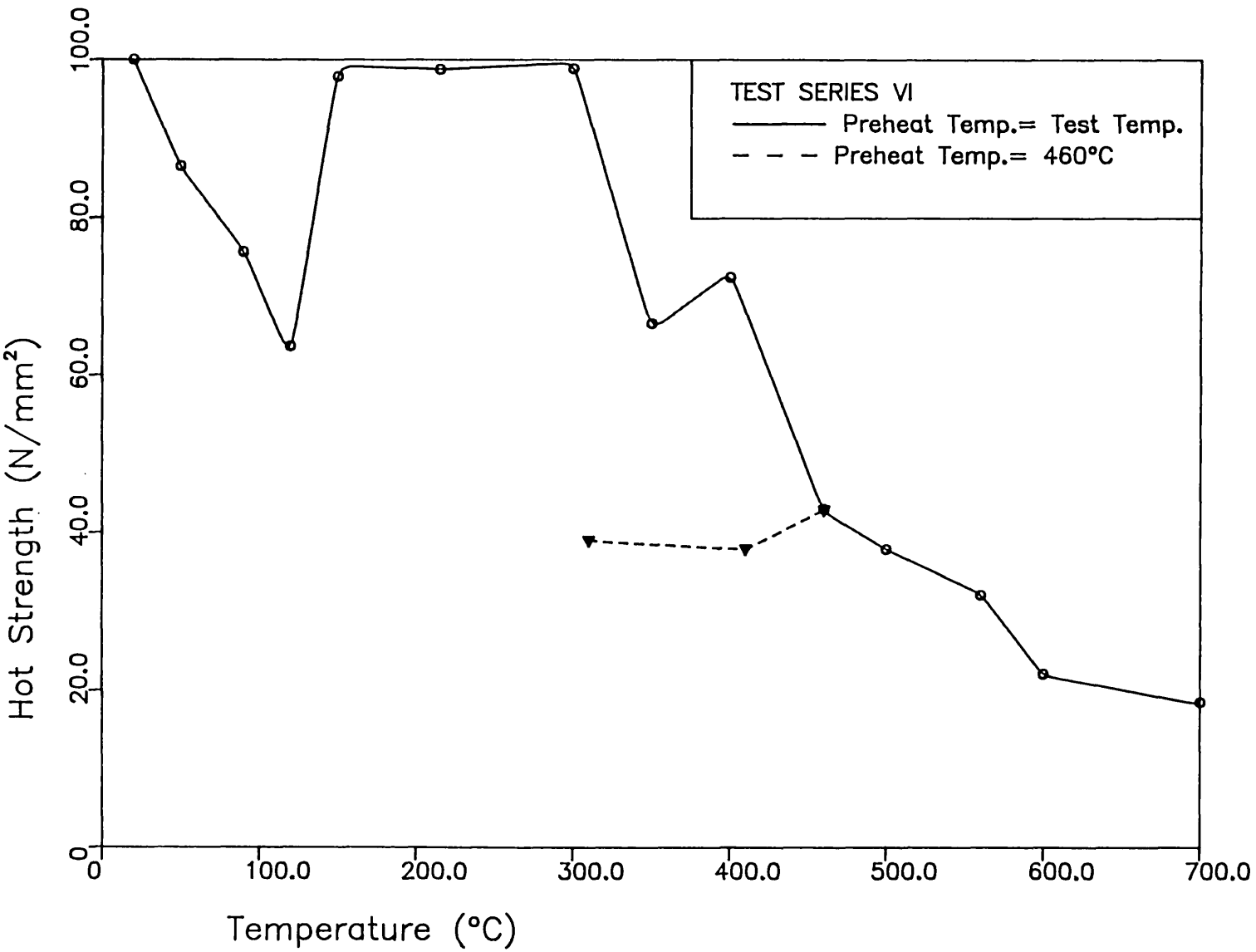

Fig.5.9 – RESIDUAL STRENGTH

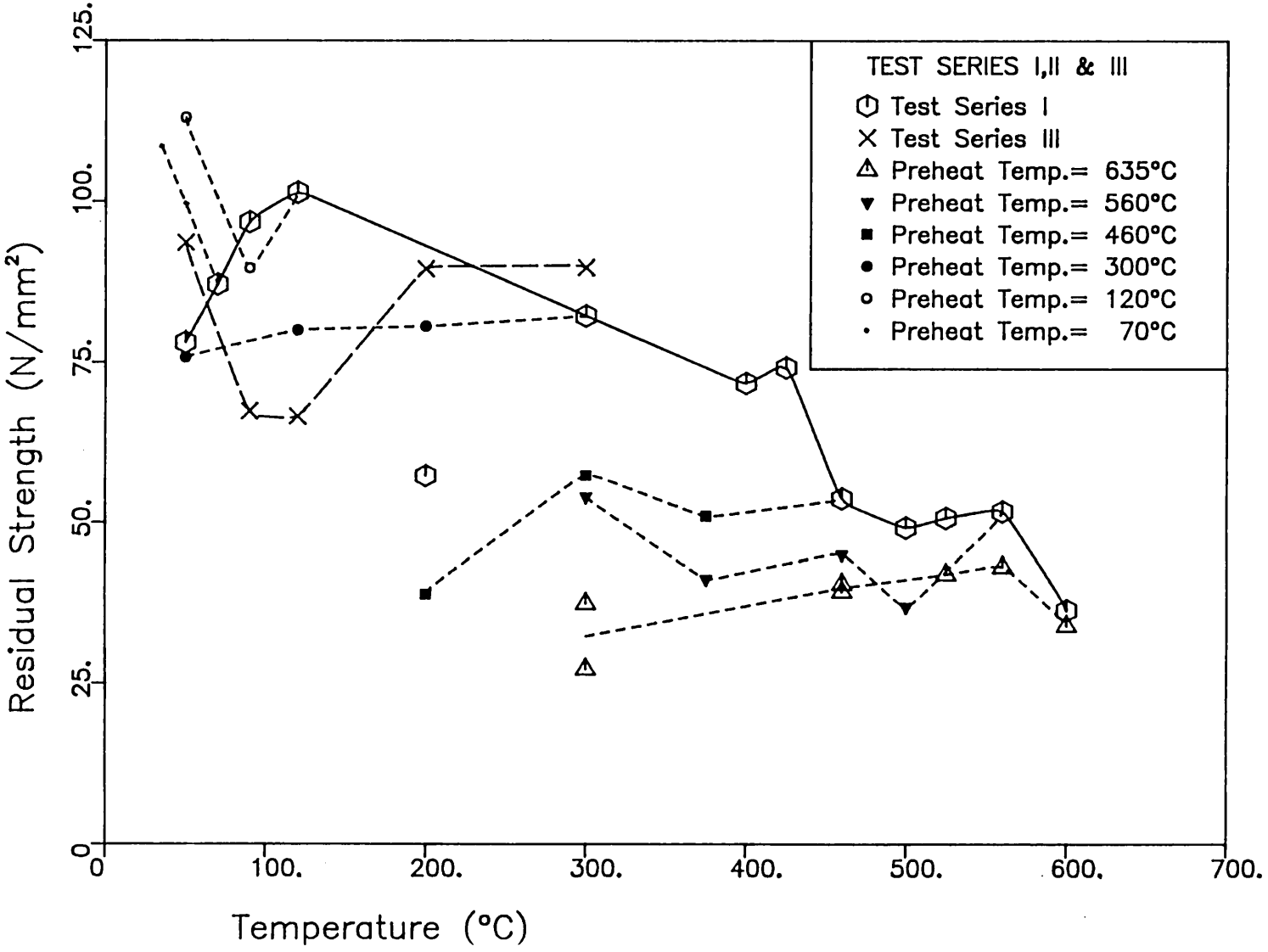

Fig.5.10 – RATIO OF STRENGTHS

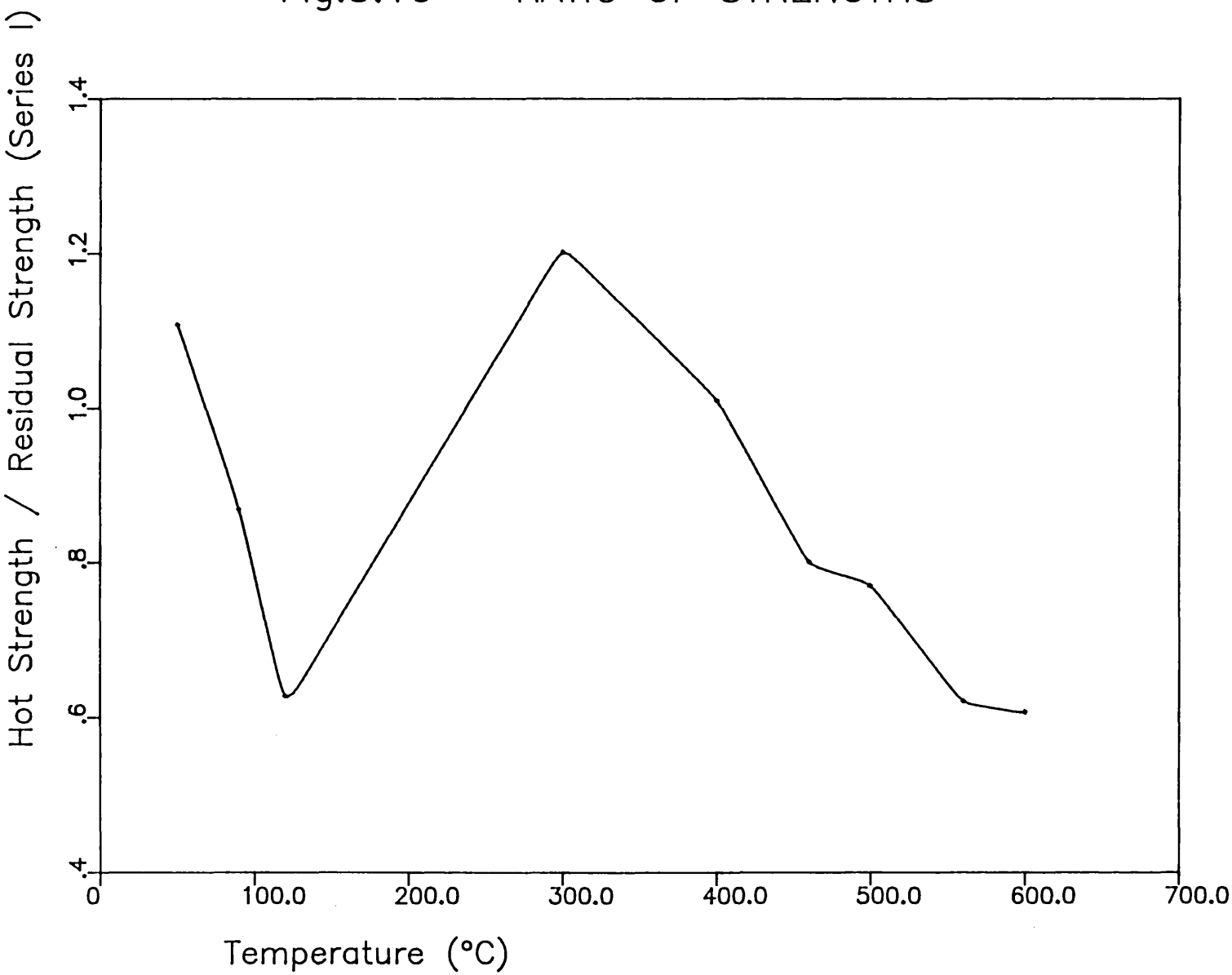

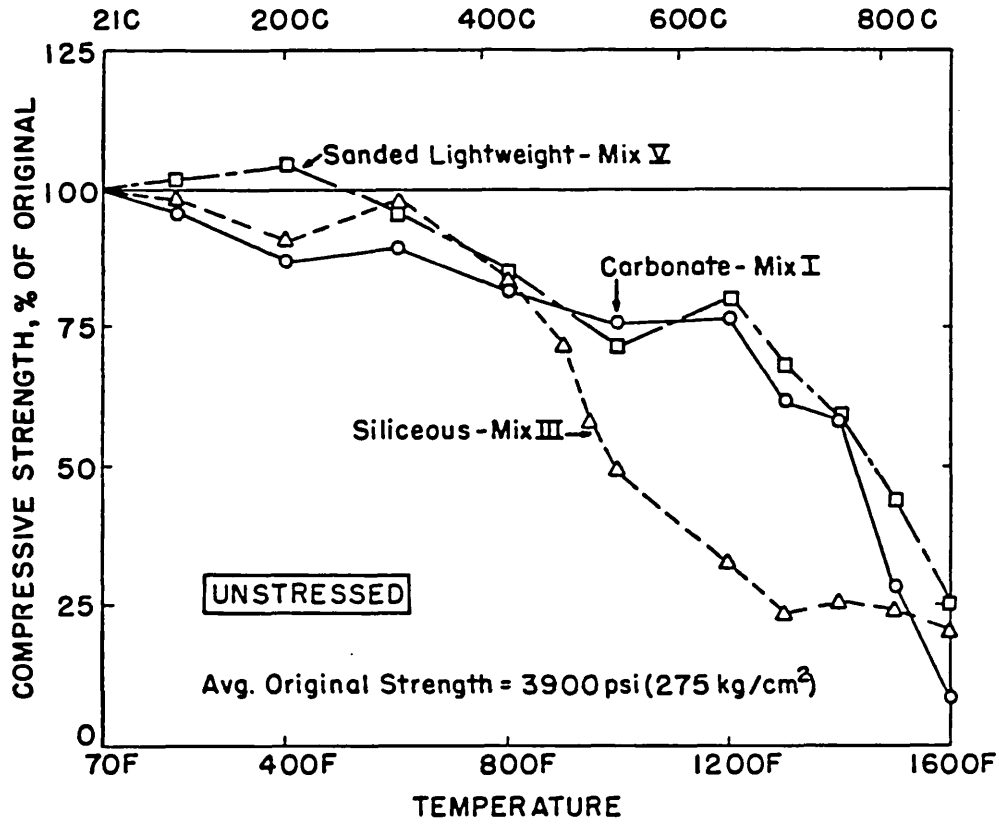

Figure 5.11(a) - EFFECT OF TEMPERATURE ON HOT STRENGTH OF CONCRETES MADE WITH DIFFERENT AGGREGATES. (FROM ABRAMS (1))

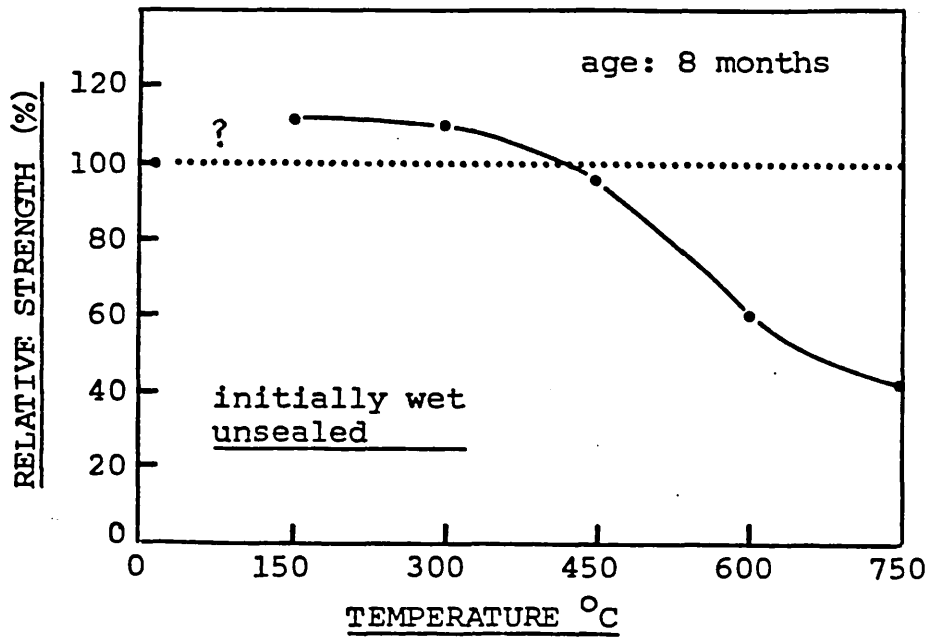

Figure 5.11(b) -EFFECT OF TEMPERATURE ON HOT STRENGTH OF CEMENT MORTAR. (FROM KHOURY (84), AFTER FISCHER (54))

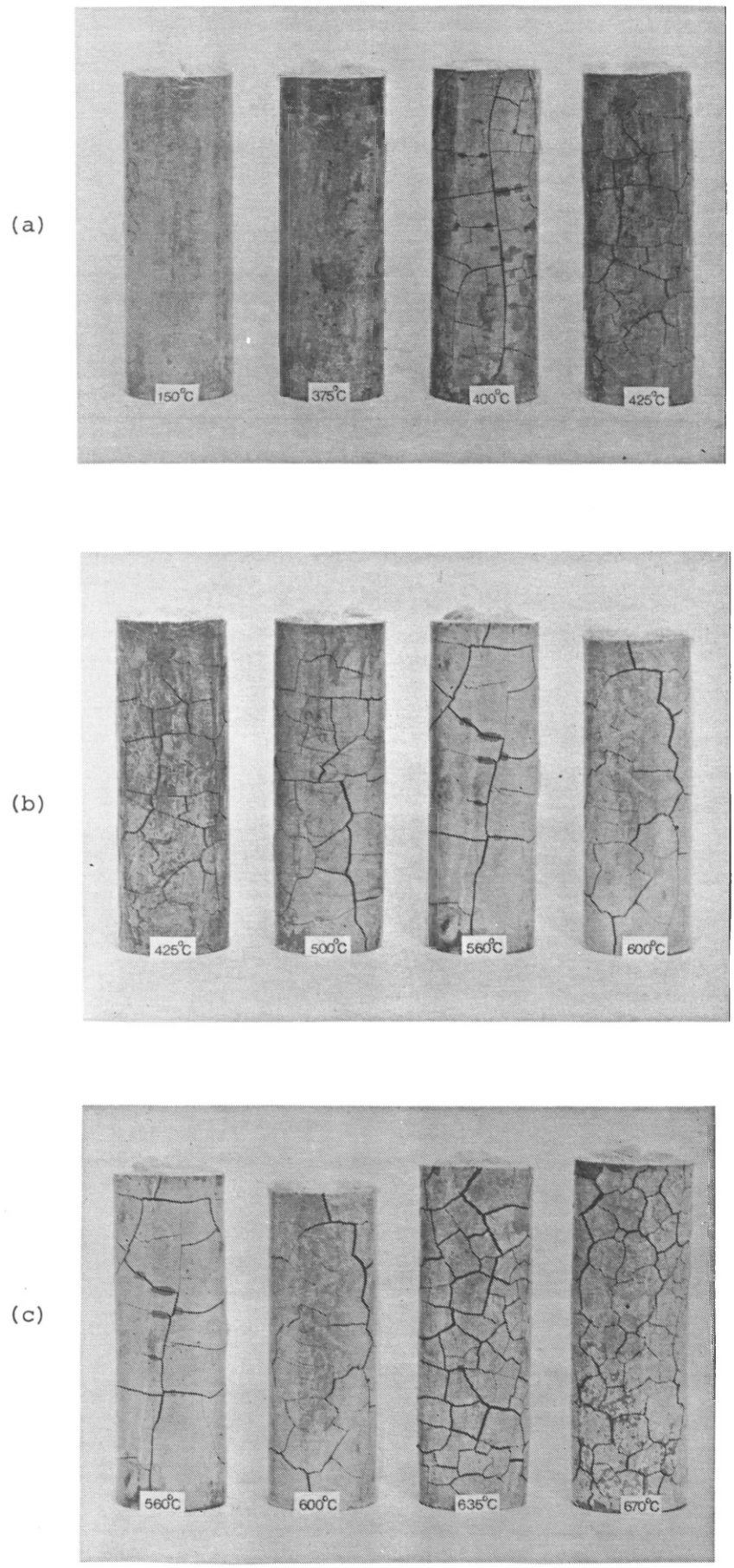

Figure 5.12 - EFFECT OF POST-COOLED EXPOSURE TO ATMOSPHERE.
NOTE (a) ONSET OF CRACKING BEYOND 400 C, (b) WHITISH HUE BEYOND 560 C, (c) SEVERE DISINTEGRATION BEYOND 635 C.

(d)

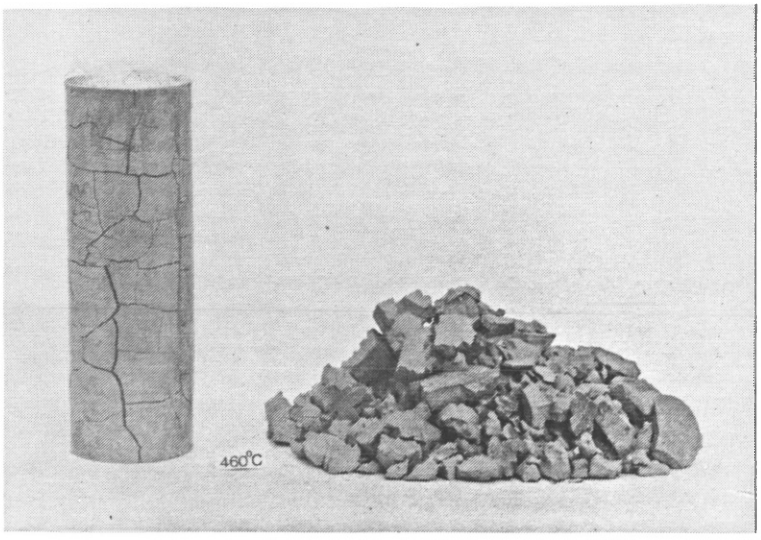

(e)

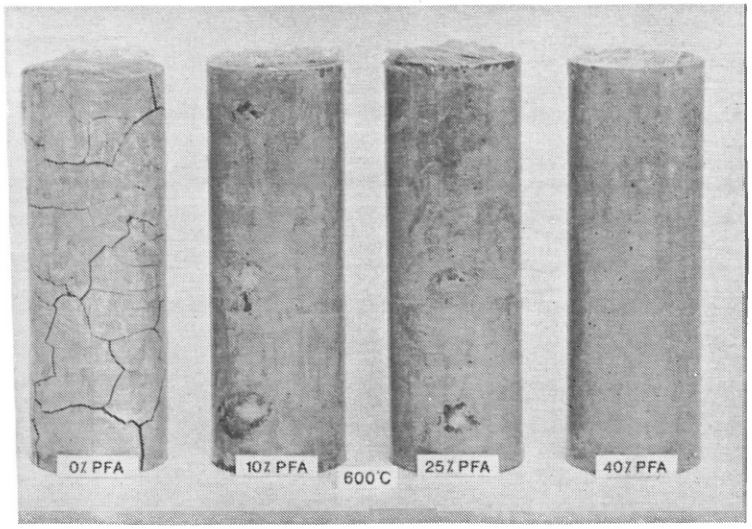

Figure 5.12(cont.) - EFFECT OF POST-COOLED EXPOSURE TO ATMOSPHERE. NOTE (d) EXTENT OF DAMAGE DUE TO REHYDRATION OF DISSOCIATED $Ca(OH)_2$, (e) EFFECT OF PARTIAL REPLACEMENT OF OPC WITH PFA.

CHAPTER 6 - SHRINKAGE AND THERMAL STRAIN

This chapter presents the shrinkage and thermal strain results from Test Series I, II and V. The analysis and interpretation of these results need to be seen in the light of two limitations. Firstly, the measured shrinkage would not reflect a true material property during the evolution of strains (unlike the measured creep), but would be dependent on the specimen size (56). This, however, does not preclude the kind of comparative investigation carried out herein on specimens of identical size. Secondly, it was not possible to isolate directly the thermal expansion strains from shrinkage strains during heating. In order to separate the strains, the coefficient of thermal expansion was equated to the measured coefficient of contraction, obtained during cooling. The above assumption seems a reasonable approximation in the light of previous experimental evidence that the cooling curve for concrete is identical to that obtained on second heating (102).

6.1. DURATION OF SHRINKAGE PHASE

As described earlier, the specimens were heated, prior to subsequent creep loading, until dimensional stability was reached. It was observed that the time required for the achievement of dimensional stability varied with the temperature concerned. Figure 6.1 shows the durations after which stability was considered to have been reached at various temperatures for the Series I tests. The figures corresponding to the points are the smallest daily strain observed - in microstrain, with contraction negative. The zeroes adjacent to some points indicate that the daily strains fluctuated minimally on both sides of zero after the duration shown. The positive strain at 670°C means that the strains immediately prior to stability were expansive.

It is clear from Figure 6.1 that, apart from temperatures around 560°C and above, the shrinkage phase occupies a duration of at least two weeks or more. Furthermore, "absolute" stability (which can be understood as minimal fluctuations about a daily strain of zero)

was achievable only above 500°C. Observations similar to this were reported by Marechal (99) for concrete and Lea and Stradling (92) for cement paste of w/c ratio 0.18.

The plot in Figure 6.1 appears to have a W-shape, with the "peaks" corresponding to temperatures where significant chemical or physical changes cause delay in dimensional stabilization. The central peak at 400°C would be related to the dissociation of $Ca(OH)_2$, while the left hand peak at 50°C is due to desorption which would be a very slow process at this temperature. The right hand peak at 670°C is probably due to the expansion of cement grains in opposition to the shrinking cement paste, as suggested by Lea and Stradling (92) and will be discussed subsequently in this chapter. The "troughs" of the W-shaped curve are temperature regimes where changes take place relatively quickly. It should be noted that the right hand trough is much lower than the left hand one, since chemical changes would occur very rapidly at temperatures of 560-635°C, whereas the left hand trough corresponds to temperatures over which the more gradual desorption of both physically and chemically bound water takes place.

6.2. INTERPRETATION OF SHRINKAGE RESULTS

The shrinkage results from the Series I tests will be analysed in this section. The initial shrinkage during air storage is calculated by measuring the weight loss of the specimen from the point of air drying to the point of testing and then using the regression line between weight loss and shrinkage in air (Figure 3.5). The thermal expansion strains were isolated from the measured strains at elevated temperature as described beforehand.

6.2.1. Variation of Shrinkage with Temperature

The evolution of strains during heating are plotted in Figure 6.2 for selected specimens. All specimens undergo an initial phase of expansive strain; however the final strains for all specimens show contraction. The shapes of these curves would be a function of the rate of heating; a very low heating rate will probably reduce if not

eliminate the initial expansive strain. The amount of strain undergone isothermally (i.e. the length of the vertical portion of the line) gives some indication of the duration to achieve dimensional stability and can be compared with Figure 6.1. The expansive strains undergone prior to stabilization at 670°C can be clearly seen.

Figure 6.3 shows the "total" strains (which includes both shrinkage and thermal expansion components) at the end of the shrinkage phase as well as the residual shrinkage strains. (Contraction is plotted as positive in this figure). The overall trend is a virtually monotonic increase in shrinkage with temperature. Two significant features are worth noting. First, the final strain at dimensional stability is a contraction for all temperatures, including one as low as 50°C. This seems to contradict the results of both Lea and Stradling (92) as well as Wittmann and Lukas (181), who obtained net expansive strains at temperatures below 100° and c.68°C respectively. However, the latter conducted their experiments under sealed conditions, which would have reduced the time-dependent contraction. The former used the very low w/c ratio of 0.18, which would have resulted in a higher proportion of unhydrated grains and a consequently lower proportion of hydrated paste; this situation could have given rise to a net expansion, not only because of the reduced amount of hydrated paste available to produce shrinkage, but also because the larger proportion of unhydrated grains would introduce an expansive effect upon heating.

The second significant feature to be noted is the plateau around 600°C with a reversal in trend at 635°C - i.e. the contraction at 670°C is less than that at 635°C. As mentioned earlier, the daily strains prior to dimensional stability at 670°C were expansive as well. The above reversal in trend has been reported by Lea and Stradling (92) as well as Harada et al (67). However, there is a considerable difference between their results (Figure 6.4), both with respect to the temperature of 'trend reversal' as well as the magnitude of the strains.

The ultimate strains on heating from Test Series V, also shown in Figure 6.4, were used to shed more light on the subject of trend

reversal. These results indicate firstly that the contraction experienced is a function of the w/c ratio of the paste, a lower w/c ratio giving a smaller contraction. Hence the results of Lea and Stradling (92), who used a w/c ratio of 0.18, show the least contraction, while the paste of w/c = 0.375 shows the greatest. It should also be noted that the greatest contraction obtained by Harada et al (67) and in the Series I tests is approximately the same; this is to be expected because the w/c ratio in both cases is 0.3.

Secondly, Figure 6.4 shows that the temperature of trend reversal is also a function of the w/c ratio. The paste of the lowest w/c ratio experiences this reversal at 491°C (92). Although two temperature points are harldy sufficient to make a judgement regarding the paste with w/c = 0.225, it seems that trend reversal has already taken place at 525°C. The Series I pastes (w/c = 0.3) show reduction in contraction at 635°C, while the paste with w/c = 0.375 does not show any trend reversal up to 725°C. The fairly high temperature of trend reversal obtained by Harada et al (67), compared to the Series I results is probably because they conducted their tests in a "dynamic" fashion, measuring the strain during a continuous increase of temperature. This approach is different to that used in the present investigation and by Lea and Stradling (92), where dimensional stability was achieved at a series of temperatures. Any "dynamic" test would tend to give higher values of temperature than a "static" one.

The dependence of the ultimate strains on heating and trend reversal temperature upon w/c ratio is most probably related to the proportions of unhydrated grains and hydrated paste. It was sought to obtain some information regarding this relationship by a microstructural investigation using scanning electron microscopy. The above investigation is reported in Chapter 9.

6.2.2. Correlation between Shrinkage and Weight Loss

The ultimate residual shrinkage is plotted against total weight loss in Figure 6.5. The plot indicates a linear relationship in the temperature range 120°C to 500°C. It is very instructive to

compare this figure with that obtained by Hobbs and Mears (73) at ambient temperatures for concrete specimens of different sizes (Figure 6.14). It must be noted that the latter curves correspond to the averages of the histories of individual specimens whose shrinkage and weight change have been continually monitored over a period of drying, whereas Figure 6.5 has been made up of the ultimate residual shrinkage and weight loss values of a number of specimens exposed to conditions that would produce different end points. Nevertheless, a certain similarity is apparent.

Hobbs and Mears (73) obtained a fairly well defined linear relationship between shrinkage and weight loss percentage above a certain value of weight loss percentage. The shrinkage per unit percentage of weight loss was much lower at weight loss percentages below this value. (See Figure 6.14). They concluded that the shrinkage taking place below this 'critical' value was controlled by capillary flow, while that taking place above this value was diffusion-controlled. The 'critical' value of weight loss percentage was called "equilibrium moisture content when moisture movement is controlled by capillary flow only".

Now Figure 6.5 also shows a fairly well defined linear region as well as a region where shrinkage per unit weight loss percentage is lower than that in this linear region. It is clear, however, that the transition is not one from capillary flow controlled shrinkage to diffusion-controlled shrinkage, because all the values of shrinkage in Figure 6.5 are ultimate residual shrinkage values, at which points both capillary flow and diffusion would have ceased at the given temperatures.

Nevertheless, the fact that the transition weight loss percentage corresponds to a temperature of 120°C suggests another kind of transition. It is clear that all physically held water would be lost in a specimen heated to dimensional stability at 120°C. The weight loss from 120°C to 500°C would be due only to the loss of chemically bound water, although some chemically bound water would be lost below 120°C as well. It may be convenient to consider that the linear portion in Figure 6.5 corresponds to shrinkage caused by the

release of chemically bound water and that this shrinkage is greater than that due to the loss of physically held water, which would be the dominant mechanism below 120°C. A temperature of 120°C could be considered as the transition point beyond which shrinkage is due to the release of chemically bound water alone.

Figure 6.14 shows a constant or reducing weight loss region beyond the diffusion-controlled linear section. This has been attributed to carbonation (73). Similarly, Figure 6.5 also seems to have such a region beyond its own linear regime, i.e. above 500°C. It may be that this too could be attributed to carbonation, which has been found to be significant in the temperature range 500°C-600°C (138).

6.3. TIME FUNCTION FOR SHRINKAGE

The evolution of shrinkage strains with time can be obtained from the strains measured during heating (Figure 6.2), the thermal expansion strains being isolated on the basis of the coefficient obtained while cooling (Figure 6.10). The shrinkage vs. time curves for 25 Series I specimens are shown in Figure 6.6, a logarithmic scale being used for the time axis. The different initial shrinkage values (due to different periods of air drying) associated with these specimens result in different starting points for the curves. The shrinkage data is also tabulated in Appendix 2.

At first sight, it may seem neither logical nor convenient to fit a mathematical expression to these curves. In the first place, there is a sudden increase in the rate of shrinkage beyond a certain point; secondly, none of these curves is an isothermal. However, a closer look at the curves indicates that above 200°C, all the shrinkage-time curves seem to follow a single path from which they diverge at different points. Furthermore, this single path is virtually linear in the log-time domain. A still closer examination of the data revealed that the points of divergence from this linear path corresponded approximately to the point of reaching maximum temperature. Hence, for temperatures above 200°C, the shrinkage-time relationship can be idealized by a logarithmic variable temperature

portion and an isothermal portion.

The logarithmic portion was idealized as

$$\epsilon_{s1} \text{ (in } \mu\epsilon) = 41174 + 24807 \ln t \qquad (6.1)$$

The isothermal portion was idealized using an exponential-type expression of the form

$$\epsilon_{s2}/\epsilon_{s2tot} = K(1-e^{\alpha t}) + (1-K)(1-e^{\beta t}) \qquad (6.2)$$

where ϵ_{s2tot} is the total shrinkage experienced in the isothermal phase.

The temperatures above 560°C showed a near horizontal deviation from the logarithmic line, hence the above expression for the isothermal portion was used for temperatures from 200°C to 560°C.

It was decided to use an exponential type expression for the isothermal portion, both because of better fits obtained over other models and also because it was consistent with the idea of a "termination" of shrinkage when dimensional stability is reached. Furthermore, it has a more realistic theoretical basis (related to diffusion mechanisms) than other formulae. (See Section 2.2.4). Although the accuracy of the expression increases with the number of terms A_i, used in the general formulation

$$\epsilon_{s2} = \sum_{i=1}^{n} A_i \qquad (6.3)$$

where $$A_i = J_i(1 - e^{\gamma_i t}) \qquad (6.4)$$

The use of two terms was deemed a suitable compromise between accuracy and simplicity (182), especially since the mathematical fitting does not extend to very long term shrinkage (16).

A least squares algorithm for optimizing non-linear parameters which was used to obtain the constants in the 3-parameter formula in equation 6.2 revealed that the values of α and β were of the same

order for all 16 curves concerned. Therefore, the average values of α and β were used in the formula, thus reducing equation (6.2) to

$$\epsilon_{sz}/\epsilon_{sztot} = K' (1-e^{\bar{\alpha}t}) + (1-K')(1-e^{\bar{\beta}t}) \qquad (6.5)$$

$$\text{where } \bar{\alpha} = \frac{1}{16} \sum_{i=1}^{16} \alpha_i \qquad (6.6)$$

$$\text{and} \qquad \bar{\beta} = \frac{1}{16} \sum_{i=1}^{16} \beta_i \qquad (6.7)$$

The values obtained for $\bar{\alpha}$ and $\bar{\beta}$ were -6.362 and -0.249; their standard deviations were 2.958 and 0.104 respectively. Hence, it was possible to use a single parameter K' to characterize the shape of the isothermal portion of the shrinkage curve and study its variation with temperature.

The fitted curves for shrinkage from 200°C to 560°C beyond 0.190 days are shown in Figure 6.7. The fit obtained, although not as good as for the 3-parameter formula, was considered adequate, with indices of correlation in all cases except two being not less than 0.95 and in 9 cases out of 16 being 0.99 or more. (The index of correlation is defined as unity less the ratio between the sums of squares of residuals and the variance of the observed values). An impression of the closeness of fit can be obtained from Figure 6.8 where selected curves have been replotted together with experimental data points.

The parameter K' has been plotted against temperature in Figure 6.9. Equation (6.5) indicates that K' is a measure of the proportion of shrinkage taking place in the early stages of the isothermal phase. This proportion is seen to be low in the temperature range 400-460°C, when the slow dissociation of $Ca(OH)_2$ will result in prolonged dimensional instability; it is high in the temperature range above 500°C, when dimensional stability is reached quickly. In the range 200-375°, K' takes a medium value.

Thus the expression for the shrinkage-time relationship can be written as

$$\left.\begin{aligned} \epsilon_s &= \epsilon_{s1}(t) \qquad (0.190 < t < t_i) \\ &= \epsilon_{s1}(t_i) + \epsilon_{s2}(t-t_i) \qquad (t > t_i) \end{aligned}\right] \tag{6.8}$$

where t_i is the time (in days) of the start of the isothermal portion; the expression is valid only beyond 0.190 days, at which time its value is zero.

$$\left.\begin{aligned} \text{i.e.} \quad \epsilon_s &= 41174 + 24807 \ln t \qquad (0.190 < t < t_i) \\ &= 41174 + 24807 \ln t_i \\ &+ \epsilon_{s2tot}(T)[K'(T)(1-e^{-6.362(t-t_i)}) + (1-K'(T))(1-e^{-0.249(t-t_i)})] \\ &\qquad\qquad (t > t_i) \end{aligned}\right] \tag{6.9}$$

The values of t_i and K' for the various temperatures are given in Table 6.1.

In concluding this section, attention should be drawn to the fact that the above method of curve fitting to variable temperature and isothermal portions may not be a universal concept applicable to drying shrinkage under all conditions. The measured drying shrinkage is not, strictly speaking, a "material" property (56), being dependent on specimen size, rate of heating and environmental factors. Nevertheless, the fairly clear demarcation between the variable temperature and isothermal portions in the temperature range 200-560°C is interesting. Further tests under different conditions (e.g. rate of heating, specimen size, initial moisture condition etc.) should be done to investigate the universality of this demarcation.

6.4. THERMAL CONTRACTION

The thermal contractions for Series I specimens are shown in Figure 6.10. It must be noted that the contraction was measured with the specimen under load, and hence the question arises as to whether any creep strains are incorporated in these measurements. Previous research (88, 152) has shown however, that thermal strains upon cooling and re-heating are not affected by load level. Hence it will be assumed that any creep strains are negligible in comparison with thermal strains.

Figure 6.10 seems to display a reasonable linearity, and hence suggests a constant coefficient of 11.60 $\mu\epsilon$/°C over the entire temperature range. This however is misleading, as will be seen from Figures 6.11 and 6.12. Figure 6.11 shows the considerable variation of the rate of contraction for a specimen cooled from 635°C to ambient temperature. The initial increase in rate (near 600°C) is probably due to the thermal inertia of the specimen, the measured temperature on the surface being lower than the temperature within, and resulting in a lower apparent rate of contraction. Apart from this, there seems to be a gradual decrease in the rate of contraction.

Figure 6.12 compares the coefficients of contraction (averaged over the entire temperature range of cooling) for Series I specimens with the coefficients for Series II specimens when being cooled from pre-heat to test temperatures. It must be remembered that the points for Series I specimens depict the upper point of the temperature range while those for Series II specimens depict the lower point. Furthermore, the Series II specimens have been cooled without load. Nevertheless, Figure 6.12 confirms the evidence from Figure 6.11 that greater contraction takes place at higher temperatures. However, in order to eliminate thermal expansion strains and obtain shrinkage strains from strains during heating, the use of an average coefficient of 11.60 $\mu\epsilon$/°C was considered sufficient.

The reduction of the rate of contraction with temperature may be purely a thermal property of the material, since most materials experience higher thermal strains at higher temperatures. On the other hand, there may be other contributory factors such as (a) swelling caused by absorption of moisture (181), (b) expansion caused by rehydration of dissociated $Ca(OH)_2$ and (c) expansion caused by thermal strain incompatibility between unhydrated cement grains and the hydrated paste. The contribution from (b) above is likely to be minimal if non-existent during the actual cooling phase itself, as indicated by the fact that the shapes of the contraction rate curves for specimens cooled from 635° and 375°C are essentially similar (Figure 6.11). On the other hand it is probably this rehydration of dissociated $Ca(OH)_2$ which caused the strain behaviour exhibited by the specimen cooled to 50°C and maintained thereat for a considerable time,

after being pre-heated to 635°C. (See Figure 6.13). This specimen failed when attempting to creep load it, indicating that the expansion had been extremely disruptive. A specimen pre-heated to 635°C and cooled back to 120°C also behaved in similar fashion.

6.5. CONCLUSION

By far the most significant influence upon shrinkage is the moisture condition of the specimen. The moisture condition at a given temperature affected the duration of the shrinkage phase. Then again, the value of ultimate residual shrinkage was found to be linearly related to total moisture loss, within the temperature range 120°C to 500°C; this range was considered to be one where shrinkage was due to the release of chemically bound water above. Shrinkage below 120°C was attributed largely to the loss of physically held water, and carbonation was thought to be taking place above 500°C. The water/cement ratio employed in the mix determined the proportion of hydrated material and thus the value of ultimate shrinkage.

The shrinkage and thermal strain behaviour is also considerably influenced by the $Ca(OH)_2$ component of the paste. It was seen that the duration of the shrinkage phase was increased considerably when the temperature was at or just above the dissociation temperature of $Ca(OH)_2$. Furthermore, if the cooling phase was protracted, the initial contraction was later modified by disruptive expansive strains resulting from the rehydration of dissociated $Ca(OH)_2$.

The time dependence of shrinkage was modelled as a logarithmic relationship in the variable temperature regime and an exponential type law in the isothermal regime.

Temperature (°C)	200	300	375	400	425	460	500	525	560
Starting point of isothermal phase, t_i (days)	0.202	0.229	0.256	0.281	0.294	0.314	0.341	0.367	0.393
Total isothermal shrinkage, ε_{s2tot} ($\mu\varepsilon$)	5205	5856	6883	6315	6136	6225	5346	4687	3476
K'	0.503	0.549	0.564	0.354	0.209	0.373	0.704	0.753	0.881

TABLE 6.1. PARAMETERS FOR ISOTHERMAL SHRINKAGE CURVES

Fig.6.1 — DURATION FOR DIMENSIONAL STABILITY

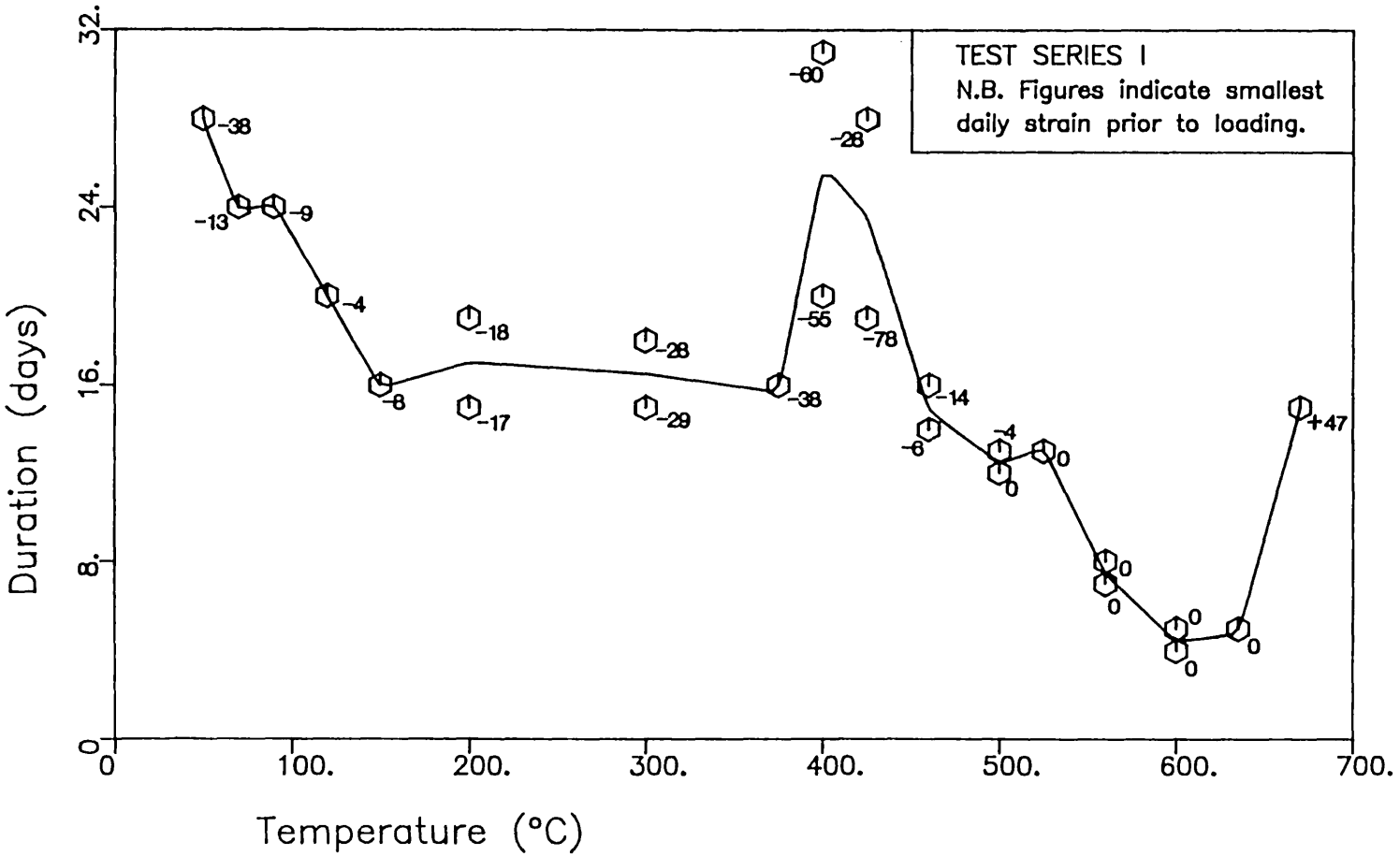

Fig.6.2 – STRAINS ON HEATING

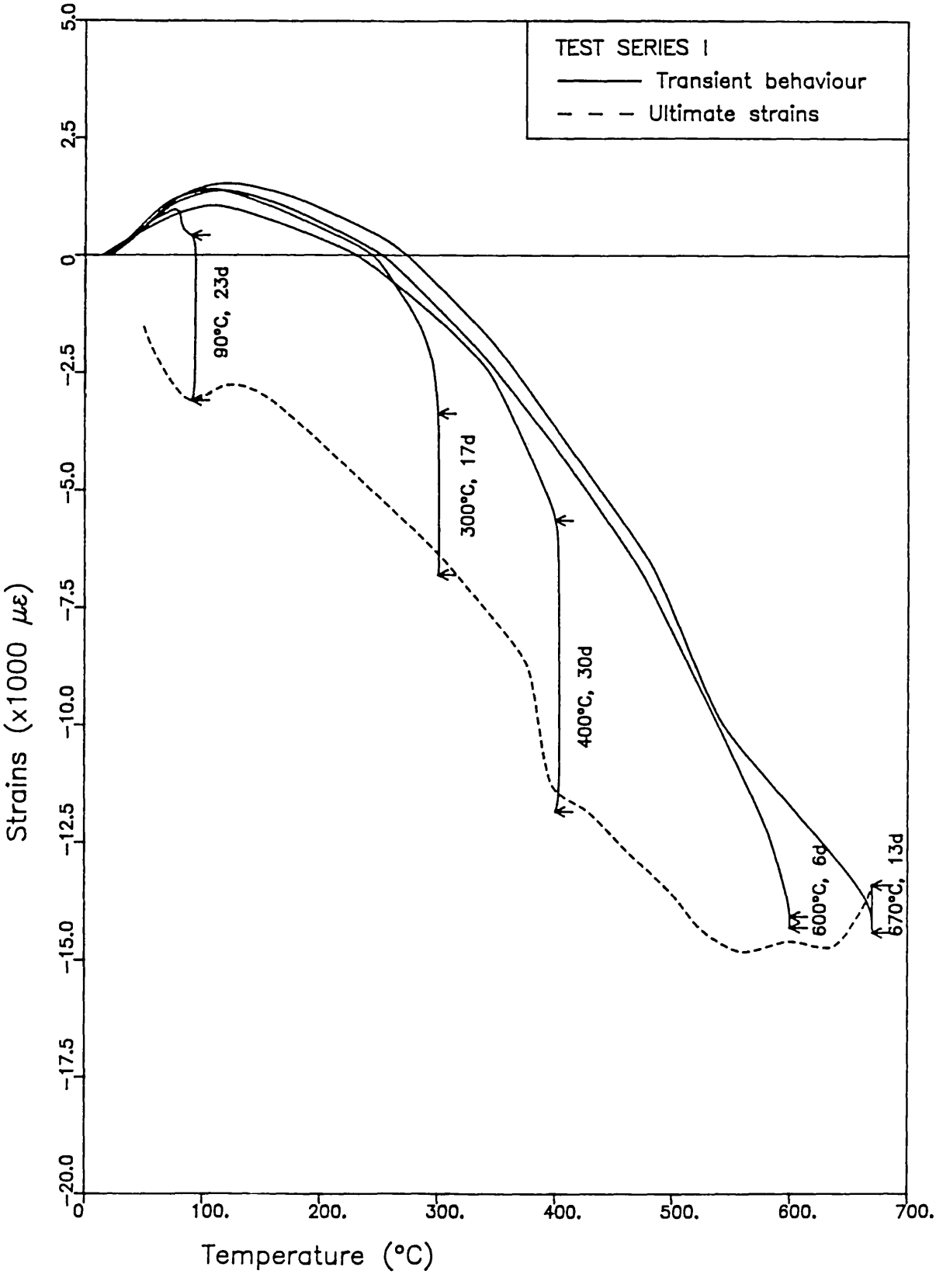

Fig.6.3 – CONTRACTIONS CAUSED BY HEATING

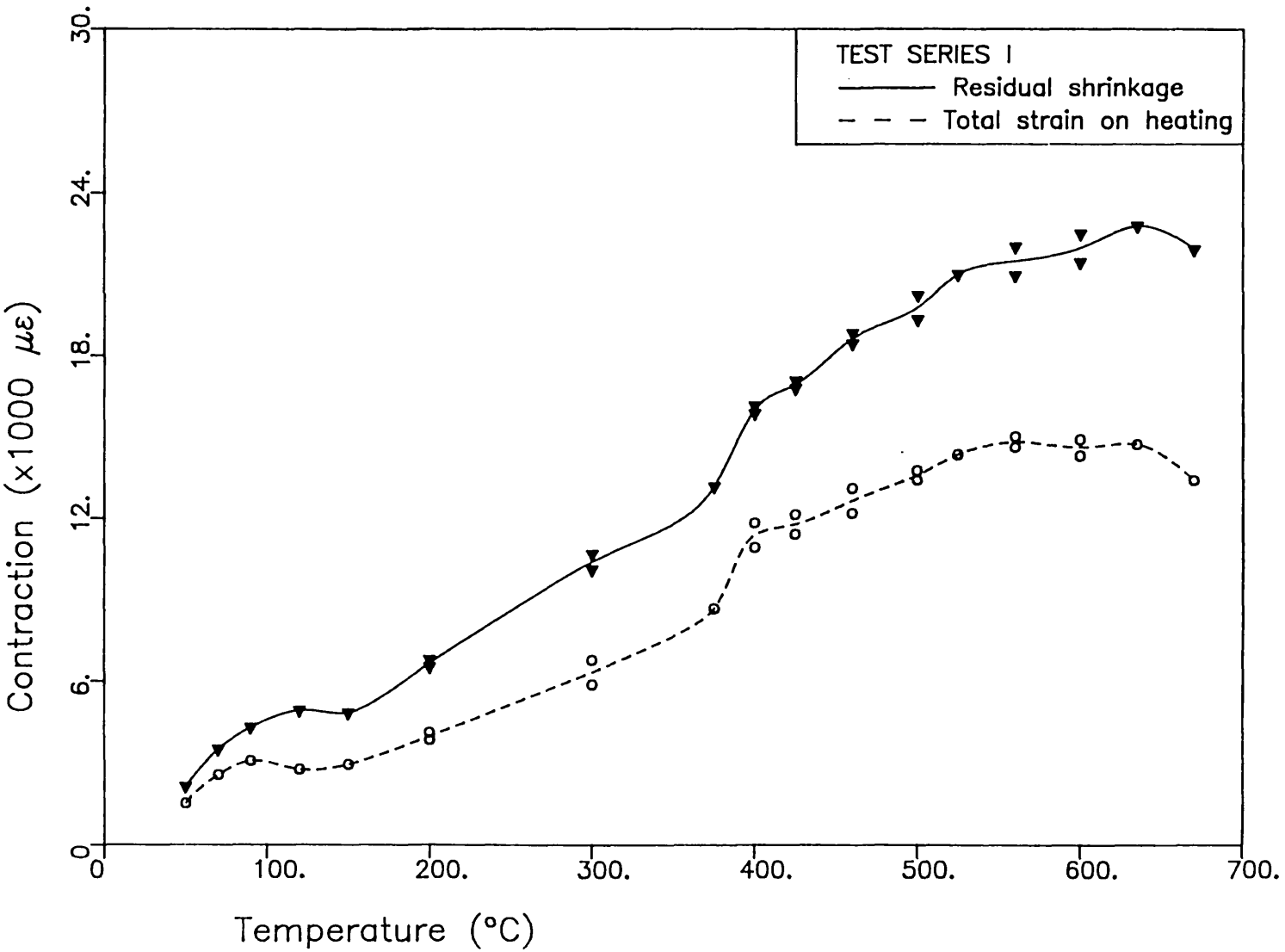

Fig.6.4 – REVERSAL OF CONTRACTION ON HEATING

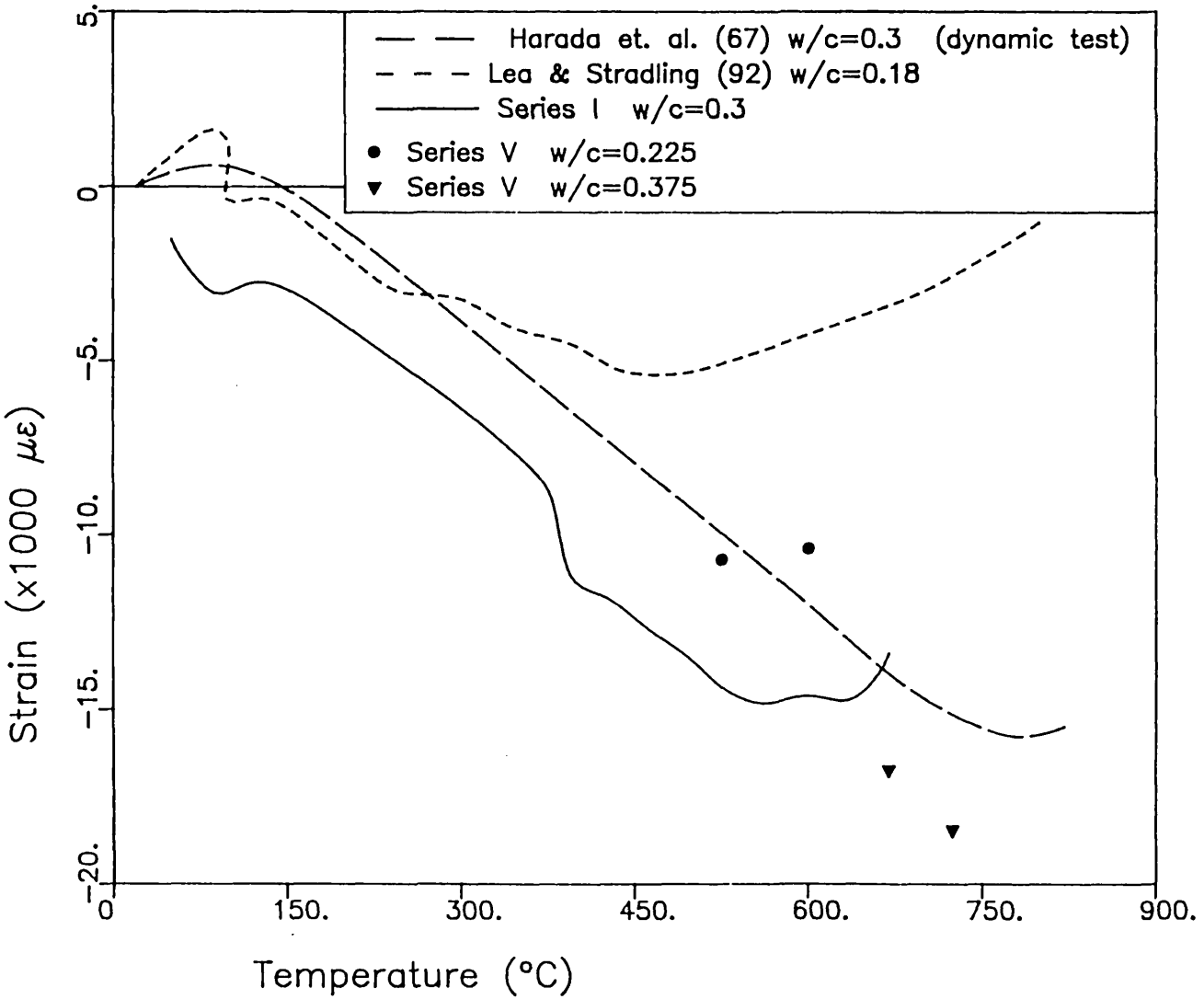

Fig.6.5 – RESIDUAL SHRINKAGE vs. WEIGHT LOSS

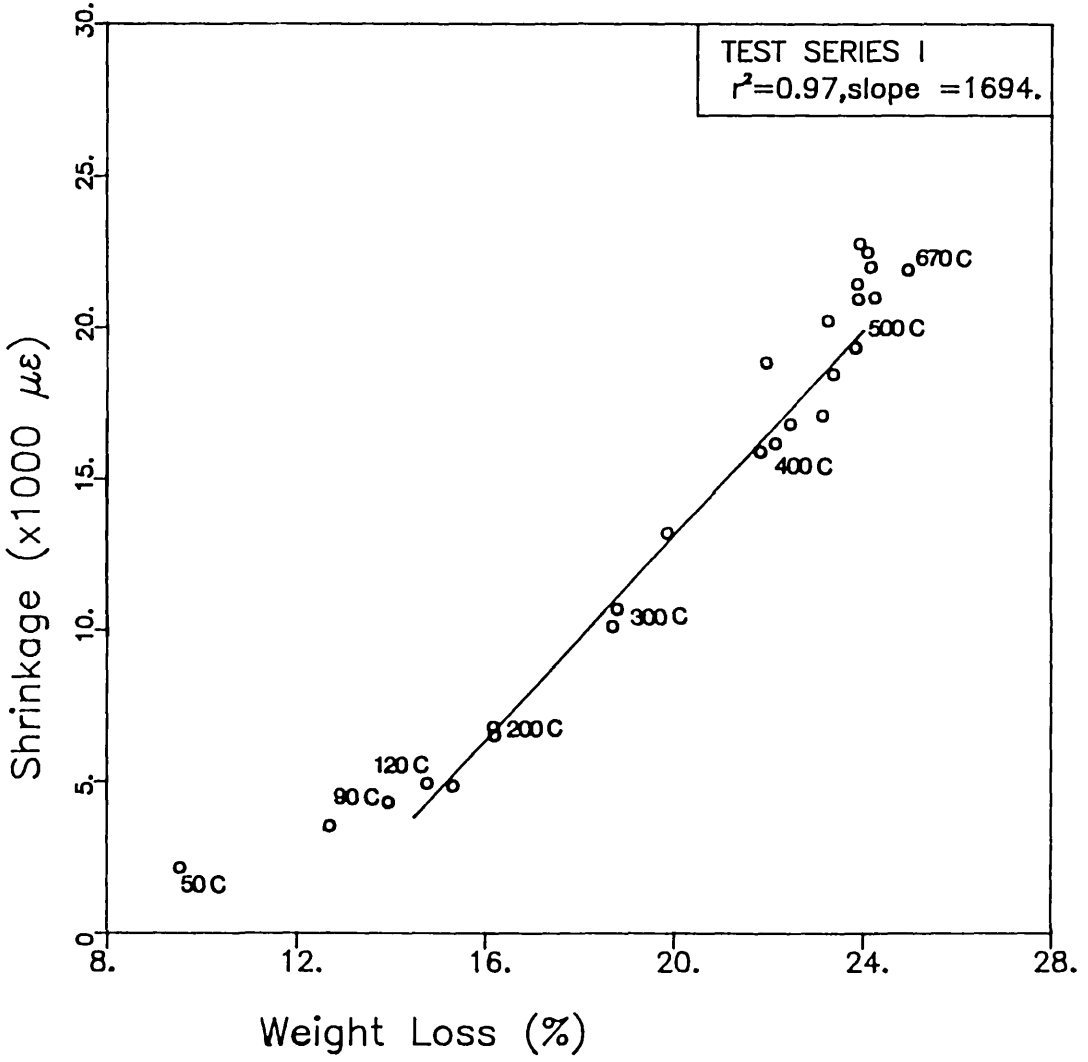

Fig.6.6 – SHRINKAGE STRAINS (EXPERIMENTAL)

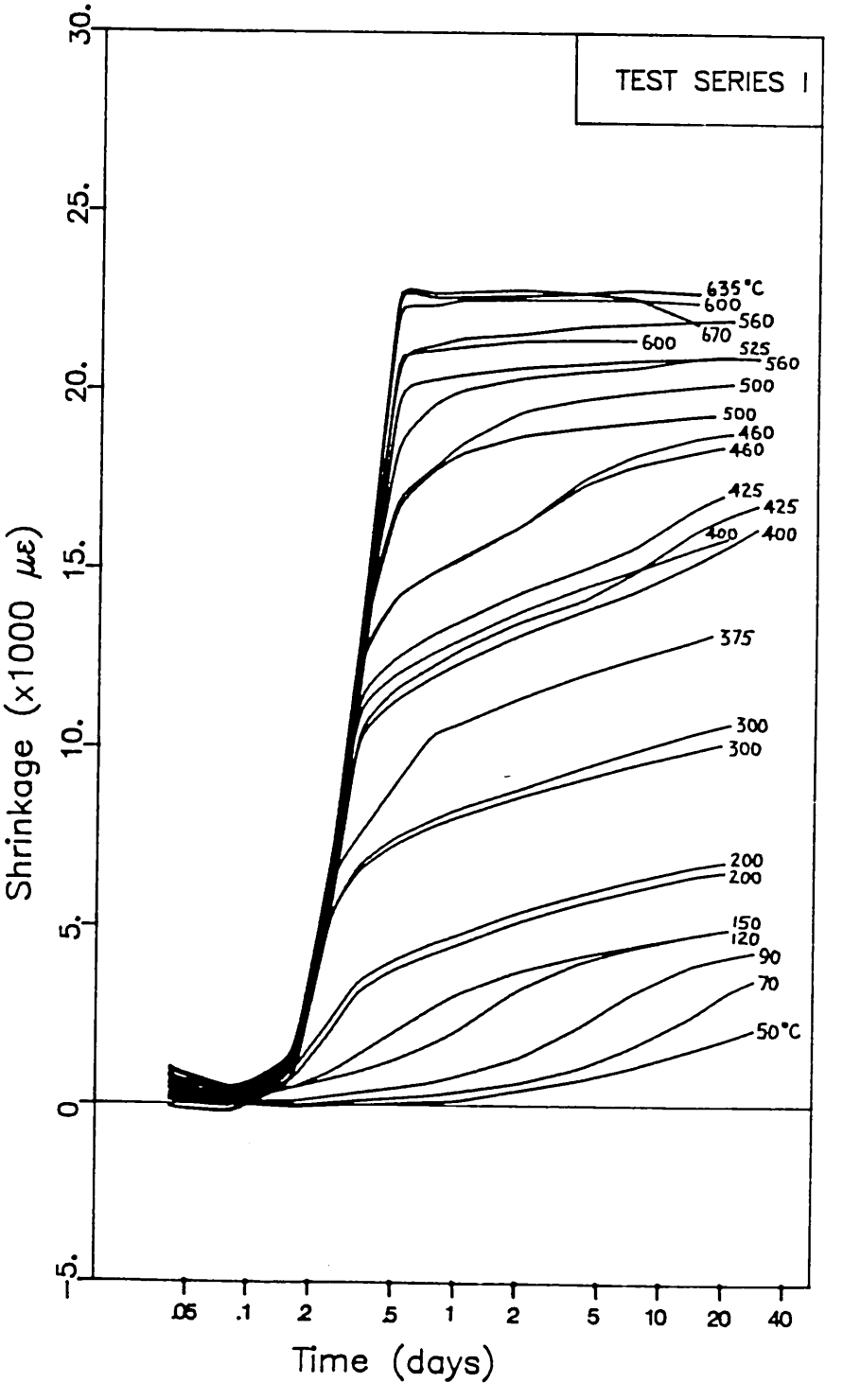

Fig.6.7 – SHRINKAGE STRAINS (IDEALIZED)

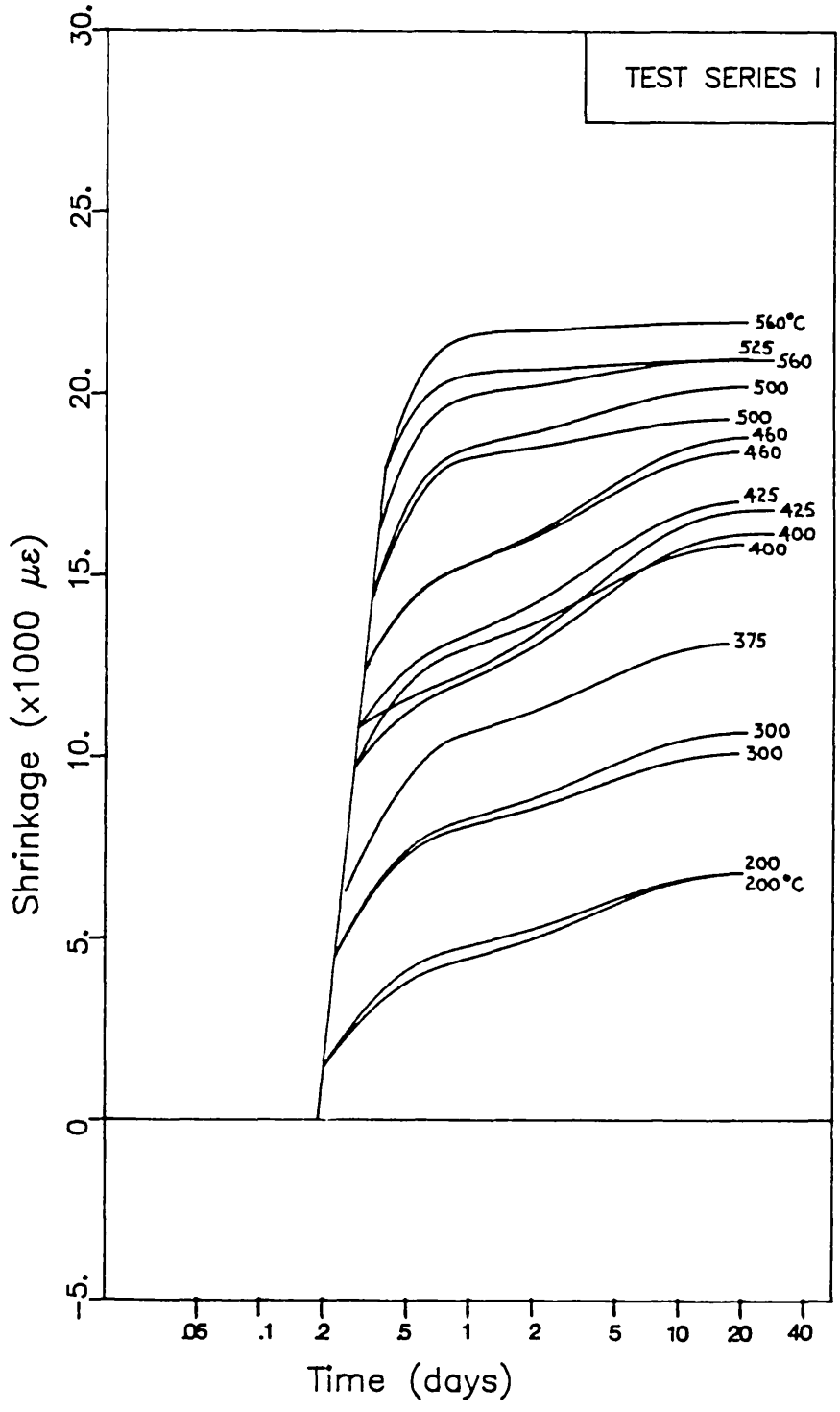

Fig.6.8 – SHRINKAGE STRAINS

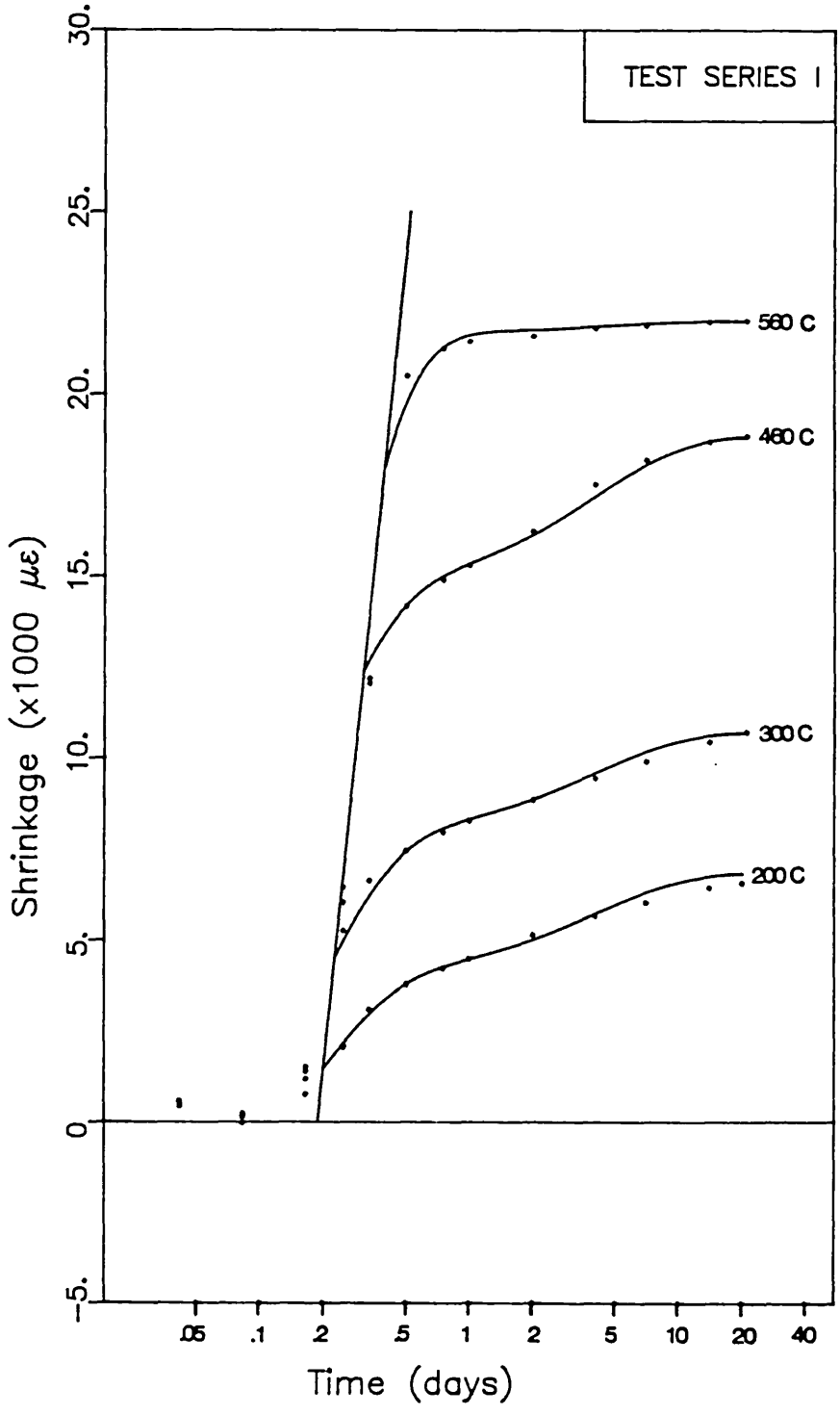

Fig.6.9 – VARIATION OF K′ WITH TEMPERATURE

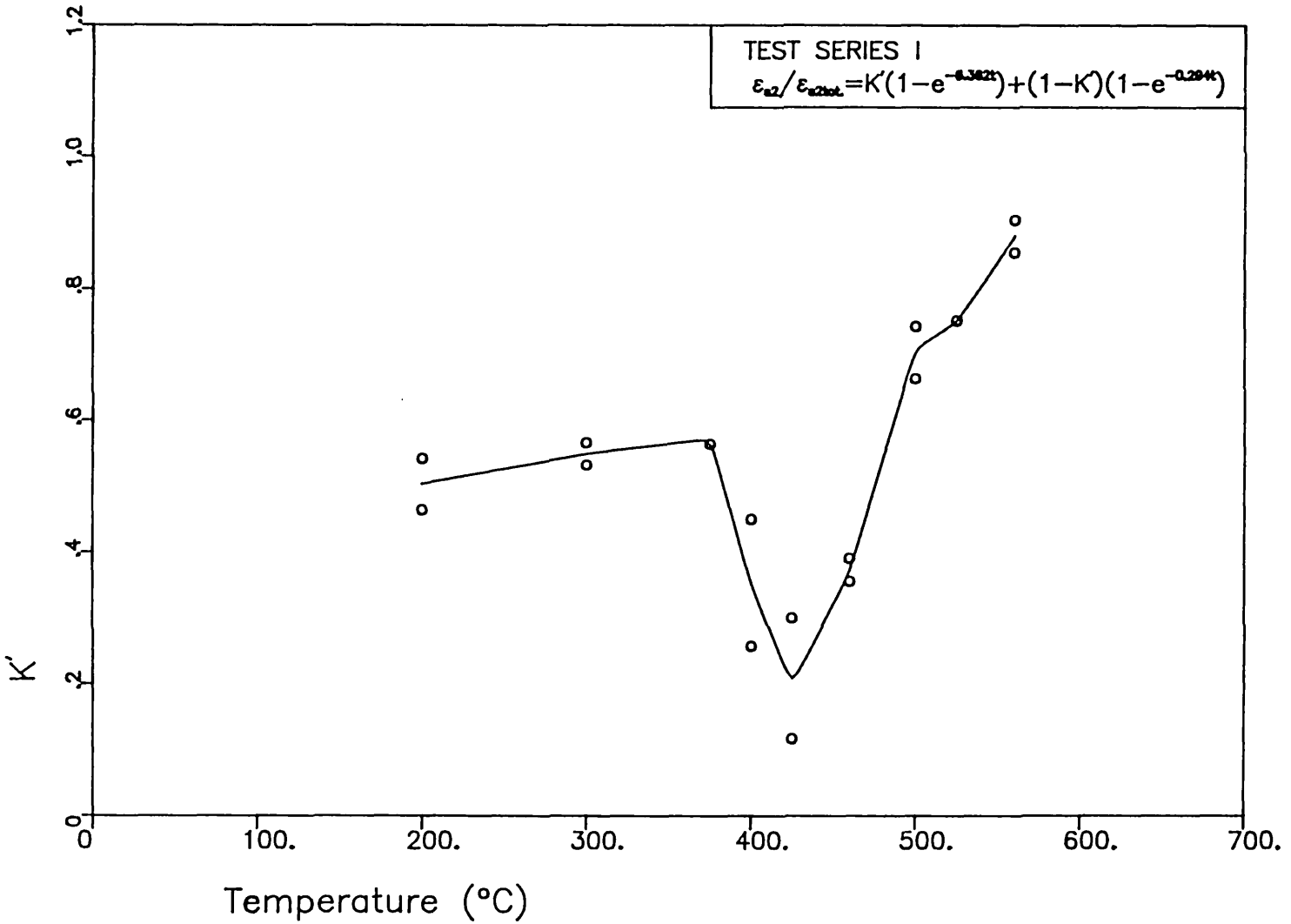

Fig.6.10 – THERMAL CONTRACTION

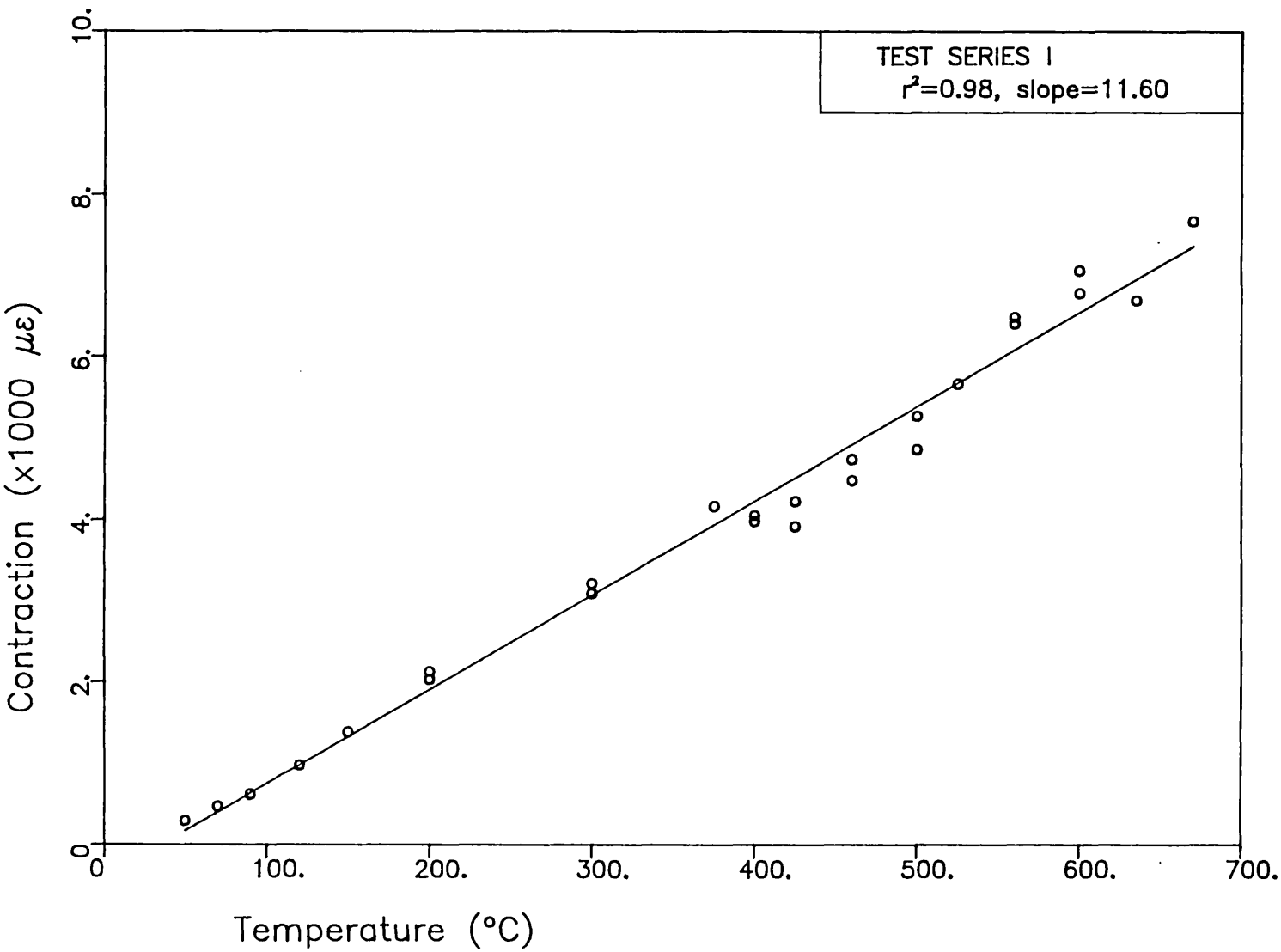

Fig.6.11 – RATE OF CONTRACTION

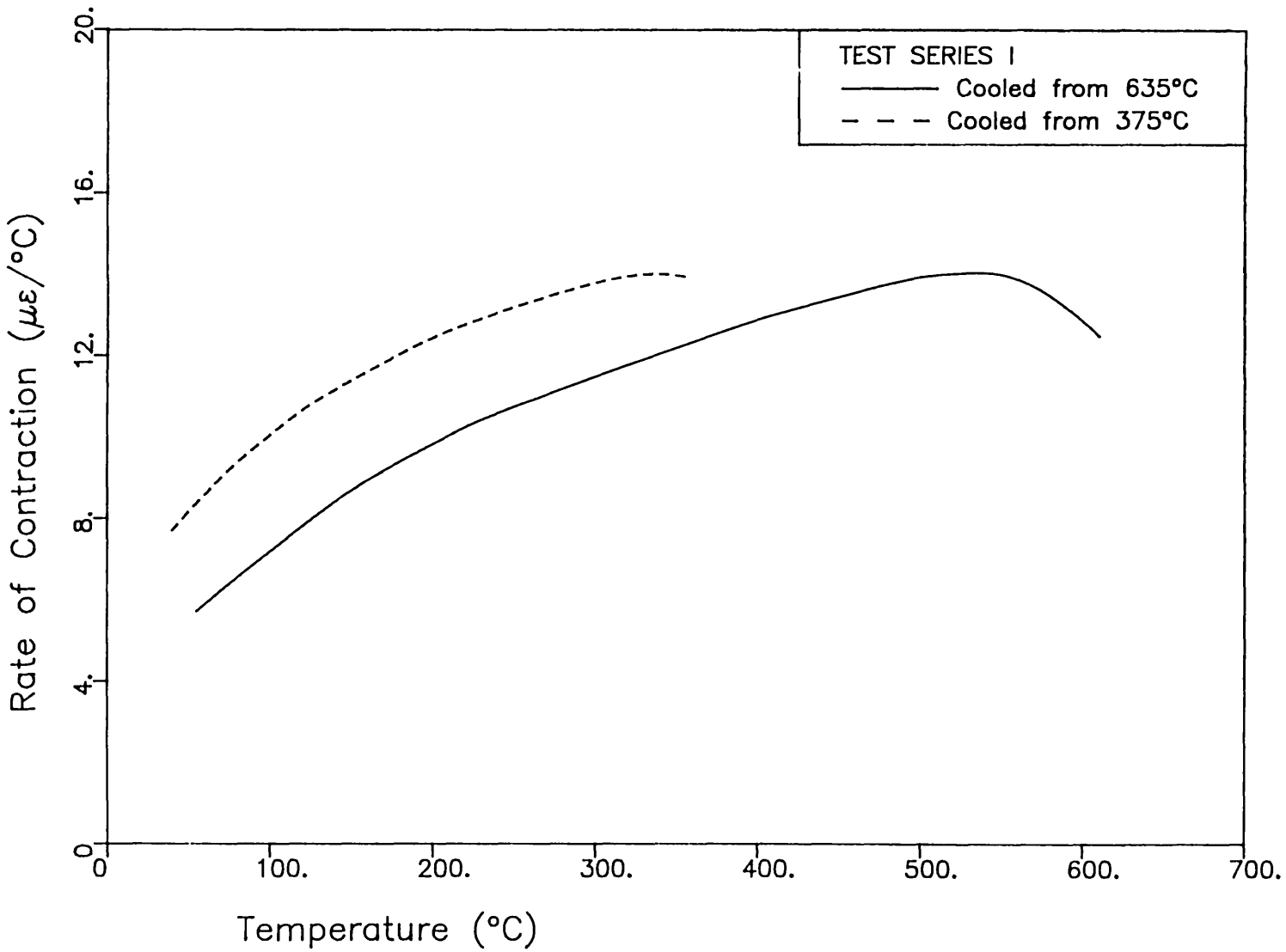

Fig.6.12 – AVERAGE COEFFICIENT OF CONTRACTION

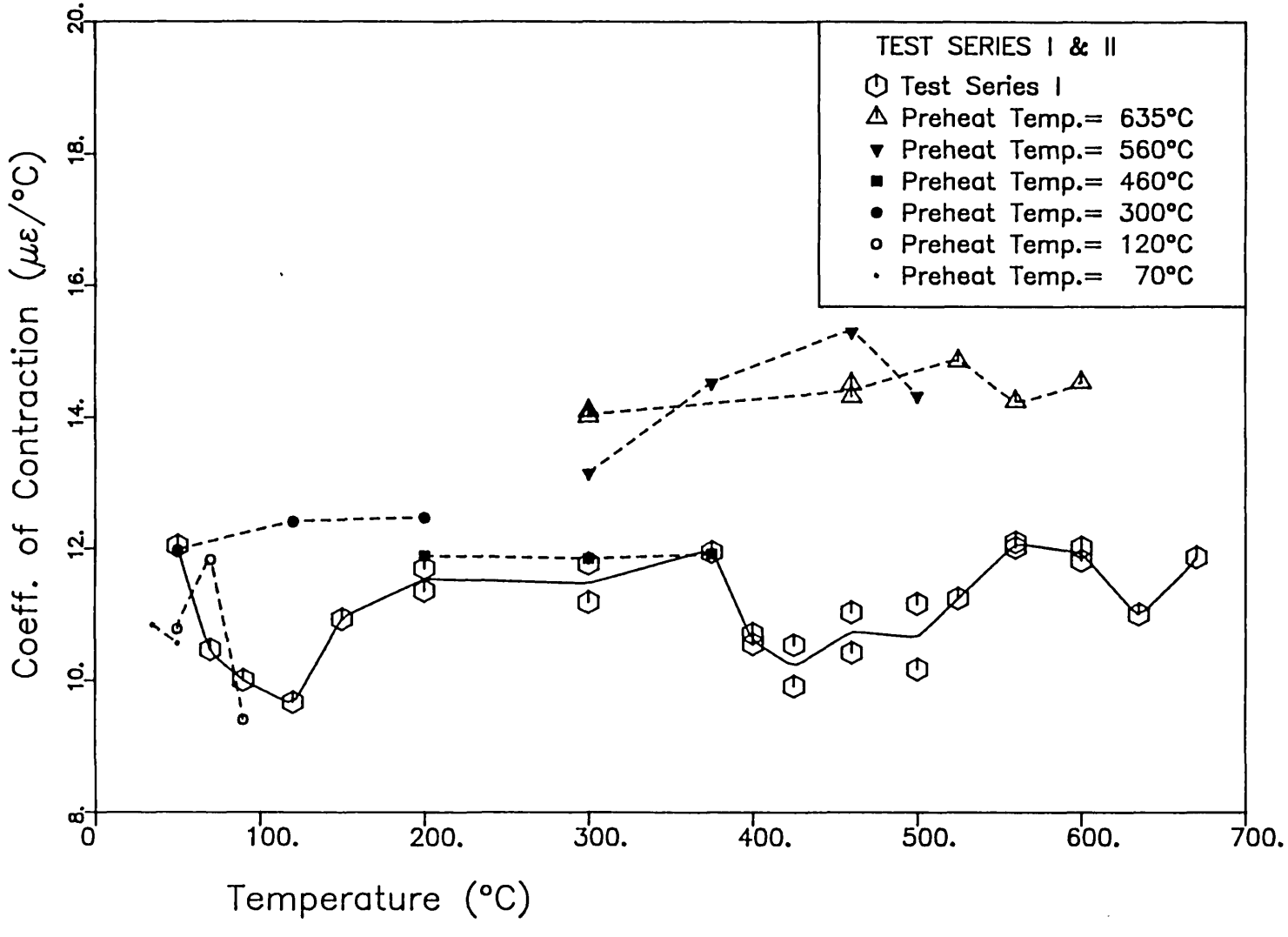

Fig.6.13 – STRAINS ON HEATING & COOLING

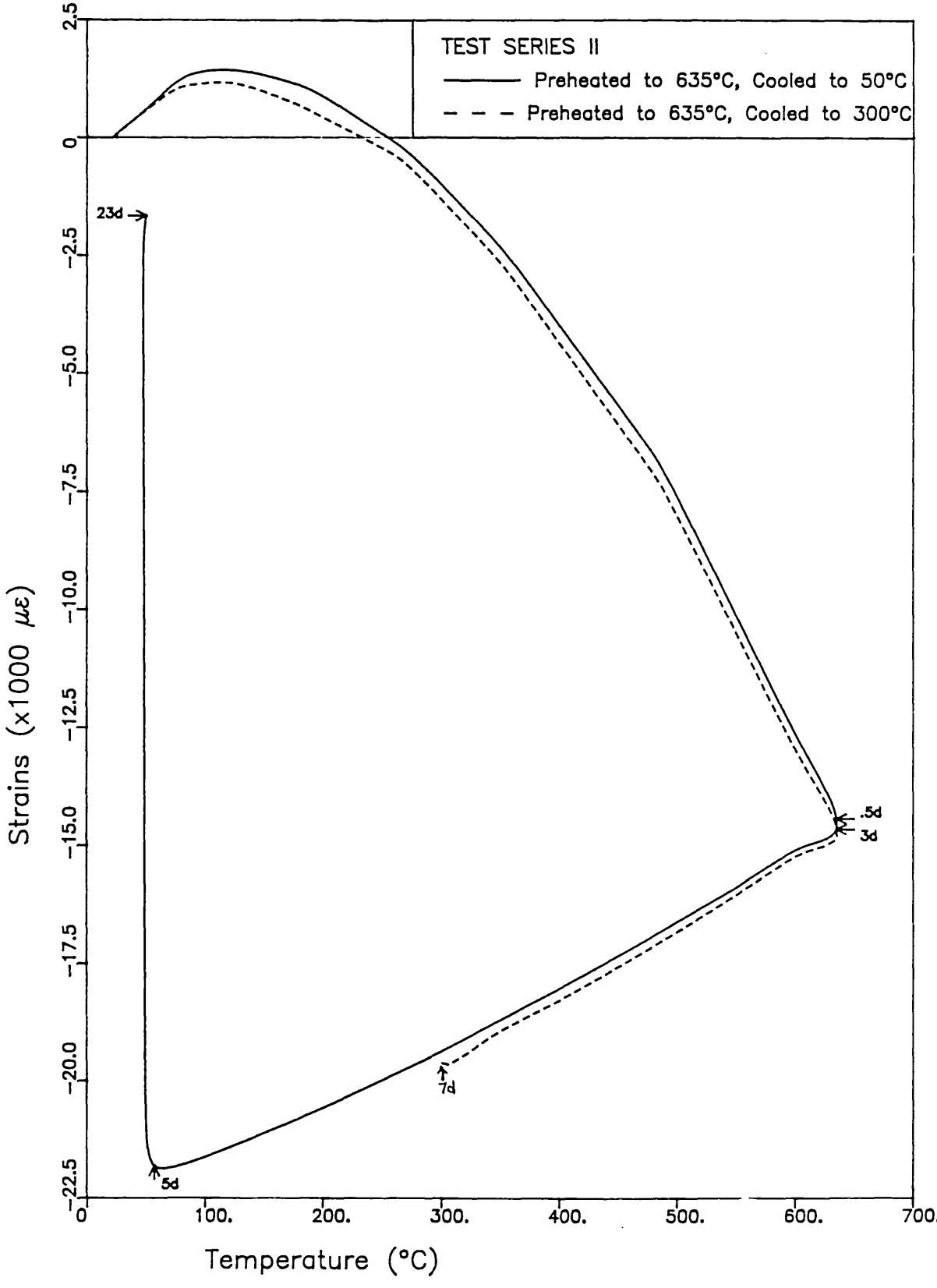

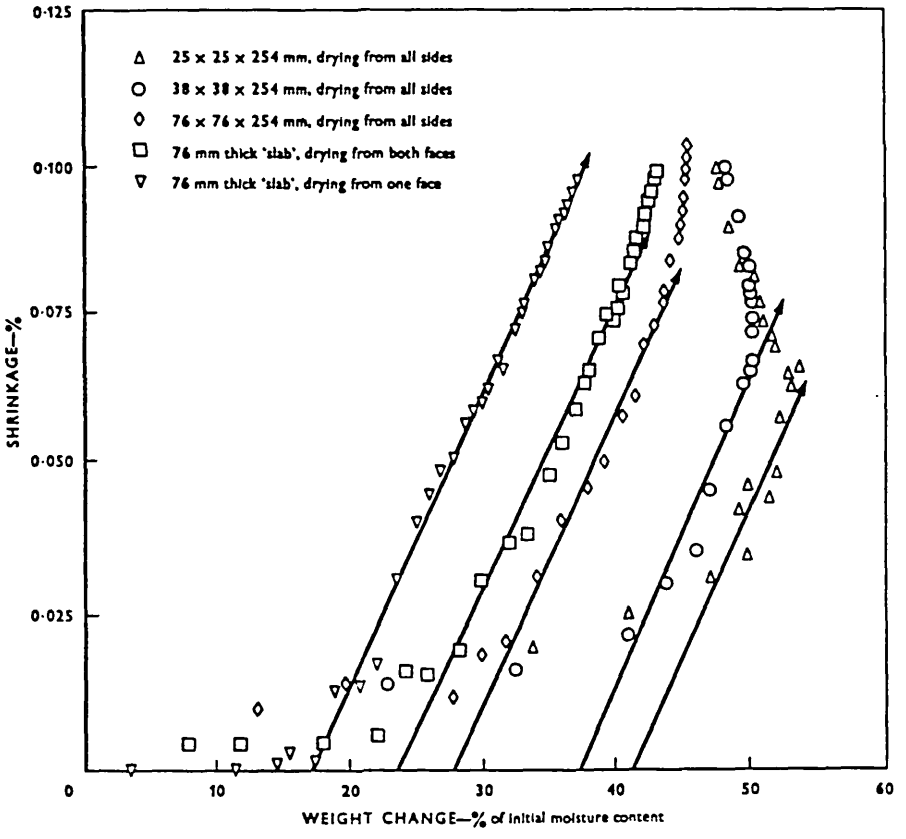

Figure 6.14 - EVOLUTION OF SHRINKAGE WITH WEIGHT CHANGE FOR CEMENT MORTAR.(FROM HOBBS & MEARS (73))

CHAPTER 7 - BASIC CREEP

The major part of the experimental programme on the creep rigs was concerned with the basic creep of hardened cement paste. This chapter sets out the results of both Series I tests, where the specimens were loaded at pre-heat temperatures, as well as Series II tests, where the specimens were loaded after being slowly cooled to temperatures lower than their pre-heat temperatures; some results from the Series V tests are also presented. The time function of basic creep is examined, confirmation being sought from other investigators' work as well. The influence of temperature is also studied, both in its directly apparent effect, as well as in its indirect effect via change in hot strength. An activation energy approach for temperature dependence is given in Chapter 8. The stress dependence of creep is investigated only in a very limited way. All the Series I and II specimens were loaded to a stress/cold strength ratio of 0.11, i.e. a stress of 10.9 N/mm^2. The raw creep data for Test Series I and II is given in Appendices 3 and 4 respectively.

7.1. EFFECT OF PRE-HEATING DURATION ON CREEP STRAINS

As indicated in Section 3.1, basic creep was assumed to be creep that took place when the unsealed specimens were loaded after dimensional stability. A stringent definition of the moisture condition at loading has been seen to be of considerable importance in the literature review (see Figure 2.1), where different pre-treatments prior to loading have been shown to have led to widely differing creep strains.

The first 3 specimens tested in the present investigation were inadvertently loaded prior to dimensional stability. The creep responses of these specimens could be used to test the importance of the criterion of dimensional stability. Furthermore, the simultaneous use of 3 furnaces, which were at different temperatures in most cases, resulted in some specimens being heated for considerable periods of time beyond dimensional stability. As a result, some replicates,

although creep tested at the same temperature, were heated for different lengths of time, albeit beyond the point of dimensional stability. This provided an opportunity of investigating the effect upon the creep strains of pre-heating durations beyond dimensional stability.

Figure 7.1 shows the above-mentioned effect of pre-heat duration upon the subsequent 1 day creep strains at selected temperatures. The specimens at 300°C, 425°C and 525°C inadvertently loaded at 4 days (i.e. prior to dimensional stability) clearly show an enhanced response over those specimens heated for periods up to dimensional stability or longer. The percentages of enhancement are 57%, 115% and 39% for the temperatures 300°C, 425°C and 525°C respectively, indicating that dimensional stability is a very important criterion for the measurement of basic creep, particularly at temperatures around 400°C where there is chemical instability for a considerable period, due to the slow dissociation of $Ca(OH)_2$. If the concurrent shrinkage is eliminated from the increased responses, the above percentages become 5%, 82% and 28% respectively.

The figure also indicates that specimens at 300°C, 400°C, 425°C and 600°C do not exhibit significant changes in their creep response when heated for periods beyond their points of dimensional stability. We can conclude, therefore, that the pre-heat duration has a significant effect on the creep response when this duration is less than the time required for dimensional stability, but has no effect beyond this point. This, in fact, greatly facilitated the experimental procedure, since the point of creep loading was time-critical only on one side of the point of dimensional stability and not both.

Figure 7.2 shows 1 day creep strains for all replicates tested. Apart from the 3 specimens at 300°C, 425°C and 525°C mentioned before, the variation between replicates ranges from negligible (1.4% at 600°C) to acceptable (17.9% at 500°C). In most cases, these variations reduce to under 5% when considering 7 day strains. This success in replication could be taken to justify the approach, described in Section 3.2, of having more points on the

temperature scale with isolated replicates, in favour of having fewer points with greater replication.

7.2. BASIC CREEP AT ELEVATED TEMPERATURES

7.2.1. Variation of Creep Response with Temperature

Figures 7.3 and 7.4 show the creep curves obtained for the Series I specimens at different temperatures up to 670°C. The curves above 525°C are shown separately because there is a manifold increase in the creep response above 600°C. However, the shapes of these curves are similar, suggesting that the type of time function for creep may be the same at all temperatures. Furthermore, all the creep responses are primary creep curves.

The influence of temperature on creep is better seen in Figures 7.5 and 7.6 where the 1- and 7-day creep strains are plotted against temperature. There are 4 points of interest in these curves. The first is a maximum at 50°C, which can be seen in Figure 7.6. It should be recalled that a strength reduction was also encountered around this temperature (see Section 5.2), which was attributed to a weaker gel structure caused by disjoining forces due to the dilatation of water layers. The creep at 50°C could be enhanced due to the same cause; in addition, the reduced strength would also contribute to an increase in creep. Furthermore, a glance at Figure 6.1 would reveal that it is difficult to achieve dimensional stability at 50°C. This would be due to slow desorption and would also tend to enhance the creep response.

Beyond this maximum at 50°C, there is a reduction in the creep response below the creep at 20°C, till a minimum is reached at 150°C. This would be due to the increased densification of the paste caused by desorption. It could be considered that the desorptive effect of temperature increasingly over-rides the thermal agitation effect at temperatures from 50°C to 150°C.

The third point of interest is the maximum at 400°C. This maximum would be due to the creep load being applied during continued

instability arising from the slow dissociation of $Ca(OH)_2$. Another glance at Figure 6.1 would show that dimensional stability is very difficult to achieve at 400°C and 425°C. Hence it is likely that specimens at 400°C and 425°C were still chemically "unstable" when creep loaded, resulting in enhanced creep strains; the specimens at 460°C may also be slightly affected by this phenomenon. The fact that the creep response diminishes beyond 400°C, up to a minimum at 500°C, would indicate that the dissociation of $Ca(OH)_2$ has little effect on the creep response, apart from situations where the creep loading takes place during the dissociation itself. Furthermore, if the points at 400, 425 and 460°C are removed, the mimimum at 500°C would vanish, indicating that it is a different kind of minimum to the one at 150°C, and further confirming that the dissociation of $Ca(OH)_2$ does not really affect the creep response in any way, unlike desorption.

The most interesting feature of Figures 7.5 and 7.6 however, is the marked increase in creep observed beyond 600°C. The 1-day creep strain at 560°C is only 2.8 times the strain at 20°C; however there is a 4.3-fold increase over the much smaller temperature range of 560°C-670°C. This marked increase in creep around 600°C has also been observed by Khoury (85) for lightweight aggregate (i.e. lytag) concrete. Gillen's tests on calcareous, siliceous and expanded-shale aggregate concrete (60) also hint at the existence of this kind of increase, but the spacing of temperature points does not emphasize it; neither does his exponential-type idealization of the temperature function give full justice to the markedness of the increase that may have resulted if more temperature points close to 600°C were employed. (See Figure 2.9a). Gross (63) also found a similar phenomenon for his gravel concrete, albeit at the lower temperature of around 400°C. The results of these three investigators have been normalized with respect to a stress/cold strength ratio of 0.1 and presented in Figure 2.2.

Based on extensive tests performed on gravel concrete (84), it can be fairly certainly concluded that the enhanced creep response beyond 400°C is due to the break-up of aggregate. However, the same cannot be said for lytag concrete at 600°C, since the aggregate is known to be stable at much higher temperatures; it is manufactured at a temperature of 1300°C. The virtually identical behaviour of the

cement paste specimens at 600°C would seem to indicate that the marked increase in creep beyond this temperature is seated in the cement paste itself.

Given that the above behaviour originates in the cement paste, it would be very instructive to find a causal link with changes taking place at the microstructural level. Two significant microstructural changes can be cited from the literature in the temperature range 600°C to 670°C. The first is an increase in the "main pore radius" of cement paste which commences around 600°C (154). The second is an expansion of anhydrous β-C_2S as it is transformed to α-C_2S (137). No marked changes from the general trends appear to take place within this temperature range in total porosity (138), micro-cracking (137), silicate polymerization (138) and dilatometry (137) of cement paste; nor are any significant thermic reactions detected by DTA (86, 137). Another change taking place in this regime, however, is the reversal of the trend of increasing shrinkage during the heating phase, described in Section 6.2, which may cause enhanced microcracking. It must be pointed out, however, that changes in pore characteristics and microcracking are irreversible with temperature, whereas evidence presented in Section 7.3 will show that this enhanced creep response above 600°C is in fact reversible with temperature. This discussion will, therefore, be further taken up in that section.

7.2.2. Evolution of Creep Response with Time

Figure 7.7 shows the ratios with respect to 1-day creep strains of the 0.1 day and 7-day creep strains. This figure gives an indication of the proportion of creep that takes place at an earlier or later time. The minima at 70°C and 400°C for the 0.1 day ratio curve suggest that a larger part of the creep takes place at a later stage; this is not surprising since these temperatures correspond to temperatures of "instability" - one due to incomplete desorption and the other due to slow dissociation of $Ca(OH)_2$. The minimum at 70°C is matched by a maximum in the 7 day ratio curve, but the one at 400°C has no corresponding maximum. The other clearly matched feature is the crest in the 0.1 day ratio curve around 90-120°C and the corresponding trough in the 7 day ratio curve. This suggests that a larger part of

the creep occurs earlier and that the response reduces faster with time, probably as a result of a more stable structure after desorption.

The 7-day ratio curve exhibits a falling trend from 200°C to 560°C, indicating that a greater proportion of creep occurs at earlier times for higher temperatures. This trend is somewhat reversed beyond 560°C, which is the region in which the creep strains show a marked increase. The 7-day ratio curve shows similarity to the curve for the n-value in the power-law idealization, shown in Figure 7.21.

7.2.3. Dependence on Stress/Hot Strength Ratio

As described previously, all the specimens were loaded to an equal stress/cold strength ratio of 0.11. The stress/hot strength ratio therefore, varied from one temperature to another and this ratio was determined using the results from the hot strength Test Series VI. Figure 7.8 shows the 7-day strains normalized to a stress/hot strength ratio of 0.11, assuming linearity between the creep response and stress/hot strength. Apart from outlying points at 400°C and the upper temperatures of 635°C and 670°C, the creep response is reasonably constant, with an average of 406.4 $\mu\epsilon$. This implies that up to around 600°C temperature affects the creep of cement paste in a way that can be correlated to the change in hot strength. It must be pointed out however, that within this broadly constant response there are familiar trends, such as the maximum at 50°C, the minimum at 120°C and an increasing trend from 120°C to 300°C. The deviation at 400°C would be due to chemical instability during loading; those beyond 600°C are due to the marked increase in creep, probably resulting from a significant change of state in the material.

The above-mentioned hypothesis regarding the stress/hot strength ratio can be looked at from another angle by plotting the 7-day creep strain against stress/hot strength ratio, irrespective of the temperature. If the point corresponding to 400°C is ignored, a fairly reasonable straight line can be drawn through the points corresponding to temperatures not greater than 600°C, as done in Figure 7.9. A least squares fit gives a coefficient of correlation, r^2, of 0.87. Furthermore, the slope obtained is 3515 $\mu\epsilon$ which corresponds

to a strain of 386.7 $\mu\epsilon$ per 0.11 stress/hot strength ratio; this compares well with the average strain in Figure 7.8. The intercept is also only 16 $\mu\epsilon$, which means that the line virtually passes through the origin.

There seems also to be a linear relationship beyond 600°C, as shown in the figure. This would give further credence to the view that there is a correlation between the way temperature affects the creep response and the way it affects hot strength. It would tend to suggest that temperature affects creep primarily in as much as it affects the structure of the material, any direct thermal effect being negligible or secondary, as is the case for strength and modulus of elasticity. However, evidence from Series II tests, described in the next section, indicate that this is not quite the case. Furthermore, discussions in Sections 8.3 and 9.4 will show that Series I creep results would depend, not only on variations in hot strength, but also on thermal effects and micro structural stabilization caused by temperature.

7.3. THE EFFECT OF HIGHER PRE-HEAT TEMPERATURES

The Series II creep tests were performed by pre-heating the specimens until dimensional stability at a given pre-heat temperature, and then cooling gently to test temperature prior to loading. The cooling phase was seen as very critical in terms of ensuring that thermal gradients within the specimen did not impair the integrity of the specimen. It should be remembered that any stresses set up would not be relieved by transitional thermal creep as in the heating phase, because such creep does not occur during cooling. Furthermore, since the specimens were being cooled without load, no assistance was available from pre-compression either.

As a test case, specimens pre-heated to 635°C and tested at 460° and 300°C were cooled at the separate rates of 1°C/minute and 0.5°C/minute. Since there was essentially no difference in either the thermal or creep strains, it was concluded that the above-mentioned rates of cooling were slow enough to preserve specimen integrity and

the cooling rate of 0.5°C/min. was used for the rest of the specimens.

The 1- and 7- day creep strains from the Series II tests are presented graphically in Figures 7.10 and 7.11 respectively. The points on the broken lines are those which have been pre-heated to the temperature at which the given line meets the solid line. The solid line represents the average creep strain at selected temperatures for the Series I tests. The immediate observation is that the higher creep experienced at higher temperatures, including the pre-heat temperature of 635°C where very high creep is observed, is not experienced after cooling to a lower test temperature. In fact, the creep strains are, in general, reduced below the Series I values at test temperature by the pre-heating. If the creep strains are normalized in terms of the response to a stress/hot strength ratio of 0.11, very definite reductions due to pre-heating are evidenced, especially at temperatures below 600°C, as seen in Figures 7.12 and 7.13. In carrying out this normalization, the hot strength of a specimen is taken to be the strength at the maximum temperature of exposure, this assumption being justified by the results in Section 5.2.

Similar observations regarding reduction in creep due to pre-heating have been made by previous investigators over a wide range of pre-heat and test temperatures (43, 100, 129, 173). Day and Gamble (43) however, reported an opposite trend for mature (i.e. 2.5 year) specimens. Marechal (100), who tested unsealed concrete up to a temperature of 500°C postulated that the reduced creep was due to the number of bonds liable to be activated being decreased. Day and Gamble (43) and Parrott (129), whose tests were on sealed cement paste specimens heated to temperatures below 100°C, attributed the reduction in creep to increased polymerization caused by the thermal treatment. Their results showed that an increasing severity of pre-treatment (in terms of temperature level and duration) resulted in a diminishing creep response. The same phenomenon is shown in the present investigation when the results are normalized with respect to stress/hot strength ratio. Figure 7.14 exemplifies this for specimens tested at 300°C after being pre-heated to various higher temperatures. The average strain for the Series I specimens at 300°C is also shown.

Concurrent investigations on the degree of polymerization, described in Chapter 9, show however, that the above reduced creep is not always accompanied by increased levels of polymerization, especially at higher temperatures. Alternatively, it is possible that moisture loss could account for the reduced creep potential. This hypothesis is investigated in Section 9.4.

It was also discovered that specimens pre-heated to temperatures of 300°C or less (i.e. 70°C, 120°C and 300°C) and cooled to lower temperatures exhibited virtually no creep when loaded. Some of them, in fact, experienced a slight expansion in later periods under load. This may be due to swelling upon re-absorption of atmospheric moisture (181). The phenomenon of zero creep after thermal pre-treatment has been reported before (119, 170). It must be noted, however, that the use of a higher stress/strength ratio may have resulted in some creep.

The 600°C temperature level is also very interesting. Not only is there a marked increase in basic creep beyond this point, but the creep at 600°C after pre-heating to 635°C is not reduced to any great extent below the Series I value, unlike the other Series II specimens. In fact, the effect of temperature on creep behaviour beyond 600°C seems to be virtually reversible.

The above phenomenological observations could shed some light on microstructural causes and mechanisms of elevated temperature creep. It is unlikely that either an increase in main pore radius (154) or enhanced microcracking are responsible for the marked increase in creep above 600°C, since these changes would be irreversible with temperature, whereas the creep response is not. A more likely cause or mechanism could be a self diffusion type phenomenon, similar to that observed in other materials such as ceramics and metals above certain critical temperatures. The close relation between creep and atomic diffusion processes forms the basis of most of the currently held theories of the creep of metals, which is normally very low below a critical temperature of around 0.3 T_m (where T_m is the melting point of the material in absolute units of temperature). Similarly creep phenomena of engineering significance are rarely encountered in

ceramics below around 0.4 T_m. Interestingly, the 600°C "critical" temperature for cement paste is around 0.5 T_m.

The creep mechanism below 600°C would probably be a structural re-adjustment type of phenomenon. This process would be enhanced by temperature, but inhibited by a higher pre-heat temperature, which would cause loss of moisture and a consequent locking together of the solid skeleton. The absence of creep below 300°C after pre-heating to higher temperatures is indicative of a temperature and perhaps stress threshold that is required to initiate creep; this would be consistent with a structural re-adjustment type of creep mechanism. The mechanism postulated above is somewhat similar to Cilosani's hypothesis (119).

7.4. TIME FUNCTION FOR BASIC CREEP

7.4.1. Choice of Time Function

Three of the formulae reviewed in Section 2.1.3 were chosen for comparison with the experimental results, namely

(i) a 2-parameter power law for creep strains, i.e.

$$\epsilon_c = At^n \qquad (7.1)$$

(ii) a 3-parameter power law for total (i.e. creep + elastic) strains, i.e.

$$\epsilon_t = P + Qt^m \qquad (7.2)$$

which is derived from Bazant's Double power law (15) with age effects being ignored;

(iii) a 2-parameter logarithmic law proposed by Day and Gamble (41) for creep strains, i.e.

$$\epsilon_c = J \log_e (1+Kt) \qquad (7.3)$$

where A, P, Q, J, K, m and n are constants for a given creep test and t is the time under load.

It must be noted that because of the errors inherent in measuring elastic strains at loads below 1.7 tons (see Section 4.4), the total strains needed for comparison with (ii) above were obtained by measuring the elastic strains for loads in excess of 1.7 tons and assuming linearity in the stress-elastic strain relationship. Formula (iii) was proposed, strictly speaking, for the flow component of creep. It is included in the comparison here because it has been suggested that total creep strains of specimens pre-heated for long durations at temperature are reasonably well fitted by it (40). This is because delayed elastic strains were considered to be associated with moisture movement; long durations of pre-heating were thought to eliminate this component to a great extent, leaving only the flow component of creep (40). It also serves to give an indication of how well a logarithmic type time function compares with the power law functions.

The fitting was done by using a least squares algorithm to optimize the parameters for each creep test. Most of the tests were performed up to a duration of 7 days and the fitting done from a time of 0.001 days up to the total duration under load. Three specimens tested at temperatures of 300°C, 460°C and 560°C respectively were kept under load for 40 days, in order to confirm the trends observed in the relatively short period of 7 days.

The results of the comparison, including the values of the parameters, are tabulated in Table 7.1 for Test Series I and Table 7.2 for Test Series II. The closeness of fit can be compared by using the Standard Error of Estimate and the Index of Correlation (52), defined as below.

$$\text{Standard Error of Estimate} = \sqrt{\frac{\text{Sum of Squares of Residuals}}{n - m}} \qquad (7.4)$$

$$\text{Index of Correlation, } i_c = \sqrt{\frac{\sum_{i=1}^{n} (y_i - \bar{y})^2 - \text{Sum of Squares of Residuals}}{\sum_{i=1}^{n} (y_i - \bar{y})^2}} \qquad (7.5)$$

where

$$\text{Sum of Squares of Residuals} = \sum_{i=1}^{n} (y_i - y_{ci})^2$$

and where

n = number of points used for the curve fitting

m = number of parameters in the formula

y_i = i^{th} observed value

y_{ci} = i^{th} calculated value (based on fitted curve)

$\bar{y}$ = mean of the observed values

It is clear from the tables that the power law functions fit the experimental results much better than do the logarithmic law, even in the case of Series II tests, where moisture movement would have been negligible if not non-existent and the flow component expected to be the predominant if not the only component of creep (40). A typical comparison of the nature of the fit obtained from the 3 formulae for a Series II specimen is shown in Figure 7.15.

In comparing formulae (i) and (ii), the tabulation indicates that (ii) gives a better fit in most cases. However, it was decided to adopt formula (i) for further analysis on the principle of parsimony, since formula (i) has only 2 parameters to formula (ii)'s 3 parameters. Furthermore, formula (i) relates to creep strain alone (as opposed to creep + elastic strain), which is what the subsequent analysis in this and the next chapter will focus on.

Formulae (i) and (iii) have also been compared using the results of Marechal (100) on quartzite concrete and Khoury (84) on lightweight aggregate (i.e. lytag) concrete. The comparison is tabulated in Table 7.3 and shown graphically for 2 typical cases in Figure 7.16. The logarithmic law performs much better for these sets of data, in some cases even giving a slightly better fit than the power law. The parameter K however, seems to decrease with temperature for Marechal's data but increase with temperature for Khoury's data.

7.4.2. Parameters of Power Law Formula

The choice of the 2 parameter power law formula to describe the time dependence of creep, especially at elevated temperatures, is

in agreement with the findings of other researchers (27, 180). The idealized creep-time relationship will be a straight line in a log-log plot and these are shown in Figure 7.17 for Series I specimens and Figure 7.18 for Series II specimens. These lines appear to be reasonably parallel to each other, implying therefore that the time function of creep is independent of temperature. However, a closer look at the parameter n, which defines the slope of the log-log plot, will indicate that it is in fact temperature dependent in a certain way, and that the time and temperature functions cannot strictly be uncoupled.

The closeness of fit obtained by using the power law formula is shown in Figure 7.19 for the 3 Series I specimens loaded for 40 days' duration. The early strains are not fitted as well as the later strains are, the former being underestimated by the formula. These early strains are fitted better in the Series II tests, as shown for a typical case in Figure 7.15. In general, the Series II results are fitted better by all the formulae than the Series I results. This may suggest that a single mechanism, such as structural re-adjustment, is operative in the Series II tests, while the Series I tests may have other contributory mechanisms, such as moisture migration as well.

The parameter A in the power law formula represents the creep at 1 day. The ratios of A to the strain at 1 day for the Series I and II specimens is shown in Figure 7.20. The proximity of these ratios to unity confirms the suitability of the power law as a time function. The tendency of the ratios for the Series I tests to lie slightly above unity shows that any underestimation of early strains is not exhibited beyond 1 day. The ratios for the Series II tests tend to lie slightly below unity.

Figure 7.21 shows the way that n is dependent on temperature. For the Series I results, the value of n increases from around 0.3 at 20°C to around 0.4 at 150°C while passing through a maximum at 70°C and a minimum at 90°C. From 150°C to 375°C the n value is sensibly constant. However it shows a falling trend from 375°C to a minimum at 560°C, whereupon it shows another increase. Some of these trends are seen in Khoury's (84) results for lytag concrete as well, where n can

be considered reasonably constant in the range 165°C to 495°C after which there is a drop to 595°C and an increase thereafter. A recent comparison (85) of the work of 3 investigators at Imperial College using the same apparatus but different materials, with a power law fitted to the creep strains beyond 1 day, also showed the above-mentioned decrease in n after a plateau over a certain temperature range. (See Figure 7.23). The Series II specimens show smaller n values than the Series I specimens, all the values being under 0.3. The 3 specimens in Series I loaded prior to dimensional stability show higher n values.

The n value is an index of the proportion of creep that would take place at earlier or later times under load, a high n value indicating protracted creep at later stages. In general, n values tend to be higher when there is dimensional instability or difficulty in achieving dimensional stability prior to loading. This is exemplified by the higher n values at 70°C, in the range 150°C-375°C and in the dimensionally unstable specimens. The specimens at 400°C and 425°C do not seem to show this. Pre-heated specimens would be very stable dimensionally and also have a reduced creep potential; hence they show comparatively lower n values. The creep increase above 600°C seems also to be associated with an increasing n value. The drop in n value from 375° to 560°C indicates that within this range, a temperature increase causes a greater proportion of creep to take place at an earlier time.

7.5. STRESS DEPENDENCE OF BASIC CREEP

Although the stress function has not been investigated in any comprehensive fashion, the few tests performed in Series V-A, where hardened cement paste of different w/c ratios were used, resulted in specimens being loaded to different stress/cold strength ratios. The resulting 1-day creep strains have been normalized on the basis of linearity of creep with stress/cold strength ratio, and shown in Figure 7.22. There is a remarkable coincidence in the strain at 525°C, justifying the above normalization and suggesting that the stress and temperature functions can be uncoupled. It is not clear whether the

differences shown at 600°C and 670°C are within experimental scatter or whether some systematic relationship is being followed. A proper experimental programme needs to be carried out to investigate the stress function, and its relation to temperature. The evidence from Figure 7.9, where creep seems to be related bi-linearly to stress/hot strength, irrespective of temperature, should also be further investigated.

One piece of additional information that Figure 7.22 gives us, however, is that 600°C seems to be the point beyond which the marked increase in creep takes place, irrespective of the w/c ratio of the paste. Although the specimens with w/c = 0.225 experienced a reversal in the ultimate strain on heating from 525°C to 600°C (See Figure 6.4), they did not show any marked increase in creep between these temperatures; conversely, although the specimens with w/c = 0.375 did not experience a reversal in the ultimate strain on heating from 670° to 725°C (Figure 6.4), they did show a large creep response at both 670°C as well as 725°C. It may be concluded therefore that the point of reversal in ultimate strain on heating has no bearing on the marked increase in creep response; instead this phenomenon appears to be a function of temperature alone, with 600°C being the critical point.

If we consider the relationship between time and stress functions, the analysis of Khoury's results in Figure 7.21 shows that the n values for specimens at 165°C, 318°C and 595°C are virtually identical, despite one stress level being double the other (84). This indicates that the stress and time functions can be uncoupled, at least within certain limits of stress and temperature.

7.6. CONCLUSION

This chapter has examined the time, temperature and stress functions of basic creep. The last has been done in a very limited fashion while the second will be considered in greater detail in the next chapter. These functions can be uncoupled in certain regimes of stress and temperature, leading to a creep formula of the type

$$\epsilon_c = K.f(T).f(\sigma).f(t) \qquad (7.6)$$

where K is a constant and f(T), f(σ) and f(t) are functions of temperature, stress and time respectively. However, they are, strictly speaking, not independent of each other.

The time function is best represented by the 2 parameter power law of the form

$$\epsilon_c = At^n \qquad (7.1)$$

where A represents creep at unit time and n is a parameter that is a function of temperature (though reasonably constant over a particular range of temperature) but seems to be independent of stress (at least at low stress levels).

The most interesting phenomenon with respect to temperature is the marked increase in creep beyond 600°C, in which region there seems to be reversibility in the effect of temperature on creep. This large increase in the creep of cement paste and lightweight aggregate concrete (85) above 600°C, suggests that a fundamental rheological property, seated in the cement paste, limits the structural use of Portland Cement based concretes to temperatures below this limit. This limit, which seems to be independent of the w/c ratio of the paste, could however be lowered if the aggregate disintegrates as in the case of gravel aggregate concrete. (See Figure 7.24).

Although the stress function has not been rigorously investigated, some pointers towards further research have been made, such as the bi-linearity between creep and the stress/hot strength ratio, and the independence of the time and stress functions of creep.

Pre-heating was seen to be a very significant factor in the subsequent creep response. On the one hand, if pre-heating was not carried out until dimensional stability was achieved, there was an increase in the creep above that value which has been defined as basic creep. Then again, if the specimens were pre-heated to a temperature higher than the test temperature, the creep response was lower than if

pre-heating was done at the test temperature itself. Furthermore, if normalized on the basis of an equal stress/hot strength ratio, the creep strain at a given test temperature was lower for higher temperatures of pre-heating. In the case of pre-heat temperatures below 300°C, no creep was observed after cooling to lower test temperatures, for the stress/cold strength level of 0.11 employed in these tests.

The creep mechanism at elevated temperatures up to 600°C, especially in the case of prior pre-heating at a higher temperature, is probably one of structural re-adjustment. At temperatures above 600°C, the mechanism is probably one of self diffusion. These mechanisms will be further discussed in Section 8.3.

Test Temp. (°C)		20	20	50	70	90	120	150	200	200	300	300	375	400	400
$\varepsilon_c = At^n$	A	246.2	226.6	244.2	161.4	177.6	163.3	121.2	141.2	173.3	281.2	322.5	394.7	683.4	680.6
	n	0.302	0.307	0.412	0.445	0.302	0.345	0.433	0.538	0.394	0.496	0.401	0.443	0.463	0.355
	Std EE	10.17	3.73	14.01	11.31	14.71	11.61	15.15	18.62	20.28	27.90	23.84	27.11	38.79	17.21
	In. Cor.	.995	.999	.996	.994	.984	.991	.978	.983	.977	.996	.990	.994	.996	.998
$\varepsilon_t = P + Qt^m$	P	615.5	559.7	738.4	659.8	983.6	837.3	785.3	924.2	931.6	1440.6	1137.7	1307.1	1834.1	2022.0
	Q	224.1	231.9	202.8	135.0	118.5	123.3	99.7	100.3	127.0	237.4	232.4	331.3	584.9	634.1
	m	0.371	0.298	0.483	0.514	0.450	0.450	0.516	0.696	0.530	0.537	0.533	0.517	0.529	0.395
	Std EE	5.58	3.74	6.75	7.22	4.51	5.60	14.15	11.56	16.82	13.19	13.43	19.59	23.72	13.92
	In. Cor.	.999	.999	.999	.998	.999	.998	.982	.994	.985	.999	.997	.997	.999	.999
$\varepsilon_c = J\ \ln(1+Kt)$	J	68.38	59.97	158.6	131.2	56.84	70.11	84.1	199.9	90.80	654.7	174.0	286.0	541.0	197.8
	K	67.30	62.63	3.97	2.42	30.81	11.60	3.43	0.90	6.85	0.31	6.47	3.15	2.68	38.4
	Std EE	34.83	21.79	38.95	24.14	33.57	28.83	22.46	29.91	36.40	69.99	55.39	61.47	101.7	67.97
	In. Cor.	.942	.971	.966	.974	.914	.942	.952	.957	.926	.985	.949	.967	.972	.964

(cont...)

TABLE 7.1. RESULTS OF CURVE FITTING FOR CREEP TEST SERIES I.

Test Temp. (°C)		425	425	460	460	500	500	525	560	560	600	600	635	670
$\varepsilon_c = At^n$	A	686.6	607.3	597.6	552.4	453.3	567.3	534.3	684.8	709.6	1000.9	1041.5	2114.9	2989.8
	n	0.335	0.307	0.366	0.344	0.323	0.321	0.333	0.314	0.236	0.300	0.282	0.361	0.345
	Std EE	43.97	14.47	37.37	25.06	17.96	24.62	22.32	27.39	10.25	14.71	32.22	75.44	49.50
	In. Cor.	.990	.998	.997	.995	.996	.996	.997	.998	.998	.999	.996	.998	.999
$\varepsilon_t = P + Qt^m$	P	1658.4	1933.1	1984.8	1858.8	1740.9	2068.5	1922.6	2277.5	1852.7	2309.0	2339.6	2976.0	3141.7
	Q	465.5	578.2	503.8	425.8	430.2	487.8	467.6	602.5	691.5	1002.1	789.7	1856.2	2832.7
	m	0.480	0.331	0.405	0.439	0.342	0.373	0.379	0.342	0.246	0.300	0.368	0.412	0.370
	Std EE	16.70	13.92	19.03	10.93	17.93	17.81	16.84	16.03	10.40	15.26	14.09	40.33	36.73
	In. Cor.	.999	.998	.999	.999	.997	.998	.998	.999	.999	.999	.999	.999	1.000
$\varepsilon_c = J\ \ln(1+Kt)$	J	244.5	137.9	548.2	208.8	148.2	195.3	199.1	410.2	113.7	284.1	287.2	894.9	942.3
	K	21.91	103.4	1.33	18.03	30.07	25.20	19.24	3.62	620.5	51.16	52.86	12.68	30.58
	Std EE	110.4	57.02	133.5	79.62	57.21	84.39	78.82	134.3	55.85	107.0	112.5	289.5	291.4
	In. Cor.	.936	.962	.968	.951	.964	.954	.958	.963	.964	.971	.957	.964	.971

TABLE 7.1. RESULTS OF CURVE FITTING FOR CREEP TEST SERIES I (CONT.).

Preheat Temp. (°C)		460		500	560				635						
Test Temp. (°C)		300	375	300	300	375	460	500	300	300	460	460	525	560	600
$\varepsilon_c = At^n$	A	204.7	221.3	231.1	229.2	249.6	405.1	415.9	269.6	346.8	392.9	448.4	413.3	677.1	1003.2
	n	0.226	0.230	0.209	0.229	0.293	0.201	0.232	0.240	0.228	0.242	0.230	0.290	0.262	0.272
	Std EE	11.02	9.83	19.30	15.81	11.61	14.54	14.89	12.12	7.24	10.32	8.98	14.55	15.30	17.23
	In. Cor.	.989	.991	.971	.983	.993	.993	.994	.993	.998	.998	.999	.997	.999	.999
$\varepsilon_t = P+Qt^m$	P	1750.4	1539.9	1805.0	1959.0	2542.7	1777.6	1831.9	2307.7	2199.9	1927.4	2230.2	1604.1	2414.0	2577.3
	Q	281.5	282.5	342.4	318.6	313.2	560.5	529.7	250.9	392.6	388.9	459.8	398.3	745.9	1001.6
	m	0.155	0.169	0.132	0.156	0.221	0.133	0.171	0.261	0.198	0.245	0.223	0.302	0.236	0.273
	Std EE	8.23	7.65	17.53	13.38	6.012	8.60	8.78	12.27	4.89	10.70	9.16	14.82	11.71	17.88
	In. Cor.	.994	.995	.978	.988	.998	.998	.998	.993	.999	.998	.999	.997	.999	.999
$\varepsilon_c = J \ln(1+kt)$	J	37.91	38.60	39.28	43.68	61.32	60.22	73.31	51.59	66.49	77.51	87.01	109.3	159.8	239.2
	K	365.3	453.6	584.4	312.6	86.64	1182.3	428.4	313.3	318.4	263.7	296.4	68.1	115.8	106.5
	StdEE	13.91	14.77	19.88	17.60	14.49	21.21	25.14	30.82	28.45	39.66	42.5	48.81	63.04	106.2
	In. Cor.	.982	.980	.969	.978	.989	.985	.984	.953	.976	.964	.968	.962	.976	.967

TABLE 7.2. RESULTS OF CURVE FITTING FOR CREEP TEST SERIES II.

Investigator		Marechal (100)						Khoury (84)									
Material		Quartzite Concrete						Lytag Concrete									
Stress/Cold strength		0.143						0.125					0.245				
Temp. (°C)		20	50	70	250	400		165	318	515	595	724	165	318	495	595	672
$\varepsilon_c = At^n$	A	38.92	80.74	58.23	86.72	158.5		142.6	193.6	326.2	702.7	8541.6	114.7	309.7	394.2	847.4	12268.
	n	0.223	0.304	0.238	0.308	0.363		0.461	0.451	0.224	0.392	0.444	0.530	0.442	0.562	0.367	0.412
	Std. EE	5.87	5.02	4.54	19.50	13.16		9.38	14.87	24.26	57.83	124.5	7.71	14.87	32.54	98.85	632.4
	In. Cor	.860	.993	.962	.906	.981		.993	.991	.959	.985	.997	.995	.996	.994	.966	.968
$\varepsilon_c = J \ln(1+kt)$	J	17.49	58.57	30.06	55.89	138.7		105.4	138.4	76.76	379.5	2800.9	126.1	209.4	503.8	409.0	3876.1
	K	4.010	1.662	2.669	2.662	1.379		3.237	3.421	84.17	6.280	17.01	1.523	3.864	1.213	8.180	21.32
	Std. EE	6.43	6.20	3.76	24.93	11.62		9.95	10.63	22.92	38.58	304.3	15.00	17.71	30.10	71.09	334.7
	In. Cor.	.832	.990	.973	.846	.985		.993	.995	.963	.993	.985	.981	.994	.995	.982	.991

TABLE 7.3. RESULTS OF CURVE FITTING FOR DATA FROM OTHER INVESTIGATORS.

Fig.7.1 – EFFECT OF PREHEATING DURATION ON 1–DAY CREEP STRAIN

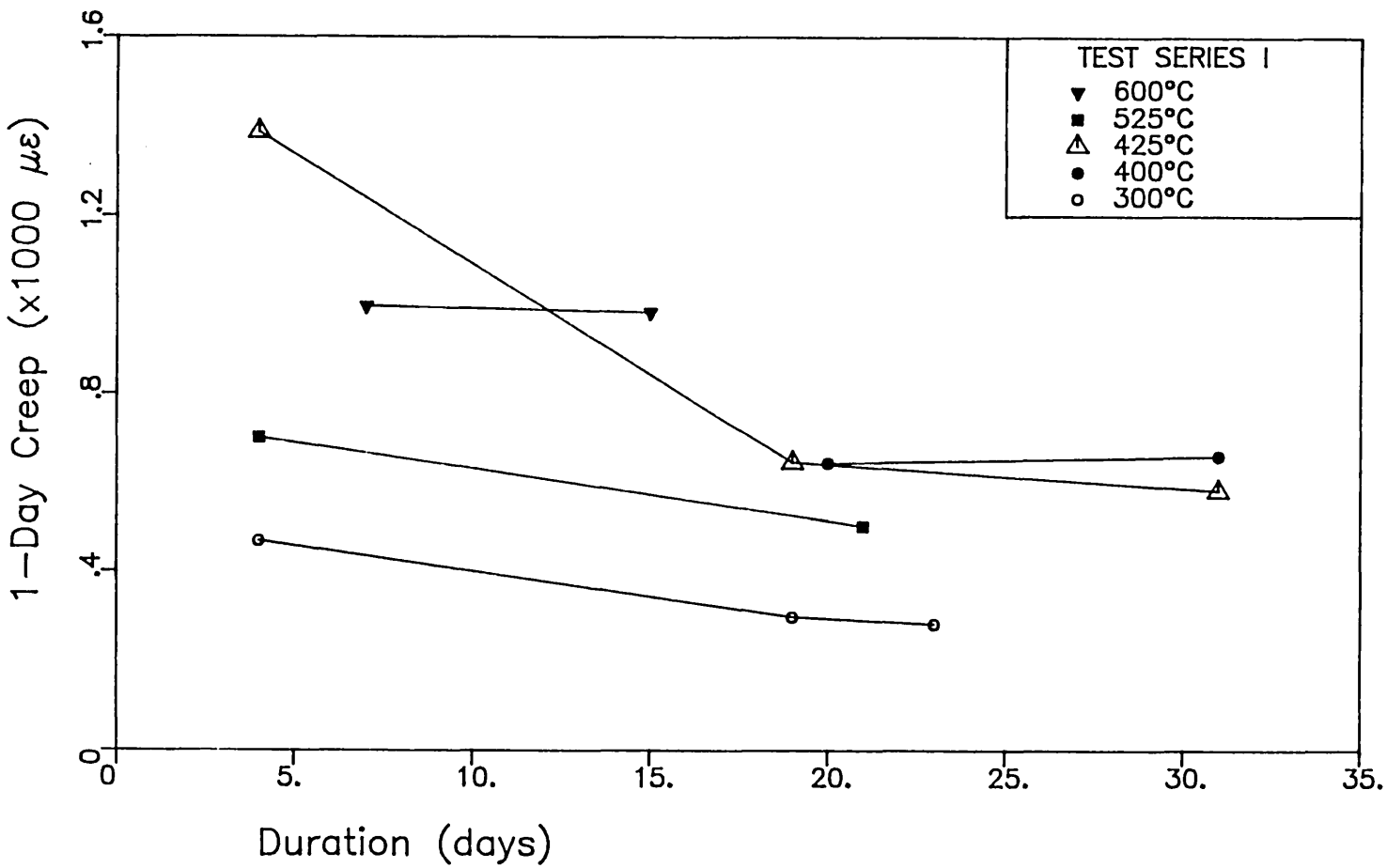

Fig.7.2 – REPLICATION – 1–DAY CREEP STRAINS

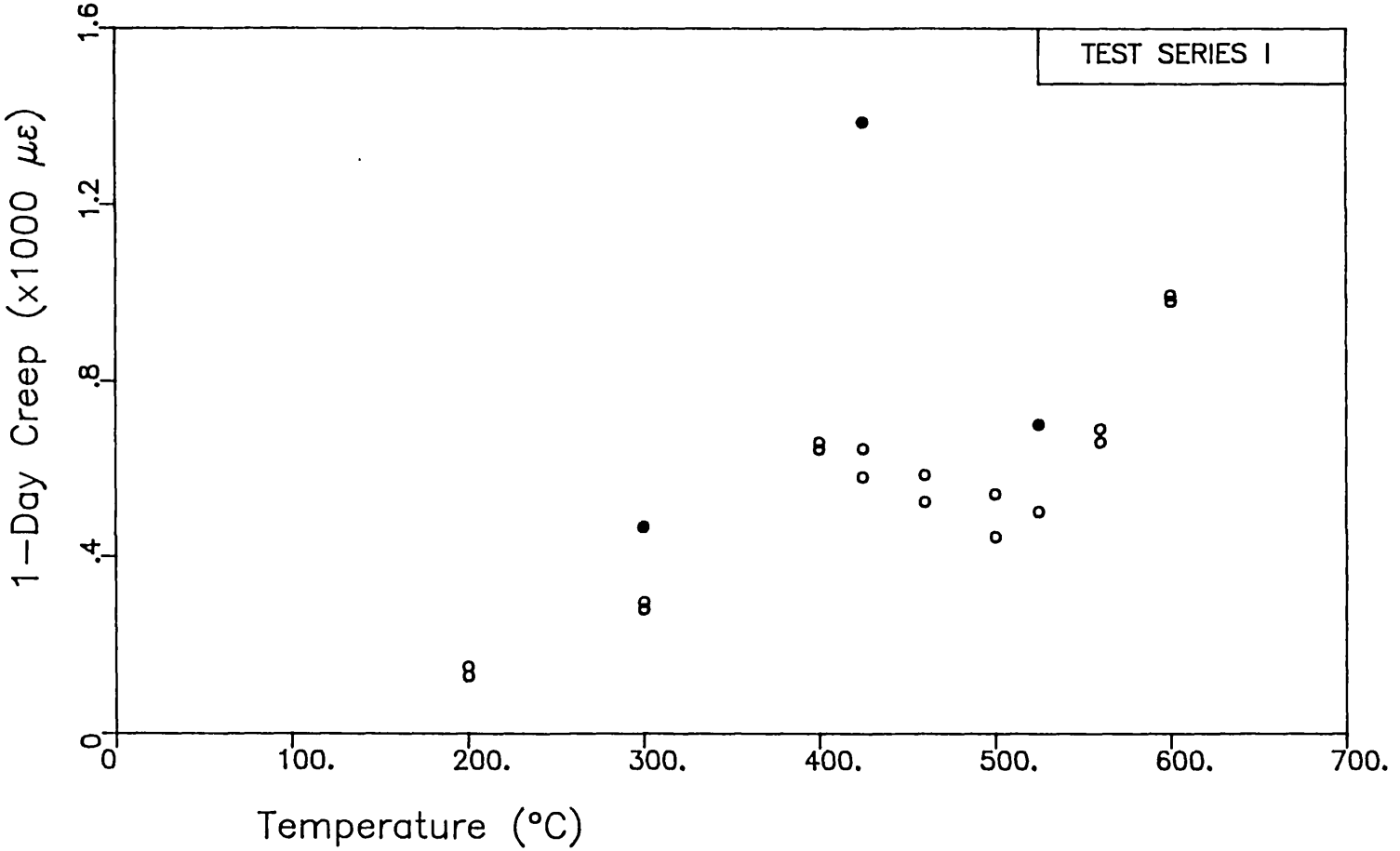

Fig.7.3 – CREEP STRAINS (EXPERIMENTAL)

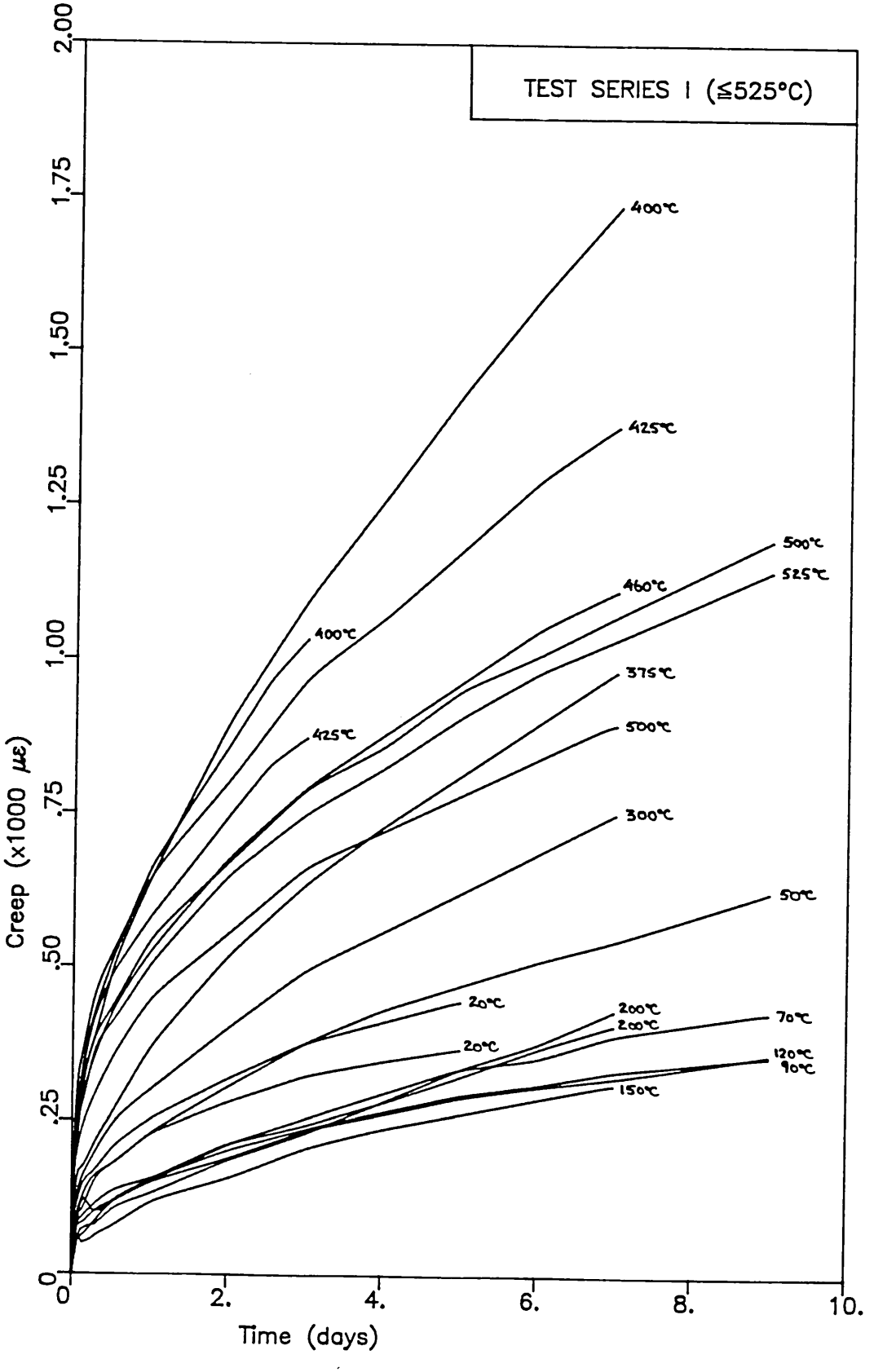

Fig.7.4 – CREEP STRAINS (EXPERIMENTAL)

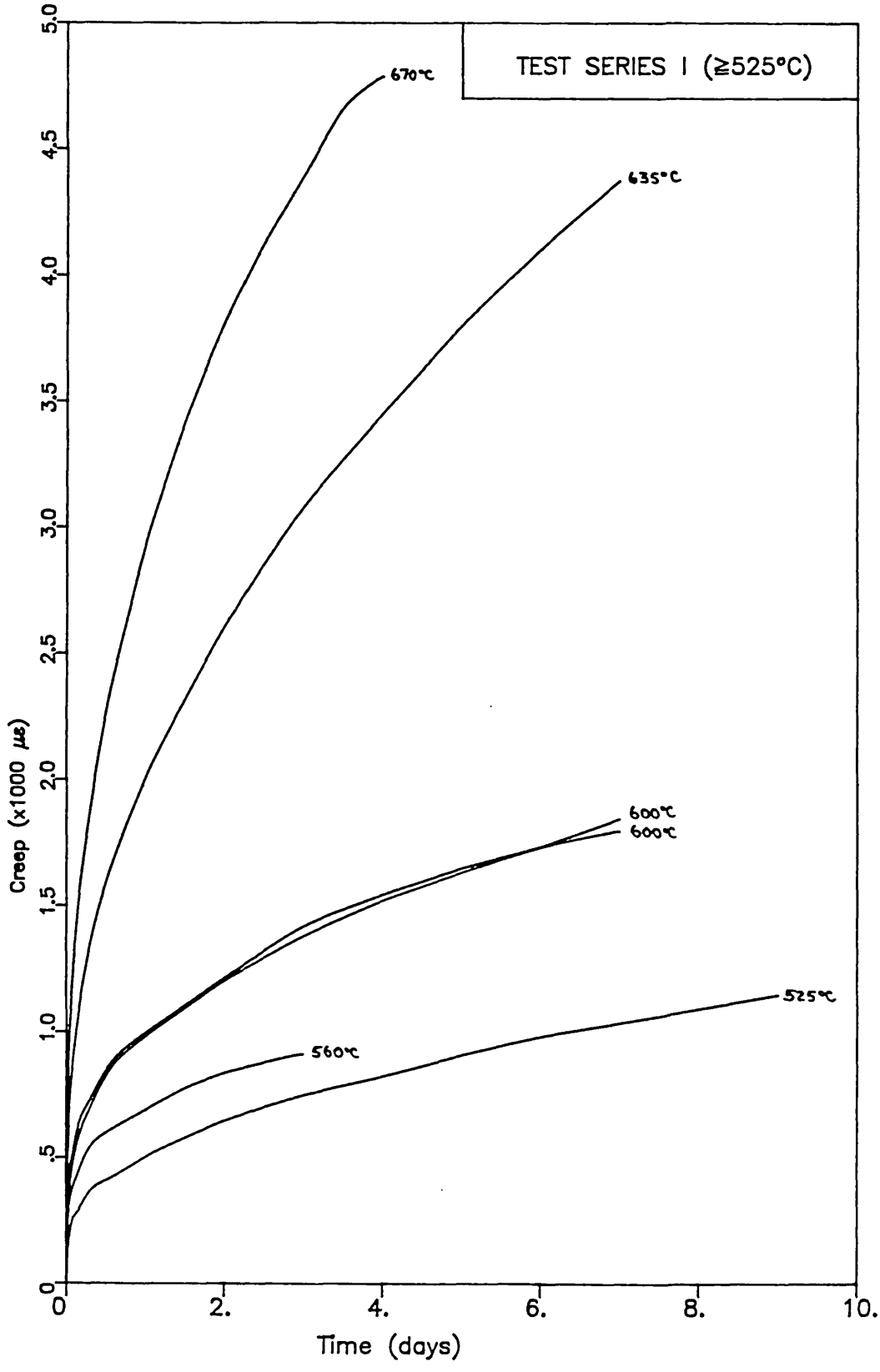

Fig.7.5 – 1–DAY CREEP STRAINS

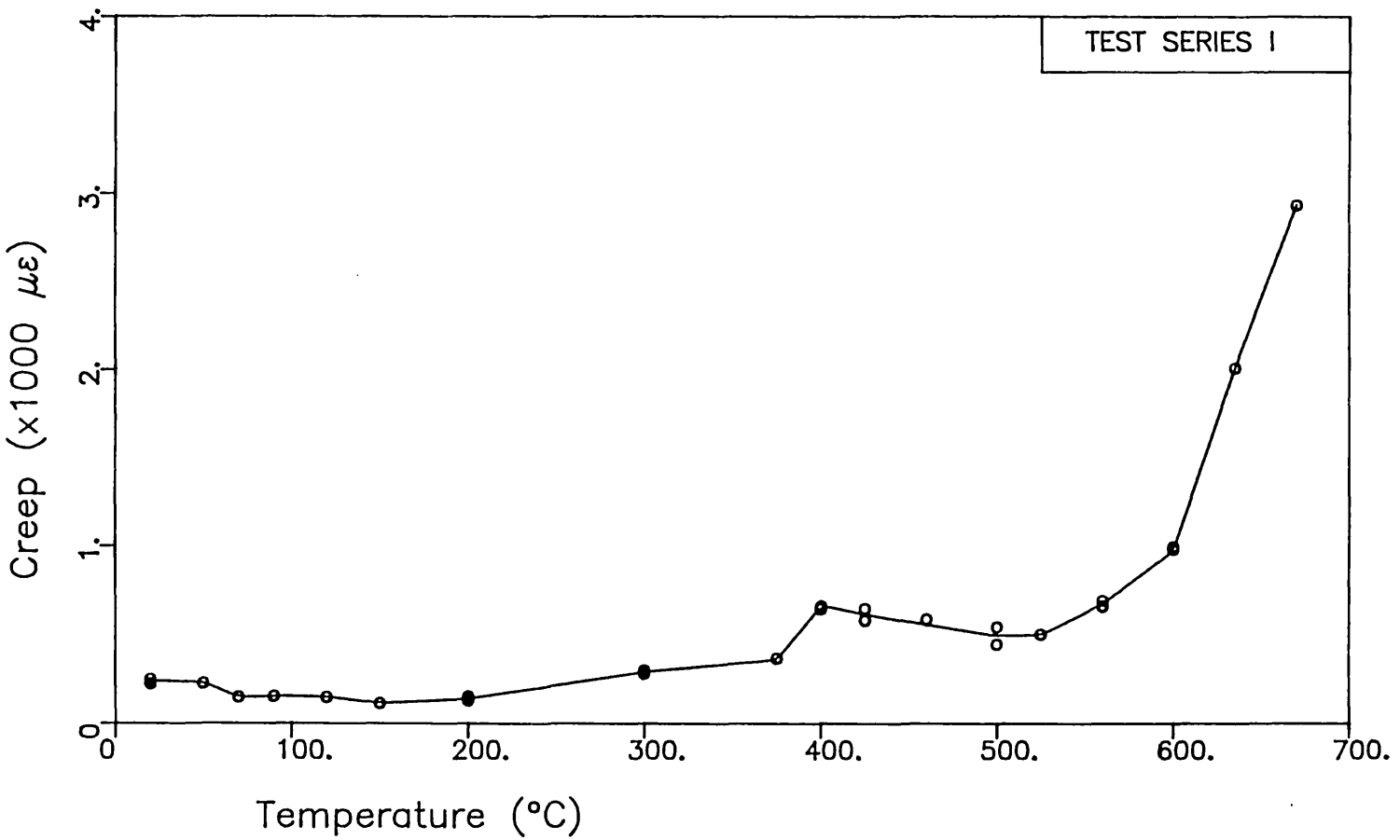

Fig.7.6 – 7–DAY CREEP STRAINS

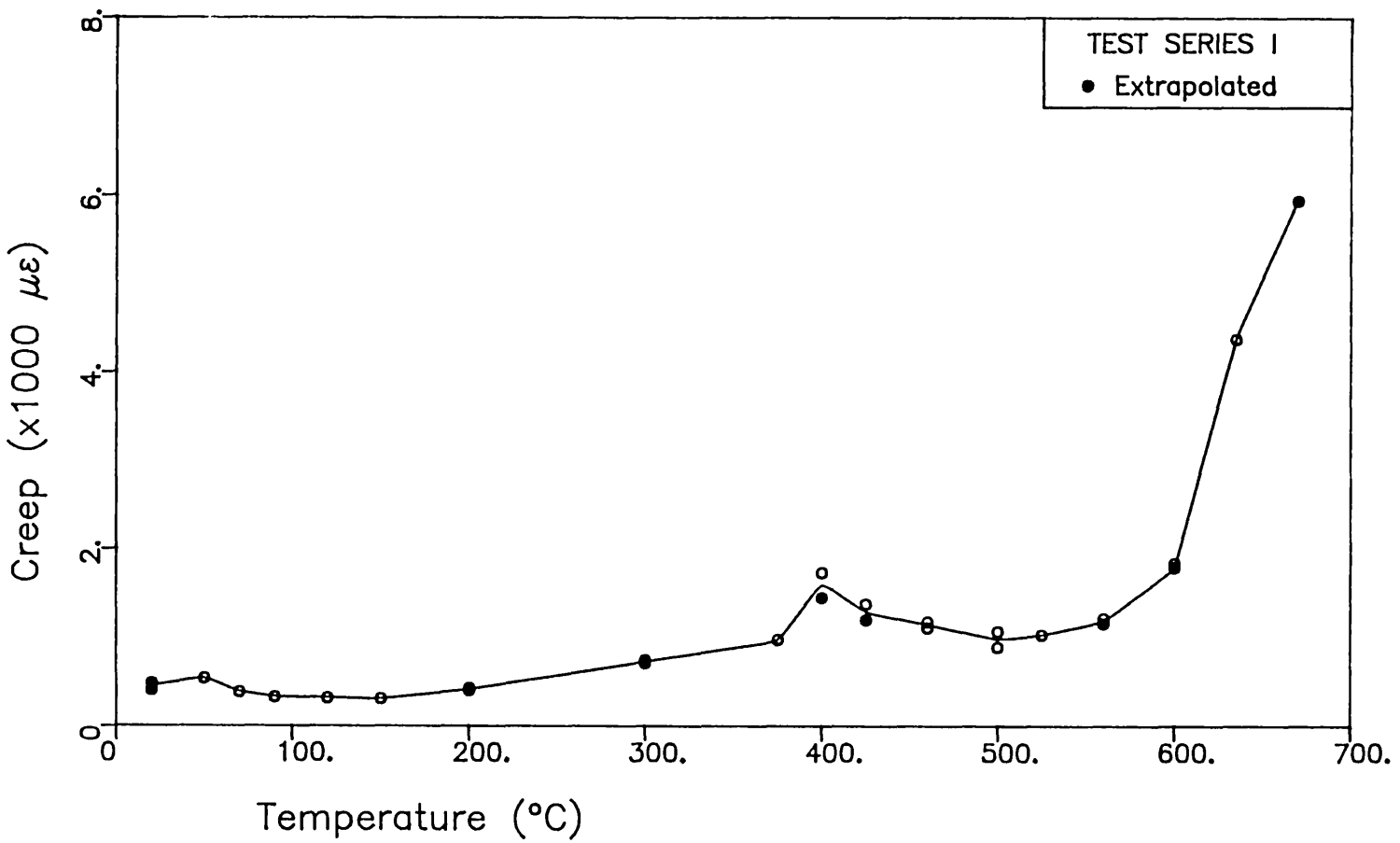

Fig.7.7 – CREEP STRAINS AS RATIOS OF 1–DAY CREEP STRAINS

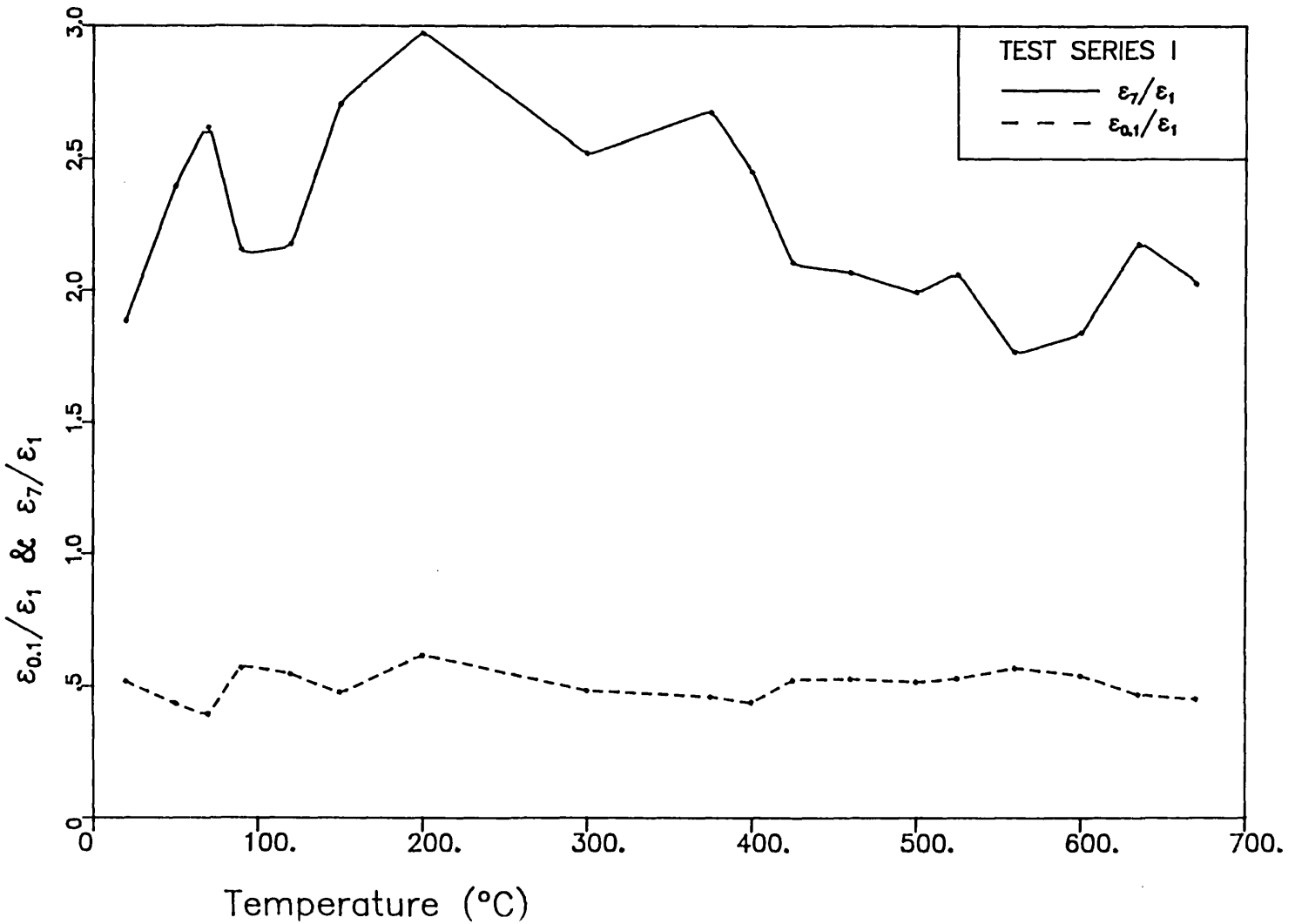

Fig.7.8 – 7–DAY CREEP NORMALIZED TO STRESS/HOT STRENGTH = 0.11

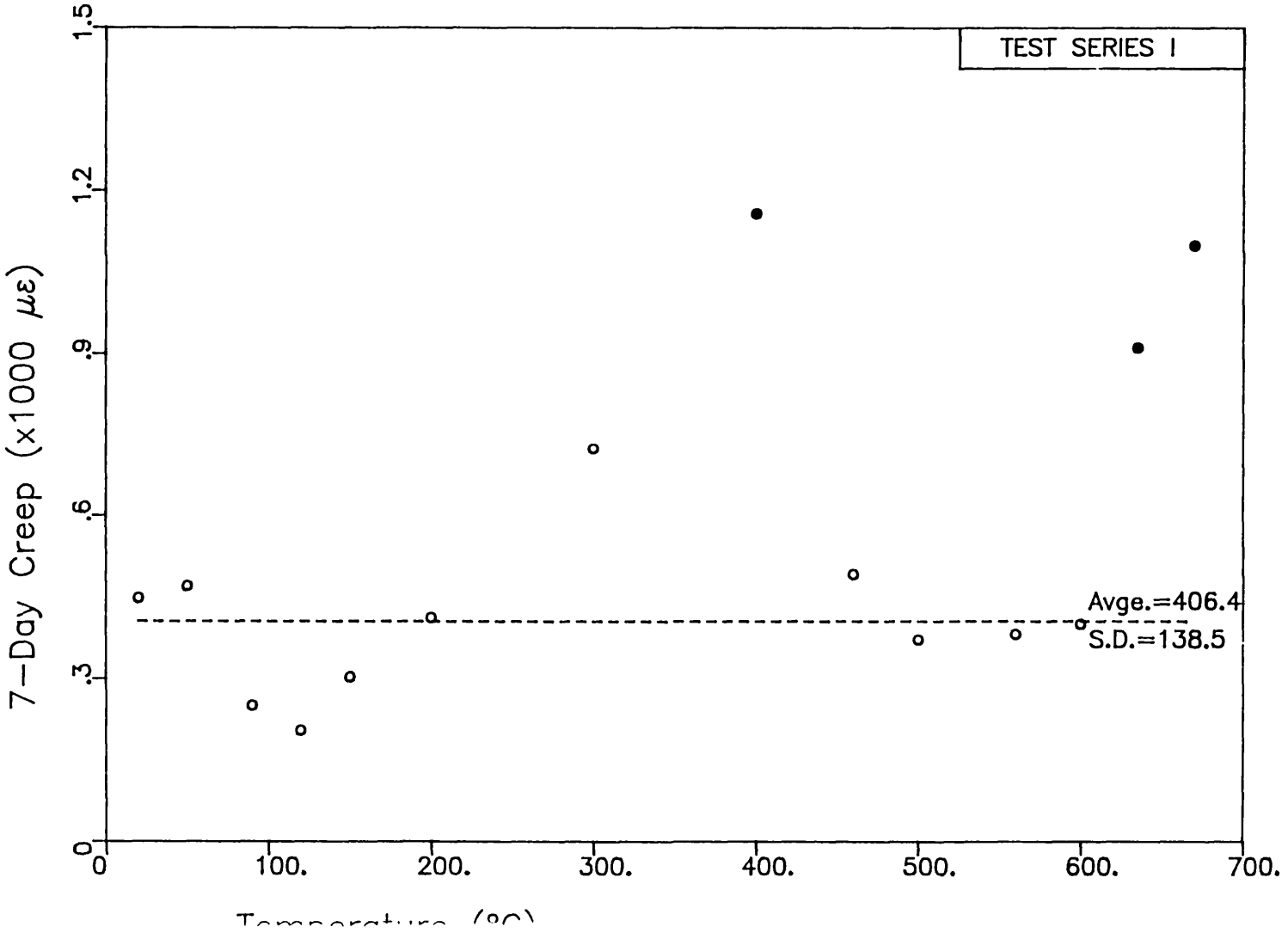

Fig.7.9 – 7–DAY CREEP STRAIN vs. STRESS/HOT STRENGTH

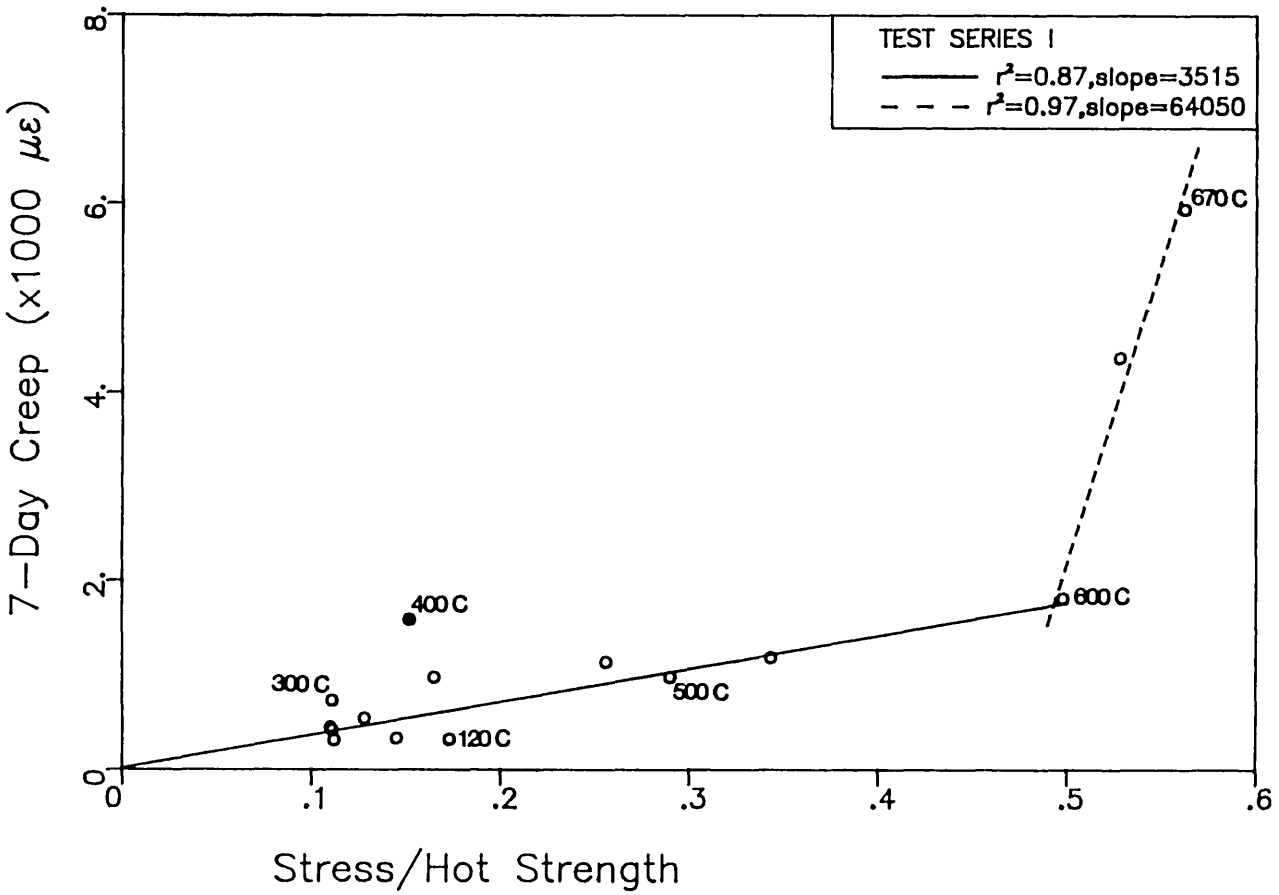

Fig.7.10 – 1–DAY CREEP STRAINS (TEST SERIES I & II)

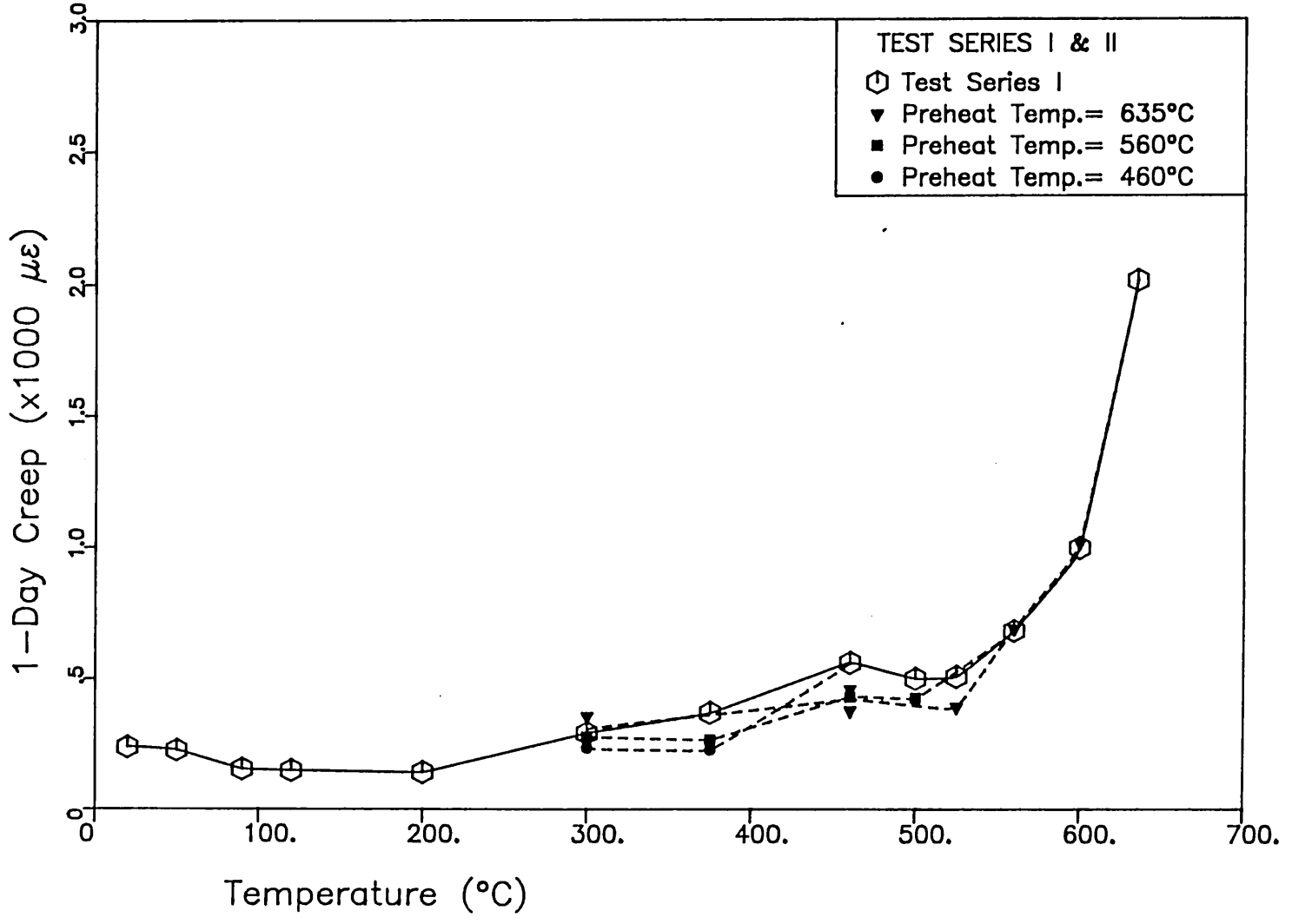

Fig.7.11 – 7–DAY CREEP STRAINS (TEST SERIES I & II)

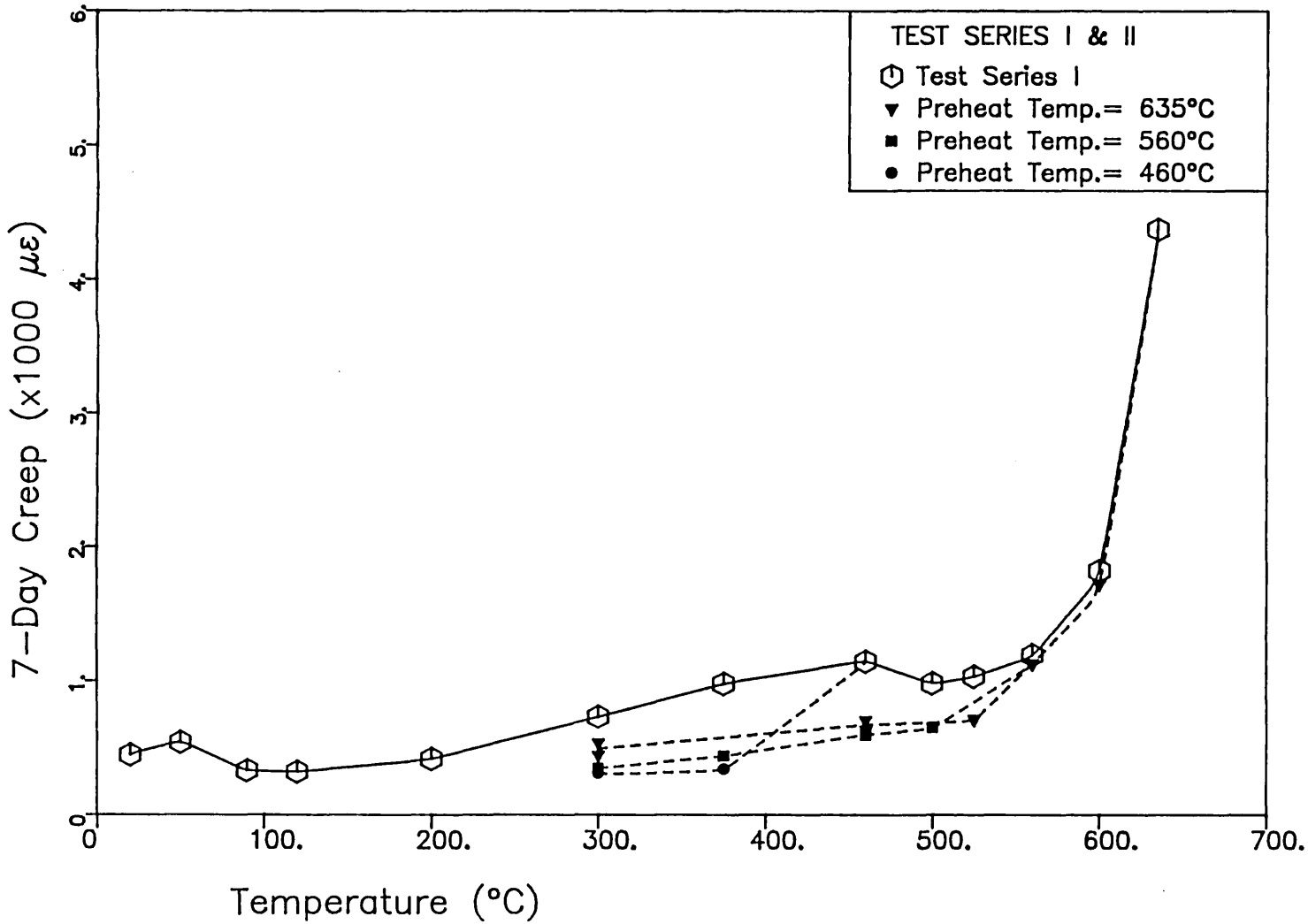

Fig.7.12 – 1–DAY CREEP (w.r.t. STRESS/HOT STRENGTH = 0.11)

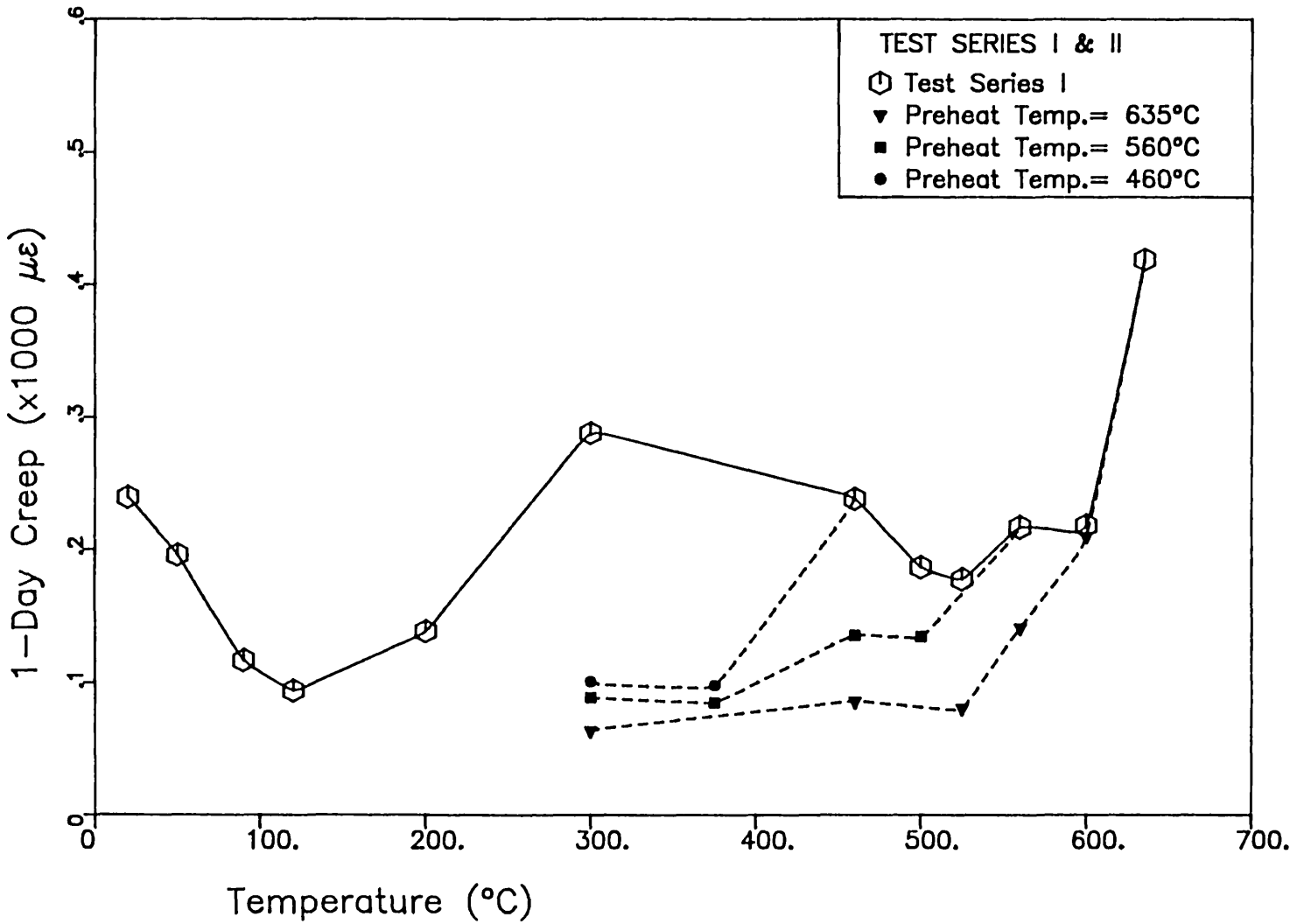

Fig.7.13 – 7–DAY CREEP (w.r.t. STRESS/HOT STRENGTH = 0.11)

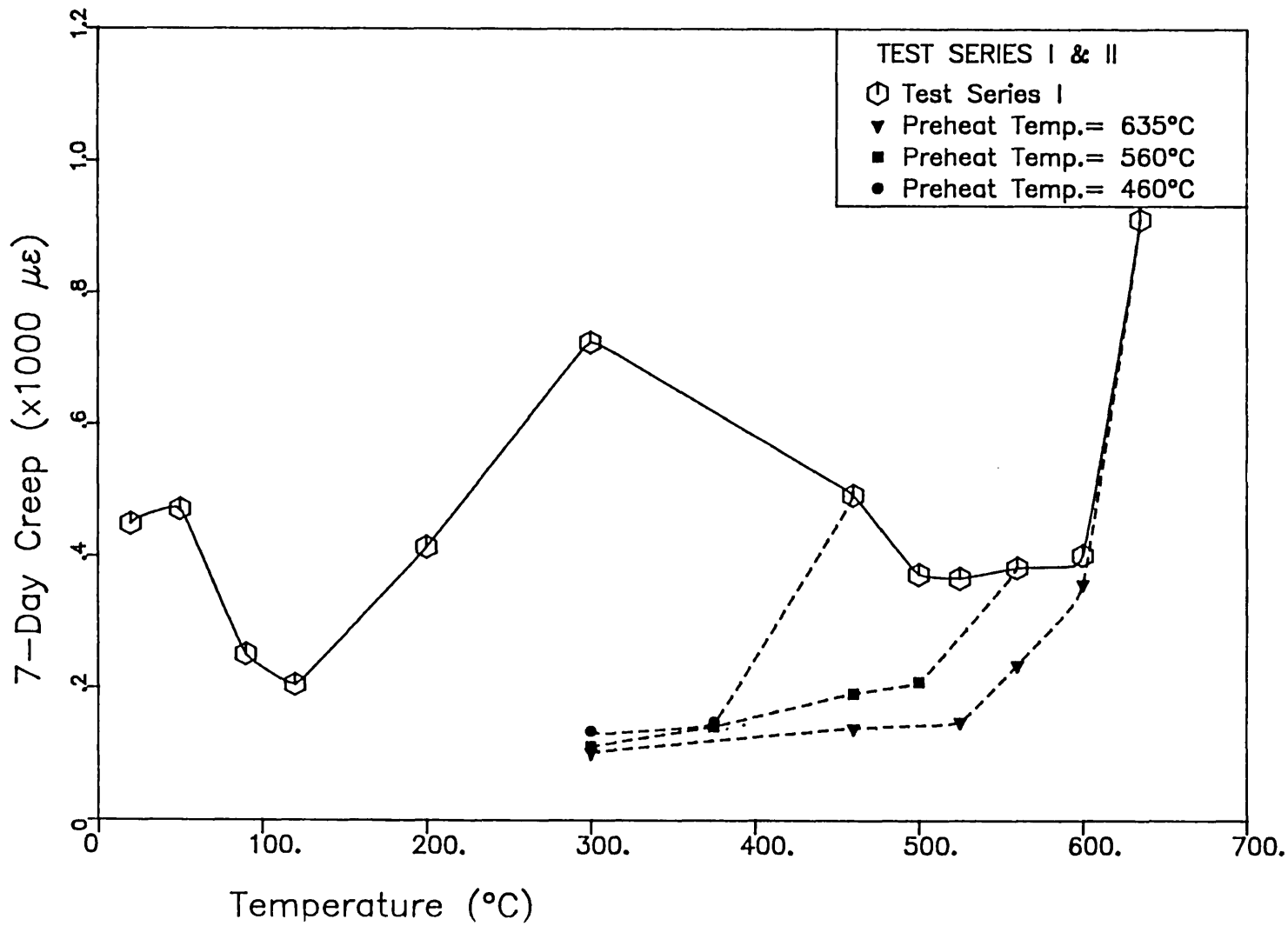

Fig.7.14 – 7–DAY CREEP AT 300°C FOR VARIOUS PREHEAT TEMPERATURES

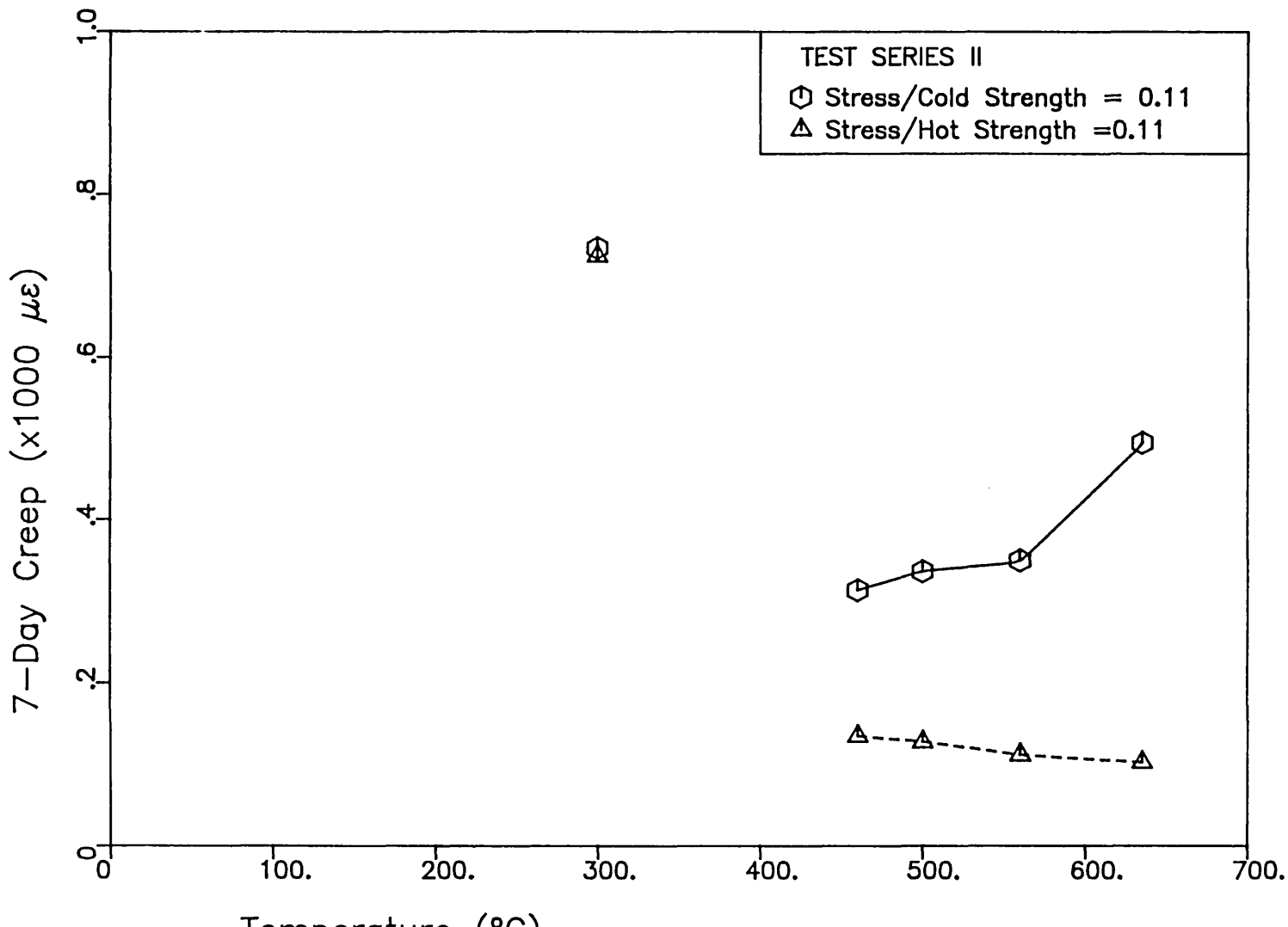

Fig.7.15 – COMPARISON OF CREEP FORMULAE

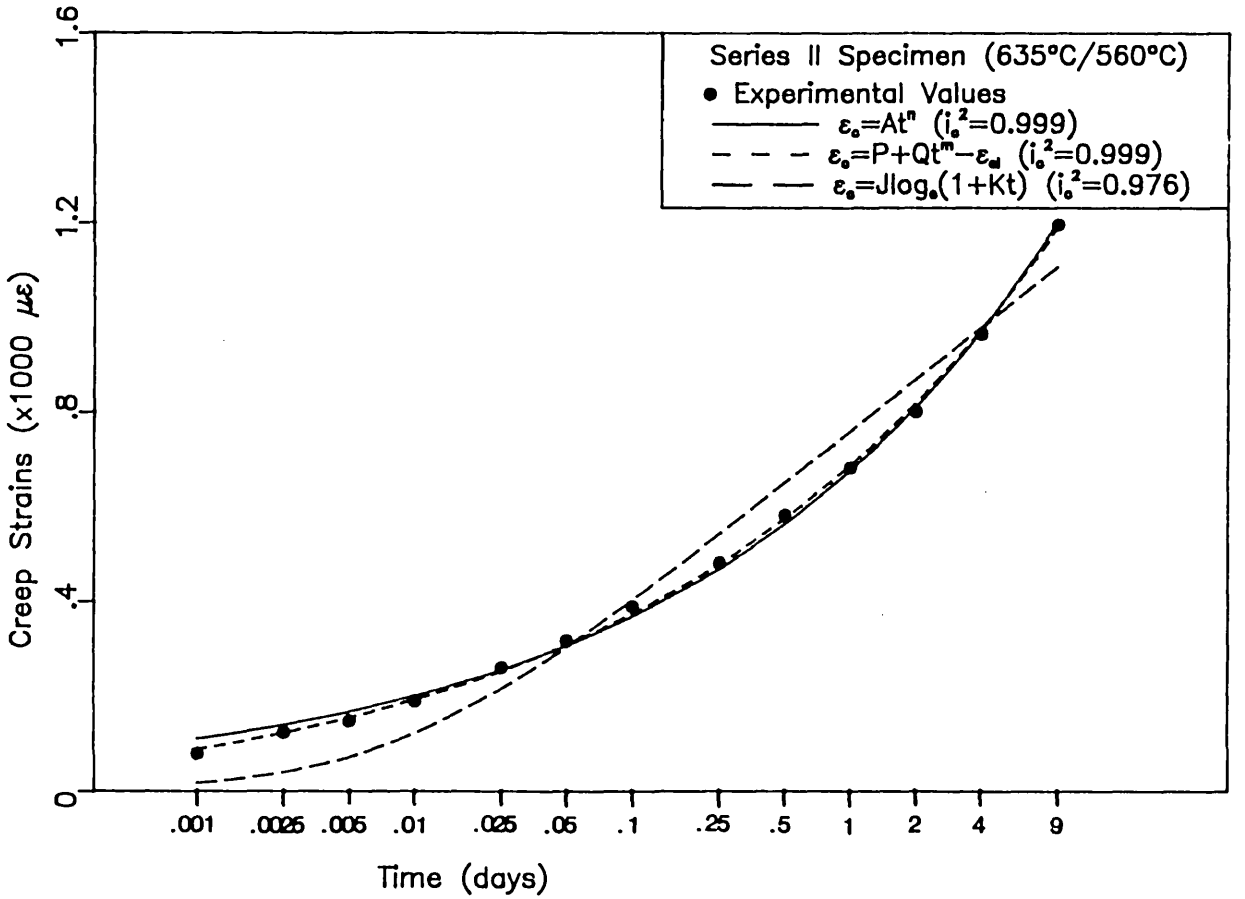

Fig.7.16 – CREEP FORMULAE FITTED TO OTHER EXPERIMENTAL DATA

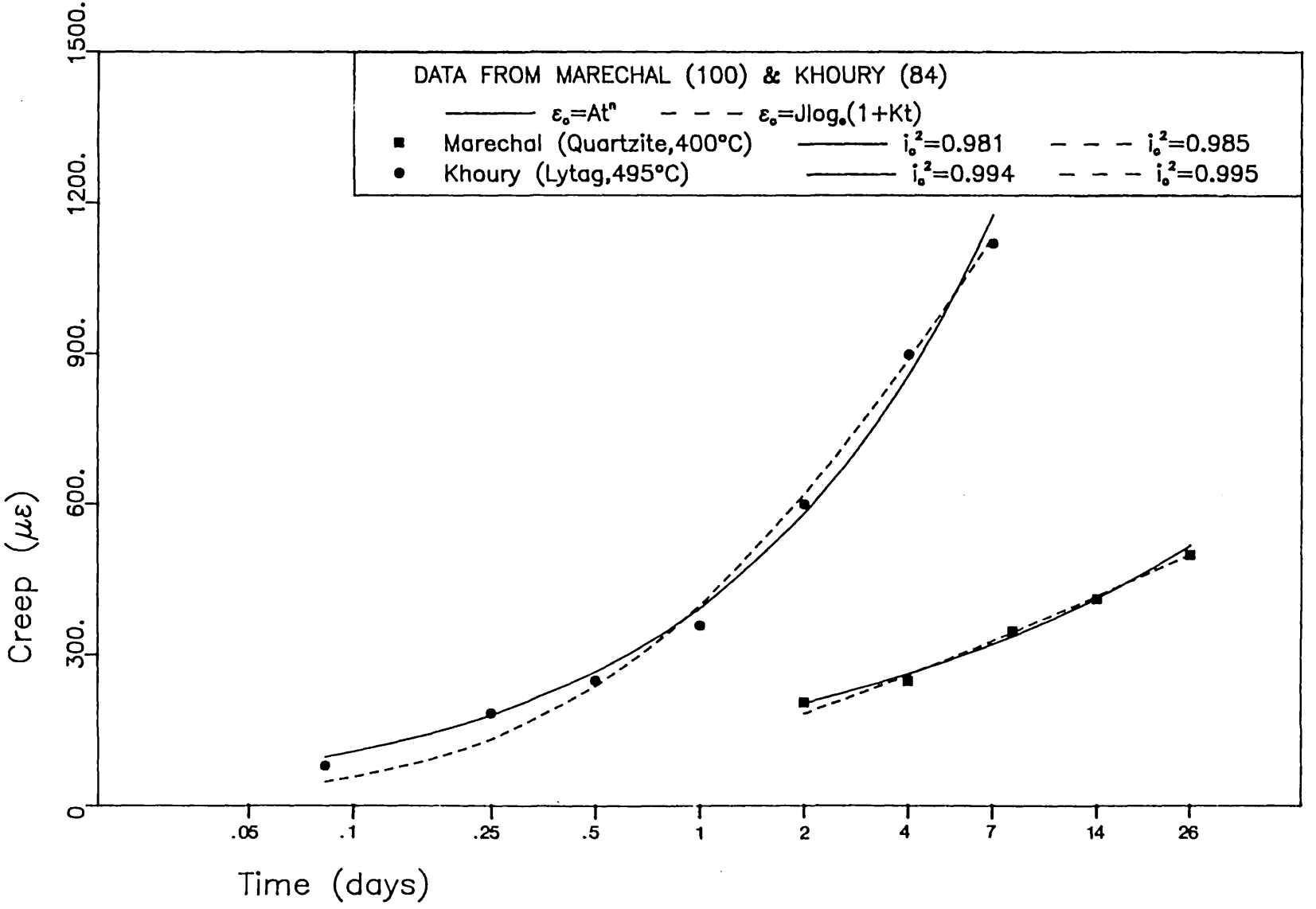

Fig.7.17 – CREEP STRAINS (IDEALIZED)

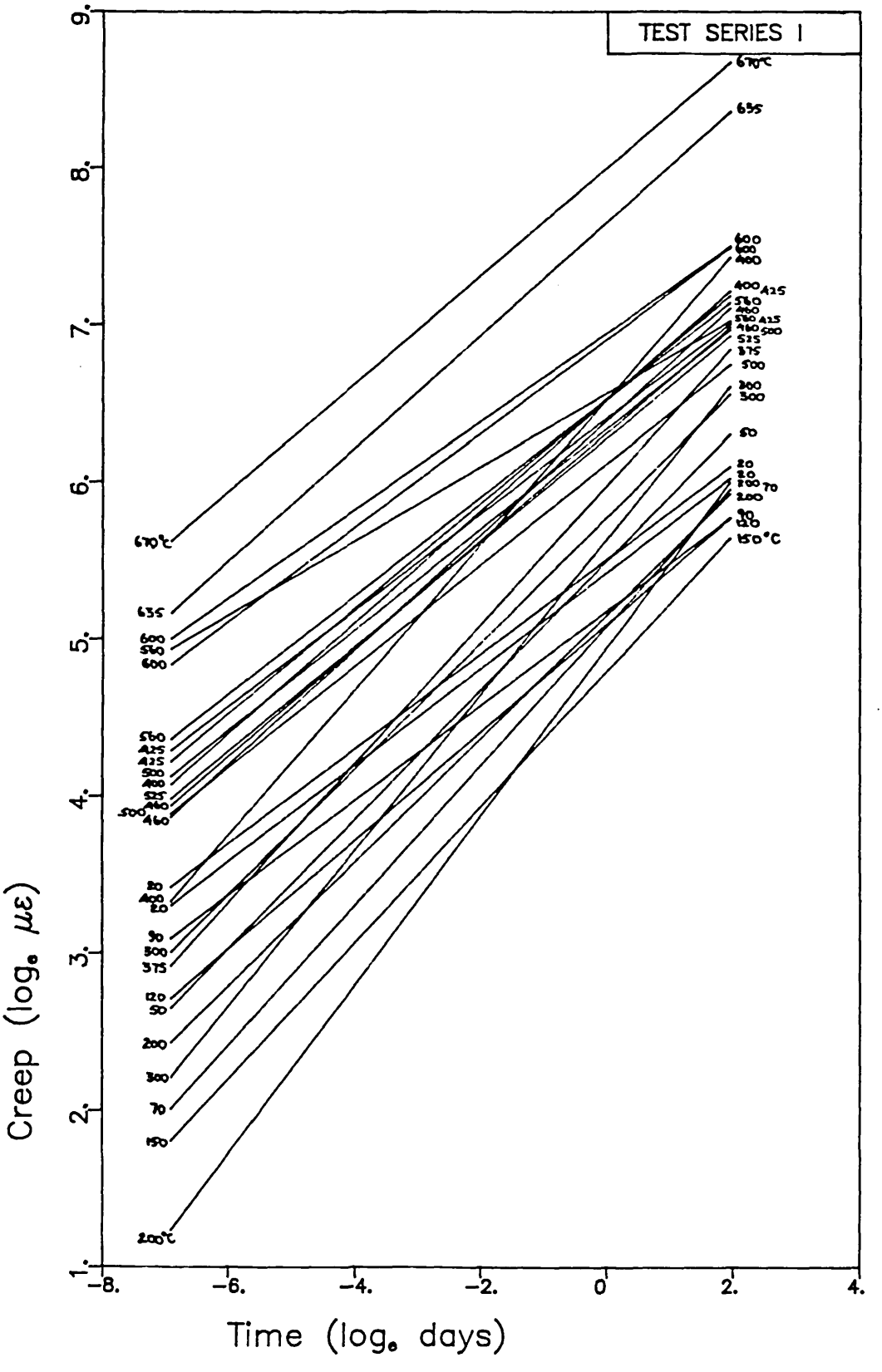

Fig.7.18 – CREEP STRAINS (IDEALIZED)

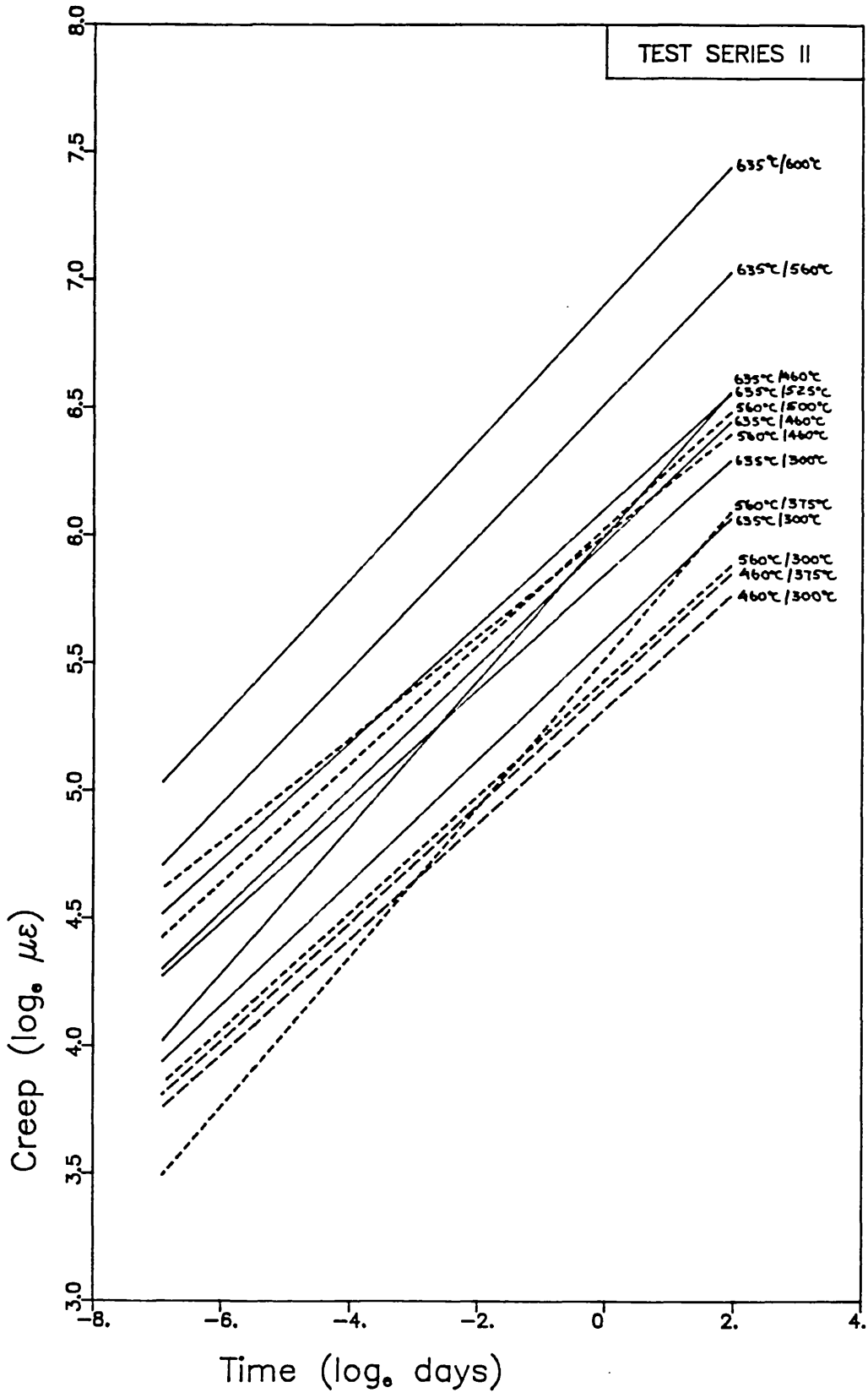

Fig.7.19 – CREEP STRAINS FITTED BY $\varepsilon_c = At^n$

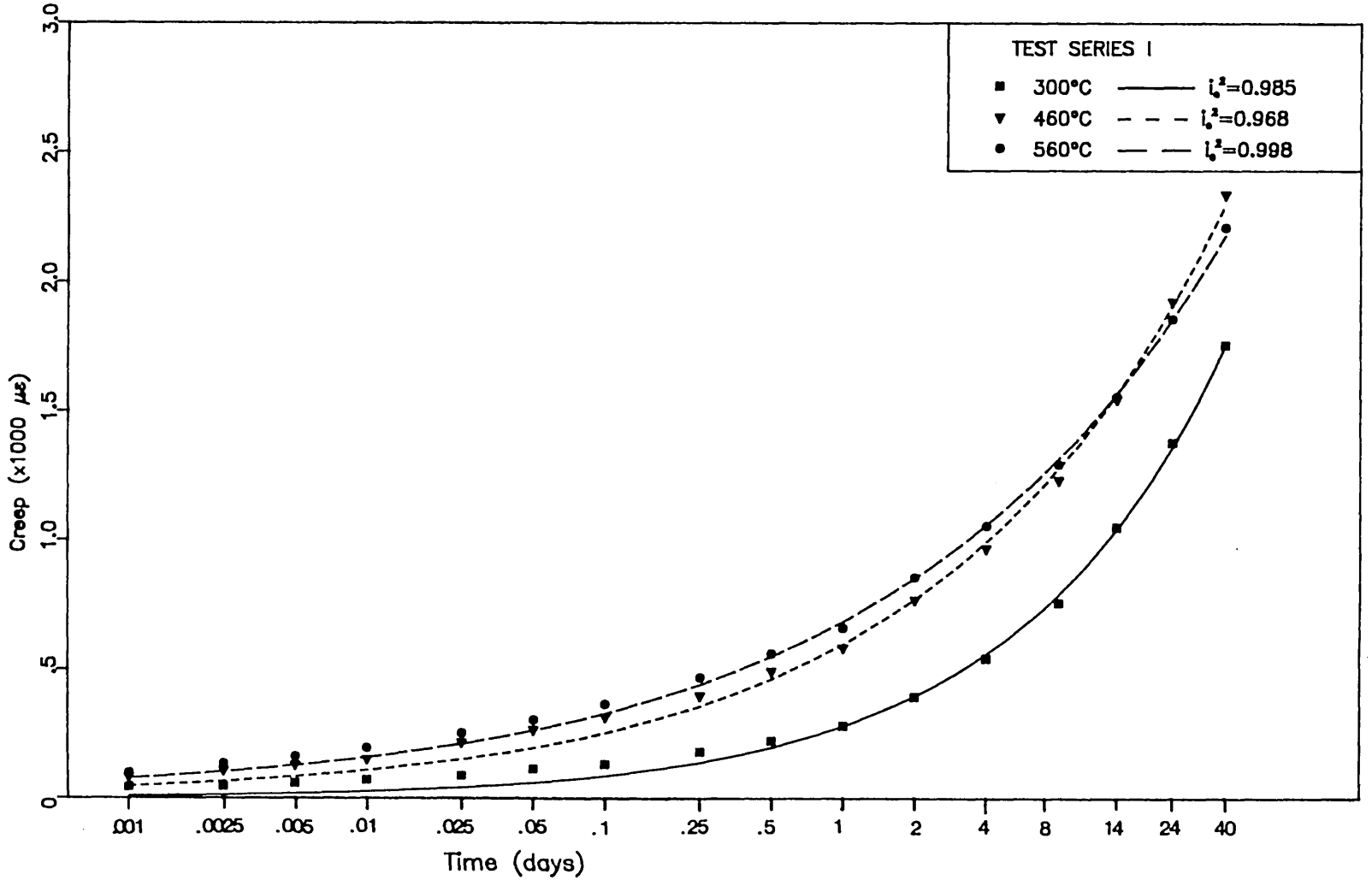

Fig.7.20 – RATIO OF "A" TO 1–DAY CREEP STRAIN

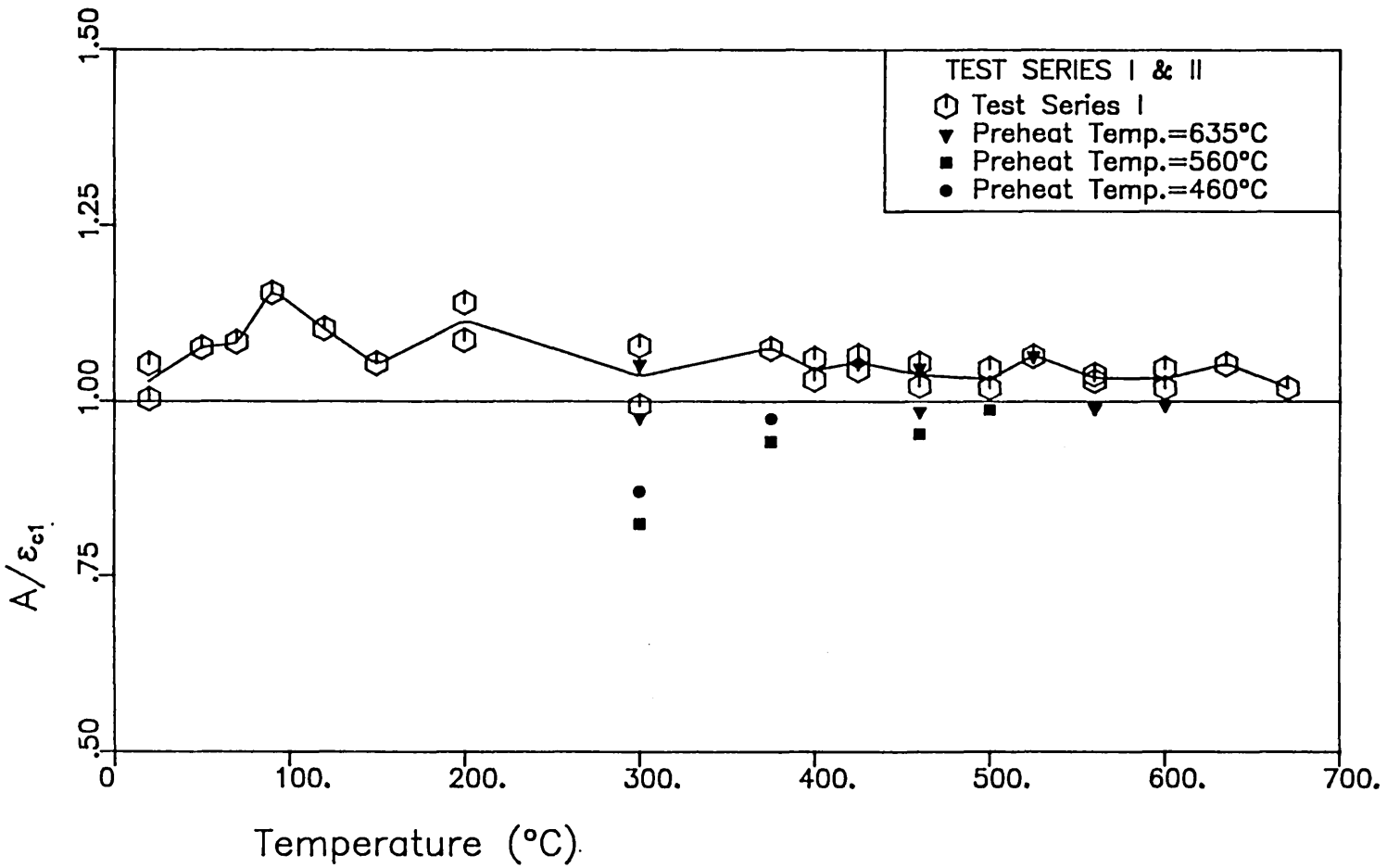

Fig.7.21 – VARIATION OF "n" WITH TEMPERATURE

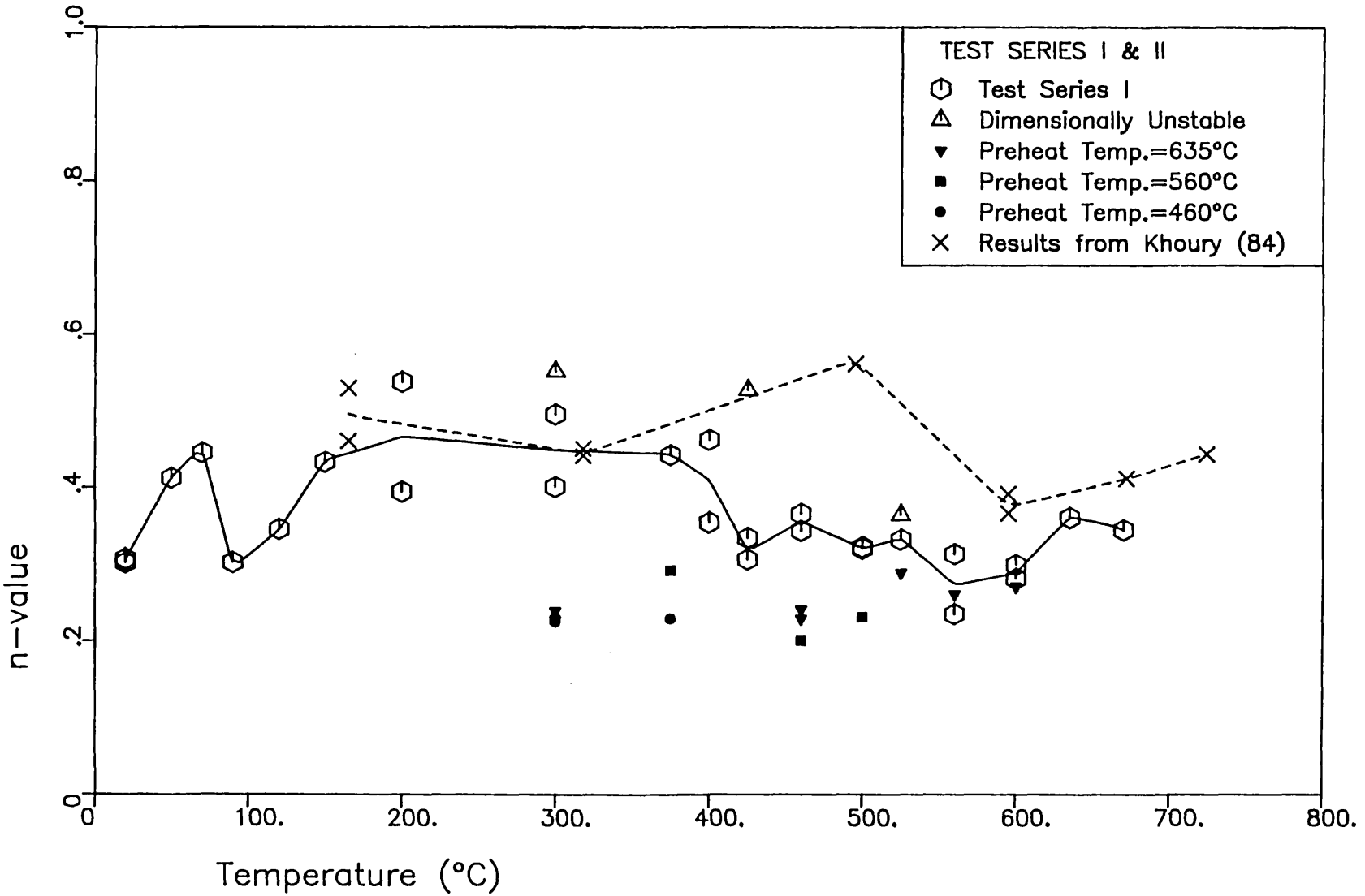

Fig.7.22– CREEP wrt STRS./COLD STRENGTH=0.1

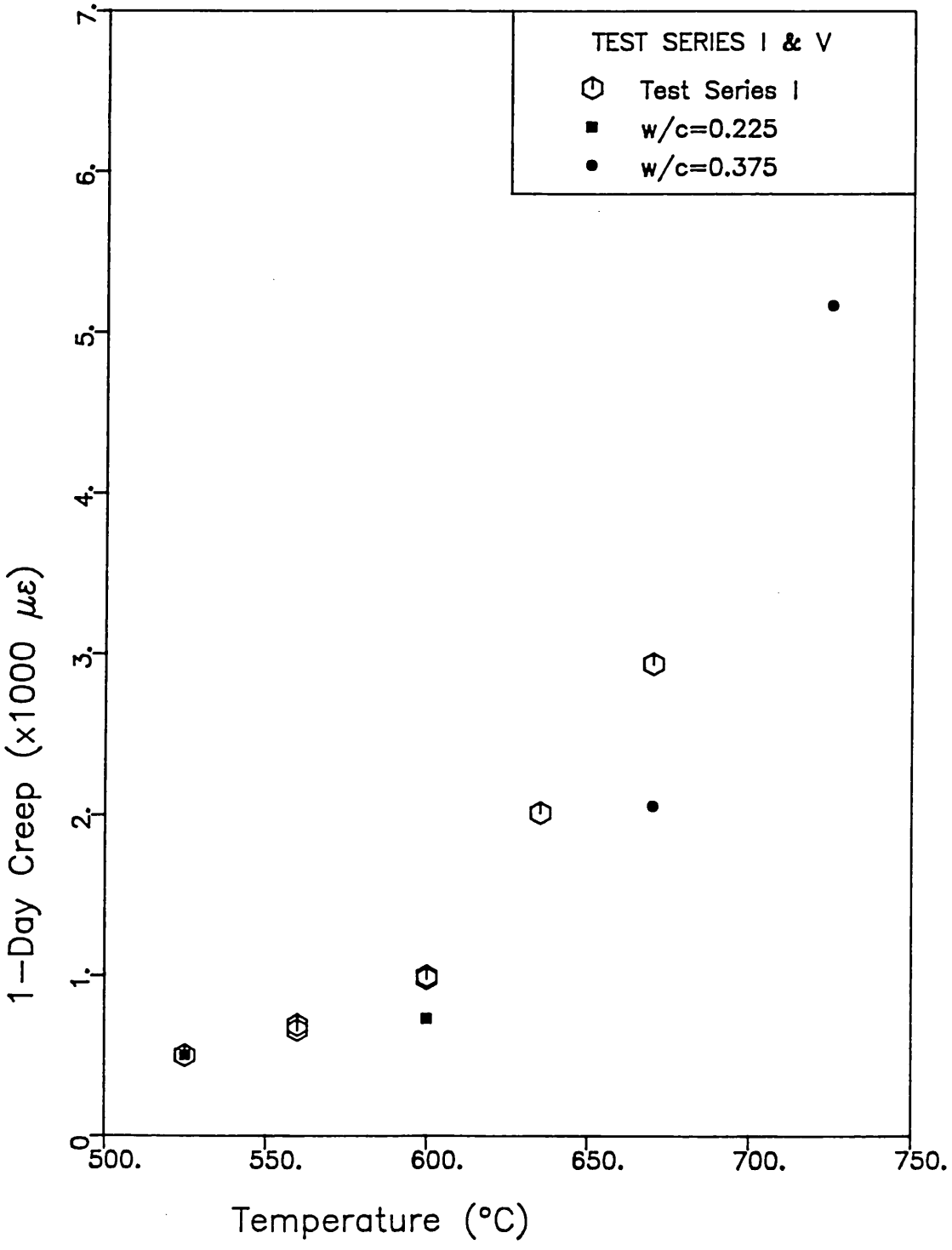

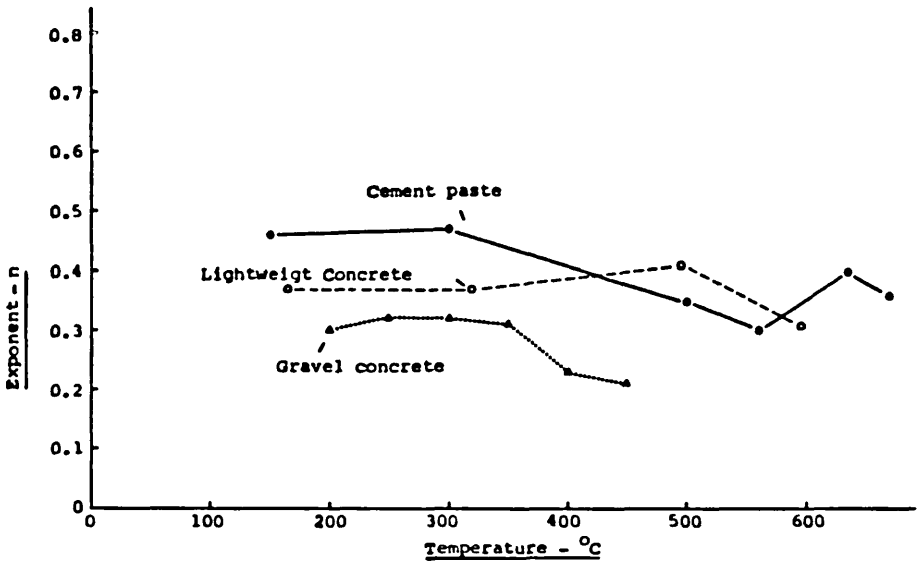

Figure 7.23 - VARIATION OF THE EXPONENT 'n' WITH TEMPERATURE FOR CEMENT PASTE AND CONCRETE.(FROM KHOURY ET AL.(85))

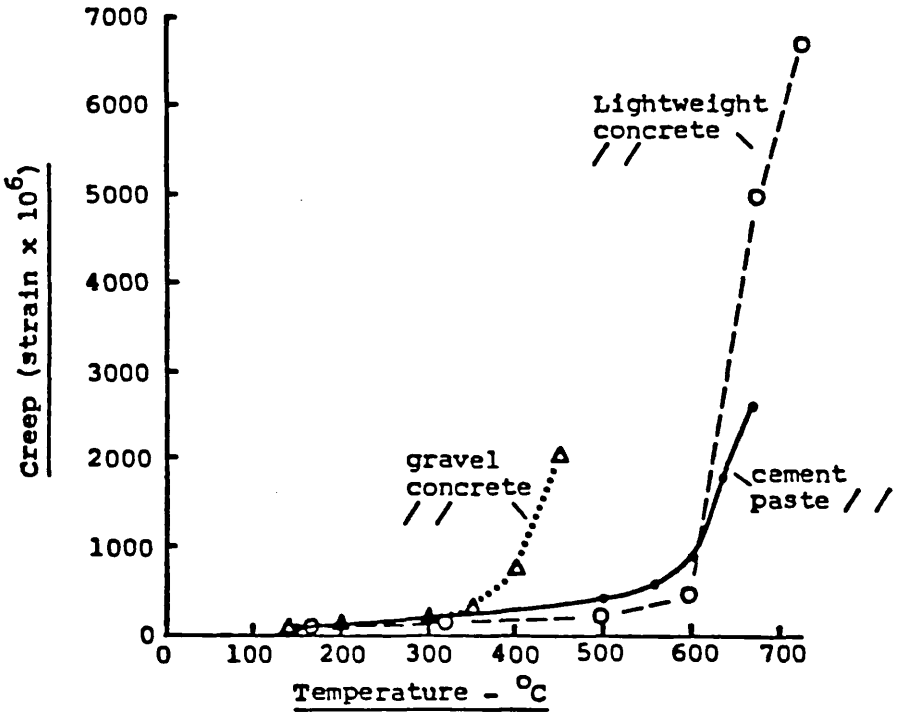

Figure 7.24 - VARIATION OF 1-DAY CREEP WITH TEMPERATURE FOR CEMENT PASTE AND CONCRETE.(FROM KHOURY ET AL.(85))

CHAPTER 8 - AN ACTIVATION ENERGY APPROACH FOR TEMPERATURE DEPENDENCE

The time and temperature dependence of basic creep would suggest its amenability to analysis by rate theory, first introduced in 1889 by Arrhenius (5) to describe the influence of temperature on the rate of inversion of sucrose. This chapter will outline rate theory as applicable to basic creep and make use of rate theory and activation energy concepts to analyse some of the experimental results.

8.1. THEORY OF RATE PROCESSES

Creeping materials have been characterized by 'elements' or 'centres' where activation processes produce creep (36, 42). These centres may take the form of dislocations in metals, whereas in concrete, the activation of a centre may be considered to be a solid-to-solid bond rupture, viscous water flow or some other physical mechanism (42).

The advantage of a rate theoretical approach is that the details of the centre are not required to be known. The approach is thermodynamic in nature and hence has to do with the overall behaviour of a large number of molecules or centres, the effects of which can be measured experimentally on the macro-level. A judicious evaluation of these quantities measured at the macro-level could, however, lead to qualitative inferences regarding microstructural mechanisms.

Even in the absence of any external force, creep centres would be subject to statistically balanced flow steps or jumps across potential barriers. These would depend on the height of the barrier - i.e. its activation free energy - denoted by E' in Figure 8.1, and the magnitude of the energy fluctuations it experiences. (The prime denotes the value of the quantity corresponding to a single centre).

We know from statistical thermodynamics that the chance, C(E'), of a centre receiving an energy fluctuation equal to its activation free energy E' can be written as

$$C(E') = (kT/h) \exp(-E'/kT) \qquad (8.1)$$

where k = Boltzmann's constant = 1.3806×10^{-23} J $^{\circ}K^{-1}$

h = Plank's constant = 1.0546×10^{-34} Js

kT/h = atomic frequency of vibration at absolute temperature T.

It should be noted that the energy term represents activation free energy and contains both enthalpy as well as entropy terms as given by

$$E' = H' - TS' \qquad (8.2)$$

where H' is the activation enthalpy
and S' is the activation entropy

The entropy changes are known to be particularly significant when a large number of atoms are involved in an activation process and S could have a large negative value (26, 40).

If we use the constants corresponding to a mole of the material, we can re-write equation (8.1) as

$$C(E) = (RT/Nh) \exp(-E/RT) \qquad (8.3)$$

where N = Arogadro No. = 6.023×10^{23} mol^{-1}

$R = N.k$ = gas costant = 8.3155 J $mol^{-1}{}^{o}K^{-1}$

As stated before, the above chance of activation is that due only to thermal energy fluctuations at a given temperature. Let us suppose that a directional force is introduced in addition, as indicated in Figure 8.1. This would change the height of the potential barrier as shown, by an amount H'_f where

$$H'_f = fd/2 \qquad (8.4)$$

where f is the force acting on a centre.

The chance of an activation in the direction of the force would then be given by

$$C(E_f) = (RT/Nh) \exp\left\{-(E - \frac{Nfd}{2})/RT\right\} \qquad (8.5)$$

and in the reverse direction by

$$C(E_b) = (RT/Nh) \exp\left\{-(E + \frac{Nfd}{2})/RT\right\} \qquad (8.6)$$

The chance of the net effect of a centre moving from an initial state A_1 to a final state C_1 will be given by

$$C(E_f)-C(E_b) = (RT/Nh)\left[\exp\left\{-(E- \frac{Nfd}{2})/RT\right\}- \exp\left\{-(E + \frac{Nfd}{2})/RT\right\}\right]$$

$$= (2RT/Nh) \exp(-E/RT) \sinh(Nfd/2RT) \qquad (8.7)$$

If the number of centres per unit volume is given by m and the contribution towards strain per activation is given by b, then the strain rate, $\dot{\epsilon}$ will be given by

$$\dot{\epsilon} = (2mbRT/Nh) \exp(-E/RT) \sinh(Nfd/2RT) \qquad (8.8)$$

Substituting for E from equation (8.2) we have

$$\dot{\epsilon} =(2mbRT/Nh) \exp(S/R) \exp(-H/RT) \sinh(Nfd/2RT) \qquad (8.9)$$

For directional forces of engineering significance, it may be assumed that the contribution from $C(E_b)$ is small compared to that from $C(E_f)$. This is tantamount to saying that

$$\sinh(Nfd/2RT) = {}^1/_2 \exp(Nfd/2RT) \qquad (8.10)$$

which is true for values of (Nfd/2RT) in excess of 1.5 or so (106).

The above simplification will allow equation (8.9) to be

written as

$$\dot{\epsilon} = (mbRT/Nh) \exp (S/R) \exp \left\{- (H - \frac{Nfd}{2})/RT\right\} \qquad (8.11)$$

or $$\dot{\epsilon} = A \exp (-Q/RT) \qquad (8.12)$$

where $A = (mbRT/Nh) \exp (S/R)$

and $$Q = H - \frac{Nfd}{2}$$

Equation (8.12) could be considered as the Arrhenius equation for creep, the temperature dependence of strain rate being expressed via an exponential term containing the measured activation energy, Q.

Q is strictly a function of the applied stress, as seen above. The "true" activation energy at zero stress can be found by extrapolation, if results from tests at several stress levels are available (42). The use of a low stress level, such as the 0.11 stress/cold strength ratio used in the present tests, would yield an experimentally measured activation energy that is close to the "true" value.

8.2. APPLICATIONS AND LIMITATIONS OF THE ARRHENIUS EQUATION

8.2.1. Using the Arrhenius Equation to Determine Activation Energy

A close examination of equation (8.12) reveals that both A and Q are functions of stress, temperature and the structure of the material (40, 140). Equation (8.12) can be re-written as

$$\dot{\epsilon} = A(\sigma,S,T) \exp \left\{-Q (\sigma,S,T)/RT\right\} \qquad (8.13)$$

where σ is the applied stress

T is absolute temperature

and S is a parameter characterizing molecular structure.

In general, A and Q have been considered as being only mildly sensitive to temperature, the main thermal effect upon creep rate arising from the exponential term (140). Furthermore, if a series of tests are conducted at the same stress level, the above parameters would be sensitive only to the structure, S.

If a material behaves like a Newtonian liquid, its strain rate will not vary with time because its structure, consisting of randomly positioned molecules, is independent of previous strain history. Under such circumstances, A and Q will be independent of the structure, S. However, most materials do not behave like Newtonian liquids, their structures changing with creep and resulting in progressively decreasing creep rates. This type of creep is called primary creep. In this sistuation, A and Q would be dependent on the structure of the material, S, which would be continuously changing with time, or more accurately, with strain. In some cases, primary creep may be followed by a period of secondary creep where the material does in fact behave like a Newtonian liquid. (See Figure 8.2).

In order to see the way that the Arrhenius equation can be used to determine the temperature dependence of creep, let us suppose that two specimens of a given material are loaded at temperatures T_1 and T_2. From equation (8.12) we can write

$$\text{for Specimen 1, } \dot{\epsilon}_1 = A_1 \exp(-Q_1/RT_1) \qquad (8.14)$$

$$\text{and for Specimen 2, } \dot{\epsilon}_2 = A_2 \exp(-Q_2/RT_2) \qquad (8.15)$$

Now we can make $A_1 = A_2$ and $Q_1 = Q_2 = Q$ if the strain rates are measured when the specimens have the same structure and undergo the same stress, provided of course that the condition of both specimens at the point of loading was identical. The temperature dependence of A and Q is considered to be negligible. The stress criterion is easy enough to achieve, by subjecting the specimens to the same external stress.

However, especially in materials such as cement paste and concrete, there is some difficulty in ensuring that the specimens have equal structures. On the one hand, 'structure' is a microstructural as opposed to a macro-level concept, and despite attempts to

characterize structure by microstructural descriptors such as a polysilicate index (40), there is considerable uncertainty in this area. The discussion in the next chapter will further highlight this uncertainty. In the absence of microstructural descriptors, the next best solution is to apply a macro-level criterion that would reflect equal structures in the specimens. Here too, there has been considerable controversy. Many researchers have measured strain rates at equal times after loading, thus implying that structure is a function of time only. This has been questioned by Day and Gamble (42) who argued that the condition of "same structure" would be better met by measuring strain rates at equal strains after loading. (See Figure 8.3). Their argument is backed up with comparative analyses of the two approaches. Apart from this, there is also the question of whether the structure of the material will change with temperature. Where the unsealed cement paste used in this investigation is concerned, this will most definitely be the case.

If however, the above difficulties can be surmounted and the strain rates at temperatures T_1 and T_2 are measured when the specimens have the same structure while being under the same stress, then because $A_1 = A_2$ and $Q_1 = Q_2 = Q$ we have

$$Q = \left\{- R/(1/T_1 - 1/T_2)\right\} \ln (\dot{\epsilon}_1/\dot{\epsilon}_2) \qquad (8.16)$$

8.2.2. Experimental Approaches for Determining Activation Energy

Historically, there have been two main experimental approaches for determining activation energy. The method proposed by Dorn (57) consists in first straining the specimen under a given stress at a temperature T_1 until a suitable point in time whereupon the temperature is suddenly raised to T_2. The creep rates both before and after the temperature rise are plotted against creep strain and the latter part of the curve extrapolated back to the point of temperature rise, to obtain the creep rates $\dot{\epsilon}_1$ and $\dot{\epsilon}_2$ as shown in Figure 8.4. Equation (8.16) can then be applied to determine the activation energy, Q.

This method seemingly has the attraction of by-passing the

necessity of deciding on a criterion for equal structures, since the measured creep rates $\dot{\epsilon}_1$ and $\dot{\epsilon}_2$ are measured at the same strain.

However, in the case of cement paste, the temperature rise itself will change the structure. In addition, where cement paste is concerned, the increase in temperature while under load induces transitional thermal creep which will give a misleading value for $\dot{\epsilon}_2$ if the creep rate extrapolation is performed on measurements soon after the temperature rise. (See Figure 8.5). A similar problem with regard to the side effects of the temperature rise itself has been reported by Mitchell et al (106) who found that the temperature change produced pore water pressures in undrained clay, which resulted in a change in effective stress, giving much higher initial creep rates.

The other method, which has the advantage of obtaining an "average" activation energy over a range of temperatures, consists in straining specimens of the material at the same stress level at several temperatures and measuring their creep rates. If the natural logarithms of creep rates corresponding to "same structures" are plotted against the reciprocal of temperature, the activation energy can be obtained from the gradient of the resulting linear regression, according to

$$\ln(\dot{\epsilon}) = \ln A - (Q/R)\frac{1}{T} \qquad (8.17)$$

It is, in fact, this method that has been adopted in the present investigation, both because of the problems inherent in Dorn's method for testing cement paste and also because the experimental procedures for the basic creep tests lent themselves to this method of analysis.

It was sought to ensure the "same structure" criterion in two ways. Firstly, the creep rates were taken as those at equal creep strains as opposed to equal time periods after loading, the former being considered to be a better criterion for similarity of structure than the latter (42).

Secondly, although specimens were tested at different

temperatures, they were all first pre-heated to one particular temperature and after dimensional stability was achieved, cooled slowly (i.e. at $^1/_2$°C per minute) to the required test temperature. Observations on strain behaviour of specimens cooled at both 1°C/min. and $^1/_2$°C/min. showed essentially no difference; hence cooling at $^1/_2$°C/min. was considered slow enough to prevent structural damage due to parasitic or gradient stresses. The above procedure therefore ensured that all specimens consisted of essentially the "same structure" at the time of loading, despite being at different temperatures; the structure would be that which was characteristic of the upper pre-heat temperature. Hence, a series of pre-heat temperatures would result in a series of activation energies corresponding to these temperatures. The variation, if any, of activation energy with temperature (in as much as temperature affects structure) can thus be obtained. The Series II creep test programme was specifically planned with this kind of analysis in view. A similar approach of reducing temperature as opposed to increasing it, has been adopted in activation energy studies of metals as well, in order to avoid annealing effects (90).

8.3. ACTIVATION ENERGY FOR BASIC CREEP OF CEMENT PASTE

8.3.1. Series II Creep Specimens

The Series II specimens were pre-heated to a particular temperature but tested at lower temperatures after slow cooling.
The Arrhenius plots for pre-heat temperatures of 635°C and 560°C are shown in Figures 8.6 and 8.7 respectively. These plots were obtained at creep strains of 200, 500 and 800 $\mu\epsilon$. The time corresponding to a particular creep strain and the creep rate at that time were obtained using the power law formula fitted to creep strains in Section 7.4. Hence from

$$\epsilon_c = At^n \qquad (7.1)$$

the time for a required creep strain of say 200 $\mu\epsilon$, t_{200} is obtained from

$$t_{200} = (200/A)^{1/n} \qquad (8.18)$$

and the creep rate at this time obtained from

$$\left[\dot{\epsilon}_c\right]_{200} = nA\,(t_{200})^{n-1} \qquad (8.19)$$

Figure 8.6, which shows the results of specimens pre-heated to 635°C, indicates that the Arrhenius plot is bilinear with a point of inflection around 525°-560°C. Furthermore, the slope of the line corresponding to the higher temperatures is around 10 times steeper than that corresponding to the lower temperature range. This reinforces the discussion in Chapter 7, where a temperature around 600°C was considered a point beyond which a different creep mechanism was brought into play.

In Figure 8.7, which shows the results of specimens pre-heated to 560°C, the points corresponding to 560°C seem to be above the linear regression line corresponding to the lower temperatures; hence these points were omitted from the linear regression. It is likely that the points at 560°C also reflect the higher activation energy mechanism.

A word of explanation is in order at this stage, regarding the limited number of Arrhenius plots, despite the fairly extensive test programme for Series II specimens. The major problem was that specimens pre-heated to temperatures of 300°C or less (i.e. 70°C, 120°C and 300°C) and cooled to correspondingly lower temperatures exhibited virtually no creep when loaded. This has already been discussed in Section 7.3, where it was conjectured that the application of a higher stress may have resulted in some creep. The creep behaviour of ceramics is also known to be characterized by a threshold stress below which no creep occurs (178).

The data from the 460°C pre-heat temperature was judged as being insufficient to be used in the analysis, not so much because only 3 temperature levels were involved, but more so because the points at 460°C were suspected of being influenced by the effects of incomplete stability prior to loading, giving rise to higher creep rates.

Where the 635°C and 560°C pre-heat temperatures were concerned, test temperatures below 300°C were not used because 2 specimens pre-heated to 635°C and cooled to 120°C and 50°C respectively showed expansive behaviour after cooling, resulting most probably from the rehydration of dissociated $Ca(OH)_2$. This has already been discussed in Section 6.4.

The net result of the limitations described above is that only 2 Arrhenius plots, corresponding to pre-heat temperatures of 635°C and 560°C, were obtained from the Series II creep tests. The values of activation energies are tabulated in Table 8.1 and shown graphically in Figure 8.8. It is clear that the activation energy for basic creep increases with creep strain in the higher temperature range. This increase of activation energy with creep strain is consistent with the observed phenomenon of a decreasing creep rate. This kind of effect would be predicted by both "exhaustion" as well as strain hardening type creep theories (57). However, it seems also that the curves in Figure 8.8 corresponding to the higher temperature range would become asymptotic to some value of activation energy, presumably corresponding to the value associated with the secondary creep stage. The curves corresponding to the lower temperature range do not vary too much with strain.

8.3.2. Series I Creep Specimens

Although the Series I creep tests were not designed to be analysed by Arrhenius plots, it was, nevertheless decided to perform such an analysis, keeping in mind the pre-conditions that would be violated. Since most concretes exposed to temperature in practice would not have been pre-heated to higher temperatures, it was thought that an Arrhenius analysis on the Series I results, if applicable, would be more useful than those on the Series II results.

Despite the variations in hot strength and paste structure that would result from specimens being heated to different temperatures prior to creep loading, the Arrhenius plots at 200,500 and 800 $\mu\epsilon$ shown in Figure 8.9 do show certain characteristic trends. Ranges of temperature corresponding to high and low activation energies are

evident, as in Figure 8.6. The coincidence between Figures 8.6 and 8.9 is especially marked in the high activation energy range as evident from the comparison in Figure 8.10. Furthermore, the values of activation energies obtained from the Series I results are very similar to those for the specimens pre-heated to 635°C, as can be seen from Table 8.1 and Figure 8.8. It must be noted that the points corresponding to 400°C, 425°C and 460°C in Figure 8.9 have been omitted from the linear regression, because these results exhibited enhanced creep rates due to incomplete stabilization prior to loading.

Great care must be exercised at this stage in order to avoid unwarranted conclusions. As will be clarified further in Section 9.4, the creep response of specimens exposed to varying temperatures, as in the case of Series I specimens, would be influenced by 3 factors, viz. (i) the Arrhenius thermal effect, (ii) variation in stress/strength ratio due to the variation in strength caused by temperature and (iii) microstructural stabilization. In general, especially at temperatures above 300°C, (i) and (ii) would tend to increase the creep potential while (iii) would tend to reduce it. Figure 8.9 contains the contributions from all 3 of these factors. Hence, although linearity very similar to Figure 8.6 is obtained in the plot, it cannot be said to correspond to the Arrhenius thermal effect. The fact that such linearity is in fact obtained can be attributed either to the thermal effect being a dominant factor which 'hides' the other two or to the possibility that factors (ii) and (iii) balance each other out. It should be brought to mind that a plot of creep against the stress/hot strength ratio for Series I specimens also produced bilinearity (Figure 7.9). This too may be a result of factors (i) and (iii) balancing each other out. For the moment, where temperature dependence is concerned, although the results from Figure 8.9 will be used in further comparisons and analyses, the plots in Figure 8.9, will be referred to as 'pseudo-Arrhenius' plots and the temperature dependence, a 'pseudo-Arrhenius' dependence.

The results below 120°C in Figure 8.9 show a marked deviation from the trend. This is probably due to the significant changes in moisture level that take place in this region. Other researchers (40, 146) have also found anomalous behaviour stemming from the influence of

moisture. (See Figure 2.8c). However, above 120°C, the Series I results show bilinearity in the pseudo-Arrhenius plots, yielding activation energies of around 25 kJ/mol in the temperature range 120°C to 525°C and around 250 kJ/mol in the temperature range 560°C to 670°C. The plots in Figures 8.6 and 8.7 for series of specimens pre-heated to 635°C and 560°C respectively should be considered as reflecting genuine Arrhenius thermal effects, because such pre-heating would equalize the strength variation and microstructural stabilization factors within each series.

8.3.3. Discussion - Arrhenius Plots and Activation Energies for Creep

The evidence from the analysis of both the Series I and II creep test results enables us to arrive at some conclusions regarding the activation energies of basic creep for cement paste. These conclusions can also be viewed in the light of the behaviour of other materials which have been better researched.

It seems that under certain conditions, the temperature dependence of basic creep for cement paste can indeed be modelled by an activation energy approach, using the Arrhenius equation. However, the nature of the Arrhenius plot is bilinear, whether the specimens have been pre-heated to 635°C and tested at lower temperatures, or tested at the pre-heat temperature itself.

Before considering this phenomenon of bilinearity, the significance of the actual values of activation energies will first be ascertained. As stated at the start of this chapter, activation energy is a thermodynamic entity that can be arrived at by macro-level measurements. However, it can give us clues regarding microstructural mechanisms that govern the observed phenomena.

The activation energy corresponding to the lower temperature range (i.e. 120°C to 525°C) is around 25 kJ/mol. It is difficult to know whether the slightly higher value of around 50 kJ/mol. obtained for the specimens pre-heated to 560°C is significant or not, in the absence of results from lower pre-heat temperatures. The value of activation energy for free water obtained from the viscosity -

temperature relationship has been found to be 14.6 kJ/mol. (146). It may seem reasonable to think that the creep mechanism in this lower temperature range is governed by or at least contributed to by the moisture condition, because this latter figure is of the same order of magnitude as our experimental activation energy. However, this is unlikely to be the case, especially where Series II specimens are concerned, since moisture stability would have been achieved at a higher temperature than the test temperature. Furthermore, the value for activation energy of around 25 kJ/mol. obtained here is almost double that for free water. It is more likely that a structural re-adjustment type of mechanism would be the dominant creep mechanism, as has been suggested in Section 7.3.

It is difficult to compare the activation energy results obtained here with the work of other investigators on cement and concrete materials, because most of their Arrhenius plots (which also would strictly have to be termed 'pseudo-Arrhenius' plots) have been based on creep rates at equal time periods as opposed to equal strains after loading. Marechal obtained activation energies ranging from 13.4 to 16.3 kJ/mol. for five pre-dried (105°C) concretes in the temperature range 20°C to 400°C, based on Arrhenius plots of creep rates at 1 day after loading (100). Reutz obtained an activation energy of 15.5 kJ/mol. for pre-dried cement paste in the range 20°C to 80°C (146). These values are lower than the activation energy for the range 120°C to 525°C obtained in the present investigation. This would, however, be due to the difference in approach stated above. The activation energy of cement paste in this investigation, based on Arrhenius plots of creep rates at an equal time period, i.e. 1 day, after loading was found to be 9.24 kJ/mol. in the above temperature range (85), which value is much lower than the value of 25 kJ/mol. obtained on the basis of creep rates at equal strains after loading.

It would be very instructive to be able to compare the activation energies of different cement bound materials, such as cement paste, cement mortar, lightweight concrete and normal concrete. The following comparisons are made of activation energies based on Arrhenius plots of creep rates at equal time periods after loading. The proximity of Reutz's value for activation energy to Marechal's

results tends to suggest that there is no essential difference between cement paste and concrete. However, Rentz's result has been obtained in the relatively small temperature range of 20°C to 80°C. On the other hand, researchers at Imperial College have found an increase in activation energy from lightweight concrete (7.53 kJ/mol.) through cement paste (9.24 kJ/mol.) to gravel concrete (12.23 kJ/mol.) in the temperature range 140°C to 300°C (85). All the researchers above performed their tests in compression. Sullivan's tests in flexure yielded activation energy values for the first 100 hours after loading of 6.89 kJ/mol. for mortar and 22.95 kJ/mol. for gravel concrete in the temperature range 100°C to 400°C (164). It is interesting that his value for mortar is close to that for cement paste (9.24 kJ/mol.) and lower than that for concrete. The particularly high value for concrete may be due partly to the break up of gravel aggregate near 400°C. Clearly there needs to be more evidence before any definite conclusions can be made with regard to the comparison attempted above.

The eight to ninefold increase in activation energy at around 525°C-560°C coincides with the sharp increase in creep described in Section 7.2. Furthermore, the specimens pre-heated to 635°C show high activation energy at higher temperatures and low activation energy at lower temperatures. This further confirms the hypothesis advanced in Section 7.3 that this sharp increase in creep, which can now be linked to a high activation energy mechanism, is indeed a thermally induced phenomenon which is reversible.

Where metals are concerned, creep at temperatures in excess of 0.5 T_m (where T_m is the melting point of the material, in absolute units) has been linked to an atomic self-diffusion mechanism, because of the close correspondence between the activation energies for creep and self-diffusion (47). A similar correlation has been observed for high temperature creep of ceramics as well (51). Figure 8.11 illustrates these relationships. The spread of activation energies ranges from 69 kJ/mol. to 477 kJ/mol. for metals and 200 kJ/mol. to 600 kJ/mol. for ceramics. The activation energy for the temperature range 560°C to 670°C obtained in the present investigation is around 250 kJ/mol., which is in fact within these ranges. Furthermore, the temperature of 560°C corresponds to around 0.5 T_m for hardened cement

paste.

The above considerations would make it seem reasonable to suggest self diffusion as the rate-controlling process for creep of hardened cement paste in the higher temperature range. The activation energy for the diffusion of oxygen in various types of glasses, which have silicate chains similar to those found in hardened cement paste, has been found to be between 275-300 kJ/mol. (163), which is similar to the values obtained in this study. The mechanism proposed is the breaking of a Si-O bond of a singly bonded oxygen atom and the subsequent interstitial motion of the oxygen ion (163). This then may well be the mechanism that governs basic creep of hardened cement paste in the temperature range 560°C to 670°C.

An alternative to the above mechanism could be a viscous flow type mechanism which is thermally induced, such as exhibited in glass. The problem with this alternative is that the activation energy for the viscous flow of glass is lower at higher temperatures (144), which is the opposite of the phenomenon observed in hardened cement paste.

The other point of interest raised by the Arrhenius plots for hardened cement paste is their bilinear nature, indicating temperature ranges of two distinct activation energies for creep. It is interesting to note that a similar phenomenon is displayed in other materials such as metals, glasses and ceramics as well.

Where metals are concerned, such a transition between activation energies for creep takes place at a temperature which is close to half the melting temperature (in absolute units); a few examples are shown in Figure 8.12a. These transitions generally indicate changes from one rate-controlling process to another (34).

The creep of glass is more conveniently described in terms of its viscosity, η, and the corresponding equation for temperature dependence would be of the form

$$\eta = A \exp (Q/RT) \qquad (8.20)$$

A plot of the natural logarithm of viscosity against the reciprocal of temperature would result in a "modified" Arrhenius-type plot and an example is shown in Figure 8.12b, where some glasses show a definite transition from one activation energy to another. However, in this case, the values of activation energy are higher in the low temperature range and lower in the high temperature range, as evident from the steepness of the lines in the plots. This is probably attributable to structural changes, the structure becoming more open as the temperature increases (144).

Transitions between low and high activation energy regimes are observed in ceramics too, as exemplified in Figure 8.12c. Here again as for metals, high activation energies are associated with greater creep observed at high temperatures. It does seem therefore, that where high temperature creep is concerned, an association of high creep with a high activation energy reflects a self-diffusion type mechanism as the rate controlling process for creep; a low activation energy associated with high creep probably indicates a viscous flow type mechanism, as exhibited in some glasses.

With the above considerations in mind, let us return to hardened cement paste. It would seem that the bilinearity in the Arrhenius plot is more likely to be due to a change in the rate controlling process of creep rather than a significant change in the structure, the change being brought about at a temperature of around 560°C. (If there is a significant change of structure involved, it is likely to be a thermally reversible re-ordering of the molecular structure). The rate controlling process for basic creep below this temperature is probably a structural re-adjustment type mechanism, while that above this temperature is likely to be a self-diffusion type mechanism.

A final comment will be made in passing. The performance of these experiments on cement paste specimens as opposed to mortar or concrete specimens has enabled us to establish that the above dual creep mechanism is seated in the cement paste itself. If tests were done on specimens having aggregate containing quartz, this bilinearity may have been attributed to the α to β quartz transform taking place at

573°C, as has actually been suggested in the literature (11). This, once again is a validation of the decision to concentrate experimentation on hardened cement paste for the purpose of this investigation.

8.4. TEMPERATURE DEPENDENCE AND THE TIME SHIFT PRINCIPLE

8.4.1. The Time Shift Principle

The time shift principle was first proposed by Schwarzl and Staverman (156) for modelling the temperature dependence of linear viscoelastic behaviour. They suggested that the difference between one isothermal creep response and another was equivalent to a horizontal shift of the response in the logarithmic time scale. Materials which obeyed such a law were called "thermorheologically simple".

In order to illustrate this principle, let us consider two isothermal creep responses at temperatures T_o and T ($> T_o$) respectively. (See Figure 8.13). If the material concerned is thermorheologically simple, the curves will have the same slope, b, and can be made to coincide with each other by a shift, parallel to the log time axis, of $\psi(T)$. Therefore the creep response at temperature T, C_T can be obtained in terms of the creep response at temperature T_o, C_{To}.

The creep strain, C_T, at time t for a specimen at temperature T is equal to that of a specimen at temperature T_o at some time t_o. Since the time shift is in the log time domain, we can write

$$C_T(\ln t) = C_{To}(\ln t + \psi(T)) \qquad (8.21)$$

where the bracket denotes functionality.

Hence we can obtain

$$\begin{aligned} C_T(\ln t) &= C_{To}\,[\ln t + \ln \phi(T)] \\ &= C_{To}\,\{\ln [t\,\phi(T)]\} \\ &= C_{To}\,(\ln \theta) \end{aligned} \qquad (8.22)$$

where $\theta = t\phi(T)$

and $\phi(T) = \exp[\psi(T)]$

Equation (8.22) can therefore predict the creep strain at a real time t after loading at a temperature T, from the creep response of the material at temperature T_o, using the modified equivalent time $t\phi(T)$.

Dorn (47) restated the above idea slightly differently by saying that equal creep strains are obtained for identical values of $\ln t + \psi(T)$. He then suggested that $\psi(T)$ could be replaced by $(-Q/RT)$ if the temperature dependence was of the Arrhenius type. Thus, the total creep strain, ϵ, would be obtained as a function of an equivalent time θ, where

$$\theta = t \exp(-Q/RT) \qquad (8.23)$$

i.e. $$\epsilon = f(\theta) = f[t \exp(-Q/RT)] \qquad (8.24)$$

The time shift principle, although developed and first used to study the creep of polymers and metals has been applied to concrete as well. Mukaddam and Bresler (109) used this principle to model creep response at different isothermal conditions as well as at different ages of loading. However, they obtained the shift function empirically on a best fit basis and it had no physical significance, unlike in Dorn's approach.

8.4.2. Application of Principle to Experimental Results

It was decided to apply the time shift principle to the experimental results, using Dorn's approach. Two limitations exist. First, linearity in Arrhenius and pseudo-Arrhenius plots was obtained only within certain temperature ranges. (See Figures 8.6, 8.7 and 8.9). It was only to these ranges that a value for activation energy could be ascribed, and the time shift principle applied.

Secondly, the value of activation energy varied with creep strain, as shown in Figure 8.8. However, as indicated earlier, the values tended towards an asymptote in the higher temperature range;

in the lower temperature range, the values were sensibly independent of creep strain. Therefore, for the purpose of this exercise, the lower temperature range activation energy was taken as the average of the 3 values at 200,500 and 800 $\mu\epsilon$; for the higher temperature range, the value at 800 $\mu\epsilon$ was adopted as the relevant value of activation energy, since it would best approximate the asymptotic value.

The object of the exercise was to verify whether the relationship between ϵ and θ was the same, irrespective of test temperature, within a given temperature range characterized by a particular activation energy. Given that a power law relationship has already been found to give the best fit for the time function of creep at various temperatures (Section 7.4), it was decided to ascertain whether a linear relationship could be obtained between ln ϵ and ln θ. Such a relationship would not only verify the time shift principle for the material, but also enable us to obtain a composite or average value for the exponent n' in the expression

$$\epsilon_c = A' \theta^{n'} \qquad (8.25)$$

within the given temperature range.

The values of θ were based on real times of 1, 4 and 7 days. Very short times after loading were not considered, because at these early times the values of activation energy may have been considerably smaller than the ones assumed. The resulting double logarithmic plots are shown in Figures 8.14 to 8.16 for the Series II specimens (corresponding to the 3 linear portions in the Arrhenius plots in Figures 8.6 and 8.7) and Figures 8.17 and 8.18 for the Series I specimens (corresponding to the 2 linear portions in the pseudo-Arrhenius plots in Figure 8.9).

The results show that there exists a single relationship between ϵ and θ, irrespective of temperature, within a given temperature range; furthermore these relationships are power law relationships of the form given in equation (8.25). Hence, not only can the temperature dependence of basic creep within certain temperature ranges be modelled by an Arrhenius or pseudo-Arrhenius type

relationship, but this relationship can also be expressed by an equivalent time concept in an "overall" power law "equivalent time" function as

$$\epsilon_c = A' \theta^{n'} \qquad (8.25)$$

where $\theta = t \exp(-Q/RT)$ (8.23)

8.5. PREDICTION OF CREEP STRAINS

8.5.1. Time-Temperature Equivalence Technique

The existence of a temperature dependence for basic creep of the form described above has two practical applications, namely the prediction of creep at higher temperatures from the creep response at a lower temperature and vice versa. The former would be relevant when test facilities at the higher temperature are not easily available or expensive to construct - i.e. when there is a temperature constraint on experimentation; the latter would be relevant when long term creep data for the lower temperature are required quickly - i.e. when there is a time constraint on experimentation. Such extrapolation techniques have also been proposed by Sullivan (165).

As described beforehand, a time-temperature equivalence based on an activation energy related time shift principle can not be obtained for the entire Series I temperature range from 20°C to 670°C. However, an example of creep strain prediction will be given from each of the two ranges 120°C to 525°C and 560°C to 670°C.

Suppose we have two specimens strained at absolute temperatures T_1 and T_2. By Dorn's argument, equal strains will be obtained at equivalent times of θ where

$$\theta = t \exp(-Q/RT) \qquad (8.23)$$

Hence we can write

$$t_1 \exp(-Q/RT_1) = t_2 \exp(-Q/RT_2) \qquad (8.26)$$

and obtain $t_2 = t_1 \exp[(Q/RT_2)-(Q/RT_1)]$ (8.27)

Given that the creep vs. time (t_1) relationship is known at a temperature T_1, equation (8.27) gives us the times, t_2, at which the same creep strains will be reached, if the test were carried out at a temperature T_2. Thus a creep vs. time relationship can be constructed for the temperature T_2.

Figure 8.19 shows how the long term strains at 560°C have been predicted from the test results of the specimen loaded at 670°C. This could be an example of there being a time constraint on experimentation; the ratio between t_2 and t_1 in equation (8.27) is 107.7, meaning that the time under load can be reduced by this factor when testing at the higher temperature.

On the other hand, Figure 8.20 shows the prediction of strains at 525°C from a test performed at 120°C. In this example the ratio between the times at the two temperatures is around 38.9. Hence, the duration of the predicted strains is also small - in this case only $^1/_4$ day from a test performed for 9 days at the lower temperature. However, there are cases when only very short term creep data is required at higher temperatures (for example, in fire resistance studies), and this may be obtained from a test of reasonable duration at a lower temperature, if there is a temperature constraint on experimentation.

8.5.2. Uncoupled Time, Temperature and Stress Functions

An alternative method of creep strain prediction is via the uncoupled time, temperature and stress functions, as expressed by

$$\epsilon_c = f_1(\sigma).f_2(T).f_3(t) \qquad (8.28)$$

where $$f_1(\sigma) = k_1(\sigma/f'_c) \qquad (8.29)$$

$$f_2(T) = k_2 \exp(-Q/RT) \qquad (8.30)$$

and $$f_3(t) = k_3 t^n \qquad (8.31)$$

where $f_1(\sigma)$, $f_2(T)$ and $f_3(t)$ refer to the stress, temperature and time functions respectively. k_1, k_2 and k_3 are constants and (σ/f'_c) is the stress/cold strength ratio. Equation (8.28) can then be written as

$$\epsilon_c = K(\sigma/f'_c) \exp(-Q/RT)\, t^n \qquad (8.32)$$

where $K = k_1.k_2.k_3$ = a constant

It must be appreciated that a rigorously theoretical justification cannot be made for the above uncoupling of functions. For example, as observed in Section 7.4, the value of the exponent n in the time function varied with temperature, although it was fairly constant over the range 150°C–375°C. Furthermore, if the temperature dependence is to be expressed by an activation energy approach, it will be a function of strain, and hence time, as discussed previously in this chapter. The effect of stress may also vary with temperature, but it has been assumed that stress function is a linear function of stress/cold strength ratio.

Despite the above limitations, the uncoupled functions approach is elegant and would be simple for designers to use. Hence, it is applied as a predictive tool within the same two temperature ranges as before – i.e. 120°C to 525°C and 560° to 670° – for the Series I specimens. The time function is uncoupled from temperature dependence by using an arithmetic mean of the n values within each range. The constant k_3 is found for each creep test by using equation (8.31) in a least squares optimization technique. The normalization of these constants with respect to a stress/cold strength ratio of unity will result in a series of products k_1k_3. These products are then fitted by equation (8.30), after transformation into the logarithmic domain. Thus we can obtain a composite constant $K = k_1.k_2.k_3$ as well as a value for Q.

The values of the constants obtained for the 2 temperature ranges studied are given in Table 8.2. It is clear that the values obtained for Q are quite different to those obtained as the values of activation energy in the more theoretically rigorous approach adopted earlier in this chapter. In fact, it is unlikely that much physical significance can be attached to the values of Q in Table 8.2; they are best regarded as empirical constants. However, the predictive capability of the formula seems reasonable, whether it be a case of predicting the time or temperature dependence of creep strain as indicated in Figures 8.21 and 8.22. As expected, the strains at

400°C, 425°C and 460°C in Figure 8.22 lie above the predicted curve, because of incomplete stabilization prior to loading at these temperatures.

8.6. CONCLUSION

In concluding this chapter, it can be said that there have been two main outcomes of the activation energy studies. Firstly, they have enabled us to establish a temperature dependence for creep. This temperature dependence could be considered to be an Arrhenius type dependence if the specimens all experienced the same upper pre-heat temperature. A similar type of relationship, termed a pseudo-Arrhenius temperature dependence was obtained, perhaps fortuitously, for the Series I specimens, which were heated to different temperatures before creep loading, for temperatures above 120°C. There were two distinct ranges of differing activation energies, with a transition temperature of around 560°C. The difference in activation energies was about an order of magnitude, i.e. 25 kJ/mol. in the lower temperature range (120°C to 525°C), compared with around 250 kJ/mol. in the higher temperature range (560°C to 670°C). It was also shown that, within the above temperature ranges, the material investigated obeyed the time shift principle of temperature dependence. This shift function was not obtained by mere empirical curve fitting, but was based on an Arrhenius or pseudo-Arrhenius type temperature dependence. Thus, it was possible to arrive at an overall power-law relationship between creep strain and equivalent time (which accounted for both temperature and time dependence), for each of the temperature ranges characterized by a particular activation energy. The establishing of the above-mentioned temperature dependence, together with the time and stress functions suggested in Chapter 7, has enabled us to propose predictive schemes for basic creep. It is likely that similar predictive schemes could be devised for mortar and concrete as well, given sufficient experimental data.

The second outcome of the activation energy studies is that they have provided clues regarding creep mechanisms at elevated

temperatures. Based on comparisons with other materials that have been better researched, it has been possible to arrive at tentative conclusions regarding these mechanisms. It is suggested that the rate controlling process of basic creep of hardened cement paste from 120°C to 560°C is a structural readjustment type of mechanism, while that from 560°C to 670°C is a self-diffusion type of mechanism.

	Strain (με) / Temp. (°C)	200	500	800
Series I	560-670	199.34	251.21	277.84
	120-525	26.18	23.06	21.46
Preheated To 635°C	525-635	229.86	260.44	276.13
	300-525	29.03	28.70	32.46
Preheated To 560°C	300-500	55.43	48.10	44.33

TABLE 8.1. ACTIVATION ENERGIES FOR CREEP OF HARDENED CEMENT PASTE (IN kJ/MOL) FOR VARIOUS CONDITIONS, TEMPERATURE RANGES AND CREEP STRAINS.

Temperature Range (°C)	120-525	560-670
n	0.4027	0.3063
Q(kJ/MOL)	9.099	91.205
K	18108	3.0643×10^9

TABLE 8.2. PARAMETERS OF EXPRESSION FOR CREEP STRAIN IN UNCOUPLED FUNCTIONS METHOD

$$\varepsilon_c = K\,(\sigma/f'_c)\,\exp\,(-Q/RT)\,t^n$$

Fig.8.1 — ENERGY BARRIERS FOR ACTIVATION PROCESSES

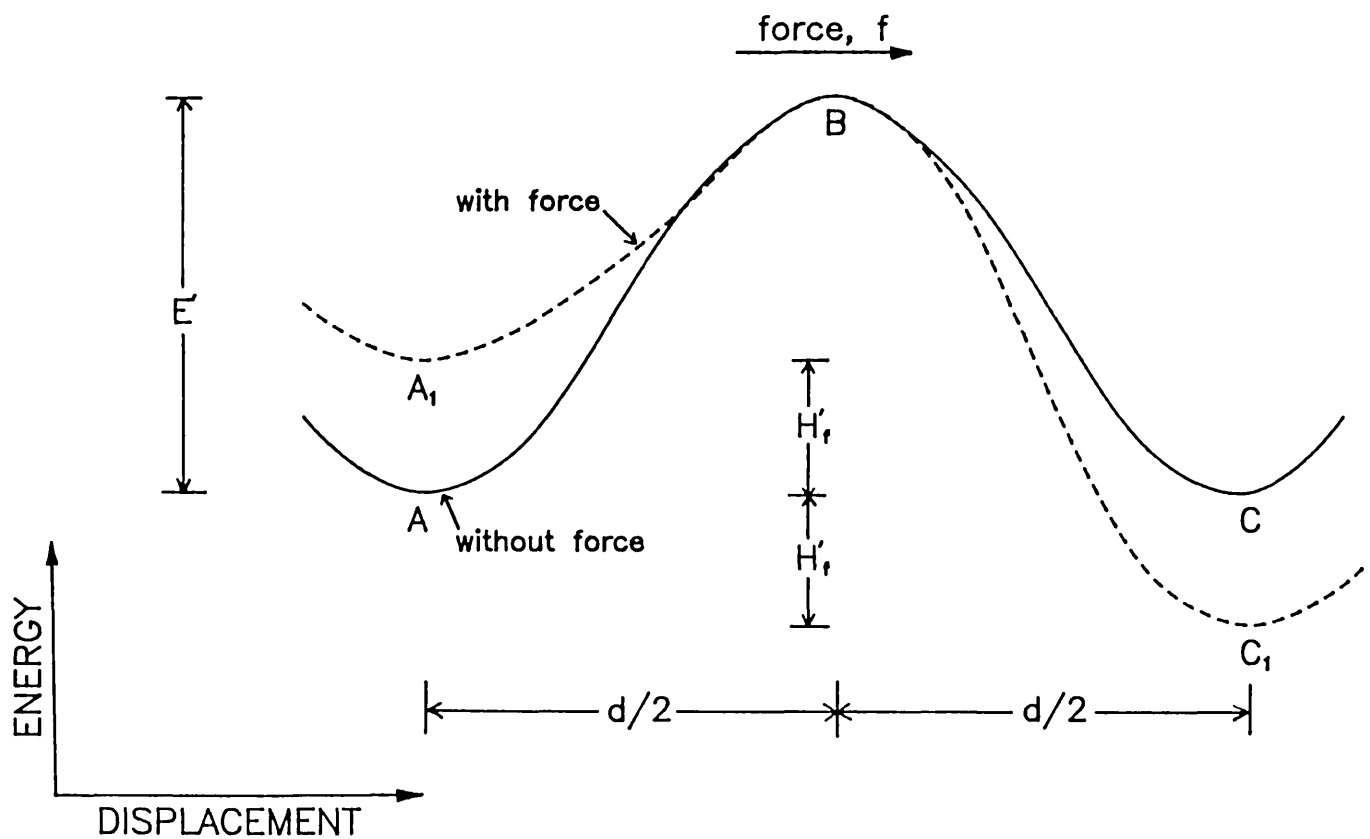

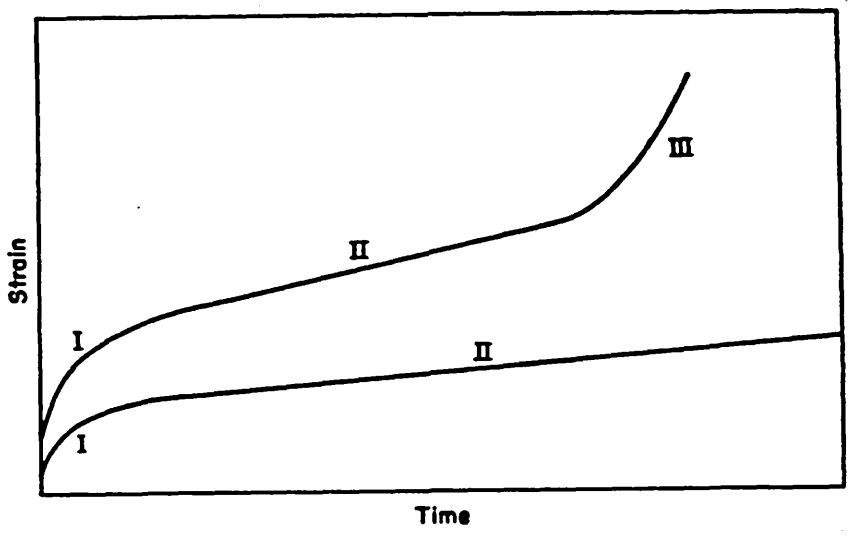

Figure 8.2 - TYPICAL CREEP CURVES FOR A VISCOELASTIC MATERIAL.
I-PRIMARY CREEP, II-SECONDARY CREEP, III-TERTIARY CREEP.

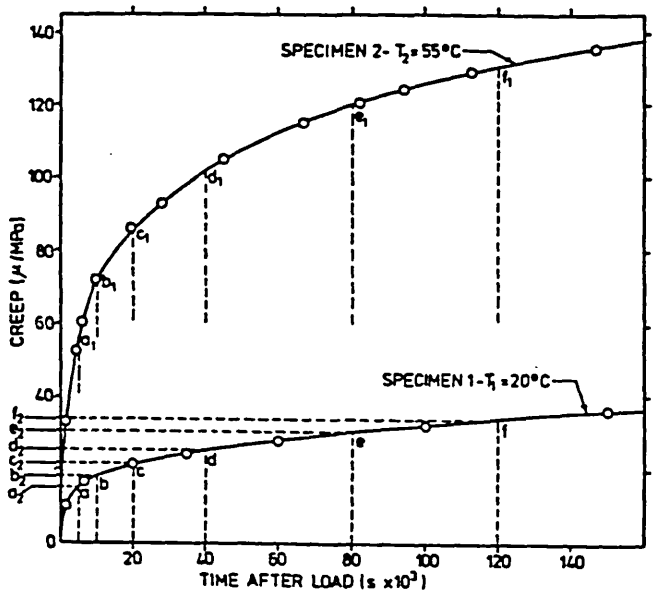

Figure 8.3 - DETERMINATION OF CREEP RATES AT EQUAL TIMES AND EQUAL STRAINS AFTER LOADING. (FROM DAY & GAMBLE (42))

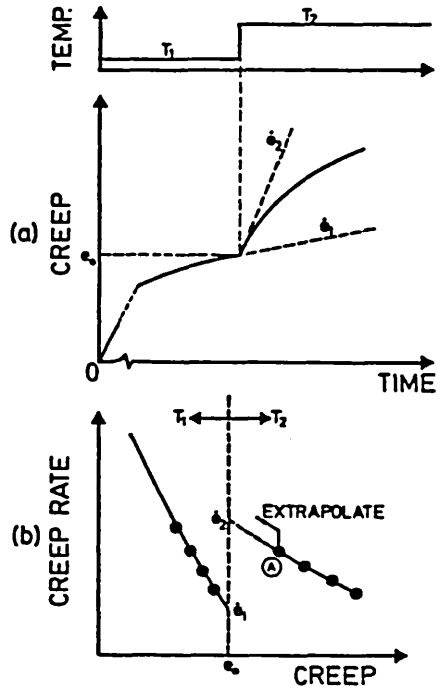

Figure 8.4 - SCHEMATIC REPRESENTATION OF DORN'S METHOD FOR DETERMINING ACTIVATION ENERGY.(FROM DAY & GAMBLE (42))

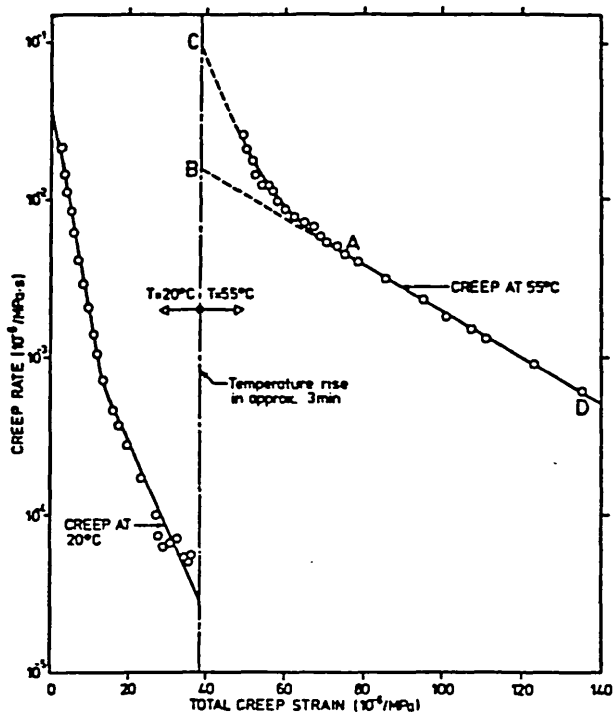

Figure 8.5 - DORN'S METHOD APPLIED TO HARDENED CEMENT PASTE.(FROM DAY & GAMBLE (42))

Fig.8.6 – ARRHENIUS PLOTS – PREHEAT TEMP.= 635°C

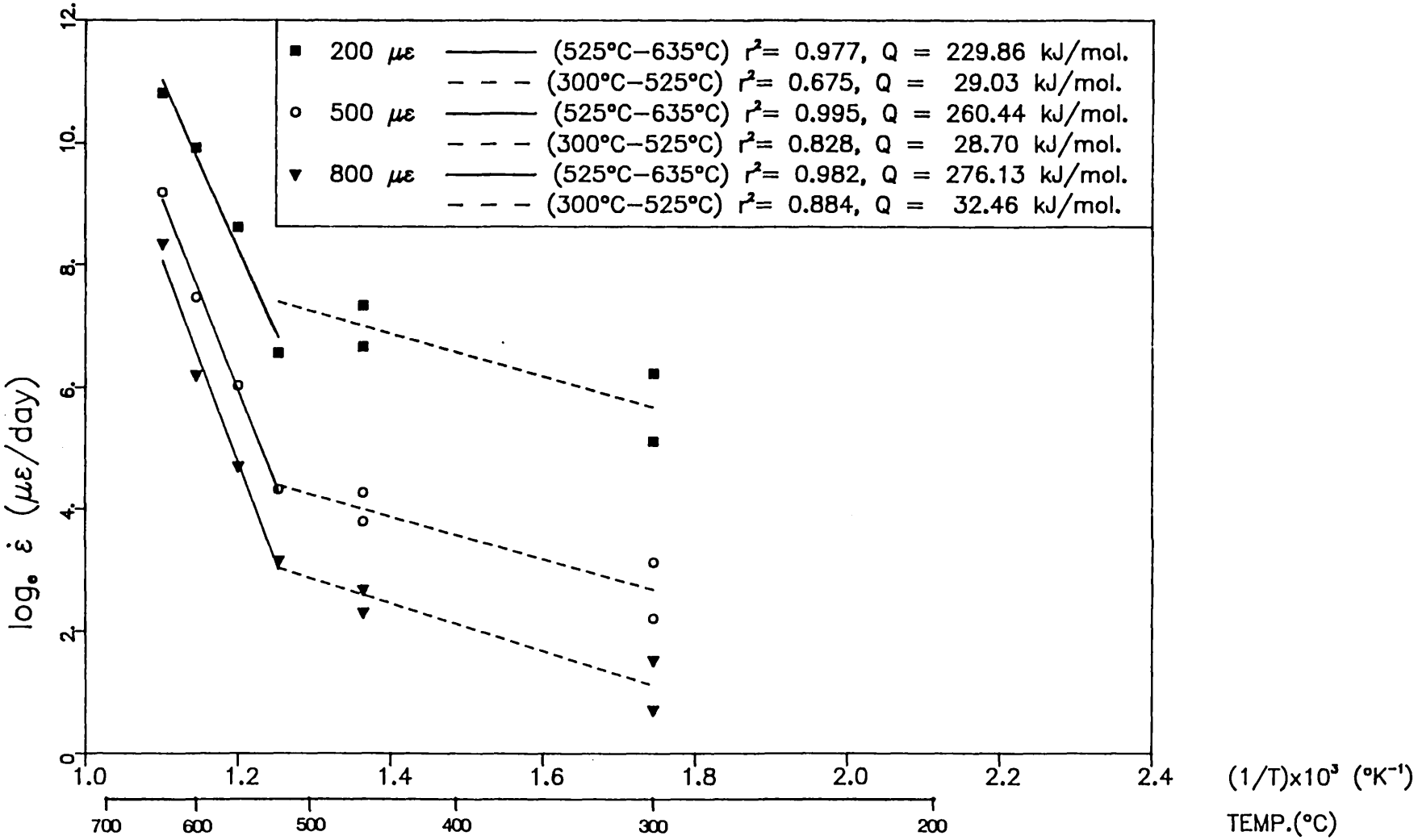

Fig.8.7 – ARRHENIUS PLOTS – PREHEAT TEMP.= 560°C

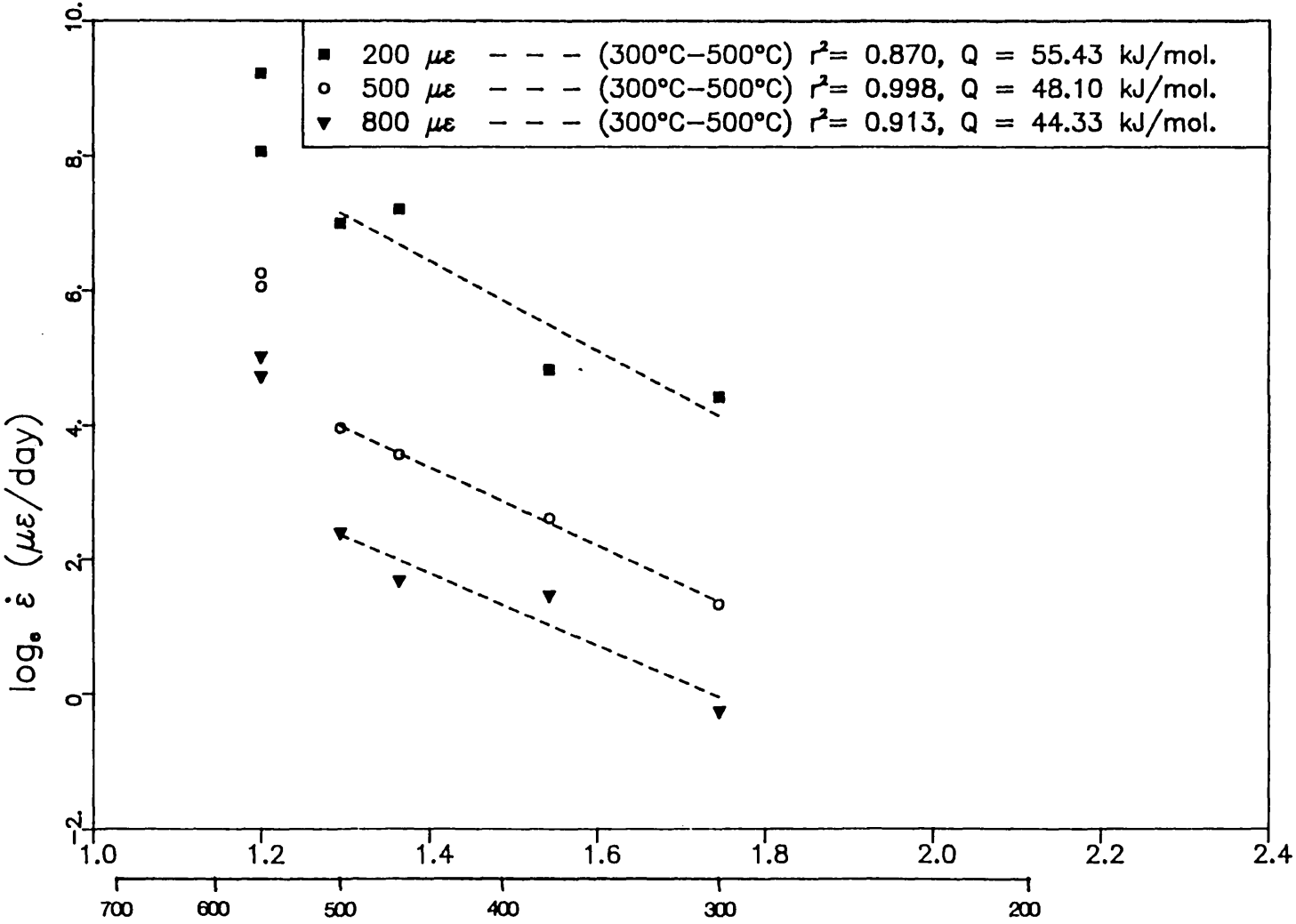

Fig.8.8 – VARIATION OF ACTIVATION ENERGY WITH CREEP STRAIN

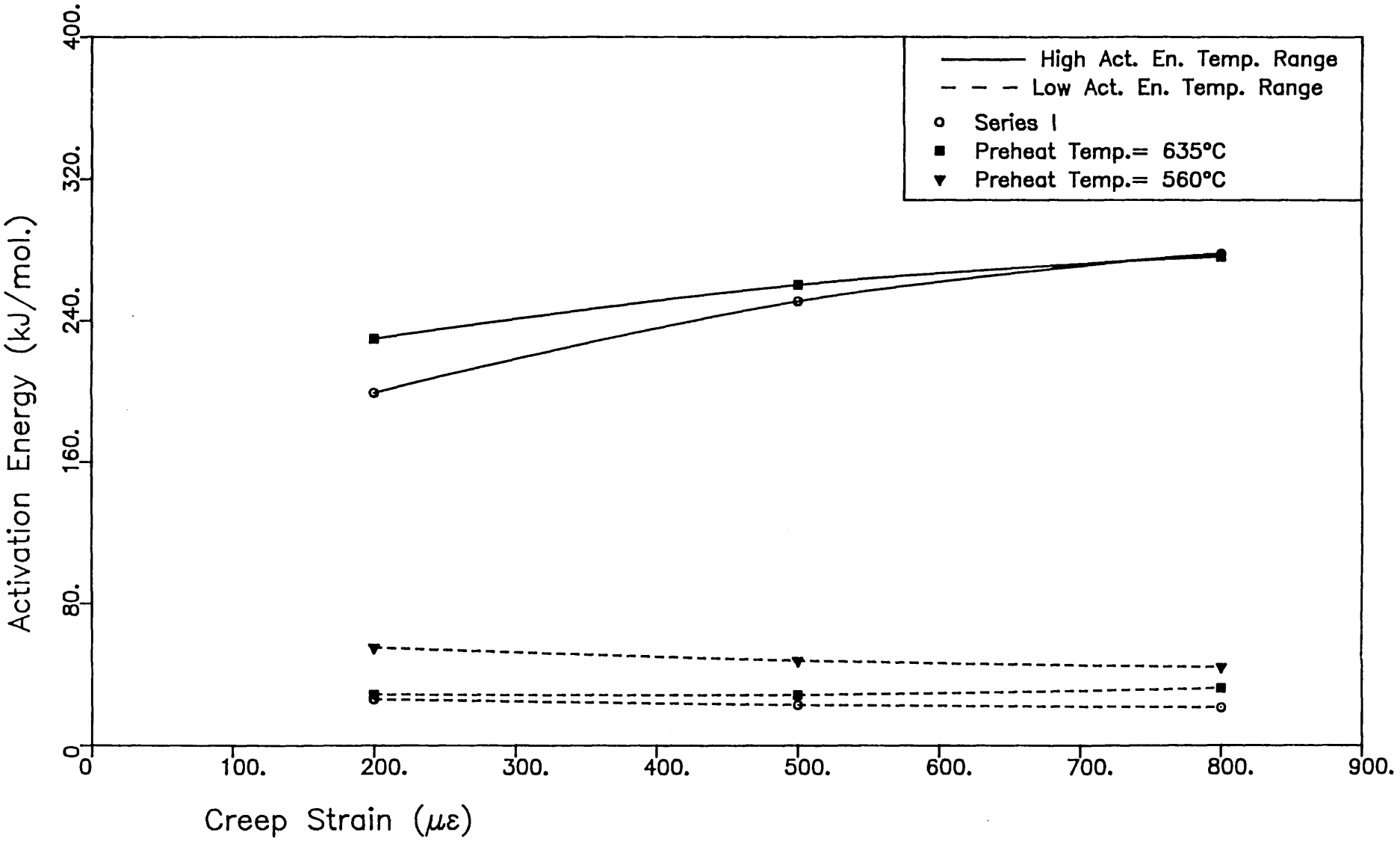

Fig.8.9 – PSEUDO–ARRHENIUS PLOTS – SERIES I

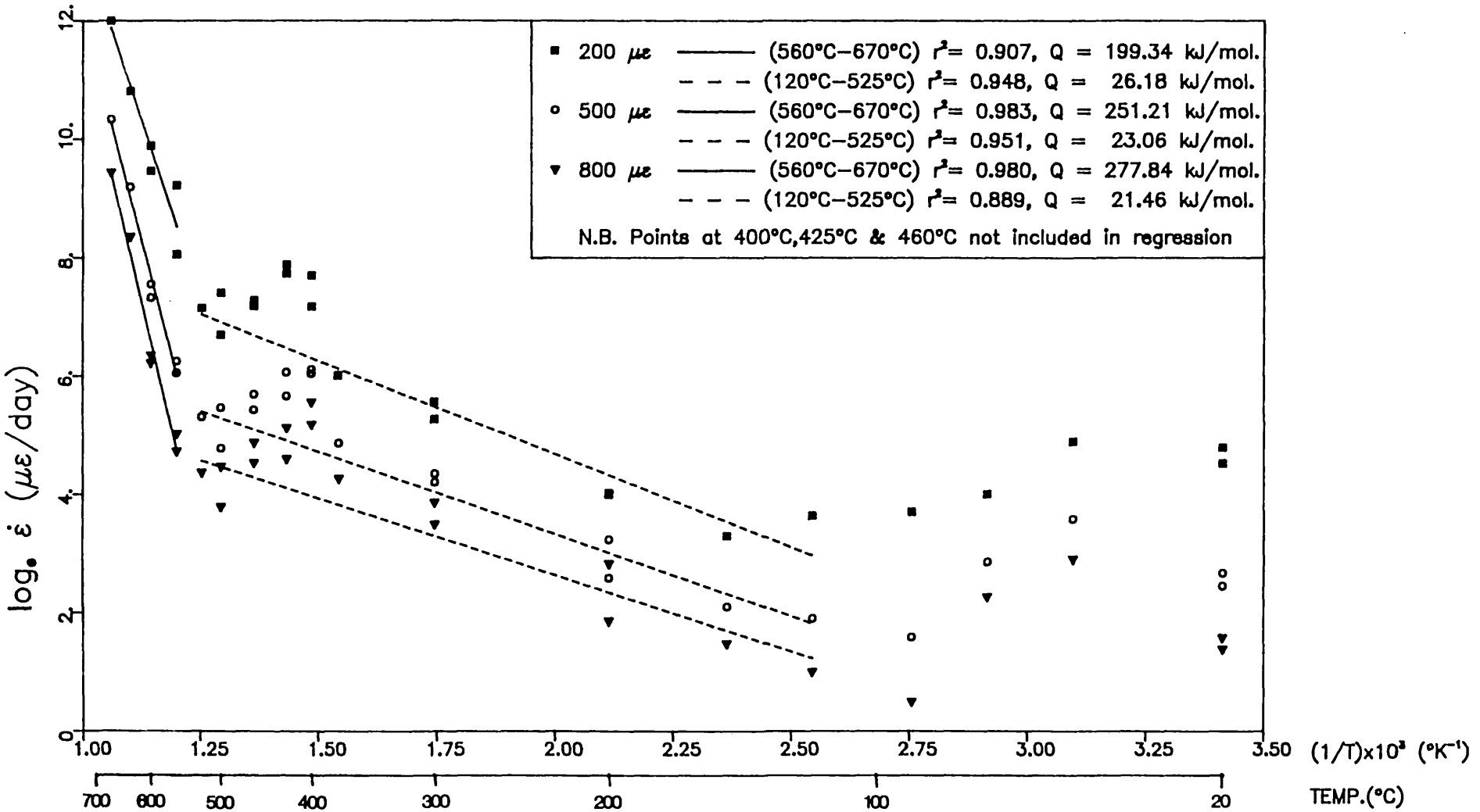

Fig.8.10 – COMPARISON OF ARRHENIUS PLOTS

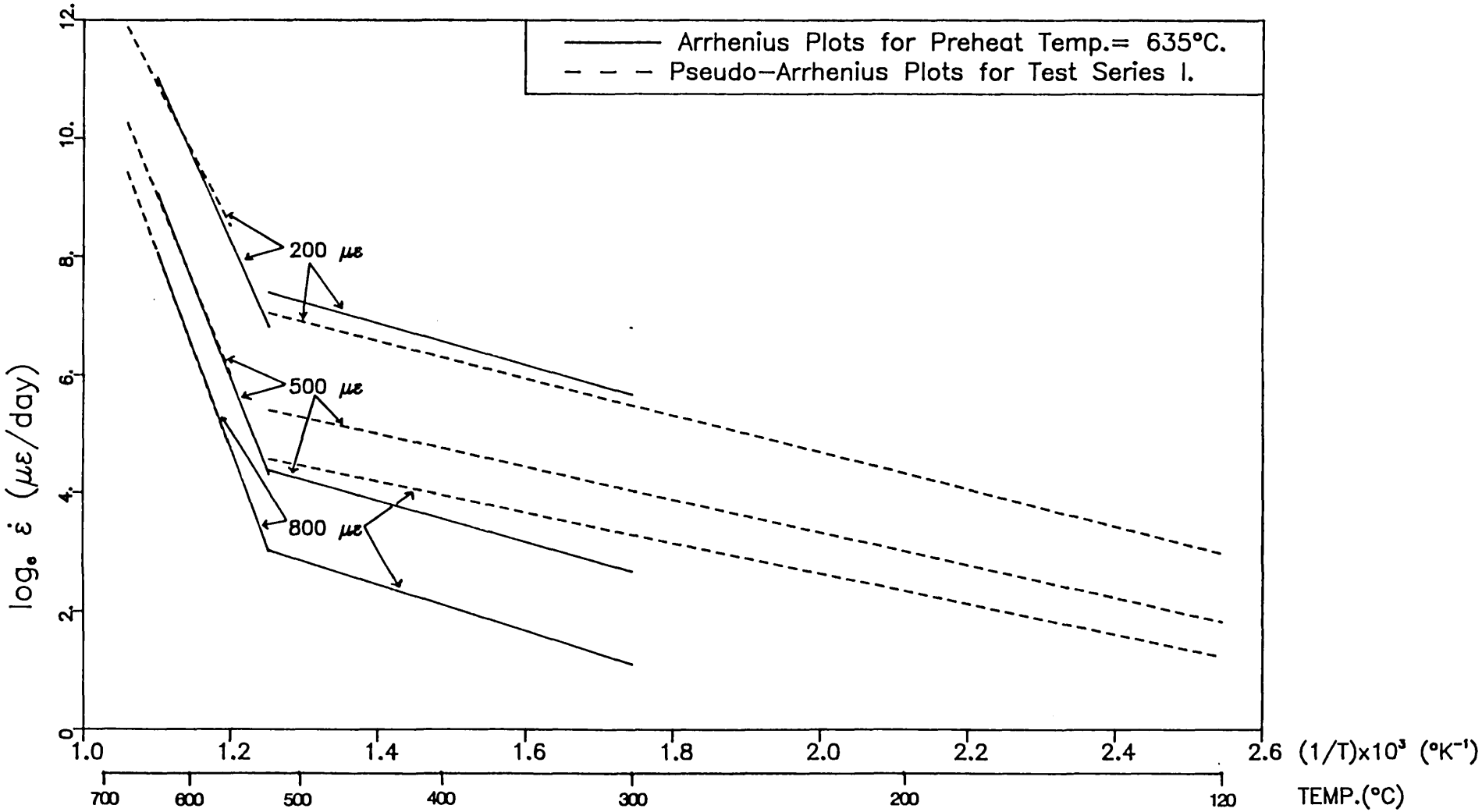

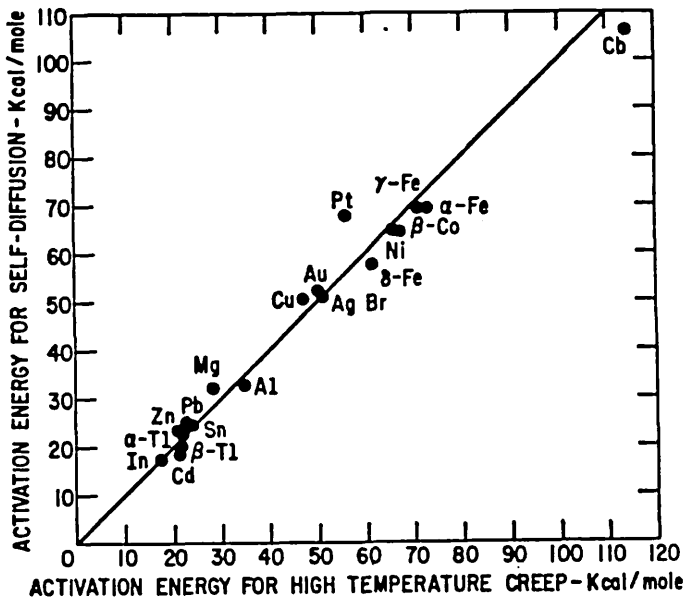

Figure 8.11(a) - CORRELATION BETWEEN ACTIVATION ENERGIES FOR SELF-DIFFUSION AND HIGH TEMPERATURE CREEP IN METALS. (FROM GAROFALO (57))

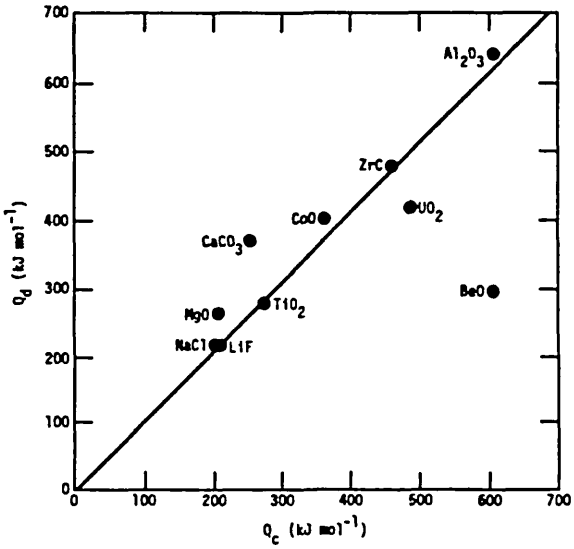

Figure 8.11(b) - CORRELATION BETWEEN THE ACTIVATION ENERGY FOR LATTICE DIFFUSION OF THE SLOWEST MOVING SPECIES, Q_d AND THE ACTIVATION ENERGY FOR CREEP, Q_c IN CERAMICS. (FROM EVANS & LANGDON (51))

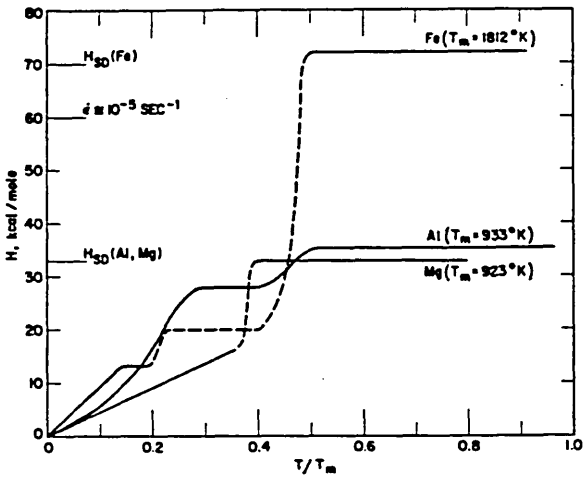

(a)

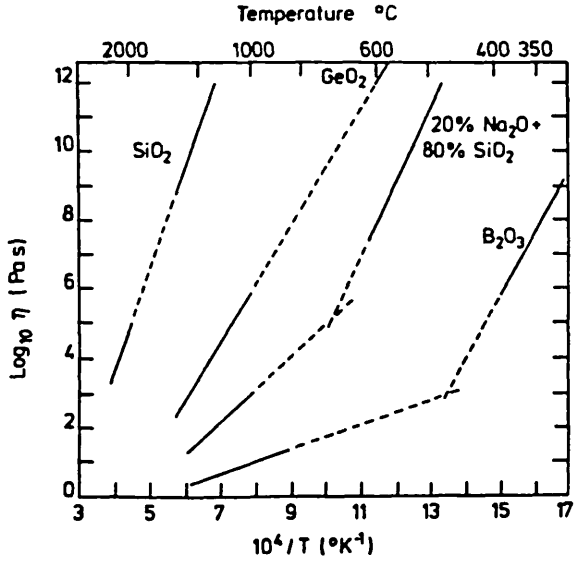

(b)

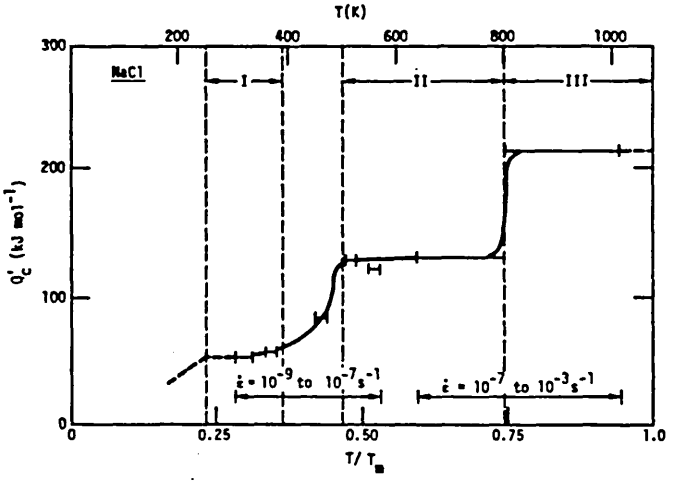

(c)

Figure 8.12 - TEMPERATURE DEPENDENCE OF ACTIVATION ENERGY FOR CREEP IN (a) METALS (FROM CONRAD(34)), (b) GLASSES (FROM RAWSON(144)) & (c) POLYCRYSTALLINE NaCl (FROM EVANS & LANGDON(51)). NOTE THAT ACTIVATION ENERGY IN (b) IS GIVEN BY THE SLOPES.

Fig.8.13 – THE TIME SHIFT PRINCIPLE

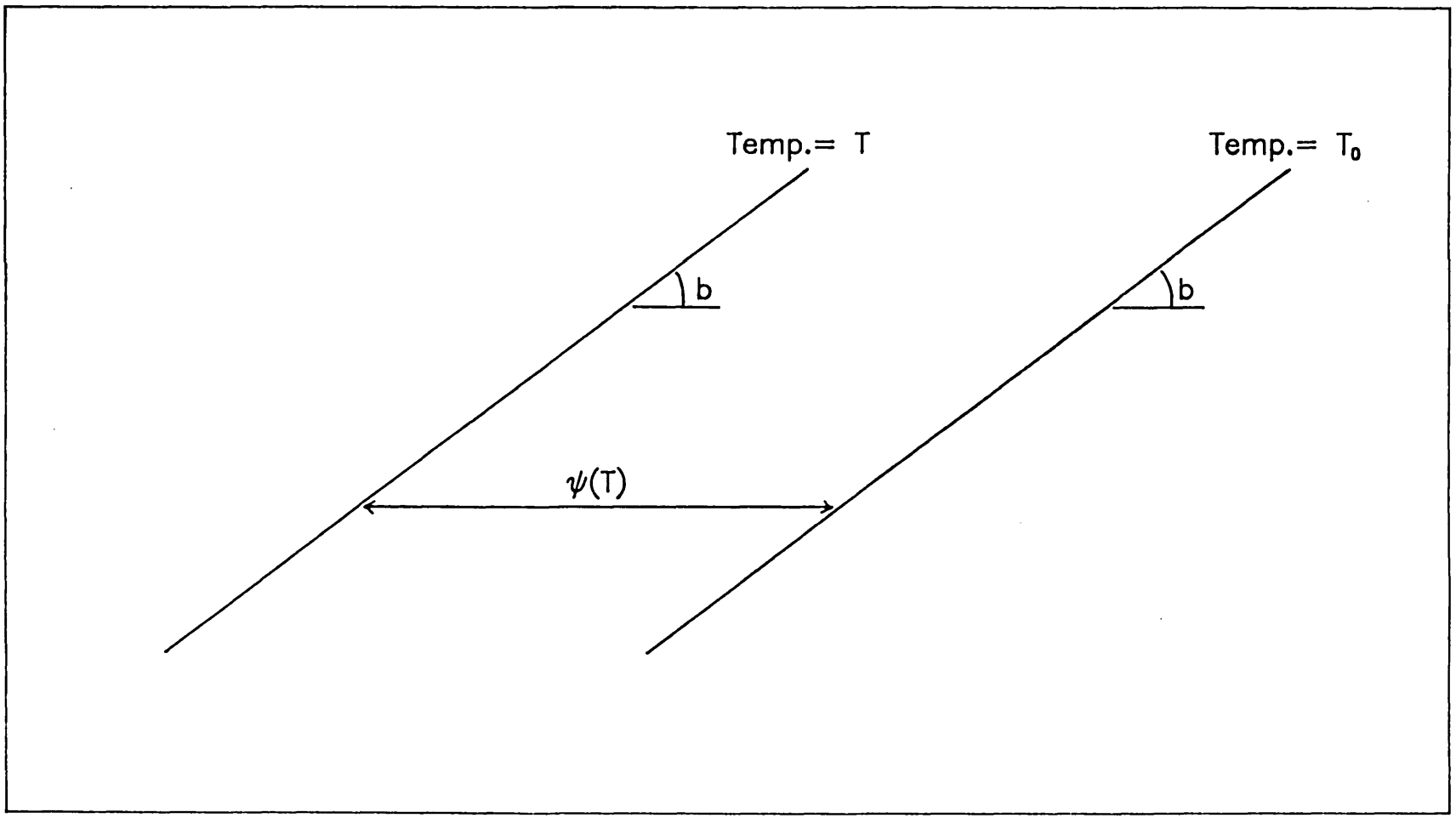

Fig.8.14 – OVERALL POWER LAW RELATIONSHIP – PREHEAT TEMP.= 635°C

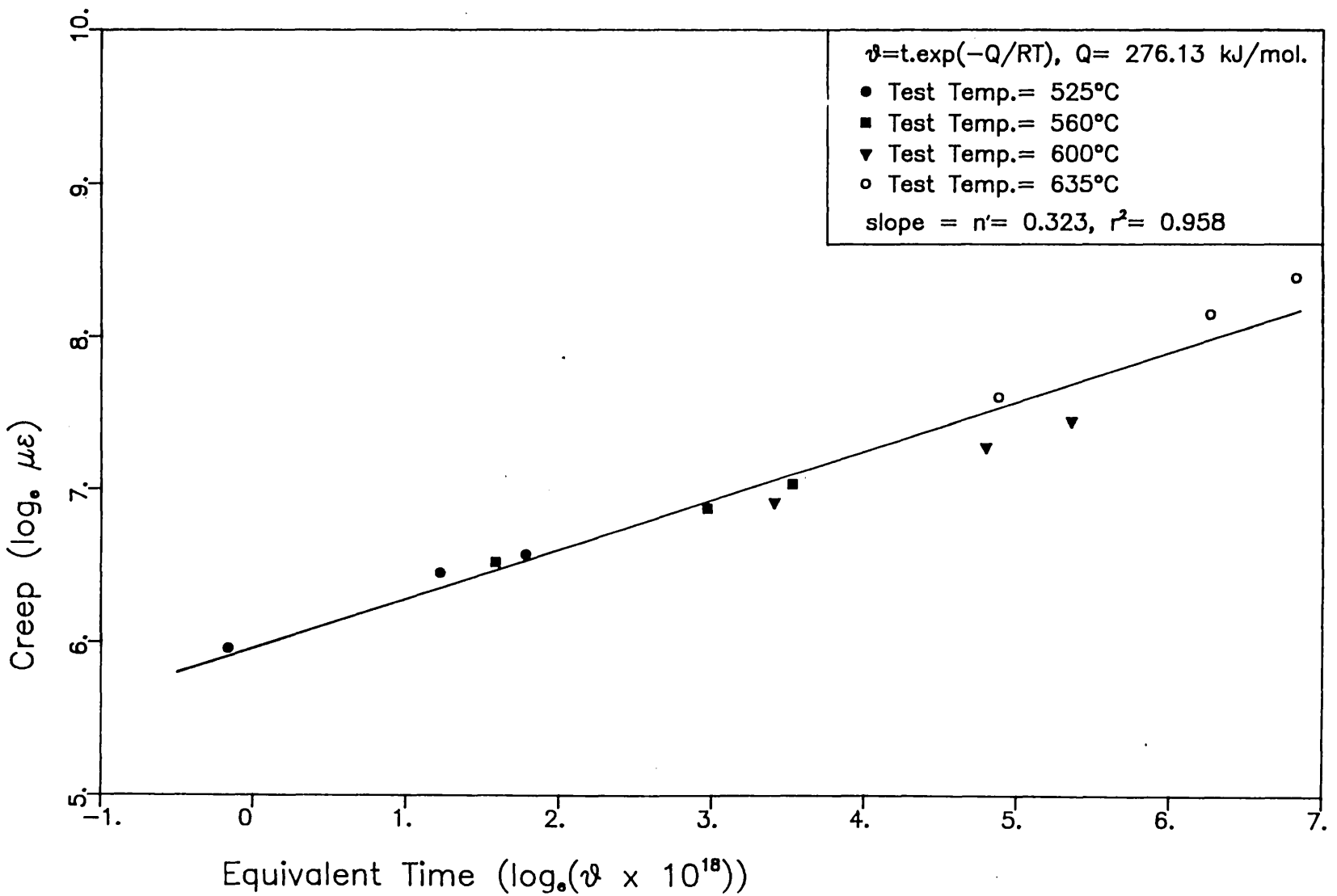

Fig.8.15 – OVERALL POWER LAW RELATIONSHIP – PREHEAT TEMP.= 635°C

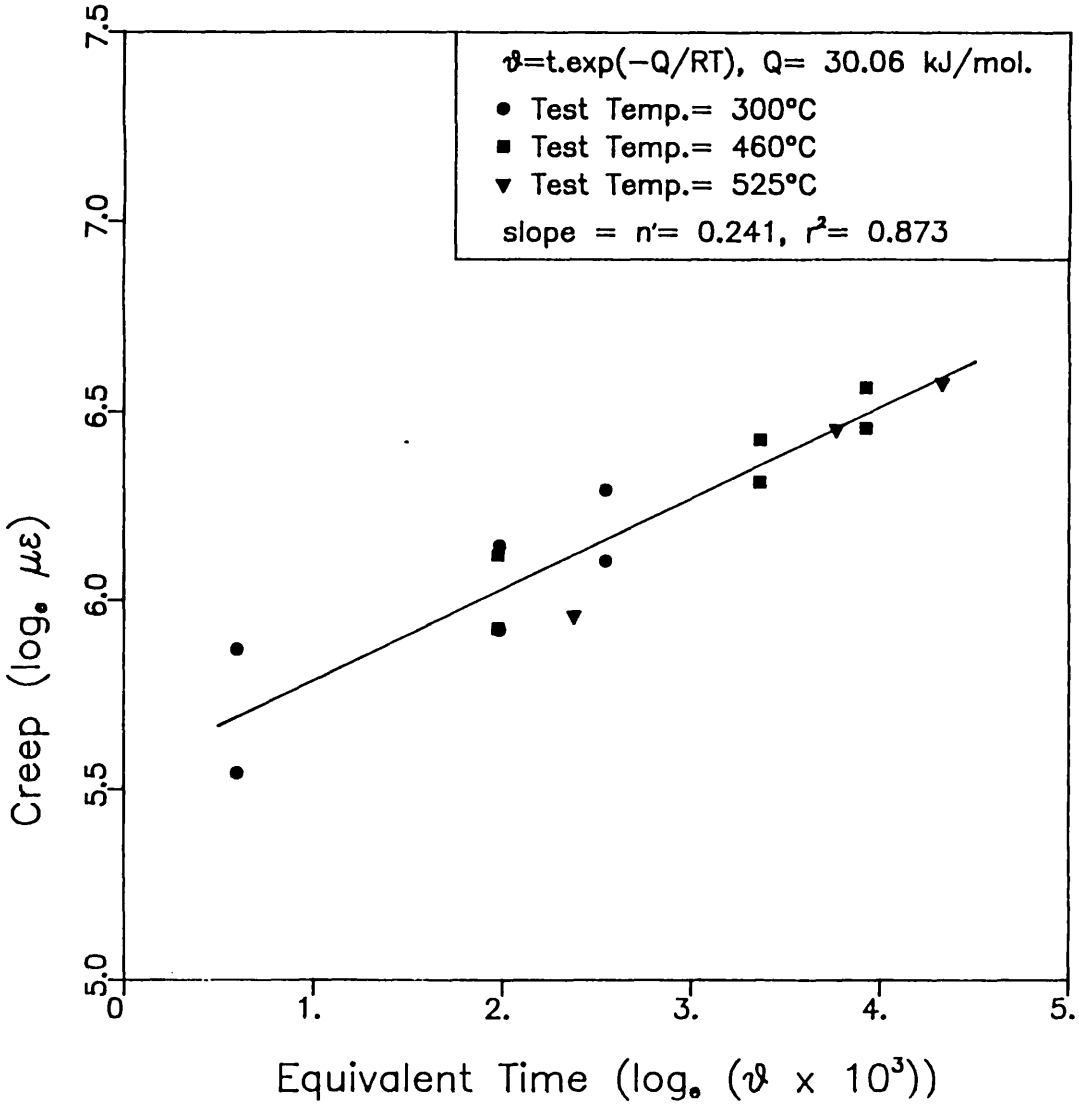

Fig.8.16 – OVERALL POWER LAW RELATIONSHIP – PREHEAT TEMP.= 560°C

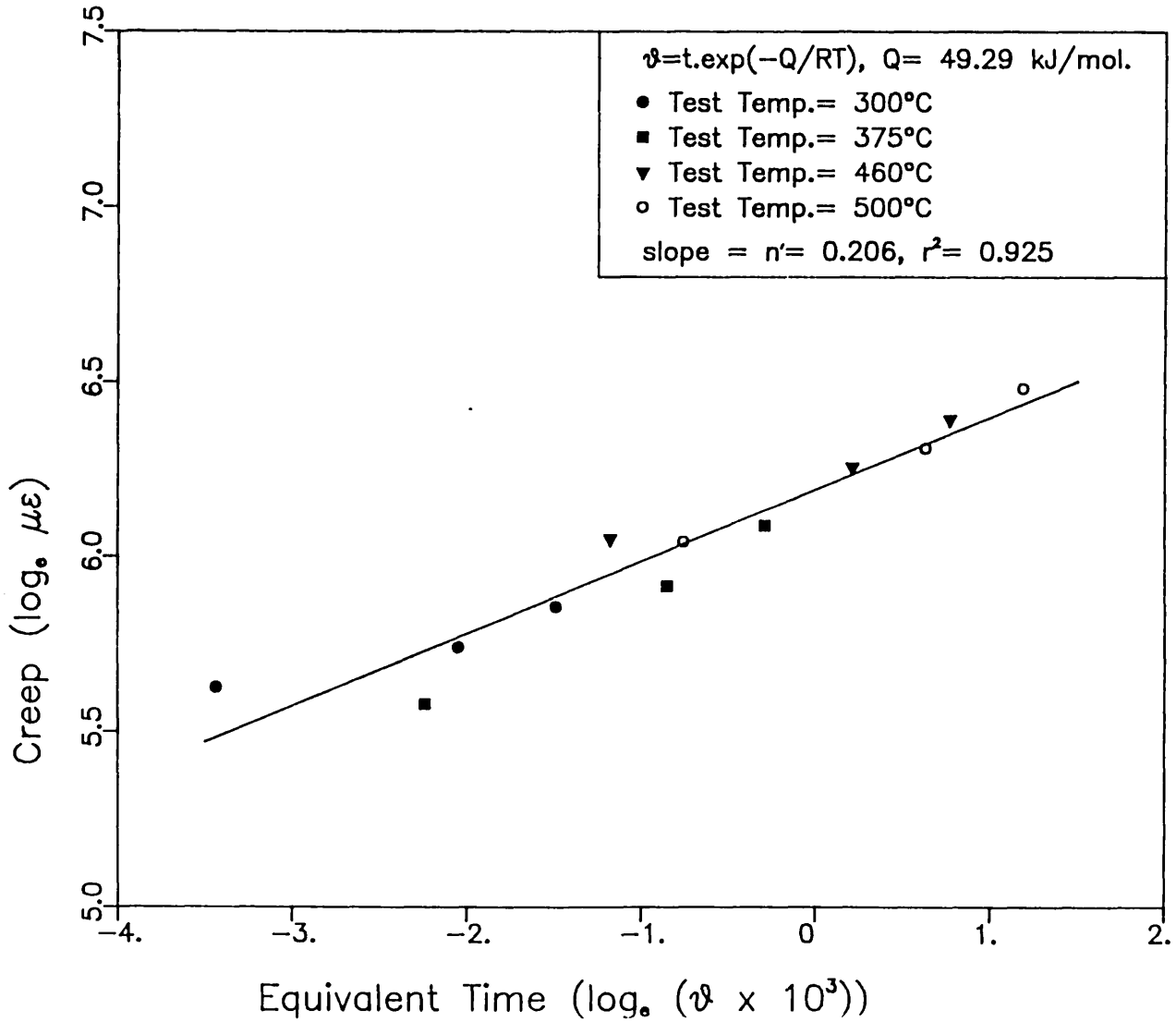

Fig.8.17 – OVERALL POWER LAW RELATIONSHIP – SERIES I

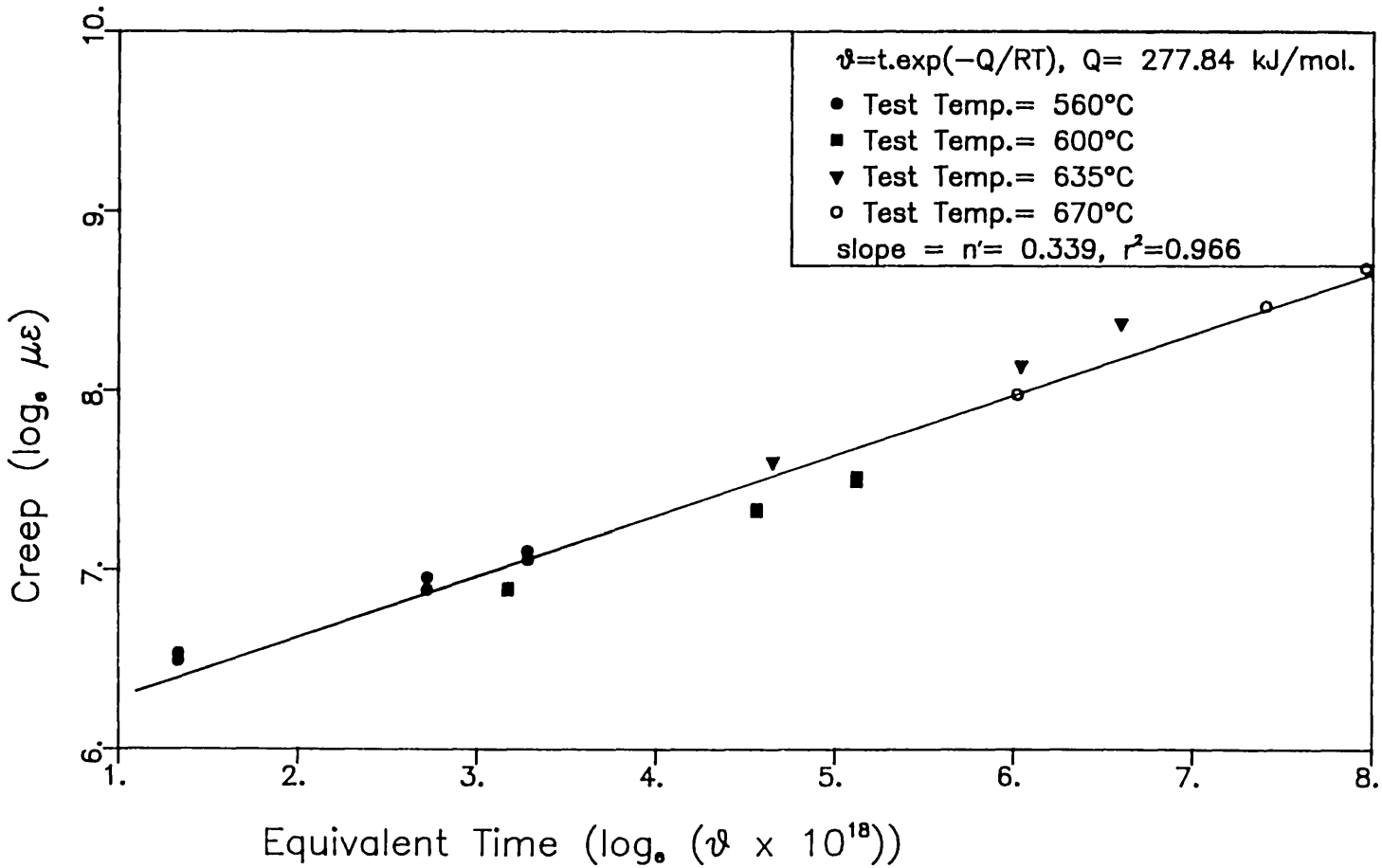

Fig.8.18 – OVERALL POWER LAW RELATIONSHIP – SERIES I

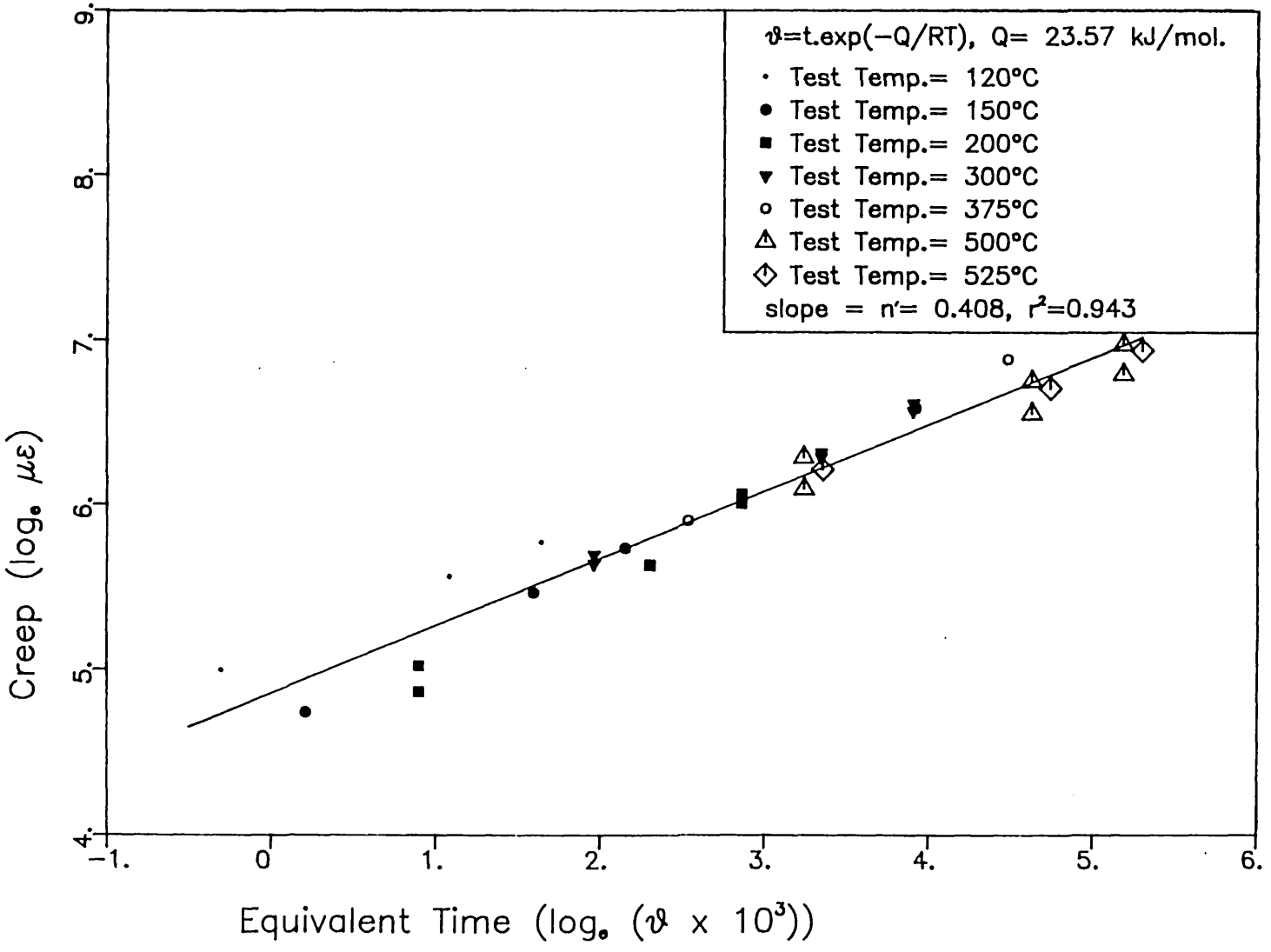

Fig.8.19—PREDICTION OF CREEP AT 560°C BY TIME—TEMPERATURE EQUIVALENCE

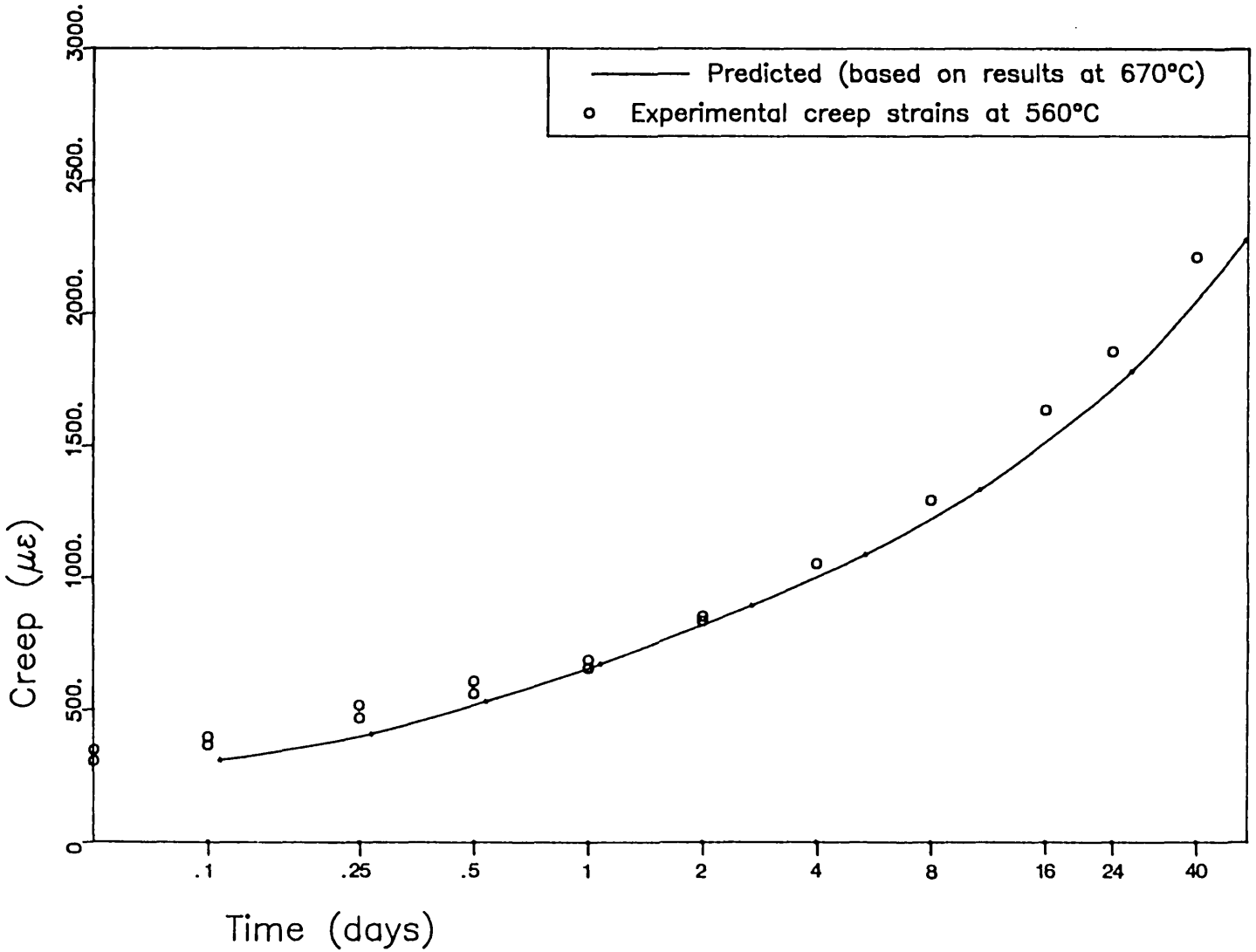

Fig.8.20—PREDICTION OF CREEP AT 525°C BY TIME—TEMPERATURE EQUIVALENCE

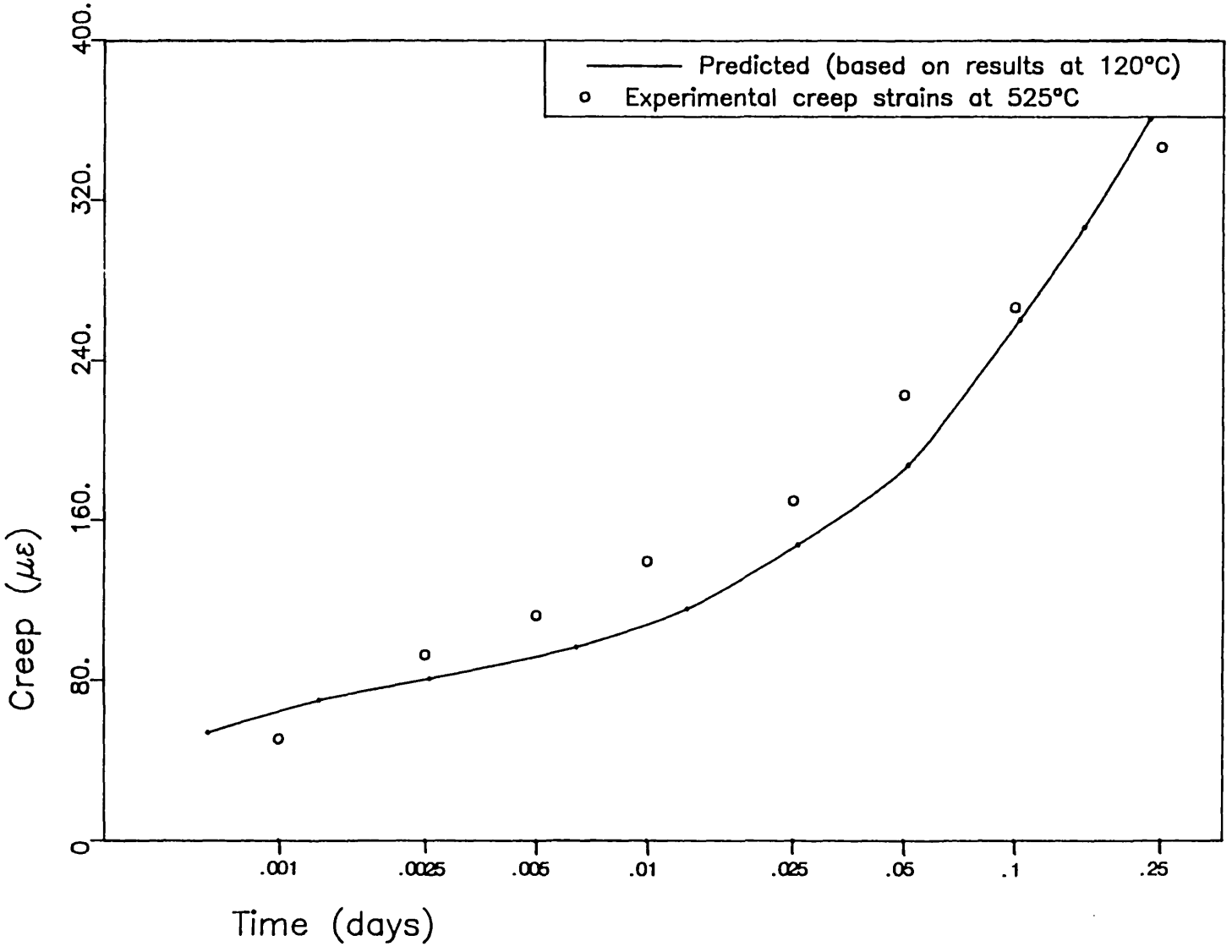

Fig.8.21—PREDICTION OF CREEP STRAINS BY UNCOUPLED FUNCTIONS METHOD

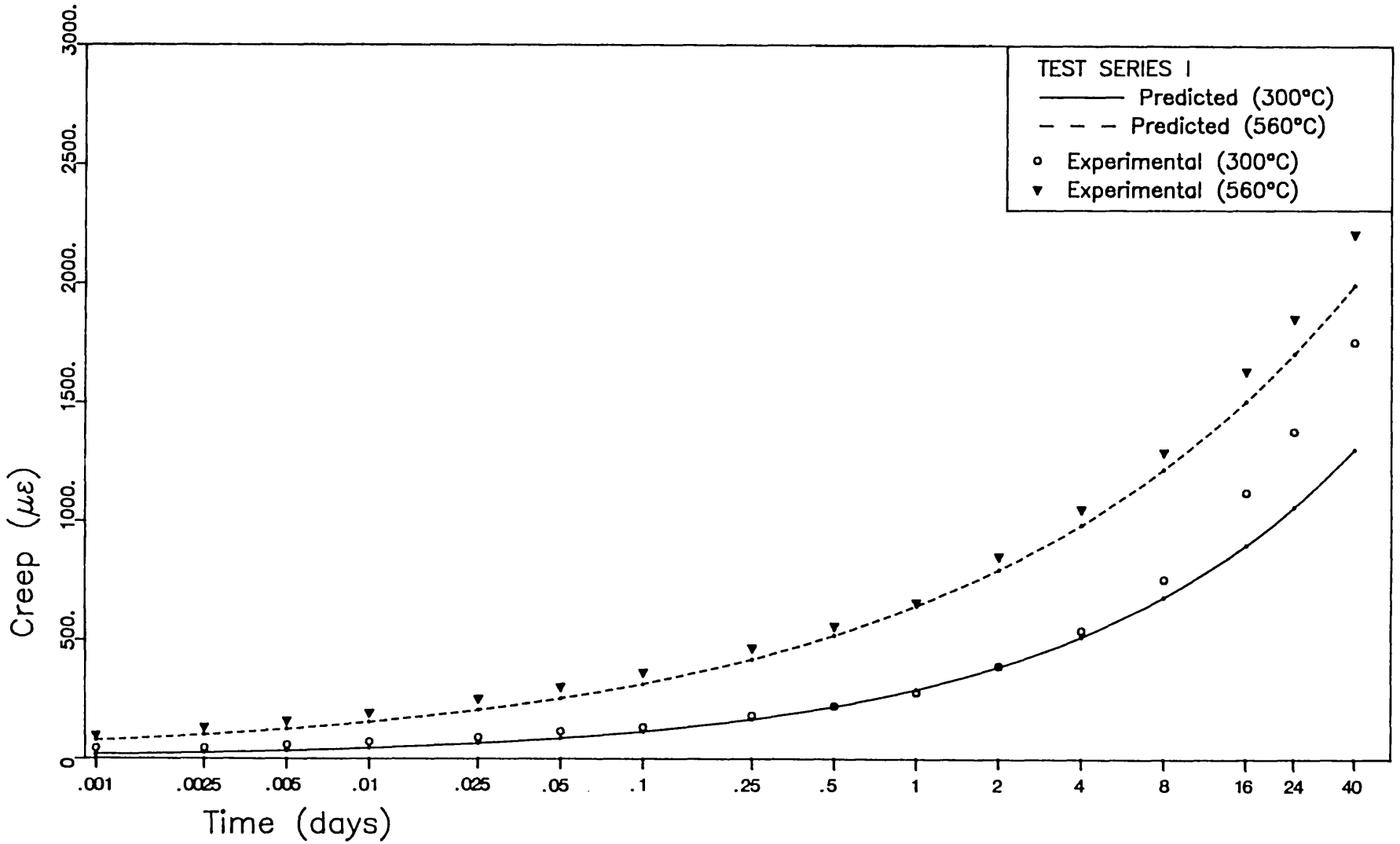

Fig.8.22–PREDICTION OF 1–DAY CREEP BY UNCOUPLED FUNCTIONS METHOD

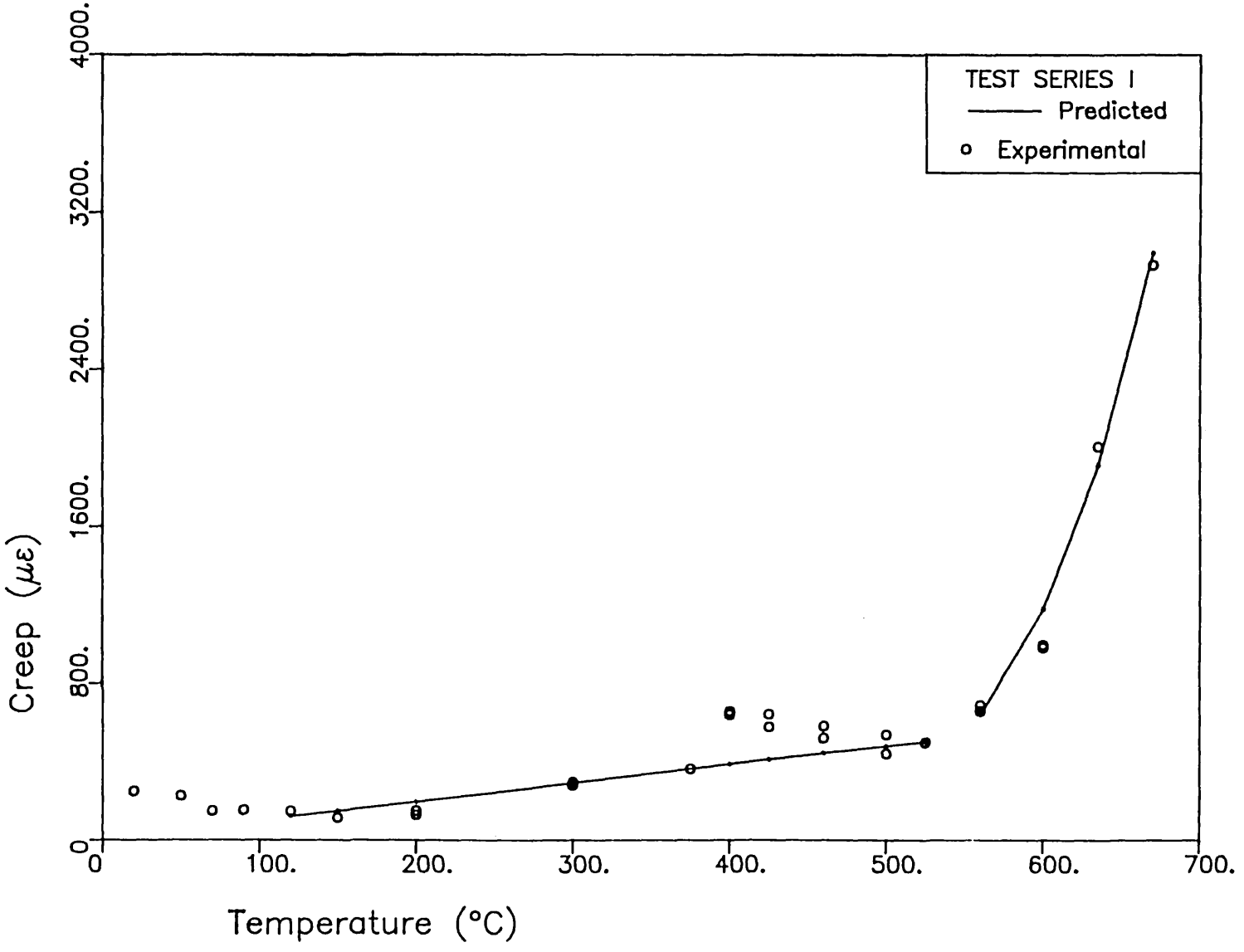

CHAPTER 9 - MICROSTRUCTURAL INVESTIGATIONS

Two kinds of investigations are reported in this chapter, namely silicate polymerization tests and scanning electron microscopy. Both kinds of tests were used to elicit information at the microstructural level of hardened cement paste, the former being chemical in nature while the latter physical.

PART I - SILICATE POLYMERIZATION TESTS

9.1. THE POLYSILICATE INDEX

The procedure for carrying out the polysilicate tests has been described in Section 3.4.3. If the spectrophotometer readings are plotted against time, the shape of the resulting reaction curves will give an indication of the degree of polymerization in the original silicate sample. For example, of the two curves shown in Figure 9.1, the sample heated to 460°C shows very little additional complexing beyond 300 seconds, whereas the one heated under load to 120°C does. The absolute absorbance values of the 2 samples should not be compared, since they merely reflect the amount of silicate dissolved by the methanolic HCl. Parrott has found that silicates in hardened cement paste with a degree of condensation of four or less make only a small contribution to the silicate complexed after 300 seconds (127, 134). Hence, the additional complexing beyond 300 seconds would be due mainly if not only to the complexing of the polysilicate fraction of the silicic acid, having a degree of condensation greater than four. Therefore the polysilicate index to be used in this investigation was chosen as the proportion of silicate not complexed by 300 seconds, which was the index used by Parrott himself (127). It must be emphasised that this is merely a convenient index suitable for making comparisons between samples. Day (40), who used a method similar to this, chose the proportion of silicate not complexed after 780 seconds as his index. He has also drawn attention to the difficulty of making quantitative comparisons between investigators.

The definition of the polysilicate index in the above fashion gives rise to the problem of defining the end point of the complexing reaction. In some cases, it seems fairly obvious that all the silicate has been complexed by 35 minutes. In other cases, especially where the proportion of polysilicate is high, the complexing reaction is clearly not complete by 35 minutes. These two cases could be exemplified by the curves in Figure 9.1. For the latter case, the end point is defined using a technique suggested by Day (40), who calculated the rate of change of absorbance at different times and found a linear relationship between complexing time and absorbance rate when plotted in logarithmic scale as shown in Figure 9.2, for the highly polymerized sample of Figure 9.1. This implies a power law relationship between absorbance rate and time of the form

$$\dot{a} = kt^n \qquad (9.1)$$

$$\text{or } \log_e(\dot{a}) = \log_e k + n \log_e t \qquad (9.2)$$

where a is the absorbance value

t is time

and k and n are constants, obtained from the regression line between the logarithms of absorbance rate and time.

The linear relationship is extrapolated to a value of absorbance rate small enough to consider that complete reaction has taken place, and the corresponding time determined. In our case, a change of 1×10^{-4} units/minute was deemed sufficiently small. Equation (9.1) was integrated to give the relationship between absorbance and time, the constant of integration being evaluated from the absorbance value at 35 minutes. The absorbance at the time when the reaction is deemed to have ceased can then be easily calculated. The polysilicate index was defined as the percentage value given by

$$P = \frac{a_{ult} - a_{300}}{a_{ult}} \times 100 \qquad (9.3)$$

where a_{ult} is the absorbance at the end of reaction and

a_{300} is the absorbance at 300 seconds.

9.2. APPROACH TO ANALYSIS OF RESULTS

The results of the polysilicate tests are presented in Table 9.1. The value tabulated is the polysilicate index, P, defined as above. The number of tests per condition range from 3 to 1, although in most cases at least 2 tests have been performed and the results found to be repeatable.

The object of the investigation was to study effects of age, temperature and load on the degree of polymerization. Furthermore, a correlation was sought between creep and microstructural changes, particularly those that reflect processes of stabilization (40, 110). Stabilization is here considered to be a phenomenon whereby the paste structure assumes a more stable configuration, in that it reduces the potential for subsequent time dependent strain.

One of the parameters considered was, of course, the degree of polymerization. However, due to the unsealed condition of the specimens, they experienced moisture loss during testing, which also may have had a stabilizing effect on the paste structure. Hence the percentage weight loss, which reflects moisture loss, was also investigated as an index of stabilization.

9.3. FACTORS AFFECTING THE DEGREE OF POLYMERIZATION

The effect of age on the degree of polymerization is shown in Figure 9.3 for ages ranging from 15 to 37 weeks. In view of the small variation indicated during this period, it was decided to consider that age had a negligible effect on the degree of polymerization within the above period of testing. The polysilicate index at 20°C was taken as the average of the values for these 4 ages. Hence, although various specimens have been treated to temperature and load regimes at different ages, it can be considered that their initial degrees of polymerization were reflected by the same polysilicate index of 7.29. It must be appreciated that all these specimens were stored in a humidity room for 14 weeks at 100% RH after casting and then air dried at around 60% RH after that. This may perhaps be the reason why the

degree of polymerization did not show a significant increase beyond 14 weeks, as found by other investigators (40, 93, 127), whose specimens were saturated throughout. The process of drying at 60% RH may not have had much effect on the polysilicate content of these well hydrated pastes; this parallels a result reported by Bentur et al (22) for a 90-day old C_3S paste subjected to shrinkage at 53% RH.

The effects of temperature and load are shown in Figure 9.4. It must be appreciated that load and temperature regimes would have been applied for differing periods as a result of constraints imposed by the method of creep testing itself. However, all specimens would have been subject to the given temperature or load for a period of not less than 7 days; changes in the degree of polymerization were expected to have levelled out over such a period.

Temperature has caused an increase in the polysilicate index up to 90°C. A comparison with Day's results for young specimens (43) indicate a similar qualitative trend in the temperature range involved. (See Figure 2.27). It is not very realistic to make quantitative comparisons, since his polysilicate descriptor was defined differently; furthermore, his thermal treatments were carried out for only 2 days and that too on saturated specimens. Nevertheless, there is a remarkable coincidence in the results at 20°C and around 50°C, but a significant divergence at 90°C.

The polysilicate index in this present investigation shows a plateau from 90°C to 120°C and then a steady decline until 460°C, where it seems to have reached an absolute minimum. It must be borne in mind that a greater number of temperature points would have given a clearer picture of the trends, especially above 120°C. However, from the evidence available it seems that unsealed cement paste undergoes an increase in the degree of polymerization with thermal treatments from 20°C to 90°C, similar to the increases reported by Day and Gamble (43) and Parrott (127) for saturated specimens. However, even at 90°C the increase is not as pronounced as for the latter specimens. Beyond 120°C, the unsealed cement paste undergoes depolymerization, as qualitatively detected by Piasta et al (138).

The broken lines in Figure 9.4 show the effect of heating the specimens under a stress/cold strength ratio of 0.11, i.e. the changes in polymerization of the Series III specimens. The evidence indicates that, at least in the temperature range 50°C to 300°C, the loading of specimens during heating enhances the degree of polymerization. (The difference in specimen size between loaded and unloaded samples was not expected to cause any significant discrepancy). This would tend to add weight to the view that load makes an actual contribution to microstructural change, as opposed to being merely a directional influence. The difference between the solid and broken lines in Figure 9.4, which is an indication of the contribution of load alone to the increase in degree of polymerization, has been plotted as the solid line in Figure 9.5. This indicates that load corresponding to a stress/cold strength ratio of 0.11 has its greatest effect at 120°C.

A few Series I and II specimens, which were loaded (also at a stress/cold strength ratio of 0.11) after heating to temperature, have been tested for polysilicate index, and the results shown in Figures 9.4 and 9.5. It is unfortunate that more specimens were not tested because the results are quite interesting. Above 460°C, loading has hardly any effect on the degree of polymerization, at which temperatures the paste is largely depolymerized anyway. At 300°C, the effect of loading for 6 weeks after heating for around 4 weeks is the same as loading during heating for around 3 weeks. It should be noted that Series II specimens give the same results as the Series I specimens at the corresponding pre-heat or upper temperature of exposure. This is true for pre-heat temperatures of 300°C as well as 460°C. (See Table 9.1). At 120°C, the two Series II specimens tested showed a greater degree of polymerization than the Series III specimen, which was heated under load. This seems to indicate that loading after thermal treatment causes a greater degree of polymerization than loading during heating. Undoubtedly more experimentation is required to substantiate this, since the result would seem to be contrary to the expected trend.

9.4. DEPENDENCE OF BASIC CREEP ON MICROSTRUCTURE AT LOADING

Attention has already been drawn to the correlation found by other authors between time dependent strain and the degree of polymerization at the start of drying or loading. The degree of polymerization has been considered, therefore, as an index of the stabilization of cement paste, affecting the potential for subsequent time-dependent strain. We shall seek to establish whether this, in fact is the case for basic creep in some Series II specimens, which were all loaded at 300°C after being pre-heated at temperatures varying from 300°C to 635°C.

Before this is done, the effect that temperature can have on the creep response should be clearly understood. Firstly, there would be an Arrhenius thermal effect that would cause an increase in creep rate with increasing temperature. Strictly speaking, this effect can be isolated only for specimens pre-heated to some equal upper temperature, but creep loaded after slow cooling to various lower temperatures.

Secondly, the exposure to temperature would induce structural changes in the material. One obvious change would be a reduction in strength (especially if we consider temperatures above 300°C), which would cause an increase in creep potential. However, the Series II basic creep results in Figures 7.10 to 7.13 show that pre-heating to higher temperatures before creep loading at a lower temperature actually reduces the creep potential. In fact, if the creep responses are normalized with respect to an equal stress/hot strength ratio, it is found that these responses are lower, the higher the pre-heat temperature. (When making the above normalization, it is assumed that the hot strength is that which corresponds to the highest temperature of exposure - see Figure 5.8).

The above evidence indicates that another kind of structural change, which causes a stabilization of the paste (in that it reduces the creep potential), is induced by exposure to temperature. It is this microstructural stabilization that we are seeking to isolate and find an index for.

The Arrhenius thermal effect can be eliminated if the analysis is performed on creep data obtained at the same temperature, which in this case is 300°C. The effect of strength reduction can be eliminated by normalizing the creep strains obtained at 300°C on the basis of an equal stress/hot strength ratio (in this case chosen as 0.11); the hot strengths at the various pre-heat temperatures are used for this normalization. The resulting differences in creep strains would be due to the variation in microstructural stabilization induced at the different pre-heat temperatures. The above ideas are schematically represented in Table 9.2.

Both the raw 1-day creep data at 300°C as well as those normalized with respect to a stress/hot strength ratio of 0.11 are plotted in Figure 9.6 against the corresponding values of P obtained for the various pre-heat temperatures. The correlation obtained is the reverse of a stabilization type correlation with temperature - i.e. higher temperatures of exposure give lower creep but also lower values of P.

On the other hand, it is instructive to plot these 1-day creep strains against the percentage weight loss, as shown in Figure 9.7. A definite stabilization-type correlation can be seen, with higher temperature giving lower creep for higher percentage weight loss. Some care should be exercised in making very definite conclusions, since many of the points are clustered in a fairly narrow band of percentage weight loss values. However, it does seem that percentage weight loss is a better stabilization index for unsealed cement paste than is the degree of polymerization, at least in the temperature range 300°C to 635°C.

It should be appreciated that the above discussion does not actually isolate the cause of microstructural stabilization; it merely suggests that percentage weight loss can be a reasonable index for the same. It is likely that this index reflects the role of moisture loss (both physically held and chemically combined) in reducing the creep potential. It must be borne in mind however, that this would be only one of the many effects of moisture loss; for example, loss of moisture would also cause weakening of the structure, leading to a reduction in

hot strength and an increase in creep potential at temperatures above 300°C and perhaps even at some lower temperatures.

9.5. DISCUSSION - STABILIZATION PROCESSES AT ELEVATED TEMPERATURES

Age (40, 93, 124), Temperature (43, 127), Drying (22) and Load (43, 110) have been found to produce stabilization in hardened cement paste, thereby reducing the potential for subsequent time-dependent strains. This effect of stabilization has been observed on specimens in both saturated as well as unsealed conditions. In all the above cases, however, thermal treatments have been applied under saturated conditions and the maximum temperature did not exceed 95°C. The degree of silicate polymerization has been found to be a fairly good index of the stabilization processes under the above conditions (22, 43, 127).

In the present investigation however, all tests were performed under unsealed conditions and the temperature range was 20°C to 670°C. In order to detect any stabilization, measured creep strains had to be corrected for strength reduction and Arrhenius thermal effects. It was found that exposure to temperature did, in fact, cause stabilization, in addition and in opposition to the above effects. However, this stabilization was not reflected in the degree of polymerization, with temperatures above 120°C actually causing depolymerization of the paste. Percentage weight loss, on the other hand, was found to be a better index of stabilization due to temperature, at least within the temperature range 300°C to 635°C.

However, more comparative studies should be undertaken with regard to percentage weight loss vis-a-vis degree of polymerization being a suitable index for microstructural stabilization in unsealed hardened cement paste. Such studies should encompass stabilization processes induced by load and also stabilization processes that take place during time-dependent strains such as creep and shrinkage.

PART II - SCANNING ELECTRON MICROSCOPY

These tests were undertaken with the intention of finding microstructural correlations with specific macro-level phenomena observed in other tests.

9.6. PROPORTION AND SIZE OF UNHYDRATED GRAINS

It was reported in Section 6.2 that both the magnitude of the strains obtained on heating as well as the temperature where reversal of contraction took place depended on the w/c ratio of the paste. It was also suggested that the relative proportions of hydrated paste to unhydrated grains were responsible for this behaviour.

Figure 9.8 shows four back scattered images of polished surfaces. Figures 9.8a to 9.8c have been taken at the same magnification of 400, and show unheated specimens of w/c ratios 0.225, 0.30 and 0.375 respectively. The white areas in the figures are unhydrated grains while the light grey areas immediately surrounding them are shells of hydrated paste.

Although some quantitative analysis would need to be performed before definite conclusions are reached, it seems that both the quantity and size of unhydrated grains increase from the 0.375 w/c ratio paste to the 0.225 w.c ratio paste; conversely, the thickness of the hydrated paste seems to decrease from Figure 9.8c to 9.8a. This then confirms the suggestion made in Section 6.2 regarding the effect of differing w/c ratios on the relative proportions of hydrated paste to unhydrated grains; it further indicates that a lower w/c ratio will result in larger grains of unhydrated material.

Figure 9.8d shows the way such pastes are likely to behave when heated. This is an image of a paste of w/c ratio 0.3 which has been heated to 525°C and resin impregnated soon after being cooled back to room temperature; hence post-cooling phenomena can be considered to have been eliminated. Although the smaller grains seem to be integral with their surrounding layers of hydrated material, the large grain on

the right hand side of the picture has been separated from its surrounding layer. Although trend reversal in contraction upon heating is shown only at 635°C (after a 'plateau' from 560°C to 635°C) for this paste of w/c = 0.3 (see Figure 6.4), it may be that cracking around unhydrated grains due to thermal incompatibility starts at even lower temperatures if the grain size is large enough. The above trend reversal is probably due to the increased expansion of the grains, following such cracking. Coupled with the evidence from Figures 9.8a to c, this suggests that pastes of lower w/c ratio experience earlier temperatures of thermal strain reversal, not only because of a larger proportion of unhydrated grains to hydrated paste, but also because the unhydrated grains are larger in size. It should be pointed out that this microstructural evidence confirms the ideas proposed by Lea and Stradling (92) over half a century ago.

9.7. CALCIUM HYDROXIDE FORMATIONS

Section 5.3 describes the remarkable phenomenon of specimen disintegration on post-cooled exposure to atmosphere after heating to temperatures above 400°C. This has been attributed to disruptive expansion caused by the rehydration of dissociated Calcium hydroxide.

In order to examine this phenomenon at a microstructural level, fracture surfaces of the 0.3 w/c ratio paste were examined using secondary electron images. These were obtained (a) before heat treatment, (b) soon after cooling back from a 7 day heat treatment at 600°C and (c) after several weeks' exposure to air subsequent to the above heat treatment; these images are shown in Figures 9.9a to 9.9c respectively.

The presence of $Ca(OH)_2$ is clearly indicated in Figure 9.9a by the fracture path having passed through cleavage planes in the hexagonal crystals, resulting in the striated appearance.

Although it is not possible to be conclusive, the $Ca(OH)_2$ formations in the bottom right hand side of Figure 9.9b seem to have ill defined edges, and may indicate that dissociation has taken place,

which would be the case in a sample examined soon after cooling back from a 7 day heat treatment at 600°C.

Figure 9.9c shows extensive cracking in the sample exposed to air after the heat treatment at 600°C. It is not possible however, to link this cracking with rehydration of dissociated $Ca(OH)_2$ on the evidence from this image alone.

In conclusion, it must be emphasised that the examination of Calcium hydroxide formations has been even less conclusive than the evidence from the back scattered images regarding the interaction of unhydrated grains and hydrated paste upon heating. However, both these areas could have potential for further investigation, as attempts to link macro-level observations with microstructural causes.

Age (wks)	15	21	29	37
Polysilicate Index, P(%)				
(1)	7.18	6.59	6.40	8.34
(2)	7.10	7.50	6.74	8.42
Average	7.14	7.05	6.57	8.38

(a) EFFECT OF AGE DURING STORAGE AT 60% RH AND 20°C ON POLYSILICATE INDEX.

Temperature (°C)	50	90	120	300	460	560	635		50	90	120	300
Unloaded	✓	✓	✓	✓	✓	✓	✓					
Loaded									✓	✓	✓	✓
Polysilicate Index,P(%)												
(1)	10.33	10.86	10.41	6.64	1.33	1.13	1.34		14.26	16.93	18.22	10.23
(2)	10.30	10.74	10.90	6.56	1.33	1.13	1.35		14.14	16.95	17.98	10.00
(3)	10.09	10.03	10.32	6.18	1.09	1.12	1.13		13.15	17.35	17.23	8.72
Average	10.24	10.54	10.54	6.46	1.25	1.13	1.27		13.85	17.08	17.81	9.65

(b) EFFECT OF HEATING ALONE AND HEATING UNDER STRESS/COLD STRENGTH = 0.11 ON POLYSILICATE INDEX.

Preheat Temp (°C)	120	120	300	300	460	460	635
Test Temp. (°C)	50	90	120	300	300	460	600
Polysilicate Index, P (%)							
(1)	20.69	20.91	9.49	9.83	1.25	1.56	1.56
(2)	20.60			9.50	1.53		
Average	20.65	20.91	9.49	9.67	1.39	1.56	1.56

(c) EFFECT OF LOADING TO STRESS/COLD STRENGTH = 0.11 AFTER DIMENSIONAL STABILITY AT TEMPERATURE ON POLYSILICATE INDEX.

TABLE 9.1. RESULTS FROM POLYSILICATE INDEX TESTS.

Cause	Testing at Temperature	Exposure to Temperature	Exposure to Temperature
Effect	Arrhenius thermal effect	Strength reduction (in general)	Microstructural stabilization
Resultant Creep Potential	Increased	Increased (in general)	Decreased
Method of Elimination	Use equal test temperatures but different pre-heat temperatures	Normalize strains w.r.t. stress/hot strength ratio	

TABLE 9.2. ISOLATION OF FACTORS AFFECTING CREEP POTENTIAL.

Fig.9.1 – TYPICAL COMPLEXING CURVES

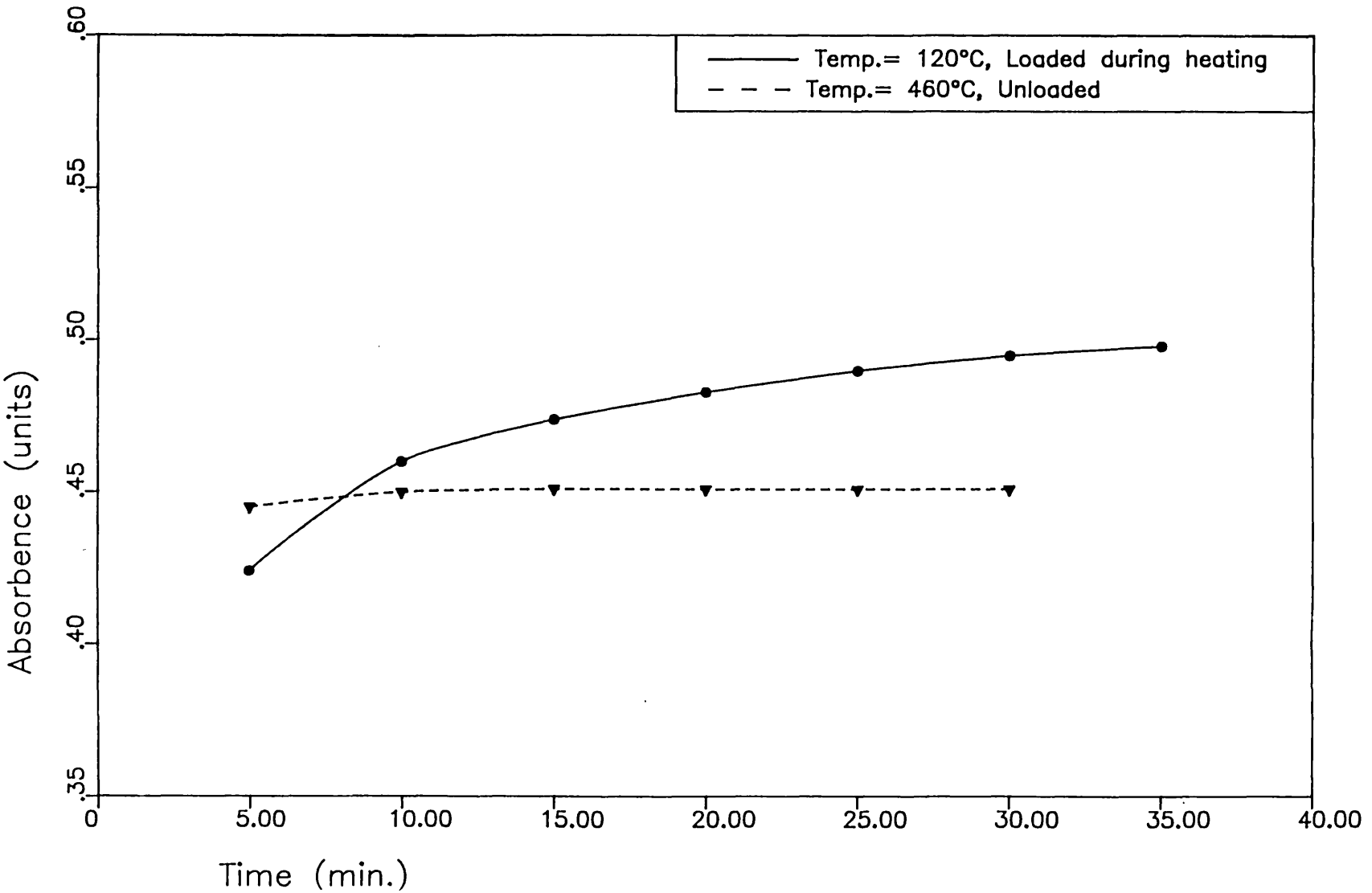

Fig.9.2—DETERMINATION OF COMPLEXING END POINT

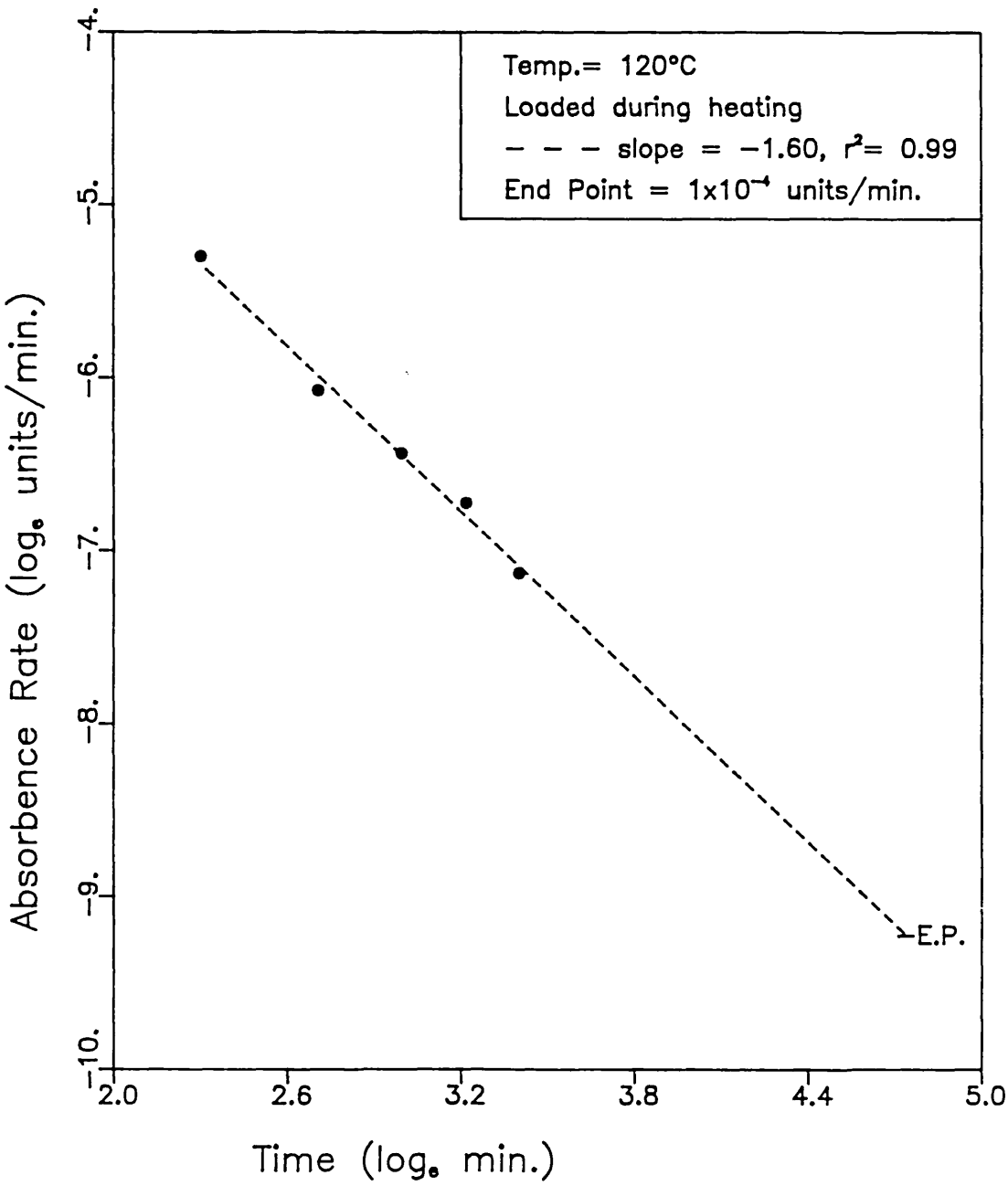

Fig.9.3 – POLYSILICATE CONTENT vs. AGE

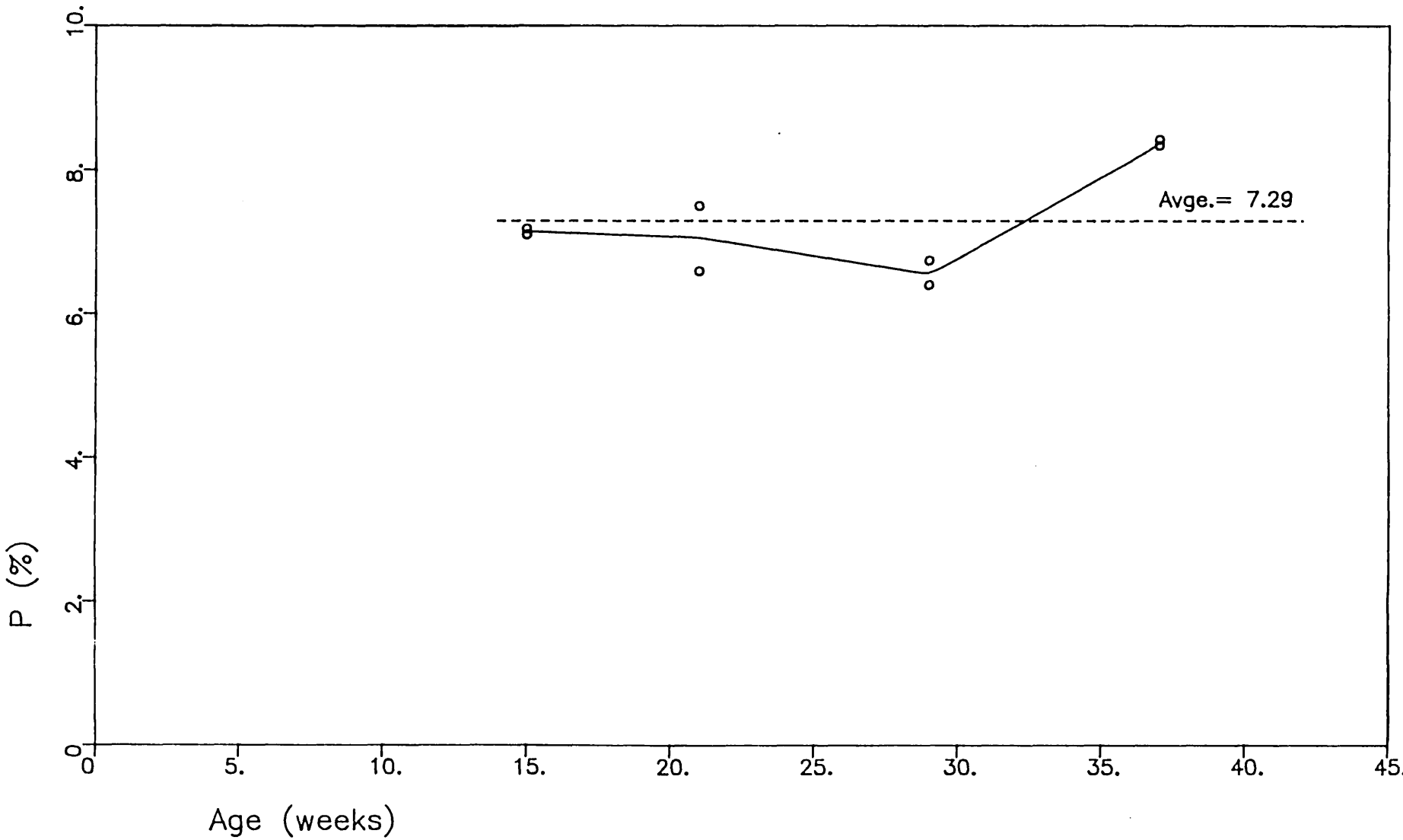

Fig.9.4 – POLYSILICATE CONTENT vs. TEMPERATURE

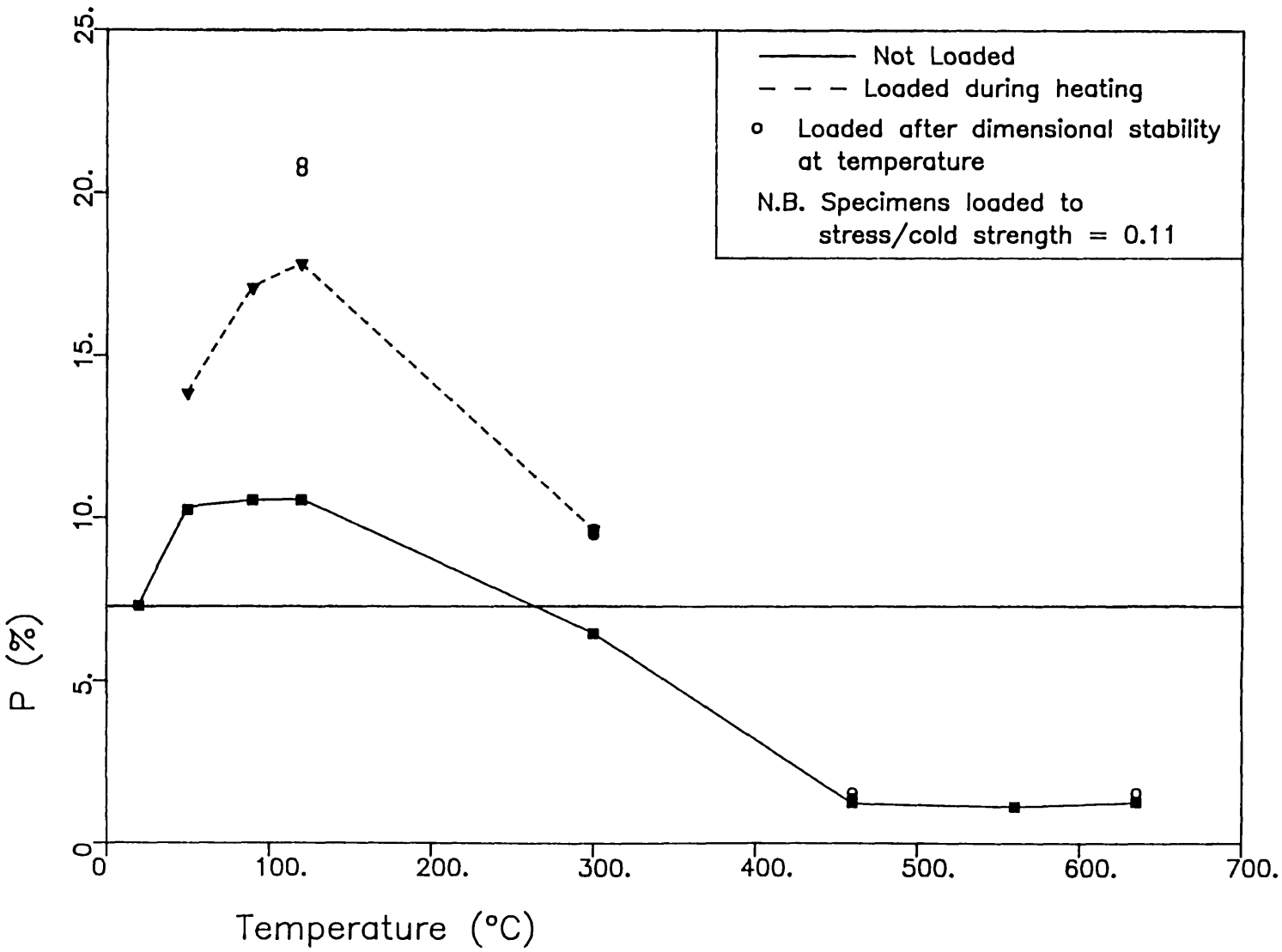

Fig.9.5 – CHANGE IN POLYSILICATE CONTENT DUE TO LOAD

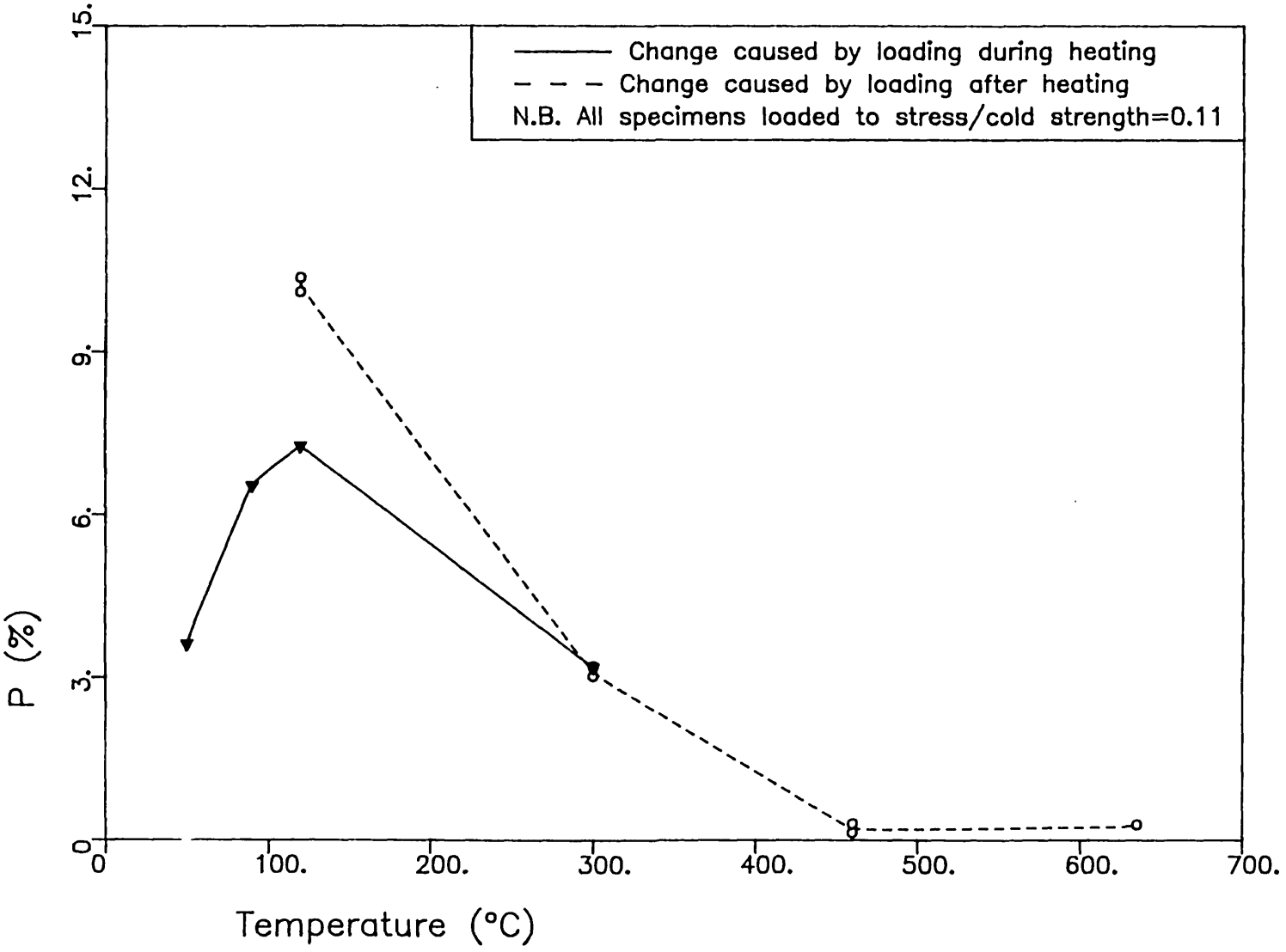

Fig.9.6 – 1–DAY CREEP STRAINS (AT 300°C) vs. POLYSILICATE CONTENT

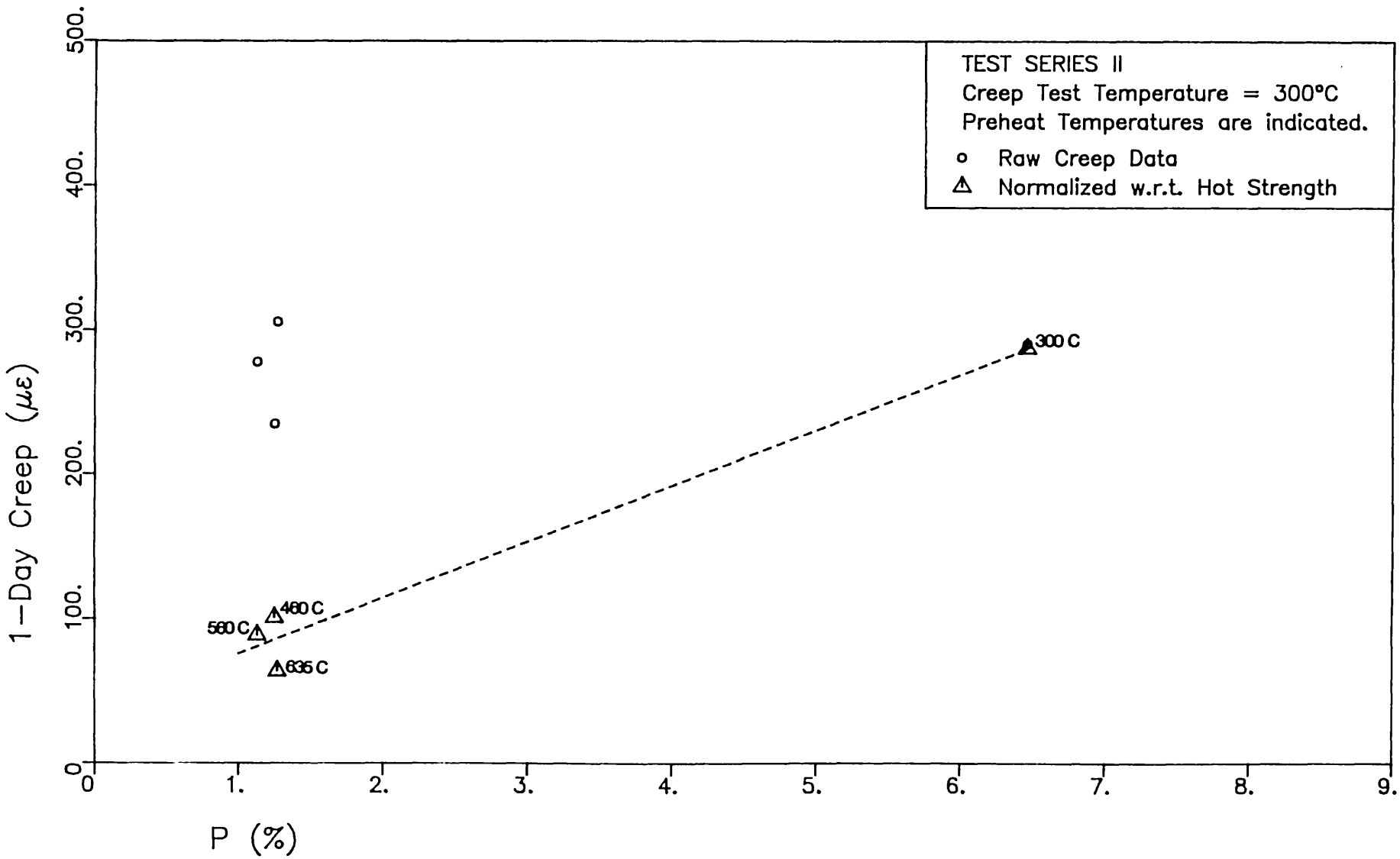

Fig.9.7 – 1–DAY CREEP STRAINS (AT 300°C) vs. WEIGHT LOSS

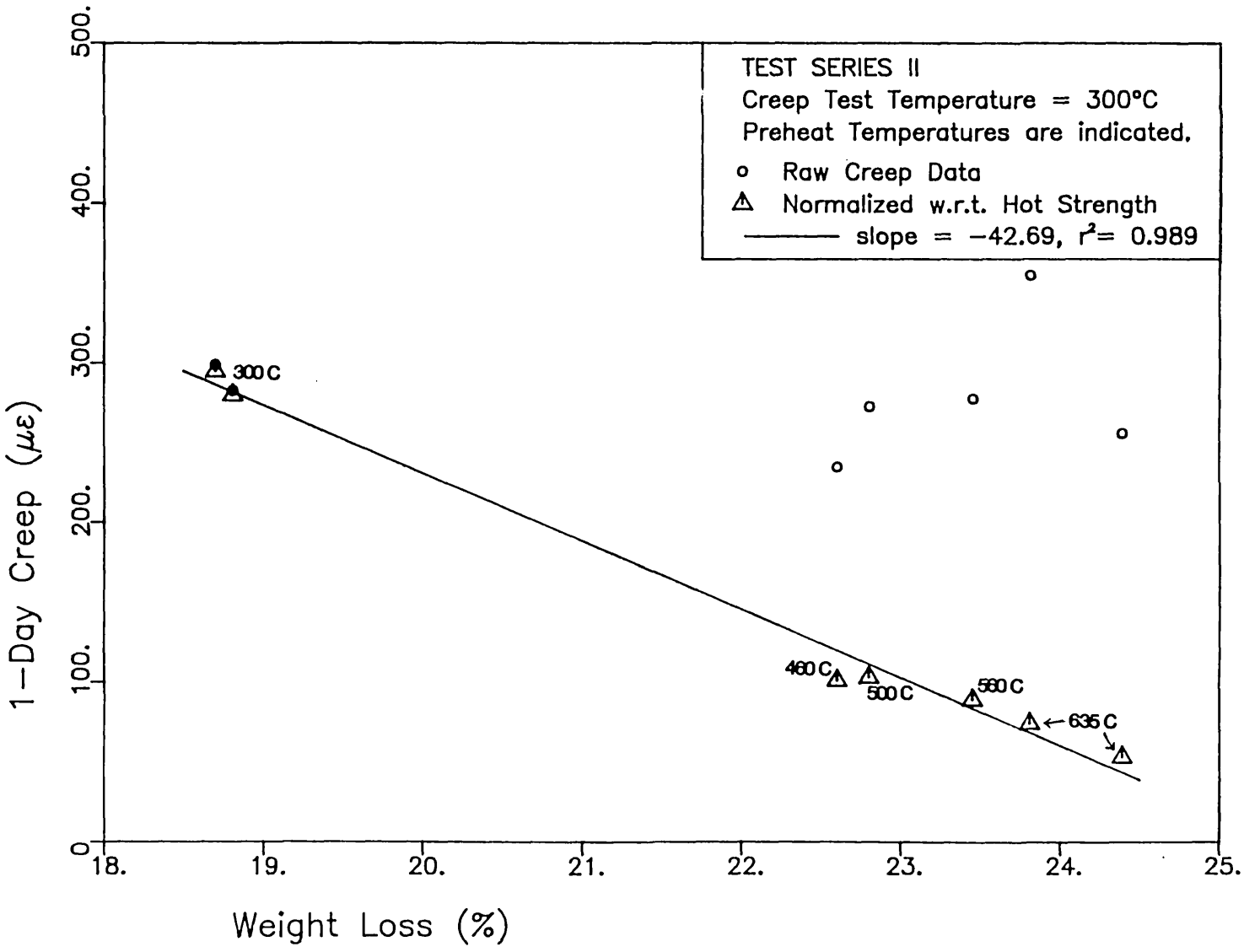

(a)

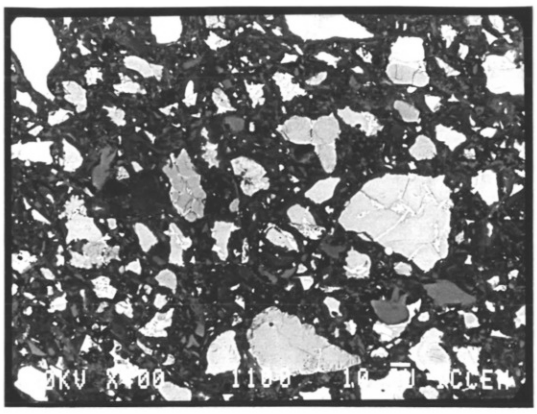

(b)

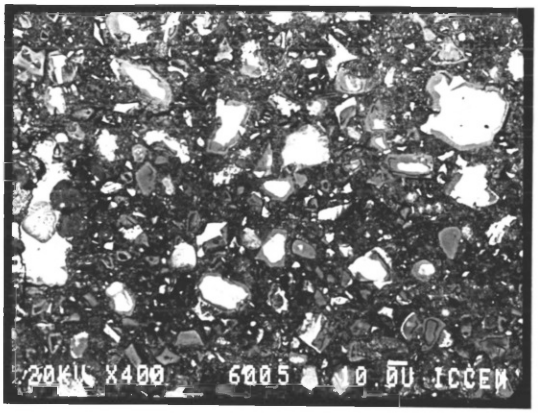

(c)

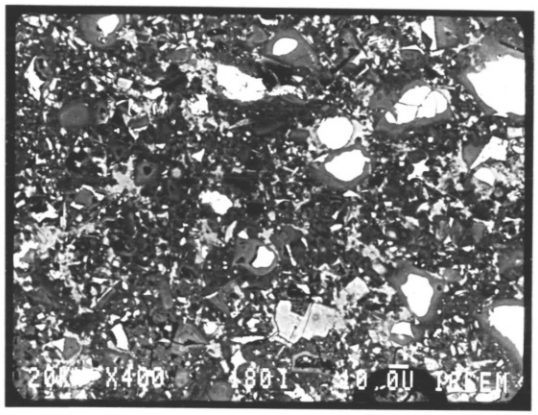

(d)

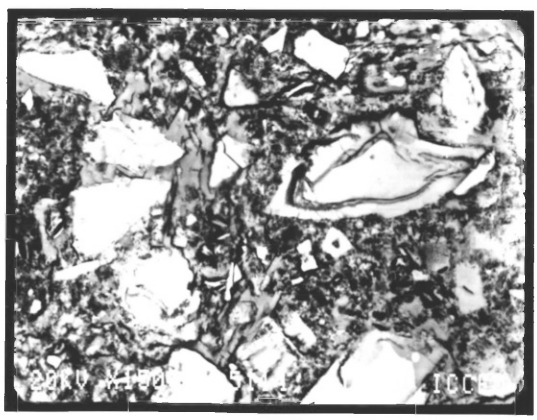

Figure 9.8 - PROPORTION AND SIZE OF UNHYDRATED GRAINS FOR OPC SAMPLES OF DIFFERING W/C RATIOS. (a)W/C=0.225,M=400x, (b)W/C=0.3,M=400x, (c)W/C=0.375,M=400x, (d)W/C=0.3, HEATED TO 525 C AND RESIN IMPREGNATED SOON AFTER COOLING, M=1500x.

(a) UNHEATED, W/C=0.3, M=4000x.

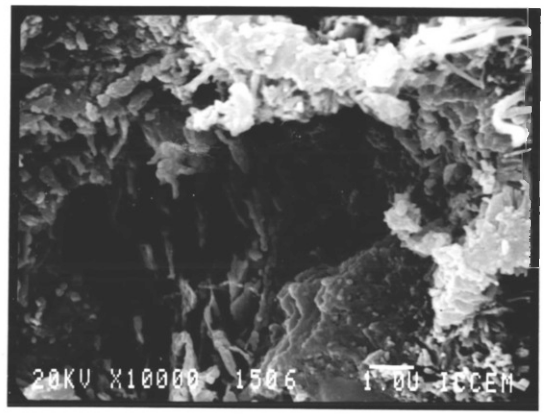

(b) HEATED TO 600 C & EXAMINED SOON AFTER COOLING, W/C=0.3, M=10000x.

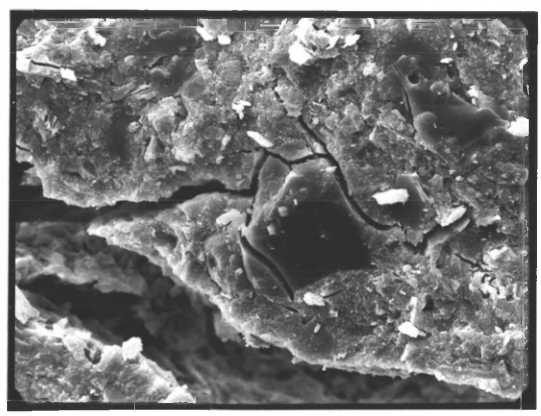

(c) HEATED TO 600 C & EXAMINED 3 WKS. AFTER COOLING, W/C=0.3, M=2000x.

Figure 9.9 - CALCIUM HYDROXIDE FORMATIONS AS AFFECTED BY HEATING TO 600 C AND SUBSEQUENT POST-COOLED EXPOSURE TO AIR.

CHAPTER 10 - MODELLING OF AGGREGATE-PASTE INTERACTION

10.1. OBJECTIVES

Thus far, this investigation has concentrated exclusively on the behaviour of hardened cement paste, for reasons specified in Section 3.1. The final stage of this thesis, however, looks at the modifying effect of aggregate inclusions upon the behaviour of the paste matrix, under thermal loading. It is sought to model this behaviour using finite element techniques. Although the modelling employed here is very elementary, some techniques and results may serve as pointers for further research.

10.1.1. Choice of Material

It has already been indicated (Section 3.1) that aggregate properties affect the response of the concrete as a whole. Examples of some of these properties are the expansive α to β transform in quartz-containing aggregate at 573°C, the thermal instability of gravel aggregate at around 400°C (84) and the chemical bond between limestone aggregate and mortar matrix at room temperature (30).

In order to obtain results of the widest generality possible, the aggregate to be used in this investigation had to meet the criteria of having a minimal degree of "specificity" while possessing characteristics representative of commonly used aggregates. These characteristics included shape, surface texture, coefficient of thermal expansion, modulus of elasticity and specific gravity. Based on the above considerations, it was decided to use roughened single sized soda-lime glass spheres of nominal diameter 12 mm as aggregate. The modulus of elasticity of soda-lime glass is 74 kN/mm^2 while the coefficient of thermal expansion is $9.2 \times 10^{-6}/°C$ (74); its specific gravity is 2.5. These values are similar to those for commonly used aggregates (118). It was expected that roughening the glass spheres would provide the kind of surface texture found on most aggregates. The spherical and single sized nature of the glass aggregates, although not characteristic or representative of normal aggregates, were con-

sidered useful for the finite element modelling described later.

The use of glass spheres, however, entails some limitations on test temperatures. The short term maximum use temperature of tempered soda-lime glass is 300°C, at which there is a tendency to densify (37). The modulus of elasticity has been found to decrease with temperature, but this is not normally significant below 200°C (12). In the light of the above considerations it was decided to limit the upper experimental temperature to 120°C, up to which temperature the modulus of elasticity was assumed to be the same as that at room temperature, and the aggregate assumed not to creep.

Having decided on the aggregate to be used, the next consideration had to do with the nature of the matrix. For the purpose of representing conventional concretes, it would have been more realistic to use a mortar mix, containing cement paste and fine aggregate, as a matrix for the aggregate inclusions. However, this would have necessitated the design and testing of such a mortar. Hence it was decided to use neat cement paste of w/c ratio 0.3 - the same material that had been used in the bulk of the present project - as the matrix. The advantage in using this cement paste mix as the matrix was that extensive creep and shrinkage results were available as inputs to the computer model from the experimental part of this project. Furthermore, it was thought that the interaction between glass spheres and neat cement paste would highlight the effects of thermal loading better than the interaction between glass spheres and a mortar mix, because the former involves a greater disparity between coefficients of thermal expansion than the latter. The volume percentage of aggregate employed was 50%, which is about the proportion of coarse aggregate in usual concrete mixes.

10.1.2. A Two-phase Material under Thermal Loading

Almost all materials experience thermal strains upon heating. If differential strains are set up within a material, these will give rise to internal stresses, which in turn may be relieved by creep.

There are two ways in which a two-phase material can

experience differential thermal strains upon heating. Firstly, there will be a thermal gradient from the surface to the central axis of the specimen. This would be especially pronounced in periods of changing temperature and would be a function of the rates of heating or cooling. This temperature gradient will cause different parts or layers of the material to expand or contract in unequal amounts, and thus set up differential thermal strains. Such differential strains would be exhibited by even a single phase or homogeneous material.

However, where a two-phase material is concerned, additional differential strains would be set up if the two phases have differing coefficients of thermal strain. These strains would be especially significant in concrete-type materials, where the cement paste undergoes contraction or shrinkage upon heating, while the aggregate experiences expansion. The stresses caused by this kind of two-phase response to heating have been called parasitic thermal stresses, while the stresses caused by thermal gradients will be called thermal gradient stresses.

Parasitic thermal stresses in concrete were first theoretically investigated by Lea and Stradling (92), who sought to gain insight into the behaviour of mortar by considering a sphere of sand surrounded by a layer of cement paste. They determined the stresses experienced in the cement paste due to a rise in temperature, using an elastic analysis. Experimental results regarding the thermal strain behaviour of cement paste were used as inputs to their theoretical model. Their calculations suggested that cement mortar would eventually break up if maintained for any length of time at a temperature of even 100°C. However, they did find experimentally that mortar briquettes in tension and concrete cubes in compression actually increased in strength up to temperatures of around 200-300°C.

Dougill (48) also investigated parasitic stresses theoretically by using Baker's lattice analogy (9). This analogy is based on the premise that load is transmitted through a concrete specimen by the thrust developed between aggregates and the interlying mortar. The resulting "thrust ring" is stabilized by tension in the mortar. Thus, a pin-jointed frame consisting of thrust and tension

elements can be taken to represent the concrete. (See Figure 10.1). Shrinkage was represented by a shortening of the mortar tension elements. A distribution of shrinkage with both space and time was assumed as simulating a temperature increase. (See Figure 10.2a). The resulting variation in strength (i.e. the external load required to rupture a lattice element) with time, due to the prescribed shrinkage, is shown in Figure 10.2c. This does actually show an initial increase in strength, as is consistent with experimental observations.

Although there was no attempt made to use any quantitative data relating to real temperatures, Dougill's studies demonstrated the usefulness of obtaining qualitative trends. He pointed out, however, that the lattice analogy was limited to elastic analyses, thus neglecting effects of creep and plastic flow in the mortar (48).

More recently, Wittmann et al (183) have modelled concrete as a two-phase material using a 2-dimensional computer generated finite element mesh for a distribution of circular aggregate inclusions in a matrix as shown in Figure 10.3. A simulated drop in temperature to -5°C was found to produce interface tensile stresses in excess of a limiting value of 3 N/mm^2 (147). This analysis too was probably a purely elastic one; however, creep strains experienced while cooling to these low temperatures would be less significant than those experienced on heating.

It would seem that the non-incorporation of creep and stress relaxation is a serious drawback in the above theoretical studies, especially in the context of the fact that cement paste and concrete exhibit large transitional thermal creep strains when heated under load (84). This is perhaps the reason for the discrepancy between the theoretical results and experimental observations of Lea and Stradling (92). If transitional thermal creep does in fact operate to relieve parasitic thermal stresses to "acceptable" levels, the high temperature strength of concrete would be dependent more on the chemical and physical changes induced in the cement paste by temperature, rather than the interaction between the aggregate and paste.

Walker et al (174) investigated the effects of both parasitic

as well as gradient stresses upon strength reduction, using rapid cyclic temperature changes from 10°C to 60°C on concretes with various coarse aggregates and mortar matrices. Their results led them to conclude that gradient stresses (assumed to be a function of the coefficient of expansion of the concrete itself) were significant in contributing to loss of strength while parasitic stresses (assumed to be a function of the difference between coefficients of expansion of mortar and coarse aggregate) were not. This conclusion is controversial and also runs counter to the theoretical investigations described beforehand. It may be that the dependence of strength on gradient stresses is heightened under conditions of rapid temperature cycling, in comparison with the dependence on parasitic stresses.

10.1.3. Choice of Model

As we have seen, the modelling of concrete as a two-phase material has progressed through various stages, from the simple analytical approach of Lea and Stradling in the 1920's (92) through the analogous model of Baker in the 1950's (9) to the finite element aggregate-matrix representation of Wittmann et al in the 1980's (183).

For the purpose of the present investigation, it was decided to use a simplifed Wittmann-type approach, which however took account of creep. The elastic solutions for stress distribution and overall strain were obtained using a finite element space discretization while the effects of creep were included using an effective modulus method. The finite element package used is described in Section 10.3 while Section 10.4 considers the incorporation of creep effects.

The main aim of this computer modelling exercise was to find the degree to which the parasitic stresses, set up by heating the two-phase concrete, were relieved by creep in the hardened cement paste. The heating was carried out at a rate of not more than 1°C/min. from 20°C to 120°C.

One of the major problems in this exercise was the checking or verification of the model. In this kind of micromechanical application, it is not possible to measure the internal stresses

experimentally. Two other alternatives can be suggested however, for checking the model. The first is to verify experimentally the degree of damage that could be expected from the stress levels obtained numerically. This may be done by measuring loss of strength or by slicing open the specimen and investigating the degree of cracking. The second method is to obtain numerically the overall strains in the specimen, which is a quantity that can, in fact, be compared with experimental values. Strictly speaking, the testing of a large number of conditions both experimentally and numerically is required for a proper verification of the model. Although this was not the case in the present investigation, the two methods above were nevertheless used to make a limited evaluation of the model.

10.2. ADDITIONAL CREEP DATA FOR MODEL

Although the time dependent phenomenon in the two-phase concrete subjected to thermal loading is better described as "stress relaxation" rather than "creep strain", the relaxation characteristics were obtained, not by direct experimentation, but by the transformation of experimental creep data. Creep tests are much easier to perform than relaxation tests, and are more reliable.

As already defined in Section 3.1, basic creep is the time dependent strain due to a load applied after dimensional stability at a given temperature has been achieved. This would be the lower bound for creep response, since loading before this point would enhance strain, as in the case of shrinkage induced creep at ambient temperature (180). The upper bound for creep response would be the condition where the load was applied right at the start of the heating regime. Not only would strains be enhanced by shrinkage but transitional thermal creep would also be experienced upon first heating; this component of creep has been found to be of considerable magnitude (84). The above ideas are schematically depicted in Figure 10.4.

In a situation where stresses are continuously developed due to thermal incompatibility upon heating, it is clear that these

stresses would give rise to the entire range of creep respones from the upper to the lower bound. It is neither practical nor even desirable to measure all these responses experimentally. The approach adopted here was to determine upper and lower bound creep curves and another intermediate point response between these bounds. The lower bound creep strains have been studied extensively as Series I tests; the upper bound results were obtained as the Series III tests by heating specimens while under load. The intermediate point was chosen as the point of reaching maximum temperature and the load applied to the specimen at this instant. (See Figure 10.4). Where the upper bound and intermediate point results were concerned, strains measured after loading would contain shrinkage and expansion strains; these were eliminated from the raw data by using the experimental results from the Series I tests.

The upper bound responses, which are in fact the results of the Series III creep tests, are shown in Figure 10.5. Temperatures from 50°C to 300°C were employed because it was originally envisaged that the numerical modelling would be performed over this range. As it is, only the 120°C data was used for the modelling. However, all the experimental results are reported. When comparing these curves with the Series I or lower bound creep curves, the difference is not merely one of magnitude but of shape as well, the upper bound curves tending to level out after some time and hence best fitted by an exponential-type relationship, as indicated in Figure 10.5.

These upper bound responses are called transient thermal creep, and is here taken to mean the load induced strain from the start of heating, through the achievement of maximum temperature, up to a total period of 7 days, although the term 'transient' is usually used in referring to the period of temperature rise only. Transient thermal creep would consist of transitional thermal creep and drying creep components. Appendix 5 gives the strains on heating under load; these are the actually measured strains, which include shrinkage and expansion components as well.

The intermediate point response was obtained only for the 120°C temperature level. The results are shown in Figure 10.6.

Since this response is midway between the upper and lower bound responses, it has been fitted by both exponential and power law curves. However, the values of the exponents have been maintained at the values obtained for the upper and lower bound curves respectively. Hence, the curves for the intermediate point in Figure 10.6 have been obtained by single parameter curve fits and they bear constant ratios to the upper and lower bound creep curves respectively. The reason for this approach will be explained later.

As stated before, verification of the model was to be performed by comparison with the overall strains in the two-phase concrete material. These strains, for both heating and cooling without load to a temperature of 120°C, are shown in Figure 10.7. It should be noted that residual contraction is shown upon cooling back to room temperature, and that the cooling phase is reasonably linear with temperature.

10.3. FINITE ELEMENT MODELLING

The finite element modelling in this study was performed by using the system FINEL (14), developed by Mr. Denis Hitchings in the Department of Aeronautics at Imperial College. The system possesses an excellent library of elements and is capable of performing a number of analyses, of which the stress analysis package is described herein.

10.3.1. Idealization and Mesh Description

The fist stage in the process of idealization was the representation of a 3-dimensional cylindrical specimen as a 2-dimensional plane stress problem as shown in Figure 10.8. This figure shows 50% of the area of the section consisting of 12 mm dia. single sized circles uniformly distributed, as representing the single sized glass spheres. A section of an actual cylinder is shown in Figure 10.9 for comparison. Although the above approximation seems rather gross, it was felt that obtaining qualitative or perhaps even semi-quantitative results from such a simple model was the most logical starting point; hence, over-complication in geometric representation

was avoided.

Given that the aggregate is taken to be uniformly distributed, it is sufficient to analyse merely a part of Figure 10.8, provided the part chosen is sufficiently representative of the whole, and correct boundary conditions are imposed. Two possibilities for smaller sections are shown in Figures 10.10a and 10.10b. It was felt that the section in Figure 10.10b, which could be called a "representative volume element", would adequately reflect longitudinal strains and internal stresses.

It is assumed that the edges O_2X_2 and O_2Y_2 in Figure 10.10b lie along the axes OX and OY in Figure 10.8 respectively. Hence the edges O_2X_2 and O_2Y_2 would be lines of symmetry; this is simulated by setting to zero the displacements in the x-direction along edge O_2Y_2 and the displacements in the y-direction along edge O_2X_2. Where edge Y_2Z_2 is concerned, all displacements in the y-direction are constrained to have the same value. A similar constraint is placed on the x-direction displacements along edge Z_2X_2. Identical boundary conditions are imposed on the section in Figure 10.10a , apart from the fact that edge Z_1X_1 is left free.

The finite element used for the stress analysis is a 2-dimensional 8 noded membrane plate element, known as PM08 in the FINEL element library. It is shown in Figure 10.11. The mid-point nodes along the edges allow them to be curved into parabolic shapes. This is particularly useful at the curved interface between aggregate and matrix. The interpolation function for displacements along the edges is parabolic as well.

The discretization of the representative volume element into PM08 finite elements is shown in Figure 10.12. A total of 113 nodes and 30 elements are employed. A particular feature of the discretization is the relatively narrow band of elements that surround the aggregate. Although these elements are in fact part of the matrix, their properties can be changed to allow for interface effects between the aggregate and matrix.

The adequacy of the degree of discretization was verified on the basis of the differences in the values of stresses at nodes shared by more than one element. In the stress analyses performed, such differences were found to be less than 2% of the maximum stress, except at nodes 15 and 68 where it was around 8%. This was considered to be sufficiently accurate and hence the degree of discretization adequate.

The adequacy of representation given by the section in Figure 10.10b was checked by comparing the overall longitudinal strains and internal stresses with a stress analysis performed on the larger section in Figure 10.10a. The maximum stress was the same for both analyses up to 3 significant digits; the difference in overall strain values was around 5%, the section in Figure 10.10a showing a larger strain, owing to the edge Z_1X_1 being free.

10.3.2. Stress Analysis Package

The stress analysis package is made up of the following modules.

ANALYSIS STRESS

GRID - Element generation, definition of material properties
ASMB - Integration and assembly of stiffness matrix (K)
BNCN - Imposes boundary conditions
CHOL - Matrix factorization
LOAD - Load vector assembly ($\underline{f}$)
SLVE - Solution for displacements ($\underline{x}$)
STRS - Calculates stresses/strains

The coefficient matrix defined is STIFFNESS (K) and the associated variable DISPLACEMENT ($\underline{x}$). The equation solved is $K\underline{x} = \underline{f}$.

ANALYSIS STRESS requires the geometry to be defined by nodal coordinates and linkages. Elements with similar properties (i.e. matrix, "interface" and aggregate) were declared consecutively by nodal linkages so that material properties could be assigned conveniently. Values for Young's Modulus and Poisson's Ratio were entered as MATERIAL

STIFFNESS, while values for the coefficients of thermal expansion were required as the MATERIAL EXPANSION inputs in the thermal load application. If a plot of the defined mesh was required, a PLOT module could be inserted after the GRID module.

The next module requiring input data was the BNCN module. Fixed displacements were used as boundary conditions to impose symmetry along edges O_2X_2 and O_2Y_2. The additional constraints of uniform deformation in the x and y directions on edges X_2Z_2 and Y_2Z_2 respectively were imposed via a user defined module, also developed in the Department of Aeronautics, inserted after the module CHOL.

Both static as well as temperature loads were used in ANALYSIS STRESS, the former being simulated as nodal point loads while the latter imposed by defining nodal temperatures.

The output from the package consists of deformations and stresses at either nodal points or element centroids. A post processing package called PLOT can be used to perform stress contouring.

A sample input for the stress analysis package is given in Appendix 6. The results of the analyses performed are reported in Section 10.5.

10.3.3. Input Data

The system of units adopted for inputting data was kN for loads and mm for length.

The modulus of elasticity of glass was taken as 74 kN/mm^2 and its Poisson's ratio 0.21; the coefficient of thermal expansion was taken as $9.2 \times 10^{-6}/°C$ (74).

Although the modulus of elasticity of hardened cement paste is reduced on exposure to temperature, it is actually increased if heated under load, as described in Section 5.1. Khoury (88) also found that the modulus of elasticity of a number of concretes at temperature was

relatively insensitive to temperature if the specimens were heated under compressive load. (See Figure 2.20). During the initial phase of heating the two-phase concrete, the expansion exhibited by the hardened cement paste matrix would cause it to experience compressive stresses. Hence, this condition would be analogous to heating under compressive load and the elastic modulus was taken as constant over the temperature and time range investigated. In any case, the maximum temperature reached was only 120°C and this approximation was considered not unreasonable. The value of 20.1 kN/mm^2 was the average obtained from the room temperature static elastic modulus tests described in Section 5.1. The Poisson's ratio, considered as equal for both elastic as well as creep strains, was taken as 0.20 (119). This value would perhaps slightly underestimate the Poisson's ratio for elastic strains and slightly overestimate the Poisson's ratio for creep strains.

Since the thermal load analysis was used to study parasitic stresses, the existence of spatial temperature differences (which would set up gradient stresses as well) was ignored, and a uniform value of temperature assigned to all the nodes at any given instant of time. In any case, the experimentally obtained maximum temperature difference between the specimen surface and axis was only 8°C.

The thermal strains for hardened cement paste were based on the average of results from 4 specimens, each heated to and maintained at 120°C for over 7 days. In taking these averages, the shrinkage in air prior to testing was also accounted for. These average values were used to estimate the thermal movement of the matrix in the two-phase concrete specimen at any given temperature or time. The coefficients of expansion could thus be calculated, with contractions being given negative values. The estimated development of thermal strains with time, in the matrix, is shown in Table 10.1.

The elastic and creep behaviour of cement paste in tension was considered to be identical to that in compression, which is of course a simplification, but not an unreasonable one (25).

10.4. SOLUTION SCHEMES FOR CREEP ANALYSIS

10.4.1. Step by Step Method

The conventional method of solving a creep problem (186, 187) is depicted schematically in Figure 10.13a. The time scale involved is divided into suitable intervals. All loads experienced during a given interval are applied at the end of that time step and an elastic analysis performed. The internal stresses thus set up are considered to produce creep during the next increment of time. These creep strains are obtained using a known creep law and imposed as "lack of fit" strains at the end of the time increment, together with other loads that may have been experienced during the increment (such as thermal loads due to a temperature change). This method consists therefore, of a succession of elastic solutions at the ends of time intervals, with creep taking place during the intervals. It is appropriately called a step-by-step method and will yield solutions both for the internal stresses as well as the overall strain at each time step. However, it was not possible to adopt this method with the current version of FINEL, which did not have a facility for inputting prescribed strains as loads.

10.4.2. Method of Superposition

As an alternative to the step-by-step method, a superposition method incorporting an effective modulus technique was adopted. Here too the time scale is divided into suitable intervals as shown in Figure 10.13b The effective modulus method (119) incorporates the effects of creep in a stress analysis by using an "effective elastic modulus" in an elastic analysis, this modulus being given by

$$E(t, \tau) = \frac{E(\tau)}{1 + \phi(t, \tau)} \qquad (10.1)$$

Here the load is considered to be applied at time τ, while the solution is required at time t. The modulus of elasticity, $E(\tau)$, can vary with the time of loading while $\phi(t, \tau)$ is the creep coefficient, which is the creep strain at time t due to loading at time τ, divided by the elastic strain at time τ. If there is no variation of elastic

modulus with age of loading, equation (10.1) can be written as

$$E(t, \tau) = \frac{E}{1 + \phi(t, \tau)} \qquad (10.2)$$

Hence, in order to obtain the creep-adjusted solution at time $t = t_n$, (n-1) solutions are carried out, the loads arising in each of the (n-1) time intervals being operated on by the corresponding effective modulus. These loads are thermal incompatibility loads and are input to ANALYSIS STRESS as LOAD TEMPERATURES with the appropriate coefficients of expansion for the two materials. The (n-1) solutions are then algebraically summed by the principle of superposition, which is assumed to hold, since the stress-strain responses are taken to be linear.

It is clear that this method is less efficient than the step-by-step method. In order to find solutions at the end of each of n time steps, this method will require n(n+1)/2 elastic solutions to be performed, compared to the n solutions for the previous method. However, the superposition method was adopted because it could be used conveniently with FINEL.

Two problems arise when trying to assign values to the creep compliance coefficients in equation (10.2).

(a) The creep does not take place under isothermal conditions. Furthermore, even after reaching constant temperature, the response will vary (i.e. reduce) with time because the specimen would not have reached stability. It is assumed that it does in fact achieve stability after 7 days.

(b) The response with time at t = 0 would be transient thermal creep, which was best fitted by an exponential type law, whereas the response at time t = 7.0 days would be basic creep, which was best fitted by a power law. It was found that a specimen loaded at t = 0.8 days (when maximum temperature was just reached) exhibited a response in between the two extremes.

These problems were solved in the following fashion.

(i) The effect of age on creep response was ignored, since the creep duration considered was only 7 days. Instead, an age-adjustment type approach (7) was used to modify the creep responses at time t = 0 and t = 0.8. i.e. if the creep compliances based on the responses at times t = 0 and t = 0.8 are called $J_1(t, \tau)$ and $J_2(t, \tau)$, the former an exponential and the latter a power expression,

$$\left.\begin{aligned} J(t, \tau) &= \alpha(\tau)\, J_1(t, \tau) \quad \tau \geqslant 0 \\ &= \beta(\tau)\, J_2(t, \tau) \quad \tau \geqslant 0.8 \end{aligned}\right\} \qquad (10.3)$$

where $\alpha(\tau)$ and $\beta(\tau)$ are reduction factors to account for the diminishing creep responses.

(ii) $\alpha(\tau)$ and $\beta(\tau)$ were obtained as follows

The responses at time t = 0 and t = 7 were modelled as

$$J_1(t) = a_1(1 - e^{ct}) \qquad (10.4)$$

and $$J_3(t) = b_1 t^n \qquad (10.5)$$

The response at time t = 0.8 was modelled as both

$$J_2(t) = a_2(1 - e^{ct}) \qquad (10.6a)$$

and $$J_2(t) = b_2 t^n \qquad (10.6b)$$

where the exponents c and n are identical to those in equations (10.4) and (10.5) respectively.

The values of α at 3 points were defined as

$$\alpha(0) = 1.0 \qquad (10.7a)$$

$$\alpha(0.8) = {}^{a_2}/_{a_1} \qquad (10.7b)$$

$$\alpha(7.0) = \frac{a_2}{a_1} \cdot \frac{b_1}{b_2} \qquad (10.7c)$$

A hyperbolic curve of the type

$$\alpha(t) = \frac{P}{(t + Q)} + R \qquad (10.8)$$

was fitted through these three points, P, Q and R being the parameters of the curve.

The shape of the β function (from t = 0.8 onwards) was assumed to follow the same shape as that of the α function, by multiplying the α values by a factor a_1/a_2. (See Figure 10.14).

(iii) The elastic or instantaneous response, J(t, t) was assumed to remain constant throughout the period (88). Hence the normalized creep compliances $\phi(t, \tau)$ could be obtained by dividing $J(t, \tau)$ by the elastic strain at room temperature.

The time period of 7 days was discretized into 13 intervals as shown in Table 10.2. However, stress and strain solutions were obtained at only 7 time steps. The effective elastic moduli, $E(t, \tau)$ for these time steps are also shown in Table 10.2, based on an original modulus E(t,t) of 20.1 kN/mm^2.

10.5. RESULTS AND CONCLUSIONS

Two kinds of analyses were performed. A static load analysis was carried out to check the behaviour of the model in the elastic range and to make comparisons with the experimentally obtained modulus of elasticity. Next, the effect of heating the two phase material to 120°C was modelled, with due consideration given to stress relief by creep. This was the main investigation. All analyses were performed on the representative volume element in Figure 10.10b.

10.5.1. Static Load Analysis

Loads corresponding to 1, 2, 3 and 4 No. 57.5 kg weights acting on the specimen through a lever arm ratio of 15:1 were applied on the edge Y_2Z_2 in Figure 10.10b as series of nodal point loads. The displacements of the edge Y_2Z_2 were obtained from an ANALYSIS STRESS and hence the strains corresponding to each 57.5 kg weight increment could be computed. These are shown in Figure 10.15, and indicate that the model behaves in a perfectly linear fashion up to a stress corresponding to 10.9 N/mm^2. The slope of the line yields a value for elastic modulus of 35.9 kN/mm^2. The experimental average for 3 specimens was 30.04 kN/mm^2. Hence the model is slightly stiffer than the real specimen under static loading.

10.5.2. Relaxation of Parasitic Thermal Stresses by Creep

As described before, heating of the two phase material will give rise to parasitic stresses, due to differential thermal movements. If creep effects are not considered, the principal stresses set up at nodes 1, 34, 38 and 7 in the matrix (see Figure 10.12) are given in Table 10.3 for a number of time steps. The overall strains are indicated as well. The contours of principal stresses at t = 7.0 days are shown in Figure 10.16.

The highest compressive and tensile stresses are experienced at node 1 during the expansion and contraction, respectively, of the paste matrix. The tensile stresses set up in the matrix are very high, i.e. around 35 N/mm^2. The radial stresses at the interface are compressive except in the early expansive phase of the paste, when a maximum tensile stress of 2 N/mm^2 is evidenced. Hence the model indicates that failure would be initiated by cracks within the paste matrix rather than by cracking at the aggregate-paste interface.

The results obtained from the superposition method for incorporating creep effects are tabulated in Table 10.4. The difference between the solutions from elastic and creep adjusted analyses for the major principal stress at node 1 is shown in Figure 10.17. Although the tensile stress at 7 days is reduced by 27%,

it is still very high and would undoubtedly cause cracking.

The difference between the solutions from elastic and creep adjusted analyses for overall strains is shown in Figure 10.18. The experimentally measured strains are also plotted here. Although the early strains (during expansion of the paste) are reduced and the later strains (during contraction of the paste) are increased by the creep adjustment, these differences are very small, compared to the differences between the elastic and creep adjusted solutions for stresses. Furthermore, there is wide discrepancy between the experimental strains and those predicted by the model.

The above results raise two important questions. The first is concerned with the efficiency of modelling, i.e. does the model reflect actual behaviour ? The high tensile stresses predicted in the model suggest that a specimen heated to 120°C for 7 days would be dramatically weakened by matrix cracks. Experimentally, it was found that such a specimen was strong enough to sustain a stress of 5.5 N/mm^2 over a further 7 days. However, another specimen heated to 120°C for 7 days and cooled back slowly to room temperature showed a strength of only 8.3 N/mm^2. The cold cylinder strength of these specimens was 27.7 N/mm^2. Furthermore the external appearance of these cylinders after cooling back to room temperature indicated cracking that seemed to radiate outwards from aggregate locations, suggesting that matrix cracks were indeed formed. (See Figure 10.19). Although one cannot exclude the possibility of these cracks having formed during cooling, the reasonable linearity of the cooling curve in Figure 10.7 suggests that cooling may not have been very disruptive. If cracking did take place at temperature itself, the experimental strains would be more expansive than the theoretical ones, which are based on linear superposition; this is in fact the case, as evident in Figure 10.18.

The second question of importance is whether this exercise has shown that parasitic thermal stresses are relaxed by creep. The theoretical studies have suggested the extent to which creep could relieve parasitic stresses. However, both experimental as well as the theoretical investigations indicate that considerable damage would be incurred by a two phase specimen of the kind used here, if sustained at

120°C, in spite of the stress relaxation.

Two contributing factors can be identified with regard to the above damage. Firstly, the use of cement paste instead of cement mortar would have greatly accentuated the differential thermal movements between matrix and inclusion. The results of Harada et al (67) indicate that commonly used mortars would experience expansion when heated, as opposed to contraction in the case of cement paste. (See Figure 2.13). Hence the parasitic thermal stresses due to the interaction between a cement mortar and aggregate would be considerably smaller than those encountered in this present investigation. This would lead us to suggest that the damage sustained by a real concrete (i.e. aggregate inclusions in a mortar matrix) heated to and maintained at 120°C would be much less than the damage caused to a specimen consisting of glass spheres in a cement paste matrix. The interaction between sand grains and hardened cement paste would of course lead to cracking, but this kind of microcracking should not be very significant in affecting overall behaviour, at least where strength is concerned.

The other factor that perhaps contributes towards the build up of disruptive tensile stresses is the rate at which the paste contracts in the process of being heated to a particular temperature. The large transient thermal creep strains (ttc) occur only during the temperature rise itself. If, on the other hand, most of the contraction takes place after the maximum temperature is attained, it will not be ttc that is involved in the stress relaxation, but rather constant temperature creep; this will be smaller in magnitude and hence less efficient in relieving stress than ttc.

Table 10.5 gives the contraction that takes place during the temperature rise itself as a ratio of the total contraction, for cement paste heated without load to various temperatures up to 300°C. It must be emphasised that these ratios would be functions of the rate of heating. However, it is very instructive to note that this ratio is negative for temperatures up to 120°C. This means that up to 120°C, it is the early compressive stresses (at node 1) which are relieved by ttc and not the subsequent disruptive tensile stresses.

It has been pointed out by Lea and Stradling (92) that the loss of concrete strength upon heating can arise from two sources, viz. (a) the effect of temperature upon the paste itself, and (b) the effect of aggregate-paste interaction due to heating. The effect of temperature upon the paste itself is shown in Figure 5.8, which indicates a minimum in strength at 120°C but a regain of original strength up to 300°C.

Where the aggregate-paste interaction is concerned, this would depend on (i) the amount of differential strain involved and (ii) the degree to which ttc is available for stress relaxation. It should be appreciated that both factor (i), which is detrimental, as well as factor (ii), which is beneficial, increase with temperature. In such a context it is difficult to predict the trend, with temperature, of the combined effect of these two factors. Experimentally, however, it is known that concrete has a strength minimum in the temperature range 50°C-100°C. (See Figure 2.17). While this has hitherto been attributed to the behaviour of the cement paste itself, it may be that the opposing factors which determine the effect of the aggregate-paste interaction also contribute towards producing this strength minimum in the above temperature range.

If the aggregate-paste interaction does in fact affect the strength of concrete at elevated temperatures, this effect would be time-dependent, especially at lower temperatures, where contraction continues to take place after the maximum temperature has been attained. This is because the internal stresses would change with time, as evident in Tables 10.3 and 10.4. Table 10.4 in fact shows a maximum point for the stresses at t = 3.0 days. Now, it is generally considered that the strength of unsealed concrete is essentially insensitive to heating duration at temperatures above 200°C, but is dependent on duration below this temperature. (See Figure 2.18a, where a strength minimum is indicated at 7 days' duration for a temperature of 105°C). Here too, this time-dependence has been attributed to the effect of temperature, with time, on the cement paste itself. However, seeing that temperatures below 200°C are those where a considerable amount of contraction takes place after the end of the temperature rise (see Table 10.5), it may be that the temperature

induced aggregate–paste interaction also contributes towards the time-dependence of concrete strength in this temperature regime.

10.6. RECOMMENDATIONS FOR FURTHER DEVELOPMENT

The two crucial aspects of this model are geometric representation and creep simulation. In the present investigation, both have been approached in a very simple manner. The following recommendations suggest improvements, and perhaps even alternatives to the approaches adopted herein.

10.6.1. Geometric Representation

The simplications made in geometric representation were (i) using a 2-dimensional model for a 3-dimensional situation, (ii) modelling the inclusions as uniformly spaced single sized discs having a percentage area equal to the volume percentage of aggregate in the specimen, and (iii) assuming the concept of a 'representative volume element'.

Although (i) seems to be a rather drastic simplification, it seems to have been used fairly successfully by other researchers in modelling concrete as a two phase composite material (183, 192). Step (iii) too does not seem unreasonable; furthermore, it has been used before in the modelling of another type of composite, namely fibre-reinforced composites (191).

However, step (ii) does not reflect realistically the true aggregate distribution across a section, as evident from a comparison between Figures 10.8 and 10.9. Although the percentage areas for both figures would be around the same, the distribution of the real aggregate in Figure 10.9 is far from uniform, as assumed in Figure 10.8. The real aggregate distribution shows widely differing aggregate spacing, ranging from areas where the aggregates actually touch each other, to others where large areas of the paste matrix are visible.

Although Figure 10.8 would give an 'average' value for aggregate spacing, it may be that the overall behaviour of the specimen is strongly influenced by either the small or the large aggregate spacing, or both. Such effects would not be reflected in the idealization made in Figure 10.8. The significance of aggregate spacing is emphasised in the research of Hsu (75), who calculated that the bond stresses due to shrinkage in a two phase material were strongly dependent on aggregate spacing, even changing sign at a spacing corresponding to around 0.45 of aggregate radius.

It should be noted that the uniform aggregate spacing in the present model is equal to the aggregate radius. This results in compressive radial stresses at node 1 (see Figure 10.12) when the matrix underwent contraction. (See Table 10.4). If the spacing were less than the above, these stresses may have been tensile, which could have suggested a completely different mode of failure initiation - i.e. by cracking at the aggregate-paste interface instead of through the paste.

Hence, it may be profitable to study the effect of aggregate spacing on the behaviour of the model. It may also be useful to evaluate Hsu's method of arriving at aggregate spacing which is based, not merely on the volume percentage of aggregate, but on a quantity termed the degree of compactness; this is defined as the ratio of percentage volume of aggregate in the mix to the percentage volume of aggregate in a fully compacted state (75). This method would result in an aggregate spacing smaller than that arrived at by the present method; however, the percentage area of aggregate would be larger than the volume percentage of aggregate in the concrete.

Another refinement that may be attempted is to represent the aggregate as discs of 2 sizes, suitably distributed. The sensitivity of the model to different configurations could also be investigated.

10.6.2. Creep Simulation

The most obvious alteration that could be made to the creep simulation is to use the step-by-step method as opposed to the

superposition method. This will be possible when the facility for inputting initial strain loading becomes available on FINEL. Furthermore, advantage can be made of the exponential type transient thermal creep functions to reduce computational effort (186).

Apart from this, more experimental data will be required, corresponding not only to different maximum temperatures, but also to different rates of heating. The lower bound or basic creep response will not be dependent on the rate of heating. However, the upper bound or ttc response will be a function of the rate of heating (33). The intermediate point response is also likely to depend on the heating rate, in as much as this rate will determine the time of load application after the commencement of heating.

Hence, there would be a series of upper bound responses, intermediate point responses and $\alpha(\tau)$ and $\beta(\tau)$ curves corresponding to different rates of heating for each maximum temperature. This data would need to be available before any simplifications or generalizations can be made.

It would also be prudent to check the accuracy of the assumed hyperbolic variation for $\alpha(\tau)$ and $\beta(\tau)$ by using creep curves from more than a single 'intermediate point'.

Another development that may need to be made is a method to account for the possibility of heating at varying rates. Situations of decreasing temperature or reheating in a regime below the maximum temperature previously reached (i.e. when no ttc is experienced) can be dealt with by considering step-wise temperature variations (190) and using the $\beta(\tau)$ curves to modify constant temperature creep responses.

Finally, it must be pointed out that the present study has considered creep and shrinkage to be functions of temperature and time only; however, they would also be dependent on the moisture condition of the paste. This may well be an important factor, especially in a micromechanical application where moisture conditions would vary not only with time but also spatially, within the specimen. Hence, this additional level of sophistication would need to be built in to the

model.

10.6.3. Other Recommendations

Although the finite element mesh was designed such that a relatively narrow band of elements surrounded the inclusion, no advantage has been made of this arrangement. Any measured or assumed variation of the interface from the rest of the matrix could be accommodated by adjusting the properties of these elements.

It would be useful to see how well the model predicts the behaviour of normal concretes, as opposed to the idealized 2 phase material used here. This would require experimental data for creep and thermal strains of mortar. Furthermore, the representation of non-regular aggregate inclusions would also pose a problem. Two approaches that have been used to date are to model the irregularity as best as possible (183) or to find some equivalent circular disc size and spacing (75).

Finally, if thermal strain and creep data are available for concrete itself, the creep simulation techniques could be used to analyse concrete structures under thermal loads, with transient thermal creep being realistically accounted for.

Time (d)	Temperature Rise (°C)	Paste Expansion (με)
0.0	0	0
0.04	19	336
0.08	57	1263
0.12	79	1601
0.20	90	1566
0.40	97	1226
0.60	99	874
0.80	100	599
1.00	100	382
1.50	100	- 70
2.00	100	- 424
3.00	100	- 866
5.00	100	-1044
7.00	100	-1044

TABLE 10.1. THERMAL STRAIN OF PASTE MATRIX.

Time, t (Days)	Time of Loading, τ (Days)													
	0.0	0.04	0.08	0.12	0.20	0.40	0.60	0.80	1.00	1.50	2.00	3.00	5.00	7.00
0.08	8.42	13.01	20.1											
0.12	6.86	10.01	14.02	20.1										
0.40	4.01	6.65	9.50	12.00	15.67	20.1								
0.80	3.46	4.66	6.05	8.54	11.63	14.79	17.38	20.1						
1.50	3.36	4.40	5.32	6.24	7.99	11.69	14.33	16.07	13.90	20.1				
3.00	3.35	4.34	5.17	5.93	7.15	9.22	10.94	13.37	12.09	13.80	14.95	20.1		
7.00	3.35	4.34	5.16	5.86	6.98	8.85	10.04	11.01	10.32	11.80	13.30	14.66	15.73	20.1

TABLE 10.2. DISCRETIZATION OF TIME FOR SUPERPOSITION METHOD AND VALUES OF EFFECTIVE ELASTIC MODULI, BASED ON AN INITIAL MODULUS OF 20.1 KN/MM^2.

	(Time (days)	0.08	0.12	0.40	0.80	1.50	3.00	7.00
Node	Strain (με)	827	1085	1029	789	515	189	117
1	σ_{11}	-14.34	-16.98	-6.478	6.232	19.22	34.67	38.13
	σ_{22}	7.029	8.321	3.175	-3.054	-9.420	-16.99	-18.69
34	σ_{11}	-13.38	-15.84	-6.042	5.812	17.93	32.34	35.56
	σ_{22}	7.958	9.421	3.595	-3.458	-10.66	-19.24	-21.16
38	$\sigma_{11} = \sigma_{22}$	-5.451	-6.453	-2.462	2.369	7.305	13.18	14.49
	σ_{12}	7.188	8.509	3.247	-3.123	-9.633	-17.38	-19.11
	σ_{r}	1.737	2.056	0.785	-0.754	-2.328	- 4.20	- 4.62
	σ_{θ}	-12.639	-14.962	-5.709	5.492	16.938	30.56	33.60
7	σ_{11}	- 4.280	- 5.066	-1.933	1.860	5.735	10.35	11.38
	σ_{22}	- 4.280	- 5.066	-1.933	1.860	5.735	10.35	11.38

TABLE 10.3. RESULTS OF ELASTIC ANALYSIS FOR 2-PHASE CONCRETE HEATED AT 1°C/MIN. TO 120°C FOR 7 DAYS.
(Note:- Subscripts 1 and 2 correspond to directions x and y respectively.)

	Time (days)	0.08	0.12	0.40	0.80	1.50	3.00	7.00
Node	Strain (με)	824	1074	1011	772	507	199	140
1	σ_{11}	-13.27	-12.18	1.808	13.79	22.50	30.2	28.0
	σ_{22}	6.577	6.276	-0.503	-6.66	-11.24	-15.44	-14.71
34	σ_{11}	-12.33	-11.12	1.975	12.93	20.82	27.73	25.54
	σ_{22}	7.425	7.016	-0.679	-7.56	-12.65	-17.30	-16.38
38	$\sigma_{11} = \sigma_{22}$	-5.086	-4.806	0.469	5.186	8.675	11.851	11.226
	σ_{12}	6.669	6.172	-0.828	-6.898	-11.331	-15.298	-14.309
	σ_{r}	1.583	1.366	-0.359	-1.712	- 2.656	- 3.447	- 3.083
	σ_{θ}	-11.755	-10.978	1.297	12.084	20.006	27.149	25.535
7	σ_{11}	- 3.985	- 3.738	0.4116	4.08	6.79	9.233	8.709
	σ_{22}	- 3.985	- 3.738	0.4116	4.08	6.79	9.233	8.709

TABLE 10.4. RESULTS OF CREEP-ADJUSTED ANALYSIS FOR 2-PHASE CONCRETE HEATED AT 1°C/MIN. TO 120°C FOR 7 DAYS.

(Note:- Subscripts 1 and 2 correspond to directions x and y respectively.)

Temp (°C)	Contraction during Temp. Rise (με)	Total Contraction at Temp. (με)	Cont. during Rise / Total Cont.	Avge.
50°C	- 614	1532	- 0.401	
90°C	- 830	3090	- 0.269	
120°C	- 333	2771	- 0.120	
200°C	410	3858	0.106	0.132
200°C	649	4123	0.157	
300°C	1968	5898	0.334	0.334
300°C	2274	6806	0.334	

TABLE 10.5. RATIOS OF CONTRACTION DURING TEMPERATURE RISE TO TOTAL CONTRACTION ON CONTINUED EXPOSURE AT MAXIMUM TEMPERATURE, WHEN HARDENED CEMENT PASTE IS HEATED WITHOUT LOAD AT 1°C/MIN.

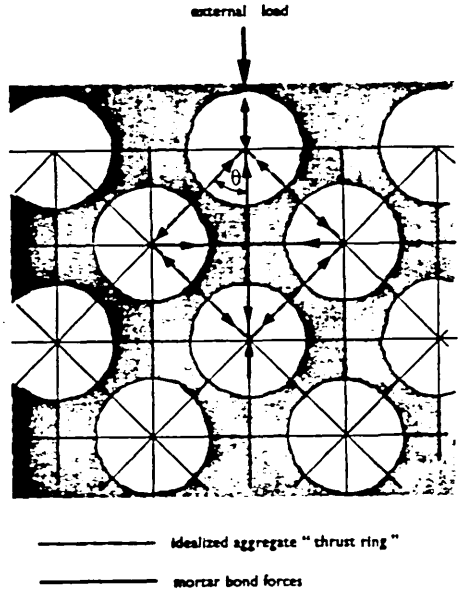

Figure 10.1 - LATTICE ANALOGY FOR CONCRETE.(FROM DOUGILL (48))

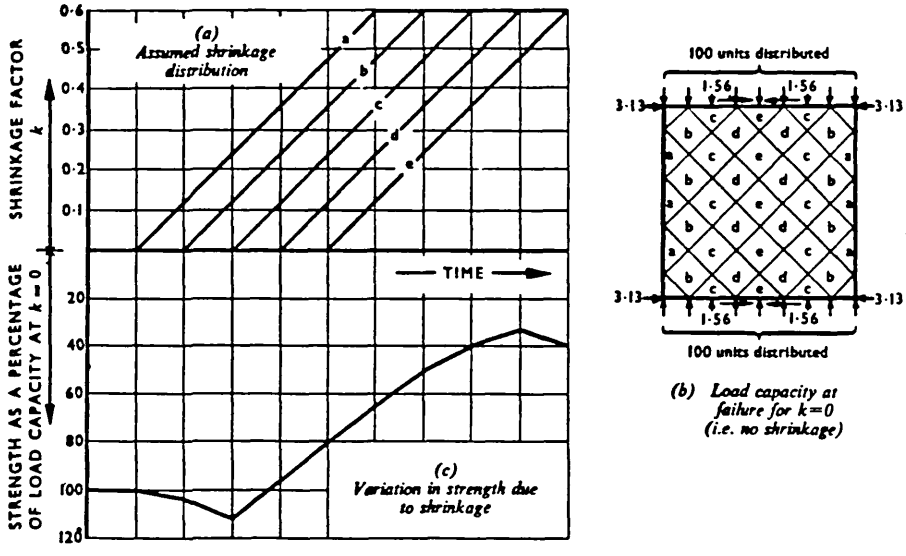

Figure 10.2 - SHRINKAGE ANALYSIS ON LATTICE STRUCTURE.(FROM DOUGILL (48))

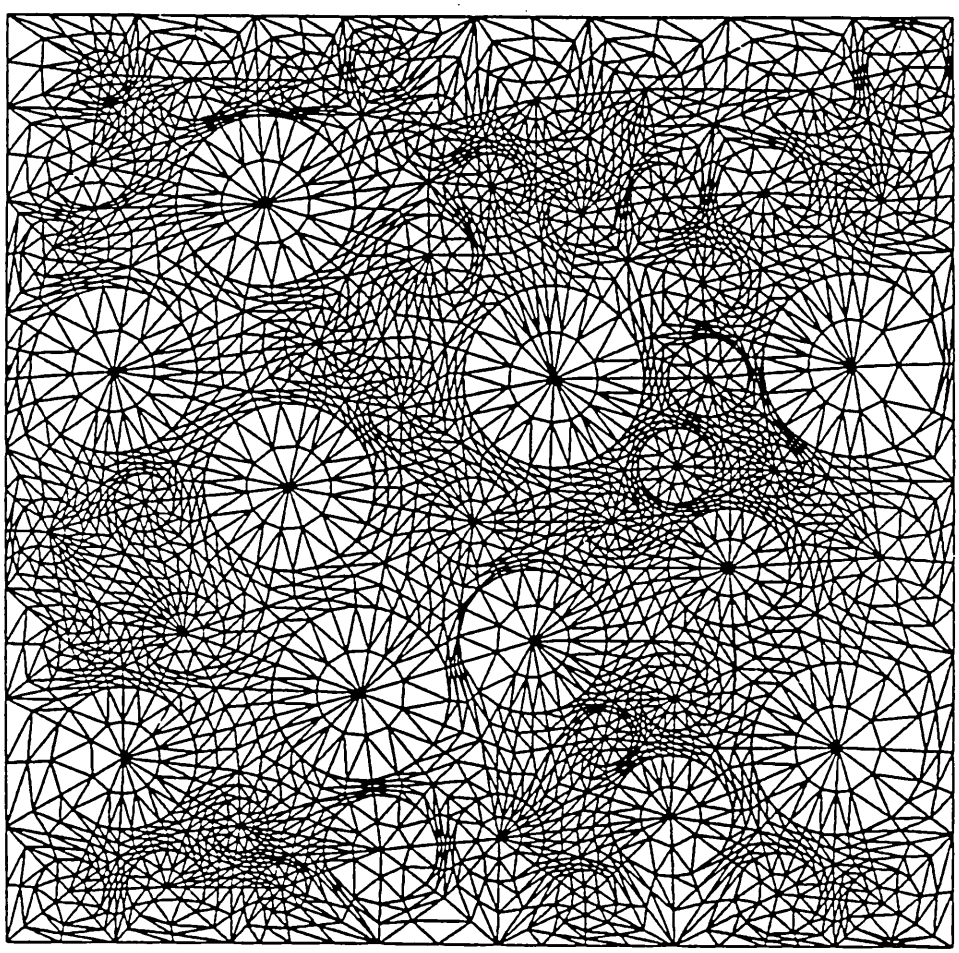

Figure 10.3 - FINITE ELEMENY MESH FOR 2-PHASE CONCRETE MATERIAL.
(FROM WITTMANN ET AL.(183))

Fig.10.4 – CREEP RESPONSES WITH VARIATION OF POINT OF LOADING

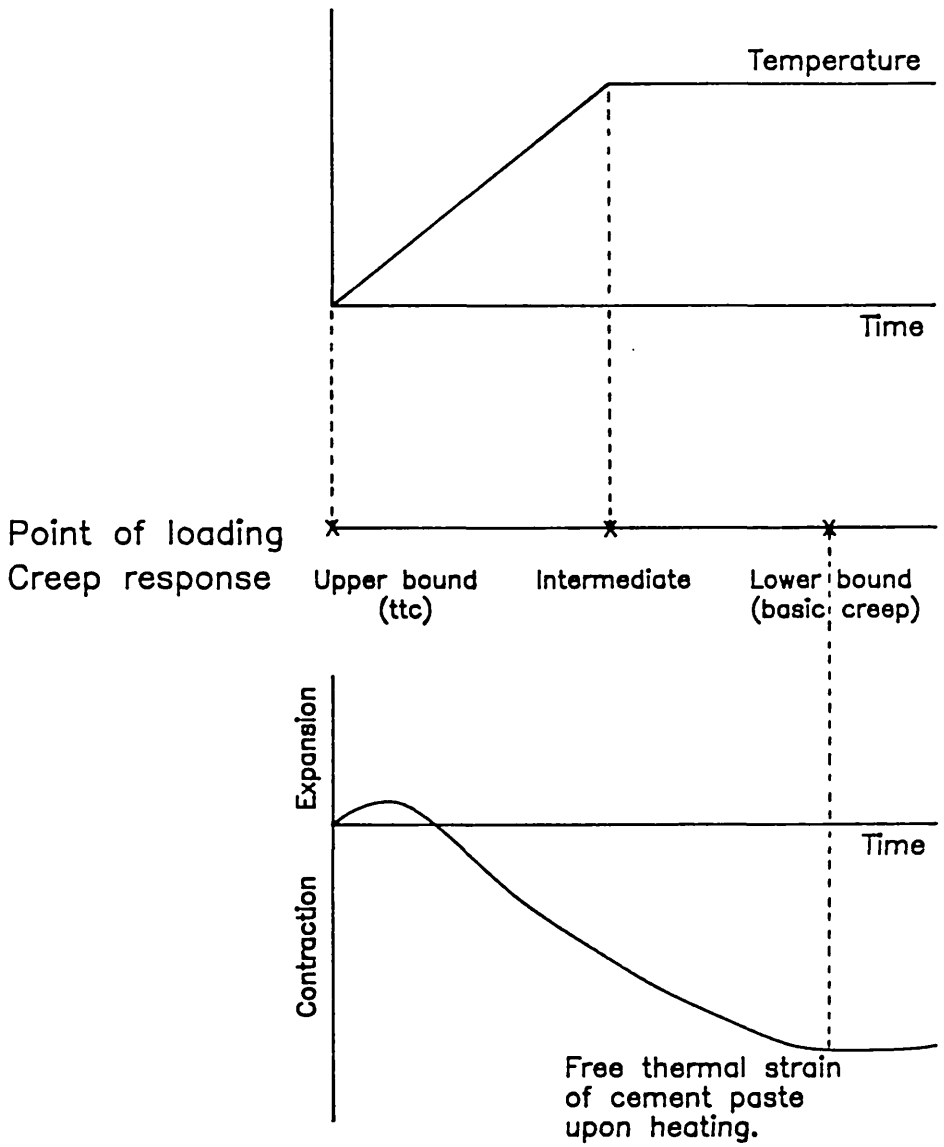

Fig.10.5 – TRANSIENT THERMAL CREEP RESPONSES

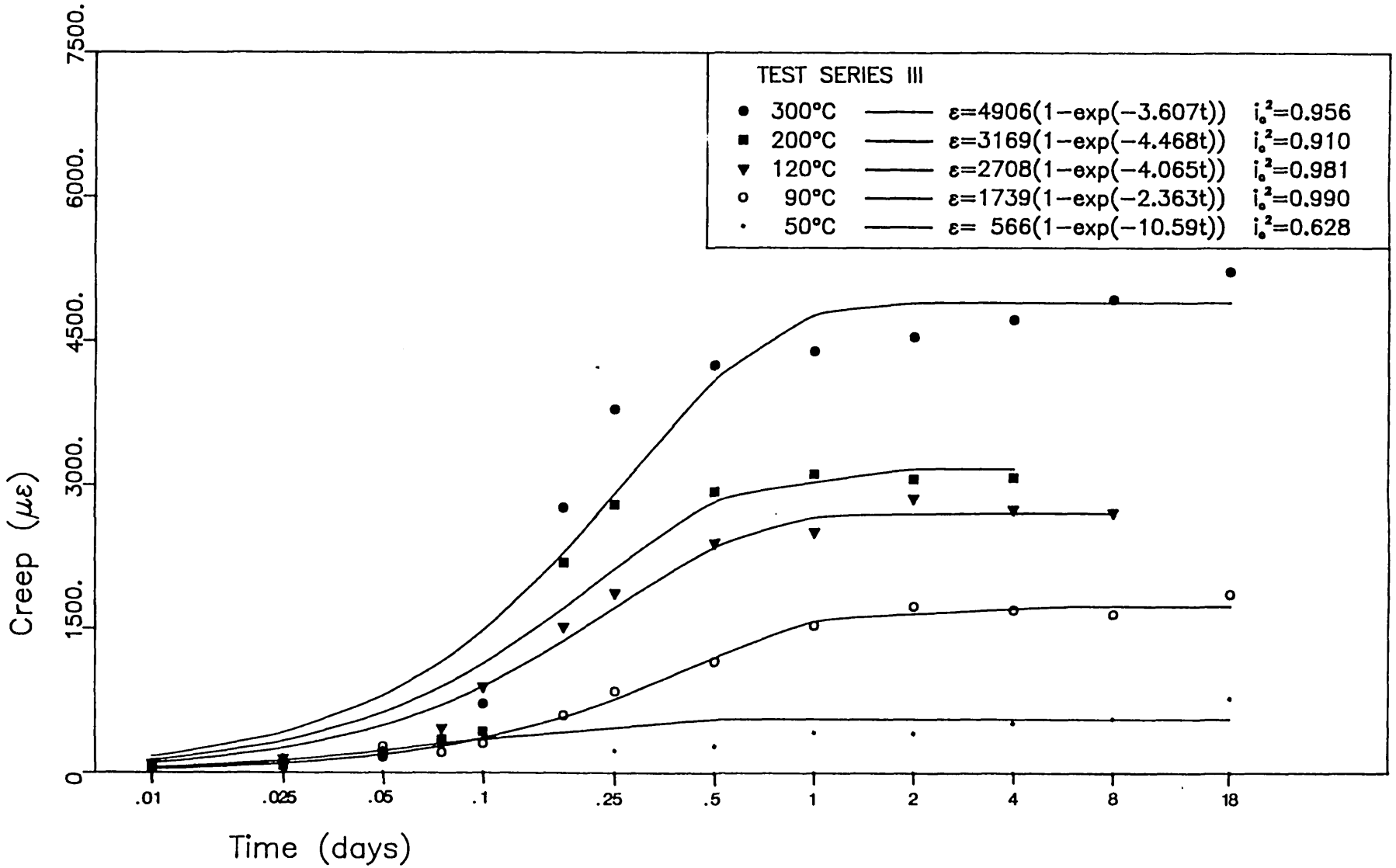

Fig.10.6 – HARDENED CEMENT PASTE CREEP STRAINS – 120°C

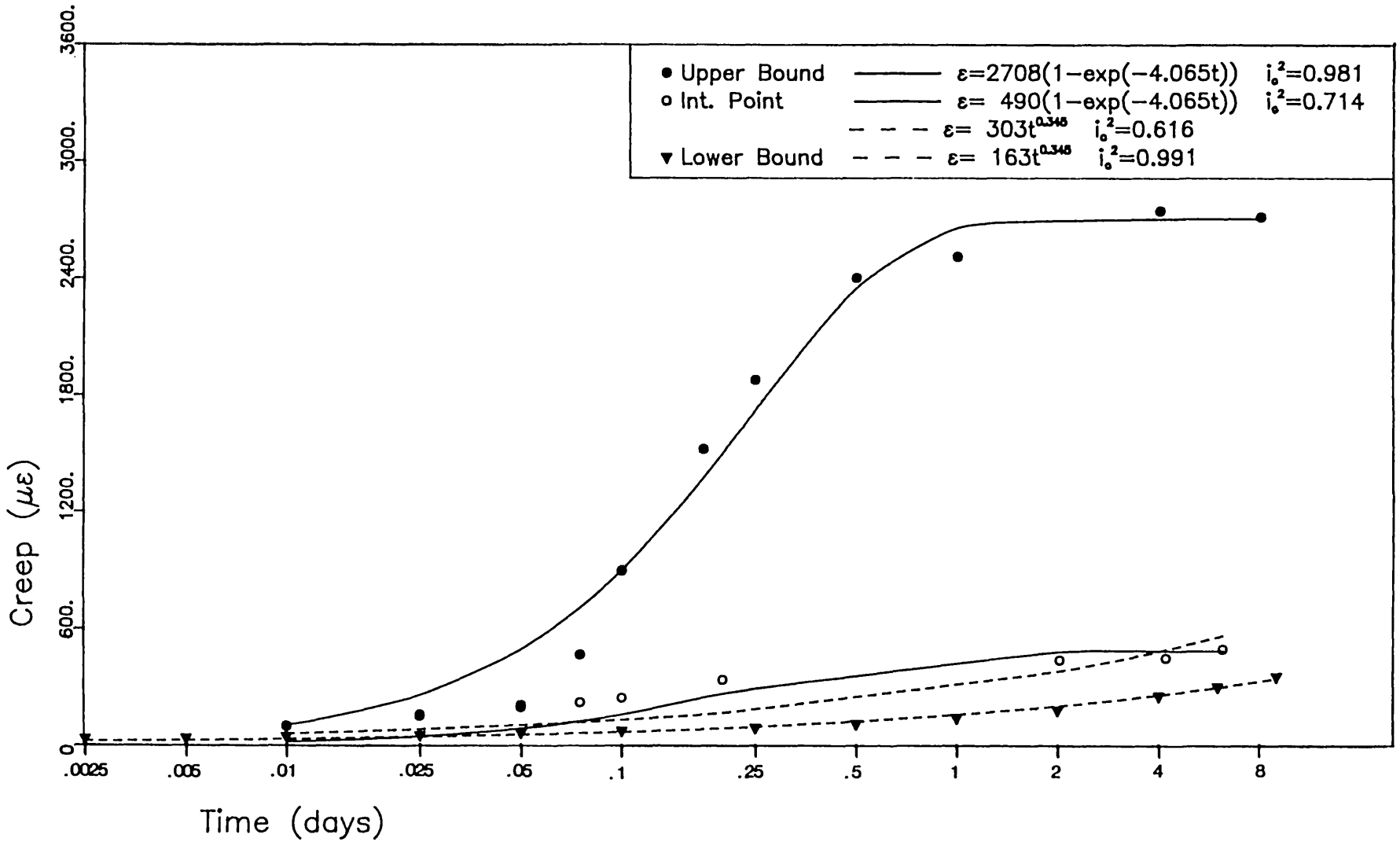

Fig.10.7 – THERMAL STRAINS FOR CONCRETE

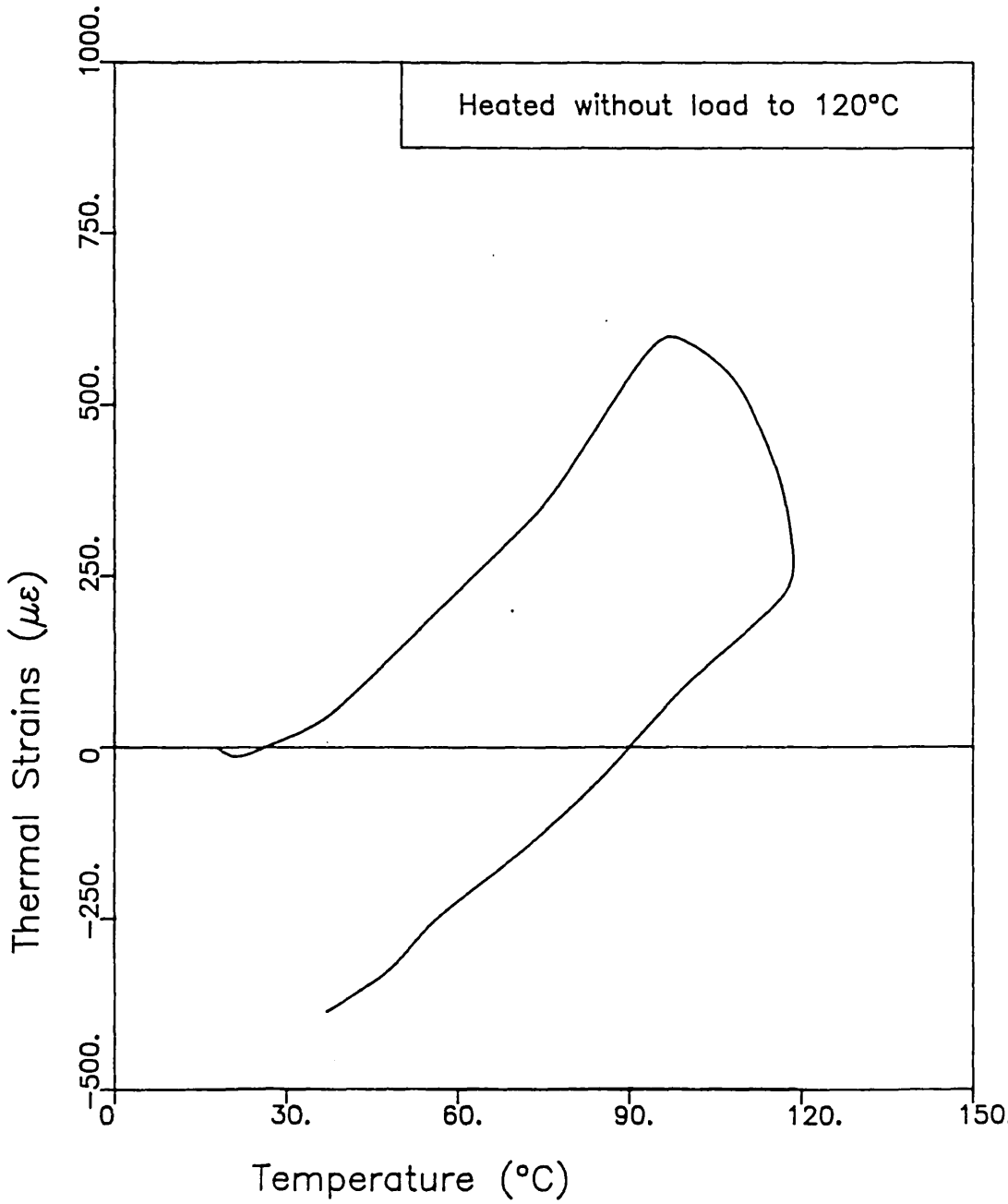

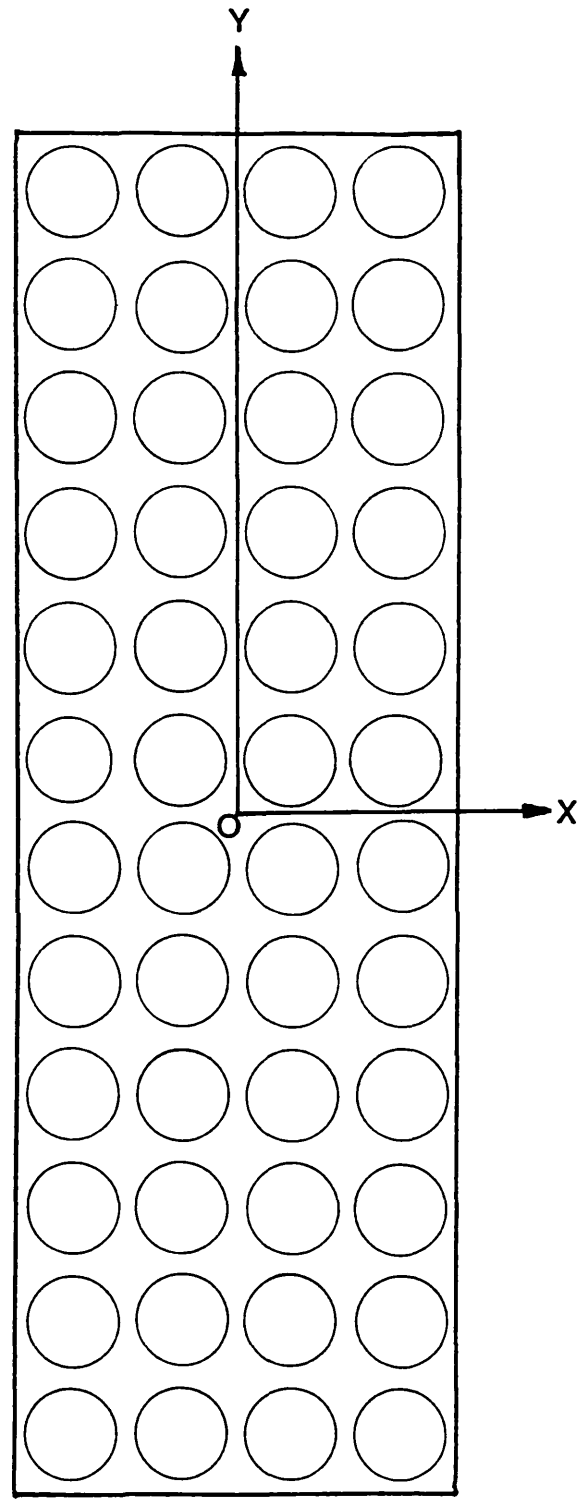

Figure 10.8 - 2-DIMENSIONAL IDEALIZATION OF SPECIMEN.

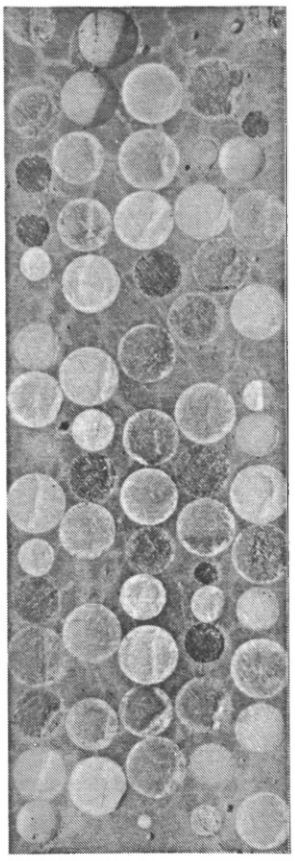

Figure 10.9 - CROSS SECTION OF ACTUAL CYLINDER, SHOWING DISTRIBUTION OF AGGREGATE INCLUSIONS.

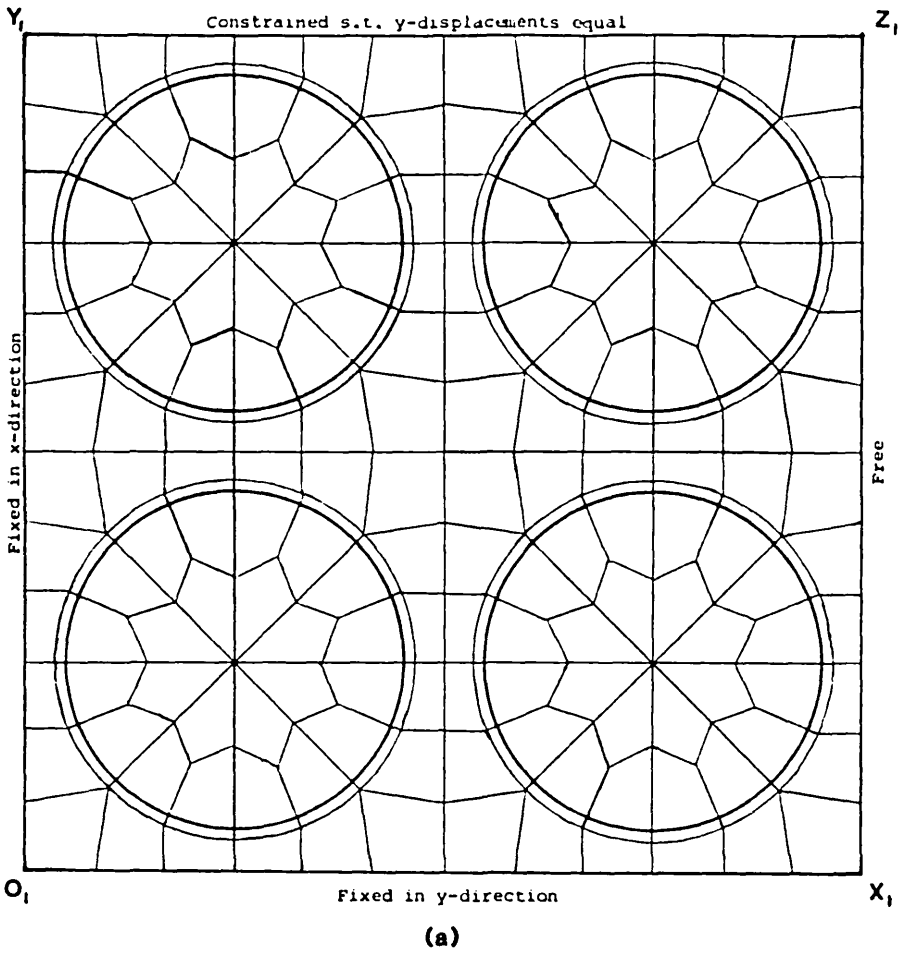

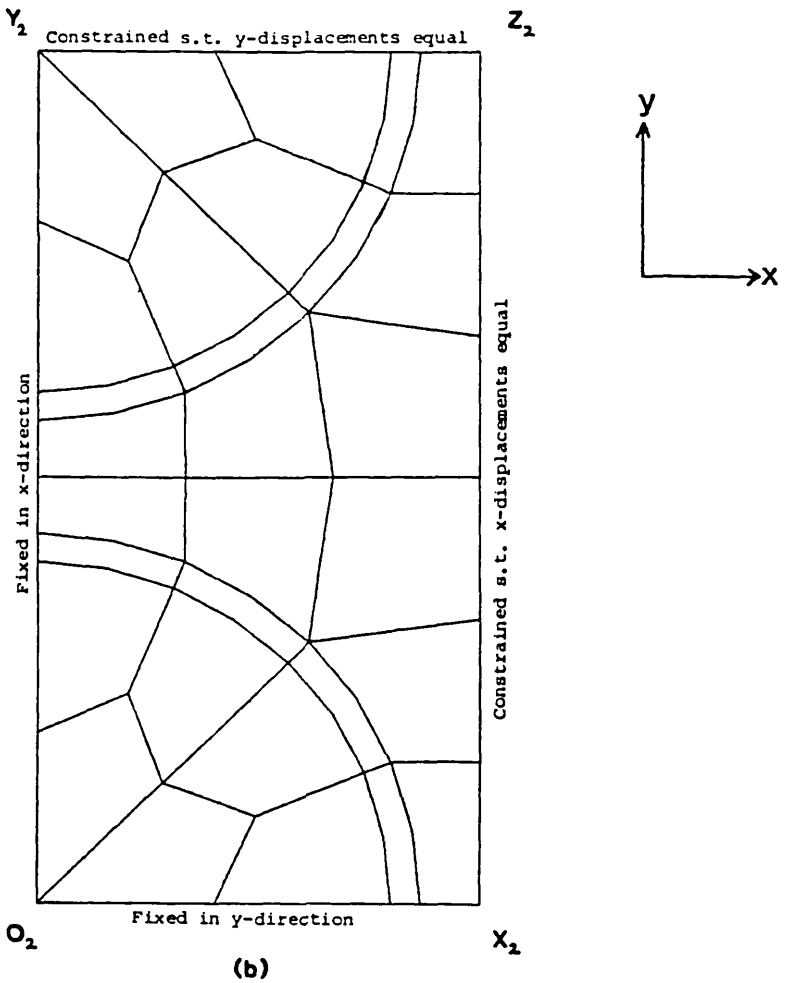

Figure 10.10 - SMALLER REPRESENTATIVE SECTIONS OF MODEL.

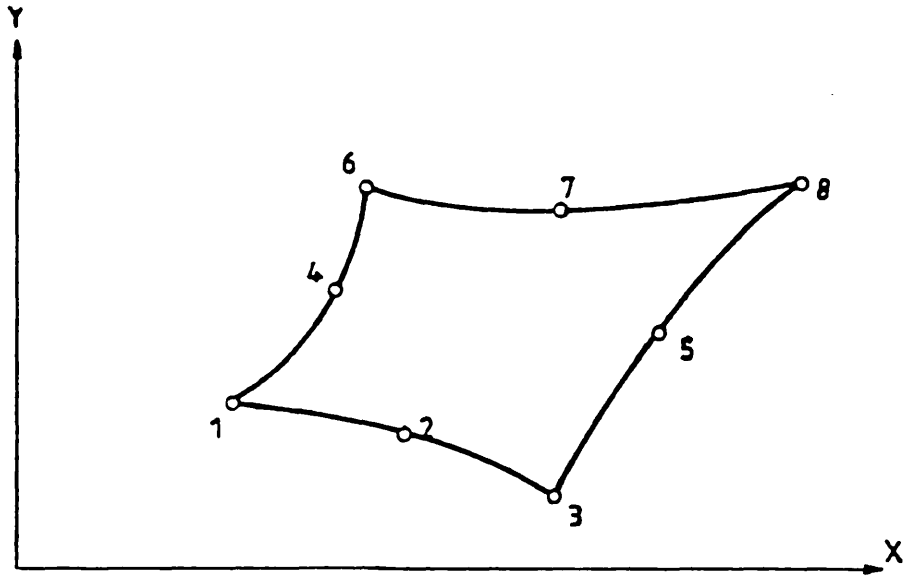

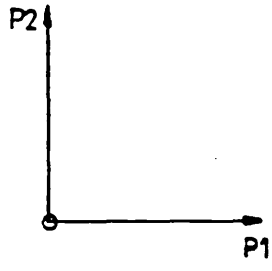

NODAL DEGREES OF FREEDOM
MATRICES - STIFFNESS
& MASS

ELEMENT PM08

Figure 10.11 - ELEMENT PM08 FROM FINEL LIBRARY.(FROM HITCHINGS (72))

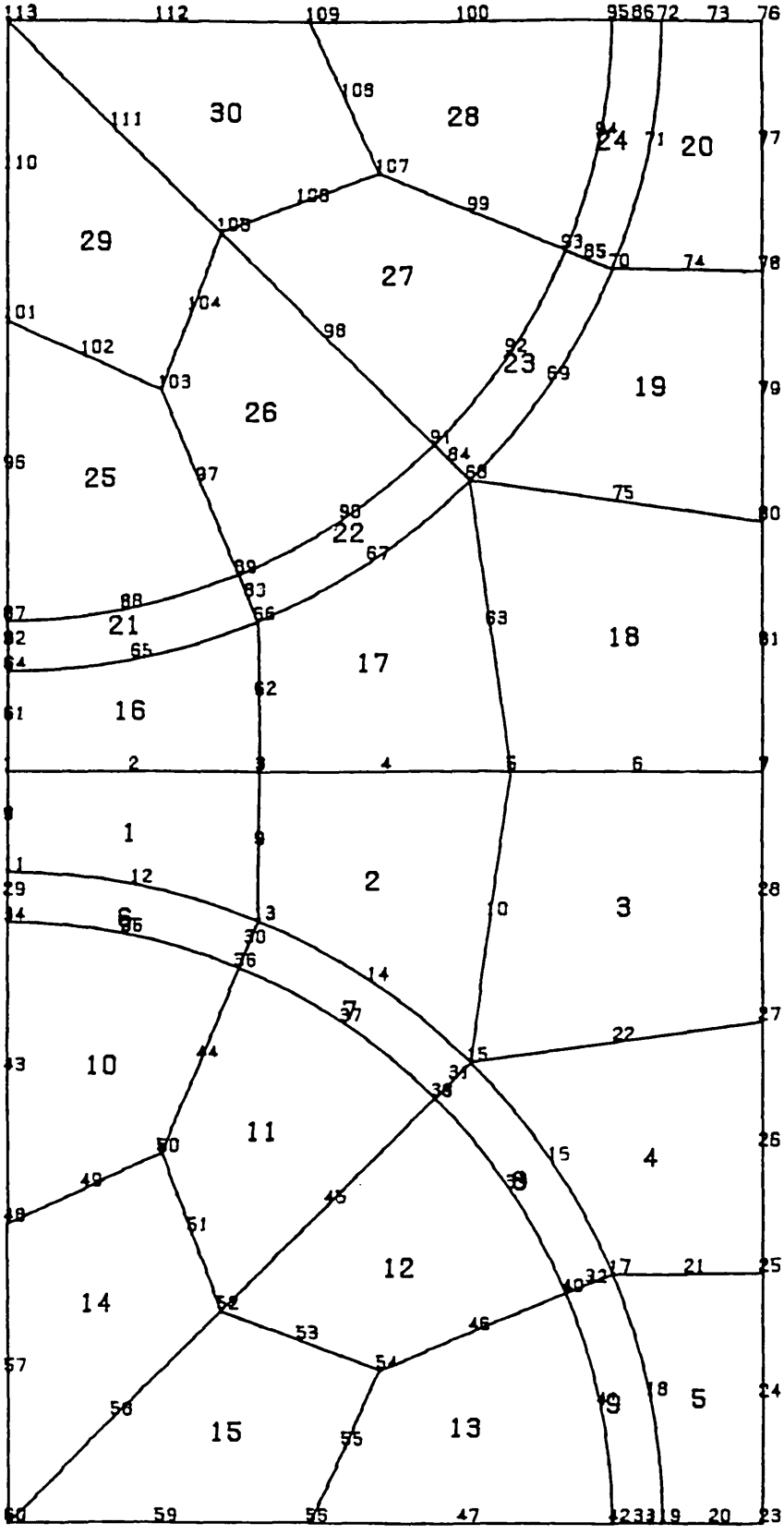

Figure 10.12 - DISCRETIZED REPRESENTATIVE VOLUME ELEMENT.

Fig.10.13 – NUMERICAL SOLUTION SCHEMES FOR CREEP ANALYSIS

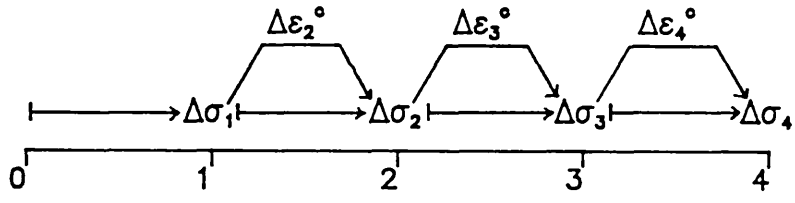

(a) Step by step method

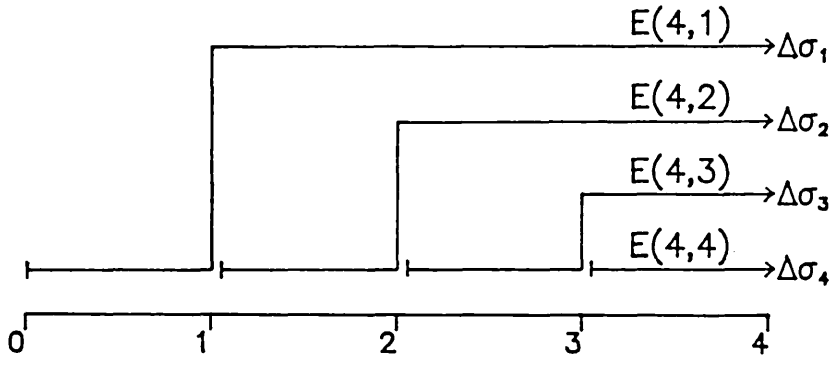

$$E(t,\tau) = E(\tau) \,/\, (1+\varphi(t,\tau))$$

(b) Superposition method

Fig.10.14 – $\alpha(\tau)$ & $\beta(\tau)$

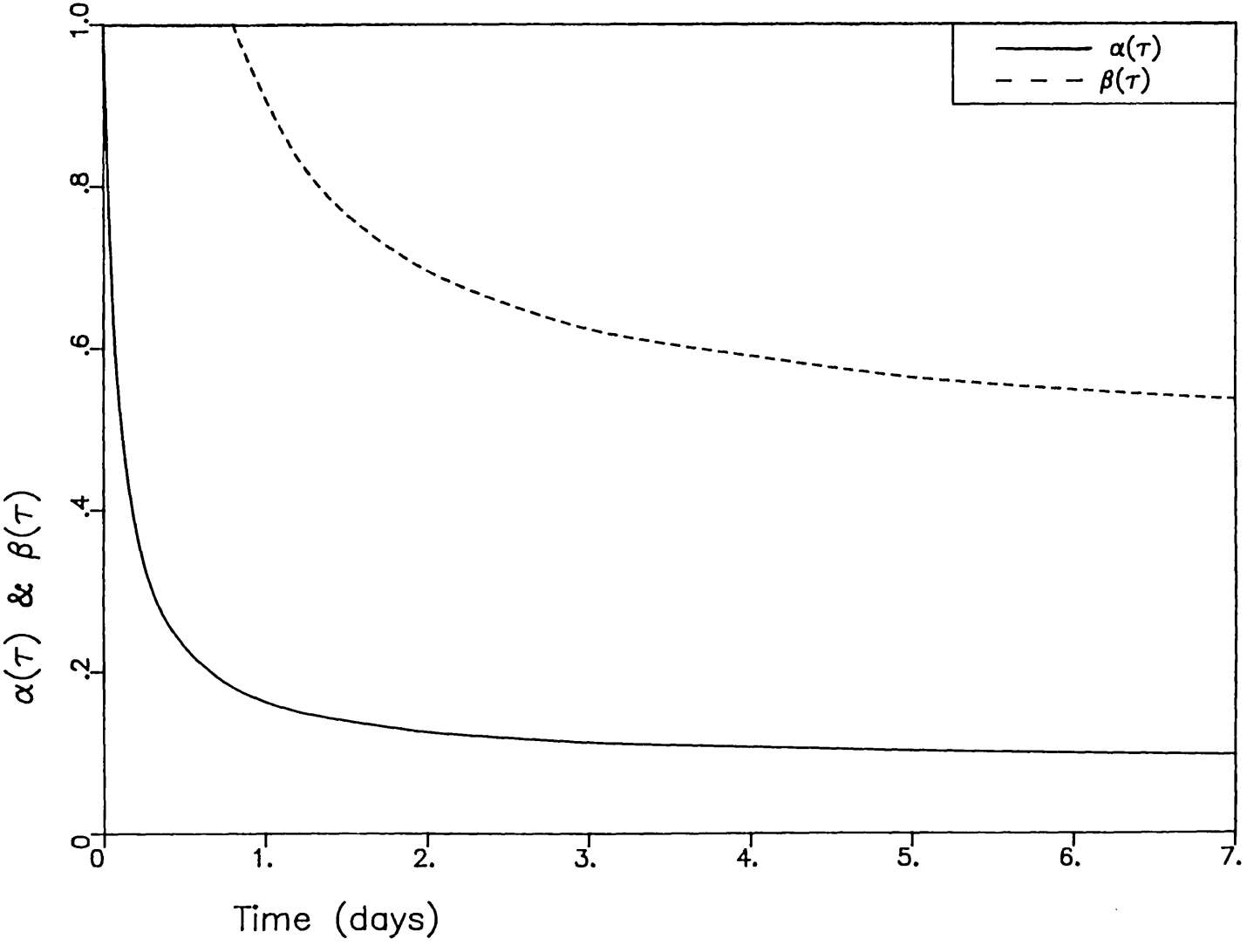

Fig.10.15 – THEORETICAL STATIC LOAD RESPONSE

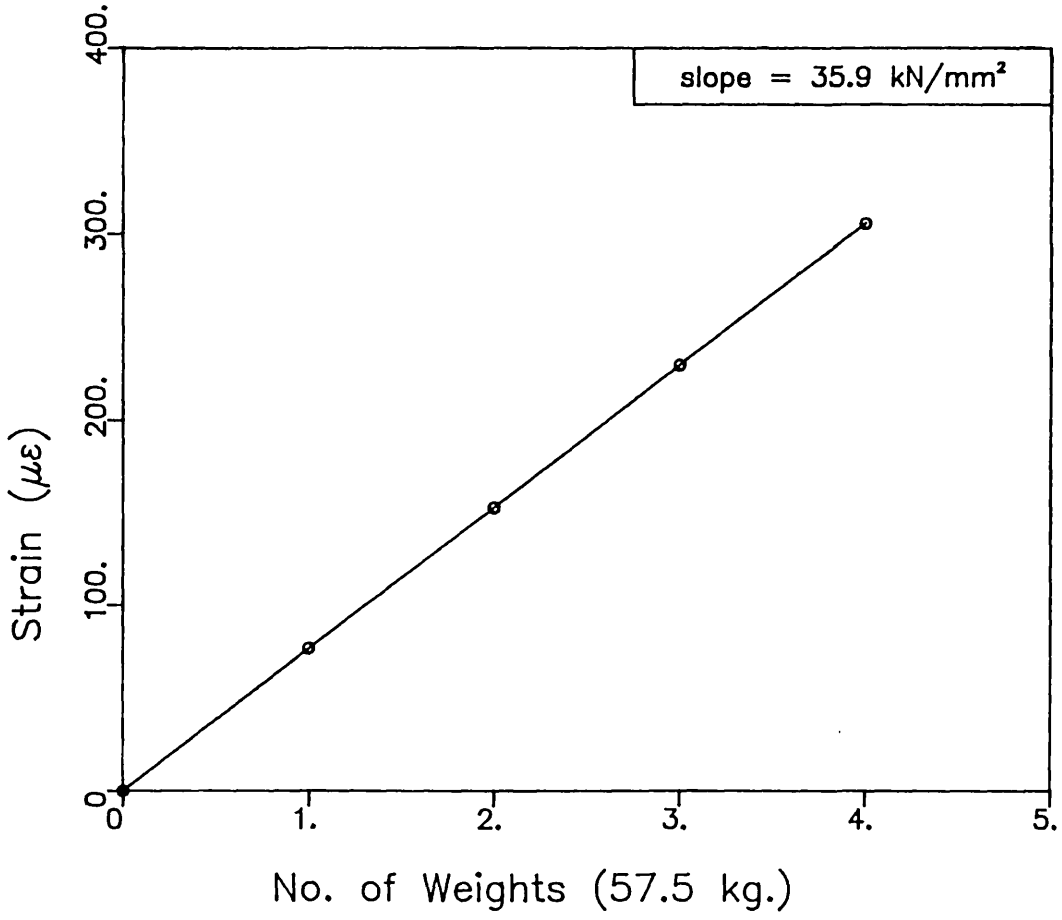

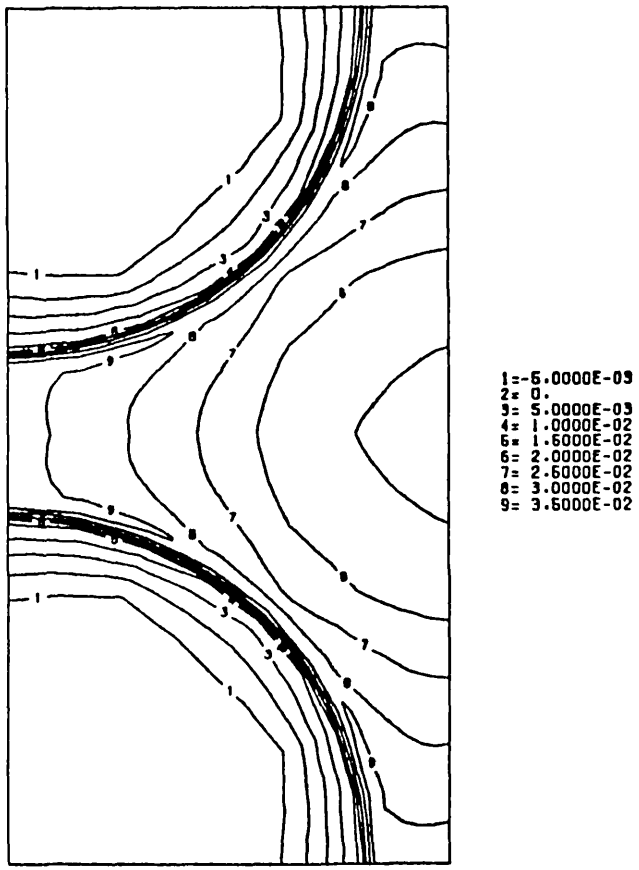

(a) MAJOR PRINCIPAL STRESS

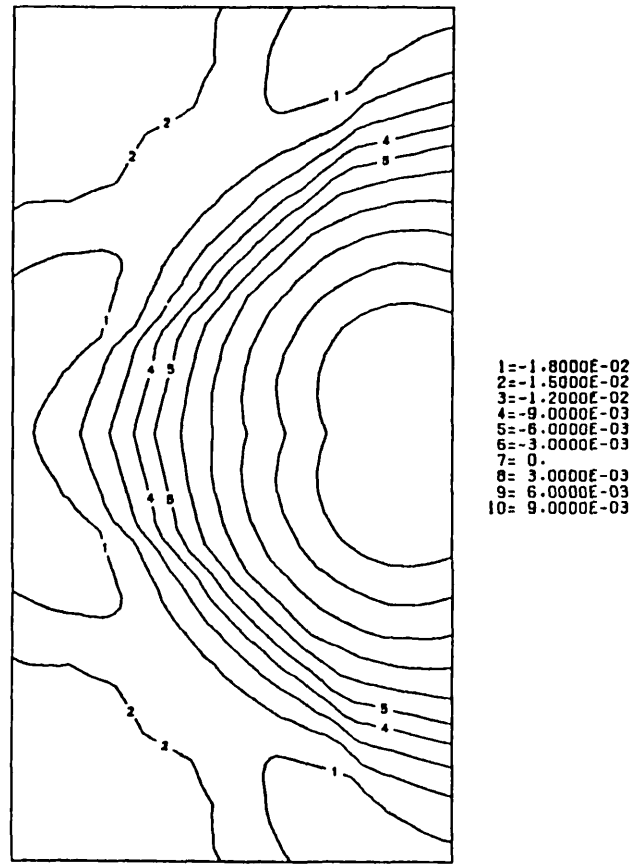

(b) MINOR PRINCIPAL STRESS

Figure 10.16 - PRINCIPAL STRESS CONTOURS FROM ELASTIC ANALYSIS AT t=7 DAYS AFTER HEATING TO 120 C AT 1 C/MIN.(STRESSES ARE IN KN/MM^2,TENSION +VE.)

Fig.10.17 – DEVELOPMENT OF MAJOR PRINCIPAL STRESS AT NODE 1

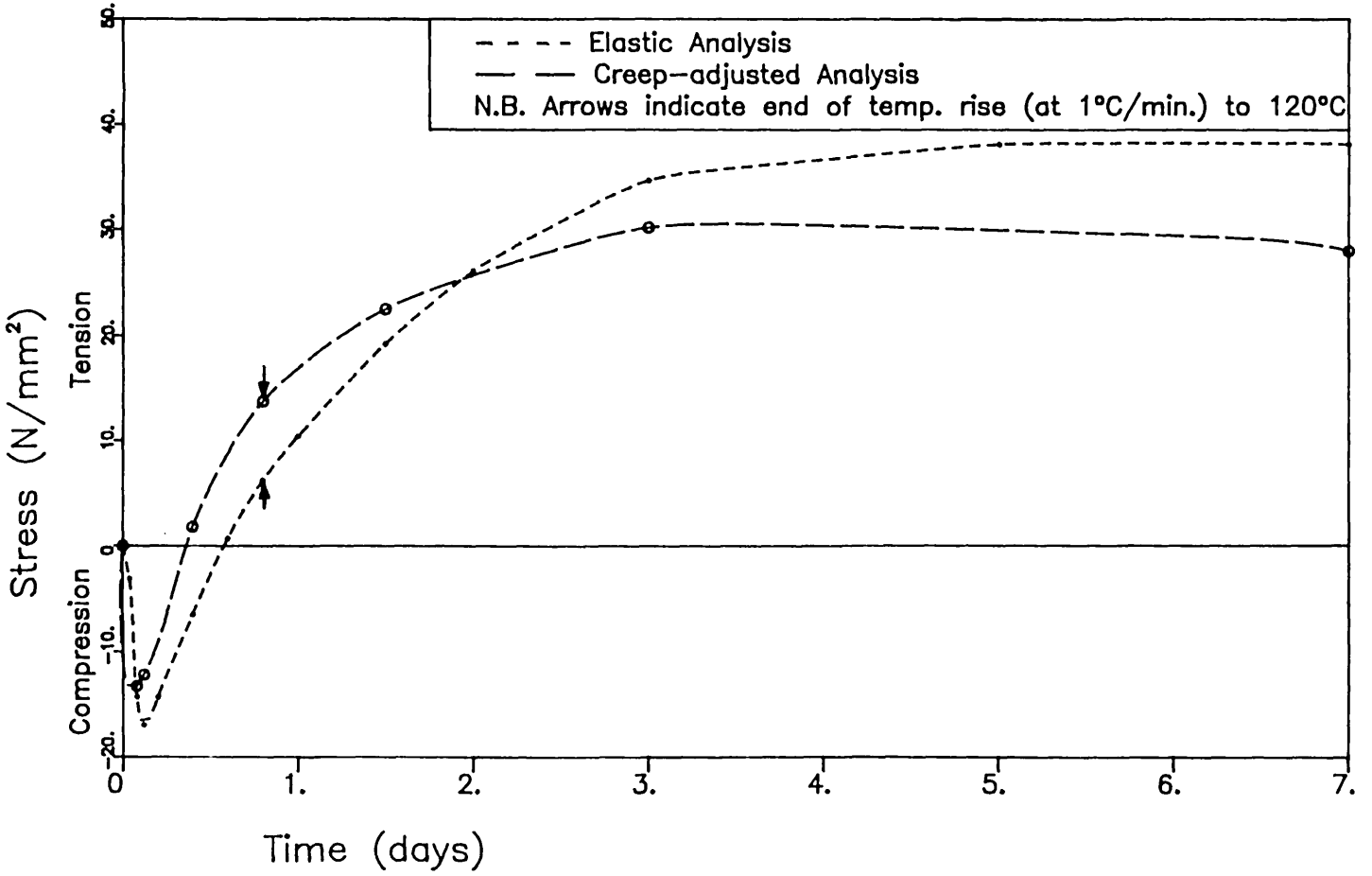

Fig.10.18 – DEVELOPMENT OF OVERALL STRAIN (AXIAL)

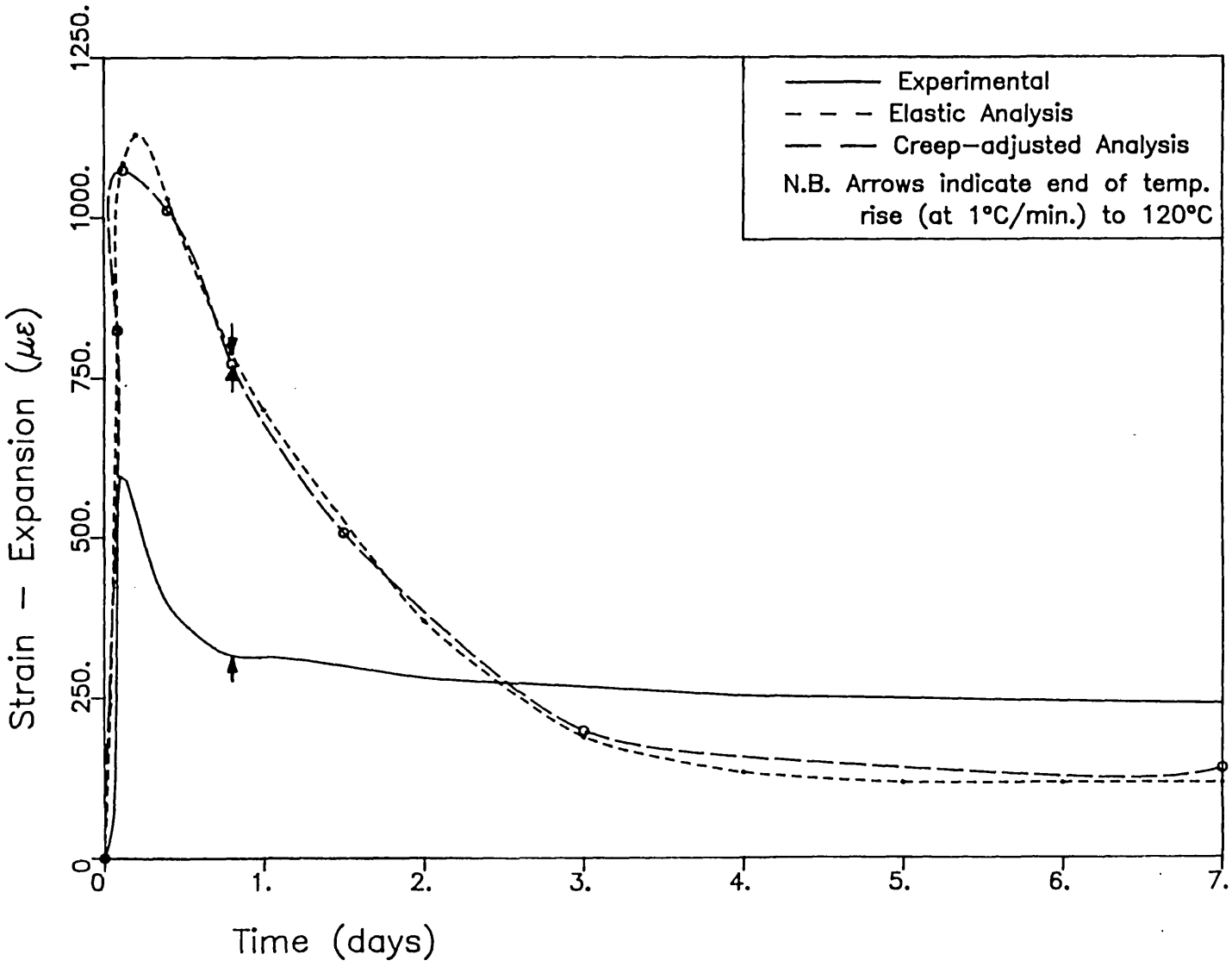

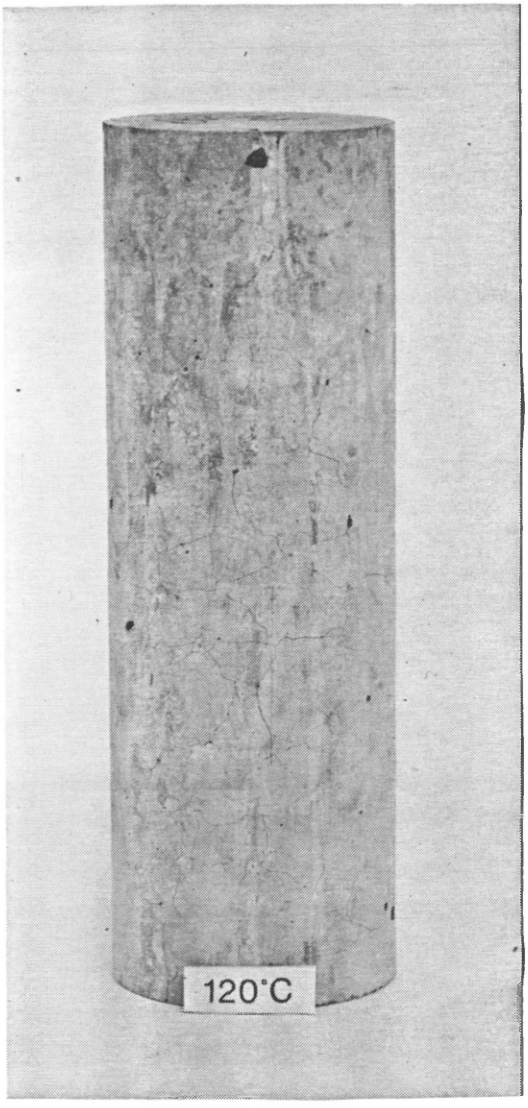

Figure 10.19 - EXTERNAL APPEARANCE OF SPECIMEN HEATED TO AND MAINTAINED FOR 7 DAYS AT 120 C BEFORE COOLING BACK TO ROOM TEMPERATURE.

CHAPTER 11 - CONCLUSIONS AND RECOMMENDATIONS

This final chapter has three sections. It first summarizes the major conclusions arrived at in Chapters 5 to 10. Next it identifies common themes running through the different results obtained in the above-mentioned chapters. Finally, it makes recommendations for future research.

11.1. SUMMARY OF MAJOR CONCLUSIONS

11.1.1. Chapter 5 - Strength and Elastic Properties

(a) Thermal drying up to a temperature of around 300°C is beneficial to both strength and static modulus of elasticity in unsealed hardened cement paste through a densification process (see Figure 5.8). The application of load also contributes to an improvement in the above-mentioned properties (see Figure 5.2). The beneficial effects of densification, either by drying or loading, are not, in general, reflected by pulse velocity measurements (see Figures 5.6 and 5.7).

(b) Strength and elasticity, especially the dynamic modulus of elasticity, show good correlation with porosity changes and moisture loss. (See Figure 5.3).

(c) Strength and elastic properties show that the over-riding effect of temperature on cement paste is 'structural' as opposed to 'thermal'; however, a slight contribution from a thermal effect may also be present. (See Figures 5.1, 5.2, 5.6, 5.7, 5.8 and 5.9).

(d) The use of hardened cement paste should be limited to 400°C, because of the disruptive expansion caused by subsequent rehydration of Calcium hydroxide, which dissociates at the above temperature. This limitation can be removed by even 10% partial replacement of the cement paste with pulverized-

fuel ash. (See Figure 5.12).

11.1.2. Chapter 6 - Shrinkage and Thermal Strain

(a) The duration of the shrinkage phase varies from one temperature to another. In temperature ranges where significant chemical or physical changes take place, cement paste experiences considerable delay in dimensional stabilization. Examples of this are desorption at temperatures below 100°C and dissociation of Calcium hydroxide at temperatures of 400°C and just above. (See Figure 6.1).

(b) The reversal of trend from contraction to expansion in the strains obtained on heating takes place at around 635°C for a cement paste with w/c = 0.3. Both the magnitude of these strains as well as the temperature of trend reversal however, are functions of the w/c ratio of the paste, depending as they do on the relative proportions of hydrated paste to unhydrated grains in the material. (See Figure 6.4).

(c) Shrinkage below 120°C is probably due to the loss of physically held water, while that above 120°C to the liberation of chemically bound moisture. The relationship between percentage weight loss and residual shrinkage is remarkably linear in the temperature range 120°C to 500°C. (See Figure 6.5).

(d) The time function for shrinkage can be approximated by a logarithmic relationship for the variable temperature portion and an exponential type expression for the isothermal portion, for shrinkage results of specimens heated to maximum temperatures from 200°C to 560°C (see Figure 6.8). The temperature dependent parameter in the isothermal expression reflects the proportion of shrinkage that would take place at an earlier or later stage at a given temperature (see Figure 6.9).

(e) The coefficient of thermal contraction of cement paste is temperature dependent, being higher at higher temperatures. (See Figure 6.11).

11.1.3. Chapter 7 - Basic Creep

(a) Although the time, temperature and stress functions of basic creep can be uncoupled in certain regimes of stress and temperature, they are, strictly speaking, interdependent.

(b) The time function is best represented by the 2 parameter power law of the form $\epsilon_c = At^n$, where A and n are parameters that are temperature and stress dependent (See Figures 7.15 and 7.19), though n only mildly so.

(c) A fundamental rheological property, seated in cement paste, limits the structural use of Portland Cement based concretes to temperatures below 600°C. There is a marked increase of creep above this temperature, in which region the creep response seems to be a state function of temperature. (See Figure 7.11).

(d) If test specimens are not pre-heated until dimensional stability is achieved prior to loading, there is an increase in the creep response above that value defined as basic creep. (See Figure 7.1).

(e) If specimens are pre-heated to a higher temperature than the test temperature, the creep response is lower than if they are pre-heated and tested at the test temperature itself (see Figure 7.11). If the creep strains are normalized on the basis of an equal stress/hot strength ratio, the responses are lower for higher temperatures of pre-heating (see Figures 7.13 and 7.14).

11.1.4. Chapter 8 - An Activation Energy Approach for Temperature Dependence

(a) Rate theory can be used to establish a temperature dependence for basic creep of cement paste. This dependence is an Arrhenius relationship for specimens pre-heated to the same upper temperature prior to testing at varying lower test temperatures. A similar relationship, obtained for specimens heated to different temperatures (above 120°C) and tested thereat, is called a pseudo-Arrhenius relationship.

(b) Cement paste exhibits two distinct temperature ranges of differing activation energies, with a transition temperature of around 560°C. The difference in activation energies was about an order of magnitude, i.e. 25 kJ/mol in the lower temperature range (120°C to 525°C), compared to around 250 kJ/mol in the higher temperature range (560°C to 670°C). (See Figures 8.6 and 8.9).

(c) Within the above temperature ranges, cement paste obeys the time shift principle. The shift function is based on an Arrhenius type temperature dependence.

(d) It is thus possible to arrive at an overall power-law relationship between creep strain and equivalent time (which accounts for both temperature and time dependence), for each of the two temperature ranges 120°C to 525°C and 560°C to 670°C. (See Figures 8.14 to 8.18).

(e) Both the time-temperature equivalence above as well as an uncoupled time, temperature and stress functions approach can be used to make predictions for basic creep. (See Figures 8.19 to 8.22).

(f) The rate controlling process of basic creep of hardened cement paste below 560°C is probably a structural readjustment type of mechanism, while that above 560°C is probably a self-diffusion type of mechanism.

11.1.5. Chapter 9 - Microstructural Investigations

(a) Age does not cause a significant change in the degree of polymerization of unsealed cement paste stored at 20°C and 60% RH from 15 to 37 weeks. Thermal treatments from 20°C to 90°C cause an increase in the polysilicate content, while temperatures beyond 120°C cause depolymerization. The loading of specimens during heating enhances the degree of polymerization, in the temperature range 50°C to 300°C. (See Figures 9.3 to 9.5).

(b) The percentage weight loss seems to be a better index of stabilization (i.e. reduction of creep potential) due to varying pre-heat temperatures than is the degree of polymerization, for unsealed cement paste at temperatures above 300°C. (See Figures 9.6 and 9.7).

(c) Scanning electron microscopy reveals that both the proportion and size of unhydrated grains increase with decreasing w/c ratio of paste. Larger grains seem to be more susceptible to separation from their shell of hydrated material upon heating, than are smaller ones (see Figure 9.8). This evidence helps to link the macro-level observations on trend reversal from contraction to expansion upon heating (see Figure 6.4) with microstructural phenomena.

11.1.6. Chapter 10 - Modelling of Aggregate-Paste Interaction

(a) The representative volume element arrived at gives a reasonable representation of specimen behaviour under static and thermal loading.

(b) It is convenient to use an age-adjustment type approach to obtain the entire spectrum of creep responses from transient thermal creep to basic creep at a given temperature.
Modification factors which vary hyperbolically with time are obtained from the upper bound (ttc), lower bound (basic creep) and intermediate point responses for a given temperature.

(See Figures 10.6 and 10.14).

(c) A superposition method using an effective modulus technique is used to account for the effects of creep in the aggregate-paste interaction. Although internal stresses arrived at by elastic analyses are reduced by creep, the model predicts significant damage by matrix cracking for the 2 phase concrete heated to and maintained at 120°C (see Figure 10.17). This is confirmed by qualitative experimental evidence.

11.2. COMMON THEMES OF INTEREST

11.2.1. Temperatures of Significance

The variety of tests performed in this project has made it possible to identify temperatures of significance where the behaviour of hardened cement paste is concerned.

A temperature of around 50°C was seen to be detrimental in general, with a minimum in static modulus of elasticity (see Figure 5.1) and a maximum in creep response (see Figure 7.6) being experienced at that temperature. This is attributed to a weakening of paste structure caused by thermally energised swelling of water layers. It should be noted that a similar minimum in hot strength occurred at the rather higher temperature of 120°C (see Figure 5.8).

This temperature of 120°C is significant because it probably marks the end of physically bound water loss. The presence of a significant amount of moisture in the paste up to this temperature probably resulted in an increasing degree of polymerization with increasing temperature; the paste experienced depolymerization beyond this temperature (see Figure 9.4). The relationship between percentage weight loss and residual shrinkage at temperatures from 120°C to 500°C showed remarkable linearity, and shrinkage in this range of temperature is probably due primarily to the liberation of chemically bound moisture (see Figure 6.5). Then again, the basic creep of hardened cement paste was found to obey an Arrhenius type temperature dependence only above 120°C, the behaviour below this

temperature deviating considerably from the trend (see Figure 8.9).

The next temperature of significance is 300°C where the static modulus of elasticity, both at temperature as well as on post-cooling, drops suddenly after being relatively constant from 200°C to 300°C (see Figures 5.1 and 5.2). The hot strength also experiences a virtually identical trend (see Figure 5.8). This temperature has been associated, at the microstructural level, with increasing porosity (148) and the onset of significant microcracking (138).

The dissociation of Calcium hydroxide at 400°C caused long delay in the achievement of dimensional stability in the temperature range 400°C to 460°C (see Figure 6.1). This made it difficult to perform truly basic creep tests at these temperatures. Furthermore, any Portland Cement paste specimens heated above 400°C were found to disintegrate on post-cooled exposure to atmosphere because of the disruptive expansion during rehydration of dissociated $Ca(OH)_2$; it was found that this could be remedied by the partial replacement of Portland Cement with PFA (see Figure 5.12).

The final temperature of interest is 560°C, beyond which a marked increase in the creep response was discovered, irrespective of the w/c ratio of the cement paste (see Figure 7.22). This parallelled the behaviour of lightweight aggregate concrete researched previously at Imperial College (85). This temperature also marked the point of bilinearity in the Arrhenius plots, the activation energy associated with the higher temperature range (560°C to 670°C) being 10 times greater than that associated with the lower temperature range (120°C to 525°C) (see Figure 8.9).

11.2.2. Densification or Stabilization

The fact that thermal and load applications caused densification or stabilization of the cement paste was evident from several aspects of this investigation.

The hot strength and residual strength showed increases in the temperature ranges 120°C to 300°C and 50°C to 120°C

respectively, to values close to or even above the cold strength, showing the beneficial effect of thermal drying (see Figures 5.8 and 5.9). The beneficial effect of drying ceased beyond 300°C, where porosity (148) and microcracking (138) are known to increase significantly. The application of load was also seen to be beneficial from a comparison of the Series III results (where load was applied during heating, constant temperature and cooling) with Series I results (where load was applied only at temperature and during cooling). The residual static elastic modulus, was higher for the Series III tests, showing a considerable increase over the modulus at room temperature (see Figure 5.2). The residual strengths for Series III specimens were however lower than those for Series I specimens, which result was difficult to explain. Then again, the static modulus of elasticity at temperature was consistently lower than that on post-cooling for Series I specimens (see Figure 5.5), pointing again to densification under load, since cooling alone, without load, to a lower test temperature from a higher one did not vary the elastic modulus very much.

The basic creep response also showed a decrease from 50°C to 150°C, mirroring the strength increase due to thermal drying (see Figure 7.6). The Series II tests however, provided the greatest evidence for stabilization by temperature. All specimens pre-heated to higher temperatures and loaded after being cooled to lower test temperatures showed less creep than if loaded after dimensional stability at these test temperatures (see Figure 7.11). In fact, if the creep strains were normalized on the basis of stress/hot strength ratio, the Series II creep responses were lower, the higher the temperature of pre-heating (see Figure 7.13). Furthermore, specimens cooled down to various test temperatures from pre-heat temperatures of 300°C or less exhibited virtually zero creep, at the stress/cold strength ratio of 0.11 employed here.

At the microstructural level, the degree of polymerization of the paste increased with thermal treatments up to 120°C, but decreased thereafter (see Figure 9.4). Loading during heating caused an increase in the degree of polymerization compared to heating without load, for temperatures from 50°C to 300°C (see Figures 9.4 and 9.5). However, the percentage moisture loss was seen to be a better index of

temperature induced stabilization (in terms of reducing the creep potential) than the polysilicate content, for unsealed cement paste at temperatures above 300°C (see Figures 9.6 and 9.7).

11.2.3. Thermal vs. Structural Effects

Temperature can affect the properties of a material in two ways. The 'structural' effect of temperature is that which is due to structural changes caused by temperature; it would, in general be a function of the maximum temperature experienced and hence history dependent. On the other hand, the 'thermal' effect of temperature is that which is due to the temperature level at the time of test and could be considered a state function.

Where unsealed hardened cement paste was concerned, all strength and elastic properties showed that the over-riding effect of temperature was structural as opposed to thermal - i.e. once the material was heated to a given temperature, its behaviour was characteristic of that temperature and not, in general, dependent on any lower temperature it was cooled to prior to testing. However the evidence seemed to indicate that a slight contribution from a thermal effect may also be present. (See Figures 5.1, 5.7 and 5.8).

Where creep was concerned, there were two structural effects induced by temperature. One was a reduction in hot strength (above 300°C) which increased the creep potential, while the other was a microstructural stabilization which reduced the creep potential. Over and above these two structural effects, there was a thermal effect which was considered to be an Arrhenius type dependence on temperature. (See Table 9.2).

The Arrhenius thermal effect was isolated for series of specimens heated to the same upper pre-heat temperature but creep tested at varying lower temperatures (see Figures 8.6 and 8.7). The microstructural stabilization effect was isolated and correlated with percentage weight loss, for specimens pre-heated to varying upper temperatures but creep loaded at the same test temperature (see Figure 9.7).

Although it is not possible to isolate these three effects in specimens heated for the first time to a series of temperatures and tested thereat (i.e. Series I specimens), such specimens did yield bilinearity in an Arrhenius plot above 120°C (see Figure 8.9) and also bilinearity in a creep vs. stress/hot strength plot (see Figure 7.9). This may have been a result of the other two effects balancing each other out in both the above cases. Hence, the Arrhenius plot in Figure 8.9 is termed a pseudo-Arrhenius relationship. It may be said however that the thermal effect influences creep much more than it does strength and elastic properties.

11.2.4. Inclusion - Matrix Interactions

One of the reasons for concentrating on hardened cement paste, as opposed to concrete, in this investigation, was to eliminate aggregate effects from the behaviour of the 'active' component in the concrete, namely the paste matrix.

However, even the cement paste itself is made up of inclusions of unhydrated grains within a matrix of hydrated paste. The effect of thermal incompatibility between these two phases was observed at the macro-level in the reversal of contraction at a particular temperature, which was dependent on the paste w/c ratio (see Figure 6.4). At the micro-level, SEM images of a heat exposed sample showed cracking between the grains and surrounding hydrated material. (See Figure 9.8). It may be instructive to perform tests on pastes where unhydrated grains have been reduced to a negligible proportion.

Where concrete is concerned, it is likely that high temperature strength during first heating is governed not so much by the aggregate-matrix interaction caused by thermal incompatibility, but rather by the weakening of the paste structure itself due to temperature. This is evident from the fact that both the cement paste tested here and concretes tested by other investigators (1, 54) lose strength significantly at the same temperature of around 300°C (see Figures 5.8 and 5.11). Thermal instability of the aggregate itself, however, would over-ride the above sources of strength reduction.

It is likely that parasitic thermal stresses set up due to thermal strain incompatibility between aggregate and matrix are relieved by creep, especially the transient thermal creep (ttc) experienced during the first heating of concrete. The efficiency of ttc in relieving stress would be functions of both the rate of heating as well as the proportion of matrix contraction (which causes the parasitic stresses) that takes place during the actual temperature rise. It has been conjectured that the strength minimum experienced around 100°C and hitherto attributed to a phenomenon seated purely in the cement paste, may be contributed to by the matrix-aggregate interaction as well.

11.3. RECOMMENDATIONS FOR FUTURE RESEARCH

The following recommendations are designed both to fill the gaps left at the end of this investigation as well as to pursue avenues opened up as a result of it. A fairly extensive set of recommendations has been made for the further development of the inclusion-matrix interaction model, in Section 10.6. They will not be repeated here.

11.3.1. The Stress Function of Basic Creep

It could be said that the time and temperature functions of the basic creep of cement paste are now fairly well understood. However, there is still scope for investigating its stress dependence, up to stresses of around 0.4 times the cold strength. Three aspects of particular interest would be (i) whether the stress function is independent or not of the temperature and time functions, (ii) whether the most useful parameter for stress dependence is the stress/cold strength or the stress/hot strength ratio and (iii) whether the stress function is linear or not.

11.3.2. The Effect of Load on the Polysilicate Content

Coupled with the above investigation of stress function, the effect of load upon the polysilicate content could be researched in greater detail. The effect of applying various stress levels during

the heating phase could be compared with that of applying them after dimensional stability has been reached at maximum temperature. It would also be interesting to find out if and how the application of load counteracts depolymerization of the paste beyond 120°C.

11.3.3. Reversible and Irreversible Components of Basic Creep

It may be instructive to obtain an idea of the way the above components of basic creep are influenced by temperature and stress, especially since irreversible creep is held by some to be a more fundamental property of cement paste and concrete than total creep. A judicious choice of a few test temperatures at which both creep and recovery are measured, together with the extensive creep data in this thesis, may enable such an analysis to be performed without much difficulty. It has been found, albeit in the case of sealed concrete, that recovery following high temperature (20°C to 96°C) creep is much smaller than the preceding creep (116).

11.3.4. Scanning Electron Microscopy Studies

More extensive investigation, of perhaps semi-quantitative nature, could yield more conclusive results than those reported in this work, regarding both the dissociation and rehydration of $Ca(OH)_2$, as well as the role of the unhydrated grain-hydrated paste interaction in reversing thermal strain around 500-600°C. Additional experimentation could include (i) the heat treating of pastes of w/c ratios of say 0.225, 0.30 and 0.375 to the same temperature of 600°C and quantifying the degree of grain-paste interface cracking from polished surface specimens and (ii) the heat treating of OPC pastes with different percentages of PFA replacement (e.g. 0%, 5%, 10%, 25%, 40%) to a temperature beyond 400°C and investigating the morphology of Calcium hydroxide formations at various stages (i.e. before heating, soon after cooling, after post-cooled exposure to air) in fracture surface specimens.

11.3.5. Activation Energy for Shrinkage

Given that it was possible to model the Series I basic creep responses above 120°C with a pseudo-Arrhenius temperature dependence, despite the specimens having different initial strengths and structures at the point of loading, it may be possible to attempt a similar analysis for shrinkage as well, given its temperature and time dependence. It is clear that only the isothermal portions of the shrinkage curves could be used for such an analysis, if it can be performed at all. Furthermore, it must be remembered that the measured shrinkage in a specimen is not a true material property, unlike the measured creep (56); rather, this measured shrinkage would depend on specimen size, environmental conditions and rate of heating. Analogies and similarities between creep and shrinkage have been drawn only because specimen and structural responses show similarities, for example in time and temperature dependence. Hence, if activation energy studies are to be undertaken for shrinkage, they will need some theoretical support as well.

11.3.6. Pre-heating as a Practical Option

This investigation has clearly demonstrated that pre-heating to a temperature higher than the temperature of loading reduces the creep potential. It is also known that the large transitional thermal creep exhibited by cement paste and concrete is removed if the material is previously heated to or above the maximum temperature to be reached under load. If it is desired to reduce the creep experienced by a structure in its lifetime, especially as in the case of pre-stressed concrete structures, practical procedures for pre-heating could be investigated. Experiments should also be carried out to verify how much of this creep potential is regained after prolonged periods at the lower loading temperature, whether ambient or otherwise. The possibility of sealing the concrete after the thermal pre-treatment, as a measure to prevent the regaining of creep potential, could also be considered. It must be kept in mind however, that creep has its beneficial effects as well, such as in stress relaxation. Hence, each application should be approached with a judicious balance being kept between the detrimental and beneficial aspects of creep, considering

not only the way it affects the structural assembly as a whole, but also the way it influences the behaviour of the heterogeneous concrete material itself.

REFERENCES

(1) ABRAMS, M. Compressive strength of concrete at temperatures to 1600 F. in ACI Special Publication SP 25. Temperature and concrete. Detroit : American Concrete Institute, 1976, pp. 33-58.

(2) ALFORD, N. McN., AND RAHMAN, A.A. An assessment of porosity and pore sizes in hardened cement pastes. J. Mater. Sci. 1981 : 16 (11), 3105-14.

(3) ANDERBERG, Y., and THELANDERSSON, S. Stress and deformation characteristics of concrete at high temperatures - 1. General discussion and critical review of literature. Lund, Sweden : Division of Structural Mechanics and Concrete Construction, Lund University of Technology, 1973. Bulletin 34.

(4) ANDERBERG, Y., and THELANDERSSON, S. Stress and deformation characteristics of concrete at high temperatures - 2. Experimental investigation and material behaviour model. Lund, Sweden : Division of Structural Mechanics and Concrete Construction, Lund University of Technology, 1976. Bulletin 54.

(5) ARRHENIUS, S. Uber die reaktionsgeschwindigkeit bei der inversion von rohrzucker durch sauren. Z. Phys. Chem. 1889 : 4, 226.

(6) ARTHANARI, S., and YU, C.W. Creep of concrete under uniaxial and biaxial stresses at elevated temperatures. Mag. Concr. Res. 1967 : 19 (60), 149-56.

(7) ARUTUNYAN, N. Kh. Some problems in the theory of creep. London : Pergamon, 1966.

(8) ASCHL. H., and MOOSECKER, W. Concrete for PCRVs : mechanical properties at elevated temperatures and residual mechanical behaviour after triaxial pre-loading. Proc. 5th Int. Conf. Struct. Mech. React. Technol. Berlin, 1979. Paper H 1/4.

(9) BAKER, A.L.L. An analysis of deformation and failure characteristics of concrete. Mag. Concr. Res. 1959 : 11 (33), 119-28.

(10) BALDWIN, R., and NORTH, M.A. A stress-strain relationship for concrete at high temperatures. Mag. Concr. Res. 1973 : 25 (85), 208-12.

(11) BALI, A. The transient behaviour of plain concrete at elevated temperatures. Ph.D. thesis, University of Aston at Birmingham, 1984.

(12) BARTENEV, G.M. The structure and mechanical properties of inorganic glasses. Groningen, Netherlands : Wolters-Noordhoff, 1970.

(13) BAZANT, Z.P., and THONGUTHAI, W. Pore pressure and drying of concrete at high temperatures. J. Eng. Mech. Div. Am. Soc. Civ. Eng. 1978 : 104 (5), 1059-80.

(14) BAZANT, Z.P., KIM, S.S., and MEIRI, S. Triaxial moisture-controlled creep tests of hardened cement paste at high temperature. Mater. Constr. 1979 : 12 (72), 447-55.

(15) BAZANT, Z.P., and OSMAN, E. Double power law for basic creep of concrete. Mater. Constr. 1976 : 9 (49), 3-11.

(16) BAZANT, Z.P., OSMAN, E., and THONGUTHAI, W. Practical formulation of shrinkage and creep of concrete. Mater. Constr. 1976 : 9 (54), 395-406.

(17) BAZANT, Z.P., and PANULA, L. Practical prediction of time-dependent deformations of concrete. Part 1 : Shrinkage. Mater. Constr. 1978 : 11 (65), 307-16.

(18) BAZANT, Z.P., and PANULA, L. Practical prediction of time-dependent deformations of concrete. Part IV : Temperature effect on basic creep. Mater. Constr. 1978 : 11 (66), 424-34.

(19) BECKER, N.K., and MACINNIS, C. A theoretical method for predicting the shrinkage of concrete. J. Am. Concr. Inst. 1973 : 70 (9), 652-7.

(20) BENTUR, A. The pore structure of hydrated cementitious compounds of different chemical composition. J. Am. Ceram. Soc. 1980 : 63 (7-8), 381-6.

(21) BENTUR, A., BERGER, R.L., LAWRENCE, F.V., MILESTONE, N.B., MINDESS, S., and YOUNG, J.F. Creep and drying shrinkage of Calcium silicate pastes. III - A hypothesis of irreversible strains. Cem. Concr. Res. 1979 : 9 (1), 83-95.

(22) BENTUR, A., MILESTONE, N.B. and YOUNG, J.F. Creep and drying shrinkage of Calcium silicate pastes. II - Induced microstructural and chemical change. Cem. Concr. Res. 1978 : 8 (6), 721-32.

(23) BLUNDELL, R., DIMOND, C., and BROWNE, R. The properties of concrete subjected to elevated temperatures. CIRIA Underwater Engineering Group, 1976.

(24) BRANSON, D.E. et al. Prediction of creep, shrinkage and temperature effects in concrete structures.
in ACI Special Publication SP 27. Designing for effects of creep, shrinkage and temperature in concrete structures. Detroit : American Concrete Institute, 1971.

(25) BROOKS, J.J., and NEVILLE, A.M. A comparison of creep, elasticity and strength of concrete in tension and in compression. Mag. Concr. Res. 1977 : 29 (40), 131-41.

(26) BROPHY, J.H., ROSE, R.M., and WULFF, J. Thermodynamics of structure. New York : Wiley, 1964.

(27) BROWNE, R., and BLUNDELL, R. The influence of loading age and temperature on the long term creep behaviour of concrete in a sealed moisture stable state. Mater. Constr. 1969 : 2 (8), 133-43.

(28) BUCKLE, E.R. Thermogravimetric analysis : the method of isobaric dehydration. J. Phys. Chem. 1959 : 63, 1231-5.

(29) CALLAHAN, J.D., and ROBINSON, G.C. Uniaxial compressive strengths of concretes for temperatures reaching 1033 K. Nucl. Eng. Des. 1978 : 45, 439-48.

(30) CAMPBELL-ALLEN, D., and DESAI, P.M. The influence of aggregate on the behaviour of concrete at elevated temperatures. Nucl. Eng. Des. 1967 : 6, 65-77.

(31) CAMPBELL-ALLEN, D., LOW, E.W.E., and ROPER, H. An investigation on the effect of elevated temperatures on concrete for nuclear vessels. Nucl. Struct. Eng. 1965 : 2, 382-8.

(32) CEB-FIP. International recommendations for the design and construction of concrete structures. London : Cement and Concrete Assn., 1970.

(33) CHERN, J.C., MARCHERTAS, A.H., and BAZANT, Z.P. Concrete creep at transient temperature : constitutive law and mechanism. Proc. 8th Int. Conf. Struct. Mech. React. Technol. Brussels, 1985. Paper H 2/5.

(34) CONRAD, H. Thermally activated deformation of metals. J. Met. 1964 : 16, 582-8.

(35) COPELAND, L.E., and KANTRO, D.L. Hydration of Portland Cement. Proc. 5th Int. Symp. Chem. Cem. Tokyo, 1968 : 2, 387-420.

(36) COTTRELL, A.H. Dislocations and plastic flow in crystals. Oxford : Clarendon Press, 1953.

(37) CREYKE, W.E.C., SAINSBURY, I.E.J., and MORRELL, R. Design with non-ductile materials. London : Applied Science, 1982.

(38) CRUZ, C.R. Apparatus for measuring creep of concrete at high temperatures. Journal of Portland Cement Assn. Research and Development Laboratories. Sep. 1968, pp. 36-42.

(39) DA SILVEIRA, A.F., and FLORENTINO, C.A. Influence of temperature on the creep of mass concrete. in ACI Special Publication SP 25. Temperature and concrete. Detroit : American Concrete Institute, 1971, pp. 173-89.

(40) DAY, R.L. An examination of the relationship between creep and microstructural change in hardened cement pastes. PhD thesis, University of Calgary, Alberta, 1979.

(41) DAY, R.L., and GAMBLE, B.R. The use of activation spectrum theory to describe creep in concrete. in F.H. Wittmann, ed. Fundamental research on creep and shrinkage of concrete. The Hague : Martins Nijhoff, 1982, pp. 15-26.

(42) DAY, R.L., and GAMBLE, B.R. The effect of changes in structure on the activation energy for the creep of concrete. Cem. Concr. Res. 1983 : 13 (4), 529-40.

(43) DAY, R.L., and GAMBLE, B.R. The effect of thermal pre-treatment on the creep of hardened cement paste. Cem. Concr. Res. 1983 : 13 (5), 638-48.

(44) DIAMOND, S. A critical comparison of mercury porosimetry and capillary condensation pore size distributions of Portland Cement pastes. Cem. Concr. Res. 1971 : 1 (5), 531-45.

(45) DIAMOND, S. Identification of hydrated cement constituents using a scanning electron microscope - energy dispersive X-ray spectrometer combination. Cem. Concr. Res. 1972 : 2 (5), 617-32.

(46) DIAMOND, S. Cement paste microstructure - an overview at several levels. Proc. Conf. on Hydraulic Cement Pastes : their structure and properties, Sheffield, 1976, pp. 2-30.

(47) DORN, J.E. Some fundamental experiments on high temperature creep. J. Mech. Phys. Solids. 1954 : 3, 85-116.

(48) DOUGILL, J.W. The effects of thermal incompatibility and shrinkage on the strength of concrete. Mag. Concr. Res. 1961 : 13 (39), 119-26.

(49) EL-JAZAIRI, B., and ILLSTON, J.M. A simultaneous semi-isothermal method of thermogravimetry and its application to cement pastes. Cem. Concr. Res. 1977 : 7 (3), 247-58.

(50) ENGLAND, G.L., and ROSS, A.D. Reinforced concrete under thermal gradients. Mag. Concr. Res. 1962 : 14 (40), 5-12.

(51) EVANS, A.G., and LANGDON, T.G. Structural ceramics. Prog. Mater. Sci. 1976 : 21, 171-441.

(52) EZEKIEL, M., and FOX, K.A. Methods of correlation and regression analysis. 3rd ed. New York : Wiley, 1959.

(53) FAHMI, H.M., BRESLER, B., and POLIVKA, M. Prediction of creep of concrete at variable temperatures. J. Am. Concr. Inst. 1973 : 70 (10), 709-13.

(54) FISCHER, R. Behaviour of cement mortar and concrete at high temperatures. Deutscher Auschuss fur Stahlbeton. 1970. Heft 214.

(55) FUNK, R., and FRYDRYCH, R. The degree of anion condensation in silicic acids and silicates.
in Highways Research Board Special Report 90, Washington, 1966, pp. 284-90.

(56) GAMBLE, B.R., and ILLSTON, J.M. Rate of deformation of cement paste and concrete during regimes of variable stress, moisture content and temperature. Proc. Conf. on Hydraulic Cement Pastes : their structure and properties, Sheffield, 1976, pp. 297-311.

(57) GAROFALO, F. Fundamentals of creep and creep rupture in metals. New York : MacMillan, 1965.

(58) GEYMAYER, H.G. Effect of temperature on creep of concrete. A literature review.
in ACI Special Publication SP 34. Concrete for nuclear reactors. Detroit : American Concrete Institute, 1972, pp. 565-89.

(59) GILKEY, H.J. The moist curing of concrete. Engineering News-Record, 1937 : 119, 630-3.

(60) GILLEN, M. Short-term creep of concrete at elevated temperatures. Fire and Materials, 1981 : 5 (4), 142-8.

(61) GLASSER, F.P., and TAYLOR, H.F.W. Miscellaneous chemical methods.
Ch : 25 in H.F.W. Taylor, ed. The chemistry of cements. Vol. 2. London : Academic Press, 1964, pp. 335-45.

(62) GROSS, H. Computer aided thermal creep analysis of concrete continua. PhD thesis, University of London, 1973.

(63) GROSS, H. High temperature creep of concrete. Nucl. Eng. Des. 1975 : 32, 129-47.

(64) HALSE, Y., PRATT, P.L., DALZIEL, J.A., and GUTTERIDGE, W.A. Development of microstructure and other properties in flyash OPC systems. Cem. Concr. Res. 1984 : 14 (4), 491-8.

(65) HANNANT, D.J. Strain behaviour of concrete up to 95°C under compressive stresses. Proc. Conf. on Pre-stressed Concrete Pressure Vessels, London, 1967, pp. 57-71.

(66) HANSEN, T.C., and ERIKSSON, L. Temperature change effect on behaviour of cement paste, mortar and concrete under load. J. Am. Concr. Inst. 1966 : 63 (4), 489-502.

(67) HARADA, T., TAKEDA, J., YAMANE, S., and FURAMURA, F. Strength, elasticity and thermal properties of concrete subjected to elevated temperatures. in ACI Special Publication SP 34. Concrete for nuclear reactors. Detroit : American Concrete Institute, 1971, pp. 377-406.

(68) HARMATHY, T.Z. Thermal properties of concrete at elevated temperatures. J. Mater. Am. Soc. Test. Mater. 1970 : 5 (1), 47-74.

(69) HARMATHY, T.Z., and BERNDT, J.E. Hydrated Portland Cement and lightweight concrete at elevated temperatures. J. Am. Concr. Inst. 1966 : 63 (1), 93-112.

(70) HAYNES, J.M. Determination of pore properties of constructional and other materials - general introduction and classification of methods. Mater. Constr. 1973 : 6 (33), 169-74.

(71) HICKEY, K.B. Creep, strength and elasticity of concrete at elevated temperatures. U.S. Bureau of Reclamation : Denver, 1967. Report No. C-1257, 17 pp.

(72) HITCHINGS, D. FINEL user's manual. London : Dept. of Aeronautics, Imperial College, 1981.

(73) HOBBS, D.W., and MEARS, A.R. The influence of specimen geometry upon weight change and shrinkage of air-dried mortar specimens. Mag. Concr. Res. 1971 : 23 (75-76), 89-98.

(74) HOLLOWAY, D.G. The physical properties of glass. London : Wykeham Publications, 1973.

(75) HSU, T.T.C. Mathematical analysis of shrinkage stresses in a model of hardened concrete. J. Am. Concr. Inst. 1963 : 60 (3), 371-89.

(76) HSU, T.T.C., and SLATE, F.O. Tensile bond strength between aggregate and cement paste or mortar. J. Am. Concr. Inst. 1963 : 60 (4), 465-85.

(77) ILLSTON, J.M. The components of strain in concrete under sustained compressive stress. Mag. Concr. Res. 1965 : 17 (50), 21-8.

(78) ILLSTON, J.M., DINWOODIE, J.M., and SMITH, A.A. Concrete, timber and metals. New York : Van Nostrand Reinhold, 1979.

(79) ILLSTON, J.M., and SANDERS, P.D. The effect of temperature change upon the creep of mortar under torsional loading. Mag. Concr. Res. 1973 : 25 (84), 136-44.

(80) ILLSTON, J.M., and SANDERS, P.D. Characteristics and prediction of creep of a saturated mortar under variable temperature. Mag. Concr. Res. 1974 : 26 (88), 169-79.

(81) JONES, R., and FACAOARU, I. Recommendations for testing concrete by the ultrasonic pulse velocity method. Mater. Constr. 1969 : 2 (10), 275-84.

(82) KAPLAN, M.F., and ROUX, F.J. Variations in the properties of concrete at elevated temperatures. Proc. 6th Int. Conf. Struct. Mech. React. Technol. Paris, 1981. Paper H 1/2.

(83) KASAMI, H., OKUNO, T., and YAMANE, S. Properties of concrete exposed to sustained elevated temperature. Proc. 3rd Int. Conf. Struct. Mech. React. Technol., London, 1975. Paper H 1/5.

(84) KHOURY, G.A. Transient thermal creep of nuclear reactor pressure vessel type concretes. PhD thesis, University of London, 1983.

(85) KHOURY, G.A., DIAS, W.P.S. and SULLIVAN, P.J.E. Deformation of concrete and cement paste loaded at constant temperatures from 140°C to 724°C. Mater. Constr. to be published, 1986.

(86) KHOURY, G.A., GRAINGER, B.N., and SULLIVAN, P.J.E. Transient thermal creep of concrete : literature review, conditions within specimen and behaviour of individual constituents. Mag. Concr. Res. 1985 : 37 (132), 131-44.

(87) KHOURY, G.A., SULLIVAN, P.J.E., and GRAINGER, B.N. Strain of concrete during first heating to 600°C under load. Mag. Concr. Res. to be published, 1986.

(88) KHOURY, G.A., SULLIVAN, P.J.E., and GRAINGER, B.N. Strain of concrete during first cooling from 600°C under load. Mag. Concr. Res. to be published, 1986.

(89) KOTTAS, R., SEEBERGER, J., and HILSDORF, H.K. Strength characteristics of concrete in the temperature range 20°C to 200°C. Proc. 5th Int. Conf. Struct. Mech. React. Technol., Berlin, 1979. Paper H 1/2.

(90) KRAUSZ, A.S., and EYRING, H. Deformation Kinetics. New York : Wiley, 1975.

(91) LANKARD, D.R., BIRKIMER, D.L., FONDRIEST, F.F., and SNYDER, M. Effects of moisture content on the structural properties of Portland Cement concrete exposed to temperatures up to 500 F.
in ACI Special Publication SP 25. Temperature and concrete. Detroit : American Concrete Institute, 1971, pp. 59-102.

(92) LEA, F.C., and STRADLING, R.A. The resistance to fire of concrete and reinforced concrete. Engineering, 1922 : 114 (2959 and 2960), 341-4, and 380-2.

(93) LENTZ, C.W. The silicate structure analysis of hydrated Portland Cement paste.
in Highways Research Board Special Report 90, Washington, 1966, pp. 269-83.

(94) L'HERMITE, R.G. Volume changes of concrete. Proc. 4th Int. Symp. Chem. Cem., Washington, 1960, pp. 659-94.

(95) LOGOTHETIS, L., and ECONOMOU, Chr. The influence of high temperatures on calibration of non-destructive testing of concrete. Mater. Constr. 1981 : 14 (79), 39-43.

(96) LOHTIA, R.D., and NASSER, K.W. Apparatus for high temperature creep tests of concrete. J. Am. Concr. Inst. 1971 : 68 (2), 114-5.

(97) MALHOTRA, H.L. Effect of temperature on the compressive strength of concrete. Mag. Concr. Res. 1956 : 8 (23), 85-94.

(98) MALHOTRA, H.L. Design of fire-resisting structures. London: Surrey University Press, 1982.

(99) MARECHAL, J.C. Le fluage du beton en fonction de la temperature. Mater. Constr. 1969 : 2 (8), 111-5.

(100) MARECHAL, J.C. Creep of concrete as a function of temperature.
in ACI Special Publication SP 34. Concrete for nuclear reactors. Detroit : American Concrete Institute, 1972, pp. 547-64.

(101) MARECHAL, J.C. Variations in the modulus of elasticity and Poisson's ratio with temperature.
in ACI Special Publication SP 34. Concrete for nuclear reactors. Detroit : American Concrete Institute, 1972, pp. 495-503.

(102) MARECHAL, J.C. Thermal conductivity and thermal expansion coefficients of concrete as a function of temperature and humidity.
in ACI Special Publication SP 34. Concrete for nuclear reactors. Detroit : American Concrete Institute, 1972, pp. 1047-57.

(103) MEARS, A.R. The effect of aggregate size and grading on initial drying shrinkage. Cement and Concrete Assn. : London, 1970. Technical Report TRA 449.

(104) MEYERS, B.L., SLATE, F.O., and WINTER, G. Relationship between time-dependent deformation and microcracking of plain concrete. J. Am. Concr. Inst. 1969 : 66 (1), 60-8.

(105) MINDESS, S., YOUNG, J.F., and LAWRENCE, F.V. Creep and drying shrinkage of Calcium silicate pastes. I - Specimen preparation and mechanical properties. Cem. Concr. Res. 1978 : 8 (5), 591-600.

(106) MITCHELL, J.K., CAMPANELLA, R.G., and SINGH, A. Soil creep as a rate process. J. Soil Mech. Found. Div. Am. Soc. Civ. Eng. 1968 : 94 (1), 231-54.

(107) MOORE, A.E. The thermal dissociation of Calcium hydroxide. Cement and Concrete Assn. : London, 1956. Technical Report TRB/233.

(108) MOTT, N.F., and NABARRO, F.R.N. Dislocation theory and transient creep. Conf. on Strength of Solids. London : Physical Society, 1948.

(109) MUKADDAM, M.A., and BRESLER, B. Behaviour of concrete under variable temperature and loading.
in ACI Special Publication SP 34. Concrete for nuclear reactors. Detroit : American Concrete Institute, 1972, pp. 771-97.

(110) MULLICK, A.K. Creep and microstructural changes in concrete.
in F.H. Wittmann, ed. Fundamental research on creep and shrinkage of concrete. The Hague : Martinus Nijhoff Publishers, 1982, pp. 49-62.

(111) NASSER, K.W. Creep of concrete at low stress-strength ratios and elevated temperatures.
in ACI Special Publication SP 25. Temperature and concrete. Detroit : American Concrete Institute, 1971, pp. 137-47.

(112) NASSER, K.W., and LOHTIA, R.P. Mass concrete properties at high temperatures. J. Am. Concr. Inst. 1971 : 68 (3), 180-6.

(113) NASSER, K.W., and LOHTIA, R.P. Creep of mass concrete at high temperatures. J. Am. Concr. Inst. 1971 : 68 (4), 276-81.

(114) NASSER, K.W., and MARZOUK, H.M. Properties of mass concrete containing fly ash at high temperatures. J. Am. Concr. Inst. 1979 : 76 (4), 537-50.

(115) NASSER, K.W., and MARZOUK, H.M. Creep of concrete at temperatures from 70 to 450 F under atmospheric pressure. J. Am. Concr. Inst. 1981 : 78 (2), 147-50.

(116) NASSER, K.W., and NEVILLE, A.M. Creep of concrete at elevated temperatures. J. Am. Concr. Inst. 1965 : 62 (12), 1567-79.

(117) NEVILLE, A.M. Creep of concrete as a function of its cement paste content. Mag. Concr. Res. 1964 : 16 (46), 21-30.

(118) NEVILLE, A.M. Properties of concrete. 3rd ed. London : Pitman, 1981.

(119) NEVILLE, A.M., DILGER, W.H., and BROOKS, J.J. Creep of plain and structural concrete. London : Construction Press, 1983.

(120) NISHIZAWA, N., and OKAMURA, H. Strength and inelastic properties of concrete at elevated temperatures. in ACI Special Publication SP 34. Concrete for nuclear reactors. Detroit : American Concrete Institute, 1972, pp. 407-21.

(121) NURSE, R.W. The dicalcium silicate phase. Proc. 3rd Int. Symp. Chem. Cem. London, 1952, pp. 56-77.

(122) ORR, C. Jr. Application of mercury porosimetry to materials analysis. Powder Technology 1969/70 : 3, 117-23.

(123) PARROTT, L.J. The effect of moisture content upon the elasticity of hardened cement paste. Mag. Concr. Res. 1973 : 25 (82), 17-20.

(124) PARROTT, L.J. An examination of the effects of age at loading upon the creep of hardened cement paste. Mag. Concr. Res. 1973 : 25 (85), 197-200.

(125) PARROTT, L.J. Lateral strains in hardened cement paste under short- and long-term loading. Mag. Concr. Res. 1974 : 26 (89), 198-202.

(126) PARROTT, L.J. Increase in creep of hardened cement paste due to carbonation under load. Mag. Concr. Res. 1975 : 27 (92), 179-81.

(127) PARROTT, L.J. Effect of a heat cycle during moist curing upon the deformation of hardened cement paste. Proc. Conf. on Hydraulic Cement Pastes : their structure and properties, Sheffield, 1976, pp. 189-204.

(128) PARROTT, L.J. Recoverable and irrecoverable deformation of heat cured cement paste. Mag. Concr. Res. 1977 : 29 (98), 26-30.

(129) PARROTT, L.J. Basic creep, drying creep and shrinkage of a mature cement paste after a heat cycle. Cem. Concr. Res. 1977 : 7 (5), 597-604.

(130) PARROTT, L.J. A study of transitional thermal creep in hardened cement paste. Mag. Concr. Res. 1979 : 31 (107), 99-103.

(131) PARROTT, L.J. Changes in saturated cement paste due to heating. Cement and Concrete Assn. : London, 1979. Technical Report 528.

(132) PARROTT, L.J. Structure and thermal creep of cement paste. Proc. 7th Int. Symp. Chem. Cem. Paris, 1980.

(133) PARROTT, L.J. Thermogravimetric and sorption studies of methanol exchange in an alite paste. Cem. Concr. Res. 1983 : 13 (1), 18-22.

(134) PARROTT, L.J., and TAYLOR, M.G. A development of the molybdate complexing method for the analysis of silicate mixtures. Cem. Concr. Res. 1979 : 9 (4), 483-8.

(135) PETZOLD, A., and ROHRS, M. Concrete for high temperatures. London : Maclaren and Sons Ltd., 1970.

(136) PHILLEO, R. Some physical properties of concrete at high temperatures. J. Am. Concr. Inst. 1958 : 54 (4), 857-64.

(137) PIASTA, J. Heat deformations of cement paste phases and the microstructure of cement paste. Mater. Constr. 1984 : 17 (102), 415-20.

(138) PIASTA, J., SAWICZ, Z., and RUDZINSKI, L. Changes in the structure of hardened cement paste due to high temperature. Mater. Constr. 1984 : 17 (100), 291-6.

(139) PICKETT, G. Effect of aggregate on shrinkage of concrete and a hypothesis concerning shrinkage. J. Am. Concr. Inst. 1956 : 52 (1), 581-90.

(140) POLIVKA, M., and BEST, C.H. Investigation of the problem of creep in concrete by Dorn's method. University of California, Berkeley, 1960. Internal Report.

(141) POMEROY, C.D. Experimental techniques and results. Ch. 5 in Z.P. Bazant and F.H. Wittmann, eds. Creep and shrinkage in concrete structures. Chichester : Wiley, 1982, pp. 111-28.

(142) POWERS, T.C. The non-evaporable water content of hardened Portland Cement paste - its significance for concrete research and its method of determination. Bull. Am. Soc. Test. Mater. 1949 : 158, 68-76.

(143) RAMACHANDRAN, V.S., FELDMAN, R.F., BEAUDOIN, J.J. Concrete science - treatise on current research. London : Heyden and Sons Ltd., 1981.

(144) RAWSON, H. Properties and applications of glass. Amsterdam : Elsevier, 1980.

(145) REICHARD, T.W. Creep and drying shrinkage of lightweight and normal weight concretes. National Bureau of Standards : Washington, 1964. Monograph 74. 30 pp.

(146) REUTZ, W. Das kriechen von zementsteins in beton und seine beeinflussung durch gleichzeitiges schwinden. Deutscher Auschuss fur Stahlbeton. Berlin, 1966. Heft 183.

(147) ROELFSTRA, P.E., SADOUKI, H., and WITTMANN, F.H. Le beton numerique. Mater. Constr. 1985 : 18 (107), 327-35.

(148) ROSTASY, F.S., WEISS, R., and WIEDEMANN, G. Changes of pore structures of cement mortars due to temperature. Cem. Concr. Res. 1980 : 10 (2), 157-64.

(149) SABRI, S., and ILLSTON, J.M. Immediate and delayed thermal expansion of hardened cement paste. Cem. Concr. Res. 1982 : 12 (2), 199-208.

(150) SACKMAN, J.L. Creep in concrete and concrete structures. Proc. Princeton Univ. Conf. on Solid Mechanics. Princeton, 1963.

(151) SAEMAN, J.C., and WASHA, G.W. Variation of mortar and concrete properties with temperature. J. Am. Concr. Inst. 1957 : 54 (5), 385-95.

(152) SAKUTA, M., KASAMI, H., and YOSHIOKA, Y. Creep, strength and thermal expansion of concrete at elevated temperatures. Proc. 5th Int. Conf. Struct. Mech. React. Technol. Berlin, 1979. Paper H 1/7.

(153) SCHNEIDER, U. Physical properties of concrete from 20°C up to melting. Betonwerk + Fertigeil-Technik. Heft 3/81.

(154) SCHNEIDER, U., and DIEDERICHS, U. Detection of cracks by mercury penetration measurements.
Ch. 3.6 in F.H. Wittmann, ed. Fracture mechanics of concrete. Amsterdam : Elsevier, 1983, pp. 207-222.

(155) SCHNEIDER, U., and WEISS, R. Kinetic considerations on the thermal destruction of cement-bound concrete and its mechanical effects. Cem. Concr. Res. 1977 : 7 (3), 259-68.

(156) SCHWARZL, F., and STAVERMAN, A.J. Time-temperature dependence of linear viscoelastic behaviour. J. Appl. Phys. 1952 : 23 (8), 838-43.

(157) SEEBERGER, J., BELLI, W., and HILSDORF, H.K. Strength characteristics of structural concrete in the temperature range 20°C to 250°C. Proc. 6th Int. Conf. Struct. Mech. React. Technol. Paris, 1981. Paper H 1/4.

(158) SIDHU, H., and LIMAYE, R.G. Creep of concrete at elevated temperatures. Indian Concrete Journal. Oct., 1983, pp. 269-73.

(159) SLATE, F.O. Microscopic observation of cracks in concrete, with emphasis on techniques developed and used at Cornell University.
Ch. 3.1 in F.H. Wittmann, ed. Fracture mechanics of concrete. Amsterdam : Elsevier, 1983, pp. 75-83.

(160) SLATE, F.O. X-ray technique for studying cracks in concrete, with emphasis on methods developed and used at Cornell University.
Ch. 3.2 in F.H. Wittmann, ed. Fracture mechanics of concrete. Amsterdam : Elsevier, 1983, pp. 85-93.

(161) SOROKA, I. Portland Cement paste and concrete. London : Macmillan, 1979.

(162) STOCKETT, A.L., SCHNEIDER, A.M., and MARDULIER, F.J. An analysis of drying shrinkage data for Portland Cement mortar and concrete. J. Mater. Am. Soc. Test. Mater. 1967 : 2, 829-42.

(163) SUCOV, E.W. Diffusion of oxygen in vitreous silica. J. Am. Ceram. Soc. 1963 : 46 (1), 14-20.

(164) SULLIVAN, P.J.E. The structural behaviour of concrete at elevated temperature. PhD thesis, University of London, 1970.

(165) SULLIVAN, P.J.E. Time-temperature extrapolation techniques as applied to concrete creep strains. Proc. 1st Int. Conf. Struct. Mech. React. Technol. Berlin, 1971. Paper H 2/2.

(166) SULLIVAN, P.J.E., KHOURY, G.A., and GRAINGER, B.N. Apparatus for measuring the transient thermal strain behaviour of unsealed concrete under constant load for temperatures up to 700°C. Mag. Concr. Res. 1983 : 35 (125), 229-36.

(167) SULLIVAN, P.J.E., and POUCHER, M.P. The influence of temperature on the physical properties of concrete and mortar in the range 20°C to 400°C.
in ACI Special Publication SP 25. Temperature and concrete. Detroit : American Concrete Institute, 1971, pp. 103-35.

(168) SULLIVAN, P.J.E., and ZAMAN, A.A. Explosive spalling of concrete exposed to high temperatures. Proc. 1st Int. Conf. Struct. Mech. React. Technol. Berlin, 1971. Paper H 1/5.

(169) THELANDERSSON, S. Mechanical behaviour of concrete under torsional loading at transient, high temperature conditions. Lund, Sweden : Division of Structural Mechanics and Concrete Construction, Lund University of Technology, 1974. Bulletin 46.

(170) THEUER, A.U. Effect of temperature on the stress deformation of concrete. Journal of Research, National Bureau of Standards. 1937 : 18 (2), 195-204.

(171) TIMUSK, J., and GHOSH, R.S. Maturing creep of Portland Cement paste. J. Am. Concr. Inst. 1971 : 68 (12), 959-63.

(172) TRUESDALE, V.W., and SMITH, C.J. The formation of molybdosilicic acids from mixed solutions of molybdate and silicate. Analyst. 1975 : 100, 203-12.

(173) VYAS, N.C., KALANI, M., and LIMAYE, R.G. Creep of concrete at different temperatures. Indian Concrete Journal. July, 1979, pp. 190-5.

(174) WALKER, S., BLOEM, D.L., and MULLEN, W.G. Effects of temperature changes as influenced by aggregates. J. Am. Concr. Inst. 1952 : 48 (4), 661-79.

(175) WALTHER, R., and PARETH, T. Rheological properties at high temperature of a concrete with crushed limestone aggregate and blast furnace cement. in F.H. Wittmann, ed. Fundamental research in creep and shrinkage of concrete. The Hague : Martinus Nijhoff, 1982, pp. 179-91.

(176) WANG, C. Creep of concrete at elevated temperatures. in ACI Special Publication SP 27. Designing for effects of creep, shrinkage and temperature in concrete structures. Detroit : American Concrete Institute, 1971, pp. 387-400.

(177) WEIGLER, H., and FISCHER, R. Influence of high temperatures on strength and deformation of concrete. in ACI Special Publication SP 34. Concrete for nuclear reactors. Detroit : American Concrete Institute, 1972, pp. 481-93.

(178) WILSHIRE, B. Creep of ceramic materials. in C.D. Pomeroy, ed. Creep of engineering materials. London : Mechanical Engineering Publications, 1978.

(179) WINSLOW, D.N., and DIAMOND, S. A mercury porosimetry study of the evolution of porosity in Portland Cement. J. Mater. 1970 : 5 (3), 564-85.

(180) WITTMANN, F.H. Creep and shrinkage mechanisms. Ch. 6 in Z.P. Bazant and F.H. Wittmann, eds. Creep and shrinkage in concrete structures. Chichester : Wiley, 1982, pp. 129-62.

(181) WITTMANN, F.H., and LUKAS, J. Experimental study of thermal expansion of hardened cement paste. Mater. Constr. 1974 : 7 (40), 247-52.

(182) WITTMANN, F.H., and LUKAS, J. The application of rate theory to time-dependent deformation of concrete. Mag. Concr. Res. 1974 : 26 (89), 191-7.

(183) WITTMANN, F.H., ROELFSTRA, P.E., and SADOUKI, H. Simulation and analysis of composite structures. Mater. Sci. Eng. 1984/85 : 68, 239-48.

(184) WITTMANN, F.H., and SETZER, M. Vergleich einiger kriech - funktionen mit versuchsergebnissen. Cem. Concr. Res. 1971 : 1 (6), 679-90.

(185) YOUNG, J.F. The microstructure of hardened Portland Cement paste.
Ch. 1 in Z.P. Bazant and F.H. Wittmann, eds. Creep and shrinkage in concrete structures. Chichester : Wiley, 1982, pp. 3-22.

(186) ZIENKIEWICZ, O.C., and WATSON, M. Some creep effects in stress analysis with particular reference to concrete pressure vessels. Nucl. Eng. Des. 1966 : 4, 406-12.

(187) ZIENKIEWICZ, O.C., WATSON, M., and KING, I.P. A numerical method of visco-elastic stress analysis. Int. J. Mech. Sci. 1968 : 10, 807-27.

(188) ZOLDNERS, N.G. Effect of high temperatures on concretes incorporating different aggregates. Proc. Am. Soc. Test. Mater. 1960 : 60, 1087-108.

(189) ZOLDNERS, N.G. Thermal properties of concrete under sustained elevated temperatures.
in ACI Special Publication SP 25. Temperature and concrete. Detroit : American Concrete Institute, 1971, pp. 1-31.

(190) ENGLAND, G.L. Numerical creep analysis applied to concrete structures. J. Am. Concr. Inst. 1967 : 64 (6), 301-11.

(191) VALLIAPPAN, S., and CURISKIS, J.I. Constitutive relationships for composite materials through micromechanics.
Ch. 31 in C.S. Desai and R.H. Gallagher, eds. Mechanics of engineering materials. Chichester : Wiley, 1984, pp. 611-632.

(192) ZAITSEV, Y. Crack propagation in a composite material.
Ch. 4.2 in F.H. Wittmann, ed. Fracture mechanics of concrete. Amsterdam : Elsevier, 1983, pp. 251-99.

APPENDIX 1 - LIST OF ITEMS OF THE CREEP TESTING MACHINE

MAIN FRAME

(1) Front post - 7.6 mm sq. x 1980 mm hollow section
(2) Rear column - 3.8 mm sq. x 1980 mm hollow section
(3) Bottom plate - 634 x 762 x 38 mm
(4) Intermediate plate - 634 x 508 x 38 mm
(5) Top plate - 634 x 399 x 38 mm
(6) Web - 482 x 82 x 38 mm
(7) Short cantilever - 69 x 82 x 38 mm
(8) Mounting - 178 x 146 x 50 mm
(9) Pulley bracket - 200 x 50 x 8 mm
(10) Column - ϕ 32 x 1680 mm
(11) Pulley - ϕ 160 x 16 mm
(12) Counterweight - 61 mm sq. x 900 mm

LEVERARM SYSTEM

(13) Leverarm - 1130 x 100 x 19 mm, Alum.
(14) Front pivot - ϕ 32 x 92 mm, KE 355
(15) Pivot at fulcrum - ϕ32 x 92 mm, KE 355
(16) Rear pivot - ϕ 32 x 92 mm, KE 355
(17) Clamp - 57 x 50 x 44 mm
(18) Vee at fulcrum - 50 x 32 x 19 mm, KE 355
(19) Block - 54 mm sq. x 100 mm
(20) Threaded arm - ϕ 25 x 610 mm
(21) Counterweight - ϕ 152 x 76 mm
(22) Bumper - 54 mm sq. x 25 mm
(23) Diaphragm - 100 x 54 x 19 mm
(24) Spacer - ϕ 16 x 10 G x 54 mm

FRONT HANGER

(25) General view of front hanger
(26) Vee at front pivot - 50 mm sq. x 38 mm, KE 355
(27) Coverplate - 242 x 50 x 16 mm, BRT MS
(28) Socket head cap screw - $^3/_8$" BSF x 85 mm

(29) Tie rod - $^3/_4$" BSF x 220 mm, EN 24

(30) Transverse beam - 140 x 60 x 50 mm, BRT MS

(31) Joint pin - ϕ 19 x 77 mm

(32) Clip

(33) Spacer - ϕ 13 x 18G x 38 mm

(34) Socket head cap screw - 5/8" x 85 mm

UPPER UNIVERSAL JOINT

(35) General view of upper universal joint

(36) Spacer - ϕ 28 x 10 G x 76 mm

(37) Joint top place - 140 x 60 x 38 mm, BRT MS

(38) Joint bottom plate - 140 x 60 x 38 mm, BRT MS

(39) Transverse beam - 140 x 60 x 50 mm, BRT MS

(40) Tie rod - 3/4" BSF x 210 mm, EN 24

(41) Bearing ball - ϕ 13 mm

(42) Spacer - ϕ 28 x 10 G x 76 mm

TITANIUM YOKE SYSTEM

(43) General view of yoke system

(44) Tie rod - ϕ 28 x 305 mm

(45) Tie rod - ϕ 19 x 475 mm

(46) Socket head cap screw - 1/8" x 57 mm

(47) Convex spherical bearing - ϕ 60 x 25 mm

(48) Spacer - ϕ 27 x 10 G x 342 mm

(49) Transverse beam - 165 x 70 x 50 mm

(50) Upper bearing plate - 165 x 100 x 40 mm

(51) Concave spherical bearing - ϕ 60 x 25 mm

(52) Circular bearing plate - ϕ 63 x 19 mm

(53) Test specimen - ϕ 62.5 x 187.5 mm

(54) Lower bearing plate - 165 x 100 x 40 mm

LOWER UNIVERSAL JOINT

(55) General view of lower universal joint

(56) Tie rod - ϕ 19 x 460 mm, EN 24

(57) Spacer - ϕ 16 x 10G x 316 mm

(58) Tie rod - ϕ 27 x 330 mm, EN 24

(59) Bolt - 3/8" BSF x 100 mm

(60) Handwheel - ϕ 150 mm

REAR HANGER AND SUSPENSION

(61) Rear hanger - 76 x 54 x 50 mm

(62) Cylindrical joint pin - ϕ 10 x 35 mm

(63) Bracket - 25 mm sq. x 41 mm

(64) Suspension - ϕ 10 x 1950 mm

FURNACE SLIDING ASSEMBLY

(67) Bolt - 5/8" BSF x 65 mm

(68) Rubber pad damper

(69) General view of furnace sliding assembly

(70) Cable

(71) Sliding tube - ϕ 63 x ϕ 32 x 250 mm

(72) Keys

(73) Upper band - ϕ 416 x 40 x 8 mm

(74) Lower band and furnace bearing ring - ϕ 416 x 40 x 8 mm

FURNACE

(75) General view of furnace - ϕ 381 x ϕ 177 x 762 mm

(76) Caposil insulating block - ϕ 380 x ϕ 177 x 60 mm

(77) Coiled coil heaters

(78) Ceramic tube - ϕ 210 x ϕ 178 x 640 mm

(79) Inner Triton ceramic fibre blanket - 13 mm thick

(80) Outer Triton ceramic fibre blanket - 13 mm thick

(81) Verticulite insulation - 60 mm thick

(82) Heated inner space - ϕ 177 x 610 mm

(83) Power supply

(84) Sindanyo asbestos cement - ϕ 380 x ϕ 177 x 60 mm

(85) Control thermocouples

(86) Zone III

(87) Mild steel skin - ϕ 381 x 762 x 2 mm

(88) Zone II

(89) Zone I

(90) Caposil insulating cap - ϕ 177 x ϕ 40 x 70 mm

STRAIN MEASURING DEVICE

(91) Location of strain measuring device

(92) Upper platen - incoloy

(93) Lower platen - incoloy

(94) Outer connecting rod - ϕ 5 mm x 71 mm, Invar

(95) Inner connecting rod - ϕ 5 mm x 56 mm, Invar

(96) Micrometer head - 13 mm travel

(97) Upper link plate - 152 x 25 x 6 mm, Alum.

(98) Lower link plate - 152 x 38 x 6 mm, Alum.

(99) Sangamo d.c. displacement transducer - 10 mm travel

(100) Collette and nut assembly

LOADS

(101) Slotted 57.5 kg weight - ϕ 300 x 100 mm

APPENDIX 2 - SHRINKAGE DATA - SERIES I

TEMP (C)	50.	70.	90.	120.	150.	200.	200.	300.	300.	375.	400.	400.
TIME (DY)												
.0000	232 (18.)	330 (18.)	386 (18.)	1013 (20.)	417 (23.)	569 (17.)	579 (17.)	660 (16.)	986 (20.)	417 (23.)	569 (17.)	0 (15.)
.0417	122 (30.)	248 (33.)	317 (34.)	947 (35.)	184 (45.)	441 (33.)	418 (33.)	583 (32.)	848 (37.)	195 (49.)	479 (33.)	-60 (27.)
.0833	-3 (38.)	10 (50.)	87 (59.)	403 (71.)	53 (83.)	-26 (73.)	17 (76.)	160 (70.)	273 (74.)	108 (87.)	51 (72.)	-160 (70.)
.1667	-77 (44.)	-31 (61.)	88 (76.)	473 (101.)	478 (118.)	765 (146.)	1020 (145.)	1399 (164.)	1434 (179.)	1268 (185.)	1403 (168.)	1163 (170.)
.2500					913 (128.)	2059 (178.)	2366 (176.)	5253 (284.)	5280 (288.)	6157 (346.)	6953 (340.)	6288 (301.)
.3330				902 (108.)		3099 (191.)	3386 (190.)	6630 (297.)	6507 (298.)		10833 (396.)	10086 (400.)
.5000				1244 (110.)		3776 (193.)	4042 (194.)	7449 (300.)	7271 (300.)		12026 (398.)	11311 (400.)
.7500	83 (47.)	267 (65.)	622 (84.)	1681 (112.)	2671 (144.)	4206 (194.)	4497 (195.)	7958 (300.)	7779 (300.)	10314 (374.)	12630 (398.)	11958 (400.)
1.0000	111 (50.)	360 (70.)	798 (90.)	2058 (120.)	3080 (150.)	4473 (200.)	4746 (200.)	8269 (300.)	8051 (300.)	10947 (375.)	12991 (400.)	12348 (400.)
2.0000	409 (50.)	617 (70.)	1321 (90.)	3220 (120.)	3736 (150.)	5130 (200.)	5393 (200.)	8838 (300.)	8627 (300.)	11390 (375.)	13819 (400.)	13164 (400.)
4.0000	711 (50.)	1048 (70.)	2203 (90.)	3994 (120.)	4168 (150.)	5655 (200.)	5901 (200.)	9437 (300.)	9118 (300.)	12036 (375.)	14492 (400.)	13836 (400.)
7.0000	1046 (50.)	1606 (70.)	3022 (90.)	4396 (120.)	4440 (150.)	6009 (200.)	6276 (200.)	9893 (300.)	9513 (300.)	12492 (375.)	14966 (400.)	14369 (400.)
14.0000	1562 (50.)	2506 (70.)	3910 (90.)	4772 (120.)	4769 (150.)	6421 (200.)	6678 (200.)	10430 (300.)	9941 (300.)	13024 (375.)	15295 (400.)	15194 (400.)
21.0000	1877 (50.)	3176 (70.)	4160 (90.)	4944 (120.)	4950 (150.)	6550 (200.)	6825 (200.)	10700 (300.)	10132 (300.)	13197 (375.)	15894 (400.)	15738 (400.)
28.0000	2135 (50.)	3517 (70.)	4311 (90.)									16172 (400.)

Note: Units are microstrain. Figures in parantheses are concurrent temperatures [illegible] C

APPENDIX 2 - SHRINKAGE DATA - SERIES I (CONT.)

TEMP (C)	425.	425.	460.	460.	500.	500.	525.	560.	560.	600.	600.	635.	670.
TIME (DY)													
.0000	970 (20.)	0 (14.)	634 (16.)	1159 (20.)	396 (23.)	892 (21.)	777 (20.)	659 (16.)	0 (14.)	871 (22.)	396 (20.)	934 (22.)	887 (22.)
.0417	842 (39.)	-72 (29.)	570 (37.)	1034 (38.)	120 (46.)	776 (39.)	654 (37.)	549 (33.)	-65 (27.)	748 (39.)	299 (37.)	802 (40.)	745 (39.)
.0833	346 (80.)	-205 (72.)	236 (73.)	494 (79.)	-35 (86.)	336 (77.)	230 (76.)	140 (73.)	-157 (70.)	344 (80.)	-58 (74.)	395 (79.)	316 (79.)
.1667	1472 (173.)	879 (168.)	1512 (168.)	1362 (176.)	1217 (178.)	1624 (171.)	1289 (170.)	1187 (169.)	928 (167.)	1380 (176.)	1104 (170.)	1379 (177.)	1477 (178.)
.2500	6556 (342.)	5631 (336.)	6450 (337.)	6530 (346.)	6503 (351.)	6871 (341.)	6373 (340.)	6032 (336.)	5636 (336.)	6588 (345.)	6174 (337.)	6553 (345.)	6572 (348.)
.3330	11138 (418.)	10200 (419.)	12053 (450.)	12177 (453.)	12560 (-)	12831 (473.)	12450 (476.)	12184 (472.)	11540 (472.)	12885 (479.)	12385 (473.)	12748 (476.)	12823 (482.)
.5000	12489 (420.)	11620 (421.)	14166 (455.)	14185 (457.)	16550 (-)	16825 (495.)	18285 (519.)	20489 (551.)	19579 (552.)	22047 (596.)	20720 (591.)	22457 (628.)	22550 (-)
.7500	13152 (421.)	12266 (422.)	14891 (456.)	14879 (457.)	17756 (500.)	17835 (495.)	19592 (522.)	21243 (553.)	20290 (554.)	22365 (596.)	21113 (600.)	22595 (628.)	22706 (-)
1.0000	13513 (425.)	12704 (425.)	15294 (460.)	15243 (460.)	18205 (500.)	18458 (500.)	19972 (525.)	21439 (560.)	20422 (560.)	22519 (600.)	21202 (600.)	22612 (635.)	22741 (670.)
2.0000	14349 (425.)	13529 (425.)	16225 (460.)	16222 (460.)	18729 (500.)	19402 (500.)	20349 (525.)	21590 (560.)	20645 (560.)	22549 (600.)	21390 (600.)	22663 (635.)	22825 (670.)
4.0000	15008 (425.)	14138 (425.)	17514 (460.)	17354 (460.)	18367 (500.)	19763 (500.)	20543 (525.)	21807 (560.)	20758 (560.)	22568 (600.)	21432 (600.)	22749 (635.)	22738 (670.)
7.0000	15611 (425.)	14911 (425.)	18188 (460.)	17895 (460.)	19122 (500.)	19952 (500.)	20661 (525.)	21879 (560.)	20863 (560.)	22565 (600.)	21442 (600.)	22844 (635.)	22610 (670.)
14.0000	16722 (425.)	16077 (425.)	18685 (460.)	18300 (460.)	19311 (500.)	20138 (500.)	20931 (525.)	21973 (560.)	20926 (560.)	22492 (600.)		22777 (635.)	21910 (670.)
21.0000	17098 (425.)	16553 (425.)	18844 (460.)	18464 (460.)	19353 (500.)	20236 (500.)	21001 (525.)	22010 (560.)	20969 (560.)				
28.0000		16821 (425.)							20957 (560.)				

Note: Units are microstrain. Figures in parantheses are concurrent temperatures in deg.C.

APPENDIX 3 - BASIC CREEP DATA - SERIES I

TEMP (C)	20.	20.	50.	70.	90.	120.	150.	200.	200.	300.	300.	375.	400.	400.
TIME (DY)														
.0010	43.	20.	25.	17.	41.	29.	13.	12.	13.	45.		26.	46.	66.
.0025	56.	36.	38.	27.	50.	35.	15.	16.	22.	47.		43.	67.	84.
.0050	61.	46.	43.	32.	53.	40.	23.	26.	32.	60.		61.	100.	116.
.0100	72.	57.	56.	40.	63.	49.	23.	35.	42.	73.	80.	86.	128.	149.
.0250	95.	74.	71.	43.	71.	54.	37.	37.	58.	91.	99.	110.	181.	200.
.0500	109.	89.	88.	50.	78.	70.	43.	47.	70.	118.	116.	146.	210.	245.
.1000	134.	113.	99.	59.	88.	81.	55.	67.	107.	136.	146.	169.	269.	306.
.2500	163.	154.	142.	78.	108.	97.	57.	77.	105.	185.	188.	203.	369.	410.
.5000	202.	177.	177.	114.	133.	116.	76.	103.	116.	226.	241.	260.	490.	509.
1.0000	251.	226.	227.	149.	154.	148.	115.	130.	152.	283.	299.	367.	644.	660.
2.0000	318.	280.	305.	210.	201.	188.	156.	185.	211.	394.	400.	517.	898.	861.
3.0000	375.	322.	375.	253.	236.	233.	204.	229.	242.	469.	492.	633.	1095.	1032.
4.0000	398.	347.	430.	313.	265.	261.	237.	281.	280.	542.	557.	728.	1262.	
5.0000	445.	368.	471.	335.	293.	289.	217.	335.	323.	602.	591.	798.	1435.	
6.0000			510.	353.	310.	307.	245.	376.	368.	670.	665.	856.	1592.	
7.0000			544.	390.	332.	322.	311.	431.	407.	717.	750.	981.	1737.	
8.0000			625.	429.	358.	361.				757.				
10.0000										871.				
12.0000										958.				
14.0000										1050.				
16.0000										1122.				
20.0000										1240.				
24.0000										1380.				
32.0000										1564.				
40.0000										1756.				

Note Units are microstrain.

APPENDIX 3 - BASIC CREEP DATA - SERIES I (CONT.)

TEMP (C)	425.	425.	460.	460.	500.	500.	525.	560.	560.	600.	600.	635.	670.
TIME (DY)													
.0010		71.	84.		47.	72.	51.	101.	140.	115.		241.	313.
.0025		100.	110.		59.	97.	93.	137.	180.	153.		315.	411.
.0050		133.	132.		89.	125.	113.	165.	204.	195.		382.	533.
.0100	213.	148.	154.	141.	111.	148.	140.	198.	241.	264.		483.	674.
.0250	245.	205.	222.	193.	151.	202.	170.	257.	296.	343.	417.	642.	896.
.0500	283.	247.	271.	218.	192.	243.	223.	308.	350.	416.	479.	788.	1088.
.1000	343.	299.	321.	264.	225.	286.	267.	369.	400.	515.	555.	947.	1333.
.2500	436.	404.	402.	341.	281.	372.	347.	471.	519.	663.	703.	1274.	1782.
.5000	520.	485.	495.	423.	348.	432.	408.	562.	609.	828.	848.	1596.	2277.
1.0000	645.	581.	585.	524.	445.	542.	502.	660.	690.	982.	995.	2009.	2934.
2.0000	803.	746.	769.	675.	554.	670.	647.	855.	837.	1202.	1213.	2610.	3818.
3.0000	966.	871.	857.	789.	659.	787.	747.	945.	912.	1377.	1416.	3079.	4394.
4.0000	1068.		968.	877.	706.	858.	823.	1054.		1520.	1543.	3453.	4787.
5.0000	1161.		1047.	946.	734.	950.	907.	1103.		1631.	1647.	3801.	
6.0000	1291.		1116.	1049.	796.	1008.	979.	1154.		1733.	1732.	4101.	
7.0000	1379.		1179.	1112.	895.	1072.	1034.	1220.		1796.	1844.	4374.	
8.0000			1234.			1196.	1146.	1293.					
10.0000			1378.					1411.					
12.0000			1464.					1495.					
14.0000			1550.					1558.					
16.0000			1649.					1636.					
20.0000			1775.					1746.					
24.0000			1926.					1858.					
32.0000			2129.					2045.					
40.0000			2341.					2213.					

Note: Units are microstrain.

APPENDIX 4 - BASIC CREEP DATA - SERIES II

PREHEAT TEMP (C)	460.	460.	500.	550.	560.	560.	560.	635.	635.	635.	635.	635.	635.	635.
TEST TEMP (C)	300.	375.	300.	300.	375.	460.	500.	300.	300.	460.	460.	525.	560.	600.
TIME (DY)														
.0010	26.	34.	40.	33.	19.	81.	69.	45.	61.	72.	90.	58.	80.	130.
.0025	46.	49.	61.	43.	30.	97.	83.	64.	77.	94.	118.	68.	125.	188.
.0050	60.	57.	75.	63.	41.	132.	102.	76.	94.	97.	133.	83.	149.	231.
.0100	64.	73.	70.	76.	47.	155.	131.	91.	119.	127.	146.	115.	191.	304.
.0250	86.	98.	97.	92.	86.	201.	178.	120.	151.	167.	177.	157.	262.	386.
.0500	106.	110.	124.	115.	108.	242.	219.	142.	177.	204.	223.	181.	319.	462.
.1000	121.	130.	148.	131.	128.	262.	256.	167.	211.	238.	272.	222.	391.	546.
.2500	150.	170.	167.	167.	178.	304.	313.	203.	260.	282.	339.	284.	483.	680.
.5000	178.	195.	203.	195.	210.	363.	372.	223.	308.	337.	395.	332.	583.	831.
1.0000	235.	227.	273.	278.	265.	425.	421.	256.	355.	375.	455.	388.	683.	1008.
2.0000	248.	280.	282.	273.	318.	475.	501.	291.	399.	442.	514.	479.	802.	1179.
3.0000	266.	276.	327.	309.	337.	495.	529.	339.	446.	515.	563.	564.	884.	1337.
4.0000	277.	289.	284.	312.	371.	522.	551.	374.	467.	552.	618.	636.	967.	1453.
5.0000	290.	319.	305.	317.	388.	553.	606.	396.	503.	584.	649.	684.	1038.	1548.
6.0000	292.		325.	335.				427.	521.	606.	672.	693.	1093.	1656.
7.0000	314.		337.	350.				448.	541.	637.	709.	718.	1132.	1724.
9.0000									570.		744.		1197.	

Note: Units are microstrain.

APPENDIX 5 - STRAINS ON HEATING UNDER LOAD - SERIES III

TEMP (C)	50.	90.	120.	200.	300.
TIME (DY)					
.0100	-18. (23.)	-64. (21.)	-53. (21.)	-27. (16.)	-42. (21.)
.0250	51. (29.)	-43. (26.)	-7. (27.)	3. (21.)	22. (27.)
.0500	210. (38.)	142. (42.)	259. (44.)	230. (38.)	303. (47.)
.0750	306. (43.)	503. (61.)	638. (67.)	727. (66.)	829. (72.)
.1000	363. (46.)	578. (70.)	616. (83.)	1045. (93.)	935. (100.)
.1750	420. (48.)	378. (80.)	115. (104.)	-1037. (158.)	-1488. (197.)
.2500	388. (49.)	99. (84.)	-325. (107.)	-2423. (186.)	-4980. (287.)
.5000	268. (49.)	-478. (86.)	-1284. (112.)	-4101. (200.)	-7289. (296.)
1.0000	68. (49.)	-1112. (86.)	-2160. (119.)	-4897. (200.)	-8216. (296.)
2.0000	-224. (49.)	-1837. (87.)	-3380. (122.)	-5502. (201.)	-8943. (296.)
4.0000	-634. (49.)	-2683. (87.)	-4209. (122.)	-6044. (201.)	-9612. (296.)
8.0000	-1188. (49.)	-3737. (88.)	-4706. (122.)		-10302. (296.)
12.0000	-1557. (49.)	-4295. (88.)			-10656. (296.)
18.0000	-1966. (49.)	-4732. (88.)			-11089. (296.)

Note: Units are microstrain. Figures in parantheses are concurrent temperatures in deg C.

APPENDIX 6 - SAMPLE INPUT DATA FOR ANALYSIS STRESS

```
;  DATA25  T=5.00
;  ----------
;
ANALYSIS STRESS
ARRAY SIZE 24000
COMM CONS EQUA TYPE
INSE OWN1 5
ELEMENT PM08  1.0
MESH COORDINATES
      .0000    7.5000      1.2500    7.5000      2.5000    7.5000      3.7500    7.5000
     5.0000    7.5000      6.2500    7.5000      7.5000    7.5000       .0000    7.0000
     2.4937    6.7526      4.7981    6.0481       .0000    6.5000      1.2681    6.3751
     2.4874    6.0052      3.6112    5.4046      4.5962    4.5962      5.4046    3.6112
     6.0052    2.4874      6.3751    1.2681      6.5000     .0000      7.0000     .0000
     6.7526    2.4937      6.0481    4.7981      7.5000     .0000      7.5000    1.2500
     7.5000    2.5000      7.5000    3.7500      7.5000    5.0000      7.5000    6.2500
      .0000    6.2500       .0000    6.0000      4.4194    4.4194      5.7743    2.3918
     6.2500     .0000      5.8847    1.1705      1.1705    5.8847      2.2961    5.5433
     3.3334    4.9888      4.2426    4.2426      4.9888    3.3334      5.5433    2.2961
     5.8847    1.1705      6.0000     .0000       .0000    4.5000      1.9134    4.6194
     3.1820    3.1820      4.6194    1.9134      4.5000     .0000       .0000    3.0000
      .7654    3.3478      1.5307    3.6955      1.8260    2.9084      2.1213    2.1213
     2.9084    1.8260      3.6955    1.5307      3.3478     .7654      3.0000     .0000
      .0000    1.5000      1.0607    1.0607      1.5000     .0000       .0000     .0000
MATERIAL STIFFNESS   20.1    .200
MATERIAL CONDUCTION    .0011
MATERIAL EXPANSION   -.00001044
MESH CONNECTIONS
     1   2   3   8   9  11  12  13     3   4   5   9  10  13  14  15
     5   6   7  10  28  15  22  27    15  22  27  16  26  17  21  25
    17  21  25  18  24  19  20  23
MATERIAL STIFFNESS   20.1    .200
MATERIAL CONDUCTION    .0011
MATERIAL EXPANSION   -.00001044
MESH CONNECTIONS
    11  12  13  29  30  34  35  36    13  14  15  30  31  36  37  38
    15  16  17  31  32  38  39  40    17  18  19  32  33  40  41  42
MATERIAL STIFFNESS   74.0    .210
MATERIAL CONDUCTION    .0014
MATERIAL EXPANSION    .00000920
MESH CONNECTIONS
    34  35  36  43  44  48  49  50    36  37  38  44  45  50  51  52
    38  39  40  45  46  52  53  54    40  41  42  46  47  54  55  56
    48  49  50  57  51  60  58  52    60  58  52  59  53  56  55  54
MESH COORDINATES
      .0000    7.5000      1.2500    7.5000      2.5000    7.5000      3.7500    7.5000
     5.0000    7.5000      6.2500    7.5000      7.5000    7.5000       .0000    8.0000
     2.4937    8.5474      4.7981    8.0519       .0000    8.5000      1.2681    8.6249
     2.4874    8.0948      3.6112    8.5054      4.5962   10.4038      5.4046   11.3888
     6.0052   12.5126      6.3751   13.7319      6.5000   15.0000      7.0000   15.0000
     6.7526   12.5063      6.0481   10.2019      7.5000   15.0000      7.5000   13.7500
     7.5000   12.5000      7.5000   11.2500      7.5000   10.0000      7.5000    8.7500
      .0000    8.7500      2.3918    8.2257      4.4194   10.5806      5.7743   12.6082
     6.2500   15.0000       .0000    8.0000      1.1705    9.1153      2.2961    9.4567
     3.3334   10.0112      4.2426   10.7574      4.9888   11.6666      5.5433   12.7039
     5.8847   13.8295      6.0000   15.0000       .0000   10.5000      1.9134   10.3806
     3.1820   11.6180      4.6194   13.0866      4.5000   15.0000       .0000   12.0000
      .7654   11.6522      1.5307   11.3045      1.8260   12.0916      2.1213   12.8787
     2.9084   13.1740      3.6955   13.4693      3.3478   14.2346      3.0000   15.0000
      .0000   13.5000      1.0607   13.9393      1.5000   15.0000       .0000   15.0000
MATERIAL STIFFNESS   20.1    .200
MATERIAL CONDUCTION    .0011
MATERIAL EXPANSION   -.00001044
MESH CONNECTIONS
     1   2   3   8   9  11  12  13     3   4   5   9  10  13  14  15
     5   6   7  10  28  15  22  27    15  22  27  16  26  17  21  25
    17  21  25  18  24  19  20  23
MATERIAL STIFFNESS   20.1    .200
MATERIAL CONDUCTION    .0011
MATERIAL EXPANSION   -.00001044
MESH CONNECTIONS
    11  12  13  29  30  34  35  36    13  14  15  30  31  36  37  38
    15  16  17  31  32  38  39  40    17  18  19  32  33  40  41  42
MATERIAL STIFFNESS   74.0    .210
MATERIAL CONDUCTION    .0014
MATERIAL EXPANSION    .00000920
MESH CONNECTIONS
    34  35  36  43  44  48  49  50    36  37  38  44  45  50  51  52
    38  39  40  45  46  52  53  54    40  41  42  46  47  54  55  56
    48  49  50  57  51  60  58  52    60  58  52  59  53  56  55  54
FIXED FREEDOMS
  19 2  20 2  23 2  33 2  42 2  47 2  56 2  59 2  60 0
   1 1   8 1  11 1  29 1  34 1  43 1  48 1  57 1
  61 1  64 1  82 1  87 1  95 1 101 1 110 1 113 1
CONS TYPE 1
```

```
CONS EQUA  1 113 2
          -1 112 2
CONS EQUA  1 112 2
          -1 109 2
CONS EQUA  1 109 2
          -1 100 2
CONS EQUA  1 100 2
          -1  95 2
CONS EQUA  1  95 2
          -1  86 2
CONS EQUA  1  86 2
          -1  72 2
CONS EQUA  1  72 2
          -1  73 2
CONS EQUA  1  73 2
          -1  76 2
CONS EQUA  1  76 1
          -1  77 1
CONS EQUA  1  77 1
          -1  78 1
CONS EQUA  1  78 1
          -1  79 1
CONS EQUA  1  79 1
          -1  80 1
CONS EQUA  1  80 1
          -1  81 1
CONS EQUA  1  81 1
          -1   7 1
CONS EQUA  1   7 1
          -1  28 1
CONS EQUA  1  28 1
          -1  27 1
CONS EQUA  1  27 1
          -1  26 1
CONS EQUA  1  26 1
          -1  25 1
CONS EQUA  1  25 1
          -1  24 1
CONS EQUA  1  24 1
          -1  23 1
LOAD TEMPERATURES
   100.0   100.0   100.0   100.0   100.0   100.0   100.0   100.0   100.0   100.0
   100.0   100.0   100.0   100.0   100.0   100.0   100.0   100.0   100.0   100.0
   100.0   100.0   100.0   100.0   100.0   100.0   100.0   100.0   100.0   100.0
   100.0   100.0   100.0   100.0   100.0   100.0   100.0   100.0   100.0   100.0
   100.0   100.0   100.0   100.0   100.0   100.0   100.0   100.0   100.0   100.0
   100.0   100.0   100.0   100.0   100.0   100.0   100.0   100.0   100.0   100.0
   100.0   100.0   100.0   100.0   100.0   100.0   100.0   100.0   100.0   100.0
   100.0   100.0   100.0   100.0   100.0   100.0   100.0   100.0   100.0   100.0
   100.0   100.0   100.0   100.0   100.0   100.0   100.0   100.0   100.0   100.0
   100.0   100.0   100.0   100.0   100.0   100.0   100.0   100.0   100.0   100.0
   100.0   100.0   100.0   100.0   100.0   100.0   100.0   100.0   100.0   100.0
   100.0   100.0   100.0
END JOB
```